



HAL
open science

Hydrolyzable polymer-based elastomers : a new strategy of antifouling coating

Laure Gevaux

► **To cite this version:**

Laure Gevaux. Hydrolyzable polymer-based elastomers : a new strategy of antifouling coating. Other [q-bio.OT]. Université de Toulon, 2019. English. NNT : 2019TOUL0011 . tel-02496991

HAL Id: tel-02496991

<https://theses.hal.science/tel-02496991>

Submitted on 3 Mar 2020

HAL is a multi-disciplinary open access archive for the deposit and dissemination of scientific research documents, whether they are published or not. The documents may come from teaching and research institutions in France or abroad, or from public or private research centers.

L'archive ouverte pluridisciplinaire **HAL**, est destinée au dépôt et à la diffusion de documents scientifiques de niveau recherche, publiés ou non, émanant des établissements d'enseignement et de recherche français ou étrangers, des laboratoires publics ou privés.

ÉCOLE DOCTORALE MER & SCIENCES (E.D. 548)

LABORATOIRE MAPIEM (E.A. 4323)

THÈSE

présentée par :

Laure GEVAUX

Soutenance prévue le : **8 Octobre 2019**

pour obtenir le grade de **Docteur**

Spécialité : Chimie

Hydrolyzable polymer-based elastomers: a new strategy of antifouling coating

THÈSE dirigée par :

M. André MARGAILLAN, Professeur, Université de Toulon

Mme Christine BRESSY, MCF/HDR, Université de Toulon

Mme Marlène NOBLET (LEJARS), IGR, Université de Toulon

Directeur

Co-directeur

Co-encadrant

JURY :

M. Etienne FLEURY, Professeur, INSA de Lyon

Mme Isabelle LINOSSIER, Professeur, Université de Bretagne Sud

Mme Valérie LANGLOIS, Professeur, Université Paris-Est

Mme Marie-Christine SAINTE CATHERINE, Expert DGA

Examineur

Rapporteur

Rapporteur

Invité

Acknowledgements

REMERCIEMENTS

Ce manuscrit est l'aboutissement de trois années de doctorat qui se sont déroulées au sein du laboratoire Matériaux Polymères Interfaces Environnement Marin (MAPIEM), à l'Université de Toulon.

Un grand merci à mes trois encadrants, André Margailan, directeur de thèse, Christine Bressy, co-directrice de thèse et Marlène Noblet, co-encadrante, vous m'avez énormément apporté sur le plan scientifique, notamment de la rigueur et de l'esprit critique. Merci de m'avoir laissé beaucoup d'autonomie et d'avoir suivi régulièrement mon travail avec intérêt. Je n'ai manqué de rien avec vous, je pense que je n'aurais pas pu espérer un meilleur encadrement et/ou meilleur soutien. Merci aussi pour tous ces autres moments de complicité en dehors du laboratoire comme au radeau, restaurants et congrès à l'étranger.

J'adresse de chaleureux remerciements à Isabelle Linossier, Valérie Langlois pour avoir accepté d'évaluer ce travail, ainsi qu'à Etienne Fleury pour sa participation à mon jury de thèse.

Je voudrais remercier la DGA pour le financement de cette thèse et notamment Marie-Christine Sainte Catherine pour être venue participer à mon 2^{ème} comité de suivi de thèse et pour sa participation à mon jury de thèse.

Merci à John Finlay, Nicholas Alfred (Université de Newcastle) et Robert Bunet (institut océanographique Paul Richard) pour les tests biologiques menés sur mes revêtements.

Je remercie également Hervé Luneau, David Pierre et Jean-Paul Lecomte de Dow pour les échantillons de catalyseurs (TIB Chemicals), pour les huiles silicones, et pour les conseils de préparation sur les élastomères silicones. Merci à l'entreprise Evonik pour m'avoir fourni des additifs divers et variés.

Merci à Jean-François Chailan et Jean-François Briand pour l'interprétation de certains de mes résultats et pour votre disponibilité chacune des fois où j'avais besoin d'un avis scientifique sur des analyses mécaniques et biologiques, respectivement.

Acknowledgements

Un grand merci à Armand Fahs et Lénaïc Belec pour m'avoir formée et aidée sur les analyses MEB-EDX et AFM.

Je remercie Fabrice Crolet, Geoffrey Nogaro et Loïc Reboul de la DGA pour l'accès à la barge d'expérimentation dans la rade de Toulon.

Merci à Gérald Culioli, Bruno Viguié, Lucile Pelloquet, Raphaëlle Barry, Isabelle Martin, Olivier Bottzeck et Sophie Berlioz pour l'aide apportée sur les différents équipements (RMN, LC/MS, confocal, lyophilisateur, DSC...). Merci aux autres membres permanents de MAPIEM notamment pour tous ces bons moments passés autour d'une galette des rois, d'une raclette ou d'un barbecue.

Un grand merci à toute l'équipe du SIM et en particulier à Jean-Michel Robert, Edwige Joliff et Mélanie Wolfs, vous m'avez aidée à de nombreuses reprises notamment sur les analyses thermiques, mécaniques et sur le turboeroder. J'ai beaucoup apprécié votre partage de conseils et de connaissances.

Merci à mon stagiaire Ismaël qui a participé à la partie synthèse de cette thèse et que j'ai eu plaisir à former. Je te souhaite bon courage pour ta thèse au Canada, ne baisse jamais les bras.

Je remercie également toutes les personnes de l'administration pour m'avoir aidée pour des services variés, notamment Anne Delarue pour l'organisation de mes congrès et Catherine Dupont pour son aide avec mes contrats d'enseignement.

A la directrice de l'ED548, Mme Muriasco, Stéphanie Moutou et la directrice de l'ED509, merci de m'avoir poussée à participer à MT180, je ne l'aurais pas fait sinon. Ça a été une expérience très intense. Merci à Patricia Casanova pour la gestion de mon dossier de thésarde et les réponses à toutes mes questions sur la formation doctorale.

Acknowledgements

Toutes les personnes ci-dessous ont aussi contribué à l'élaboration de cette thèse, car elles m'ont permis de rester bien dans ma tête, pour cela je leur en suis reconnaissante.

Je remercie tous ceux avec qui nous avons passé de bons moments, que ce soit dans le cadre de congrès, au laboratoire, lors de soirées apéro plage, lors de concerts, de restos, notamment mon petit ismo (#bobu #allocoo #atiékééé #déguéé #muffin #monmogo), Nesrine (#mamachicha #tadjine #onsenttonparfumàdeskm #tapremièreetdernièrefoisauski), Margaux (#lapetitemeuflapluscostaudquejeconnaisse), Elora, Vitalys, Sigrid, etc. et la team MIO/PROTEE.

René, mon cher René, merci d'avoir rallongé ta thèse d'un an juste pour rester un peu plus longtemps avec moi, ma 3^{ème} année n'aurait vraiment pas été pareil sans toi, tu as une très belle âme, je te remercie de m'avoir supportée 24h/24. Ta patience et ton calme avec moi m'ont souvent laissée agréablement perplexe. Tu es un frère parfois un tout petit peu hypocrite mais on va dire que je te pardonne (#René #leshybridescestlavenir #documentairesanimaliers #saveurarc-en-ciel #cestchimiqueousynthétique #ilfautoccuperwiviàlaplage #Scih*bçamarchepaaasaprès4ansdethèse). Merci pour avoir apporté ta bonne humeur à toutes les soirées et merci aussi pour m'avoir beaucoup appris sur Word 😊.

Coqueletto, je suis triste que tu partes avant ma soutenance, tu auras été mon alter ego masculin, insupportable et ronchon à la fois mais très attachant malgré tout. Merci de m'avoir dit que je ne finirai jamais ma thèse en 3 ans, ça m'a beaucoup stimulé je dois dire. Poulette Sarah latina, tu as été une très belle rencontre (d'habitude j'ai un peu de mal avec les latinas^^), ta joie insatiable est ta plus belle qualité, j'ai adoré t'avoir en soirée même si j'aime pas quand tu mets des musiques espagnoles.

Mon petiot Nathan, merci pour ta fraîcheur et ton innocence qui m'ont presque fait oublier mon âge à certains moments. J'aurais aimé faire plus de soirées avec toi mon fillot. Je te souhaite en tout cas une très bonne expérience de thèse, que tu as déjà brillamment entamée et j'espère que tu auras toi aussi, sous ton aile, de nouveaux petits petiots.

Acknowledgements

Brenoir, ta rareté (#noiroublanc #albinos #primatepoilu #allergiesàtout&nimportequoi), ta démarche originale, ton teint palo et ton humour de professor ont fait que tu as fini par beaucoup me charmer. Le doute m'habitait au début sur ton cas mais finalement j'ai fini par t'adopter, tu as été une belle rencontre et j'espère qu'avec Isis vous vivrez heureux avec beaucoup de bébés albinos noirs mexicains (#hybridesunpeuchelou).

Merci aux anciens qui ne sont plus parmi nous mais avec qui j'ai aussi passé de très bons moments (à Londres entre autres) avec notamment Aurélie, Laurie et Riri (même si c'était pas facile tous les jours^^).

Enfin, je remercie toute ma famille, et en particulier ma popotte, mon pounet et mes frère & sœur Stéphane et Virginie pour avoir toujours été là pour moi, pour m'avoir soutenue dans chacune de mes décisions. C'est grâce à vous que je suis là aujourd'hui. Merci à ma grande BF, Marie Toquigon, tu as aussi toujours été là pour moi, malgré la distance, tu es et resteras toujours mon petit ange gardien.

VALORIZATION OF THE PHD WORK

Scientific papers

- Gevaux L., Lejars M., Margaillan A., Briand, J.-F.; Bunet, R.; Bressy C., « Hydrolyzable additive-based silicone elastomers: a new approach for antifouling coatings », *Polymers*, **2019**, 11, 305.
- Gevaux L., Lejars M., Margaillan A., Bressy C., « Water erodible coatings based on a hydrolyzable PDMS/polyester network », *Material Today Communications*, **2018**, 17, 517-526.

Oral presentations

- Gevaux L., Lejars M., Margaillan A., Bressy C., « Water erodible silicone/polyester networks for antifouling applications », 26th day of PACA Chemistry (26^{ème} Journée de la Chimie PACA), University of Nice Sophia Antipolis, France, 26 April **2019**.
- Gevaux L., Lejars M., Margaillan A., Bressy C., « Water erodible coatings based on a hydrolyzable PDMS/polyester network for marine application », 19th International Congress on Marine Corrosion and Fouling (ICMCF), Florida Institute of Technology (FIT), Melbourne, Florida, 24- 29 June **2018**.
- Gevaux L., Lejars M., Margaillan A., Bressy C., « Ma Thèse en 180 Secondes », 12th Scientific Days (La Recherche fait son Show), Toulon, France, 10 April **2018**.
- Gevaux L., Lejars M., Margaillan A., Bressy C., « Elastomère silicone hydrolysable: une nouvelle approche de revêtement antifouling », 45th days of the study of polymers (45^{ème} Journées d'études des polymers, JEPO), Gravelines, France, 1-6 October **2017**.

Posters

- Gevaux L., Lejars M., Margaillan A., Bressy C., « Hydrolyzable additive polymers embedded in a silicone elastomer for antifouling applications », 26th day of PACA Chemistry (26^{ème} Journée de la Chimie PACA), University of Nice Sophia Antipolis, France, 26 April **2019**.
- Gevaux L., Lejars M., Margaillan A., Bressy C., « Hydrolyzable additive-based silicone elastomers: «a new approach of antifouling coatings », 19th International Congress on Marine Corrosion and Fouling (ICMCF), Florida Institute of Technology (FIT), Melbourne, Florida, 24- 29 June **2018**.

ACRONYMS AND SYMBOLS

▪ Polymers

P(CL- <i>co</i> -VL)	Poly(ϵ -caprolactone- <i>co</i> - δ -valerolactone)
P(MDO- <i>co</i> -TBSM- <i>co</i> -MMA)	Poly(2-methylene-1,3-dioxepane- <i>co</i> -methyl methacrylate- <i>co</i> -tributylsilyl methacrylate)
P(MMA-TBMSiMA)	Poly(methyl methacrylate- <i>tert</i> -butyldimethylsilyl methacrylate)
P(PA- <i>co</i> -RA- <i>co</i> -IPA)	Poly(phtalic acid- <i>co</i> -ricinoleic acid- <i>co</i> -isophtalic acid ester anhydride)
PAA	Poly(acrylic acid)
PAAm	Polyacrylamide
PBAT	Poly(butylene adipate- <i>co</i> -terephthalate)
PBS	Poly(butylene succinate)
PCB	Poly(carboxybetaine)
PCL	Poly(ϵ -caprolactone)
PDES	Poly(diethoxysilane)
PDMS	Poly(dimethylsiloxane)
PE	Poly(ethylene)
PEA	Poly(ethylene adipate)
PEC	Poly(ethylene glycol- <i>co</i> -citric acid)
PEG	Poly(ethylene glycol)
PEO	Poly(ethylene oxide)
PES	Poly(ethylene succinate)
PGA	Poly(glycolide)
PGS	Poly(glycerol sebacate)
PGSL	Poly(glycerol, sebacate and lactic acid)
PHB	Poly(hydroxybutyrate)
PHEMA	Poly(2-hydroxyethyl methacrylate) (HEMA)
PHFP	Poly(hexafluoropropylene)
PLA	Poly(lactide)
PLGA	Poly(lactide- <i>co</i> -glycolide)
PMATM2	poly(bis(trimethylsilyloxy)methylsilyl methacrylate)
PMETA	Poly(2-(methylacryloyloxy)ethyl trimethylammonium chloride)
PMMA-PBMA	Poly(methyl methacrylate- <i>co</i> -butyl methacrylate)
PMPC	Poly(2-methacryloyloxyethyl phosphorylcholine)
POC	Poly(1,8-octanediol citrate)
PPSC	Poly((1,2-propanediol-sebacate)-citrate)
PS	Poly(styrene)
PSB	Poly(sulfobetaine)
PTFE	Poly(tetrafluoroethylene)
PTMC	Poly(trimethylene carbonate)

Acronyms and symbols

PU	Poly(urethane)
PVA	Poly(vinyl alcohol)
PVC	Poly(vinyl chloride)
PVF	Poly(vinyl fluoride)
PVP	Poly(N-vinyl pyrrolidone)
PXS	Poly(xylitol sebacate)

▪ Other chemical compounds

AIBN	2,2'-azobis(2-methylpropionitrile)
BD	1,4-butanediol
BiND	Bismuth neodecanoate
CDCl ₃	Deuterated chloroform
CPDB	2-cyano-2-propyl dithiobenzoate
Cu ₂ O	Dicopper oxide
DBTDL	Dibutyltin dilaurate
DCOIT	4,5-dichloro-2- <i>n</i> -octyl-4-isothiazoline-3-one
DMHA	<i>N,O</i> - di-methacryloylhydroxylamin
DMSO- <i>d</i> ₆	Deuterated dimethyl sulfoxide
DOTDL	Dioctyl tin dilaurate
EG	Ethylene glycol
ES40	Ethyl polysilicate
HPMA	<i>N</i> -(2-hydroxypropyl)-methacrylamide
IPTES	(3-isocyanatopropyl)triethoxysilane
IPTMS	(3-isocyanatopropyl)trimethoxysilane
MDO	1,3-dioxepane monomer
QAS	Quaternary ammonium-based compounds
SnOctII	2-ethylhexanoate catalyst
TBSM	Tributylsilyl methacrylate
TBT	Tributyltin
TEOS	Tetraethoxysilane
THF- <i>d</i> ₈	Deuterated tetrahydrofuran
TIPSiMA	Triisopropylsilyl methacrylate
ZnO	Zinc oxide

▪ Characterization techniques

AFM	Atomic force microscope
CA	Contact angle

Acronyms and symbols

CLSM	Confocal laser scanning microscopy
DCA	Dynamic contact angle
DMA	Dynamic mechanical analysis
DSC	Differential scanning calorimetry
EDX	Energy dispersive X-Ray spectroscopy
FTIR-ATR	Fourier-transform infrared Attenuated Total Reflectance
NMR	Nuclear magnetic resonance
SEC	Size exclusion chromatography
SEM	Scanning electron microscopy
TD-SEC	Triple detection- size exclusion chromatography
TGA	Thermogravimetric analysis

▪ Other acronyms

AF	Antifouling
AFS convention	International convention on the control of harmful antifouling systems on ships
ASW	Artificial seawater
BPD	Biocidal Product Directive
CDP	Controlled Depletion Polymers
CDPR	California Department of Pesticide Regulation
d.w.	Deionized water
ECHA	European Chemicals Agency
FIR	Friction increase rate
FR	Fouling Release
FRC	Fouling Release Coating
HLB	Hydrophilic-Lipophilic Balance
IMO	International Maritime Organization
IPN	Interpenetrating network
NEO	Neopentyl glycol
NPA	Natural product antifoulant
OWRK	Owens-Wendt-Rabel-Kaelble
RAFT	Reversible addition-fragmentation chain transfer
ROP	Ring opening polymerization
RTV	Room Temperature Vulcanization
SFE	Surface free energy
SLIPS	Slippery Lubricant-Infused Porous Surface
SPC	Self-Polishing Coating
X3	Hempasil X3

Acronyms and symbols

▪ Symbols

$\Delta\theta$	Hysteresis water contact angle
D	Diffusion coefficient
ΔH_m	Enthalpy of melting
dn/dc	Refractive index increment
\bar{D}	Dispersity
E'	Elastic modulus
E^*	Effective elastic modulus
F	Force
f	Functionality
F_{adh}	Maximum adhesion force
M/I	Monomer/initiator molar ratio
M_c	Interchain molar mass
M_n	Number average molar mass
M_w	Mass average molar mass
R	Tip radius
R_a	Arithmetic average of the surface roughness
R_z	Absolute average value of the 5 highest peaks and 5 lowest peaks
SiO_xOH_y	Siliceous phase
$\tan \delta$	Dissipation factor
T_g	Glass transition temperature
t_i	Immersion time
T_m	Melting temperature
t_R	Reaction time
T_α	α relaxation temperature
w	Mass fraction
X_c	Crystallinity
δ	Hansen parameter
θ_{hex}	Static n-hexadecane contact angle
θ_w	Static water contact angle
$\theta_{w,adv}$	Advancing water contact angle
$\theta_{w,rec}$	Receding water contact angle
λ	Wavelength
γ_S	Surface free energy
γ_S^P	Polar component of the surface free energy
γ_S^D	Dispersive component of the surface free energy

TABLE OF CONTENTS

INTRODUCTION 1

Chapter I State-of-the-art 9

I.1. Introduction 9

I.2. Marine fouling 10

 I.2.1. Impact of biofouling on human activities 10

 I.2.2. Biofouling as a process 10

I.3. Overview of the antifouling strategies 13

 I.3.1. Biocidal antifouling strategy 13

 I.3.2. Biocide-free antifouling coatings 16

I.4. Focus on biocidal antifouling coatings 22

 I.4.1. Commercial biocidal antifouling coatings 22

 I.4.1.1. Description of the biocidal coating composition 23

 I.4.1.1.1. Insoluble-matrix coating 23

 I.4.1.1.2. Soluble-matrix coating 24

 I.4.1.1.3. Self-polishing coatings 25

 I.4.1.2. Specific properties of the erodible biocidal coatings 30

 I.4.1.2.1. Erosion process 30

 I.4.1.2.2. Release process 32

 I.4.1.2.3. Other surface physico-chemical properties 34

 I.4.2. Advances made on erodible antifouling coatings at the research state 35

I.5. Focus on fouling release coatings 45

 I.5.1. Commercial fouling release coatings 45

 I.5.1.1. Description of the FRC composition 46

 I.5.1.1.1. Elaboration of conventional silicone elastomers 46

 I.5.1.1.1.1. Peroxide-induced crosslinking of polysiloxane 46

 I.5.1.1.1.2. Condensation cure system 47

 I.5.1.1.1.3. Addition cure system 49

 I.5.1.2. Improvement of the FRCs 49

Table of contents

<i>I.5.1.3.</i>	<i>Specific properties of FRCs</i>	<i>57</i>
<i>I.5.1.3.1.</i>	<i>Surface properties.....</i>	<i>57</i>
<i>I.5.1.3.1.1.</i>	<i>Contact angles</i>	<i>57</i>
<i>I.5.1.3.1.2.</i>	<i>Surface free energy.....</i>	<i>58</i>
<i>I.5.1.3.1.3.</i>	<i>Smoothness</i>	<i>60</i>
<i>I.5.1.3.2.</i>	<i>Bulk properties.....</i>	<i>61</i>
<i>I.5.1.3.2.1.</i>	<i>Softness.....</i>	<i>61</i>
<i>I.5.1.3.2.2.</i>	<i>Coating thickness</i>	<i>63</i>
<i>I.5.1.3.3.</i>	<i>Ecotoxicity in the aquatic environment</i>	<i>63</i>
I.5.2.	Advances made on FRCs at the academic research state.....	64
<u>I.6.</u>	<u>Hydrolyzable polymers as potential candidates for novel hybrid FRCs</u>	<u>75</u>
I.6.1.	Hydrolyzable polymers	75
<i>I.6.1.1.</i>	<i>Linear hydrolyzable polymers.....</i>	<i>75</i>
<i>I.6.1.2.</i>	<i>Hydrolyzable networks.....</i>	<i>78</i>
<i>I.6.1.2.1.</i>	<i>Hydrolyzable in the polymeric chains</i>	<i>79</i>
<i>I.6.1.2.2.</i>	<i>Hydrolyzable in the crosslinks</i>	<i>83</i>
I.6.2.	Kinetics of hydrolysis.....	84
<u>I.7.</u>	<u>Conclusion.....</u>	<u>86</u>
<u>I.8.</u>	<u>Bibliographical references.....</u>	<u>87</u>
Chapter II	Hydrolyzable polymer additive-based silicone elastomers.....	109
<u>II.1.</u>	<u>Introduction</u>	<u>109</u>
<u>II.2.</u>	<u>Hydrolyzable polymer additives.....</u>	<u>110</u>
II.2.1.	Requirements for the hydrolyzable polymer additives.....	110
II.2.2.	Preparation of polymer additives.....	113
II.2.3.	Physico-chemical properties of the hydrolyzable polymer additives.....	114
II.2.4.	Hydrolysis mechanisms of the polymer additives	115
<i>II.2.4.1.</i>	<i>Hydrolysis mechanism of PCL-based polymers.....</i>	<i>115</i>
<i>II.2.4.2.</i>	<i>Hydrolysis mechanism of PMATM2</i>	<i>116</i>
II.2.5.	Wettability properties of the hydrolyzable polymer additives.....	117
<u>II.3.</u>	<u>Preparation of silicone-based coatings</u>	<u>118</u>

Table of contents

II.3.1. Choosing a model system	118
<i>II.3.1.1. Choice of the PDMS oil</i>	<i>119</i>
<i>II.3.1.2. Choice of the crosslinker</i>	<i>119</i>
<i>II.3.1.3. Choice of the catalyst.....</i>	<i>120</i>
II.3.2. Blend with additives	120
<i>II.3.2.1. Choice of the additive amount</i>	<i>120</i>
<i>II.3.2.2. Choice of the solvent.....</i>	<i>121</i>
<i>II.3.2.3. Formulation process</i>	<i>121</i>
<u>II.4. Characterization of coatings.....</u>	<u>122</u>
II.4.1. Mass loss test.....	123
II.4.2. Surface properties	126
<i>II.4.2.1. Preliminary study on PDMS.....</i>	<i>126</i>
<i>II.4.2.2. Roughness measurements</i>	<i>131</i>
<i>II.4.2.3. Contact angle measurements and surface free energies.....</i>	<i>133</i>
<i> II.4.2.3.1. Dynamic water contact angles</i>	<i>133</i>
<i> II.4.2.3.2. Surface free energy.....</i>	<i>137</i>
<i> II.4.2.3.3. Modified time lag method</i>	<i>139</i>
<i>II.4.2.4. Infrared spectroscopy</i>	<i>140</i>
II.4.3. Bulk properties.....	149
<i>II.4.3.1. Differential scanning calorimetry analyses.....</i>	<i>149</i>
<i>II.4.3.2. Elastic modulus.....</i>	<i>151</i>
<u>II.5. Conclusion.....</u>	<u>154</u>
<u>II.6. Bibliographical references.....</u>	<u>157</u>
Chapter III Hydrolyzable PDMS/polyester hybrid networks.....	163
<u>III.1. Introduction</u>	<u>163</u>
<u>III.2. Hydrolyzable copolymers</u>	<u>164</u>
III.2.1. Preparation of the hydrolyzable copolymers	164
<i>III.2.1.1. Synthesis of poly(D,L-lactide-co-glycolide).....</i>	<i>164</i>
<i>III.2.1.2. Synthesis of PLGA-b-PDMS-b-PLGA</i>	<i>166</i>
<i>III.2.1.3. Poly(ϵ-caprolactone)-based polymers</i>	<i>168</i>

Table of contents

III.2.2.	Physico-chemical properties of the (co)polymers	169
III.2.2.1.	General description of the polymers.....	169
III.2.2.2.	Wettability of the polyester-based polymers	170
III.3.	Elaboration of PDMS/polyester hybrid networks	171
III.3.1.	Preparation of polyester macrocrosslinkers	173
III.3.1.1.	Preliminary investigations.....	173
III.3.1.1.1.	Alkoxysilanization reaction of polyester-based polymers.....	173
III.3.1.1.2.	Influence of the alkoxysilane functions.....	174
III.3.2.	Formation of PDMS/polyester hybrid networks	177
III.3.2.1.	Preliminary investigations.....	177
III.3.2.1.1.	Co-solvent	177
III.3.2.1.2.	Molar mass of the polyester-based polymer	178
III.3.2.1.3.	Catalyst amount	180
III.3.2.1.4.	Formulation preheating	180
III.3.2.1.5.	Curing conditions	180
III.3.2.1.6.	Conclusion on the optimal parameters.....	181
III.3.2.2.	Final coatings formulations.....	185
III.3.3.	Elaboration of self-crosslinked polyester-based networks	185
III.3.4.	Residue extraction test.....	186
III.3.5.	Thermal degradation of the networks.....	188
III.4.	Conclusion.....	195
III.5.	Bibliographical references.....	197
Chapter IV	Characterization of the PDMS/polyester hybrid networks	200
IV.1.	Introduction	200
IV.2.	Physico-chemical properties at $t_i=0$.....	201
IV.2.1.	Surface physico-chemical properties	201
IV.2.1.1.	Microstructure of the coating surface	201
IV.2.1.2.	Surface chemistry	208
IV.2.1.3.	Surface micromechanics	212
IV.2.2.	Thermo-mechanical bulk properties.....	223

Table of contents

IV.2.2.1.	Thermal properties of the networks	223
IV.2.2.2.	Viscoelastic properties of the networks	225
IV.2.2.2.1.	Viscoelastic behavior at ambient temperature.....	226
IV.2.2.2.2.	Influence of the temperature on the viscoelastic properties of the networks	227
IV.2.3.	Summarization of the key findings of the surface/bulk physico-chemical properties	233
IV.3.	Physico-chemical properties during immersion	235
IV.3.1.	Static immersion	235
IV.3.1.1.	Mass loss test (and water uptake test).....	235
IV.3.1.2.	Roughness	240
IV.3.1.3.	Wetting properties.....	243
IV.3.1.3.1.	Dynamic contact angle measurements	243
IV.3.1.3.2.	Surface free energy.....	251
IV.3.1.4.	Mechanical properties	256
IV.3.2.	Dynamic immersion.....	256
IV.4.	Conclusion.....	264
IV.5.	Bibliographical references.....	267
Chapter V	Antifouling and fouling release properties of the coatings.....	271
V.1.	Introduction	271
V.2.	Static field test	271
V.2.1.1.	Antifouling efficacy duration.....	273
V.2.1.2.	Identification of the type of fouling organisms	281
V.2.1.3.	Fouling release properties.....	287
V.3.	Biological assays.....	292
V.3.1.	Biological assay on <i>A. amphitrite</i> cypris larvae	292
V.3.1.1.	Settlement of <i>A. amphitrite</i> on the hydrolyzable additive-based PDMS coatings.	292
V.3.2.	Bioassays on diatoms and algal spores	293
V.3.2.1.	Diatoms <i>Navicula incerta</i>	294
V.3.2.1.1.	Initial attachment of diatoms on the PDMS/polyester hybrid networks	294
V.3.2.1.2.	Removal of diatoms on the PDMS/polyester hybrid networks	295
V.3.2.2.	<i>Ulva</i> spores.....	296

Table of contents

V.3.2.2.1.	Green alga <i>Ulva rigida</i>	296
V.3.2.2.2.	Green alga <i>Ulva linza</i>	297
V.4.	Conclusion	301
V.5.	Bibliographical references	303
Chapter VI	Experimental section	307
VI.1.	Synthesis protocols	307
VI.1.1.	Controlled radical polymerization	307
VI.1.2.	Ring opening polymerization	307
VI.1.3.	Silanization reactions	309
VI.2.	Preparation of polymer additive films	311
VI.3.	Analyses of the polymers	311
VI.3.1.	Nuclear Magnetic Resonance Spectroscopy.....	311
VI.3.1.1.	PMATM2	312
VI.3.1.2.	PLGA.....	314
VI.3.1.3.	PCL	315
VI.3.1.4.	PLGA- <i>b</i> -PDMS- <i>b</i> -PLGA	318
VI.3.1.5.	PCL- <i>b</i> -PDMS- <i>b</i> -PCL.....	320
VI.3.1.6.	Alkoxysilane-terminated polymers	322
VI.3.1.7.	¹ H NMR kinetics of the hydrolysis of trialkoxysilane functions.....	327
VI.3.2.	Size exclusion chromatography.....	329
VI.3.3.	Physico-chemical properties	330
VI.3.3.1.	Contact angle measurements	330
VI.3.3.1.1.	Dynamic contact angles.....	330
VI.3.3.1.2.	Surface free energy.....	331
VI.3.4.	Thermal properties.....	332
VI.3.4.1.	Differential scanning calorimetry analysis.....	332
VI.3.4.2.	Thermogravimetric analysis.....	333
VI.4.	Formulation of coatings	333
VI.4.1.	Formulation recipe of hydrolyzable additive-based PDMS coatings.....	333
VI.4.2.	Formulation recipe of the PDMS/polyester hybrid networks-based coatings.....	334

Table of contents

VI.5. Characterization of the PDMS-based coatings	336
VI.5.1. Physico-chemical properties	336
VI.5.1.1. Contact angle measurements	336
VI.5.1.1.1. Modified time lag method	336
VI.5.1.1.2. Dynamic contact angles.....	337
VI.5.1.1.3. Surface free energy.....	337
VI.5.1.2. Roughness measurements	337
VI.5.1.3. Infrared spectroscopy	337
VI.5.2. Residue extraction test.....	338
VI.5.3. Scanning electron microscopy.....	338
VI.5.4. Confocal laser scanning microscopy	338
VI.5.5. Thermo-mechanical properties	339
VI.5.5.1. Dynamic mechanical analysis.....	339
VI.5.5.2. Differential scanning calorimetry analysis.....	339
VI.5.5.3. Thermogravimetric analysis.....	340
VI.5.5.4. Atomic force microscope.....	340
VI.6. Erosion properties.....	341
VI.6.1. Water uptake test	341
VI.6.2. Mass loss test.....	341
VI.6.3. Thickness loss test	342
VI.7. Antifouling properties.....	343
VI.7.1. Field test	343
VI.7.2. Bioassays	344
VI.7.2.1. Larval barnacle culture and settlement assay of <i>A. Amphitrite</i> Cyprids.....	344
VI.7.2.2. Settlement and removal assays of diatom <i>N. incerta</i>	345
VI.7.2.3. Settlement and removal assays of <i>Ulva</i> spores.....	345
VI.8. Bibliographical references.....	349
CONCLUSION AND PERSPECTIVES.....	351

INTRODUCTION

Immersed surfaces such as ship hulls are subject to the accumulation of a large community of marine species (bacteria, alga, mollusks etc.) referred as biofouling. This biofouling causes serious issues for the naval industry such as accelerated ship hull damages, drag increase which leads to more fuel consumption and maneuverability loss. The ships also require more dry-docking periods to clean all the biofouling. It has been reported that the US navy annually spent US\$180-260 million to maintain all their ship hulls cleaned [1]. The important expenditures related to the biofouling issue justify the massive research done on the development of long-time efficient antifouling (AF) systems.

To avoid fouling and maintain the hull performance, AF coatings represent the most effective solution. US\$60 billion of fuel saving, 384 million tones reduction in carbon dioxide and 3.6 million tones reduction in Sulphur dioxide emissions are estimated to be achieved thanks to the use of AF coatings [2].

The self-polishing copolymer-based antifouling coatings (SPCs) based on tributyltin (TBT) groups, introduced in the seventies, were very successful. Their action mechanism relied on a constant release of toxic tin oxides induced by a controlled erosion of the coating. Due to their high toxicity, especially on non-targeted species [3], TBT-based coatings were banned by the International Maritime Organization (IMO) in 2008 [4]. They were then substituted, on one hand, by erodible coatings containing less toxic biocides (mainly copper biocides associated with synthetic booster biocides), and on the other hand, by “non-stick” silicone Fouling Release Coatings (FRCs) which rely on surface physico-chemical properties to decrease the adhesion of marine organisms.

Even if these two types of coatings show an AF efficacy between 3 to 5 years [5], they still display major drawbacks. The biocidal AF coatings are subject to worldwide regulations such as the Biocidal Products Directive (BPD) in Europe or the Federal Insecticide, Fungicide, and Rodenticide Act (FIFRA) in the United States Of America, which tend to reduce or even ban the use of certain biocides in AF coatings [6,7]. The main drawbacks of Fouling Release Coatings are their low

Introduction

antifouling efficacy during idle periods as their AF activity is based on a cleaning effect during navigation. Besides, FRCs are also more expensive than biocidal paints [8].

The aim of this PhD project is to develop new antifouling coatings that combine the chemistry of the FRCs and SPCs, without using any biocides. These hybrid coatings are based on silicone elastomers, like those used in FRCs, but they are modified by the addition of water hydrolyzable polymer additives (1st strategy) or modified by the use of water hydrolyzable macrocrosslinkers (2nd strategy). Polymers with hydrolyzable ester functions in side-groups or in the main chain were selected as water hydrolyzable polymer additives to develop FRCs with evolving surface properties during water immersion. Polyesters with hydrolyzable ester functions only in their main chains were selected to develop erodible hybrid silicone/polyester networks. Both strategies are expected to inhibit or limit the adhesion of marine organisms by creating ambiguous surfaces.

The term “ambiguous” can describe surfaces that can reorganize themselves in contact with water or surfaces that can renew themselves through chemical reactions occurring at the solid/liquid interface. Ambiguous coatings can also result from heterogeneous surfaces exhibiting hydrophilic and hydrophobic micro- or nanophases. Numerous studies have indeed built on this concept of amphiphilic surfaces, demonstrating the broad applicability of this strategy to control biofouling [9–12].

Chapter I is a state-of-art of all the existing AF coatings both in the industry and academic research worlds. Erodible biocidal AF coatings and FRCs are described in details since they represent the main AF coatings on the market. Chapter I also gives an overview of hydrolyzable polymers or networks which could be good candidates for novel hybrid AF coatings.

Chapter II deals with the strategy of adding hydrolyzable polymers into a poly(dimethylsiloxane) (PDMS) elastomer. The silicone elastomer provides a low surface energy and a low elastic modulus that favor the non-adhesion and easy removal of marine organisms while the hydrolyzable polymer additives modify the surface chemistry with their hydrolysis ability and/or their amphiphilic nature. The surface properties of these additives-based FRCs were studied in terms of mass loss, wettability, roughness, surface chemistry and viscoelastic properties to

Introduction

understand the influence of the hydrolyzable polymer additives on the silicone matrix. These results will give us matter to discuss how these coatings can provide antifouling properties while immersed in seawater.

Chapter III deals with the strategy of crosslinking bis-silanol poly(dimethylsiloxane) chains with hydrolyzable polyesters crosslinkers to obtain ambiguous and erodible coatings. Different statistical and triblock macrocrosslinkers were first synthesized with various molar masses and molar compositions. Then, the optimization of the crosslinking conditions of the polymers was studied to design PDMS/polyester hybrid networks.

The chemical and mechanical properties of these peculiar PDMS/polyester hybrid networks are investigated in Chapter IV to clarify the microstructure of these networks. Self-crosslinked polyesters and PDMS elastomers were synthesized and used as references to provide a clear understanding and interpretation of the results. A mass loss test as well as a thickness loss test were performed to evaluate the erosion properties of the hybrid coatings.

Chapter V describes the antifouling (AF) and fouling release (FR) properties of the different coatings (from Chapter II and Chapter III) thanks to a marine field test in the Toulon bay and several biological assays. The AF results are correlated to the physico-chemical properties disclosed in the previous chapters. This Chapter V is essential to compare the two strategies and conclude on the most promising antifouling solution.

Finally, Chapter VI describes the experimental protocols of the polymers syntheses, the coatings formulations and the coatings characterizations.

Introduction

1. Schultz, M.P.; Bendick, J.A.; Holm, E.R.; Hertel, W.M. Economic impact of biofouling on a naval surface ship. *Biofouling* **2011**, *27*, 87–98.
2. Goler, H.; Erdogan, O. Increasing Operational Efficiency of High Speed Ro-Ro Vessels Via New Hull Coating Technologies. *SSRN Journal* **2017**.
3. Fent, K. Worldwide Occurrence of Organotin from Antifouling Paints and Effects in the Aquatic Environment. In *Antifouling Paint Biocides*; Konstantinou, I.K., Ed.; The Handbook of Environmental Chemistry; Springer Berlin Heidelberg: Berlin, Heidelberg, **2006**; pp. 71–100 ISBN 978-3-540-32844-5.
4. Gipperth, L. The legal design of the international and European Union ban on tributyltin antifouling paint: Direct and indirect effects. *Journal of environmental management* **2008**, *90 Suppl 1*, S86-95.
5. Yebra, D.M.; Kiil, S.; Dam-Johansen, K. Antifouling technology—past, present and future steps towards efficient and environmentally friendly antifouling coatings. *Progress in Organic Coatings* **2004**, *50*, 75–104.
6. Pereira, M.; Ankjaergaard, C. 10 - Legislation affecting antifouling products. In *Advances in Marine Antifouling Coatings and Technologies*; Hellio, C., Yebra, D., Eds.; Woodhead Publishing Series in Metals and Surface Engineering; Woodhead Publishing, **2009**; pp. 240–259 ISBN 978-1-84569-386-2.
7. Senda, T. International Trends in Regulatory Aspects. In *Ecotoxicology of Antifouling Biocides*; Arai, T., Harino, H., Ohji, M., Langston, W.J., Eds.; Springer Japan: Tokyo, **2009**; pp. 23–34 ISBN 978-4-431-85708-2.
8. Lejars, M.; Margailan, A.; Bressy, C. Fouling Release Coatings: A Nontoxic Alternative to Biocidal Antifouling Coatings. *Chem. Rev.* **2012**, *112*, 4347–4390.
9. Finlay, J.A.; Fletcher, B.R.; Callow, M.E.; Callow, J.A. Effect of background colour on growth and adhesion strength of *Ulva* sporelings. *Biofouling* **2008**, *24*, 219–225.
10. Krishnan, S.; Wang, N.; Ober, C.K.; Finlay, J.A.; Callow, M.E.; Callow, J.A.; Hexemer, A.; Sohn, K.E.; Kramer, E.J.; Fischer, D.A. Comparison of the Fouling Release Properties of Hydrophobic Fluorinated and Hydrophilic PEGylated Block Copolymer Surfaces: Attachment Strength of the Diatom *Navicula* and the Green Alga *Ulva*. *Biomacromolecules* **2006**, *7*, 1449–1462.
11. Weinman, C.J.; Finlay, J.A.; Park, D.; Paik, M.Y.; Krishnan, S.; Sundaram, H.S.; Dimitriou, M.; Sohn, K.E.; Callow, M.E.; Callow, J.A.; et al. ABC Triblock Surface Active Block Copolymer with Grafted Ethoxylated Fluoroalkyl Amphiphilic Side Chains for Marine Antifouling/Fouling-Release Applications. *Langmuir* **2009**, *25*, 12266–12274.
12. Gudipati, C.S.; Greenlief, C.M.; Johnson, J.A.; Prayongpan, P.; Wooley, K.L. Hyperbranched fluoropolymer and linear poly(ethylene glycol) based amphiphilic crosslinked networks as efficient antifouling coatings: An insight into the surface compositions, topographies, and morphologies. *J. Polym. Sci. A Polym. Chem.* **2004**, *42*, 6193–6208.

Chapter I	State-of-the-art	9
I.1.	Introduction	9
I.2.	Marine fouling	10
I.2.1.	Impact of biofouling on human activities	10
I.2.2.	Biofouling as a process	10
I.3.	Overview of the antifouling strategies	13
I.3.1.	Biocidal antifouling strategy	13
I.3.2.	Biocide-free antifouling coatings	16
I.4.	Focus on biocidal antifouling coatings	22
I.4.1.	Commercial biocidal antifouling coatings	22
I.4.1.1.	<i>Description of the biocidal coating composition</i>	23
I.4.1.1.1.	<i>Insoluble-matrix coating</i>	23
I.4.1.1.2.	<i>Soluble-matrix coating</i>	24
I.4.1.1.3.	<i>Self-polishing coatings</i>	25
I.4.1.2.	<i>Specific properties of the erodible biocidal coatings</i>	30
I.4.1.2.1.	<i>Erosion process</i>	30
I.4.1.2.2.	<i>Release process</i>	32
I.4.1.2.3.	<i>Other surface physico-chemical properties</i>	34
I.4.2.	Advances made on erodible antifouling coatings at the research state	35
I.5.	Focus on fouling release coatings	45
I.5.1.	Commercial fouling release coatings	45
I.5.1.1.	<i>Description of the FRC composition</i>	46
I.5.1.1.1.	<i>Elaboration of conventional silicone elastomers</i>	46
I.5.1.1.1.1.	<i>Peroxide-induced crosslinking of polysiloxane</i>	46
I.5.1.1.1.2.	<i>Condensation cure system</i>	47
I.5.1.1.1.3.	<i>Addition cure system</i>	49
I.5.1.2.	<i>Improvement of the FRCs</i>	49
I.5.1.3.	<i>Specific properties of FRCs</i>	57
I.5.1.3.1.	<i>Surface properties</i>	57
I.5.1.3.1.1.	<i>Contact angles</i>	57
I.5.1.3.1.2.	<i>Surface free energy</i>	58
I.5.1.3.1.3.	<i>Smoothness</i>	60
I.5.1.3.2.	<i>Bulk properties</i>	61
I.5.1.3.2.1.	<i>Softness</i>	61

Chapter I. State-of-the-art

I.5.1.3.2.2. Coating thickness	63
I.5.1.3.3. Ecotoxicity in the aquatic environment	63
I.5.2. Advances made on FRCs at the academic research state	64
I.6. <u>Hydrolyzable polymers as potential candidates for novel hybrid FRCs</u>	75
I.6.1. Hydrolyzable polymers	75
I.6.1.1. Linear hydrolyzable polymers.....	75
I.6.1.2. Hydrolyzable networks.....	78
I.6.1.2.1. Hydrolyzable in the polymeric chains	79
I.6.1.2.2. Hydrolyzable in the crosslinks	83
I.6.2. Kinetics of hydrolysis	84
I.7. <u>Conclusion</u>	86
I.8. <u>Bibliographical references</u>	87

Chapter I State-of-the-art

I.1. Introduction

This bibliographical chapter gives a global overview of the antifouling (AF) technologies developed from the past decade.

In the first instance, the marine fouling organisms and their colonization process are presented as well as their impact on the marine industry and on the environment. In the second part, the different AF solutions are listed, among them, the biocidal antifouling coatings and the biocide-free antifouling coatings.

The commercial biocidal AF coatings are the most employed coatings in the marine industry. Their chemical compositions and action mechanisms are investigated to understand the key parameters influencing the most their antifouling ability such as the erosion and leaching rates. A focus on academic research made through the past decade gives further perspectives of erodible antifouling coatings.

The commercial biocide-free Fouling Release Coatings (FRCs) are then reviewed, from their elaboration to their physico-chemical properties which are responsible for their self-cleaning ability. The advanced research on new FRCs highlights a willingness of combining different antifouling mechanisms to increase the AF and FR activities of FRCs during idle periods. These more complex coatings can be designated as “hybrid” coatings due to their various chemical compositions and mechanisms of action intended to provide multifunctional antifouling coatings.

The last part deals with degradable polymers as potential candidates for improving FRCs, which is the main subject of this PhD work. The presented hydrolyzable polymers are not necessarily materials encountered in the antifouling field but their properties could be interesting for this application.

I.2. Marine fouling

I.2.1. Impact of biofouling on human activities

Biofouling in the marine environment is a very large community of micro- and macroorganisms (also called biofoulants) which develop onto immersed surfaces like ship hulls, propeller blades, pipelines, off-shore platforms, heat exchangers among others [1–4]. It is an inevitable natural process that causes serious issues such as increasing the hydrodynamic drag of ships [5]. The macrofouling accumulates on ship hulls and makes the surface rougher and even knobby. This roughness modifies the hydrodynamic profile of ship hulls by increasing their drag resistance [6]. To compensate the loss of speed, which can be up to 40 % [7], the vessel will increase its fuel consumption leading to the release of supplementary greenhouse gases. Another consequence of biofouling is the need for frequent dry-docking to scrape the heavy fouling. Up to 200-400 tons of fouling biomass are sometimes removed from boats [8]. The fouling accumulation on vessels also leads to the transport of marine organisms to new geographical zones causing uncontrolled invasions by foreign species. Biofouling can even promote surface corrosion, materials discoloration and deterioration [9].

I.2.2. Biofouling as a process

Biofouling occurs rapidly on a submerged surface. The four general stages of biofouling are described in Figure I-1.

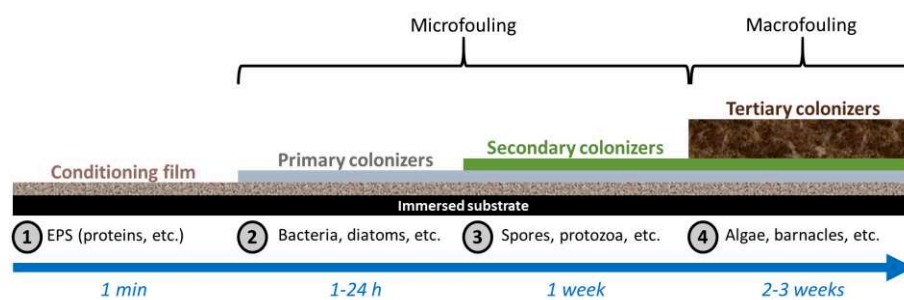


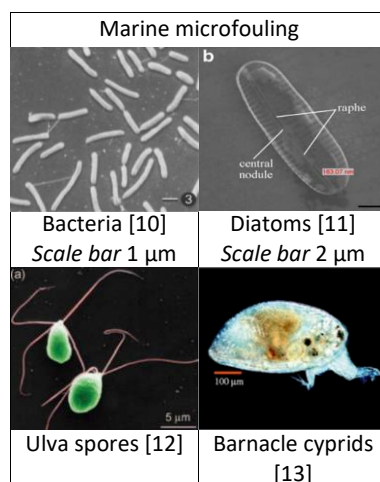
Figure I-1. The four steps of marine organisms' settlement.

The first step of biofouling consists in the formation of an organic layer. The organic compounds such as polysaccharides, proteins, phospholipids or nucleic acids, also called

Chapter I. State-of-the-art

extracellular polymeric substances or adhesive exudates, are adsorbed on the surface [9]. They enable microorganisms such as bacteria to stick to the surface, and are a source of nutrients for their growth (stage 2). After one week, a more complex community of multicellular colonizers including spores of macroalgae, protozoa, marine fungi and barnacle cyprids develops (stage 3). Stages 2 and 3 are referred to as microfouling. Some common fouling microorganisms, quoted in Table I-1, are often used for settlement and removal bioassays to evaluate antifouling (AF) and fouling release (FR) properties of coatings.

Table I-1 : Frequent marine microorganisms.



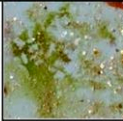
The following step (stage 4), induced and stimulated by the existing microfouling, leads to the rapid growth and metamorphosis of macroorganisms such as larvae of barnacles, bryozoans, mollusks, tunicates, mussels among others [14]. The most common macrofouling species found in the Toulon bay (France) are given in Table I-2.

Oceans and seas water present various physico-chemical characteristics that can influence the settlement of biofouling. Water temperatures ranging from -2°C to $+35^{\circ}\text{C}$ will affect the growth of bacteria, diatoms and barnacles. It is generally observed that fouling is more severe in the tropics with a greater species diversity within the fouling population than in temperate zones [3]. Salinity has also a major contribution on the biofouling settlement. It varies from 32 to 38 g salt/kg water on a worldwide scale; the highest concentration of salts is found in the Mediterranean Sea with up to 38 g salt/kg [15]. Stanley et al. have acknowledged that salts

Chapter I. State-of-the-art

such as NaCl, LiCl, MgCl₂ are essential for bacteria growth because they participate in the physiological processes of marine bacteria development [16]. Other parameters such as pH, dissolved gases (O₂, CO₂), water turbulence, sunlight, water depth and pollution, will influence both the biofouling organisms and the substrate [3].

Table I-2. Several common macroorganisms attached on various test panels in static conditions (photographs taken from the Toulon bay in France).

		Macrofouling		
Plants fouling	Algae			
		Green algae	Brown algae	Red algae
		Animal fouling	Hard shell organisms	
Barnacles	Tubeworms			Spirorbis
Grass or bush type organisms				
	Encrusting bryozoans		Hydroids	
Spineless organisms				
		Sponges	Ascidians	Tunicates

It is worth noticing that there are more than 4000 fouling species in the oceans and seas with different adhesion mechanisms [7,17]. This massive diversity of species makes it difficult to tackle biofouling. Thus, it is a great challenge for researchers to find antifouling systems that target the widest range of marine species.

I.3. Overview of the antifouling strategies

To prevent biofouling on navy ships or different immersed structures, several technologies are available. The most widespread strategy is the use of biocidal antifouling paints applied on ship hulls, which prevent fouling colonization by releasing biocidal substances at the coating/water interface. In 2009, this technology represented 95 % of the worldwide market of antifouling systems [7]. Although biocidal coatings remain the most widespread antifouling solution, their toxicity towards non-targeted marine species is a huge problem to the environment. That is why other antifouling paints, free of biocides, were developed and compete with the biocidal paints. It is also possible to find active antifouling systems which are not necessarily paints such as ultrasonic or electrochemical systems and cleaning robots.

I.3.1. Biocidal antifouling strategy

Biocidal coatings are used on ships hulls since the twentieth century. The first self-polishing co-polymer paints, patented in 1977, contained tributyltin (TBT) moieties chemically bonded to a poly(methyl methacrylate) matrix (Figure I-2). It was the most efficient AF coating at that time [18]. The antifouling mechanism relies on an ion-exchange between the coating and the seawater which leads to the controlled release of TBT salts in the marine environment. However, the highly toxicity of TBT was proved to be a disaster on the marine ecosystem with oysters and other mollusks malformations at very low concentrations (10 to 20 ng.L⁻¹) [19,20].

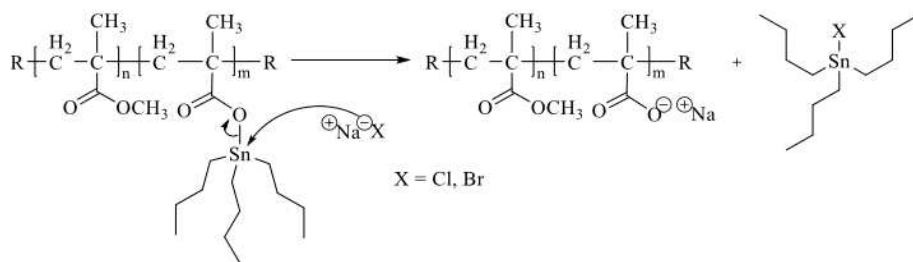


Figure I-2. Mechanism of action of TBT-based SPCs: leaching of TBT moiety from SPC consisting of tributyltin methacrylate methyl methacrylate with aqueous chloride or bromide [21].

For this reason, TBT-based coatings were definitely banned in 2008 by the International Maritime Organization (IMO) [22]. This huge decision was followed by a wave of restrictions towards toxic molecules used in antifouling paints [23]. The willingness to preserve the aquatic

Chapter I. State-of-the-art

environment is motivated by the multiple dramatic consequences assessed by many researchers over the years [19,24–26]. Biocidal substances have been thoroughly investigated by the European Chemicals Agency (ECHA) for risks to the human health and to the environment. In 2019, only ten biocides are approved in the Biocidal Product Regulation (BPR) for antifouling applications. Their approval is valid until the next process of permissions in 2026.

Despite these strict legislations on antifouling products [27], biocidal paints still remain the most commercialized paints in the antifouling market. Depending on the countries, the biocide regulations can be different, some biocides are banned in some countries but not in others. For instance, the Swedish Chemicals Agency has reduced the allowed copper content in the antifouling paints of leisure boats (down to 8.5 wt.%) and forbidden the use of booster biocides in the east coasts of the Baltic Sea [28].

- Biocidal antifouling coatings

The AF efficacy of biocidal coatings relies on the more or less controlled release of biocides. Once immersed in water, the biocides contained in the AF coatings are solubilized and released. The small voids left by the biocides in the coating form a leached layer (Figure I-3).

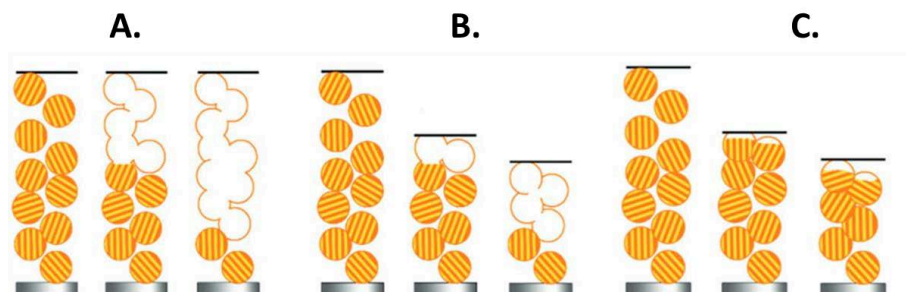


Figure I-3. Illustration of the forming leached layer in insoluble-matrix (A), soluble-matrix (B) and self-polishing (C) coatings after different immersion times in seawater [29].

Biocidal antifouling coatings can be divided into three categories depending on their binder/matrix and their resulting mechanism of action:

- A. Insoluble-matrix coatings, also called hard coatings, where the binder is insoluble and the biocides release depends only on the diffusion of water within the coating, and

Chapter I. State-of-the-art

their further dissolution in seawater. The leached layer thickness increases over time, leading to a quick decrease of the biocides release.

- B. Soluble-matrix coatings, also called ablative coatings or Controlled Depletion Polymers (CDPs) coatings, where the binder can be dissolved by seawater leading to an erosion of the coating and a decrease of the leached layer thickness. However, the process is not well controlled thus the release of biocides is not constant over time.
- C. Self-Polishing Coatings (SPCs), where the binder can be hydrolyzed in seawater and became soluble overtime leading to a controlled erosion of the coating, a constant leached layer thickness and thus a constant release of biocides over time.

These three types of biocidal AF coatings are commercially available. Their composition and mechanisms of action will be thoroughly detailed in § I.4.1.1.

- Biocides

There are two types of biocides: the heavy metal biocides and the booster biocides (organic molecules). Among the BPR approved biocides, dicopper oxide, also named cuprous oxide or copper (I) oxide (Cu_2O), is the most used in commercially available biocidal AF coatings. The other authorized biocides in 2019 in Europe are:

- *N*-[dichloro(fluoro)methyl]sulfanyl-*N*-(dimethylsulfamoyl)-4-methylaniline (Tolyfluanid);
- 4-bromo-2-(4-chlorophenyl)-5-(trifluoromethyl)-1*H*-pyrrole-3-carbonitrile (Tralopyril or Econeal);
- 4,5-dichloro-2-*n*-octyl-4-isothiazoline-3-one (DCOIT);
- 5-[1-(2,3-dimethylphenyl)ethyl]-1*H*-imidazole (Selektope or Medetomidine);
- bis(1-hydroxy-1*H*-pyridine-2-thionato-*O,S*)copper (copper pyrrithione, CuPT);
- *N*-[dichloro(fluoro)methyl]sulfanyl-*N*-(dimethylsulfamoyl)aniline (Dichlofluanid);
- zinc;*N*-[2-(sulfidocarbothioylamino)ethyl]carbomodithioate (Zineb);
- copper thiocyanate (CuSCN);
- copper flakes.

Bis(2-pyridylthio) zinc 1,1'-dioxide (zinc pyrrithione, ZnPT), copper (metallic) and free radicals (generated in situ from water) are currently waiting for approval.

Chapter I. State-of-the-art

Copper compounds efficiently prevent the attachment of barnacles, tubeworms and some algae [30]. Medetomidine, Zineb, Tralopyril and DCOIT are often designated as booster biocides since they are generally used in synergy with copper biocides to achieve protection against a larger community of fouling species.

The biocides can either be embedded in the matrix in their pure form or encapsulated [31–34]. Biocides can also be tethered (covalently bonded) to the polymeric matrix to eliminate release of biocides into the surrounding water [35–37]. The AF efficacy relies on sufficient bioavailability of the active compound upon contact between the organism and the coating.

The impact of biocides on the aquatic environment was highlighted by several research studies with toxic effects on various marine species [38–40]. The presence of high levels of booster biocides and TBT in the marine sediments is also very alarming as they will probably stay there for decades.

- Less toxic molecules

Numerous publications report the development of less toxic active molecules with antifouling and antimicrobial properties which might partially or fully replace the traditional copper biocides. Some alternatives are surfactants (Tween 85) [41,42], enzymes (chitinase, lipase, esterase) [43], quaternary ammonium-based compounds (QAS) [44–46] or natural product antifoulants (NPAs) such as phenolic compounds (thymol, eugenol, tara tannin, etc.) [47,48]. These NPAs are promising active molecules because they demonstrated a narcotic effect on nauplii of *Balanus Amphitrite* [49–51] Other NPAs such as macrocyclic lactones are used as anti-parasitic or pesticide agents [52]. Even though these “greener” molecules show promising antifouling properties, they still exhibit a toxic effect, thus, they will be subject to the same regulation as biocides.

1.3.2. Biocide-free antifouling coatings

Due to the environmental issues of biocidal antifouling coatings, more environmentally friendly solutions have been explored. Five reviews on more ecological antifouling coatings were published since 2010 highlighting the desire to substitute the biocidal antifouling coatings [53–57]. These coatings could be divided into three categories based on their chemistry.

- PDMS-based Fouling Release Coatings

Poly(dimethylsiloxane)-based Fouling Release Coatings (PDMS-based FRCs) are non-toxic commercially available antifouling coatings. Their efficacy relies on a dual mode of action: a non-stick effect and a detaching effect (Figure I-4) [57]. This dual mode of action is achieved thanks to the specific properties of PDMS elastomers, such as low surface free energy, low elastic modulus, and smoothness. The low surface free energy minimizes interactions (van der Waals, electrostatic and Lewis acid-bas interactions) between the fouling organisms and the PDMS surface, thus limiting their adhesion strength [58]. The low elastic modulus facilitates the interfacial slippage between the fouling organism and the PDMS surface, since the PDMS can deform when subjected to mechanical strains [59].

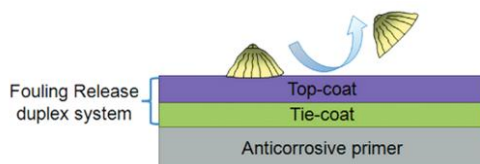


Figure I-4. Schematic illustration of Fouling Release Coatings [57].

PDMS-based FRCs are also known for their drag reduction ability. Any physical object such as a vessel being propelled through the water has drag associated with it. In fluid dynamics, drag is defined as the force that opposes forward motion through the fluid and is parallel to the direction of the fluid flow [60]. The drag of a ship that moves in the water consists of two major components: the wave-making drag and skin frictional drag. PDMS-based FRCs are able to reduce this latter drag component thanks to their smoothness which leads to significant fuel savings.

PDMS-based FRCs show limits in their use as antifouling coatings (Figure I-5). Due to their non-stick properties, they may suffer from poor adhesion onto the ship hulls despite the use of a tie-coat. Mechanical damages of the soft silicone coating such as cutting and tearing can also frequently occur on the ship sides caused by anchor chains or mooring impact. These issues also happen for biocide-based coatings but they are much more critical for PDMS-based FRCs as their efficacy (fouling release and drag reduction) only relies on the surface physico-chemical properties [61].

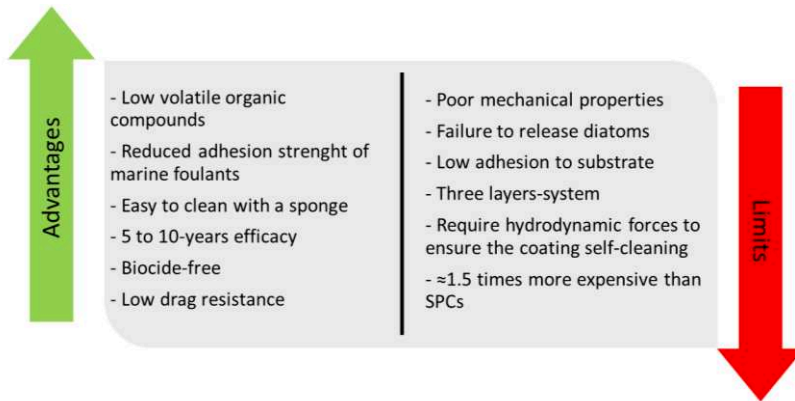


Figure I-5. Advantages and limits of PDMS-based FRCs.

As FRCs are one of the main commercially available AF coatings, their elaboration and mechanism of action will be thoroughly described in § 1.5.

- Superhydrophobic coatings

Superhydrophobic coatings are materials which repel water in a manner that the water droplet rolls on the surface like a pearl [62–65]. This very low surface wettability is traduced by a very high water contact angle $\theta_w \geq 150^\circ$. Some examples of superhydrophobic surfaces can be obtained thanks to:

- the fixation of nanoparticles (silver, gold, carbon nanotubes, copper) onto a substrate [63,66,67];
- the addition of fluorinated polymers that generate a surface segregation [64,68];
- plasma treatments [69,70];
- the nano- or micro-texturation of the coating via photolithography or embossing processes [71–75].

The resulting coatings have the ability to reduce the surface contact between the fouling organism and the substrate and/or reduce the number of interactions between the fouling organism and the substrate. These coatings usually follow the Cassie–Baxter theory such that a water drop is floating above the surface asperities. Another notable characteristic of these coatings is their very low water contact angle hysteresis ($\Delta\theta \leq 5^\circ$) which corresponds to the difference between the advancing and receding contact angles [76].

Chapter I. State-of-the-art

This traduces the stable state of the pearl-shaped water droplet while moving on the solid surface. Thus, this traduces the minimum of interaction between a mobile water droplet and the solid surface.

Although these superhydrophobic surfaces are a very promising ecological AF solution, their manufacturing process as well as their application on large-scale ship hulls are very expensive and/or difficult to implement.

- Slippery Lubricant-Infused Porous Surface (SLIPS)

SLIPS are porous materials in which are infused non-reactive lubricant oils, often silicone or fluorinated oils. SLIPS exhibit excellent liquid-repellency and slippery properties which enables drag reduction up to 16 % and a good FR performance [77–79]. Although their wettability properties are similar to those of the superhydrophobic coatings (such as very high θ_w and very low $\Delta\theta$), they do not have the same action mechanisms. In the case of SLIPS, the water repellency comes from the repulsive hydrophobic lubricant layer whereas in the case of superhydrophobic coatings, the water repellency comes from the water droplets floating above the surface protrusions. Besides, they do not necessarily exhibit contact angles higher than 150° but rather between 105 and 150° [80,81].

Given that the AF mechanism of SLIPS technology depends mainly on the uppermost mobile lubricant layer, this AF efficacy is rapidly limited by the lubricant depletion. SLIPS were thus improved to increase their long-term stability. Self-secretion or resupply of the lubricant by “vascularization” of the material (with internal channel networks) in the polymer bulk enable to prolong the life-time of SLIPS. This is why they are often called self-healing or self-replenishing coatings [77,78].

- Xerogel-based coatings

Xerogel-based coatings [82] also named sol-gel coatings represent another category of fouling release coatings. They are comprised of a thin organically modified silica layer obtained by polycondensation of various alkoxy silanes, such as tetraethoxysilane (TEOS). Although they are water-based formulations, they still exhibit low surface free energy of 20-25 mJ/m² [83–85].

Chapter I. State-of-the-art

The commercially available xerogel coating patented as AquaFast in 2012 can be applied via roller, brush or spraying to all sort of surfaces including cameras and equipment of offshore oil extraction platforms [86,87]. It was also applied to over 100 ship hulls in Lake Ontario, showing continued success in the field. The advantages of xerogels are their transparency and thin thickness (10-60 μm against 125-500 μm for conventional PDMS elastomers) [7]. They have a superior wear-resistance and elastic modulus (10^2 - 10^4 MPa) compared to PDMS elastomers. The main drawback of these thin xerogel coatings is that they cannot undergo similar deformation to the soft PDMS-based FRCs and thus their release of hard fouling will be more dependent on the hydrodynamic forces [83].

- Hydrogel coatings

Hydrogel materials are hydrophilic polymer networks that can absorb high quantity of water (60-99 wt.%) [88]. Hydrogel-based coatings are known to strongly prevent cells and proteins adsorptions and to display antifouling activity on zoospores or barnacle cypris [89]. Poly(2-hydroxyethyl methacrylate) (HEMA), polyether glycol (PEG), polyacrylamide (PAAm) and polyvinyl alcohol (PVA) are mainly used for hydrogel coatings. Their softness (10 kPa-1MPa), hydration and swelling ability (up to 300-350 %) create a thick “water-like” layer with a high surface free energy ($\gamma_s = 58$ -60 mJ/m^2) [90]. This “water-fictive” barrier dissuades the adhesion of microorganisms. Due to their very low elastic modulus, hydrogels are mechanically weak which limits their application in antifouling coatings.

- Amphiphilic coatings

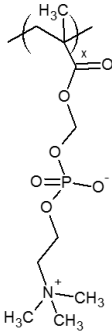
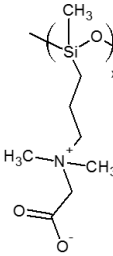
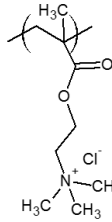
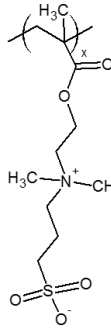
Amphiphilic coatings contain both hydrophobic and hydrophilic polymers. This dual function provides an ambiguous surface towards marine organisms [91]. Different chemistries allow this dual property such as hard-soft polyurethane-PDMS coatings, polyethylene glycol (PEG), PDMS, polypeptide, zwitterionic copolymer additives-based coatings or hyperbranched crosslinked PEG/fluorinated networks. These amphiphilic coatings are promising in the field of marine AF coatings and some are already used in commercially available marine coatings. The detailed composition and surface/bulk properties of these amphiphilic systems will be discussed in § 1.5.2.

Chapter I. State-of-the-art

- Ions-based coatings

Coatings with grafted zwitterionic or cationic polymers can generate antibacterial and antifouling surfaces [92]. The potential of Poly(2-(methacryloyloxy)ethyl trimethylammonium chloride) (**PMETA**), poly(2-methacryloyloxyethyl phosphorylcholine) (**PMPC**), polycarboxybetaine (**PCB**) and polysulfobetaine (**PSB**) as matrix for marine AF coatings was reported into the literature (Table I-3). These ions-based coatings reduce or suppress biofilm formation and are resistant to protein adhesion [93–95]. Their mechanism of action is the formation of a hydrated layer (with a zeta potential \approx 0) that strongly reduces electrostatic attractions with the marine organisms [96,97].

Table I-3. Polyzwitterionic polymers with antifouling and antimicrobial properties.

			
Poly(2-methacryloyloxy)ethyl phosphorylcholine (PMPC)	Carboxybetaine functionalized polysiloxane (PDMS-g-CB)	Poly(2-methacryloyloxy)ethyl trimethylammonium chloride (PMETA)	Polymethacrylate sulfobetaine (PMSB)

I.4. Focus on biocidal antifouling coatings

Biocidal coatings are the most commercialized antifouling systems. As briefly described in § 1.3.1, there are three types of biocidal coatings based on the polymer matrix: insoluble matrix- coatings, soluble matrix- and Self-Polishing Copolymer-based coatings (SPCs). All coatings contain biocides at a percentage which vary among suppliers or research studies. In the following sections, the commercially available SPCs are exhaustively listed as they are the most performing coatings. In addition, the advances made on SPCs at the research state are then discussed to show novel promising hybrid SPCs.

I.4.1. Commercial biocidal antifouling coatings

The main commercially available SPC and CDP coatings produced from the largest suppliers are listed in Table I-4. Both the polymer matrix or binder and the type and amount of biocides vary among suppliers. The amount of biocides used in commercial SPCs/CDPs vary between 10 and 60 wt.% in total. The quantitative composition of biocidal antifouling paints can be summarized as follows [98]:

- Matrix or polymer binder (20–30 wt.%);
- Main biocides (15–40 wt.%);
- Co- or booster biocides (4–5 wt.%);
- Erosion additives like zinc oxide (5–15 wt.%);
- Pigments (3–4 wt.%);
- Plasticizers (2–5 wt.%);
- Catalysts (0.5–2 wt.%);
- Solvents (15–20 wt.%).

I.4.1.1. Description of the biocidal coating composition

I.4.1.1.1. *Insoluble-matrix coating*

Insoluble-matrix coatings are made of acrylics, epoxy, polyurethane, vinyls or chlorinated rubber [99] and contain high loadings of biocides. Their strengths lie on their good mechanical properties. The water diffuses through the pores that are left empty by the dissolution of biocidal particles and go on to dissolve the next ones. For these coatings, the thickness of the leached layer increases with time since the polymer is insoluble (Figure I-6).

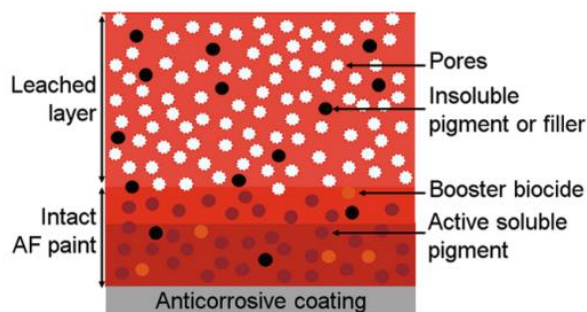


Figure I-6. Schematic representation of the insoluble-matrix coating once exposed to water[57].

Therefore, it becomes harder for biocides deeply embedded in the matrix to be dissolved by water and released at the coating/water interface. The biocide release rate is thus drastically reduced after a short immersion period (6 to 12 months) resulting in a progressive loss of antifouling protection. Another drawback is the voids left by the released biocides which generate surface roughness and promote biofouling settlement [57]. These insoluble coatings are typically used on leisure boat hulls as their service life does not exceed 24 months [100]. The companies providing this coating technology are for example Boero Paints, Nautix etc.

1.4.1.1.2. Soluble-matrix coating

Soluble-matrix AF or ablative coatings are mainly composed of rosin, a natural resin containing 85-90% of long unsaturated fatty acids [99]. These coatings have a leached layer which decreases over time thanks to the hydration/dissolution of the rosin matrix (Figure I-7).

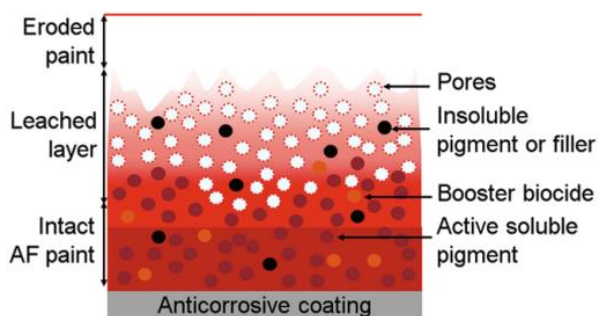


Figure I-7. Schematic representation of the soluble-matrix coating once exposed to water [57].

However, the renewal of the surface is not entirely controlled and can generate surface asperities. The AF efficacy of traditional soluble-matrix coatings usually last between 12 months to 36 months. These rosin-based coatings also show some surface imperfections after removing them from water like the presence of some cracks partly due to the surface oxidation [101]. Other issues associated to this technology are that the biocide release is not as constant as in the SPCs, they show low activity during idle times and they display poor self-smoothing (Figure I-8) [102].

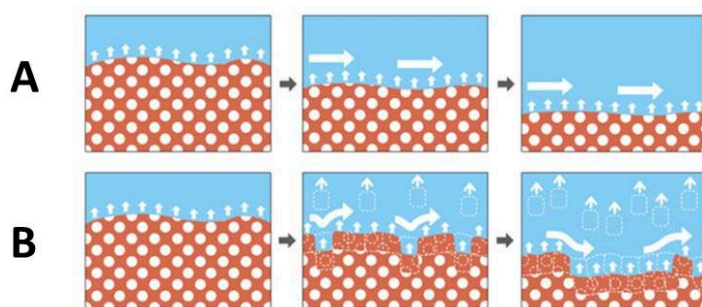


Figure I-8. Comparison of the surface renewal between SPCs (A) and CDPs (B) (from Ecoloflex SPC Nippon paint technical report).

Chapter I. State-of-the-art

To increase the antifouling efficacy durability and limit their surface defects of soluble-matrix systems, plasticizers, fibers and reinforcing synthesized resins such as vinyl chloride/vinyl acetate copolymers are used in addition to rosin [100,103,104]. These improved soluble-matrix coatings are designated by controlled depletion polymers (CDPs) and can be effective for periods up to 60 months. The commercial paints providing this coating technology are for example Interspeed from International paint, SeaForce 60 from Jotun, EcoFleet from PPG, Bioflex 800 from Nippon paint and SeaVoyage from Sherwin Williams (Table I-4).

1.4.1.1.3. Self-polishing coatings

The Self-Polishing Copolymer-based coatings (SPCs) display the most controlled and predictable surface erosion in water (Figure I-9).

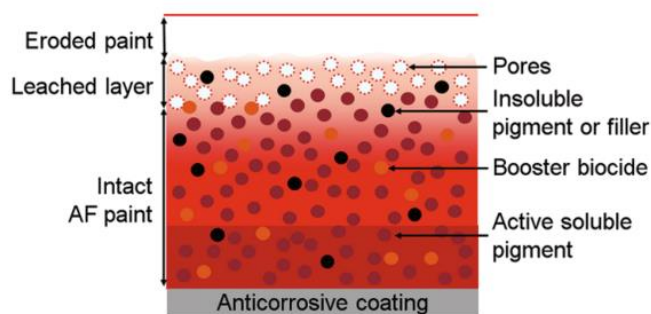
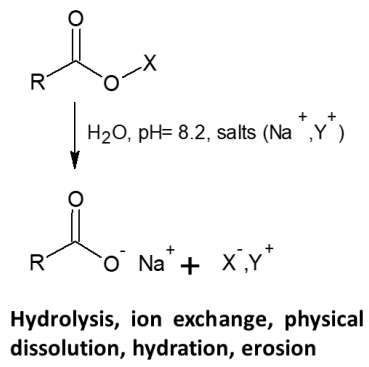


Figure I-9. Schematic representation of the self-polishing copolymer-based coating once exposed to water [57].

Contrary to the soluble matrix where the binder is “washed” from the surface, the binder from SPCs undergoes a hydrolysis/ion-exchange reaction (Figure I-10). The thickness of the leached layer is constant over time meaning that the biocides release rate and the erosion rate exhibit similar kinetics. The SPCs are based on silylated polyacrylate, zinc or copper polyacrylate. SPCs can be effective for periods up to 90 months. The commercial paints providing this coating technology are for example Intersmooth from International paint, SeaForce 90 from Jotun, SailAdvance from PPG, Ecoloflex from Nippon paint and SeaFlo Neo from Chugoku Marine Paint (Table I-4).



BINDER SYSTEMS	-X
SA-SPC Silyl acrylate polymer	$ \begin{array}{c} \text{R}^2 \\ \\ \text{---Si---} \\ \\ \text{R}^2 \end{array} $
CA-SPC Copper acrylate polymer	$ \text{---Cu---O---C(=O)---R} $
ZA-SPC Zinc-acrylate polymer	$ \text{---Zn---O---C(=O)---R} $

Figure I-10. Common polyacrylate binders for SPCs.

Chapter I – State-of-the-art

Table I-4. Chemical composition of commercially available biocidal antifouling coatings (the main companies).

Company	Paint name	Main biocides (amount wt.%)	Binder (when known)	Specifications
Hempel	Oceanic + 73902	Cu ₂ O (25-50), Zineb (5-10), CuO (≤ 1), copper (< 1)	Zinc carboxylate and acrylic binders	60 months sailing interval
	Oceanic + 73952	Cu ₂ O (25-50), Zineb (5-10), CuO (≤ 1), copper (< 1)	Zinc carboxylate and acrylic binders	60 months sailing interval
	Globic 6000	Cu ₂ O (25-35), CuPT (1-3), CuO (≤ 1), copper (< 1)	Nano acrylate technology	60 months sailing interval
	Globic 7000	Cu ₂ O (25-50), Zineb (3-5), CuPT (1-3), CuO (≤ 1), copper (< 1)	Nano acrylate technology	60 months sailing interval
	Globic 8000	Cu ₂ O (25-50), Zineb (3-5), CuPT (1-3), CuO (1-3), copper (< 1)	Nano acrylate technology	90 months sailing interval
	Globic 9000	Cu ₂ O (25-50), CuPT (1-3), CuO (1-3), copper (1-3),	Nano acrylate technology	90 months sailing interval
	Globic 9500S	Cu ₂ O (25-50), CuPT (3-5), CuO (1-3), copper (< 1), medetomidine (< 0.1)	Nano acrylate technology	90 months sailing interval
	Globic 9500M	Cu ₂ O (25-50), CuPT (3-5), Zineb (3-5), CuO (1-3), copper (1-2.5), DCOIT (< 1)	Nano acrylate technology	90 months sailing interval
	Dynamic 9000 79900	Cu ₂ O (25-50), CuPT (3-5), CuO (1-3), copper (< 1)	Hydrolysing silyl acrylate	90 months sailing interval
	Dynamic 9000 79950	Cu ₂ O (25-50), CuPT (3-5), CuO (1-3), copper (< 1)	Hydrolysing silyl acrylate	90 months sailing interval
	Dynamic 8000	Cu ₂ O (25-50), Zineb (3-5), CuPT (1-3), CuO (1-3), copper (< 1)	Hydrolysing silyl acrylate	90 months sailing interval
International	Interswift 6600	Cu ₂ O (25-50), Zineb (1.0-10)	Copper acrylate resin (1.0-10 wt.%) with rosin (1.0-10 wt.%)	
	Interswift 6800HS	Cu ₂ O (25-50), Zineb (1.0-2.5), CuPT (1.0-2.5), CuO (1-2.5)	Copper acrylate with rosin (10-25 wt.%)	
	Intersmooth 360 SPC	Cu ₂ O (25-50), ZnPT (1.0-10), CuO (1.0-10)	Copper acrylate technology	
	Intersmooth 365 SPC	Cu ₂ O (40-50), ZnPT (2.5-5)	Acrylic copper polymer (10-20 wt.%)	
	Intersmooth 7460HS SPC	Cu ₂ O (25-50), CuPT (2.5-10), CuO (1.0-2.5)	Copper acrylate resin (amount not indicated) with rosin amine (1-2.5 wt.%)	
	Intersmooth 7465HS SPC	Cu ₂ O (> 50), CuPT (2.5-10)	Copper acrylate technology	
	Intersmooth 7465Si SPC	Cu ₂ O (25-50), CuPT (2.5-10), CuO (1.0-2.5)	Silyl acrylate polymer technology	
	Intersmooth 7475Si SPC	Cu ₂ O (30-40), CuPT (2.5-5), CuO (1.0-2.5)	Silyl acrylate polymer technology	
	Intersmooth 7670 SPC	ZnPT (2.5-10), Tralopyril (2.5-10)	Copper acrylate technology	
	Intercept 7000	Cu ₂ O (25-50), CuPT (2.5-10), CuO (1.0-2.5)	Lubyon Technology, rosin (2.5-10 wt.%), acrylic copolymer (2.5-10 wt.%)	
	Intercept 8500 LPP	Cu ₂ O (25-50), CuPT (2.5-10), CuO (1.0-2.5)	Lubyonand silyl methacrylate technology	
	Interspeed 640	Cu ₂ O (25-50)	Rosin (10-25 wt.%)	
	Interspeed 5640	ZnPT (2.5-10), Tralopyril (2.5-10)	CDP, rosin (10-25 wt.%)	
	Interspeed 6200	Cu ₂ O (10-25), Zineb (2.5-10)	CDP, rosin (10-25 wt.%)	
	Interspeed 6400	Cu ₂ O (25-50), Zineb (2.5-10), CuO (1.0-2.5)	CDP, rosin (10-25 wt.%)	
	Interspeed 6400NA	Cu ₂ O (25-50), CuO (1.0-10)	CDP	
	Interspeed 5617	Cu ₂ O (10-25)	CDP, rosin (10-25 wt.%)	30 months sailing interval
	Interspeed 5100	Cu ₂ O (1.0-10), Zineb (1.0-10)	Traditional cuprous oxide self-polishing antifouling, rosin (10-25 wt.%)	
	Interspeed 5992	Copper thiocyanate (7-25)	Rosin (5-10 wt.%)	30 months sailing interval
Interflex 8700 SPC	ZnPT (5-10), Tralopyril (5-10)	Copper acrylate technology		
Jotun	SeaForce Active	Cu ₂ O (10-30), Zineb (1-10), CuPT (1-3)	Acrylic, hydrolyzing antifouling coating, rosin (1-10 wt.%)	60 months sailing interval
	SeaForce Active	Cu ₂ O (30-60), Zineb (1-10) Copper thiocyanate (0-3)	Acrylic, hydrolyzing antifouling coating, rosin (1-10 wt.%)	90 months sailing interval
	SeaForce 90	Cu ₂ O (25-50), Zineb (1-5), CuPT (1-3),	Ion-exchange antifouling technology, rosin (1-10 wt.%)	60 months sailing interval

Chapter I – State-of-the-art

	SeaForce 300AV	Cu ₂ O (25-50), DCOIT (0-3)	Ion-exchange antifouling technology, rosin (1-10 wt.%)	36 months sailing interval
	SeaForce 30	Cu ₂ O (10-30), Zineb (1-10)	Ion-exchange antifouling technology, rosin (1-10 wt.%)	36 months sailing interval
	SeaForce 30M	Cu ₂ O (10-23), Zineb (1-10)	Ion-exchange antifouling technology, rosin (10-25 wt.%)	36 months sailing interval
	SeaConomy 900	Cu ₂ O (25-50), Zineb (1-10)	Metal carboxylate ion-exchange technology, rosin (10-25 wt.%)	60 months sailing interval
	SeaConomy 700	Cu ₂ O (10-23), Zineb (1-10)	Metal carboxylate ion-exchange technology, rosin (10-25 wt.%)	36 months sailing interval
	SeaForce 60	Cu ₂ O (25-50), Zineb (1-5), copper thiocyanate (0-3)	Rosin (0-10 wt.%)	60 months sailing interval
	SeaForce 60M	Cu ₂ O (25-50), Zineb (1-10)	Rosin (10-25 wt.%)	60 months sailing interval
	SeaForce Shield	Cu ₂ O (10-23), Zineb (1-10)	3 rd generation ion exchange antifouling	60 months sailing interval
	SeaMate	Cu ₂ O (30-60), CuPT (1-3), Zineb (1-5)	Silyl technology, rosin (0-5 wt.%)	90 months sailing interval
	SeaMate M	Cu ₂ O (25-50), CuPT (1-3), Zineb (1-5)	Silyl technology, rosin (0-10 wt.%)	90 months sailing interval
	SeaMate NB	Cu ₂ O (25-50), CuPT (1-3), Zineb (1-5)	Silyl technology, rosin (0-10 wt.%)	90 months sailing interval
	SeaQuantum PRO U	Cu ₂ O (25-35), CuPT (1-5), Zineb (2-5)	Silyl acrylate technology	90 months sailing interval
	SeaQuantum PLUS S	Cu ₂ O (35-50), CuPT (1-5)	Silyl acrylate technology	90 months sailing interval
	SeaQuantum CLASSIC S	Cu ₂ O (35-50), CuPT (1-5)	Silyl acrylate technology	90 months sailing interval
	SeaQuantum ULTRA S	Cu ₂ O (35-50), CuPT (1-5)	Silyl acrylate technology	90 months sailing interval
	SeaQuantum STATIC	Cu ₂ O (35-50), CuPT (1-5)	Silyl acrylate technology	90 months sailing interval
	SeaQuantum PLUS S	Cu ₂ O (35-50), CuPT (1-5)	Silyl acrylate technology	90 months sailing interval
	SeaQuantum X200-1	Cu ₂ O (35-50), CuPT (1-5)	Silyl acrylate technology	90 months sailing interval
	SeaQuantum X200-2	Cu ₂ O (35-50), CuPT (1-5)	Silyl acrylate technology	90 months sailing interval
	SeaQuantum X200-3	Cu ₂ O (35-50), CuPT (1-5)	Silyl acrylate technology	90 months sailing interval
	SeaQuantum X200-S	Cu ₂ O (40-50), CuPT (1-2.5), DCOIT (1-2.5)	Silyl acrylate technology	90 months sailing interval
PPG	Alphagen 240	Cu ₂ O (35-50), DCOIT (1-3)		
	Alphagen 230			
	SigmaGlide 1290			8 % fuel saving, 7 years (service life)
	Sigma Nexeon			2.5 % fuel saving
	EcoFleet 290	Cu ₂ O (25-50), DCOIT (1-3)		Up to 60 months in-service period
	EcoFleet 530	Cu ₂ O (20-41), DCOIT (0.1-2.5)	Rosin (10-20 wt.%)	Up to 60 months in-service period
	EcoFleet 690	Cu ₂ O (35-50), Zineb (5-10)		Up to 60 months in-service period, best performance for low speed vessels
	Sigma Sailadvance RX and GX		Lubricant (slippery surface technology)	90 months sailing interval
	Sigma Sailadvance DX 800		Silyl acrylate technology	Fuel savings up to 7 %
	Sigma Nexeon 710	ZnPT (5-15), tralopyril (1-5)		Fuel savings of 2.5 %, 25 % smoother
Chugoku Marine Paint	Seaflo Neo CF Premium	CuPT (1-5), medetomidine (0.1-1)	Zinc acrylate polymer	FIR= 7 % (speed loss of only 1 %)
	Seaflo Neo SL Z	Cu ₂ O (40-50), CuPT (1-5)	Innovative hydrolysis polymer	FIR= 1.2%, ultra-smooth surface
	Seaflo Neo 500 Z	Cu ₂ O (30-40), CuPT (1-5), CuO (0.1-1)		
	Sea Grandprix CF-10		Zinc acrylate employing ionomer technology	
	Sea Grandprix 1000L	Cu ₂ O (40-50), CuPT (1-5), CuO (0.1-1), copper (0.1-1)	Advanced silyl polymer with highly hydrolysis activity	90 months at 24 knots
	Sea Grandprix 2000A	Cu ₂ O (40-50), CuPT (1-5)	Silylated polymethacrylate	60 months
	Sea Grandprix 950L			60 months (250 µm dry film), FIR= 5.6 %
	Sea Grandprix 900L			90 months, FIR= 6.9 %
	Sea Grandprix 880HS			90 months, FIR= 6.9 %
	Sea Grandprix 770HS			60 months, FIR=7.9 %

Chapter I – State-of-the-art

	Sea Grandprix 660HS Sea Grandprix 500HS Sea Grandprix 330HS	Cu ₂ O (30-40), CuO (0.1-1), DCOIT (0.1-1) Cu ₂ O (40-50), CuO (1-5), CuPT (1-5)	Zinc acrylate polymer	FIR= 10.7 % 36 months, up to 60 months if low risk fouling areas
Nippon paint marine	Aquaterras (1000/2000/6000/8000)			Biocide-free, 10 % fuel saving, amphiphilic micro-domain SPC
	Bioflex 800	Cu ₂ O (5-25), Diuron (1-10), CuPT (1-5)	CDP that contains paraffin waxes (1-10 wt.%), rosin (1-10 wt.%)	
	Ecoloflex SPC 100HS			
	Ecoloflex SPC 200	Cu ₂ O (25-40), CuPT (0.5-1)	Silyl acrylate copolymer, contains paraffin waxes (1-10 wt.%), rosin (1-10 wt.%)	
	Ecoloflex SPC 250 HyB	Cu ₂ O (20-50), CuPT (1-10)	Copper silyl acrylate copolymer, contains paraffin waxes (1-5 wt.%)	
	Ecoloflex SPC 400 HyB	Cu ₂ O (20-50), CuPT (1-5)	Copper silyl acrylate copolymer	
Transocean	Cleanship 293 Cleanship 297			Suitable for slow speed vessels Suitable for slow speed vessels
	Cleanship 291	Cu ₂ O (25-50), Diuron (2.5-10)	Rosin (10-25 wt.%)	SPC, hybrid binder, 60 months of service life
	Transocean optima			Ablative coating, 18-24 months of service life
	Transocean Longlife		Mixed matrix type	30 months sailing interval, not suitable for stationary or slow steaming vessels
	Armada	Hydrolyzable silylacrylic polymer		60 months sailing interval
Sherwin Williams	SeaVoyage 100	Cu ₂ O (10-25), CuPT (0-5)	Rosin (10-25 wt.%)	CDP
	SeaVoyage copper free	ZnPT (1-8.1), Tralopyril (1-9.2)	Rosin (10-25 wt.%)	
	Seaguard ablative AF coating	Cu ₂ O (49), CuO (0-5)	Polyamide polymer, rosin (0-10 wt.%)	Use on vessels with service speed exceeding 10 knots

Cu₂O= dicopper oxide, CuO= copper II oxide (ECHA product type 08), ZnPT= zinc pyrithione, CuPT= copper pyrithione, FIR= friction increase ratio.

1.4.1.2. Specific properties of the erodible biocidal coatings

1.4.1.2.1. *Erosion process*

The physico-chemical properties of the water in which the coating is immersed are undeniably affecting the erosion process but in the following text the focus is done on the nature of the polymers.

The mechanisms of CDP and SPC coatings are based on a hydration/ dissolution and hydration/hydrolysis processes, respectively. In other words, in one case the erosion is physically induced while in the other the erosion is chemically induced. In addition, depending on the nature of the hydrolyzable polymers, the coating can undergo either surface or bulk erosion [105–107]. Surface erosion occurs when hydrolytic cleavage of polymer chains is faster than the water penetration. On the opposite, bulk erosion occurs when the diffusion of water into the bulk material is faster than the hydrolysis process [105]. Many aliphatic polyesters such as poly(lactide) (PLA) and poly(ϵ -caprolactone) PCL undergo bulk degradation.

The advantages of surface erosion are the linear erosion profile, which traduces a gradual surface renewal, and the conservation of the intrinsic mechanical properties. On the contrary, bulk erosion can lead to a massive swelling with no mass loss for a certain amount of time followed by a fast failure of the material (Figure I-11). The sudden material failure would drastically reduce the coating life time. Besides, bulk erosion generates porosity which can be source of hiding places for marine organisms. For antifouling applications, surface erosion is thus more suitable. A family of polymers that can undergo surface erosion is for example the poly(anhydride)s as long as the applied thickness is higher than 100 μm (L_{critical}) according to Burkersorda et al. [108].

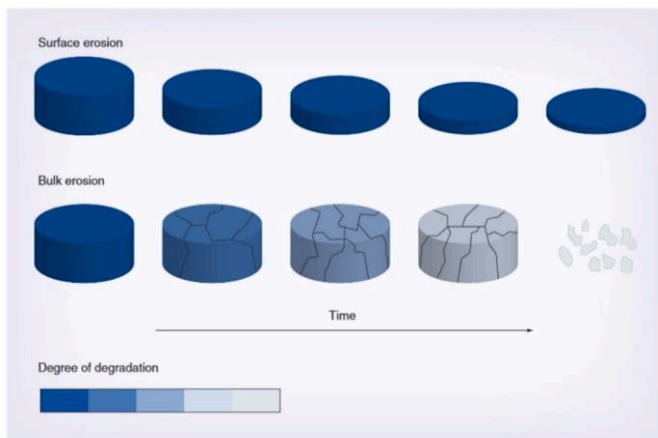


Figure I-11. Schematic illustration of surface and bulk erosion processes [106].

The key parameters that influence the erosion rate are:

- 1) the polarity of the polymer or permeability to water or affinity to water

The polarity of the polymer depends on the polymer chemical composition. The presence of hydroxyl, amine or carboxylic groups (hydrophilic groups) will be more favorable to water absorption than alkyl groups (hydrophobic groups). This will markedly impact the erosion rate given that the polymers first needs to be hydrated before being hydrolyzed or dissolved [109].

- 2) the polymer crystallinity

Semi-crystalline polymers possess tightly packed phases (crystalline phases) which are less accessible to degradants [110]. On the contrary amorphous regions will favor water diffusion owing to their random arrangement that gives open access to water. Thus, amorphous regions will degrade first leaving the more crystalline regions.

- 3) the polymer microstructure

Polymers selected in commercial SPC coatings are mainly copolymers. Copolymers are often made of two monomers, A and B. These copolymers can be statistical (random) copolymer or diblock copolymers. In statistical copolymers there is three possible linkages, A-A, A-B and B-B. These different linkages can lead to different reactivities towards water leading to different erosion rates [111].

Bressy's group studied the influence of the monomer nature, molar monomer ratio (A/B), the copolymer architecture (random or block) and the molar mass of the polymers on the erosion rate of some poly(trialkylsilyl methacrylate)s [57,112]. For instance, they showed the steric hindrance of the pending groups on monomer units was responsible for lower hydrolysis rates. They also reported that a random copolymer displayed a higher erosion rate ($4.40 \pm 0.10 \mu\text{m/d}$) than a diblock copolymer ($0.38 \pm 0.06 \mu\text{m/d}$) with the same A/B molar ratio, similar molar masses and in the same immersion conditions. And finally, they highlighted that low molar mass values ($M_w < 40,000 \text{ g/mol}$) could enhance the water solubilization of the hydrolyzed polymer.

These different parameters can thus tailor the hydrolysis kinetics of the polymer and thus the erosion rate. It is important to notify that the life of an erodible AF coating is determined by its initial dry film thickness and its erosion rate upon immersion time.

The erosion rates of commercial SPC coatings such Hempel Globic, nterspeed, Intersmooth and Seaquantum range from 0.08 to $0.26 \mu\text{m/d}$ (or 2.12 to $7.64 \mu\text{m/month}$) in natural seawater at 25°C and 25 knots for a minimum immersion time of 200 days (internal data). These erosion rates were found to be the most suitable rates to guarantee AF efficacy varying from 60 to 90 months with dry average thickness of $[75-160] \mu\text{m} \times 2$ (according to the product data sheets from Chugoku, PPG, Jotun and Hempel).

1.4.1.2.2. Release process

The main interest of erodible biocidal coatings is that the dissolution front of the biocides coincides with the dissolution/hydrolysis front of the polymer matrix. This is what allows a more progressive renewal of the leached layer. The erodible coatings display a more constant biocide leaching rate than the insoluble coatings which makes a more durable AF efficacy (Figure I-12).

An American study revealed the effect of temperature, immersion time, immersion conditions and resin nature of various copper based-AF coatings [113]. They showed that by increasing the temperature of the seawater from 1 to 26°C , the Cu leaching rates varied from 0.26 to $0.65 \mu\text{g/cm}^2/\text{d}$. Moreover, they showed that between the first and the 8^{th} immersion month, the leaching rate decreased by 2 to 5 times. Leaching rates fluctuations were also observable

depending on the resin nature (rosin, ester gum or coumarone-indene). They revealed a huge gap between laboratory assays and field tests with Cu leaching rates going from 0.5 $\mu\text{g}/\text{cm}^2/\text{d}$ to 10 $\mu\text{g}/\text{cm}^2/\text{d}$ or more. Finally, they agreed on a constant leaching rate of 10 $\mu\text{g}/\text{cm}^2/\text{d}$ to be the minimum efficient leaching rate for the prevention of fouling. Burant et al. further studied the Cu discharging into surface waters from California marinas [114]. They modeled the copper leaching rates under various scenari from copper-based AF coatings and highlighted that the copper leaching rate from recreational vessels was comprised between 0.5 to 25 $\mu\text{g}/\text{cm}^2/\text{d}$. The CDPR (California Department of Pesticide Regulation) authorized a 9.5 $\mu\text{g}/\text{cm}^2/\text{d}$ Cu leaching rate as a maximum allowable leach rate, entered into force on July, 2018.

The release rate of copper and zinc from SPCs has been estimated from 2 to 50 $\mu\text{g}/\text{cm}^2/\text{d}$ in artificial sea water (ASW) depending on the polymer matrix and the initial biocide content in the dry coating [115]. The rosin dissolution rate from a CDP in seawater could reach 50 $\mu\text{g}/\text{cm}^2/\text{d}$ after 4 days of immersion [116].

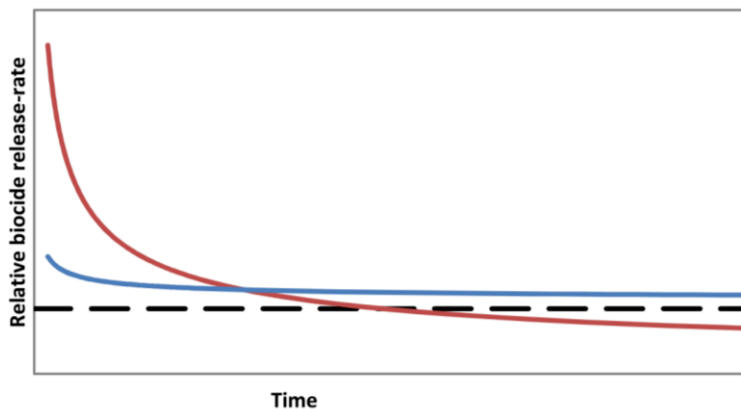


Figure I-12. Comparison between a traditional insoluble matrix antifouling coating (red line) and a self-polishing antifouling coating (blue line). Considering that both coatings contain a similar amount of biocide initially. A minimum effective biocide release rate is indicated by a dashed line Data from Hempel technical report.

Most of the released compounds are metal biocides. For instance, a study done by the San Diego Regional Water Quality Control Board estimated that 98% of Cu in Shelter Island Yacht Basin was due to its leaching from copper-based AF coatings [117].

Copper biocides are not the only source of cupric ions (Cu^{2+}), Cu^{2+} also comes from the hydrolysis of the copper acrylate polymer. The degradation products of this hydrolyzable polymer is thus also considered toxic. This is not the case for silyl acrylate polymers which do not have an apparent toxicity towards marine species [118]. Zinc oxide (ZnO) is widely used in antifouling paints as a filler to help the erosion process of the coating. Although it is not listed as a biocidal compound in the BPR (PT21), it is considered as a booster biocide that increases the copper toxicity by 200x [119]. Waterman et al. also pointed out that erodible “biocide-free” coatings containing ZnO still exerted acute toxic effect on non-target organisms and could not thus be regarded as “biocide-free”. According to them, ZnO should be restricted to values below 10 %. Other released compounds are polymer backbones, polymers, oligo- or monomers, plasticizers and pigments. These latter compounds received minor attention compared to the leached biocides [98].

1.4.1.2.3. Other surface physico-chemical properties

Erodible coatings exhibit roughness values around 0.33 and 0.47 μm which are higher to that of FRCs (0.077-0.116 μm) [60]. This roughness can be source of additional frictional drag. Some values of friction increase rate (FIR) from commercial coatings are quoted in Table I-4. The self-polishing participates to the smoothing of the surface with immersion time which can limit the frictional drag of biocide-based AF coatings.

The water contact angle of SPCs are around 80-90° [120,121]. Once immersed, SPCs can turn even more hydrophilic (down to 60°, [121]) due to the hydration and hydrolysis of the polymer which ends up more soluble in the water. The surface free energies of SPCs (not yet immersed in water) are usually between 33 and 36 mJ/m^2 (with $\gamma_S^P \approx 5-9 \text{ mJ}/\text{m}^2$) against 23-26 mJ/m^2 (with $\gamma_S^P \leq 2 \text{ mJ}/\text{m}^2$) for FRCs traducing the more hydrophilic and water swelling nature of SPCs [60].

I.4.2. Advances made on erodible antifouling coatings at the research state

Since 2010, researchers have further broadened the choices of polymer binders for erodible antifouling coatings. Their objective was to explore novel copolymer microstructure to design efficient AF erodible coatings containing lower amounts of biocides. In the following section, four categories of recent polymers used for AF coatings are reported: **(i)** polymers with hydrolyzable main chains, **(ii)** polymers with hydrolyzable pendant groups, **(iii)** polymers combining **(i)** and **(ii)**, and **(iv)**. hydrolyzable polymer networks.

(i) Polymers with hydrolyzable main chains

Biodegradable polyesters can be considered as promising binders for antifouling paints to prevent major environmental pollution [121–124]. They usually possess the following characteristics to be suitable for paint applications:

- Solubility in most common organic solvents;
- Compatibility with fillers and other additives;
- Controlled degradation;
- And molecule release.

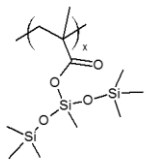
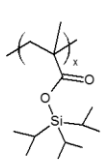
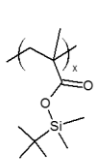
Solubility and compatibility of hydrolyzable polymers in the paint formulations are usually not problematic as long as the solvent and additives are not source of undesired chemical reactions. Xylene, ethylene acetate, methyl isobutyl ketone or THF are the most employed solvents in paints [125–129].

Biodegradable polyesters have been extensively studied by Réhel's and Zhang's groups. Fäy et al. studied coatings degradation to compare the antifouling efficacy of surface erodible-coatings and bulk erodible-coatings [105]. The poly(phtalic acid-co-ricinoleic acid-co-isophtalic acid ester anhydride) (P(PA-co-RA-co-IPA) copolymer (Figure I-13, **A**) exhibited a surface erosion and displayed the second higher erosion rate behind poly(methyl methacrylate-co-butyl methacrylate) (PMMA-PBMA)/rosin-based coating (with bulk erosion process) in distilled water. However, the field tests revealed P(PA-co-RA-co-IPA) was totally eroded after 2 months due to the different physico-chemical properties of the natural seawater (pH, salinity and presence of microorganisms). Poly(ϵ -caprolactone-co- δ -valerolactone) P(CL-co-VL) (Figure I-13, **B**) and PMMA-PBMA rosin-based paints (with bulk erosion process) were more suitable antifouling binders.

(ii) Polymers with hydrolyzable pendant groups

Bressy's group synthesized block and random copolymers of poly(methyl methacrylate- *tert*-butyldimethylsilyl methacrylate) (P(MMA-TBMSiMA)) and compared their erosion rate to a TBT-based-coating reference in dynamic conditions [112]. The resulting erosion rates were very similar to the TBT-coating for diblock copolymers containing 21-27 mol.% of hydrolyzable silylated groups with an erosion of 0.37-0.38 $\mu\text{m}/\text{day}$. The glass transition temperature of PMMA was essential to maintain a good mechanical stability and good film properties of the resulting coatings. Its presence also aimed for adjusting the erosion profiles. Bressy's group has also studied the erosion profiles of trialkylsilyl polymethacrylate copolymers [112]. Some examples of poly(tri-alkylsilyl methacrylate)s with hydrolyzable side groups are presented in Table I-5. Hydrolytic degradations of the side groups is strongly dependent on the size of the alkyl group linked to the silicone atom [120]. The steric hindrance of the pendant moiety is responsible for lower hydrolysis kinetics. For instance, poly(bis(trimethylsilyloxy)methylsilyl methacrylate) (PMATM2) is less hindered than poly(triisopropylsilyl methacrylate) (TIPSiMA) and thus degrades faster.

Table I-5. Hydrolyzable poly(trialkylsilyl methacrylate)s.

		
Poly(bis(trimethylsilyloxy)methylsilyl methacrylate) (PMATM2)	Poly(triisopropylsilyl methacrylate) (TIPSiMA)	Poly(<i>tert</i> -butyldimethylsilyl methacrylate) (TBMSiMA)

A new polymer based on zinc acrylate monomer (zinc 3-(allyloxy)propanoate, ZnAA) was investigated to improve the SPC resin fluidity and stability (Figure I-14) [127]. The polymers based on 1 to 3 mol.% of this monomer unit demonstrated good self-polishing properties under dynamic artificial seawater conditions.

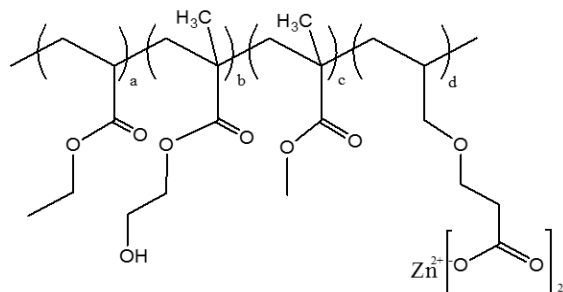


Figure I-14. Self-polishing copolymer resin containing ethyl acrylate (EA), 2-hydroxyethylmethacrylate (HEMA), methyl methacrylate (MMA) and zinc 3-(allyloxy)propanoate (ZnAA) monomers [132].

Other polymers with hydrolyzable side groups are poly(cationic-zwitterionic ester)s such as poly(carboxybetaine ester) [133,134]. The hydrolytic cleavage of a portion of their side chain carrying the bactericidal quaternary ammonium salts revealed a new functionality: the zwitterionic form with non-fouling properties (Figure I-15). In this manner, even after hydrolysis the polymer still has an antifouling effect.

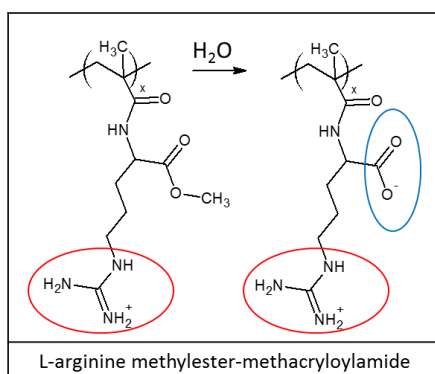


Figure I-15. Switchable cationic-zwitterionic polymer through hydrolysis in water.

(iii) Copolymers combining hydrolyzable backbones and hydrolyzable pendant groups

Zhou et al. combined monomers with hydrolyzable pendant groups and hydrolyzable backbones in a triblock copolymer poly(2-methylene-1,3-dioxepane -co- methyl methacrylate -co- tributylsilyl methacrylate) referred as P(MDO-co-TBSM-co-MMA) (in Figure I-16)[124].

Chapter I – State-of-the-art

Such copolymers favored a surface erosion and provided excellent antifouling properties for 4 months with up to 20 wt.% of 1,3-dioxepane monomer (MDO) (cf. Table I-6). The ultimate objective is to find a balance of hydrophilic/hydrophobic polymers so that the resulting coating degrade itself in a progressive way [135].

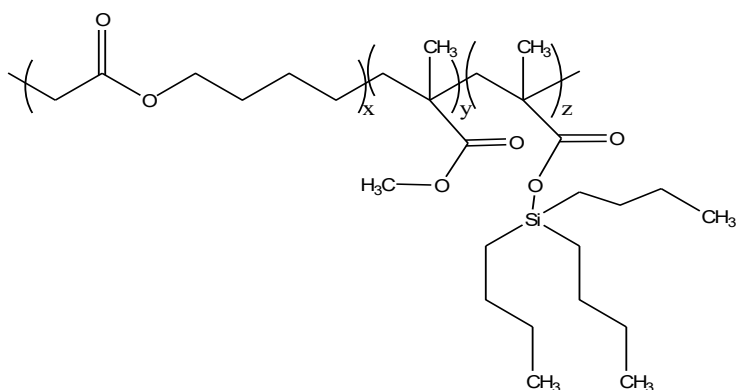


Figure I-16. Degradable P(MDO-co-TBSM-co-MMA) [124].

Other monomers used for SPC are presented in the review of Xie et al. (Figure I-17) [29].

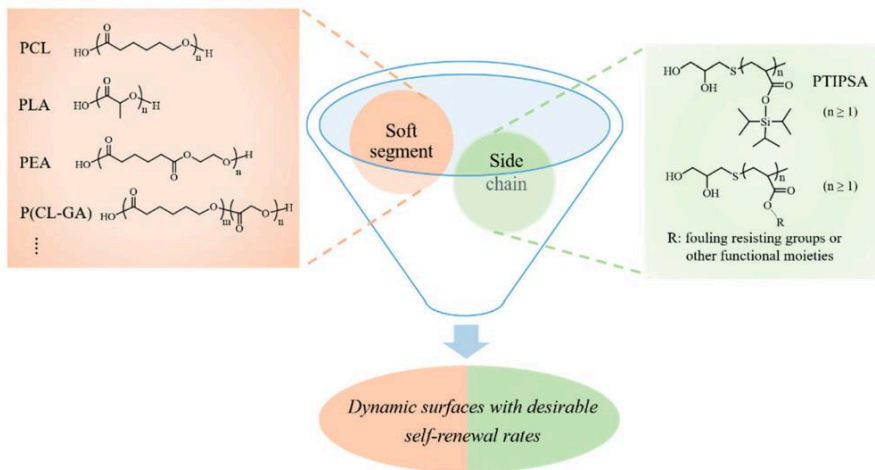


Figure I-17. Examples of monomers hydrolyzed in their backbones and in their pendant groups [29].

(iv) Hydrolyzable networks

Monomers can also be polymerized in a network thanks to the addition of crosslinking agents. Xie et al. designed a biodegradable copolymer based on MDO and on a tertiary carboxybetaine ester monomer (TCB) to make a degradable polymer resistant to proteins. 7-methacryloyloxy-4-methylcoumarin (MAMC) was used to photo-crosslink the above polymer and develop a polyfunctional coating with a hydrolysis-induced zwitterion which is able to inhibit the adhesion of marine bacteria (Figure I-18) [125]. The resulting mass loss was of 0.5-2.5 mg/cm² after 30 days in ASW, 25°C (cf. Table I-6).

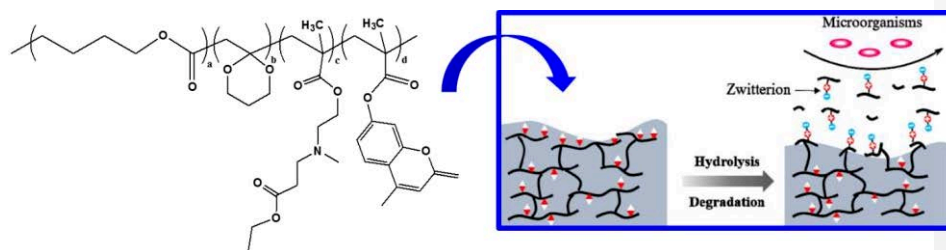


Figure I-18. Biodegradable copolymer with hydrolysis-induced zwitterions for antibiofouling [125].

Chapter I – State-of-the-art

Hydrogel coatings based on a terpolymer of methyl methacrylate (MMA), acrylic acid (AA), tributylsilyl methacrylate (TBSM) or triisopropylsilyl methacrylate (TIPSM) of 13,000-31,000 g/mol were tested in marine field tests (Figure I-19) [136,137]. Both the type of hydrolyzable monomer content and the crosslinking degree was investigated. Results highlighted that with no crosslinking, the polymers leach out making it impossible to create a durable hydrogel layer and thus cannot prevent the fouling. On the other hand, the crosslinking of *ca.* 26 mol.% of hydrolyzable monomers (either TBSM or TIPSM groups) can form a good, soft, thin and dynamic hydrogel on the surface making the adsorption of proteins more difficult on it. The self-peeling resulted from the hydrolysis of the network dangling groups (either TBSM or TIPSM groups) and allowed thickness changes of 10.6-15 μm/month in ASW. However, an over-crosslinking can significantly reduce the self-peeling rate, which could alter the surface renewal and antifouling property.

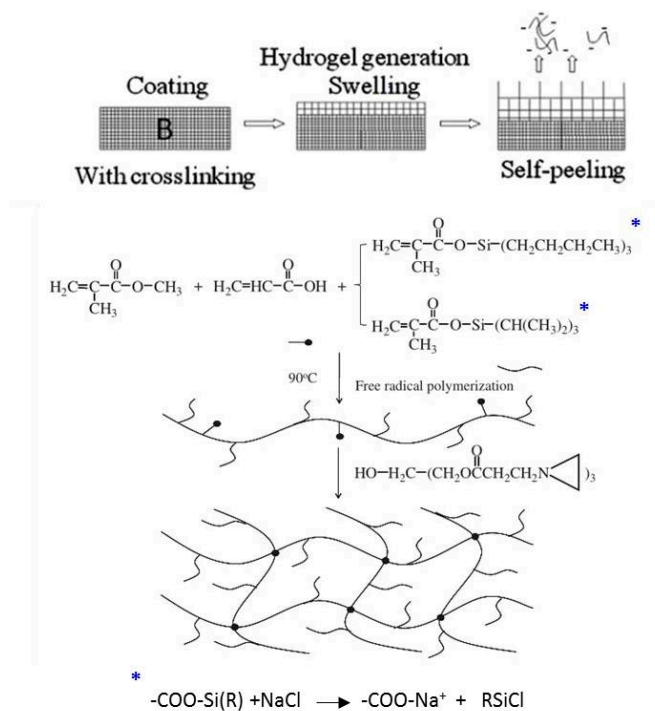


Figure I-19. Schematic of a hydrogel self-peeling coating immersed in seawater [136,137].

Chapter I – State-of-the-art

Table I-6 gives leaching and/or erosion rates of some erodible antifouling coatings at the research and development stages from 2010 until today. This table highlights the various nature of erodible polymers and the effort to substitute copper biocides by less toxic compounds such as the DCOIT booster biocide, NPAs or QAS-based compounds.

Globally, it shows that by changing the polymer binder (which are usually less toxic than copper acrylate), similar toxicant leaching rates (LR) and erosion rates (ER) to those of the commercial SPCs (LR \approx 10 $\mu\text{g}/\text{cm}^2/\text{d}$, ER \approx 0.10-0.30 $\mu\text{m}/\text{d}$ or 8 $\mu\text{m}/\text{month}$) could be obtained.

In this table, polymers are classified as rosin-based (pink), acrylate-based (purple), poly(ester)s-based (green) and poly(urethane)-based (blue) polymers.

Table I-6. Some examples of erodible coatings at the academic research state from 2010 until today.

	Erodible/ soluble matrix or self-polishing polymer	Specialty additives (other than biocides)	Substances with biocidal activity (and mass %)	Leaching/release rate	Erosion rate/thickness loss/mass loss	Ref.
Rosin-based	Rosin with co-binder styrene acrylic copolymer - CDP	Chalk, castor oil gel, oleic acid, chlorinated paraffin	Zinc tannate (tara tannin) 27-35 % w/v	2.5 µg/cm ² /d of leached total poly(phenol) and 1-2 µg/cm ² /d of leached Zn ²⁺		[49]
	Rosin (10-15%), metal-acrylate	Zinc oxide: 12-15%, inorganic fibers (Hempel Olympic 86950)	Copper pyrithione: 10-25%, cupric oxide: 1% copper < 1% and Zineb 5-10 %	13 ± 1.8 µg/cm ² /d of Cu and 5.6 ± 0.5 µg/cm ² /d of Zn in ASW*		[138]
	Rosin (90%)	Co-solvent mix (10%)	Ivermectin (0.1% w/v) (macrocyclic lactones)	Between 0.68 ± 0.2 ng/cm ² /d and 2.95 ± 0.38 ng/cm ² /d	2.10 ⁻⁵ cm/d (=0.2 µm/d)	[52]
	Mixture of rosin and phenolic resin (10-20 wt%)	Chlorinated paraffin as plasticizer, red iron oxide, barium sulfate, talc, zinc oxide + formulation additives	Copolymer of styrene sulfonate with maleic acid or copolymer of vinyl acetate with maleic acid or copolymer of styrene with acrylic acid (complexation of anionic polyelectrolytes with Cu ²⁺ and/or phosphonium groups) - 3 to 12 wt.%	0.02 to 0.1 % of released Cu ²⁺ compared to the total theoretical release of Cu ²⁺	One paint: 0.27 µm/day the other paint < 0.1 µm/d	[139]
	Fully hydrogenated rosin (Foral AX-E) (18.4- 18.5 % in the total formulation) + PBMA-PMMA copolymer (2%, neocryl) (possible poly(silyl acrylate) as a metal resinate)	Zeolite dehydrated agent (sylosiv A4) (2.9 % in the total formulation) and other additives	Zineb Nautec (8-9 % in the total formulation), cuprous oxide (45-46 % in the total formulation)		Over 18 months, at 9-13-18 knots, polishing rate = 12;13;16 µm/month	[140]
	Silylated acrylic copolymer and rosin (28-52 % wet weight), other binder systems are also shown	Starch with glucoamylase (0.5-1-2.4-5-10 % wet weight), pigments etc.	Copper pyrithione, copper omadine (3-6 % wet weight)		3.5-5.3 (µm/10,000 nautical miles)	[141]
Acrylate-based	PMMA-PBMA with rosin (mixture of abietic and dehydroabiatic acids) (16.3 wt%) "polyacrylic paint" compared to P(CL-VL) matrix (16.3 wt%)	TiO ₂ , BaSO ₄ , other paint additives	Chlorhexidine (4.5 wt%), zinc peroxide ZnO ₂ (10 wt.%) and Tween 85 (6 wt%)	7 µg/cm ² /d for zinc peroxide and 2 µg/cm ² /d for chlorhexidine	Bulk erosion rate of 0.45 µm/week	[122]
	Network based on statistical copolymer PMMA (methyl methacrylate)-PAA acrylic acid-PTBSM (tributylsilyl methacrylate)	Crosslinker XAMA7 (aziridine reacts with carboxylic acid)			15 µm/month for the non-crosslinked copolymer	[137]
	Copolymer pMMA-b-pHEMA-b-PEA with zinc acrylate monomer)				0.03-0.2 µm/month, ASW, 15 knots, 5 weeks duration	[132]
	Poly(MDO-co-TBSM-co-MMA) (90 wt.%) random copolymer		DCOIT (10 wt.%)	55-120 µg/cm ² /d after 30 days (DCOIT) in dynamic conditions	1.6-8.1 µm/month in ASW, 25°C, 90 days (thickness loss) and 0.1-0.6 mg/d (degradation rate)	[124]

Chapter I – State-of-the-art

	Erodible/ soluble matrix or self-polishing polymer	Specialty additives (other than biocides)	Substances with biocidal activity (and mass %)	Leaching/release rate	Erosion rate/thickness loss/mass loss	Ref.
Polyester-based	MDO (2-methylene-1,3-dioxepane), TCB (tertiary carboxybetaine ester) and MAMC (7-methacryloyloxy-4-methylcoumarin)-based polymer				0.5-2.5 mg/cm ² mass loss after 30 days in ASW, 25°C	[125]
	Poly(ϵ -caprolactone-co- δ -valerolactone) (P(CL-VL)) (80/20)		Zinc pyrithione (photodegradable) and copper thiocyanate	6-8 μ g/cm ² /d before 10 days and 2-4 μ g/cm ² /d after 45 days		[142]
	Poly(ϵ -caprolactone-co- δ -valerolactone) (P(CL-VL))	Tween 80 (3% w/w), Span 85 (3% w/w), PEG-silane (3% w/w)(surface modifier), CaCO ₃ , fillers, pigments	Copper thiocyanate CuSCN (31 wt.% in the dry coating)	0.06-0.58-3.05 μ g/cm ² /month (control= 0.18 μ g/cm ² /month) for /Span/Tween/PEG-based coatings respectively	0.45 μ m/week (bulk erosion) Cf. Lorient et al.	[143]
	PCL- <i>b</i> -PDMS- <i>b</i> -PCL	Polyamide waxes, TiO ₂ , ZnO, CaCO ₃	Dichlorofluanid, Zinc pyrithione, copper thiocyanate		16% M _n loss after 350 days in d.w.* (copolymer hydrolytic degradation)	[126]
Polyurethane-based	QAS-modified poly(urethane) network	Trifunctional silicate cross-linker, desmodur polyisocyanate	Butyl/decyl or octadecyl bis(2-hydroxyethyl) methyl ammonium biocide		8 to 20 % mass loss after 24 weeks in distilled water	[144]
	Poly(propylene carbonate) polyurethane		DCOIT (4,5-dichloro-2-octyl-isothiazolone), 10 wt.% (+ 0/1/5/10/20)	Release rate of DCOIT= 0.08 to 0.77 mg/m ² /d	Hydrolysis rate= 0.012-0.051 g/(m ² d) in ASW	[145]
	Silyl acrylate based poly(urethane) with PCL, PEA (poly(ethylene adipate) and PLA		DCOIT (10 wt.%)	Release rate of DCOIT= 10-50 μ g/cm ² /d	0.3-4 .10 ⁻³ g/cm ² mass loss after 90 days in ASW, 25°C	[121]
	Degradable poly(urethane) with copolyester oligomer of ϵ -caprolactone (CL) and glycolide (GA)		DCOIT (4,5-dichloro-2-octyl-isothiazolone), 10 wt%		0.001-0.07 g/175 days (mass loss), ASW, 25°C	[146]
	Micellar core-shell acrylique poly(urethane) (PAA- <i>b</i> -PS- <i>b</i> -PU- <i>b</i> -PS-PAA)				8-10 μ m/month in ASW, dynamic conditions	[131]

*ASW= artificial sea water, d.w.= deionized water

I.5. Focus on fouling release coatings

Before 2008, publications about biocide-based antifouling coatings prevailed over publications about FRCs (Figure I-20). But this trend was reversed after 2008 indicating researchers and industrials paid more attention to these systems [57,147,148]. Indeed, the total sales of FRCs significantly rose following the adoption of the IMO-AFS convention entered in force in 2008 (convention to control the use of harmful antifouling systems on ships), and are currently estimated to 5-10 % by volume for commercial shipping [149,150].

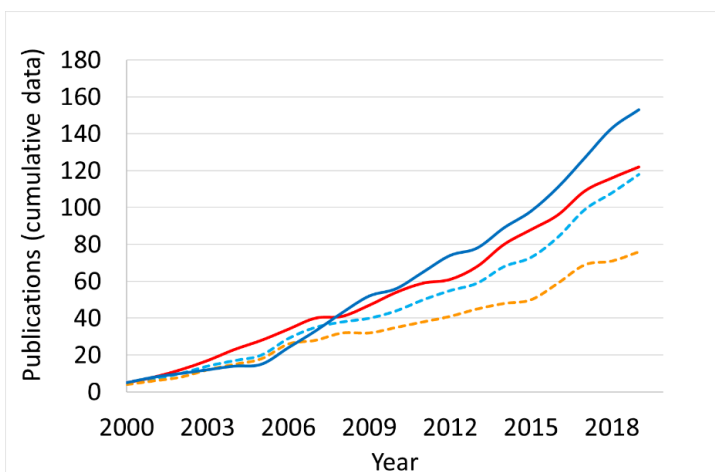


Figure I-20. Total publications (articles, conference papers, patents and reviews) on fouling release coatings (dark blue line), biocide-based antifouling coatings (red line), silicone-based coatings (dotted blue line) and self-polishing coatings (dotted orange line) from 2000 to 2019, based on a Reaxys search of the terms “fouling release coatings”, “biocide-based antifouling coatings”, “silicone-based coatings” and “self-polishing coatings”, respectively.

I.5.1. Commercial fouling release coatings

FRCs are mainly based on silicone elastomers which are defined as non-toxic, non-stick and slippery coatings. Their specific properties, i.e. low surface free energy, low elastic modulus, and low roughness, contribute to the easy detachment of the settled fouling organisms thanks to the hydrodynamic forces during sailing. The service life of an FRC can vary from 5 to 10 years depending on its composition and the navigation schedule of the ship. Table 1.9 gives an overview of the commercially available FRCs.

Chapter I – State-of-the-art

Different strategies are used by the supplier for improving the AF efficiency of silicone elastomers. Fluorinated or amphiphilic additives and also biocides could be added to the PDMS network.

I.5.1.1. Description of the FRC composition

I.5.1.1.1. Elaboration of conventional silicone elastomers

Silicone elastomers are a class of organic-inorganic materials with an alternation of silicon-oxygen atoms in the main chain. Each silicon atom carries two alkyl pendant groups, usually methyl groups. The elastomer material is obtained through the crosslinking of high molar masses polysiloxane chains carrying reactive end-chain functions such as –hydroxyl, -amino, -alkoxy, vinyl and hydrosilylated functions essential for the curing process.

Most of silicone elastomers are prepared using three different crosslinking routes: (i) peroxide-induced free radical reactions of vinyl-functionalized polysiloxane oil (High Temperature Vulcanization), (ii) condensation reactions of hydroxyl, amino- or alkoxy-terminated polysiloxane oil (Room Temperature Vulcanization, RTV), and (iii) hydrosilylation or addition cure of vinyl and hydrosilylated polysiloxane oil [151]. The crosslinking of silicone elastomers can be very challenging for the FRCs manufacturers given that the conditions of application on ship hulls are not always ideal (for example at very low temperature).

I.5.1.1.1.1. Peroxide-induced crosslinking of polysiloxane

High consistency rubbers (HCRs) are made of very high molar mass vinyl-based PDMS (50,000 to 200,000 g/mol) [152]. HCRs are crosslinked via free radical reactions at high temperature. A typical drawback of the peroxide cure reaction is the formation of a heterogeneous crosslinking due to the random distribution of vinyl groups [153]. The network may contain numerous dangling chains and entanglements between neighboring chains which can weaken the elastomer mechanical properties [152]. Additional fillers can be required to improve mechanical properties

Chapter I – State-of-the-art

I.5.1.1.1.2. Condensation cure system

The condensation cure is a nucleophilic substitution reaction occurring on the silicon atom in presence of a catalyst (Figure I-21). To form crosslinks, a hydroxyl-terminated polysiloxane is reacting at room temperature with small quantities of tri- or tetrafunctional silanes ($RSiX_3$ or SiX_4) such as the ones presented in Table I-7. The amount of crosslinking agents as well as the nature of their leaving groups will influence the crosslinking density and the cure rate, respectively. Low molecular weight alcohols are generated during this process.

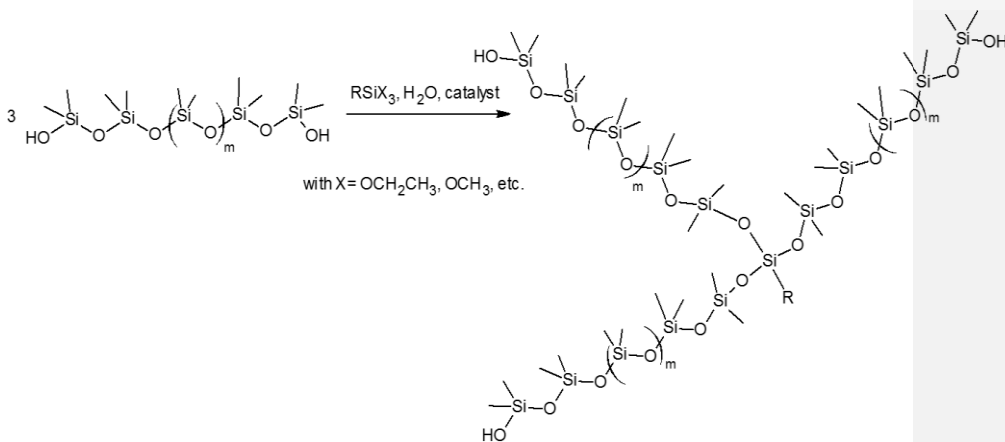


Figure I-21. Condensation cure of bis-silanol-terminated poly(dimethylsiloxane) oil.

Table I-7. Typical crosslinking agents for condensation cure silicone elastomers.

	<p style="text-align: center;">$n = 2, 3, 4 \dots$</p>
Tetraethoxysilane (TEOS)	Ethyl polysilicate (ES40)

The nucleophilic substitution reactions in the condensation crosslinking process requires a catalyst which can be either an acid, a base, a tin or a titanium alkoxy/acyloxy derivative.

Chapter I – State-of-the-art

Some examples of catalysts used to elaborate silicone elastomers are presented in Figure I-22.

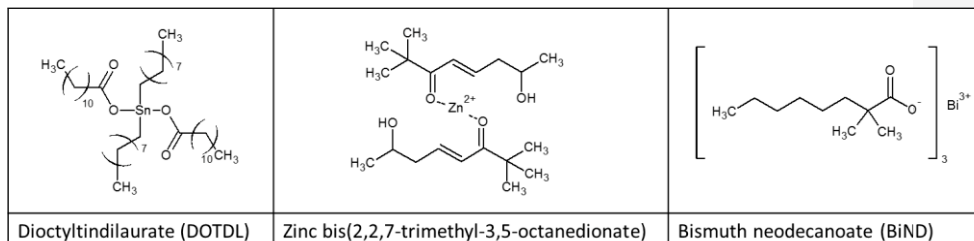


Figure I-22. Typical catalysts used for condensation cure silicone elastomers.

Moisture is also a requisite co-catalyst in the tin catalysis mechanism given that dioctyl tin dilaurate (DOTDL) or dibutyltin dilaurate (DBTL) compounds need to be first hydrolyzed before producing the true catalytic species that will attack the silanol functions. The condensation cure can generate by-products such as ethanol or methanol depending on the nature of the crosslinking agent.

RTV11 is an example of two-part PDMS systems cured by condensation cure manufactured by Momentive performance materials. The first part is the base resin comprises bis-silanol PDMS (10,000 cps, $M_{n,SEC} = 34$ kg/mol, $M_{w,SEC} = 70$ kg/mol by SEC, $\bar{D} = 2.1$ with PS standards in toluene, intern data), the ES40 crosslinking agent and calcium carbonate filler. The second part called the curing agent comprises the DBTDL catalyst.

However, the use of tin catalysts poses a threat to the marine environment reported as toxicants [154]. The tin content in crosslinkable organosilane polymers-based coatings was restricted to 0.1 % by European legislation (EU 276/2010) for various industrial applications [155].

Alternatives to tin compounds are zinc complex or bismuth carboxylate catalysts (Figure I-22) or trifluoroacetic acid [156]. The bismuth neodecanoate (BiND) used by Martinelli et al. is a more innocuous catalyst but is 3 times less reactive than tin compounds and also 2 to 3 times more expensive [128,157]. This is why 1 wt.% of BiND (in the total dry

Chapter I – State-of-the-art

formulation) is added in their total dry PDMS coatings against the usual 0.1 wt.% of organotin catalyst.

I.5.1.1.1.3. Addition cure system

The addition cure or hydrosilylation cure is a very widely used process for the preparation of silicone elastomers. Two complementary polymers containing Si-H groups and Si-CH=CH₂ groups lead to the crosslinking reaction in presence of platinum catalysts such as Karstedt's catalyst or Speier's catalyst at elevated temperatures, e.g. 160°C (Figure I-23) [153,158]. An example of addition cure system is the liquid silicone rubber obtained with vinyl telechelic PDMS (between 10,000 and 50,000 g/mol) and a short Si-H PDMS crosslinker [152].

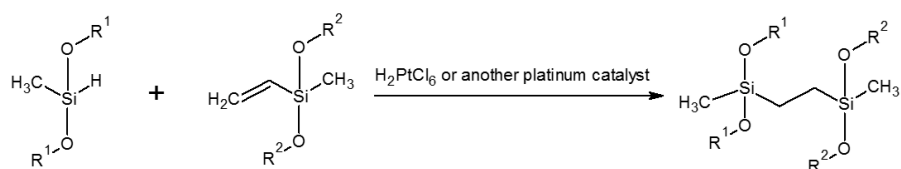


Figure I-23. Hydrosilylation cure of silicone elastomers.

Two commercial PDMS elastomers Silastic T2 (50,000 cps) and Sylgard 184 (5,100 cps, $M_{n,SEC} = 32$ kg/mol, $M_{w,SEC} = 46$ kg/mol, $D = 1.5$ with PS standards in toluene, intern data) from Dow were often used as standards of comparison for antifouling applications. They consist in two-part PDMS system cured by platinum-catalyzed hydrosilylation from a mixture of the base resin and a curing agent. Contrary to RTV11, there is no release of by-products during the cure. The addition reaction is although very sensitive to contaminants such as oleophilic compounds [159].

I.5.1.2. Improvement of the FRCs

As discussed in § I.3.2., silicone elastomer-based coatings are a promising ecological antifouling alternative [57]. Nevertheless, the economic cost/benefit analyses were still not comparable to SPC coatings [37]. The rise of ECHA regulations limit the use of biocides and so it gives an opportunity for FRCs to attract more attention.

Low γ_s , low roughness and low elastic modulus are important parameters for fouling release properties but are not enough to achieve long-term antifouling properties in static conditions [160]. In this section, the main methods used to improve the AF/FR performance of the commercially available FRCs are enumerated. Two main chemical routes can lead to improved FRCs such as: (i) additive-based FRCs (i) and (ii) biocide-based FRCs.

(i) Additives-based FRCs

The most common way to improve conventional FRCs is to design amphiphilic FRCs. In this technology, non-reactive surface-active block copolymers are added to the PDMS coating in small amounts (less than 10 %) [161,162]. The addition of amphiphilic additives does not modify the bulk softness and surface smoothness of the FRCs. However, it changes the surface chemistry: FRCs are able to exhibit “mosaic chemical structures” with hydrophilic and hydrophobic domains (Figure I-24). The resulting surfaces are often referred as “ambiguous surfaces” inhibiting the adhesion of microorganisms depending on the size of juxtaposed domains.

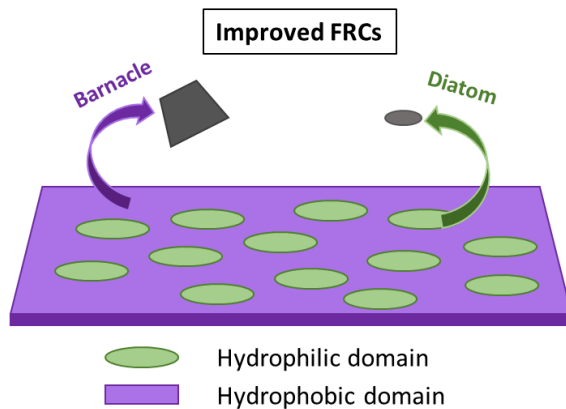


Figure I-24. Schematic representation of amphiphilic FRCs.

The hydrophilic domains are often made of poly(ethylene glycol) (PEG) segments and the hydrophobic domains are often made of perfluoropolyether or PDMS segments.

Thanks to the time lag method, Noguier et al. revealed the diffusion ability of small PDMS-PEG block copolymers (amphiphilic additives) through a PDMS-based FRC (4 wt.% of the total weight in the dry film) by mean of the Fick’s first law of diffusion [127].

Chapter I – State-of-the-art

The resulting amphiphilic surface can minimize the chemical and electrostatic adhesion of a larger community of marine species [164–168]. In a patent from Hempel, a non-reactive polyether modified PDMS oil named Tego glide 435 provided by Evonik Industries was used at 3 wt.% relative to the dry coating in an enzyme-based FRC [169]. HempasilX3 and SilicOne77450 are defined as a hydrogel-based PDMS elastomer and may also use these type of amphiphilic compounds (seen in Table I-8).

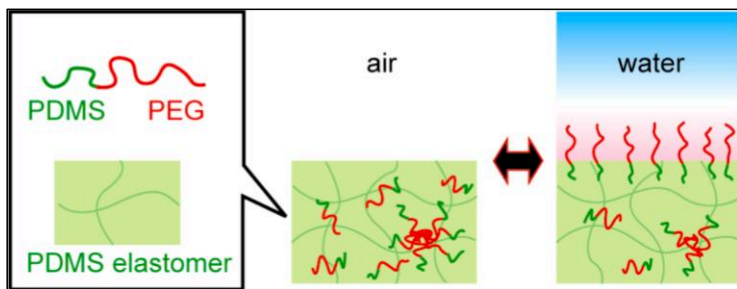


Figure I-26. PDMS-*b*-PEG additive migration towards the surface in contact with water [163].

An amphiphilic additive (named FR355, a silicone/acrylic hybrid polymer, from Wacker) was introduced in an Akzo Nobel patent. Its possible molecular structure is shown in Figure I-27, A [170]. The coexistence of anchoring mobile siloxane chains (exposing the alkyl groups at the interface) and liquid-crystal like rigid structure of perfluorinated chains at the top surface was proved to display higher removal percentage of *Ulva* sporelings and barnacles than the PDMS elastomer control, and also reduced the settlement of cyprid barnacles [171,172]. Intersleek 1100SR may use the same technology (Table I-8).

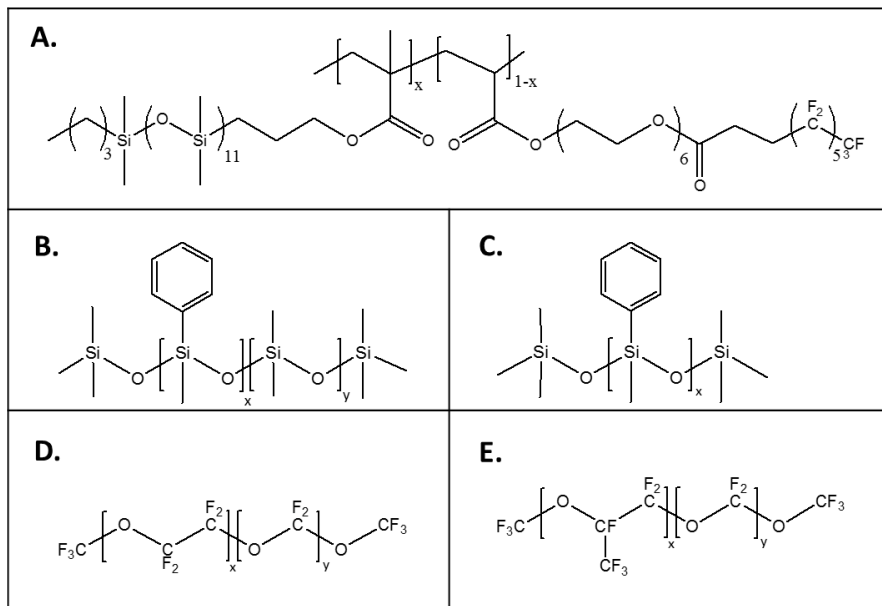


Figure I-27. Common oil additives used in FRCs.

Hydrophobic oils can also be found in some FRCs such as phenyl-modified PDMS oils (Figure I-27, **B** and **C**) [161], fluorinated oils such as Krytox oils (Krytox 100, Krytox K7 from DuPont) used in SLIPS [173], Fomblin (perfluoropolyether) PFPE lubricants (Figure I-27, **D** and **E**, from Solvay) [174], FluorolinkE (from Solvay) or Demnum S200 oils (from Daikin Industries) [170]. These oils are usually added to conventional condensation cure PDMS formulations in percentages varying from 2 to 10 wt.% to enhance the AF properties. After 14 weeks of immersion in tropical sites, coatings containing these kind of fluorinated oils were at least 2 times less fouled than the PDMS control. These liquid-infused FRCs can thus achieve strong reduction of adhesion strength of marine macrofouling onto the immersed coating. [173].

Akzo Nobel also introduced a novel FRC called Intersleek 1001 (Table I-8) containing lanolin oils (1-30 wt.%) [175]. These oils contain one or several sterols and long chain fatty esters. Their efficacy was demonstrated in different marine locations with 10 % less fouling compared to a fluoropolymer-based commercial FRC after 10 months.

(ii) Biocide-based FRCs

FRCs containing copper pyriithione as biocide are also commercially available (Hempaguard X5 and X7, Table I-8). The combination of biocides with the active hydrogel technology aims for increasing AF properties over time (Figure I-28). Their biocide content (≤ 10 wt.%) remains inferior to those of SPCs.

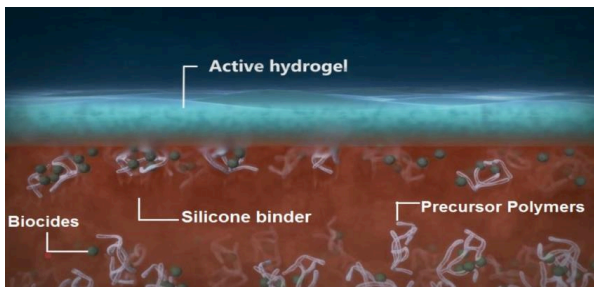


Figure I-28. Actiguard technology: a third generation of fouling release (Hempel technical report, [176]).

Chapter I – State-of-the-art

Table I-8. Commercially available Fouling Release Coatings.

Company	Top-coat	Binder	Specifications
Chugoku Marine Paints	Bioclean HB	Silicone elastomer	R _v = 46 μm FIR= 1.0 %, R _s = 45 μm, % smoother than conventional FRCs
	BiocleanPlus	Silicone elastomer with PEGylated polymers	
	Bioclean R	Silicone elastomer	
	Bioclean SG	Silicone elastomer	
	Bioclean SG-R	Silicone elastomer	
Fujifilm Hunt Smart Surfaces	Surface Coat	Siloxane & silicones (60-80 wt.%), silicone fluid (5-10 wt.%) and RTV silicone rubber (3-7 wt.%) in part A	Efficient at speed ≥ 8 knots, 6 to 10 % fuel savings
International Paint	Intersleek737	Silicone elastomer	Efficient at speed >15 knots and for high activity vessels, 4 % fuel savings vs SPCs
	Intersleek 970	Silicone elastomer with fluoropolymer and PEG	For all vessel types, efficient at speed >10 knots, 9 % fuel savings vs SPCs
	Intersleek 1100SR	Silicone elastomer with advanced fluoropolymer and PEG	For all vessel types, efficient at speed >6 knots, 10 % fuel savings vs SPCs
	Intersleek 1001	Bio-renewable sterols (long chain waxy sterols)	6 % fuel savings, 60 % less in VOC, minimum 5 years of FR efficacy
Nippon Paint	Ecolosilk	Silicone elastomer	Efficient at speed >15 knots
PPG	SigmaGlide 1290	Silicone elastomer with a dynamic surface regeneration, contains PDMS oils (methyl-terminated, hydroxyl-terminated or PEG ether-terminated) (20-50 wt.% in the hardener pot)	8 % fuel savings, 7 years of service life
Sherwin Williams	SeaGuard Surface Coat		Efficient at speed ≥10 knots, 6-10 % fuel savings
Transocean	Ultima System		Efficient for fast vessels

Chapter I – State-of-the-art

Company	Top-coat	Binder	Specifications
Hempel	Hempasil X3 87500	Silicone condensation-cured elastomer with a hydrogel microlayer	Efficient at speed >8 knots and activity>50%, 8 % fuel savings
	Hempaguard X5 89700	Silicone condensation-cured elastomer, contains CuPT (5-7.1 wt.% in part A) and glycolethers (10-25 wt.% in part B)	Efficient at speed >8 knots, enables up to 60 static days, 8 % fuel savings vs SPCs
	Hempaguard X7 89900	Silicone condensation-cured elastomer with a hydrogel microlayer, contains CuPT (5-10 wt.% in part A)	No speed limitation, enables up to 120 static days, 8 % fuel savings vs SPCs
	SilicOne 77450	Silicone condensation-cured elastomer with a hydrogel microlayer	For yacht
Jotun	SeaQuest	Silicone elastomer that contains amphiphilic oils	
	SeaLion Repulse	Silicone elastomer	Efficient at high speed and high activity, 4 % fuel savings vs the mean market
	SeaLion Resilient	Epoxy polysiloxane	Efficient at high speed, for high activity vessels, 1.5 % fuel savings
Adaptive Surface Technologies	SLIPS N1x	Lubricant-infused porous material	8 % fuel saving vs traditional AF coatings

I.5.1.3. Specific properties of FRCs

I.5.1.3.1. *Surface properties*

I.5.1.3.1.1. Contact angles

Poly(dimethylsiloxane) surfaces are known to be water repellent. Their hydrophobicity is traduced by a high-water contact angle (between 105-110°) which is maintained even after a long immersion time. The low electrostatic and dipolar interactions between the Si-O-Si backbone and the water molecules are responsible for this high-water contact angle. Dynamic contact angles can give other information such as the ability of the surface to reorganize after water contact or a surface heterogeneity [177]. The water advancing contact angle ($\theta_{w,adv}$) is governed by the hydrophobic functions or domains at the surface of the coating whereas the water receding contact angle ($\theta_{w,rec}$) is affected by the hydrophilic functions or domains. Usually, the $\theta_{w,adv}$ and $\theta_{w,rec}$ of PDMS elastomers are very similar indicating their high resistance to surface reorganization in contact with water. This can be traduced by a low contact angle hysteresis ($\Delta\theta = \theta_{w,adv} - \theta_{w,rec} \leq 40^\circ$) [178].

Table I-9 displays the wettability properties of some well-known commercial FRCs. Among them, Intersleek 1100SR and Hemptasil X3 show interesting behaviors after water exposure. Their receding contact angles are lower than 70° suggesting a surface chemical heterogeneity likely due to the presence of the hydrophilic PEG functionalities. Intersleek 900 showed surprisingly lower water contact angle given that it is a fluoropolymer-based coating, this can probably come from the influence of pigments and/or fillers from the paint formulation.

Chapter I – State-of-the-art

Table I-9. Comparison of the wettability properties between different FRCs: RTV11, Silastic T2, Intersleek 700, Intersleek 900, (fluoropolymer technology), Intersleek 1100SR (amphiphilic technology) and Hempasil X3, (hydrogel technology).

	θ_w (°)	$\theta_{w,adv}$ (°)	$\theta_{w,rec}$ (°)
RTV11 [179,180]	104.2±1.9	103	94
Silastic T2 [181,182]	109	115.1±3.8	68.7±2.2
Intersleek 700 [183]	99±1		
Intersleek 900 [183]	76.45±1.95		
Intersleek 1100SR (*intern data)	108.2±3.9*	110.3±0.3*	56.6±2.3*
Hempasil X3 [168,184]	95.8±1.2	96±1	23±1

It is worth noting that some species prefer to settle on hydrophobic coatings such as green algal zoospores diatoms *Navicula perminuta* or *Amphora*. Their settlement are 3 times more important on hydrophobic surfaces ($\theta_w = 116^\circ$) than on hydrophilic surfaces ($\theta_w < 15^\circ$) [185,186]. Thus, this shows the limitation of FRCs in the marine environment.

I.5.1.3.1.2. Surface free energy

PDMS chains have a remarkable chain flexibility. The free orientation of the siloxane backbone enables a very low energy of rotation of Si-O-Si (0 kJ/mol) against 14 kJ/mol for C-C in poly(ethylene) (PE) and more than 20 kJ/mol in poly(tetrafluoroethylene) (PTFE) [187]. This backbone flexibility promotes the packing of methyl groups at the surface to adopt the lowest surface free energy [188]. A surface with a low-surface free energy is known to limit the chemical interactions with fouling organisms. The Baier curve exhibits the most preferred intervals of surface free energy (20-30 mJ/m²) to minimize these adhesion forces (Figure I-29).

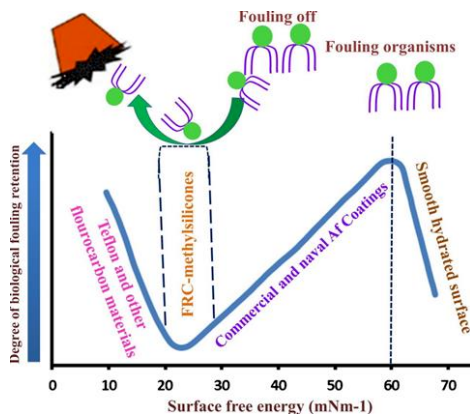


Figure I-29. The Baier curve of adhesion strength vs. surface free energy applied in antifouling paints where Baier curve minimum values improve biofouling detachments [189].

Surface free energies of standard PDMS elastomers such as RTV11 are usually around 25 mJ/m² (Table I-10), these low values are the reason why liquids have difficulties to wet PDMS surfaces. Indeed, to wet a solid surface, the liquid must have a surface tension lower than the surface free energy of the solid surface.

According to the Owens-Wendt-Radel-Kaelble (OWRK) theory, it is possible to divide the surface free energy into two components: the polar and the dispersive component ($\gamma_S = \gamma_S^D + \gamma_S^P$). In this way, Owens et al. evaluated the dispersion contribution ($\gamma_S^D = 19.0-20.5$ mJ/m²) and polar contribution ($\gamma_S^P = 1.2-1.6$ mJ/m²) of PDMS which confirmed its dispersive nature and its very low polarity [188]. Chemical bonding and electrostatic interactions involved in the attachment of marine species onto surfaces can be minimized by using non-polar dispersive surfaces [190]. The dispersive and hydrophobic nature of PDMS coatings makes it hard for biofoulants to strongly adhere since interactions are mostly van der Waals and London forces (weak energy interactions) rather than polar interactions (hydrogen bonding and permanent dipoles). These weak interactions allow to remove biofoulants from the surface with a lower strength leading to a better fouling release ability.

Chapter I – State-of-the-art

Table I-10. Comparison of the surface free energies between different FRCs: RTV11, Silastic T2, Intersleek 700, Intersleek 900, (fluoropolymer technology), Intersleek 1100SR (amphiphilic technology) and Hempasil X3, (hydrogel technology).

	γ_s (mJ/m ²)	γ_s^D (mJ/m ²)	γ_s^P (mJ/m ²)
RTV11 [191]	25.1	22.7	2.4
Silastic T2 [192]	23.3±0.4	23.2±0.4	0.20±0.05
Intersleek 700 [183]	33.91±0.81	33.56±0.83	0.26±0.26
Intersleek 900 [168]	30.08 ± 1.14		
Intersleek 1100SR (internal data*)	27.5*		
Hempasil X3	25.7±2.5*	24.2±1.6*	1.4±0.8*

Due to their low surface free energy, FRCs have difficulties to strongly adhere on the substrate. Warrick introduced the “abhesive” character of silicone materials related to the unbound PDMS that migrate at the silicone material/substrate interface and prevent the silicone material to adhere on a substrate [193]. To overcome this drawback, many solutions are available on the market. Materials which can bond both to the substrate and to the silicone elastomer are used to form an intermediate layer (often called tie-coat or link layer). The molecules with this dual function can be alkoxypolysilicate, alkylborates, vinylalkoxysilanes or silyalkylphosphates. They enhance the adhesion on various materials such as metallic or ceramic surfaces.

I.5.1.3.1.3. Smoothness

FRCs display a smooth surface traduced by low roughness values (0.077-0.116 μm or less) [60]. A smooth surface will favor drag reduction. FRCs are known to cause approximatively 5.6 % less skin frictional drag over time than traditional biocidal antifouling paints at the same sailing speed [194]. In addition, FRCs recorded reduced skin frictional drag between 9 and 22% at different velocities (6.5–22.7 knots) relative to some commercial SPCs [114].

Göler et al. have also compared the performances of SPCs and FRCs applied on 8 high-speed Ro-Ro vessels. They have estimated an average speed loss of 3 % with 12 % fuel consumption for SPCs against 1 % speed loss with 5 % fuel consumption for FRCs [195]. FRCs are thus very efficient when it comes to decrease the ship hull drag.

Nonetheless, there can be different sources of FRC roughness [196]:

Chapter I – State-of-the-art

- the application technique (brush, roller, airless spray gun);
- the paint additives (filled/unfilled);
- the chosen cured-system (hydrosilylation/polycondensation);
- the amount of crosslinking agent/catalyst;
- the water immersion duration.

These parameters can make the roughness vary from the nano- to the microscopic scale. For example, Bullock et al. reported an increase of roughness on RTV11 after water exposure. This was due to the voids left by CaCO_3 fillers, phenomenon called “pitting erosion” [197]. The roughness changed from 45 to 104 nm after 3 months in water.

Beigbeder et al. observed an increase of roughness during immersion for an unfilled hydrosilylation-cured PDMS system [198]. This sudden change was reported to be due to a siloxane backbone reorganization.

Some studies also showed the impact of polydiethoxysilane crosslinking agents (TEOS, ES40) on the surface properties [199–202]. These compounds favors the formation of siliceous phase on the surface due to silanol or alkoxy silane functions coming from the self-condensation of alkoxy silane crosslinking agent but also from the non-crosslinked end-chains (silanol) or even hydrolysis of near surface siliceous phase [197,199,202]. These siliceous phases referred as $(\text{SiO}_x\text{OH}_y)$ phase or silica domains (SiO_2) can result in a roughness increase from 0.27 nm to 21.1 nm for a TEOS-cured system after 8.5 months of water immersion [199]. Black et al. showed that an increase of tin-catalyst concentration could raise the self-condensation of TEOS resulting in micrometer-size particles, and thus a microroughness [203].

1.5.1.3.2. Bulk properties

1.5.1.3.2.1. Softness

Another characteristic of FRCs is their softness, traduced by a low elastic modulus (Table I-11).

Chapter I – State-of-the-art

Table I-11. Comparison of the elastic modulus between different FRCs: RTV11, Silastic T2, Intersleek 700, Intersleek 900, (fluoropolymer technology), Intersleek 1100SR (amphiphilic technology) and Hempasil X3, (hydrogel technology).

	E' (MPa)
RTV11 [204]	1.8±0.3
Silastic T2 [192]	1.4
Intersleek 700 [176]	1.1
Intersleek 900 [161,176]	3.15±0.42
Intersleek 1100SR [205]	0.84
Hempasil X3 [161]	1.89±0.18

Brady et al. demonstrated that adhesion depended not only on the surface free energy but also on the elastic modulus (Young's modulus) as shown in Figure I-30 [206]. The linear relation between relative adhesion and $(E \cdot \gamma_c)^{1/2}$ indicates that a minimum of adhesion is achieved with a minimum of $(E \cdot \gamma_c)^{1/2}$.

Fluorine-based polymers like poly(tetrafluoroethylene) (PTFE) are also interesting for fouling release applications [207] but their very high glass transition temperature (T_g) and/or very high elastic modulus (0.5 GPa) make them less efficient for pull-off fracture mechanisms [187,206,208]. Besides, their very low solubility in most organic solvents make them hard to formulate in antifouling paints.

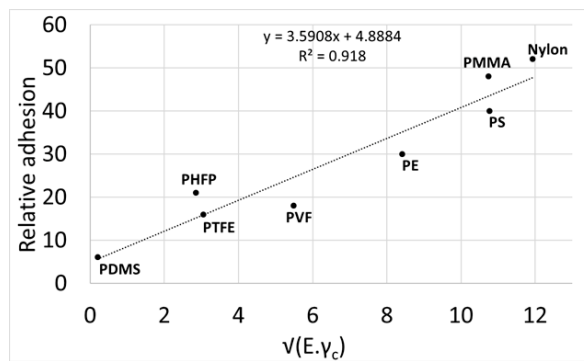


Figure I-30. Relative adhesion (dimensionless) as a function of the square root of the product of critical surface energy (γ_c) and elastic modulus (E) of different polymer [209].

Chapter I – State-of-the-art

The elastic modulus depends on the crosslinking density of elastomers. Wang et al. observed a variation from 0.57 to 3.7 MPa with PDMS elastomers by changing the [base:curing agent] ratio from 33:1 to 5:1 [210].

Kendall's theory showed that the force to detach a hard object from a surface, called the pull-off force ($F_{\text{pull-off}}$, N), depends on the bulk modulus (E' , MPa), the work of adhesion (w_a , J/m²) and the coating thickness (d , m). This pull-off force is the lowest when the bulk modulus and work of adhesion are low and the coating film thickness is high (**Eq. 1**) [211].

$$F_{\text{pull-off}} \propto w_a^{1/2} K^{1/2} d^{-1/2} \quad \text{Eq. 1}$$

With their low elastic modulus, FRCs can deform themselves and remove the hard macrofouling by interfacial slippage of the macrofouling adhesive [59]. In contrast, more rigid materials cannot release fouling by the same peeling mechanism.

1.5.1.3.2.2. Coating thickness

The coating thickness also plays an important role in the removal of fouling organisms from FRCs [212]. As seen with Kendall's theory (in § 1.5.1.3.2.1), the pull-off force, measured with pseudo-barnacles (models of live barnacles), has been shown to be inversely proportional to the coating thickness (as long as the coating thickness is inferior to 4 mm) [211]. However, further testing using live species of barnacles did not find the same relationship between coating thickness and pull-off force. This different trend could be explained by the difference of detachment and fracturing mechanisms between the natural basal plates of barnacles and those of pseudo-barnacles [212,213]. It has also been reported that below 100 µm dry film thickness, barnacles can "cut through" to the underlying substrate and thus establish a strong adhesion. In another study, the release of *Ulva* sporelings could be increased with a higher thickness of PDMS coatings [59]. The preferred dry thickness of a FR top-coat (for a good cost-effectiveness) is around 140-200 µm [214].

1.5.1.3.3. Ecotoxicity in the aquatic environment

The content of unbound silicone oils in fouling release coatings can range from 1 to 10 % which is why FRCs release 4,000 tons of PDMS compounds in the marine environment every year

Chapter I – State-of-the-art

[193,215]. This non-negligible amount of waste triggers some concerns towards the safety of the aquatic ecosystem. Some researchers have demonstrated that PDMS do not present any risks to free swimming species or benthic organisms as silicone oils go directly in the sediments due to their extreme low water solubility and thus could not bioaccumulate in marine species.

Nendza et al. mentioned that at high quantity of PDMS oil or species (stabilized in water thanks to the addition of surfactants) might cause adverse physico-mechanical effects to organisms such trapping, suffocation or respiratory system occlusions [216]. But all these effects were never encountered in real conditions given that PDMS oils could barely stay in suspension in the water without surfactant help due to their high octanol-water partition coefficient. At the end, no toxicity effect on physiological functions of crustaceans and other marine species was detected. PDMS does not bioaccumulate because of their low concentration and low permeability into biological membranes [217]. Although PDMS fluids are persistent macromolecules in the sediments, they are considered innocuous to marine species [193,216,217].

I.5.2. Advances made on FRCs at the academic research state

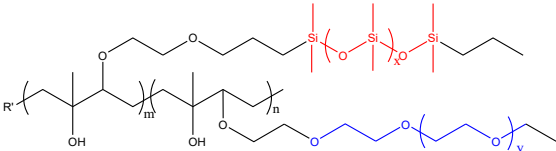
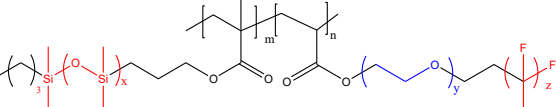
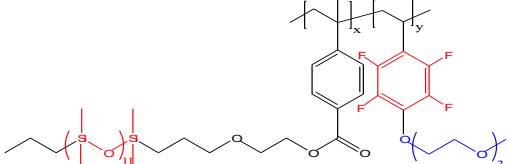
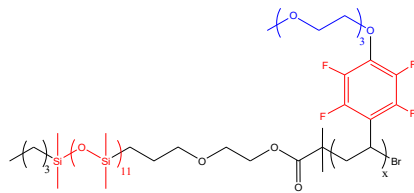
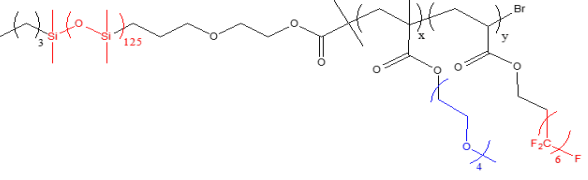
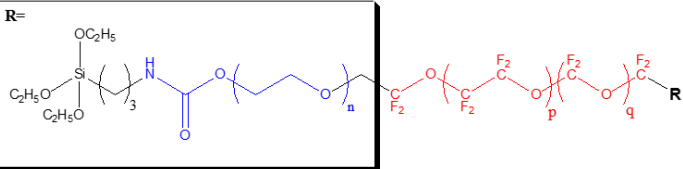
One of the most promising way to improve FRCs was found to be the addition of amphiphilic copolymers as already found on the market [91]. But there is also more and more research on FRCs with crosslinked amphiphilic networks. In the following text, these two topics are developed. A global overview of all the possible categories of hybrid FRCs (among them the amphiphilic copolymer additives and the amphiphilic networks) is also made at the end of this section to show the new trends in the academic research.

▪ Amphiphilic copolymers additives

Galli et al. has compiled numerous way to design non-toxic amphiphilic copolymers and their effect on marine biofouling [91]. These polymers are reported to provide a surface-active coating upon immersion able to confuse organisms during settlement and immersion. Polymer architectures comprising PDMS, PEG and fluorine moieties are widely investigated for FRCs applications, some examples of these amphiphilic copolymers are shown in Table I-12 and their antifouling activities are thoroughly described in Table I-13.

Chapter I – State-of-the-art

Table I-12. Examples of amphiphilic polymers for AF applications (hydrophilic and hydrophobic moieties are indicated with blue and red colors respectively).

<p>A</p> 	[218]
<p>B</p> 	[165]
<p>C</p> 	[157]
<p>D</p> 	[219]
<p>E</p> 	[220]
<p>F</p> 	[166]

To understand the parameters that affect the most the AF and FR properties of PDMS elastomers, Galli *et coll.* have studied the impact of the monomer unit ratio (e.g. fluoroalkyl/PEG units ratio), the molar mass of block copolymer-based additives and the monomer units sequencing in copolymers [220]. The best AF and FR results were attributed to the lower molar mass block copolymers and block copolymers with fluoroalkyl/PEG methacrylate units molar ratios from 50:50 to 60:40. The loading of amphiphilic additives was also investigated with loading varying from 1 to 20 % relative to the PDMS content. Improved AF abilities with less than 5 wt.% of amphiphilic additives were reported [157,163,171,219–221].

Murthy et al. have demonstrated that PEG-PDMS-based additives with long siloxane segments showed the best ability to reduce biofilm formation due to the easier migration toward the surface [222].

Although PEG is still the most employed hydrophilic polymer for antifouling applications, others can be encountered such as poly(zwitterionic)s [223], oligopeptides [224–227], poly(acrylic acid) [228], polysaccharides [229], poly(2-hydroxyethyl methacrylate) (PHEMA) [230] and poly(N-vinyl pyrrolidone) (PVP). These hydrophilic polymers could replace PEG given that they also strongly inhibit the protein adsorption.

▪ Amphiphilic networks

Amphiphilic networks come from the crosslinking of reactive hydrophilic polymers with reactive hydrophobic silicone oils. A major advantage of this approach is to reduce the leaching of additives into the aquatic environment.

Grunlan's group have described the mechanisms involved in these crosslinked amphiphilic coatings as follows [231]:

- 1) Migration of PEG-based polymers towards the surface;
- 2) Enrichment of PEG onto the surface (arriving from the bulk) driven by the affinity of hydrophilic functions with the surrounding water;
- 3) Swelling and solvation of the PEG-domains resulting in voluminous amphiphilic "tails" acting like a hydrated barrier.

Chisholm et al. described a condensation cure silicone elastomer with fluorinated pendant groups attached to the crosslinked PDMS backbone as well as freely dangling PEG segments (Figure I-31) [232]. The aim of this hybrid network is to stabilize the FR property by avoiding the leaching of the amphiphilic chains.

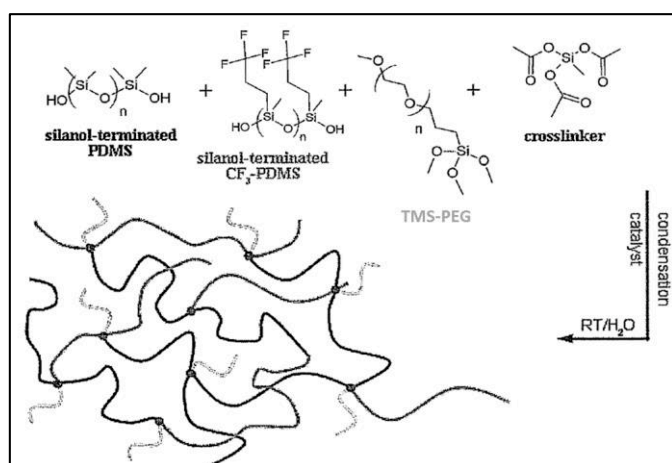


Figure I-31. Amiphilic crosslinked material for fouling release applications [232].

Amiphilic coatings can also be obtained by crosslinking amiphilic polymers into a FR system. For instance, a lot of work on epoxy-, poly(urethane) (PU) or poly(urea)-based coatings were investigated for antifouling applications (Figure I-32, a., b., c., d.).

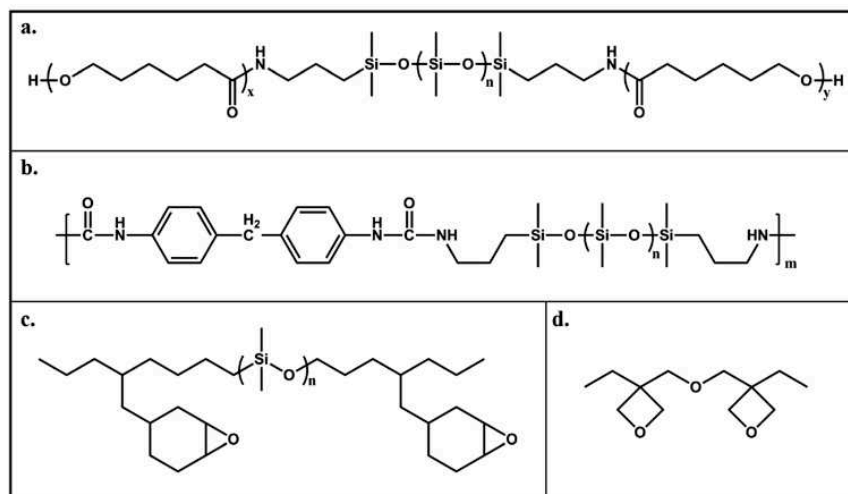


Figure I-32. Examples of poly(urethane) (a), poly(urea) (b), epoxy (c) and oxetane (d) prepolymers for FR applications [174].

Copolymerization or crosslinking of these prepolymers (Figure I-32) with PDMS segments gives rise to phase separation with hydrogen bonded hard domains and soft silicone domains (Figure I-33, A). These crosslinked amphiphilic networks have in common to generate a heterogeneous complex surface morphology upon immersion.

The resulting interconnected networks exhibit a low surface free energy ($\gamma_s=25-29$ mJ/m²) thanks to the silicone domains and a heterogeneous surface chemistry thanks to the polyester domains. These coatings also show superior mechanical properties (with elastic modulus superior to 80 MPa) and improve the adhesion of the coating to the substrate (adhesion to substrate > 1.0 MPa) [233–240]. These properties make the coating more resistant to mechanical damages, and thus extend the coating stability in water durable. Some PDMS–epoxy coatings were immersed for 60 days in seawater and cleaned with water to evaluate the biofouling detachment performance. The biofoulants (slime and settlement of barnacles, oysters, polychaetes and ascidines) were much more easily detached from the PDMS–epoxy coatings than from the control unmodified epoxy coating [241]. However, after 90 days immersion, a residual amount of biofoulants was left even after the washing procedure. This fact was attributed to the surface reorganization; hard segments of the ester and urethane moieties migrate to

the water interface changing the polymer surface energy and heterogeneity, and consequently the adhesion strength of the organisms increases.

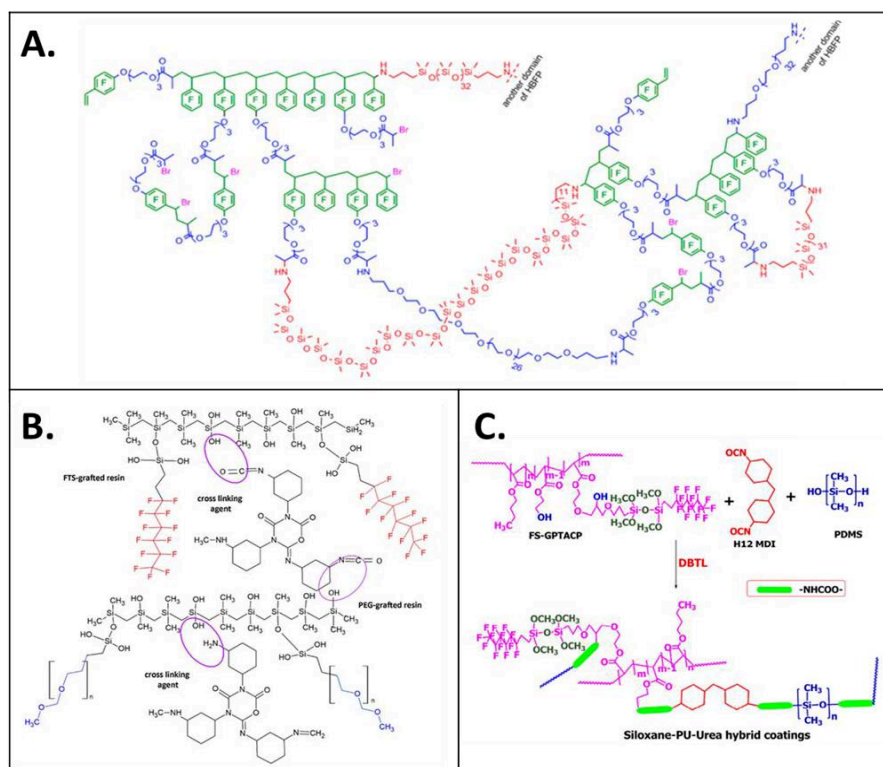


Figure I-33. Example of amphiphilic networks for fouling release and antifouling applications [242–244].

Pollack et al. studied a hyperbranched fluoropolymer-PDMS-PEG terpolymer network [242] (Figure I-33, B). AFM analyses were conducted before and after immersion revealing a phase separation between the hydrophilic domains and hydrophobic domains. The ethoxylated (EG) domains can form rough and rigid phases easily swollen by water. These EG domains thus display high surface energy known to affect the adhesion of gluing proteins coming from microorganisms and allows both a reduced settlement and easy removal of microorganisms [245]. The fluorine-rich domains show high modulus and low surface energy with water repellent properties and the surrounding soft PDMS regions display a smooth surface with low surface energy.

Chapter I – State-of-the-art

They displayed variable wettability ($\theta_w = 57\text{-}117^\circ$) and topographical (RMS roughness = 210-790 nm) properties depending on the fluoropolymer/PDMS/PEG mass ratio.

Crosslinked polysiloxane networks with antifouling and antimicrobial properties were patented by the NDSU Research Foundation [246,247]. In the last case, Boudjouk et al. described a hybrid FRC containing biocidal moieties which were either hydrolyzable such as Triclosan moiety (Figure I-34, **A & B**, encircled in red) or non-cleavable such as the QAS segment (Figure I-34, **A**, framed in green). The FRC also contained “texturizing” moieties such as PDMS backbones (Figure I-34, **A & B**, framed in blue) and fluorinated pendant groups (Figure I-34, **B**, framed in purple). This highlights the desire to design multifunctional coatings.

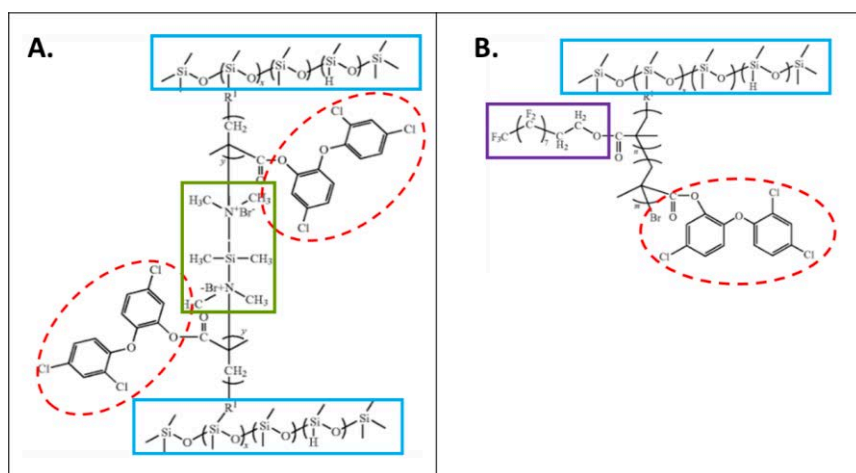


Figure I-34. Polysiloxane-based network with an antifouling activity [246].

A Reaxys bibliographical research has indicated 190 scientific published papers dealing with hybrid FRCs from 2010 to today. Table I-13 shows the antibiofouling activities of some of those novel FRCs. They were classified into different categories: the amphiphilic FRCs (blue), the nanoparticles-based FRCs (purple), the textured FRCs (orange), the polyelectrolytes-based FRCs (dark red), the biocide-based FRCs (pink) and the oil-infused FRCs (green). These hybrid FRCs displayed similar or different surface/bulk physico-chemical properties compared to a conventional FRC but often with improved antifouling activities.

Some general trends could be highlighted from this table for each hybrid FRCs categories. The nanoparticles-based FRCs could drastically modify the water contact angles (up to 167°) compared to a conventional FRC. They could also exhibit very low surface free energies 9-24 mJ/m² and release toxic nanoparticles in seawater (with release rate much lower than those of SPCs). All these effects enabled the decrease of bacteria settlement. Textured FRCs showed targeted antifouling activities towards specific species depending on the shape and dimensions of the texturation. Polyelectrolytes could easily disrupt the protein adhesion and biofilm formation certainly thanks to their electrically neutral surface. Oil-infused FRCs strongly decreased the settlement of hard fouling in particular thanks to their very low elastic modulus (< 1MPa) and their ability to leach oils. Some oils may become part of the elastomer to reduce the premature leaching of oils and so increase the AF effectiveness duration [263].

Table I-13. Some examples of hybrid fouling release coatings from the past decade.

	Elastomer matrix	Additional compounds	Fouling release and antifouling performance of the experimental coating (bioassays and/or field tests)	Surface/bulk properties	Ref.
Amphiphilic FRCS	Poly(styrene)-block-poly(ethylene- <i>ran</i> -butylene)-block-poly(styrene) (SEBS) thermoplastic elastomer (Kraton MD6945)	Polystyrene _{28k} -block-poly(ethylene- <i>ran</i> -butylene) _{25k} -block-polyisoprene _{20k} with PDMS (17-39 mol.% attached) and PEG side chains (11-38 mol.% attached) (cf. Table I-12, A)	<ul style="list-style-type: none"> ↘ settlement of diatoms <i>Navicula</i>, ↘ settlement of <i>Ulva linza</i> sp. → removal of <i>Ulva linza</i> sp., compared to Silastic T2 (control) 	$\theta_{w,adv} = 93-103^\circ$ and $\theta_{w,rec} = 19-34^\circ$ $E' = 1.2 \pm 0.3$ MPa	[218]
	PDMS elastomer (bis-silanol PDMS, ES40, DBTDA)	Amphiphilic copolymers of a methacrylic monomer (SiMA) carrying a polysiloxane side chain and an acrylic monomer (ZA, 10–85 mol.%) with a mixed poly(ethylene glycol) (PEG)-fluoroalkyl side chain (copolymer loading= 1 and 4 wt.%) (cf. Table I-12, B)	<ul style="list-style-type: none"> → settlement of <i>B. amphitrite</i> cyprids ↗ or → removal of <i>B. amphitrite</i> cyprids ↗ removal of <i>Ulva linza</i> sp., compared to the PDMS control Field test: less hard-fouling compared with PDMS and similar microbial and weed fouling compared to PDMS and Intersleek 700 (after 18 weeks in Brattans, Sweden) 	$\theta_w = 97-104^\circ$ (PDMS: $\theta_w = 114^\circ$) $\gamma_s = 20.4-23.6$ mJ/m ² at $t_i = 0$ and $\gamma_s = 23.-29.2$ mJ/m ² at $t_i = 7$ days (in water) $\gamma_s^d = 17.7-23.1$ mJ/m ² at $t_i = 0$ and $\gamma_s^d = 17.4-22.1$ mJ/m ² at $t_i = 7$ days (in water) $\gamma_s^p = 0.5-3.0$ mJ/m ² at $t_i = 0$ and $\gamma_s^p = 4.2-8.0$ mJ/m ² at $t_i = 7$ days (in water) RMS ≈ 1 nm (very smooth)	[165,248]
	PDMS elastomer (bis-silanol PDMS, ES40, BiND)	4-(triethyleneglycol monomethyl ether)-2,3,5,6-tetrafluorostyrene (39 and 77 mol.%) and poly(dimethyl siloxane) vinylbenzoate (cf. Table I-12, C)	<ul style="list-style-type: none"> ↘ settlement of <i>Ulva linza</i> sp. (÷3) ↗ removal of <i>Ulva linza</i> sp. (×10), compared to PDMS control 	$\theta_w = 99-113^\circ$ (PDMS: $\theta_w = 110^\circ$) $\gamma_s = 22.6-25.9$ mJ/m ² (PDMS: $\gamma_s = 23.3$ mJ/m ²) $\gamma_s^d = 22.6-25.6$ mJ/m ² (PDMS: $\gamma_s^d = 23.3$ mJ/m ²) $\gamma_s^p = 0-1.3$ mJ/m ² (PDMS: $\gamma_s^p = 0$ mJ/m ²)	[157]
	PDMS elastomer (bis-silanol PDMS, ES40, BiND)	Poly(dimethylsiloxane) block (degree of polymerization 11) and a poly(4-(triethyleneglycol monomethyl ether)-2,3,5,6-tetrafluorostyrene) block (average degree of polymerisation 71) (copolymer loading 4 wt.%) (cf. Table I-12, D)	<ul style="list-style-type: none"> ↘ settlement of <i>B. amphitrite</i> cyprids ↗ removal of juveniles of <i>B. improvisus</i>, compared to the PDMS control 	$\theta_w = 112 \pm 1^\circ$ (PDMS: $\theta_w = 110 \pm 1^\circ$) $\gamma_s = 23.1$ mJ/m ² (PDMS: $\gamma_s = 23.3$ mJ/m ²) $\gamma_s^d = 23.1$ mJ/m ² (PDMS: $\gamma_s^d = 23.3$ mJ/m ²) $\gamma_s^p = 0$ mJ/m ² (PDMS: $\gamma_s^p = 0$ mJ/m ²) $E' < 2$ MPa	[219]
	PDMS elastomer (bis-silanol PDMS, ES40, BiND)	Block copolymers containing oligo(ethylene glycol) (PEGMA) and fluoroalkyl (AF6) side chains with composition ratios from 50/50 to 60/40 for AF6/PEGMA. (copolymer loading= 4 wt.%) (cf. Table I-12, E)	<ul style="list-style-type: none"> → removal of diatoms <i>Navicula incerta</i>, ↘ settlement of <i>Ulva linza</i> ↗ removal of <i>Ulva linza</i>, compared to the PDMS control 	RMS = 1.8 nm	[220]
	Crosslinked network coatings based on PFPE/PDMS/acrylic polyols with DBTDL	α,ω -triethoxysilane terminated perfluoropolyether (PFPE) oligomer (cf. Table I-12, F) and α,ω -triethoxysilane terminated poly(dimethyl siloxane) (PDMS)	<ul style="list-style-type: none"> ↘ settlement of bacteria <i>Escherichia coli</i> ↘ settlement of diatom <i>Navicula</i> (÷3) compared to both PDMS resin and acrylic polyol. 	$\theta_w = 102.2-107.8^\circ$ (PDMS resin: $\theta_w = 112.8 \pm 2.8^\circ$, acrylic polyol: $\theta_w = 85.1 \pm 1.5^\circ$) $\gamma_s = 19.3-21.7$ mJ/m ² (PDMS resin: $\gamma_s = 19.4$ mJ/m ² , acrylic polyol: 38.8 mJ/m ²) $E' = 19.91-47.49$ MPa (PDMS resin: $E' = 308.72$ MPa, acrylic polyol: $E' = 104.73$ MPa) $(E' \cdot \gamma_c)^{1/2} = 19.95-32.10$ (PDMS resin: $(E' \cdot \gamma_c)^{1/2} = 77.39$, acrylic polyol: $(E' \cdot \gamma_c)^{1/2} = 63.78$)	[249]

Chapter I – State-of-the-art

	Elastomer matrix	Additional compounds	Fouling release and antifouling performance of the experimental coating (bioassays and/or field tests)	Surface/bulk properties	Ref.
Nanoparticles-based FRCS	PDMS elastomer	CuO, CTAB-capped (cetyl trimethylammonium bromide) CuO and ZnO nanoparticles (0.1 wt.%)	→ settlement of <i>Bacillus flexus</i> bacteria compared to the PDMS control. → settlement of diatom <i>Navicula</i> compared to the PDMS control Field test: 68-80 % less fouling compared with PDMS (after 45 days)	$\theta_w = 78-119^\circ$ (PDMS $\theta_w = 94^\circ$) Leaching rates: 8.2 ng/cm ² /d for CuO, 6.45 ng/cm ² /d for CuO-CTAB and 59.4 ng/cm ² /d for ZnO	[250]
	PDMS elastomer	SiO ₂ -doped ZnO nanospheres (0.5 wt.%)	→ settlement of <i>Micrococcus sp.</i> , <i>Pseudomonas putida</i> strains of bacteria and <i>Aspergillus niger</i> fungi → removal of <i>Ulva linza</i> compared to PDMS control	$\theta_w = 167 \pm 2^\circ$, $\gamma_s = 9.24$ mJ/m ² $R_a = 0.11 \pm 0.01$ μm , $E' = 2-4$ MPa	[251]
	PDMS elastomer (Sylgard 184)	Organomodified montmorillonite (OMMT) nanofillers (1 or 2 wt.%)	→ removal of <i>Ulva linza</i> compared to PDMS control	$\theta_w =$ from $102 \pm 2^\circ$ to $93 \pm 0.2^\circ$ after 120 h in d.w. $E' = 3.5-4$ MPa against 2.5 MPa for PDMS control $R_a = 60$ nm ($R_z = 20.1$ nm for PDMS) After 6 days in d. w.: $R_z = 30$ nm ($R_z = 251.9$ nm for PDMS) = no increase of nanoroughness after immersion.	[252]
	PDMS elastomer	MWCNTs-OH/Fe ₂ O ₃ (1 % of the pigment volume concentration) Phenylmethyl silicone oil (9 wt.%)	→ settlement of biofilm compared to the PDMS control. → removal (80-90%) of biofilm (against 60% for PDMS control). Field test: Good AF/FR properties after 8 months of immersion	$\theta_w = 117.8-123.1^\circ$ $\gamma_s = 24.2-21.9$ mJ/m ² $E' = 0.68-0.84$ MPa Roughness= 0.891-6.068 μm Breaking elongation 257%-189%	[253]
	PDMS elastomer	Silicon carbide nanowire composite (0.5 wt.%)	→ settlement of <i>B. subtilis</i> , <i>S. aureus</i> , <i>P. aureginosa</i> , <i>E. coli</i> , <i>C. albicans</i> (yeast), <i>A. niger</i> (fungi) compared to PDMS control Field test: No biofouling after 90 days of immersion	$\theta_w = 153^\circ$ $\gamma_s = 11.25$ mJ/m ² (13.5 mN/m after 7 days in d.w.), $E' = 1.9$ MPa, RMS= 2.4 nm, Hardness shore A= 31.4 \pm 0.7	[254]
	Interpenetrating polymer network (IPNs) based on a silicone elastomer and a hydrogel network made of poly(propyl acrylamide)	Silver nanoparticles (0.5-3 wt.%)	→ <i>Chlorella</i> , <i>Phaeodactylum</i> and <i>Navicula</i> algae settlement compared to PDMS	Reduction of contact angles after 10 min of immersion of 9-10° for the IPNs.	[255]
Textured FRCS	PDMS elastomer with biomimetic structured surface replicated from natural Trifolium leaf (terrestrial plant)	Poly(3-sulfopropylmethacrylate) (PSPMA) brushes grafted onto the textured silicon wafer	→ settlement of <i>Chlorella</i> and <i>Nannochloropsis maritima</i> microalgae compared to flat Sylgard 184	Microtextured surface	[256]
	Textured (0.2-1000 μm) PDMS surface (round or square texture shape)		→ settlement of diatoms <i>Nitzschia closterium</i> and <i>Amphora sp.</i> , → settlement of <i>Ulva sp.</i> , → settlement of <i>Saccostrea glomerata</i> oyster for 100 μm -texturation, → settlement of <i>Bugula neritina</i> bryozoan for 4 μm texturation, → settlement of <i>Amphibalanus reticulatus</i> barnacle for 40-80 μm texturation compared to PDMS control Field test: after 6 months loss of the deterrent effect but FR property still good.	Microtextured surface	[257]

Chapter I – State-of-the-art

	Elastomer matrix	Additional compounds	Fouling release and antifouling performance of the experimental coating (bioassays and/or field tests)	Surface/bulk properties	Ref.
	Biomimetic shark skin surface (OH- or CH ₃ -terminated silicon wafer Sharklet AF™)		↘ adhesion of the mussel protein on coatings with higher riblet height (5 μm) and OH-functionalized Sharklet silicone.	Riblet features height: 1-5 μm θ _w =90-101° for CH ₃ -terminated Sharklet and θ _w =5-8° for OH-terminated Sharklet	[258]
Polyelectrolyte-based FRCs	Tethered quaternary ammonium salt (QAS) in a curable PDMS	QAS-functional alkoxy silane	↘ settlement and ↗ removal of <i>Cellulophaga lytica</i> , <i>Halomonas pacifica</i> bacteria and diatom <i>Navicula incerta</i> compared to PDMS and FRCs.		[259]
	Interpenetrating network of PDMS (IPN) and UV-crosslinked zwitterionic polymer	Zwitterionic polymers: poly(carbobetaine methacrylate) poly(sulfobetaine methacrylate)	↘ adsorption of fibrinogen protein compared to PDMS	θ _{air/water} = 30-33° (60.5±4.5° for PDMS) Zeta potential 0 mV for zwitterionic -based IPN against -90 mV for PDMS. Water uptake= 64-112 %	[96]
Biocide-based FRCs	Cationic polysiloxane	Cleavable Triclosan quaternary ammonium salts hydrophobic perfluoroalkyl groups	↘ biofilm retention compared to RTV silicone with four tested marine bacteria (<i>H. marina</i> , <i>H. pacifica</i> , <i>C. lytica</i> and <i>P. atlantica</i>).	E' = 0.88-1.4 MPa	[260]
	PDMS elastomer (60-80 wt.%)	Enzymes such as Savinase, alcanase, pectin methyl esterase, Papain/PEG-papain (0.05-1 wt.%), poly(oxyalkylene) modified silicone oil or fluorinated oil (2-4 wt.%), encapsulated biocides: DCOIT, copper pyriithione (1-6 wt.%)	Field test: variable fouling results depending on the formulations (after 24 months on raft in Singapore)		[261]
	PDMS elastomer	Surfactant (salts of long chain unsaturated poly(aminoamide)s and acid esters) (0.6 wt.%), Tralopyril (13.9 wt.%)	Not studied	Leaching rate of Tralopyril: 5.6-11.0 μg/cm ² /d	[262]
Oil-infused FRCs	PDMS elastomer	DMS-T15 (3,780 g/mol) and DMS-T05 (770 g/mol) silicone oils with 5 to 10 wt.% <u>Control</u> : Ecoflex (platinum catalyst based silicone kit) with 6.5 wt.% of Silicone Thinner	↘ adhesion strength of Barnacle (<i>A. amphitrite</i>) on the experimental coating compared to Ecoflex	E' = 30.8 kPa (against 35.7 kPa for Ecoflex)	[263]
	PDMS elastomer (RTV11, GE1, RTV511)	DMSC15 (carbinol(hydroxyl)terminated poly(dimethylsiloxane), MW 1000 g/mol, 20% non-siloxane) and FMS123 (poly-3,3,3-trifluoropropylmethylsiloxane, MW 3000) silicone oils (≤ 10 wt.%)	↘ adhesion of <i>Balanus eburneus</i> (barnacle) compared to the PDMS control		[264]
	RTV11	Siloxane oil (DMS-T31, Gelest) and a non-ionic surfactant (0.5-4 wt.%) and/or α-tocopherol antioxidant (1.5 wt.%)	Algae biofilm Mussel adhesion Bacterial adhesion (<i>Marinobacter hydrocarbonclasticus</i>)	θ _w ≥ 90° (control: θ _w = 102.2°) γ _s = 25.82-26.71 mJ/m ² R _g = 15.914 nm R _q = 20.211 nm E' = 280-318 Pa	[249,265]

I.6. Hydrolyzable polymers as potential candidates for novel hybrid FRCs

In this section, a focus is made on main-chain hydrolyzable polymers that could be used as degradable binders for novel FRCs. Most of the polymers presented in this section come from pharmaceutical and biomedical related papers. Indeed, many biomedical systems use biocompatible hydrolyzable polymers, for example, to control the drug release or to control the resorption of soft scaffold tissues [106,266,267].

To adapt these polymers to the marine antifouling field, some properties will be examined. Ideally, the potential candidates should undergo gradual hydrolytic degradations, should be non-toxic to the marine environment, biodegradable, amorphous or with low crystallinity to favor water absorption, and should be compatible with polysiloxanes. Gathering all these criteria in one polymer is challenging, which is why, hydrolyzable polymer networks are also discussed afterwards given that they enable the design of complex chemical structures with more tunable erosion profiles.

Finally, a special attention will be paid to the hydrolysis kinetics of a series of polymers. This information is also important for Chapter II and III to find the polymers with the most suitable hydrolysis kinetics for controlling the renewal of the coating surface by erosion. The final aim of these candidates will be to add new physico-chemical properties on the surface of a FRC.

I.6.1. Hydrolyzable polymers

Hydrolyzable polymers were largely investigated in scientific reviews [268–271] due to their biodegradable and biocompatible properties. They can be employed in a wide range of applications: packaging, agriculture, medicine and also more and more in marine coatings.

I.6.1.1. Linear hydrolyzable polymers

The aliphatic polyesters represent a very wide family of linear polymers which hydrolyze in their backbone. They comprise poly(hydroxyalkanoate)s, synthesized from hydroxyacids (HO-R-COOH) and poly(alkene dicarboxylic acid)s or poly(alkene diol)s, prepared by polycondensation of diols and diacids or ring opening polymerization (ROP).

Chapter I – State-of-the-art

Poly(glycolide) (PGA) is the simplest linear aliphatic polyester. It is prepared by ring opening polymerization of the cyclic glycolide at high temperatures. Its low solubility in most organic solvents and its fast hydrolysis kinetics limit its applications.

Poly(lactide) (PLA) is more hydrophobic than PGA due to the presence of -CH₃ side groups. The lactide monomer has two optical forms: L-lactide and D-lactide. The resulting polymers (PLLA and PDLA) have very different crystallinity and so different hydrolysis rates. Their outstanding biocompatibility makes them very suitable for biomedical applications (such as bioresorbable implant materials) [272]. Glycolide monomers are often copolymerized with lactide monomers to achieve more tunable hydrolytic degradations, the resulting copolymer is poly(lactide-co-glycolide) PLGA [273–276].

Another well studied aliphatic polyester is poly(ϵ -caprolactone) (PCL). It is obtained from the ring-opening polymerization of ϵ -caprolactone in presence of tin octoate catalyst. PCL is a hydrophobic, semi-rigid material at room temperature. PCL can be degraded easily by enzymes and fungi and has a very slow hydrolytic degradation.

Many other polymers are hydrolyzable in their backbone such as poly(amide)s, poly(urethane)s, poly(hydroxyalcanoate)s, poly(carbonate)s, poly(anhydride)s and poly(saccharide)s. Some of them are detailed in Figure I-35 with their associated properties in Table I-14.

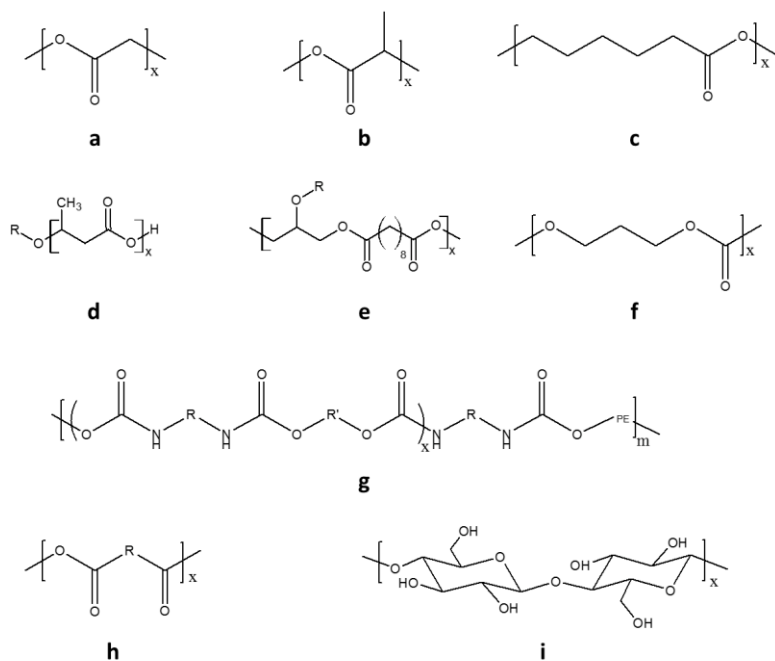


Figure I-35. Chemical structure of some polymers hydrolyzable in their backbone: poly(glycolide) (a) poly(lactide) (b), poly(ϵ -caprolactone) (c), poly(ϵ -hydroxybutyrate) (d), poly(butylene succinate) (e), poly(trimethylene carbonate) (f), poly(ester-urethane)(g), poly(anhydride) (h) and cellulose (i).

Chapter I – State-of-the-art

Table I-14. Characteristics of some polymers hydrolyzable in their backbone.

Polymer	Properties (T_m , T_g , E' , X_c)*	Description	Ref.
PGA (Figure I-35, a) Poly(glycolide)	T_m = 220-225°C, T_g = 35-40°C, E' =1-10 GPa, X_c = 45-55%	Good mechanical properties but rapidly lost upon immersion. Fast hydrolysis. Insoluble in most organic solvents	[277,278]
PLA (D,L or L) (Figure I-35, b) Poly(lactide)	T_m = 220-225°C, T_g = 63.8°C, Tensile strength= 30-70 MPa, variable crystallinities	Hydrophobic polymer, hard and white or transparent. Very stiff materials, Biocompatible. Brittleness and poor thermal stability and bulk erosion	[272,279,280]
PCL (Figure I-35, c) Poly(caprolactone)	T_m = 60-65°C, T_g = -60°C, Tensile strength= 23 MPa, X_c = 50-70%	Semi-rigid and semi-crystalline material. Slow degradation rate in distilled water.	[130]
PHB (Figure I-35, d) Poly(hydroxybutyrate)	T_m = 177°C, T_g = 4°C, E' = 1.7 GPa, X_c > 50%	Brittle material. Degradable by numerous microorganisms	[281]
PBS (Figure I-35, e) Poly(butylene succinate)	T_m = 90-120°C, T_g = -45/-10°C Tensile strength= 23-34 MPa, X_c = 34-45%	Better processability than PGA and PLA. Similar mechanical behavior to PE and PP. Insufficient biocompatibility	[282]
PTMC (Figure I-35, f) Poly(trimethylene carbonate)	T_g =-26 to -15°C E' = 3-6 MPa X_c = 0%	Surface erosion. Rubbery materials, poor mechanical performance (flexible and soft). Enzymatic and microbial degradation	[267,283]
Poly(ester-urethane) (Figure I-35, g)	Tensile strength= 9.3 GPa	Presence of hard and soft segments. Good mechanical properties. Waterborne systems. Toxicity of isocyanates (chain extender). Slow rate of hydrolytic degradation	[267,284,285]
Poly(anhydride) (Figure I-35, h)	T_m = 65-240°C, T_g = -20-60°C, X_c > 50%	Two hydrolyzable sites in the repeating unit. Non-toxic degradation products. High crystallinity and fast degradation (weight loss: 0.3-2.3 mg/h in PBS, 37°C)	[271,286]
Cellulose (Figure I-35, i)	$E' \geq 10$ GPa	Infusible and insoluble in most solvents Needs to be transformed to be processable	[287-289]

* T_m corresponds to the melting temperature, T_g corresponds to the glass transition temperature, E' corresponds to the elastic modulus and X_c corresponds to the degree of crystallinity.

1.6.1.2. Hydrolyzable networks

The need for biodegradable networks for medical implants or drug delivery systems was fulfilled by the design of soft and elastic materials with biodegradable properties [266,267]. Biodegradable polymers such as PLA or PGA were widely studied for biomedical application but their stiffness has rapidly limited their use [290].

Many polymeric networks were thus successfully produced with a wide range of mechanical properties and degradation profiles. Some polymeric networks can exhibit complex molecular architectures to diversify the hydrolytic degradation behaviors.

In the following paragraphs, the networks that are hydrolyzable in their polymer main chains are distinguished from the ones that are hydrolyzable in their crosslinks nodes.

Chapter I – State-of-the-art

1.6.1.2.1. Hydrolyzable in the polymeric chains

One way to design degradable networks is to crosslink hydrolyzable polymers. The crosslinks may be either physical or chemical [267]. Physical crosslinks encountered in poly(ester-urethane) or poly(urethane) elastomers are formed by clusters of crystallized hard segments while the surrounding chains are in an amorphous state [291]. These “pseudo-crosslinks” formed by hard segments can dissociate with temperature and recover (reversible process). These physically crosslinked elastomers are also named thermoplastic elastomers. On the contrary, chemical crosslinks are irreversible due to covalent bonding of different prepolymers. To make a 3D elastomer network, there should be at least one multifunctional molecule or macromolecule.

Scott et al. highlighted the benefits of having crosslinked polymers rather than linear polymers during a hydrolysis process [282]:

- the hydrolysis of a linear polymer leads to 2 chains which induces low mass losses but fast material failure (for example the hydrolytic degradation of a semi-crystalline copolyester led to 1.7 % weight loss and 66.1 % of strength loss [292])
- the crosslinked polymer undergoes a random scission of its chains which gives a more gradual mass loss while still maintaining the network integrity since the polymers are all attached one to another.

Nevertheless, it was also mentioned that a tightly crosslinked network would increase its hydrolysis resistance since the bulk diffusion of water is difficult. Thus the crosslinking density is a parameter to shorten or extend the lifetime of biodegradable elastomers in aqueous media [282,293].

In a review, Tham et al. reported a wide range of polyol-based biodegradable elastomers [294]. Examples of hydrolyzable networks are poly(glycerol sebacate) (PGS) [295,296], poly(1,8-octanediol citrate) (POC) [290,297,298] or poly(xylitol sebacate) (PXS). These two polymers can be synthesized through a polycondensation reaction which produces degradable hydrogels. Their low elastic moduli, 0.28 ± 0.03 MPa for PGS, 1.8-14 MPa for POC and 0.8 MPa for PXS, make them suitable for engineering soft tissues [267].

Chapter I – State-of-the-art

Younes et al. reported that the lowest the glass transition temperature (T_g) of a prepolymer is, the lowest the T_g of the resulting elastomer will be. This will favor the water degradation due to the amorphousness of the polymer as long as the surrounding aqueous medium has a temperature above the T_g of the elastomer [299].

The use of a hydrolyzable interpenetrating polymer networks (IPN) based on poly(D,L-lactide)- diol (PLA-diOH) and poly(methyl methacrylate) (PMMA) was introduced by Rohman et al. [300]. With this approach they were able to find an intermediate mass loss profile between the PLA single and PMMA single networks (Figure I-36).

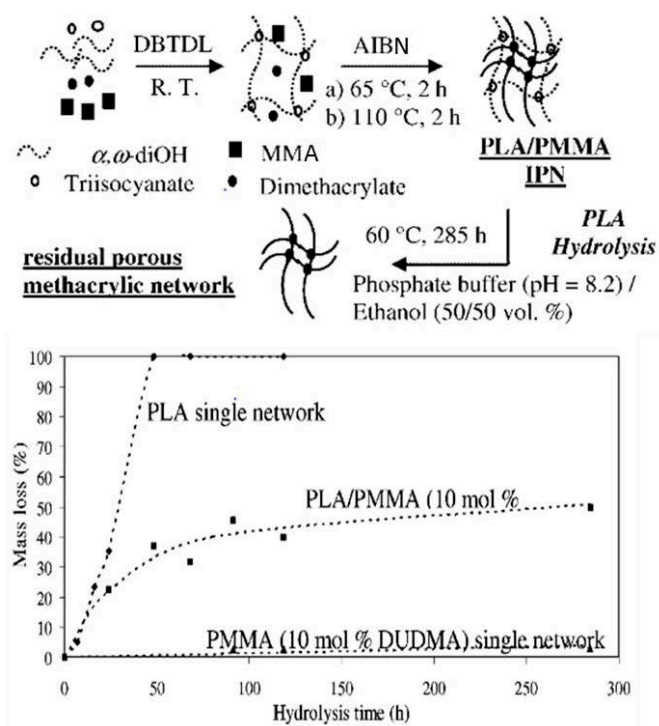


Figure I-36. Designing of PLA/PMMA IPNs [300].

A review from Brzeska et al. deals with biodegradable crosslinked poly(urethane) [301]. Polyols and isocyanates are covalently bonded via urethane bonds and can be further hydrolyzed and/or metabolized in non-toxic products. An example of a crosslinked PU prepared by crosslinking copolymerization of *N*-(2-hydroxypropyl)-methacrylamide (HPMA)

Chapter I – State-of-the-art

and the *N,O*- dimethacryloylhydroxylamin (DMHA) crosslinker was described by Chivukula et al. [302] (Figure I-37).

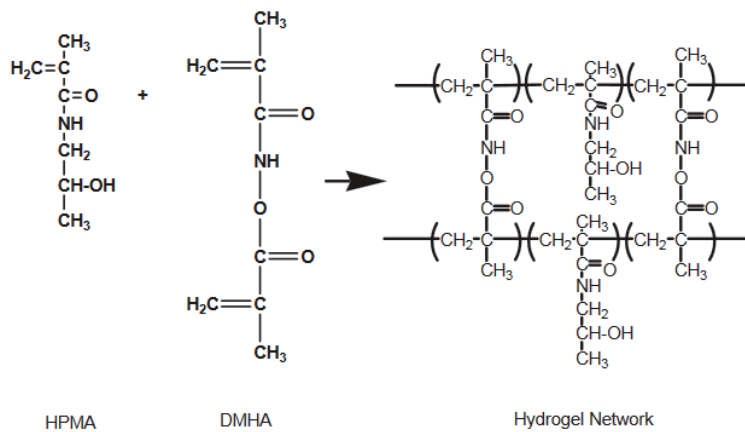


Figure I-37. Example of a hydrolyzable PU network [302].

Amphiphilic macromonomers based on a poloxamer made of poly(ethylene glycol) (PEG) and poly(propylene glycol) (PPG) were functionalized with lactide, glycolide, ϵ -caprolactone and methacrylic anhydride monomers to form a hydrogel with hydrolyzable junctions (Figure I-38). The covalently crosslinked polymer networks provided a biocompatible system with the ability to tune the stiffness of the network (from 138 to 263 kPa) and to tailor its degradation kinetics (from several weeks up to more than a year) depending on the nature of the oligoester [298].

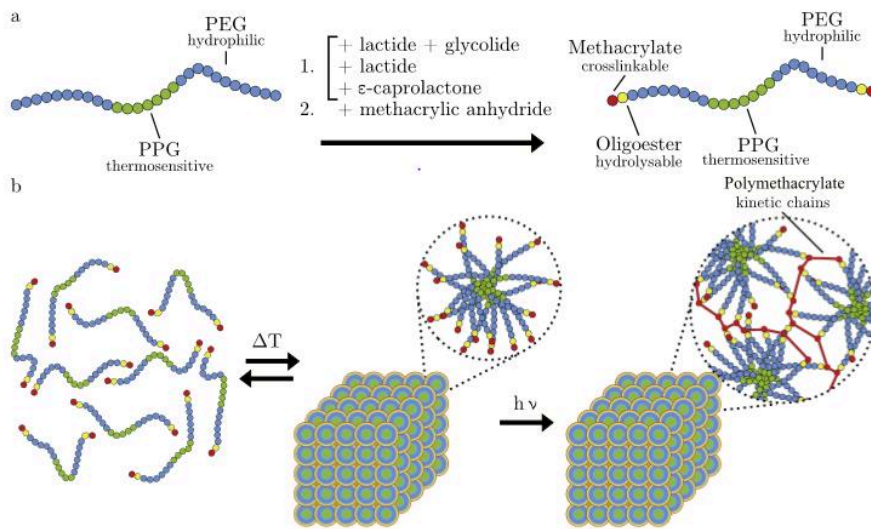


Figure I-38. Amphiphilic macromonomers based on a poloxamer (PEG-*b*-PPG-*b*-PEG) with hydrolyzable junctions [303].

1.6.1.2.2. Hydrolyzable in the crosslinks

Another way to design hydrolyzable networks is to use degradable crosslinkers [304]. A recent study developed lactone-based star-shaped crosslinkers (Figure I-39) [305]. The mechanical properties of the polyester network were tunable and competitive with a conventional elastomer and could undergo fast hydrolytic degradation in presence of a cutinase enzyme.

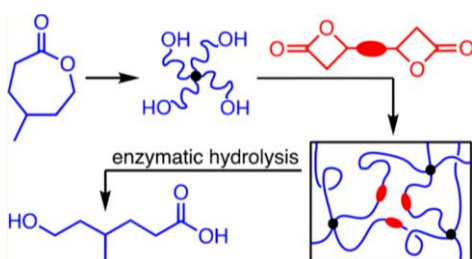


Figure I-39. Hydrolyzable star-shaped polyester elastomer [305].

Stubbe et al. synthesized a hydrogel polymer network based on hydroxyethylmethacrylate (HEMA) and dextran molecules (Figure I-40) [306]. In these networks, the crosslinks are hydrolyzable carbonate ester bonds formed between methacrylate groups and dextran molecules. This system is suitable for drug delivery applications.

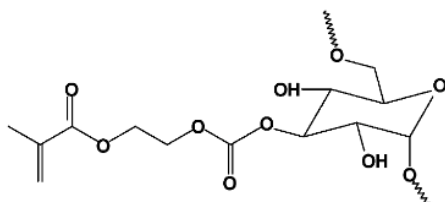


Figure I-40. Chemical structure of the glucopyranose substituted with HEMA to achieve a hydrolyzable gel [306].

Multifunctional monomers such as poly(ϵ -caprolactone) diol (PCL-diol) or triol (PCL-triol) (Figure I-41) in a PU network can provide various crosslinking density. Incorporation of PEG can increase the water uptake. All these composition parameters can tune the hydrolysis rate of polymer network [307].

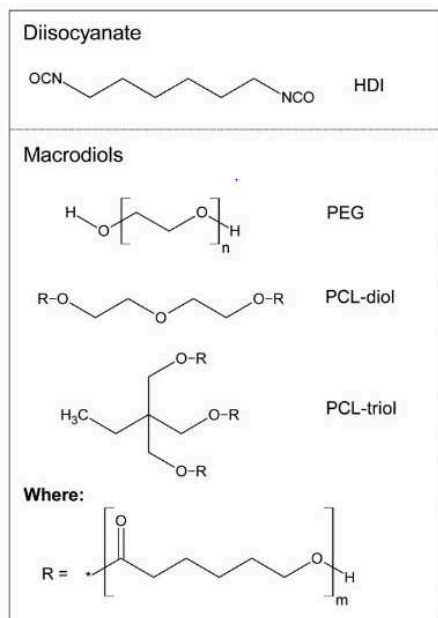


Figure I-41. Molecular structures of diisocyanate and macrodiols for the preparation of a hydrolyzable poly(urethane) [307].

I.6.2. Kinetics of hydrolysis

The hydrolysis rate of a polymer is related to several parameters such as hydrophilicity, molar mass, crystallinity and availability of hydrolyzable functions [110]. It is possible that during the hydrolysis process, the released degradation products decrease the pH value and thus enable an auto-catalyzed hydrolysis [109].

The surrounding environment in which the polymer is immersed will also influence the kinetics of degradation, in particular temperature, pH, presence of enzymes or microorganisms. Rutkowska et al. observed that the degradation of PCL was faster in seawater (in the Baltic sea) than in a buffered salt solution at 37°C [308,309]. After 8 weeks PCL was already destroyed in seawater whereas the weight change in the buffered salt solution was 11 to 20 % after 10 weeks. This was attributed to a hotter water between may-august playing an

Chapter I – State-of-the-art

important role in the PCL degradation, as well as mechanical stress and enzymatic degradation in seawater. Table I-15 shows hydrolysis rates of a series of hydrolyzable polymers.

Table I-15. Hydrolysis kinetics of various polymers.

Polymer (X_c = crystallinity)	Average molar mass, M_n (g/mol)	Immersion conditions	Mass loss % after x weeks (w)/ days (d)/hours (h)	Ref.
PLA (amorphous)	2,700	Distilled water	7% (50d) – 10% (150d) – 20% (350d)	[126]
PLA	9,000	Distilled water	17% (50d) – 56% (350d)	[126]
PLA- <i>b</i> -PDMS- <i>b</i> -PLA	2150- <i>b</i> -2300- <i>b</i> -2150	Distilled water	15% (50d) – 38% (350d)	[130]
PLA- <i>b</i> -PDMS- <i>b</i> -PLA	9400- <i>b</i> -2300- <i>b</i> -9400	Distilled water	15% (50d) – 34% (350d)	[130]
PLA diol	5,000	Solution PBS (pH= 7,4, T= 37°C)	5% (60d) – 30% (80d)– 60% (120d)	[279]
PLA diol	20,000	Solution PBS (pH= 7,4, T= 37°C)	<5% (60d) – 60% (120d)- 100% (180d)	[279]
PLLA	65,000	Natural conditions	20% (90 w)	[310]
PDLLA-C	8,870 (\bar{D} =1,57)	Solution PBS (pH= 7,4, T= 37°C)	20% (8 w) 55% (16 w)	[311]
PLGA/Tegomer	19,000 Tegomer = 2,400	PBS solution (pH= 7,4, T= 37°C)	20% (20d) – 70% (60d)	[312]
PLGA/Tegomer	40,000 Tegomer = 2,400	PBS solution (pH= 7,4, T= 37°C)	50% (20d) – 75% (60d)	[312]
PLGA (55/45)	unknown	Water, 37°C, pH= 7.4	40% (3 w) – 68% (5 w)	[313]
Cellulose- <i>g</i> -PLLA	50,000 (PLA) ≈ 36,000 (cellulose)	PBS solution (pH= 7,4, T= 37°C)	PLLA : 4% (30d) Cellulose : 5% (30d) Copolymer : 15-45% (30d)	[287]
PCL (X_c =54%)	2,900	Distilled water	1% (50d) – 15% (150d) – 22% (350d)	[130]
PCL- <i>b</i> -PDMS- <i>b</i> -PCL (X_c =33%)	3,400- <i>b</i> -2,300- <i>b</i> -3,400	Distilled water	5% (50d) – 35% (150d) – 40% (350d)	[130]
PCL- <i>b</i> -PDMS- <i>b</i> -PCL (X_c =16%)	1,700- <i>b</i> -2,300- <i>b</i> -1,700	Distilled water	1% (50d) – 10% (150d) – 10% (350d)	[130]
Crosslinked polyglycerol sebacate (PGS)	18,300 ± 1 620	PBS solution (pH= 7,4, T= 37°C)	17±6% (60d)	[314]
Poly(glycerol sebacate) (PGS)		PBS solution (pH= 7,4, T= 37°C)	35% (20d) – 75% (50d)- 85% (60d)	[295]
PGS	6,500 (\bar{D} =3,5)	20 mL of 0,1 mM NaOH at 37°C	15% (70d)	[315]
Poly(butylene succinate) (PBS), X_c =48%	M_n = 63,300	NaOH solution (2M), 40°C	18% (48h)	[316]
PBS	M_w = 1.16.10 ⁵	pH= 14, 37°C, 150 rpm	30% (400h)	[317]
PES (poly(ethylene succinate), X_c = 40%)	M_w = 8.7.10 ⁴ (\bar{D} =2,1)	pH= 14, 37°C	13% (2d), 26% (4d)	[318]
Poly(butylene adipate-co-terephthalate) (PBAT) (X_c =14%)	75,000	Distilled water, 60°C, 30 rpm PBS solution, 37°C	70% (200d), 50% (400d) 50% (31d)	[319]
Poly(ethylene adipate) (X_c =74±5%)	40,000	Sea water from bay/ocean, 25°C	100±0% (28d)/ 57±14% (28d)	[320]
Poly(ethylene succinate) (PEC) (X_c =61±5%)	30,000		2±1% (28d)/5±2% (28d)	
PCL (X_c =63±5%)	110,000		100±0% (28d)/ 67±21% (28d)	
P(3-hydroxybutyrate) (X_c =65±5%)	350,000		41±16% (28d)/ 23±13% (28d)	
PPSC (20/10/9)		PBS solution (pH= 7,4, T= 37°C)	42% (8d) – 60% (12d) – 90% (14d)	[321]
Poly((1,2-propanediol-sebacate)-citrate)		PBS solution (pH= 7,4, T= 37°C)	20% (20d) – 35% (60d) – 42% (80d)	[322]
PGSL Poly(glycerol, sebacate and lactic acid)		PBS solution (pH= 7,4, T= 37°C)	20% (20d) – 35% (60d) – 42% (80d)	[322]
PEC elastomer (PEG/CA=citric acid), molar ratio= 10/9	1,200 (prepolymers)	PBS solution (pH= 7,4, T= 37°C)	60% (60h)	[323]
PBAT (X_c =14%)	75,000	PBS solution (pH= 7,4, T= 37°C)	50% (31d)	[319]
Poly(butylene adipate-co-terephthalate)		PBS solution (pH= 7,4, T= 37°C)	50% (31d)	[319]
PLGA 75/25 (F1, F2) and 50/50 (F3, F4)	F1: 4,300 (\bar{D} =14,8) F2: 9,200 (\bar{D} =6,4) F3: 4,200 (\bar{D} =8,9) F4: 7,600 (\bar{D} =4,5)	PBS solution (pH= 7,4, T= 37°C)	40% (70d) for F1 70% (70d) for F2 20% (40d) for F1 80% (70d) for F4	[324]

I.7. Conclusion

This chapter gave us great insight on the two main commercially available antifouling coatings: SPCs and FRCs. SPCs are the most commercialized antifouling paints. Their excellent inhospitable behavior towards aquatic organisms is due to a well-controlled matrix degradation and a constant release of biocides. Fouling release coatings are also promising antifouling systems thanks to their easy removal of fouling organisms allowed by low adhesion forces between the coating and the fouling species.

Nevertheless, SPCs and FRCs both showed their limits such as biocide content restrictions for SPCs and reduced antifouling efficacy in static conditions for FRCs. Advanced academic research highlighted that successful antifouling properties could be obtained with multifunctional surface-active coatings based on less toxic compounds. This opens up many possibilities of new hybrid antifouling coatings.

Easy processed hydrolyzable polymers such as PCL and PLA are widely used in the biomedical field. Their copolymerization and/or crosslinking can provide complex polymeric architectures with tunable hydrolytic degradations. Thus, an opportunity is drawn to use them as erodible binders to improve FRCs and provide a multifunctional antifouling coating.

I.8. Bibliographical references

1. Flemming, H.-C. Biofouling in water systems – cases, causes and countermeasures. *Applied Microbiology and Biotechnology* **2002**, *59*, 629–640.
2. Townsin, R.L.; Spencer, D.S.; Mosaad, M. Rough propeller penalties. *Society of Naval Architects and Marine Engineers-Transactions* **1985**, *93*.
3. Benson, P.H.; Brining, D.L.; Perrin, D.W. Marine Fouling and Its Prevention. *Marine Technology* **1973**, *8*.
4. Horbund, H.M.; Freiburger, A. Slime films and their role in marine fouling: A review. *Ocean Engineering* **1970**, *1*, 631–634.
5. Lindholdt, A.; Dam-Johansen, K.; Olsen, S.M.; Yebra, D.M.; Kiil, S. Effects of biofouling development on drag forces of hull coatings for ocean-going ships: a review. *Journal of Coatings Technology and Research* **2015**, *12*, 415–444.
6. Candries, M.; Atlar, M.; Mesbahi, E.; Pazouki, K. The Measurement of the Drag Characteristics of Tin-free Self-polishing Co-polymers and Fouling Release Coatings Using a Rotor Apparatus. *Biofouling* **2003**, *19*, 27–36.
7. Ciriminna, R.; Bright, F.V.; Pagliaro, M. Ecofriendly Antifouling Marine Coatings. *ACS Sustainable Chemistry & Engineering* **2015**, *3*, 559–565.
8. Railkin, A.; Ganf, T.; Manylov, O. *Marine Biofouling: Colonization Processes and Defenses*; CRC Press, 2003; ISBN 978-0-8493-1419-3.
9. Yebra, D.M.; Kiil, S.; Dam-Johansen, K. Antifouling technology—past, present and future steps towards efficient and environmentally friendly antifouling coatings. *Progress in Organic Coatings* **2004**, *50*, 75–104.
10. Dempsey, M.J. Marine bacterial fouling: A scanning electron microscope study. *Marine Biology* **1981**, *61*, 305–315.
11. Wang, J.; Cao, S.; Du, C.; Chen, D. Underwater locomotion strategy by a benthic pennate diatom *Navicula* sp. *Protoplasma* **2013**, *250*, 1203–1212.
12. Callow, J.A.; Callow, M.E. The Ulva Spore Adhesive System. In *Biological Adhesives*; Smith, A.M., Callow, J.A., Eds.; Springer Berlin Heidelberg: Berlin, Heidelberg, 2006; pp. 63–78 ISBN 978-3-540-31048-8.
13. Phang, I.Y.; Aldred, N.; Clare, A.S.; Vancso, G.J. Towards a nanomechanical basis for temporary adhesion in barnacle cyprids (*Semibalanus balanoides*). *Journal of The Royal Society Interface* **2008**, *5*, 397–402.
14. Kristensen, J.B.; Meyer, R.L.; Laursen, B.S.; Shipovskov, S.; Besenbacher, F.; Poulsen, C.H. Antifouling enzymes and the biochemistry of marine settlement. *Biotechnology Advances* **2008**, *26*, 471–481.
15. Ocean salinity Available online: <https://www.sciencelearn.org.nz/resources/686-ocean-salinity> (accessed on Mar 25, 2019).
16. Stanley, S.O.; Morita, R.Y. Salinity Effect on the Maximal Growth Temperature of Some Bacteria Isolated from Marine Environments. *Journal of Bacteriology* **1968**, *95*, 169–173.
17. Almeida, E.; Diamantino, T.C.; de Sousa, O. Marine paints: The particular case of antifouling paints. *Progress in Organic Coatings* **2007**, *59*, 2–20.
18. Milne, A.; Hails, G., Marine paint, **1977**, US4021392A.
19. Alzieu, C. Environmental impact of TBT: the French experience. *Science of The Total Environment* **2000**, *258*, 99–102.

20. Fent, K. Worldwide Occurrence of Organotin from Antifouling Paints and Effects in the Aquatic Environment. In *Antifouling Paint Biocides*; Konstantinou, I.K., Ed.; The Handbook of Environmental Chemistry; Springer Berlin Heidelberg: Berlin, Heidelberg, **2006**; pp. 71–100 ISBN 978-3-540-32844-5.
21. Damon, C.A. Hydrogen Peroxide: Toward a New Generation of Marine Antifouling Materials. **140**.
22. Gipperth, L. The legal design of the international and European Union ban on tributyltin antifouling paint: Direct and indirect effects. *Journal of environmental management* **2008**, *90 Suppl 1*, S86-95.
23. Capt. Ahmed Saad Hassan Noufal; Capt. Mohamed Hussein Nassar Hassan The Impact of Implementing the International Convention on the Control of Harmful Anti-fouling Systems in Ships (AFS Convention) on the Marine Environment. *Journal of Shipping and Ocean Engineering* **2016**, *6*.
24. Bellas, J. Comparative toxicity of alternative antifouling biocides on embryos and larvae of marine invertebrates. *Science of The Total Environment* **2006**, *367*, 573–585.
25. Batista-Andrade, J.A.; Caldas, S.S.; de Oliveira Arias, J.L.; Castro, I.B.; Fillmann, G.; Primel, E.G. Antifouling booster biocides in coastal waters of Panama: First appraisal in one of the busiest shipping zones. *Marine Pollution Bulletin* **2016**, *112*, 415–419.
26. Ytreberg, E.; Karlsson, J.; Eklund, B. Comparison of toxicity and release rates of Cu and Zn from anti-fouling paints leached in natural and artificial brackish seawater. *Science of The Total Environment* **2010**, *408*, 2459–2466.
27. Pereira, M.; Ankjaergaard, C. Legislation affecting antifouling products. In *Advances in Marine Antifouling Coatings and Technologies*; Elsevier, 2009; pp. 240–259 ISBN 978-1-84569-386-2.
28. Bighiu, M.A.; Eriksson-Wiklund, A.-K.; Eklund, B. Biofouling of leisure boats as a source of metal pollution. *Environmental Science and Pollution Research* **2017**, *24*, 997–1006.
29. Xie, Q.; Pan, J.; Ma, C.; Zhang, G. Dynamic surface antifouling: mechanism and systems. *Soft Matter* **2019**, *15*, 1087–1107.
30. Voulvoulis, N.; Scrimshaw, M.D.; Lester, J.N. Comparative environmental assessment of biocides used in antifouling paints. *Chemosphere* **2002**, *47*, 789–795.
31. Hart, R.L.; Virgallito, D.R.; Work, D.E., Microencapsulation of biocides and antifouling agents, **2009**, US7550200B2.
32. Miale, J.B.; Miale, A.; Porter, R.P., Anti-fouling marine paints containing microencapsulated anti-fouling agents and the process of microencapsulation, **1981**, US4253877.
33. Wallström, E.; Jespersen, H.T.; Schaumburg, K. A new concept for anti-fouling paint for Yachts. *Progress in Organic Coatings* **2011**, *72*, 109–114.
34. Faÿ, F.; Linossier, I.; Legendre, G.; Vallée-Réhel, K. Micro-Encapsulation and Antifouling Coatings: Development of Poly(lactic acid) Microspheres Containing Bioactive Molecules. *Macromolecular Symposia* **2008**, *272*, 45–51.
35. Carbone-Howell, A.L.; Stebbins, N.D.; Uhrich, K.E. Poly(anhydride-esters) Comprised Exclusively of Naturally Occurring Antimicrobials and EDTA: Antioxidant and Antibacterial Activities. *Biomacromolecules* **2014**, *15*, 1889–1895.
36. Ma, J.; Ma, C.; Yang, Y.; Xu, W.; Zhang, G. Biodegradable Polyurethane Carrying Antifoulants for Inhibition of Marine Biofouling. *Industrial & Engineering Chemistry Research* **2014**, *53*, 12753–12759.

Chapter I – State-of-the-art

37. Pinori, E.; Elwing, H.; Berglin, M. The impact of coating hardness on the anti-barnacle efficacy of an embedded antifouling biocide. *Biofouling* **2013**, *29*, 763–773.
38. Thomas, K. The environmental fate and behaviour of antifouling paint booster biocides: A review. *Biofouling* **2001**, *17*, 73–86.
39. Konstantinou, I.K.; Albanis, T.A. Worldwide occurrence and effects of antifouling paint booster biocides in the aquatic environment: a review. *Environment International* **2004**, *30*, 235–248.
40. Batista-Andrade, J.A.; Caldas, S.S.; Batista, R.M.; Castro, I.B.; Fillmann, G.; Primel, E.G. From TBT to booster biocides: Levels and impacts of antifouling along coastal areas of Panama. *Environmental Pollution* **2018**, *234*, 243–252.
41. Carreau, D.; Vallée-Réhel, K.; Linossier, I.; Quiniou, F.; Davy, R.; Compère, C.; Delbury, M.; Faÿ, F. Development of environmentally friendly antifouling paints using biodegradable polymer and lower toxic substances. *Progress in Organic Coatings* **2014**, *77*, 485–493.
42. Faÿ, F.; Linossier, I.; Legendre, G.; Vallée-Réhel, K. Micro-Encapsulation and Antifouling Coatings: Development of Poly(lactic acid) Microspheres Containing Bioactive Molecules. *Macromolecular Symposia* **2008**, *272*, 45–51.
43. Olsen, S.M.; Pedersen, L.T.; Laursen, M.H.; Kill, S.; Dam-Johansen, K. Enzyme-based antifouling coatings: a review. *Biofouling* **2007**, *23*, 369–383.
44. Charnley, M.; Textor, M.; Acikgoz, C. Designed polymer structures with antifouling–antimicrobial properties. *Reactive and Functional Polymers* **2011**, *71*, 329–334.
45. Bellotti, N.; del Amo, B.; Romagnoli, R. Quaternary Ammonium “Tannate” for Antifouling Coatings. *Ind. Eng. Chem. Res.* **2012**, *51*, 16626–16632.
46. He, W.; Zhang, Y.; Li, J.; Gao, Y.; Luo, F.; Tan, H.; Wang, K.; Fu, Q. A Novel Surface Structure Consisting of Contact-active Antibacterial Upper-layer and Antifouling Sub-layer Derived from Gemini Quaternary Ammonium Salt Polyurethanes. *Scientific Reports* **2016**, *6*, 32140.
47. Qian, P.-Y.; Li, Z.; Xu, Y.; Li, Y.; Fusetani, N. Mini-review: Marine natural products and their synthetic analogs as antifouling compounds: 2009–2014. *Biofouling* **2015**, *31*, 101–122.
48. Qian, P.-Y.; Xu, Y.; Fusetani, N. Natural products as antifouling compounds: recent progress and future perspectives. *Biofouling* **2009**, *26*, 223–234.
49. Bellotti, N.; del Amo, B.; Romagnoli, R. Tara tannin a natural product with antifouling coating application. *Progress in Organic Coatings* **2012**, *74*, 411–417.
50. Pérez, M.; García, M.; Blustein, G. Evaluation of low copper content antifouling paints containing natural phenolic compounds as bioactive additives. *Marine Environmental Research* **2015**, *109*, 177–184.
51. Bellotti, N.; del Amo, B.; Romagnoli, R. Caesalpinia Spinosa Tannin Derivatives for Antifouling Formulations. *Procedia Materials Science* **2012**, *1*, 259–265.
52. Pinori, E.; Berglin, M.; Brive, L.M.; Hulander, M.; Dahlström, M.; Elwing, H. Multi-seasonal barnacle (*Balanus improvisus*) protection achieved by trace amounts of a macrocyclic lactone (ivermectin) included in rosin-based coatings. *Biofouling* **2011**, *27*, 941–953.
53. Gittens, J.E.; Smith, T.J.; Suleiman, R.; Akid, R. Current and emerging environmentally-friendly systems for fouling control in the marine environment. *Biotechnology Advances* **2013**, *31*, 1738–1753.

54. Buskens, P.; Wouters, M.; Rentrop, C.; Vroon, Z. A brief review of environmentally benign antifouling and foul-release coatings for marine applications. *Journal of Coatings Technology and Research* **2013**, *10*, 29–36.
55. Magin, C.M.; Cooper, S.P.; Brennan, A.B. Non-toxic antifouling strategies. *Materials today* **2010**, *13*, 36–44.
56. Pradhan, S.; Kumar, S.; Mohanty, S.; Nayak, S.K. Environmentally Benign Fouling-Resistant Marine Coatings: A Review. *Polymer-Plastics Technology and Materials* **2019**, *58*, 498–518.
57. Lejars, M.; Margaillan, A.; Bressy, C. Fouling Release Coatings: A Nontoxic Alternative to Biocidal Antifouling Coatings. *Chem. Rev.* **2012**, *112*, 4347–4390.
58. Zeriouh, O.; Reinoso-Moreno, J.V.; López-Rosales, L.; Cerón-García, M. del C.; Sánchez-Mirón, A.; García-Camacho, F.; Molina-Grima, E. Biofouling in photobioreactors for marine microalgae. *Critical Reviews in Biotechnology* **2017**, *37*, 1006–1023.
59. Chaudhury, M.K.; Finlay, J.A.; Chung, J.Y.; Callow, M.E.; Callow, J.A. The influence of elastic modulus and thickness on the release of the soft-fouling green alga *Ulva linza* (syn. *Enteromorpha linza*) from poly(dimethylsiloxane) (PDMS) model networks. *Biofouling* **2005**, *21*, 41–48.
60. Mirabedini, S.M.; Pazoki, S.; Esfandeh, M.; Mohseni, M.; Akbari, Z. Comparison of drag characteristics of self-polishing co-polymers and silicone foul release coatings: A study of wettability and surface roughness. *Progress in Organic Coatings* **2006**, *57*, 421–429.
61. Townsin, R.L.; Anderson, C.D. Fouling control coatings using low surface energy, foul release technology. In *Advances in Marine Antifouling Coatings and Technologies*; Elsevier, 2009; pp. 693–708 ISBN 978-1-84569-386-2.
62. Yang, W.; Li, J.; Zhou, P.; Zhu, L.; Tang, H. Superhydrophobic copper coating: Switchable wettability, on-demand oil-water separation, and antifouling. *Chemical Engineering Journal* **2017**, *327*, 849–854.
63. Ma, M.; Hill, R.M. Superhydrophobic surfaces. *Current Opinion in Colloid & Interface Science* **2006**, *11*, 193–202.
64. Li, X.-M.; Reinhoudt, D.; Crego-Calama, M. What do we need for a superhydrophobic surface? A review on the recent progress in the preparation of superhydrophobic surfaces. *Chemical Society Reviews* **2007**, *36*, 1350.
65. Cho, K.L. Development of Superhydrophobic Coatings. 250.
66. Han, J.T.; Kim, B.K.; Woo, J.S.; Jang, J.I.; Cho, J.Y.; Jeong, H.J.; Jeong, S.Y.; Seo, S.H.; Lee, G.-W. Bioinspired Multifunctional Superhydrophobic Surfaces with Carbon-Nanotube-Based Conducting Pastes by Facile and Scalable Printing. *ACS Applied Materials & Interfaces* **2017**, *9*, 7780–7786.
67. Chapman, J.; Regan, F. Nanofunctionalized Superhydrophobic Antifouling Coatings for Environmental Sensor Applications—Advancing Deployment with Answers from Nature. *Advanced Engineering Materials* **2012**, *14*, B175–B184.
68. Friesen, C.M.; Améduri, B. Outstanding telechelic perfluoropolyalkylethers and applications therefrom. *Progress in Polymer Science* **2018**, *81*, 238–280.
69. Tsougeni, K.; Vourdas, N.; Tserepi, A.; Gogolides, E.; Cardinaud, C. Mechanisms of Oxygen Plasma Nanotexturing of Organic Polymer Surfaces: From Stable Super Hydrophilic to Super Hydrophobic Surfaces. *Langmuir* **2009**, *25*, 11748–11759.
70. Fernández-Blázquez, J.P.; Fell, D.; Bonaccorso, E.; Campo, A. del Superhydrophilic and superhydrophobic nanostructured surfaces via plasma treatment. *Journal of Colloid and Interface Science* **2011**, *357*, 234–238.

Chapter I – State-of-the-art

71. Scardino, A.J.; de Nys, R. Mini review: Biomimetic models and bioinspired surfaces for fouling control. *Biofouling* **2011**, *27*, 73–86.
72. Myan, F.W.Y.; Walker, J.; Paramor, O. The interaction of marine fouling organisms with topography of varied scale and geometry: a review. *Biointerphases* **2013**, *8*, 30.
73. Salta, M.; Wharton, J.A.; Blache, Y.; Stokes, K.R.; Briand, J.-F. Marine biofilms on artificial surfaces: structure and dynamics. *Environmental Microbiology* **2013**, *15*, 2879–2893.
74. Kirschner, C.M.; Brennan, A.B. Bio-Inspired Antifouling Strategies. *Annual Review of Materials Research* **2012**, *42*, 211–229.
75. Yan, Y.Y.; Gao, N.; Barthlott, W. Mimicking natural superhydrophobic surfaces and grasping the wetting process: A review on recent progress in preparing superhydrophobic surfaces. *Advances in Colloid and Interface Science* **2011**, *169*, 80–105.
76. Eral, H.B.; 't Mannetje, D.J.C.M.; Oh, J.M. Contact angle hysteresis: a review of fundamentals and applications. *Colloid and Polymer Science* **2013**, *291*, 247–260.
77. Li, J.; Ueda, E.; Paulssen, D.; Levkin, P.A. Slippery Lubricant-Infused Surfaces: Properties and Emerging Applications. *Advanced Functional Materials* **2019**, *29*, 1802317.
78. Howell, C.; Vu, T.L.; Lin, J.J.; Kolle, S.; Juthani, N.; Watson, E.; Weaver, J.C.; Alvarenga, J.; Aizenberg, J. Self-Replenishing Vascularized Fouling-Release Surfaces. *ACS Applied Materials & Interfaces* **2014**, *6*, 13299–13307.
79. Amini, S.; Kolle, S.; Petrone, L.; Ahanotu, O.; Sunny, S.; Sutanto, C.N.; Hoon, S.; Cohen, L.; Weaver, J.C.; Aizenberg, J.; et al. Preventing mussel adhesion using lubricant-infused materials. *Science* **2017**, *357*, 668–673.
80. Wei et al. - 2016 - Silicone Oil-Infused Slippery Surfaces Based on Sol-Gel Process-.pdf.
81. Scarratt, L.R.J.; Zhu, L.; Neto, C. How Slippery are SLIPS? Measuring Effective Slip on Lubricated Surfaces with Colloidal Probe Atmoc Force Microscopy. *Langmuir* **2019**, *35*, 2976–2982.
82. Finlay, J.A.; Bennett, S.M.; Brewer, L.H.; Sokolova, A.; Clay, G.; Gunari, N.; Meyer, A.E.; Walker, G.C.; Wendt, D.E.; Callow, M.E.; et al. Barnacle settlement and the adhesion of protein and diatom microfouling to xerogel films with varying surface energy and water wettability. *Biofouling* **2010**, *26*, 657–666.
83. Sokolova, A.; Cilz, N.; Daniels, J.; Stafslie, S.J.; Brewer, L.H.; Wendt, D.E.; Bright, F.V.; Detty, M.R. A comparison of the antifouling/foul-release characteristics of non-biocidal xerogel and commercial coatings toward micro- and macrofouling organisms. *Biofouling* **2012**, *28*, 511–523.
84. Destino, J.F.; Gatley, C.M.; Craft, A.K.; Detty, M.R.; Bright, F.V. Probing Nanoscale Chemical Segregation and Surface Properties of Antifouling Hybrid Xerogel Films. *Langmuir* **2015**, *31*, 3510–3517.
85. Damon, C.A.; Gatley, C.M.; Beres, J.J.; Finlay, J.A.; Franco, S.C.; Clare, A.S.; Detty, M.R. The performance of hybrid titania/silica-derived xerogels as active antifouling/fouling-release surfaces against the marine alga *Ulva linza* : *in situ* generation of hypohalous acids. *Biofouling* **2016**, *32*, 883–896.
86. Bennett, S.M. (73) Assignee: this syster of State. 46.
87. Detty, M.R.; Ciriminna, R.; Bright, F.V.; Pagliaro, M. Environmentally benign sol-gel antifouling and foul-releasing coatings. *Acc. Chem. Res.* **2014**, *47*, 678–687.
88. Murosaki, T.; Ahmed, N.; Ping Gong, J. Antifouling properties of hydrogels. *Science and Technology of Advanced Materials* **2011**, *12*, 064706.

89. Finlay, J.A.; Callow, M.E.; Ista, L.K.; Lopez, G.P.; Callow, J.A. The Influence of Surface Wettability on the Adhesion Strength of Settled Spores of the Green Alga *Enteromorpha* and the Diatom *Amphora*. *Integr Comp Biol* **2002**, *42*, 1116–1122.
90. Yandi, W.; Mieszkin, S.; Martin-Tanchereau, P.; Callow, M.E.; Callow, J.A.; Tyson, L.; Liedberg, B.; Ederth, T. Hydration and Chain Entanglement Determines the Optimum Thickness of Poly(HEMA-*co*-PEG₁₀ MA) Brushes for Effective Resistance to Settlement and Adhesion of Marine Fouling Organisms. *ACS Applied Materials & Interfaces* **2014**, *6*, 11448–11458.
91. Galli, G.; Martinelli, E. Amphiphilic Polymer Platforms: Surface Engineering of Films for Marine Antibiofouling. *Macromolecular Rapid Communications* **2017**, 1600704.
92. Higaki, Y.; Kobayashi, M.; Murakami, D.; Takahara, A. Anti-fouling behavior of polymer brush immobilized surfaces. *Polym J* **2016**, *48*, 325–331.
93. Cheng, L.; Liu, Q.; Lei, Y.; Lin, Y.; Zhang, A. The synthesis and characterization of carboxybetaine functionalized polysiloxanes for the preparation of anti-fouling surfaces. *RSC Advances* **10**.
94. Yang, W.J.; Cai, T.; Neoh, K.-G.; Kang, E.-T.; Teo, S.L.-M.; Rittschof, D. Barnacle Cement as Surface Anchor for “Clicking” of Antifouling and Antimicrobial Polymer Brushes on Stainless Steel. *Biomacromolecules* **2013**, *14*, 2041–2051.
95. Francolini, I.; Vuotto, C.; Piozzi, A.; Donelli, G. Antifouling and antimicrobial biomaterials: an overview. *APMIS* **2017**, *125*, 392–417.
96. Dundua, A.; Franzka, S.; Ulbricht, M. Improved Antifouling Properties of Polydimethylsiloxane Films via Formation of Polysiloxane/Polyzwitterion Interpenetrating Networks. *Macromol. Rapid Commun.* **2016**, *37*, 2030–2036.
97. Cheng, L.; Liu, Q.; Lei, Y.; Lin, Y.; Zhang, A. The synthesis and characterization of carboxybetaine functionalized polysiloxanes for the preparation of anti-fouling surfaces. *RSC Adv.* **2014**, *4*, 54372–54381.
98. Watermann, B.; Eklund, B. Can the input of biocides and polymeric substances from antifouling paints into the sea be reduced by the use of non-toxic hard coatings? *Marine Pollution Bulletin* **2019**, *144*, 146–151.
99. Yebra, D.M.; Kiil, S.; Dam-Johansen, K. Antifouling technology—past, present and future steps towards efficient and environmentally friendly antifouling coatings. *Progress in Organic Coatings* **2004**, *50*, 75–104.
100. Almeida, E.; Diamantino, T.C.; de Sousa, O. Marine paints: The particular case of antifouling paints. *Progress in Organic Coatings* **2007**, *59*, 2–20.
101. Pei, X.; Ye, Q. Development of Marine Antifouling Coatings. In *Antifouling Surfaces and Materials*; Zhou, F., Ed.; Springer Berlin Heidelberg: Berlin, Heidelberg, 2015; pp. 135–149 ISBN 978-3-662-45203-5.
102. Chambers, L.D.; Stokes, K.R.; Walsh, F.C.; Wood, R.J.K. Modern approaches to marine antifouling coatings. *Surface and Coatings Technology* **2006**, *201*, 3642–3652.
103. Oikonomou, E.K.; Iatridi, Z.; Moschakou, M.; Damigos, P.; Bokias, G.; Kallitsis, J.K. Development of Cu²⁺- and/or phosphonium-based polymeric biocidal materials and their potential application in antifouling paints. *Progress in Organic Coatings* **2012**, *75*, 190–199.
104. Muthukrishnan, T.; Dobretsov, S.; De Stefano, M.; Abed, R.M.M.; Kidd, B.; Finnie, A.A. Diatom communities on commercial biocidal fouling control coatings after one year of immersion in the marine environment. *Marine Environmental Research* **2017**, *129*, 102–112.

105. Faÿ, F.; Linossier, I.; Peron, J.J.; Langlois, V.; Vallée-Rehel, K. Antifouling activity of marine paints: Study of erosion. *Progress in Organic Coatings* **2007**, *60*, 194–206.
106. Bat, E.; Zhang, Z.; Feijen, J.; Grijpma, D.W.; Poot, A.A. Biodegradable elastomers for biomedical applications and regenerative medicine. *Regenerative Medicine* **2014**, *9*, 385–398.
107. Göpferich, A.; Tessmar, J. Polyanhydride degradation and erosion. *Advanced Drug Delivery Reviews* **2002**, *54*, 911–931.
108. von Burkersroda, F.; Schedl, L.; Göpferich, A. Why degradable polymers undergo surface erosion or bulk erosion. *Biomaterials* **2002**, *23*, 4221–4231.
109. Göpferich, A. Mechanisms of polymer degradation and erosion. *Biomaterials* **1996**, *17*, 103–114.
110. Huang, S.J.; Edelman, P.G. An overview of biodegradable polymers and biodegradation of polymers. In *Degradable Polymers*; Scott, G., Gilead, D., Eds.; Springer Netherlands: Dordrecht, 1995; pp. 18–28 ISBN 978-94-010-4253-6.
111. Tamada, J.A.; Langer, R. Erosion kinetics of hydrolytically degradable polymers. *Proceedings of the National Academy of Sciences* **1993**, *90*, 552–556.
112. Bressy, C.; NGuyen, M.N.; Tanguy, B.; Ngo, V.G.; Margailan, A. Poly(trialkylsilyl methacrylate)s: A family of hydrolysable polymers with tuneable erosion profiles. *Polymer Degradation and Stability* **2010**, *95*, 1260–1268.
113. Ketchum, B.H.; Ferry, J.D.; Redfield, A.C.; Burns, A.E. Evaluation of AntiFouling Paints by Leaching Rate Determinations. *Industrial & Engineering Chemistry* **1945**, *37*, 456–460.
114. Burant, A.; Zhang, X.; Singhasemanon, N. Antifouling Paint Biocide Monitoring and Modeling To Support Mitigation. In *Pesticides in Surface Water: Monitoring, Modeling, Risk Assessment, and Management*; ACS Symposium Series; American Chemical Society, 2019; Vol. 1308, pp. 491–517 ISBN 978-0-8412-3410-9.
115. Ytreberg, E.; Karlsson, J.; Eklund, B. Comparison of toxicity and release rates of Cu and Zn from anti-fouling paints leached in natural and artificial brackish seawater. *Science of The Total Environment* **2010**, *408*, 2459–2466.
116. Peres, R.S.; Baldissera, A.F.; Armelin, E.; Alemán, C.; Ferreira, C.A. Marine-friendly antifouling coating based on the use of a fatty acid derivative as a pigment. *Materials Research* **2014**, *17*, 720–727.
117. Goh, K.S.; Gan, J.; Young, D.F.; Luo, Y. *Pesticides in Surface Water: Monitoring, Modeling, Risk Assessment, and Management*; ACS Publications, 2019;
118. Bressy, C.; Hellio, C.; Nguyen, M.N.; Tanguy, B.; Maréchal, J.-P.; Margailan, A. Optimized silyl ester diblock methacrylic copolymers: A new class of binders for chemically active antifouling coatings. *Progress in Organic Coatings* **2014**, *77*, 665–673.
119. Watermann, B.T.; Daehne, B.; Sievers, S.; Dannenberg, R.; Overbeke, J.C.; Klijnsstra, J.W.; Heemken, O. Bioassays and selected chemical analysis of biocide-free antifouling coatings. *Chemosphere* **2005**, *60*, 1530–1541.
120. Lejars, M.; Margailan, A.; Bressy, C. Synthesis and characterization of diblock and statistical copolymers based on hydrolyzable siloxy silylester methacrylate monomers. *Polymer Chemistry* **2014**, *5*, 2109.
121. Ma, C.; Xu, W.; Pan, J.; Xie, Q.; Zhang, G. Degradable Polymers for Marine Antibiofouling: Optimizing Structure To Improve Performance. *Ind. Eng. Chem. Res.* **2016**, *55*, 11495–11501.
122. Carteau, D.; Vallée-Réhel, K.; Linossier, I.; Quiniou, F.; Davy, R.; Compère, C.; Delbury, M.; Faÿ, F. Development of environmentally friendly antifouling paints using

- biodegradable polymer and lower toxic substances. *Progress in Organic Coatings* **2014**, *77*, 485–493.
123. Chen, S.; Ma, C.; Zhang, G. Biodegradable polymers for marine antibiofouling: Poly(ϵ -caprolactone)/poly(butylene succinate) blend as controlled release system of organic antifoulant. *Polymer* **2016**, *90*, 215–221.
124. Zhou, X.; Xie, Q.; Ma, C.; Chen, Z.; Zhang, G. Inhibition of Marine Biofouling by Use of Degradable and Hydrolyzable Silyl Acrylate Copolymer. *Industrial & Engineering Chemistry Research* **2015**, *54*, 9559–9565.
125. Xie, Q.; Xie, Q.; Pan, J.; Ma, C.; Zhang, G. Biodegradable Polymer with Hydrolysis-Induced Zwitterions for Antibiofouling. *ACS Applied Materials & Interfaces* **2018**, *10*, 11213–11220.
126. Azemar, F.; Faÿ, F.; Réhel, K.; Linossier, I. Development of hybrid antifouling paints. *Progress in Organic Coatings* **2015**, *87*, 10–19.
127. Camós Noguera, A.; Olsen, S.M.; Hvilsted, S.; Kiil, S. Diffusion of surface-active amphiphiles in silicone-based fouling-release coatings. *Progress in Organic Coatings* **2017**, *106*, 77–86.
128. Galli, G.; Barsi, D.; Martinelli, E.; Glisenti, A.; Finlay, J.A.; Callow, M.E.; Callow, J.A. Copolymer films containing amphiphilic side chains of well-defined fluoroalkyl-segment length with biofouling-release potential. *RSC Adv.* **2016**, *6*, 67127–67135.
129. Yao, J.; Chen, S.; Ma, C.; Zhang, G. Marine anti-biofouling system with poly(ϵ -caprolactone)/clay composite as carrier of organic antifoulant. *Journal of Materials Chemistry B* **2014**, *2*, 5100.
130. Azemar, F.; Faÿ, F.; Réhel, K.; Linossier, I. Control of hydration and degradation properties of triblock copolymers polycaprolactone-*b*-polydimethylsiloxane-*b*-polycaprolactone. *Journal of Applied Polymer Science* **2014**, *131*, 1–8.
131. Jo, J.-H.; Ko, H.-C.; Kim, B.-W.; Park, H.; Lee, I.; Chun, H.-H.; Jo, N.-J. Micellar core-shell-type acrylic-polyurethane hybrid materials with self-polishing property. *Composite Interfaces* **2016**, *23*, 797–805.
132. Kim, S.-M.; Kim, A.Y.; Lee, I.; Park, H.; Hwang, D.-H. Synthesis and Characterization of Self-Polishing Copolymers Containing a New Zinc Acrylate Monomer. *Journal of Nanoscience and Nanotechnology* **2016**, *16*, 10903–10907.
133. Xu, G.; Liu, P.; Pranantyo, D.; Neoh, K.-G.; Kang, E.-T. Dextran- and Chitosan-Based Antifouling, Antimicrobial Adhesion, and Self-Polishing Multilayer Coatings from pH-Responsive Linkages-Enabled Layer-by-Layer Assembly. *ACS Sustainable Chemistry & Engineering* **2018**, *6*, 3916–3926.
134. Li, G.; Cheng, G.; Xue, H.; Chen, S.; Zhang, F.; Jiang, S. Ultra low fouling zwitterionic polymers with a biomimetic adhesive group. *Biomaterials* **2008**, *29*, 4592–4597.
135. Dai, G.; Xie, Q.; Ma, C.; Zhang, G. Biodegradable Poly(ester-*co*-acrylate) with Antifoulant Pendant Groups for Marine Anti-Biofouling. *ACS Applied Materials & Interfaces* **2019**, *11*, 11947–11953.
136. Hong, F.; Xie, L.; He, C.; Liu, J.; Zhang, G.; Wu, C. Effects of hydrolyzable comonomer and cross-linking on anti-biofouling terpolymer coatings. *Polymer* **2013**, *54*, 2966–2972.
137. Xie, L.; Hong, F.; He, C.; Ma, C.; Liu, J.; Zhang, G.; Wu, C. Coatings with a self-generating hydrogel surface for antifouling. *Polymer* **2011**, *52*, 3738–3744.
138. Ytreberg, E.; Karlsson, J.; Eklund, B. Comparison of toxicity and release rates of Cu and Zn from anti-fouling paints leached in natural and artificial brackish seawater. *Science of The Total Environment* **2010**, *408*, 2459–2466.

Chapter I – State-of-the-art

139. Oikonomou, E.K.; Iatridi, Z.; Moschakou, M.; Damigos, P.; Bokias, G.; Kallitsis, J.K. Development of Cu²⁺- and/or phosphonium-based polymeric biocidal materials and their potential application in antifouling paints. *Progress in Organic Coatings* **2012**, *75*, 190–199.
140. Gillard, M.; Cattiaux, A coating composition, *EP2399963A1*, **2011**, 52.
141. Olsen, S.M.; Kiil, S., Enzyme-based self-polishing, *WO2010089378A1*, **2010**, 22.
142. Lorient, M.; Linossier, I.; Vallée-Réhel, K.; Faÿ, F. Influence of Biodegradable Polymer Properties on Antifouling Paints Activity. *Polymers* **2017**, *9*, 36.
143. Faÿ, F.; Gouessan, M.; Linossier, I.; Réhel, K. Additives for Efficient Biodegradable Antifouling Paints. *International Journal of Molecular Sciences* **2019**, *20*, 361.
144. Coneski, P.N.; Weise, N.K.; Fulmer, P.A.; Wynne, J.H. Development and evaluation of self-polishing urethane coatings with tethered quaternary ammonium biocides. *Progress in Organic Coatings* **2013**, *76*, 1376–1386.
145. Chen, Y.; Liu, Z.; Han, S.; Han, J.; Jiang, D. Poly(propylene carbonate) polyurethane self-polishing coating for marine antifouling application. *Journal of Applied Polymer Science* **2016**, *133*.
146. Ma, C.; Xu, L.; Xu, W.; Zhang, G. Degradable polyurethane for marine anti-biofouling. *Journal of Materials Chemistry B* **2013**, *1*, 3099.
147. Eduok, U.; Faye, O.; Szpunar, J. Recent developments and applications of protective silicone coatings: A review of PDMS functional materials. *Progress in Organic Coatings* **2017**, *111*, 124–163.
148. Zhang, X.; Brodus, D.; Hollimon, V.; Hu, H. A brief review of recent developments in the designs that prevent bio-fouling on silicon and silicon-based materials. *Chemistry Central Journal* **2017**, *11*, 18.
149. Bressy, C.; Lejars, M. Marine fouling: an overview. *The Journal of Ocean Technology* **2014**, *9*, 19–28.
150. Sonak, S.; Pangam, P.; Giriyan, A.; Hawaldar, K. Implications of the ban on organotins for protection of global coastal and marine ecology. *Journal of Environmental Management* **2009**, *90*, S96–S108.
151. Owen, M.J. Elastomers: Siloxane. In *Encyclopedia of Materials: Science and Technology*; Elsevier, 2001; pp. 2480–2482 ISBN 978-0-08-043152-9.
152. Stricher, A.M.; Rinaldi, R.G.; Barrès, C.; Ganachaud, F.; Chazeau, L. How I met your elastomers: from network topology to mechanical behaviours of conventional silicone materials. **2015**, 14.
153. Brook, M.A. Silicon in organic, organometallic, and polymer chemistry /; Michael A. Brook. **2000**.
154. Pretti, C.; Oliva M.; Mennillo F.; Barbaglia M.; Funel M.; Yasani B.R.; Martinelli E.F; Galli G., *Ecotoxicology and Environmental Safety* **98**, **2013**, 250-256.
155. Commission Regulation (EU) No 276/2010, *Official journal of the European Union*, 31 March **2010**, 86, 7-12.
156. Mincheva, R.; Beigbeder, A.; Pettitt, M.E.; Callow, M.E.; Callow, J.A.; Dubois, P. Metal-free anti-biofouling coatings: the preparation of silicone-based nanostructured coatings via purely organic catalysis. *Nanocomposites* **2016**, *2*, 51–57.
157. Martinelli, E.; Hill, S.D.; Finlay, J.A.; Callow, M.E.; Callow, J.A.; Glisenti, A.; Galli, G. Amphiphilic modified-styrene copolymer films: Antifouling/fouling release properties against the green alga *Ulva linza*. *Progress in Organic Coatings* **2016**, *90*, 235–242.

158. Andriot, M.; DeGroot, J.V.; Meeks, R.; Wolf, A.T.; Leadley, S.; Garaud, J.L.; Gubbels, F.; Lecomte, J.P.; Lenoble, B.; Stassen, S.; et al. Silicones in Industrial Applications. 106.
159. Wynne, K.; Swain, G.; Fox, R.; Bullock, S.; Uilk, J. Two silicone nontoxic fouling release coatings: Hydrosilation cured PDMS and CaCO₃ filled, ethoxysiloxane cured RTV11. *Biofouling* **2000**, *16*, 277–288.
160. Townsin, R.L.; Anderson, C.D. Fouling control coatings using low surface energy, foul release technology. In *Advances in Marine Antifouling Coatings and Technologies*; Elsevier, 2009; pp. 693–708 ISBN 978-1-84569-386-2.
161. Camós Nogue, A.; Olsen, S.M.; Hvilsted, S.; Kiil, S. Field study of the long-term release of block copolymers from fouling-release coatings. *Progress in Organic Coatings* **2017**, *112*, 101–108.
162. Nogue, A.C. *Experimental investigation of the behaviour and fate of block copolymers in fouling-release coatings*; Technical University of Denmark (DTU): Kgs. Lyngby, 2016;
163. Inutsuka, M.; Yamada, N.L.; Ito, K.; Yokoyama, H. High Density Polymer Brush Spontaneously Formed by the Segregation of Amphiphilic Diblock Copolymers to the Polymer/Water Interface. *ACS Macro Letters* **2013**, *2*, 265–268.
164. Martinelli, E.; Suffredini, M.; Galli, G.; Glisenti, A.; Pettitt, M.E.; Callow, M.E.; Callow, J.A.; Williams, D.; Lyall, G. Amphiphilic block copolymer/poly(dimethylsiloxane) (PDMS) blends and nanocomposites for improved fouling-release. *Biofouling* **2011**, *27*, 529–541.
165. Martinelli, E.; Sarvothaman, M.K.; Alderighi, M.; Galli, G.; Mielczarski, E.; Mielczarski, J.A. PDMS network blends of amphiphilic acrylic copolymers with poly(ethylene glycol)-fluoroalkyl side chains for fouling-release coatings. I. Chemistry and stability of the film surface. *Journal of Polymer Science Part A: Polymer Chemistry* **2012**, *50*, 2677–2686.
166. Sun, X.; Zhang, F.; Chen, Y.; Cheng, Z.; Su, Y.; Hang, J.; Jin, L.; Li, N.; Shang, D.; Shi, L. Preparation and properties of crosslinked network coatings based on perfluoropolyether/poly(dimethyl siloxane)/acrylic polyols for marine fouling-release applications. *Journal of Applied Polymer Science* **2015**, *132*, n/a-n/a.
167. Krishnan, S.; Wang, N.; Ober, C.K.; Finlay, J.A.; Callow, M.E.; Callow, J.A.; Hexemer, A.; Sohn, K.E.; Kramer, E.J.; Fischer, D.A. Comparison of the Fouling Release Properties of Hydrophobic Fluorinated and Hydrophilic PEGylated Block Copolymer Surfaces: Attachment Strength of the Diatom *Navicula* and the Green Alga *Ulva*. *Biomacromolecules* **2006**, *7*, 1449–1462.
168. zhang, J.; Lin, C.; Wang, L.; Zheng, J.; Xu, F.; Sun, Z. Study on the correlation of lab assay and field test for fouling-release coatings. *Progress in Organic Coatings* **2013**, *76*, 1430–1434.
169. Olsen, S.M.; Yebra, D.M. Polysiloxane-based fouling release coats including enzymes *AU2012278332B2*, **2014**.
170. Williams, D.N.; Edward, N.I. Anti-fouling compositions with a fluorinated alkyl- or alkoxy-containing polymer or oligomer. *US8771798B2* **2014**.
171. Mielczarski, J.A.; Mielczarski, E.; Galli, G.; Morelli, A.; Martinelli, E.; Chiellini, E. The Surface-Segregated Nanostructure of Fluorinated Copolymer–Poly(dimethylsiloxane) Blend Films. *Langmuir* **2010**, *26*, 2871–2876.
172. Marabotti, I.; Morelli, A.; Orsini, L.M.; Martinelli, E.; Galli, G.; Chiellini, E.; Lien, E.M.; Pettitt, M.E.; Callow, M.E.; Callow, J.A.; et al. Fluorinated/siloxane copolymer blends for fouling release: chemical characterisation and biological evaluation with algae and barnacles. *Biofouling* **2009**, *25*, 481–493.

Chapter I – State-of-the-art

173. Aizenberg, J.; Aizenberg, M.; Cui, J.; Dunn, S.S.; Hatton, B.; Howell, C.; Kim, P.; Wong, T.-S.; Yao, X. Slippery self-lubricating polymer surfaces 2014.
174. Nurioglu, A.G.; Esteves, A.C.C.; de With, G. Non-toxic, non-biocide-release antifouling coatings based on molecular structure design for marine applications. *J. Mater. Chem. B* **2015**, *3*, 6547–6570.
175. Tyson, B.V.; Reynolds, K.J. Fouling-resistant composition comprising sterols and/or derivatives thereof.
176. Sørensen, K.F.; Hillerup, D.; Blom, A.; Olsen, S.M. ActiGuard: Novel technology to improve long-term performance of silicone-based Fouling Defence coatings. 10.
177. Duong, T.H.; Briand, J.-F.; Margailan, A.; Bressy, C. Polysiloxane-Based Block Copolymers with Marine Bacterial Anti-Adhesion Properties. *ACS Applied Materials & Interfaces* **2015**, *7*, 15578–15586.
178. Park, J.Y.; Ahn, D.; Choi, Y.Y.; Hwang, C.M.; Takayama, S.; Lee, S.H.; Lee, S.-H. Surface chemistry modification of PDMS elastomers with boiling water improves cellular adhesion. *Sensors and Actuators B: Chemical* **2012**, *173*, 765–771.
179. Al-Juhni, A.A.; Newby, B.Z. Incorporation of benzoic acid and sodium benzoate into silicone coatings and subsequent leaching of the compound from the incorporated coatings. *Progress in Organic Coatings* **2006**, *56*, 135–145.
180. Filip, N.; Pustam, A.; Ells, V.; Grosicki, K.M.T.; Yang, J.; Oguejiofor, I.; Bishop, C.D.; DeMont, M.E.; Smith-Palmer, T.; Wyeth, R.C. Fouling-release and chemical activity effects of a siloxane-based material on tunicates. *Marine Environmental Research* **2016**, *116*, 41–50.
181. Sokolova, A.; Cilz, N.; Daniels, J.; Stafslie, S.J.; Brewer, L.H.; Wendt, D.E.; Bright, F.V.; Detty, M.R. A comparison of the antifouling/foul-release characteristics of non-biocidal xerogel and commercial coatings toward micro- and macrofouling organisms. *Biofouling* **2012**, *28*, 511–523.
182. Hoipkemeier-Wilson, L.; Schumacher, J.F.; Carman, M.L.; Gibson, A.L.; Feinberg, A.W.; Callow, M.E.; Finlay, J.A.; Callow, J.A.; Brennan, A.B. Antifouling Potential of Lubricious, Micro-engineered, PDMS Elastomers against Zoospores of the Green Fouling Alga *Ulva* (Enteromorpha). *Biofouling* **2004**, *20*, 53–63.
183. Dobretsov, S.; Thomason, J.C. The development of marine biofilms on two commercial non-biocidal coatings: a comparison between silicone and fluoropolymer technologies. *Biofouling* **2011**, *27*, 869–880.
184. Thorlaksen, P.C.W.; Yebra, D.M.; Catala, P. Hydrogel-based third generation fouling release coatings. **2010**.
185. Finlay, J.A.; Bennett, S.M.; Brewer, L.H.; Sokolova, A.; Clay, G.; Gunari, N.; Meyer, A.E.; Walker, G.C.; Wendt, D.E.; Callow, M.E.; et al. Barnacle settlement and the adhesion of protein and diatom microfouling to xerogel films with varying surface energy and water wettability. *Biofouling* **2010**, *26*, 657–666.
186. Cassé, F.; Swain, G.W. The development of microfouling on four commercial antifouling coatings under static and dynamic immersion. *International Biodeterioration & Biodegradation* **2006**, *57*, 179–185.
187. Kim, J.; Chaudhury, M.K.; Owen, M.J. Hydrophobicity loss and recovery of silicone HV insulation. *IEEE Transactions on Dielectrics and Electrical Insulation* **1999**, *6*, 695–702.
188. Owen, M.J. The Surface Activity of Silicones: A Short Review. *Industrial & Engineering Chemistry Product Research and Development* **1980**, *19*, 97–103.

189. Selim, M.S.; Shenashen, M.A.; El-Safty, S.A.; Higazy, S.A.; Selim, M.M.; Isago, H.; Elmarakbi, A. Recent progress in marine foul-release polymeric nanocomposite coatings. *Progress in Materials Science* **2017**, *87*, 1–32.
190. Jr, R.F.B.; Singer, I.L. Mechanical factors favoring release from fouling release coatings. *Biofouling* **2000**, *15*, 73–81.
191. Truby, K.; Wood, C.; Stein, J.; Cella, J.; Carpenter, J.; Kavanagh, C.; Swain, G.; Wiebe, D.; Lapota, D.; Meyer, A.; et al. Evaluation of the performance enhancement of silicone biofouling-release coatings by oil incorporation. *Biofouling* **2000**, *15*, 141–150.
192. Evariste, E.M.L. Effects of non-biocidal coating technologies on colonisation by ectocarpoid algae. 337.
193. Warrick, E.L.; Pierce, O.R.; Polmanteer, K.E.; Saam, J.C. Silicone Elastomer Developments 1967–1977. *Rubber Chemistry and Technology* **1979**, *52*, 437–525.
194. Wang, X.; Olsen, S.M.; Andres Martinez, E.; Olsen, K.N.; Kiil, S. Drag resistance of ship hulls: effects of surface roughness of newly applied fouling control coatings, coating water absorption, and welding seams. *Journal of Coatings Technology and Research* **2018**, *15*, 657–669.
195. Goler, H.; Erdogan, O. Increasing Operational Efficiency of High Speed Ro-Ro Vessels Via New Hull Coating Technologies. *SSRN Journal* **2017**.
196. Howell, D.; Behrends, B. A review of surface roughness in antifouling coatings illustrating the importance of cutoff length. *Biofouling* **2006**, *22*, 401–410.
197. Bullock, S.; Johnston, E.E.; Willson, T.; Gatenholm, P.; Wynne, K.J. Surface science of a filled polydimethylsiloxane-based alkoxy silane-cured elastomer: RTV11. *Journal of colloid and interface science* **1999**, *210*, 18–36.
198. Beigbeder, A.; Jeusette, M.; Mincheva, R.; Claes, M.; Brocorens, P.; Lazzaroni, R.; Dubois, P., On the effect of carbon nanotubes on the wettability and surface morphology of hydrosilylation-curing silicone coatings, *Journal of Nanostructured Polymers and Nanocomposites*, **2009**, *5*, 23, 37–43.
199. Berglin, M.; Wynne, K.J.; Gatenholm, P. Fouling-release coatings prepared from α,ω -dihydroxypoly(dimethylsiloxane) cross-linked with (heptadecafluoro-1,1,2,2-tetrahydrodecyl)triethoxysilane. *Journal of Colloid and Interface Science* **2003**, *257*, 383–391.
200. Wynne, K.J.; Ho, T.; Johnston, E.E.; Myers, S.A. Surface science and stability of networks prepared from hydroxy-terminated polydimethylsiloxane and methyltriethoxysilane. *Applied Organometallic Chemistry* **1998**, *12*, 763–770.
201. Ogoshi, T.; Fujiwara, T.; Bertolucci, M.; Galli, G.; Chiellini, E.; Chujo, Y.; Wynne, K.J. Tapping Mode AFM Evidence for an Amorphous Reticular Phase in a Condensation-Cured Hybrid Elastomer: α,ω Dihydroxypoly(dimethylsiloxane)/Poly(diethoxysiloxane) /Fumed Silica Nanoparticles. *Journal of the American Chemical Society* **2004**, *126*, 12284–12285.
202. Johnston, E.; Bullock, S.; Uilk, J.; Gatenholm, P.; Wynne, K.J. Networks from α,ω -Dihydroxypoly(dimethylsiloxane) and (Tridecafluoro-1,1,2,2-tetrahydrooctyl)triethoxysilane: Surface Microstructures and Surface Characterization. *Macromolecules* **1999**, *32*, 8173–8182.
203. Black, E.P.; Ulibarri, T.A.; Beaucage, G.; Schaefer, D.W.; Assink, R.A.; Bergstrom, D.F.; Giwa-Agbomeirele, P.A.; Burns, G.T. Sol–Gel-Derived Silica–Siloxane Composite Materials: Effect of Reaction Conditions in Polymer-Rich Systems. In *Hybrid Organic-*

- Inorganic Composites*; Mark, J.E., Lee, C.Y.-C., Bianconi, P.A., Eds.; American Chemical Society: Washington, DC, **1995**; Vol. 585, pp. 237–246 ISBN 978-0-8412-3148-1.
204. Arce, F.T.; Avci, R.; Beech, I.B.; Cooksey, K.E.; Wigglesworth-Cooksey, B. Modification of Surface Properties of a Poly(dimethylsiloxane)-Based Elastomer, RTV11, upon Exposure to Seawater. *Langmuir* **2006**, *22*, 7217–7225.
 205. Benschop, H.O.G.; Guerin, A.J.; Brinkmann, A.; Dale, M.L.; Finnie, A.A.; Breugem, W.-P.; Clare, A.S.; Stübing, D.; Price, C.; Reynolds, K.J. Drag-reducing riblets with fouling-release properties: development and testing. *Biofouling* **2018**, *34*, 532–544.
 206. Brady, R.F. Properties which influence marine fouling resistance in polymers containing silicon and fluorine. *Progress in Organic Coatings* **1999**, *35*, 31–35.
 207. Drummond, C.J.; Georgaklis, G.; Chan, D.Y.C. Fluorocarbons: Surface Free Energies and van der Waals Interaction. *Langmuir* **1996**, *12*, 2617–2621.
 208. *Silicone surface science*; Advances in silicon science; 1st ed.; Springer: New York, **2012**; ISBN 978-94-007-3875-1.
 209. Brady, R.F., A fracture mechanical analysis of fouling release from nontoxic antifouling coatings. *Progress in Organic Coatings* **2001**, *43*, 188-192
 210. Wang, Z.; Volinsky, A.A.; Gallant, N.D. Crosslinking effect on polydimethylsiloxane elastic modulus measured by custom-built compression instrument. *Journal of Applied Polymer Science* **2014**, *131*.
 211. Kohl, J.G.; Singer, I.L. Pull-off behavior of epoxy bonded to silicone duplex coatings. *Progress in Organic Coatings* **1999**, *36*, 15–20.
 212. Singer, I.L.; Kohl, J.G.; Patterson, M. Mechanical aspects of silicone coatings for hard foulant control. *Biofouling* **2000**, *16*, 301–309.
 213. Sun, Y.; Guo, S.; Walker, G.C.; Kavanagh, C.J.; Swain, G.W. Surface elastic modulus of barnacle adhesive and release characteristics from silicone surfaces. *Biofouling* **2004**, *20*, 279–289.
 214. Holberg, S.; Losada, R. Fouling-release coatings for steam condensers in thermal power plants. *Heat Exchanger Fouling and Cleaning* **2017**, *6*, 177-182.
 215. Stevens, C.; Powell, D.E. Fate Baseline and Effects of Polydimethylsiloxane (PDMS) in Marine Environments. *Marine Pollution Bulletin* **2001**, *42*, 8.
 216. Nendza, M. Hazard assessment of silicone oils (polydimethylsiloxanes, PDMS) used in antifouling-/foul-release-products in the marine environment. *Marine Pollution Bulletin* **2007**, *54*, 1190–1196.
 217. Kuo, A.C. Poly (dimethylsiloxane). *Polymer data handbook* **1999**, 411–435.
 218. Sundaram, H.S.; Cho, Y.; Dimitriou, M.D.; Finlay, J.A.; Cone, G.; Williams, S.; Handlin, D.; Gatto, J.; Callow, M.E.; Callow, J.A.; et al. Fluorinated Amphiphilic Polymers and Their Blends for Fouling-Release Applications: The Benefits of a Triblock Copolymer Surface. *ACS Appl. Mater. Interfaces* **2011**, *3*, 3366–3374.
 219. Oliva, M.; Martinelli, E.; Galli, G.; Pretti, C. PDMS-based films containing surface-active amphiphilic block copolymers to combat fouling from barnacles *B. amphitrite* and *B. improvisus*. *Polymer* **2017**, *108*, 476–482.
 220. Wenning, B.M.; Martinelli, E.; Mieszkin, S.; Finlay, J.A.; Fischer, D.; Callow, J.A.; Callow, M.E.; Leonardi, A.K.; Ober, C.K.; Galli, G. Model Amphiphilic Block Copolymers with Tailored Molecular Weight and Composition in PDMS-Based Films to Limit Soft Biofouling. *ACS applied materials & interfaces* **2017**, *9*, 16505–16516.
 221. Yao, M.; Fang, J. Hydrophilic PEO-PDMS for microfluidic applications. *J. Micromech. Microeng.* **2012**, *22*, 025012.

222. Murthy, R.; Bailey, B.M.; Valentin-Rodriguez, C.; Ivanisevic, A.; Grunlan, M.A. Amphiphilic silicones prepared from branched PEO-silanes with siloxane tethers. *Journal of Polymer Science Part A: Polymer Chemistry* **48**, 4108–4119.
223. Lin, Y.; Zhong, W.; Dong, C.; Zhang, C.; Feng, X.; Zhang, A. Synthesis and Antifungal Activities of Amphiphilic PDMS-b-QPDMAEMA Copolymers on *Rhizoctonia solani*. *ACS Appl. Bio Mater.* **2018**, *1*, 2062–2072.
224. Leng, C.; Buss, H.G.; Segalman, R.A.; Chen, Z. Surface Structure and Hydration of Sequence-Specific Amphiphilic Polypeptides for Antifouling/Fouling Release Applications. *Langmuir* **2015**, *31*, 9306–9311.
225. Calabrese, D.R.; Wenning, B.; Finlay, J.A.; Callow, M.E.; Callow, J.A.; Fischer, D.; Ober, C.K. Amphiphilic oligopeptides grafted to PDMS-based diblock copolymers for use in antifouling and fouling release coatings. *Polym. Adv. Technol.* **2015**, *26*, 829–836.
226. Patterson, A.L.; Wenning, B.; Rizis, G.; Calabrese, D.R.; Finlay, J.A.; Franco, S.C.; Zuckermann, R.N.; Clare, A.S.; Kramer, E.J.; Ober, C.K.; et al. Role of Backbone Chemistry and Monomer Sequence in Amphiphilic Oligopeptide- and Oligopeptoid-Functionalized PDMS- and PEO-Based Block Copolymers for Marine Antifouling and Fouling Release Coatings. *Macromolecules* **2017**.
227. van Zoelen, W.; Buss, H.G.; Ellebracht, N.C.; Lynd, N.A.; Fischer, D.A.; Finlay, J.; Hill, S.; Callow, M.E.; Callow, J.A.; Kramer, E.J.; et al. Sequence of Hydrophobic and Hydrophilic Residues in Amphiphilic Polymer Coatings Affects Surface Structure and Marine Antifouling/Fouling Release Properties. *ACS Macro Lett.* **2014**, *3*, 364–368.
228. Røn, T.; Javakhishvili, I.; Hvilsted, S.; Jankova, K.; Lee, S. Ultralow Friction with Hydrophilic Polymer Brushes in Water as Segregated from Silicone Matrix. *Advanced Materials Interfaces* **2016**, *3*, 1500472.
229. Bauer, S.; Arpa-Sancet, M.P.; Finlay, J.A.; Callow, M.E.; Callow, J.A.; Rosenhahn, A. Adhesion of Marine Fouling Organisms on Hydrophilic and Amphiphilic Polysaccharides. *Langmuir* **2013**, *29*, 4039–4047.
230. Yoshikawa, C.; Goto, A.; Tsujii, Y.; Fukuda, T.; Kimura, T.; Yamamoto, K.; Kishida, A. Protein Repellency of Well-Defined, Concentrated Poly(2-hydroxyethyl methacrylate) Brushes by the Size-Exclusion Effect. *Macromolecules* **2006**, *39*, 2284–2290.
231. Hawkins, M.L.; Rufin, M.A.; Raymond, J.E.; Grunlan, M.A. Direct observation of the nanocomplex surface reorganization of antifouling silicones containing a highly mobile PEO-silane amphiphile. *Journal of Materials Chemistry B* **2014**, *2*, 5689.
232. Chisholm, B.J.; Fargo, W.; Christianson, D.A. Amphiphilic fouling release coatings. *US8820257B2* **2014**, *29*.
233. Liu, C.; Xie, Q.; Ma, C.; Zhang, G. Fouling Release Property of Polydimethylsiloxane-Based Polyurea with Improved Adhesion to Substrate. *Industrial & Engineering Chemistry Research* **2016**, *55*, 6671–6676.
234. Galhenage, T.P.; Webster, D.C.; Moreira, A.M.S.; Burgett, R.J.; Stafslie, S.J.; Vanderwal, L.; Finlay, J.A.; Franco, S.C.; Clare, A.S. Poly(ethylene) glycol-modified, amphiphilic, siloxane–polyurethane coatings and their performance as fouling-release surfaces. *Journal of Coatings Technology and Research* **2017**, *14*, 307–322.
235. Gapeeva, A.; Holken, I.; Adelung, R.; Baum, M. *Characterization of a polydimethylsiloxane-polythiourethane polymer blend with potential as fouling-release coating*; 2017;
236. Joshi, R.G.; Goel, A.; Mannari, V.M.; Finlay, J.A.; Callow, M.E.; Callow, J.A. Evaluating fouling-resistance and fouling-release performance of smart polyurethane surfaces: An

- outlook for efficient and environmentally benign marine coatings. *Journal of Applied Polymer Science* **2009**, *114*, 3693–3703.
237. Sommer, S.; Ekin, A.; Webster, D.C.; Stafslie, S.J.; Daniels, J.; VanderWal, L.J.; Thompson, S.E.M.; Callow, M.E.; Callow, J.A. A preliminary study on the properties and fouling-release performance of siloxane–polyurethane coatings prepared from poly(dimethylsiloxane) (PDMS) macromers. *Biofouling* **2010**, *26*, 961–972.
238. Xie, Q.; Ma, C.; Liu, C.; Ma, J.; Zhang, G. Poly(dimethylsiloxane)-Based Polyurethane with Chemically Attached Antifoulants for Durable Marine Antibiofouling. *ACS Applied Materials & Interfaces* **2015**, *7*, 21030–21037.
239. Santiago, A.; Irusta, L.; Schäfer, T.; Corres, A.; Martin, L.; González, A. Resistance to protein sorption as a model of antifouling performance of Poly(siloxane-urethane) coatings exhibiting phase separated morphologies. *Progress in Organic Coatings* **2016**, *99*, 110–116.
240. Liu, D.; Wu, G.-M.; Kong, Z.-W. Preparation and characterization of a polydimethylsiloxane-modified, epoxy-resin-based polyol dispersion and its crosslinked films. *J. Appl. Polym. Sci.* **2017**, *134*, n/a-n/a.
241. Rath, S.K.; Chavan, J.G.; Sasane, S.; Jagannath; Patri, M.; Samui, A.B.; Chakraborty, B.C. Two component silicone modified epoxy foul release coatings: Effect of modulus, surface energy and surface restructuring on pseudobarnacle and macrofouling behavior. *Applied Surface Science* **2010**, *256*, 2440–2446.
242. Pollack, K.A.; Imbesi, P.M.; Raymond, J.E.; Wooley, K.L. Hyperbranched Fluoropolymer-Polydimethylsiloxane-Poly(ethylene glycol) Cross-Linked Terpolymer Networks Designed for Marine and Biomedical Applications: Heterogeneous Nontoxic Antibiofouling Surfaces. *ACS Applied Materials & Interfaces* **2014**, *6*, 19265–19274.
243. Barletta, M.; Aversa, C.; Pizzi, E.; Puopolo, M.; Vesco, S. Design, manufacturing and testing of anti-fouling/foul-release (AF/FR) amphiphilic coatings. *Progress in Organic Coatings* **2018**, *123*, 267–281.
244. Sebastin, A.Y.; Mohanty, S.; Nayak, S.K. Synthesis and characterization of eco-friendly siloxane-semifluorinated polyurethane coatings for underwater application. *J. Appl. Polym. Sci.* **2019**, *136*, 47720, 1-11.
245. Gudipati, C.S.; Greenlief, C.M.; Johnson, J.A.; Prayongpan, P.; Wooley, K.L. Hyperbranched fluoropolymer and linear poly(ethylene glycol) based amphiphilic crosslinked networks as efficient antifouling coatings: An insight into the surface compositions, topographies, and morphologies. *J. Polym. Sci. A Polym. Chem.* **2004**, *42*, 6193–6208.
246. Boudjouk, P.; Johnson, T. Polysiloxanes with anti-fouling activity. *US 8820257B2* **2011**, 17.
247. Thorlaksen, P.C.W.; Strand, S.; Blom, A.; Bork, U. Fouling control coating compositions, *US9534121B2*. **2017**, 14.
248. Martinelli, E.; Sarvothaman, M.K.; Galli, G.; Pettitt, M.E.; Callow, M.E.; Callow, J.A.; Conlan, S.L.; Clare, A.S.; Sugiharto, A.B.; Davies, C.; et al. Poly(dimethyl siloxane) (PDMS) network blends of amphiphilic acrylic copolymers with poly(ethylene glycol)-fluoroalkyl side chains for fouling-release coatings. II. Laboratory assays and field immersion trials. *Biofouling* **2012**, *28*, 571–582.
249. Akuzov, D.; Vladkova, T.; Zamfirova, G.; Gaydarov, V.; Nascimento, M.V.; Szeglat, N.; Grunwald, I. Polydimethyl siloxane coatings with superior antibiofouling efficiency in laboratory and marine conditions. *Progress in Organic Coatings* **2017**, *103*, 126–134.

Chapter I – State-of-the-art

250. Gomathi Sankar, G.; Sathya, S.; Sriyutha Murthy, P.; Das, A.; Pandiyan, R.; Venugopalan, V.P.; Doble, M. Polydimethyl siloxane nanocomposites: Their antifouling efficacy in vitro and in marine conditions. *International Biodeterioration & Biodegradation* **2015**, *104*, 307–314.
251. Selim, M.S.; Shenashen, M.A.; Elmarakbi, A.; Fatthallah, N.A.; Hasegawa, S.; El-Safty, S.A. Synthesis of ultrahydrophobic and thermally stable inorganic–organic nanocomposites for self-cleaning foul release coatings. *Chemical Engineering Journal* **2017**, *320*, 653–666.
252. Beigbeder, A.; Labruyère, C.; Viville, P.; Pettitt, M.E.; Callow, M.E.; Callow, J.A.; Bonnaud, L.; Lazzaroni, R.; Dubois, P. Surface and Fouling-Release Properties of Silicone/Organomodified Montmorillonite Coatings. *Journal of Adhesion Science and Technology* **2011**, *25*, 1689–1700.
253. Ba, M.; Zhang, Z.; Qi, Y. The influence of MWCNTs-OH on the properties of the fouling release coatings based on polydimethylsiloxane with the incorporation of phenylmethylsilicone oil. *Progress in Organic Coatings* **2019**, *130*, 132–143.
254. Selim, M.S.; Yang, H.; Wang, F.Q.; Fatthallah, N.A.; Li, X.; Li, Y.; Huang, Y. Superhydrophobic silicone/SiC nanowire composite as a fouling release coating material. *Journal of Coatings Technology and Research* **2019**.
255. Tian, S.; Jiang, D.; Pu, J.; Sun, X.; Li, Z.; Wu, B.; Zheng, W.; Liu, W.; Liu, Z. A new hybrid silicone-based antifouling coating with nanocomposite hydrogel for durable antifouling properties. *Chemical Engineering Journal* **2019**, *370*, 1–9.
256. Wan, F.; Pei, X.; Yu, B.; Ye, Q.; Zhou, F.; Xue, Q. Grafting Polymer Brushes on Biomimetic Structural Surfaces for Anti-Algae Fouling and Foul Release. *ACS Appl. Mater. Interfaces* **2012**, *4*, 4557–4565.
257. Vucko, M.J.; Poole, A.J.; Carl, C.; Sexton, B.A.; Glenn, F.L.; Whalan, S.; de Nys, R. Using textured PDMS to prevent settlement and enhance release of marine fouling organisms. *Biofouling* **2014**, *30*, 1–16.
258. Yang, H.; Zhang, W.; Chen, T.; Huang, S.; Quan, B.; Wang, M.; Li, J.; Gu, C.; Wang, J. Direct Experimental Evidence of Biomimetic Surfaces with Chemical Modifications Interfering with Adhesive Protein Adsorption. *Molecules* **2018**, *24*, 27.
259. Majumdar, P.; Crowley, E.; Htet, M.; Stafslie, S.J.; Daniels, J.; VanderWal, L.; Chisholm, B.J. Combinatorial Materials Research Applied to the Development of New Surface Coatings XV: An Investigation of Polysiloxane Anti-Fouling/Fouling-Release Coatings Containing Tethered Quaternary Ammonium Salt Groups. *ACS Comb. Sci.* **2011**, *13*, 298–309.
260. Chisholm, B. J.; Boudjouk, P.; Thomas, J.; Christianson, S.J., Antifouling materials containing cationic polysiloxanes, *US8278400B2*, **2010**.
261. Olsen, S.M.; Yebra, D.M., Polysiloxane-based fouling release coats including enzymes, *US2014/0134146A1*, **2014**.
262. Jones, P.K.; Hawkins, I.; M. Curry, A.; Li, Z.; Sinclair-Day, J.D., Biocidal foul release coating systems, *US2014/0141263A1*, **2014**.
263. Shivapooja, P.; Cao, C.; Orihuela, B.; Levering, V.; Zhao, X.; Rittschof, D.; López, G.P. Incorporation of silicone oil into elastomers enhances barnacle detachment by active surface strain. *Biofouling* **2016**, *32*, 1017–1028.
264. Kavanagh, C.J.; Swain, G.W.; Kovach, B.S.; Stein, J.; Darkangelo-Wood, C.; Truby, K.; Holm, E.; Montemarano, J.; Meyer, A.; Wiebe, D. The Effects of Silicone Fluid Additives

- and Silicone Elastomer Matrices on Barnacle Adhesion Strength. *Biofouling* **2003**, *19*, 381–390.
265. Vladkova, T.G.; Dineff, P.D.; Zlatanov, I.Y.; Kathioli, S.; Ramasammy, V.; Vasudeva, P.S.M. Composition coating for biofouling protection **2008**.
266. du Toit, L.C.; Choonara, Y.E.; Kumar, P.; Pillay, V. Polymeric networks for controlled release of drugs: a patent review. *Expert Opinion on Therapeutic Patents* **2016**, *26*, 703–717.
267. Tran, R.; Dey, J.; Gyawali, D.; Zhang, Y.; Yang, J. Biodegradable Elastomeric Polymers and MEMS in Tissue Engineering. *Biomaterials for MEMS*; Chiao, J.-C., Ed.; Pan Stanford Publishing, **2011**, ISBN 978-981-4241-46-5.
268. Vroman, I.; Tighzert, L. Biodegradable Polymers. *Materials* **2009**, *2*, 307–344.
269. Chandra, R.; Rustgi, R., Biodegradable polymers, *Prog. Polym. Sci.* **1998**, *23*, 1273-1335.
270. Ginjupalli, K.; Shavi, G.V.; Averineni, R.K.; Bhat, M.; Udupa, N.; Nagaraja Upadhya, P. Poly(α -hydroxy acid) based polymers: A review on material and degradation aspects. *Polymer Degradation and Stability* **2017**, *144*, 520–535.
271. Kumar, N.; Langer, R.S.; Domb, A.J. Polyanhydrides: an overview. *Advanced Drug Delivery Reviews* **2002**, *54*, 889–910.
272. Madhavan Nampoothiri, K.; Nair, N.R.; John, R.P. An overview of the recent developments in polylactide (PLA) research. *Bioresource Technology* **2010**, *101*, 8493–8501.
273. Park, T.G. Degradation of poly(lactic-co-glycolic acid) microspheres: effect of copolymer composition. *Biomaterials* **1995**, *16*, 1123–1130.
274. Choi, S.H.; Park, T.G. Synthesis and characterization of elastic PLGA/PCL/PLGA tri-block copolymers. *Journal of Biomaterials Science, Polymer Edition* **2002**, *13*, 1163–1173.
275. Makadia, H.K.; Siegel, S.J. Poly Lactic-co-Glycolic Acid (PLGA) as Biodegradable Controlled Drug Delivery Carrier. *Polymers* **2011**, *3*, 1377–1397.
276. Gentile, P.; Chiono, V.; Carmagnola, I.; Hatton, P. An Overview of Poly(lactic-co-glycolic) Acid (PLGA)-Based Biomaterials for Bone Tissue Engineering. *International Journal of Molecular Sciences* **2014**, *15*, 3640–3659.
277. Siparsky, G.L.; Voorhees, K.J.; Miao, F. Hydrolysis of polylactic acid (PLA) and polycaprolactone (PCL) in aqueous acetonitrile solutions: autocatalysis. *Journal of Polymers and the Environment* **1998**, *6*, 31–41.
278. Chu, C.C. Hydrolytic degradation of polyglycolic acid: Tensile strength and crystallinity study. *Journal of Applied Polymer Science* **1981**, *26*, 1727–1734.
279. Wiggins, J.S.; Hassan, M.K.; Mauritz, K.A.; Storey, R.F. Hydrolytic degradation of poly(D,L-lactide) as a function of end group: Carboxylic acid vs. hydroxyl. *Polymer* **2006**, *47*, 1960–1969.
280. Xu, K.; Kozluca, A.; Denkbaş, E.B.; Pişkin, E. Synthesis of PDLLA homopolymers with different molecular weights. *J. Appl. Polym. Sci.* **1996**, *59*, 561–563.
281. Bonartsev, A.P.; Myshkina, V.L.; Nikolaeva, D.A.; Furina, E.K.; Makhina, T.A.; Boskhomdzhiev, A.P.; Ivanov, E.A.; Iordanskii, A.L.; Bonartseva, G.A. Biosynthesis, biodegradation, and application of poly(3-hydroxybutyrate) and its copolymers - natural polyesters produced by diazotrophic bacteria. *M* **2007**, *13*.
282. Scott, G., Degradable Polymers: Principles and Applications; *Springer Science & Business Media*, **2002**; ISBN 978-1-4020-0790-3.
283. Fukushima, K. Poly(trimethylene carbonate)-based polymers engineered for biodegradable functional biomaterials. *Biomaterials Science* **2016**, *4*, 9–24.

284. Fabbri, M.; Gigli, M.; Gamberini, R.; Lotti, N.; Gazzano, M.; Rimini, B.; Munari, A., Hydrolysable PBS-based poly(ester urethane)s thermoplastic elastomers. *Polymer Degradation and Stability* **2014**, *108*, 223-231.
285. Bogdanov, B.; Toncheva, V.; Schacht, E.; Finelli, L.; Sarti, B.; Scandola, M. Physical properties of poly(ester-urethanes) prepared from different molar mass polycaprolactone-diols. *Polymer* **1999**, *40*, 3171–3182.
286. Göpferich, A.; Langer, R. The influence of microstructure and monomer properties on the erosion mechanism of a class of polyanhydrides. *Journal of Polymer Science Part A: Polymer Chemistry* **1993**, *31*, 2445–2458.
287. Yan, C.; Wu, J.; Zhang, J.; He, J.; Zhang, J. Hydrolytic degradation of cellulose-graft-poly(l-lactide) copolymers. *Polymer Degradation and Stability* **2015**, *118*, 130–136.
288. Eichhorn, S.J.; Young, R.J. The Young's modulus of a microcrystalline cellulose. *Cellulose* **2001**, *8*, 197–207.
289. Yamanaka, S.; Watanabe, K.; Kitamura, N.; Iguchi, M.; Mitsuhashi, S.; Nishi, Y.; Uryu, M. The structure and mechanical properties of sheets prepared from bacterial cellulose. *J Mater Sci* **1989**, *24*, 3141–3145.
290. Tran, R.T.; Thevenot, P.; Gyawali, D.; Chiao, J.-C.; Tang, L.; Yang, J. Synthesis and characterization of a biodegradable elastomer featuring a dual crosslinking mechanism. *Soft Matter* **2010**, *6*, 2449.
291. Stokes, K.; McVenes, R.; Anderson, J.M. Polyurethane Elastomer Biostability. *Journal of Biomaterials Applications* **1995**, *9*, 321–354.
292. Fredericks, R.J.; Melveger, A.J.; Dolegiewitz, L.J. Morphological and structural changes in a copolymer of glycolide and lactide occurring as a result of hydrolysis. *Journal of Polymer Science: Polymer Physics Edition* **1984**, *22*, 57–66.
293. Yeh, Y.-C.; Ouyang, L.; Highley, C.B.; Burdick, J.A. Norbornene-modified poly(glycerol sebacate) as a photocurable and biodegradable elastomer. *Polymer Chemistry* **2017**, *8*, 5091–5099.
294. Tham, W.H.; Wahit, M.U.; Abdul Kadir, M.R.; Wong, T.W.; Hassan, O. Polyol-based biodegradable polyesters: a short review. *Reviews in Chemical Engineering* **2016**, *32*.
295. Zhang, X.; Jia, C.; Qiao, X.; Liu, T.; Sun, K. Porous poly(glycerol sebacate) (PGS) elastomer scaffolds for skin tissue engineering. *Polymer Testing* **2016**, *54*, 118–125.
296. Chen, Q.-Z.; Bismarck, A.; Hansen, U.; Junaid, S.; Tran, M.Q.; Harding, S.E.; Ali, N.N.; Boccaccini, A.R. Characterisation of a soft elastomer poly(glycerol sebacate) designed to match the mechanical properties of myocardial tissue. *Biomaterials* **2008**, *29*, 47–57.
297. Kang, Y.; Yang, J.; Khan, S.; Anissian, L.; Ameer, G.A. A new biodegradable polyester elastomer for cartilage tissue engineering. *Journal of Biomedical Materials Research Part A* **2006**, *77A*, 331–339.
298. Yang, J.; Webb, A.R.; Ameer, G.A. Novel Citric Acid-Based Biodegradable Elastomers for Tissue Engineering. *Advanced Materials* **2004**, *16*, 511–516.
299. Younes, H.M.; Bravo-Grimaldo, E.; Amsden, B.G. Synthesis, characterization and in vitro degradation of a biodegradable elastomer. *Biomaterials* **2004**, *25*, 5261–5269.
300. Rohman, G.; Grande, D. Mesoporous Polymeric Materials Tailored from Oligoester-Derivatized Interpenetrating Polymer Networks. *Macromol. Symp.* **2008**, *267*, 21–26.
301. Brzeska, J. Biodegradable Polyurethanes Cross-Linked by Multifunctional Compounds *Current Organic Synthesis*, *14* **2017**, *6*, 778-784(7).

Chapter I – State-of-the-art

302. Chivukula, P.; Dušek, K.; Wang, D.; Dušková-Smrčková, M.; Kopečková, P.; Kopeček, J. Synthesis and characterization of novel aromatic azo bond-containing pH-sensitive and hydrolytically cleavable IPN hydrogels. *Biomaterials* **2006**, *27*, 1140–1151.
303. Melchels, F.P.W.; Blokzijl, M.M.; Levato, R.; Peiffer, Q.C.; Ruijter, M. de; Hennink, W.E.; Vermonden, T.; Malda, J. Hydrogel-based reinforcement of 3D bioprinted constructs. *Biofabrication* **2016**, *8*, 035004.
304. Thomas, A.A.; Kim, I.T.; Kiser, P.F. Symmetrical biodegradable crosslinkers for use in polymeric devices. *Tetrahedron Letters* **2005**, *46*, 8921–8925.
305. De Hoe, G.X.; Zumstein, M.T.; Tiegs, B.J.; Brutman, J.P.; McNeill, K.; Sander, M.; Coates, G.W.; Hillmyer, M.A. Sustainable Polyester Elastomers from Lactones: Synthesis, Properties, and Enzymatic Hydrolyzability. *Journal of the American Chemical Society* **2018**, *140*, 963–973.
306. Stubbe, B.G.; Horkay, F.; Amsden, B.; Hennink, W.E.; De Smedt, S.C.; Demeester, J. Tailoring the Swelling Pressure of Degrading Dextran Hydroxyethyl Methacrylate Hydrogels. *Biomacromolecules* **2003**, *4*, 691–695.
307. Polo Fonseca, L.; Bergamo Trinca, R.; Isabel Felisberti, M. Thermo-responsive polyurethane hydrogels based on poly(ethylene glycol) and poly(caprolactone): Physico-chemical and mechanical properties: ARTICLE. *J. Appl. Polym. Sci.* **2016**, *133*.
308. Rutkowska, M.; Jastrzębska, M.; Janik, H. Biodegradation of polycaprolactone in sea water. *Reactive and Functional Polymers* **1998**, *38*, 27–30.
309. Rutkowska, M.; Krasowska, K.; Heimowska, A.; Kowalczyk, M. Degradation of the blends of natural and synthetic copolyesters in different natural environments. *Macromol. Symp.* **2003**, *197*, 421–430.
310. Stolt, M.; Krasowska, K.; Rutkowska, M.; Janik, H.; Rosling, A.; Södergård, A. More on the poly(L-lactide) prepared using ferrous acetate as catalyst. *Polym. Int.* **2005**, *54*, 362–368.
311. Rahaman, Md.H.; Tsuji, H. Hydrolytic degradation behavior of stereo multiblock and diblock poly(lactic acid)s: Effects of block lengths. *Polymer Degradation and Stability* **2013**, *98*, 709–719.
312. Porjazoska, A.; Kayaman-Apohan, N.; Karal-Yilmaz, O.; Cvetkovska, M.; Baysal, K.; Baysal, B.M. Synthesis and characterization of glycolide, L-lactide, and PDMS-based terpolymers as a support for cell cultures. *Journal of Biomaterials Science, Polymer Edition* **2002**, *13*, 1119–1134.
313. Mei, F.; Peng, Y.; Lu, S.; Sun, F.; Zhang, Y.; Ge, C.; Zhang, Y.; Gu, H.; Wang, Y.; Zhao, X.; et al. Synthesis and Characterization of Biodegradable Poly(lactic-co-glycolic acid). *Journal of Macromolecular Science, Part B* **2015**, *54*, 562–570.
314. Wang, Y.; Ameer, G.A.; Sheppard, B.J.; Langer, R. A tough biodegradable elastomer. *Nature Biotechnology* **2002**, *20*, 602.
315. Nijst, C.L.E.; Bruggeman, J.P.; Karp, J.M.; Ferreira, L.; Zumbuehl, A.; Bettinger, C.J.; Langer, R. Synthesis and Characterization of Photocurable Elastomers from Poly(glycerol-co-sebacate). *Biomacromolecules* **2007**, *8*, 3067–3073.
316. Jin, T.-X.; Liu, C.; Zhou, M.; Chai, S.; Chen, F.; Fu, Q. Crystallization, mechanical performance and hydrolytic degradation of poly(butylene succinate)/graphene oxide nanocomposites obtained via in situ polymerization. *Composites Part A: Applied Science and Manufacturing* **2015**, *68*, 193–201.

317. Dai, X.; Qiu, Z. Crystallization kinetics, morphology, and hydrolytic degradation of novel biobased poly(butylene succinate-co-decamethylene succinate) copolyesters. *Polymer Degradation and Stability* **2017**, *137*, 197–204.
318. Qiu, S.; Zhang, K.; Su, Z.; Qiu, Z. Thermal behavior, mechanical and rheological properties, and hydrolytic degradation of novel branched biodegradable poly(ethylene succinate) copolymers. *Polymer Testing* **2018**, *66*, 64–69.
319. Sangroniz, A.; Gonzalez, A.; Martin, L.; Irusta, L.; Iriarte, M.; Etxeberria, A. Miscibility and degradation of polymer blends based on biodegradable poly(butylene adipate-co-terephthalate). *Polymer Degradation and Stability* **2018**, *151*, 25–35.
320. Kasuya, K.; Takagi, K.; Ishiwatari, S.; Yoshida, Y.; Doi, Y. Biodegradabilities of various aliphatic polyesters in natural waters. *Polymer Degradation and Stability* **1998**, *59*, 327–332.
321. Lei, L.; Ding, T.; Shi, R.; Liu, Q.; Zhang, L.; Chen, D.; Tian, W. Synthesis, characterization and in vitro degradation of a novel degradable poly((1,2-propanediol-sebacate)-citrate) bioelastomer. *Polymer Degradation and Stability* **2007**, *92*, 389–396.
322. Sun, Z.-J.; Wu, L.; Huang, W.; Zhang, X.-L.; Lu, X.-L.; Zheng, Y.-F.; Yang, B.-F.; Dong, D.-L. The influence of lactic on the properties of Poly (glycerol–sebacate–lactic acid). *Materials Science and Engineering: C* **2009**, *29*, 178–182.
323. Ding, T.; Liu, Q.; Shi, R.; Tian, M.; Yang, J.; Zhang, L. Synthesis, characterization and in vitro degradation study of a novel and rapidly degradable elastomer. *Polymer Degradation and Stability* **2006**, *91*, 733–739.
324. Lu, L.; Garcia, C.A.; Mikos, A.G. In vitro degradation of thin poly(DL-lactic-co-glycolic acid) films. *J. Biomed. Mater. Res.* **1999**, *46*, 236–244.

Chapter II	Hydrolyzable polymer additive-based silicone elastomers	109
II.1.	Introduction	109
II.2.	Hydrolyzable polymer additives	110
II.2.1.	Requirements for the hydrolyzable polymer additives	110
II.2.2.	Preparation of polymer additives	113
II.2.3.	Physico-chemical properties of the hydrolyzable polymer additives	114
II.2.4.	Hydrolysis mechanisms of the polymer additives	115
II.2.4.1.	Hydrolysis mechanism of PCL-based polymers	115
II.2.4.2.	Hydrolysis mechanism of PMATM2	116
II.2.5.	Wettability properties of the hydrolyzable polymer additives	117
II.3.	Preparation of silicone-based coatings	118
II.3.1.	Choosing a model system	118
II.3.1.1.	Choice of the PDMS oil	119
II.3.1.2.	Choice of the crosslinker	119
II.3.1.3.	Choice of the catalyst	120
II.3.2.	Blend with additives	120
II.3.2.1.	Choice of the additive amount	120
II.3.2.2.	Choice of the solvent	121
II.3.2.3.	Formulation process	121
II.4.	Characterization of coatings	122
II.4.1.	Mass loss test	123
II.4.2.	Surface properties	126
II.4.2.1.	Preliminary study on PDMS	126
II.4.2.2.	Roughness measurements	131
II.4.2.3.	Contact angle measurements and surface free energies	133
II.4.2.3.1.	Dynamic water contact angles	133
II.4.2.3.2.	Surface free energy	137
II.4.2.3.3.	Modified time lag method	139
II.4.2.4.	Infrared spectroscopy	140
II.4.3.	Bulk properties	149
II.4.3.1.	Differential scanning calorimetry analyses	149
II.4.3.2.	Elastic modulus	151
II.5.	Conclusion	154

II.6. Bibliographical references.....157

Chapter II Hydrolyzable polymer additive-based silicone elastomers

II.1. Introduction

It was previously mentioned in Chapter I that since the ban of TBT-SPC, the industrial and academic researchers have focused more and more their research works on developing hydrophobic fouling release coatings (FRCs) which prevent the accumulation of biofouling thanks to a self-cleaning effect under hydrodynamic conditions. With the exception of few fluorine-based polymers, PDMS elastomers have been the most used polymers for fouling release purposes due to their low values of surface energy, elastic modulus and surface roughness.

Many researches have been devoted to the addition of different kinds of surface-active compounds in fouling release coatings to decrease the amount of biofouling [1]. Various articles described the improved biofouling inhibition abilities thanks to the use of non-reactive amphiphilic copolymers in FRCs, mainly based on non-hydrolyzable fluorinated, siloxane and oxyalkylane moieties [1–7]. Long-term fouling release protection of these coatings were proved to be dictated by both the hydrophobic and the hydrophilic blocks of the amphiphilic additives. This strategy is revolutionary for FRCs since the physico-chemical properties of the surface are significantly modified with relatively small amounts of additives (≤ 10 wt.%) while the advantageous bulk properties of PDMS elastomers (i.e. low elastic modulus) are maintained.

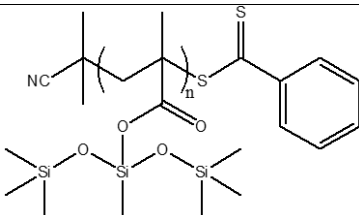
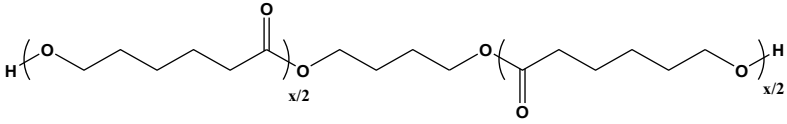
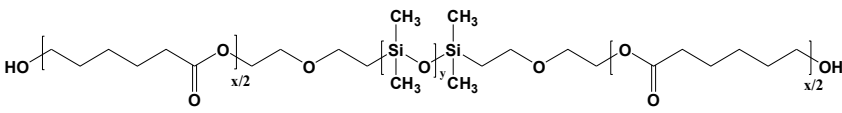
In this PhD work, novel surface-active FRCs are designed with the introduction of hydrolyzable polymer additives in a silicone elastomer. These hydrolyzable polymer additives are expected to migrate more or less quickly towards the upper surface, creating some hydrophilic and/or hydrolyzable regions among the hydrophobic PDMS phase. Thus, these coatings would behave as chemical evolving surfaces which improve the fouling release and antifouling properties during static periods, without the use of biocides.

In the first part, the criteria which helped us to select three polymer additives as surface-active and hydrolyzable polymer additives are presented. Their physico-chemical properties and hydrolysis kinetics are described and discussed.

Chapter II. Hydrolyzable polymer additive-based silicone elastomers

Among the three polymers, one is a synthetic poly(bis(trimethylsilyloxy)methylsilyl methacrylate) (PMATM2) (A), the second one is a commercial poly(ϵ -caprolactone) (PCL) (B) and the last one is a commercial triblock copolymer PCL-*b*-PDMS-*b*-PCL (C) (Table II-1).

Table II-1. Chemical structures of the three hydrolyzable polymer additives

A	
B	
C	

In the second part, the formulation conditions of the cured PDMS system are studied. The blend of 5 to 20 wt.% of the hydrolyzable polymer additives into the PDMS matrix is also described.

In the last part, the resulting coatings were physically and chemically characterized to evaluate their surface properties before and after water immersion. A mass loss test will give information on the kinetics of hydrolysis and releasing of the embedded hydrolyzable polymer additives. The bulk properties are also studied such as the elastic modulus since it is a key parameter for fouling release properties.

II.2. Hydrolyzable polymer additives

II.2.1. Requirements for the hydrolyzable polymer additives

To obtain hydrolyzable polymer additive-based silicone elastomers, the polymer additives needed to fulfill a certain number of requirements:

1) To be hydrolyzable

The hydrolysis property is directly related to the water uptake of a polymer. The more water a polymer will absorb, the more hydrolytic cleavages it will undergo. This is why the crystallinity of the polymer is an essential parameter to consider. It is well-known that amorphous regions in a polymer are faster hydrated than crystalline regions [8]. Generally, a glass transition temperature below the temperature of the surrounding aqueous medium favors the water diffusion within the polymer bulk thanks to its non-organized and mobile chains structure that gives numerous access paths. A low crystallinity will also favor a fast hydrolysis. The hydrolysis kinetics and mechanism of the pure polymer are essential to predict the durability of the polymer in an aqueous media. Nevertheless, the hydrolysis of the polymer additives incorporated in the hydrophobic PDMS elastomer will necessarily be limited by the slow water progression within the PDMS. The ultimate goal of the addition of hydrolyzable polymers in a hydrophobic matrix is to generate a chemically unstable surface. This instability can either come from the detachment and release of small degradation products and/or the apparition of hydrophilic functions after the hydrolysis reaction. Polymers with hydrolyzable backbones (PCL and PCL-*b*-PDMS-*b*-PCL) and hydrolyzable pendant groups (PMATM2) were chosen according to their various hydrolysis kinetics shown in Chapter I (§ 1.6.2.).

2) To have a low toxicity towards the aquatic environment

Marine pollution is a serious worldwide concern coming partly from the accumulation of plastics on the seabed and ocean floors. It is thus really important to choose the less toxic and persistent polymers to limit harmful effects in the marine compartment. Marine biodegradable polymers are the most preferred candidates for this application.

3) To be compatible with the silicone elastomer

Marabotti et al. mentioned the incompatibility between a copolymer and a polymer matrix as a trigger for surface segregation [9]. To avoid phase separation issues between a (homo)polymer additive (other than PDMS) and a silicone matrix, the molar mass of the polymer additive should be the lowest possible ($< 4,000$ g/mol). A possible solution to avoid major incompatibility is to use PDMS-based diblock (AB) or triblock (ABA) copolymers [4].

In this PhD work, a triblock copolymer (PCL-*b*-PDMS-*b*-PCL) containing a PDMS central block and polyester side blocks will be tested as an additive for novel FRCs. Its corresponding polyester homopolymer (A) which is the poly(ϵ -caprolactone), was used to conclude on the necessity of a PDMS flexible block for the additive dispersion in the silicone elastomer.

A poly(silyl methacrylate) was also selected (PMATM2), its siloxane pendant groups can guarantee its good compatibility in the PDMS elastomer.

The final objectives are the best dispersion of the polymer additives within the silicone matrix and the conservation of silicone elastic properties. To optimize the dispersion, a good solvent for both the silicone oil and the hydrolyzable polymer additives must be chosen.

4) To be able to diffuse within the silicone elastomer

The diffusion of the hydrolyzable polymer additives towards the surface is essential to replenish the surface with molecules from the bulk of the coating. In this way, it would maintain the amphiphilic character of the coating surface. The parameters influencing the diffusion process are mainly the molar mass and chemical nature of the polymer additive. For example, non-reactive PDMS homopolymers can diffuse in a PDMS elastomer with diffusion rates from 2.10^{-12} m²/s to 8.10^{-12} m²/s with molecular weight ranging from 3,000 to 5,000 g/mol [10–12]. According to Noguez et al., diblock copolymer additives (PEG-*b*-PDMS) were able to diffuse in a PDMS elastomer with diffusion rates superior to 5.10^{-12} m²/s as long as the molecular weight did not exceed 4,000 g/mol [4].

The addition of a PDMS block or siloxane pendant groups within a (co)polymer can thus markedly enhance the migration of the copolymer additive within a PDMS elastomer. The comparison of the surface physico-chemical properties between the PCL and PCL-*b*-PDMS-*b*-

PCL-based PDMS coatings will show the benefit or not of the presence of a PDMS flexible anchoring group in the additive.

In brief, taking into account the previous criteria, three polymers with variable chemical structures (ABA or A), molar mass, crystallinity and therefore different hydrolysis kinetics were selected.

II.2.2. Preparation of polymer additives

Poly(bis(trimethylsilyloxy)methylsilyl methacrylate) (PMATM2) was synthesized by Radical Addition-Fragmentation Chain Polymer Transfer (RAFT) already described by Lejars et al. [13] (Figure II-1). The RAFT polymerization is a controlled radical polymerization which enables to obtain a polymer with a targeted molecular weight and a narrow dispersity.

The presence of a Chain Transfer Agent (CTA) establishes an equilibrium between dormant and active chains. In this way, all polymer chains will grow in a similar way contrary to conventional radical polymerization in which the chains grow randomly and result in a wide dispersity. The polymerization of MATM2 in anhydrous xylene was performed at 75°C for 20h to achieve a conversion of 96 %. The resulting polymer was not precipitated in methanol as previous assays of precipitation have led to the premature hydrolysis of PMATM2. For this reason, PMATM2 was kept in the xylene reaction mixture under argon before immediate formulation to preserve it from hydrolysis. The remaining monomer (4 mol.%) were thus not removed from the final polymer. The final number-average molar mass was 5,500 g/mol (the target value was 5,000 g/mol) with a dispersity value of 1.26. The amount of hydrolyzed pendant groups was estimated at 3 mol.% by ¹H NMR with the appearance of peaks at 0.25-0.27 ppm (the hydrolysis may have occurred during the NMR tube preparation or the storage).

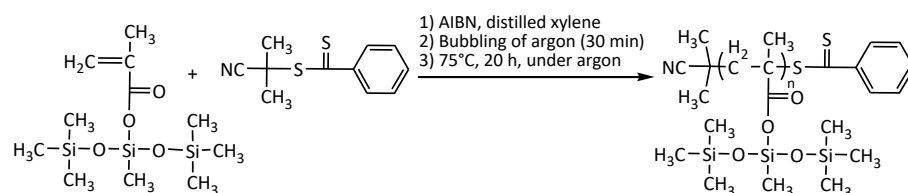


Figure II-1. Synthesis of poly(bis(trimethylsilyloxy)methylsilyl methacrylate) with cyanoisopropyl dithiobenzoate as CTA.

Chapter II. Hydrolyzable polymer additive-based silicone elastomers

Commercial PCL and PCL-*b*-PDMS-*b*-PCL were used as received without further purification. OH-terminated PCL (or PCL diol) was a white soft material from Perstrop with a molar mass of 3,000 g/mol according to the technical data sheet. PCL-*b*-PDMS-*b*-PCL was a waxy solid shaped into pellets received from Evonik.

II.2.3. Physico-chemical properties of the hydrolyzable polymer additives

The three polymer additives displayed molar masses below 10,000 g/mol according to the size exclusion chromatography (SEC) (Table II-2). The PCL-*b*-PDMS-*b*-PCL triblock copolymer with blocks of respective molar masses 2,300-*b*-2,200-*b*-2,300 exhibited a lower crystallinity ($X_c = 28\%$) than a PCL of 4,000 g/mol ($X_c = 77\%$) and a PCL of 2,000 g/mol ($X_c = 60\%$) due to its central PDMS block which brings flexibility to the polymer chain. PCL and PCL-*b*-PDMS-*b*-PCL are semi-crystalline polymers with melting temperature (T_m) values around 50–55°C, while PMATM2 is totally amorphous. At room temperature, this methacrylic polymer is very sticky, and has a glass transition temperature (T_g) value at -20°C.

Table II-2. Characterization data of the polymer additives.

	PCL	PCL- <i>b</i> -PDMS- <i>b</i> -PCL	PMATM2
$M_{n,NMR}$ (g/mol)	3,000	6,800	5,700
$M_{n,SEC}$ (g/mol)	2,800 ^b	7,300 ^a	5,500 ^b
Dispersity, \bar{D}	1.28 ^b	1.32 ^a	1.26 ^b
T_g (°C)	-60 ^c	n.d. ^d	-20 ^e
T_m (PCL) (°C)	51	52-56	-
$\Delta H_{m,sample}$ (PCL) (J/g)	87	57	-
X_c (PCL)(%) ^f	62	28	0

^a Determined by SEC (toluene, PS standards);

^b Determined by TD-SEC (THF) with $dn/dc = 0.044$ mL/g in THF for PMATM2 and $dn/dc = 0.071$ mL/g in THF for PCL [13,14];

^c Determined by modulated DSC;

^d Not determined for both blocks; ^e Determined by conventional DSC;

^f Degree of crystallinity $X_c(\%) = \frac{w(\text{PCL}) \times \Delta H_m \times 100}{\Delta H_m^0}$ with $\Delta H_m^0 = 139.3 \frac{\text{J}}{\text{g}}$ and $w(\text{PCL}) = 0.68$ (mass fraction of PCL) for PCL-*b*-PDMS-*b*-PCL [8].

II.2.4. Hydrolysis mechanisms of the polymer additives

The knowledge of the hydrolysis mechanism is essential to explain the degradation kinetics of the polymers in their pristine state.

II.2.4.1. Hydrolysis mechanism of PCL-based polymers

PCL-based polymers belong to the family of aliphatic polyesters which undergo hydrolytic cleavages within their main chains in seawater (Figure II-2 and Figure II-3). Their hydrolytic degradation follows three steps:

- (i) Water diffuses through the amorphous phases of the polymer (hydration step);
- (ii) Once the water reaches some available ester functions, it divides the chain into oligomers or monomers of caproic acid;
- (iii) These degradation products (oligomers or monomers of caproic acid) can self-catalyse the hydrolytic reactions thanks to the accumulation of carboxylic acid functions within the bulk before being released in the water.

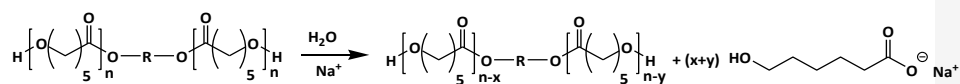


Figure II-2. Hydrolysis reaction of poly(ϵ -caprolactone) in seawater.

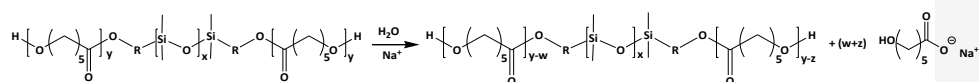


Figure II-3 Hydrolysis reaction of PCL-*b*-PDMS-*b*-PCL in seawater.

PCL is a hydrophobic semi-crystalline polymer whose hydrolysis strongly depends on its crystallinity. PCL was considered to undergo a bulk erosion in demineralized water [15]. Nonetheless, this assumption was contradicted by Lim et al., as they observed negligible changes in M_w for a PCL suggesting a surface erosion after 14 days at 37°C in a 0.5 M of sodium hydroxide ($M_w(\text{PCL}) = 118,000 \text{ g/mol}$, $X_c(\text{PCL}) = 44.2\text{-}62.2 \%$) [16].

Chapter II. Hydrolyzable polymer additive-based silicone elastomers

PCL is often used in combination with other hydrolyzable polymers to form binders for Self-Polishing Coatings in research papers [17–22]. Its low hydrolysis kinetics can be interesting to obtain the desired hydrolysis profile and thus achieve long-lasting antifouling effect through an erosion process.

According to Azemar et al., PCL (3,000 g/mol) and PCL-*b*-PDMS-*b*-PCL (\approx 2,850-*b*-2,300-*b*-2,850) hydrolyzed very slowly. Around 2 wt.% and 17 wt.% of $M_{n,SEC}$ loss was shown after 50 days in deionized water [8]. Hydrolytic kinetics of other PCL-based polymers are also detailed in Table II-3.

Table II-3. Hydrolysis kinetics for PCL-based polymers in deionized water (taken from [8]).

Polymer	M_n (g/mol)	X_c (%)	Mass loss (%) (20 d)	Mass loss (%) (150 d)	Mass loss (%) (350 d)
PCL3000	2900	54	1	15	24
PCL- <i>b</i> -PDMS- <i>b</i> -PCL	1700- <i>b</i> -2300- <i>b</i> - 1700	16	1	10	11
PCL- <i>b</i> -PDMS- <i>b</i> -PCL	3400- <i>b</i> -2300- <i>b</i> - 3400	33	5	35	45

II.2.4.2. Hydrolysis mechanism of PMATM2

Contrary to PCL, PMATM2 undergoes a hydrolytic degradation of its pendant groups in seawater (Figure II-4). As an amorphous polymer, PMATM2 degrades faster than PCL. The complete hydrolysis of PMATM2 leads to the formation of poly(methacrylic acid) (PMAA). To assess its hydrolytic degradation, PMATM2 was immersed in distilled water at ambient temperature. After 9 days, it exhibited 30 wt.% of mass loss. The test was not continued further given that the surface displayed many cracks and was starting to fall into small pieces as it became brittle.

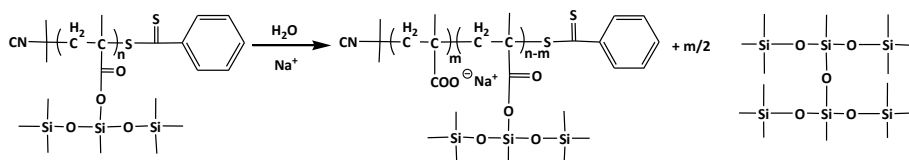


Figure II-4. Hydrolysis reaction of PMATM2 in seawater.

II.2.5. Wettability properties of the hydrolyzable polymer additives

The wettability of the three polymer additives was compared with the PDMS elastomer. The advancing contact angle highlights the contribution of the hydrophobic phases at the polymer surface while the receding contact angle highlights the contribution of the hydrophilic phases at the polymer surface (Figure II-5, **A**), as reported by Duong et al. [23].

The three polymers are hydrophobic with water advancing contact angle ($\theta_{w,adv}$) values higher than 100° , similar to the PDMS reference (Figure II-5, **B**). The most hydrophobic polymers were PMATM2 and PCL-*b*-PDMS-*b*-PCL with $\theta_{w,adv}$ values around 115° . This result can be explained by a denser surface coverage of dimethylsiloxane functions which have reoriented towards the polymer surface thanks to their flexible siloxane chains.

The three hydrolyzable polymers also showed water receding contact angles ($\theta_{w,rec}$) around $40-55^\circ$ against 96° for the PDMS elastomer (Figure II-5, **B**). The resulting contact angle hysteresis values ($\Delta\theta = \theta_{w,adv} - \theta_{w,rec}$) of the hydrolyzable polymers are thus higher than that of the PDMS elastomer. This difference of $\Delta\theta$ can be due to different reasons: **(i)** surface heterogeneities (microphase separation or roughness), **(ii)** chemical surface modifications caused by a molecular reorganization or **(iii)** by hydrolysis reactions.

In the case of PCL, the polar functionalities such as hydroxyl (-OH) or carbonyl (-C=O) functions were certainly reoriented towards the surface/water interface **(ii)**, explaining the higher contact angle hysteresis compared to PDMS reference.

In the case of PCL-*b*-PDMS-*b*-PCL, the higher $\Delta\theta$ can be due to both **(i)** and **(ii)** given that there could be both hydrophobic and hydrophilic blocks at the surface/water interface (surface microphase segregation).

In the case of PMATM2, the large contact angle hysteresis is mainly explained by the fast hydrolysis of the siloxane pendant groups **(iii)** leading to the apparition of carboxylic acid functionalities at the surface/water interface.

Thanks to these dynamical contact angles (DCA) measurements, it will be possible to know if the hydrolyzable polymer additives are present on the PDMS elastomer and/or migrate towards its surface, while comparing with the PDMS reference.

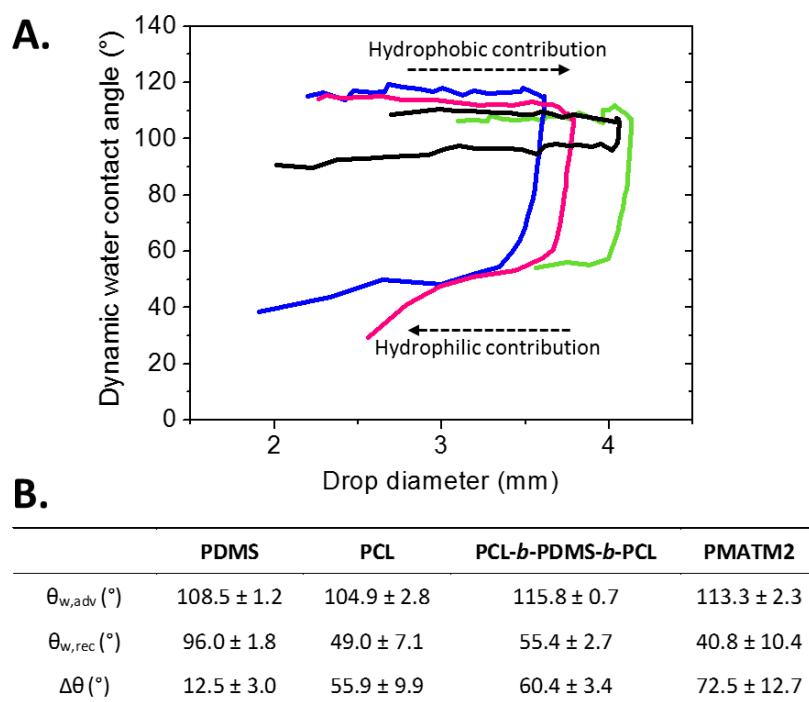


Figure II-5. (A.) Hysteresis curves of water contact angles of PDMS elastomer (black line), PCL (green line), PCL-*b*-PDMS-*b*-PCL (blue line) and PMATM2 (pink line). (B.) DCA values of the polymer additives films in comparison with the PDMS elastomer reference (contact angle values are the average of 3 advancing and receding cycles).

II.3. Preparation of silicone-based coatings

In this chapter, a silicone elastomer is chosen as the binder for the hydrolyzable polymer additives. The choice of the compounds used to form the silicone elastomer are commented in the following text.

II.3.1. Choosing a model system

A PDMS model system is used in this PhD project as a simplified representation of a conventional FRC. This model system intends to reduce the amount of components commonly

Chapter II. Hydrolyzable polymer additive-based silicone elastomers

used in antifouling paints (such as pigments, fillers, etc.) to reduce complexity while interpreting the analyses. Indeed, the main purpose was to only evaluate the impact of the hydrolyzable polymer additives on the silicone elastomer surface and bulk properties.

The model system can be described as a mixture of a bis-silanol PDMS oil, a crosslinker, a catalyst and some solvent. For all coatings prepared in this PhD work, no biocide is added.

II.3.1.1. Choice of the PDMS oil

The molar mass of the bis-silanol PDMS was chosen based on a commercial filled PDMS model: the condensation cure RTV11. This commercial silicone elastomer is often used as a control for FRCs assessment. To obtain a similar elastic modulus to RTV11, it was decided to select a PDMS oil within the same range of molar mass. RTV11 was centrifuged to separate the fillers from the PDMS oil. The number-average molar mass of the PDMS oil was found to be 33,700 g/mol ($\bar{M}_n = 2.1$) by size exclusion chromatography (SEC) in toluene using polystyrene standards. It was decided to select a bis-silanol PDMS of 23,700 g/mol ($\bar{M}_n = 1.8$) to form the condensation-cured silicone network. The apparent molar mass between crosslinks (M_c) was shown to have very small influence on the diffusion coefficient (D) of small molecules (with D proportional to $M_c^{0.2}$) [24]. A hydrosilylation-cured PDMS would have been conceivable too but as it often requires a higher reaction temperature (varying from 65 to 180°C), thus a room temperature vulcanized PDMS by condensation was more convenient to process.

II.3.1.2. Choice of the crosslinker

The crosslinker or curing agent was the same as the one used in RTV11 elastomer. It consists in an alkoxy-based polysilicate or polydiethoxysiloxane (PDES). This crosslinker exhibits a molar mass of 744 g/mol making it less volatile than the commonly used tetraethoxysilane (TEOS). After complete hydrolysis of the ethoxysiloxane functions, the crosslinker can react with the bis-silanol PDMS oil.

The PDMS:crosslinker mass ratio was an important parameter as it influences the stiffness of the silicone elastomer. Indeed, the more crosslinker is added, the more rigid the network will be. For example, with a 100:3 mass ratio (PDMS/crosslinker from Sylgard 184, Dow Corning), the resulting elastic modulus was 0.5 MPa whereas with 100/20, the resulting elastic modulus

Chapter II. Hydrolyzable polymer additive-based silicone elastomers

was 3.6 MPa [25]. According to the composition of some silicone-based FRCs, it is possible to find PDMS/crosslinker mass ratios ranging from 100/2 to 100/15 [2,26–29]. In this PhD work, the targeted elastic modulus was ≈ 1 MPa, achieved by a PDMS/PDES ratio of 100/4.4.

II.3.1.3. Choice of the catalyst

The catalyst used in this PhD work is dioctyltin dilaurate (DOTDL). Tin-based catalysts are known to be the efficient catalysts for the hydrolysis and condensation reactions of organosilane-based systems [30]. It should be mentioned that tin-based catalysts are generally mutagenic or reprotoxic [31], this is why only a very small amount of tin-based catalyst was added in our formulations (0.1 wt.% relative to the PDMS oil). The European regulation has fixed a limit of 0.1 wt.% of tin content in RTV11 [32]. The tin-based catalyst used in this PhD work has a tin content of 15.5-17 % which gives a tin percentage in the elastomer lower than 0.02 %. At this level, the Sn toxicity should not intervene in the antifouling effect.

After exposition to seawater, the PDMS elastomer exhibits a white layer probably due to side reactions involving the crosslinker and/or tin catalyst (Figure II-6). The causes of this white layer will be further discussed in § II.4.2.3.1. To limit this phenomenon, all the analyses were performed in deionized water.

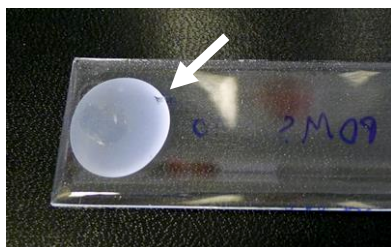


Figure II-6. Photograph of a seawater droplet left on the condensation cure PDMS overnight causing white bloom on surface beneath it.

II.3.2. Blend with additives

II.3.2.1. Choice of the additive amount

The amount of hydrolyzable polymer additives was varied from 5 to 15 wt.%. Given that PMATM2 showed a better compatibility in the silicone elastomer, 20 wt.% was also tested.

Chapter II. Hydrolyzable polymer additive-based silicone elastomers

These amounts were chosen based on what is commonly found in the literature for additive-containing FRCs as previously mentioned in Chapter I (§ I.5.1.2.). The additive loading had to be sufficient to influence the PDMS surface chemistry but not excessive to preserve its elastomer properties.

II.3.2.2. Choice of the solvent

Commercial silicone elastomers such as RTV11, RTV2, etc. usually do not contain solvent. In this study, it was necessary to add solvent to dissolve the polymer additives. For two substances to be miscible, their solubility parameter, δ , (also referred as solubility parameter or Hildebrand value) must be similar. The solubility parameter of xylene ($\delta = 8.9 \text{ cal}^{1/2} \cdot \text{cm}^{-3/2}$) shows that it is an excellent solvent for PDMS ($\delta = 7.3 \text{ cal}^{1/2} \cdot \text{cm}^{-3/2}$) and good solvent for PCL ($\delta = 19.5 \text{ cal}^{1/2} \cdot \text{cm}^{-3/2}$) [33,34]. The lower affinity between PCL and xylene is explained by the greater presence of polar forces in PCL ($\delta_p = 4.8 \text{ cal}^{1/2} \cdot \text{cm}^{-3/2}$). The solubility parameter of PMATM2 is unknown but it bears bulky apolar $-\text{SiMe}_3$ groups which help the PMATM2 to be dissolved by xylene.

To provide the best film-forming properties of the coatings, the solvent was tested with different loading from 10 to 40 wt.%. Below 20 wt.%, the polymer additives could not be properly dissolved in the pre-solution. Above 30 wt.%, the resulting coating showed an uneven thickness due to the very low formulation viscosity and the important solvent evaporation that both disturbed the film formation. The amount used in the additive-based coatings ranged from 21 to 26 wt.% in the total formulation depending on the additive content.

II.3.2.3. Formulation process

A pre-mixture of the polymer additives in xylene was slowly added in the PDMS oil. To maximize the dispersion of PCL-based polymers and PMATM2 within the PDMS oil, the resulting mixture was stirred at 1500 rpm for 20 minutes. The catalyst was added dropwise with a clean pipette. The formulations were not placed under vacuum, as it is usually advised in the technical data sheet to remove air bubbles, to avoid any macrophase separation. The solvent content was chosen specially to limit the entrapment of air bubbles thanks to a low viscosity of the formulation.

Chapter II. Hydrolyzable polymer additive-based silicone elastomers

In the following analysis, the nomenclature of the coatings is YYY-BX, where YYY is the type of hydrolyzable polymer additives (PCL for the PCL homopolymer, TGO for the triblock PCL-*b*-PDMS-*b*-PCL and M3T for the PMATM2 homopolymer), B stands for blend, and X corresponds to the mass fraction of the hydrolyzable additive polymer within the dry coating (Figure II-7).

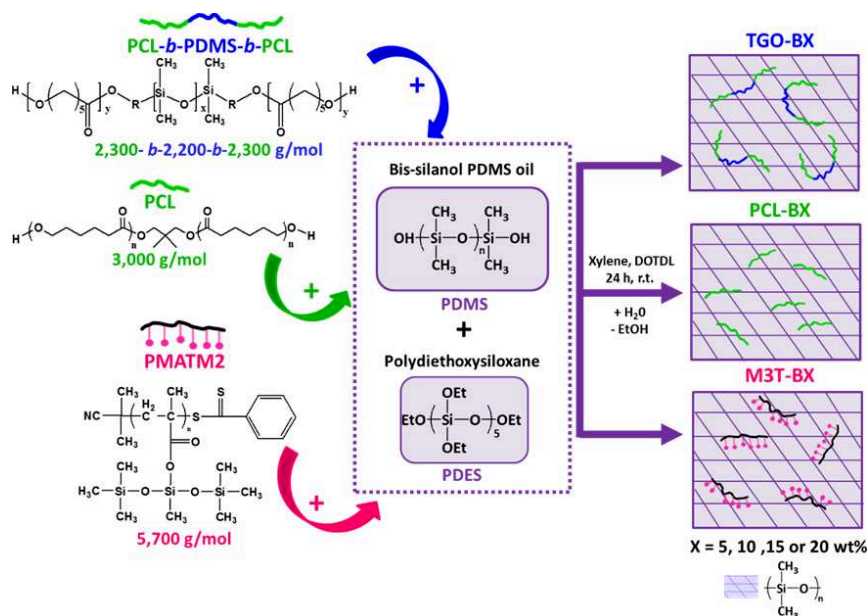


Figure II-7. General pathway for the preparation of hydrolyzable additive-based silicone elastomers.

II.4. Characterization of coatings

As a first step, a hydrolytic degradation test was investigated to evaluate the hydrolysis kinetics of the hydrolyzable polymer additives embedded in the silicone elastomer. Then, surface characterizations of the coatings were carried out to determine the chemical and physical changes during immersion in deionized water. The bulk properties were investigated through DSC analysis to study the influence of the additives on the PDMS thermal properties. Finally, the viscoelastic properties were evaluated before and after a long-term water exposure to observe the impact the water aging on the coatings elastic moduli.

II.4.1. Mass loss test

The additives-based silicone elastomers coated on glass slides were immersed in distilled water at room temperature for 32 weeks to assess the ability of the hydrolyzable polymer additives to hydrolyze when embedded in a hydrophobic elastomer. Aliphatic polyesters such as PCL are expected to degrade very slowly through a bulk erosion [8], whereas PMATM2, bearing silylated ester groups as hydrolyzable pendant groups, is known to quickly hydrolyze [13]. The predominance of the PDMS matrix within our coatings may slow down the water diffusion due to its hydrophobic nature [35]. Nevertheless, the well-known mobility of siloxane bonds does not prevent the migration or diffusion of small polymers inside its bulk.

Figure II-8 shows that the PDMS elastomer coatings comprising PCL or PCL-*b*-PDMS-*b*-PCL exhibited a maximum mass loss values between 0.43 ± 0.02 wt.% and 0.56 ± 0.04 wt.% which was comparable to the additive-free PDMS reference mass loss (0.55 ± 0.04 wt.%) during 32 weeks of immersion. This low mass loss can be due to the loss of tin-compounds or the loss of silica-formed particles or the release of uncrosslinked compounds [36].

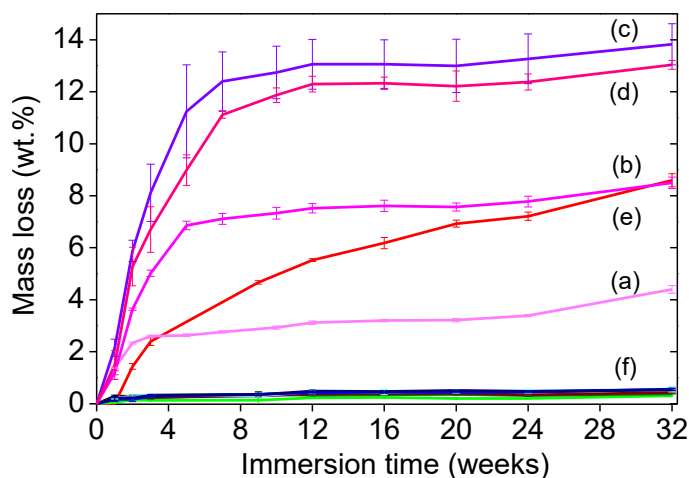


Figure II-8. Mass loss (wt.%) in deionized water at room temperature of (a) M3T-B5, (b) M3T-B10, (c) M3T-B15, (d) M3T-B20, (e) commercial HEMPASIL X3 and (f) the other coatings based on PCL and PCL-*b*-PDMS-*b*-PCL as well as the PDMS reference without additives.

Chapter II. Hydrolyzable polymer additive-based silicone elastomers

The coatings comprising PMATM2 showed a plateau reached after 12 weeks. M3T-B5, M3T-B10, M3T-B15, and M3T-B20 showed mass losses of 3.4 ± 0.1 wt.%, 7.8 ± 0.2 wt.%, 13.3 ± 0.9 wt.%, and 12.4 ± 0.3 wt. % respectively, after 24 weeks of immersion. The mass loss mostly corresponds to the weight fraction of the pendant ester groups released from the blend once hydrolyzed (the cleavable side groups of MATM2 repeating unit correspond to 74 wt.% of the repeating unit molar mass). Thus, this result indicates that some poly(methacrylic acid) (PMAA) chains coming from the PMATM2 hydrolysis remained within the elastomer coatings after 24 weeks of immersion.

A change of color was also observed for M3T-BX coatings upon immersion: the coatings have gone from pink to almost transparent (Figure II-9). This pink color came from the PMATM2 and more particularly to the dithiobenzoate moiety of the PMATM2 backbone. A quick TD-SEC analyses were carried out on the degradation products obtained from the immersion waters of M3T-B15 after 24 weeks of immersion (after lyophilization of the degradation products). The TD-SEC analysis showed 2 peaks: one at an elution volume of 17.65 mL, probably corresponding to the cleaved pendant groups, the other one at [19.21-20.71] mL, probably corresponding to the CPDB RAFT agent as it showed a high peak intensity at $\lambda = 380$ nm with the UV detector (while the initial PMATM2 was eluted at 15.75 mL). This analysis suggests the PMAA was not released at this stage of immersion (24 weeks) and that the color change of coatings came from the cleavage and release of dithiobenzoate moiety.

After 32 weeks of immersion, the mass losses reached 4.4 ± 0.1 wt.%, 8.5 ± 0.2 wt.%, 13.8 ± 0.8 wt.%, and 13.0 ± 0.2 wt. % for M3T-B5, M3T-B10, M3T-B15, and M3T-B20, respectively. The increase of mass loss values at 32 weeks suggests a partial release of PMAA from the coating.

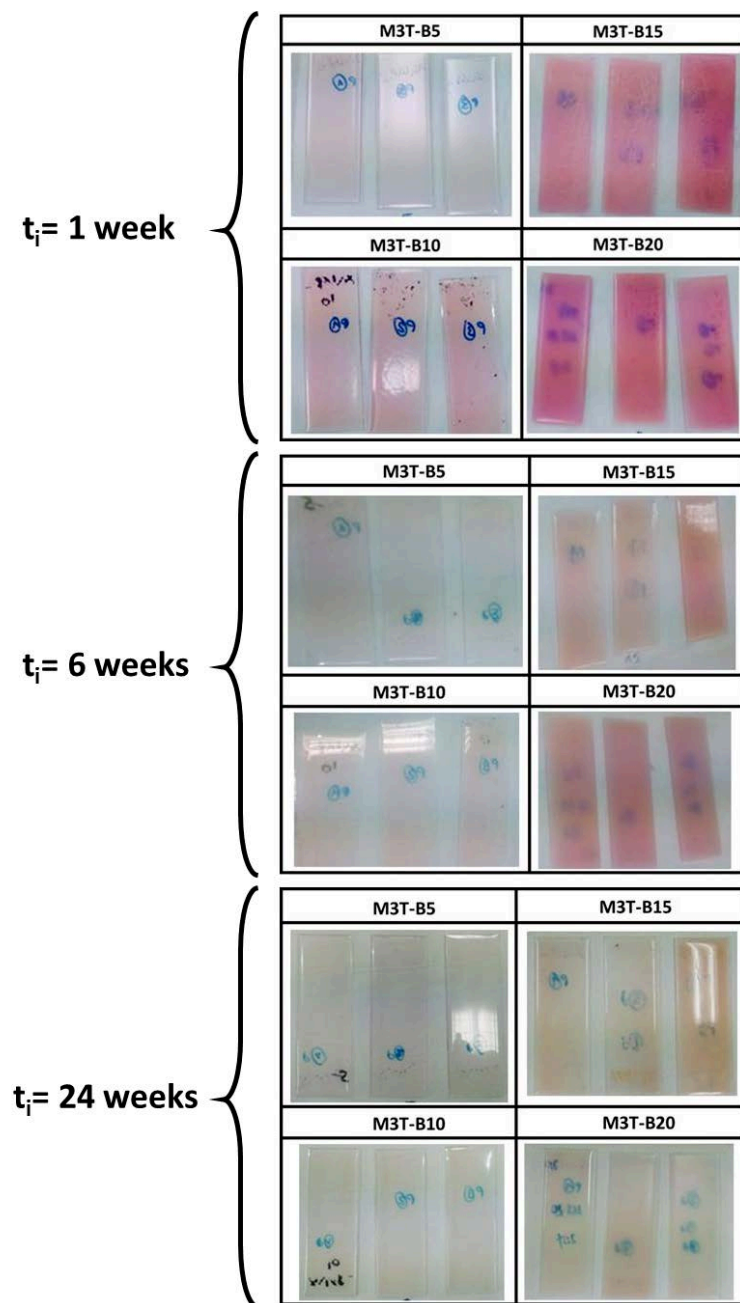


Figure II-9. M3T-BX coated glass slides after different immersion times in deionized water.

Chapter II. Hydrolyzable polymer additive-based silicone elastomers

The commercial hydrogel-based FRC Hemptasil X3 from Hempel (X3) forms a hydrogel layer on the extreme surface [37]. To our knowledge, this coating does not contain any hydrolyzable polymer but exhibits a non-negligible mass loss (up to 8 wt.%) which is due to the leaching of non-bonded (co)polymers.

With this mass loss test, two different kinetics profiles of hydrolysis have been observed for PMATM2 and the PCL-based additives embedded in a silicone matrix. PCL and PCL-*b*-PDMS-*b*-PCL are known to hydrolyze slowly (cf. Table II-3) and their blend in a silicone elastomer reduces even more their hydrolysis kinetics suggesting they are trapped in the hydrophobic silicone matrix with a limited mobility towards the surface and/or access to water. Regarding PMATM2, the siloxane pendant groups may have helped the polymer to migrate faster towards the surface and replenish the surface. M3T-BX showed a reservoir effect of PMATM2 after 12 weeks.

II.4.2. Surface properties

The surface characterization of the coatings is essential to understand the surface segregation/enrichment in hydrolyzable polymer additives. To detect the presence of the hydrolyzable polymer additives on the surface of the silicone elastomer, several analyses were conducted upon water immersion: contact angle measurements, monitoring of the surface chemistry by infrared spectroscopy with attenuated total reflectance (FT-IR ATR) and roughness measurements.

II.4.2.1. Preliminary study on PDMS

A preliminary study was performed to evaluate the dynamic contact angles (DCA) of the PDMS reference during 16 weeks of immersion.

Figure II-10 shows the DCA cycles of PDMS at different immersion times (t_i). At $t_i=0$, the PDMS reference showed values comparable to what is found in the literature as shown in Chapter I (§ I.5.1.2.1.1.) with $\theta_{w,adv} = 108.5 \pm 1.2^\circ$, $\theta_{w,rec} = 96.0 \pm 1.8^\circ$ and $\Delta\theta = 12.5 \pm 3.0^\circ$.

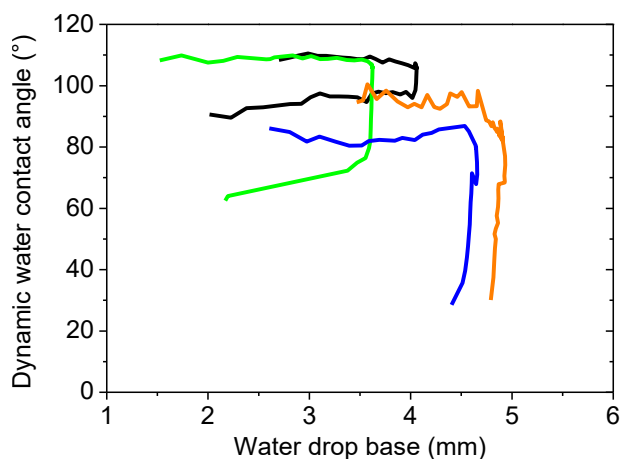


Figure II-10. Advancing/receding water contact angle cycles of the PDMS reference at $t_i = 0$ (black line), $t_i = 2$ weeks (green line), $t_i = 9$ weeks (blue line) and $t_i = 16$ weeks (orange line).

After 2 weeks, $\theta_{w,adv}$ was not modified while $\theta_{w,rec}$ was decreased to $66^\circ \pm 11^\circ$. After 9 weeks, $\theta_{w,adv}$ dropped to 90° while $\theta_{w,rec}$ was barely measurable given that the water droplet never retracted (strongly attached to the surface). At 16 weeks, $\theta_{w,adv}$ increased to 90° while $\theta_{w,rec}$ was still hardly measurable. This unstable wettability behavior was obviously abnormal for such material and certainly due to the rise of a white layer on the surface after immersion (Figure II-11).



Figure II-11. PDMS coating (on a PVC substrate) partially immersed (right side of the panel) in deionized water for 24 h and subsequently dried for 20 min (the immersed area is shown with the white arrow).

Some studies have highlighted the impact of polydiethoxysilane crosslinking agents (TEOS, ES40) on the surface properties [38–41]. These compounds favored the formation of siliceous phases on the surface due to silanol or alkoxy silane functions coming from the self-condensation of alkoxy silane crosslinking agent but also from the non-crosslinked end-chains (silanol) or even the formation of near surface siliceous phases [36,38,41]. These siliceous phases referred as SiO_xOH_y phase or silica domains (SiO_2) can result in a roughness increase which would explain the change of PDMS wettability after water immersion.

Another analysis was able to highlight the growing of this white layer of particles upon water immersion (Figure II-12). Indeed, it was observed by confocal laser scanning microscopy (CLSM) a rising fluorescence intensity on top of the PDMS surface after immersion in deionized water at different times. The protocol of this analysis is described in the experimental section (§ VI.5.4.).

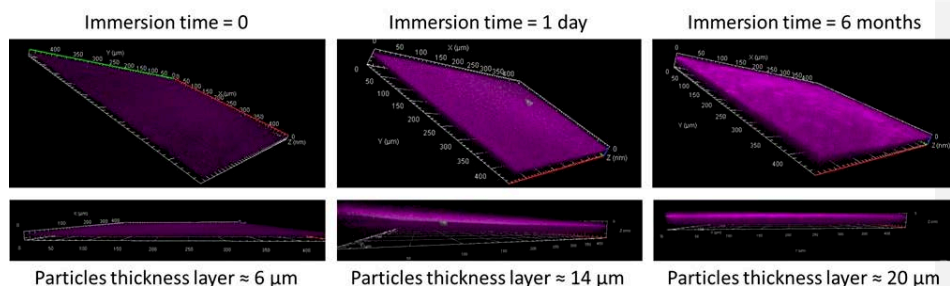


Figure II-12. Evolution of the particles layer thickness on top of the 1-mm thick PDMS reference coating upon static immersion in deionized water. Images are obtained by CLSM ($\times 20$) with a He-Ne laser ($\lambda_{\text{excitation}} = 594 \text{ nm}$ and $\lambda_{\text{emission}} = 633 \text{ nm}$).

A similar phenomenon was observed by Havrilla et al.[42]. They explained that in the virgin material, the tin appeared homogeneously distributed throughout the material but after aging the 4 mm-thick PDMS foam at 50°C for 1 month, it exhibited a $75 \mu\text{m}$ -tin-rich layer on its surface. Thus, the residual tin catalyst could migrate to the surface. This phenomenon poses concerns for the antifouling application as it would bring undesired toxicity onto the PDMS coating. The presence of tin compounds could also induce unwanted chemical reactions with marine salts.

To further elucidate the nature of these particles, PDMS coatings were immersed in three different types of water (ultrapure water, deionized water and artificial seawater). A carbon-based adhesive was placed onto the surface of the immersed coating to remove any particles formed and then was analyzed by scanning electron microscopy with energy dispersive X-ray spectroscopy (SEM-EDX) (Figure II-13).

Figure II-13 shows that the immersion of the PDMS coating in deionized water and artificial seawater led to numerous particles (mainly calcium-based particles) while the immersion of the PDMS coating in ultrapure water showed only a few amount of particles.

Chapter II. Hydrolyzable polymer additive-based silicone elastomers

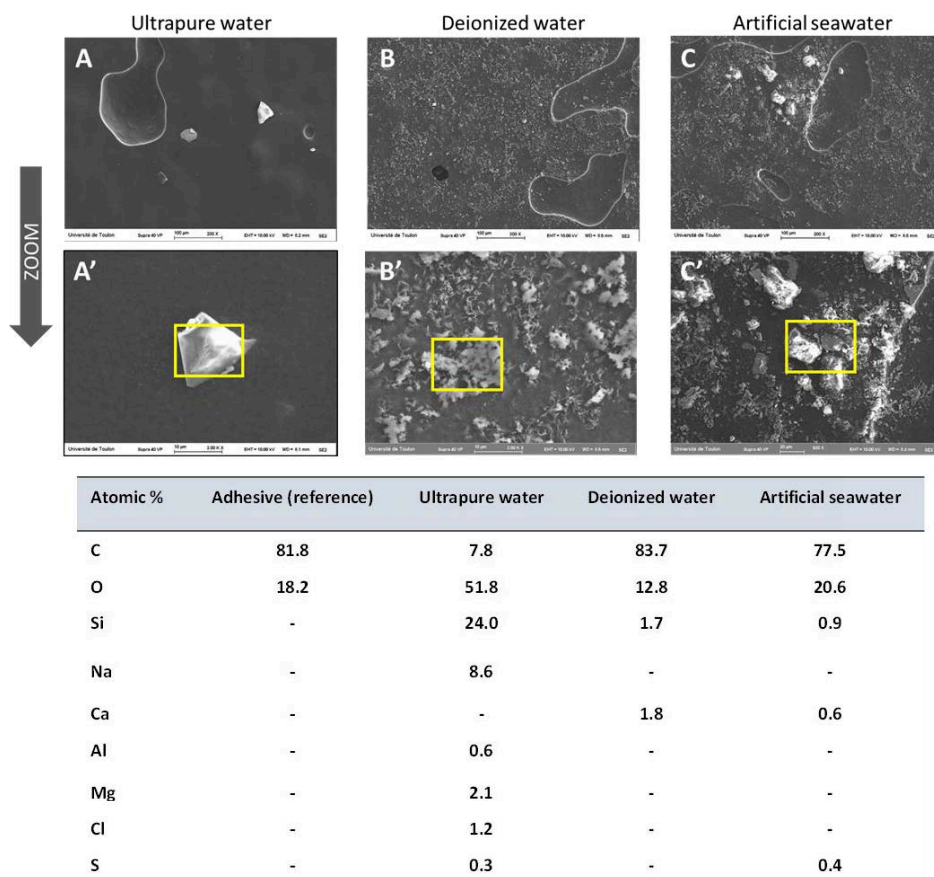


Figure II-13. SEM images of the white layer taken for each coating using a carbon adhesive, after 4 days of immersion, at different magnifications: x200 (A, B, C), x2,000 (A', B') and x500 for C'. The table displays the EDX analysis with the atomic compositions corresponding to the areas framed in yellow.

Given the absence of tin in particles observed by SEM-EDX, the white layer can be attributed to siliceous phases and salts rather than tin-based compounds.

PDMS coatings immersed in the three different aqueous media showed, in most cases, decreasing static water contact angle with large standard deviations during 14 days of immersion (Table II-4). This revealed the unpredictable wettability of the PDMS for short immersion periods occurring no matter what the water composition was.

Chapter II. Hydrolyzable polymer additive-based silicone elastomers

Table II-4. Static water contact angles of identical PDMS coatings immersed in different aqueous media after several immersion times (before measurement, the coatings were gently rinsed with ultrapure water and dried for 4 h).

Immersion time (days)	Ultrapure water	Deionized water	Artificial seawater
0	$\theta_w = 108.3 \pm 0.8^\circ$	$\theta_w = 105.9 \pm 2.6^\circ$	$\theta_w = 110.0 \pm 0.8^\circ$
4	$\theta_w = 109.0 \pm 2.3^\circ$	$\theta_w = 135.0 \pm 6.1^\circ$	$\theta_w = 72.1 \pm 7.5^\circ$
7	$\theta_w = 98.5 \pm 0.9^\circ$	$\theta_w = 104.4 \pm 2.3^\circ$	$\theta_w = 84.2 \pm 4.1^\circ$
14	$\theta_w = 86.2 \pm 1.1^\circ$	$\theta_w = 64.2 \pm 6.3^\circ$	$\theta_w = 94.2 \pm 12.1^\circ$

Due to these observations, the following DCA, surface free energy and roughness investigations were performed in ultrapure water to limit as much as possible this phenomenon and they were also not pursued beyond 3 weeks of immersion since the receding contact angle started to decrease because of the formation of the siliceous layer.

II.4.2.2. Roughness measurements

The roughness measurements are another manner to reveal the presence of the polymer additives on the surface by comparison with the PDMS reference. The surface segregation between the polymer additive and the silicone matrix could indeed lead to an irregular surface topography.

All the coatings were prepared by casting the formulations on glass slides. R_a , the arithmetic average of the surface roughness was measured for all coatings. All the values were measured with a profilometer according to the standard ISO 4288-1996, and are the average of 3 measurements per coating before and after water immersion (Table II-5, Cf. experimental section in chapter VI). The roughness measurements after immersion were performed 6 h after withdrawal from the ultrapure water to let the coatings dry.

Chapter II. Hydrolyzable polymer additive-based silicone elastomers

Table II-5. Coatings roughness values (R_a) at $t_i=0$ and at $t_i=9$ weeks (5 weeks for M3T-BX).

	R_a at $t_i=0$ (μm)	R_a at $t_i=9$ weeks
PDMS	0.13 ± 0.01	0.9 ± 0.1
X3	0.13 ± 0.01	0.24 ± 0.05
PCL-B5	0.28 ± 0.01	2.6 ± 0.5
PCL-B10	0.4 ± 0.1	2.5 ± 0.4
PCL-B15	0.2 ± 0.1	2.7 ± 0.2
TGO-B5	0.42 ± 0.01	1.0 ± 0.7
TGO-B10	1.4 ± 0.3	1.0 ± 0.2
TGO-B15	1.5 ± 0.2	1.6 ± 0.7
M3T-B5	0.6 ± 0.1	1.2 ± 0.4
M3T-B10	0.25 ± 0.02	1.3 ± 0.4
M3T-B15	0.5 ± 0.2	2.1 ± 0.5
M3T-B20	0.5 ± 0.2	8.3 ± 0.9

Before immersion, all the coatings exhibit R_a below $0.6 \mu\text{m}$ except for TGO-B10 and TGO-B15. The presence of PCL blocks on the surface and/or right underneath may explain why TGO-B10 and TGO-B15 values of roughness were slightly higher at *ca.* $1.5 \mu\text{m}$. PCL blocks located on or right underneath the surface may have generated roughness by deforming the PDMS surface. Regarding all the other coatings, the polymer additives did not influence significantly the surface topography. For PCL-BX, R_a is under $0.5 \mu\text{m}$, this would mean the PCL additives were mainly located in the bulk and did not disrupt the surface smoothness of PDMS. Based on the R_a values of M3T-BX, PMATM2 seemed to have no influence on the surface topography probably due to its soft amorphous state at ambient temperature which simulates the PDMS smoothness.

After 9 weeks of immersion, an increase of roughness (from $R_a \approx 0.5$ to $R_a \approx 2 \mu\text{m}$) was observed for all the coatings except for the commercial FRC. To avoid misinterpretations of this roughness increases, it should be reminded the presence of siliceous phases or salt particles onto the condensation cured systems (preliminary study, § II.4.2.1.).

The M3T-BX exhibited brittle surfaces with the presence of cracks on it after only 1 week of immersion and which kept increasing after 5 weeks of immersion (Figure II-14). This made the roughness analysis difficult to realize as the cracks were randomly distributed on the coatings. This observation confirms the depletion of PMATM2 after its hydrolysis. The small pieces of coatings removed from the surface were sources of roughness (R_a could reach $\approx 8 \mu\text{m}$ in some areas after 5 weeks).



Figure II-14. Apparition of cracks on the M3T-BX coatings after 5 weeks

II.4.2.3. Contact angle measurements and surface free energies

Contact angle measurements give information about the hydrophilic or hydrophobic nature of the coating surface, in other words, their wetting properties influenced either by their surface chemistry, their surface heterogeneity and/or their potential chemical reorganization after water exposure. It further enables the determination of the surface free energy (SFE) of the coating when the analysis is performed with more than one probe liquid.

II.4.2.3.1. *Dynamic water contact angles*

The aim of dynamic contact angle (DCA) analysis was to assess whether the hydrolyzable polymer additives are located at the surface rather than trapped in the bulk of the coating. In the case of TGO-BX and PCL-BX coatings, this information is valuable since the mass loss test was not sufficient to assess if polyester segments were present or not on the surface.

As a reminder, PDMS surfaces are known to be hydrophobic and very resistant to surface reorganization in contact with water, resulting in a low contact angle hysteresis ($\Delta\theta = \theta_{w,adv} - \theta_{w,rec}$), i.e. the advancing water contact angle ($\theta_{w,adv}$) and the receding water contact angle ($\theta_{w,rec}$) are broadly similar [38].

▪ Hydrolyzable polymer additives-based coatings

- Before immersion

Figure II-15 shows that all advancing contact angles were around 105-110° indicating that all the coatings were hydrophobic before immersion. The hydrogel-based commercial FRC displayed a $\theta_{w,adv}$ slightly lower than the experimental coatings in accordance to literature results ($\theta_{w,adv} = 96 \pm 1^\circ$) [43].

As expected, the PDMS reference showed a $\theta_{w,rec}$ of $96.0 \pm 1.8^\circ$ which means there was no significant surface reorganization. PCL-BX had $\theta_{w,rec}$ around 70-90° suggesting the very small amount of PCL present on the surface given that it is very closed to the $\theta_{w,rec}$ of the PDMS reference and higher than the $\theta_{w,rec}$ of the pure PCL which was of $49 \pm 7.1^\circ$ (cf. § II.2.5).

The $\theta_{w,adv}$ of M3T-BX were even up to 115° probably due to the trimethylsilyl groups of PMATM2 which amplify the coating hydrophobicity.

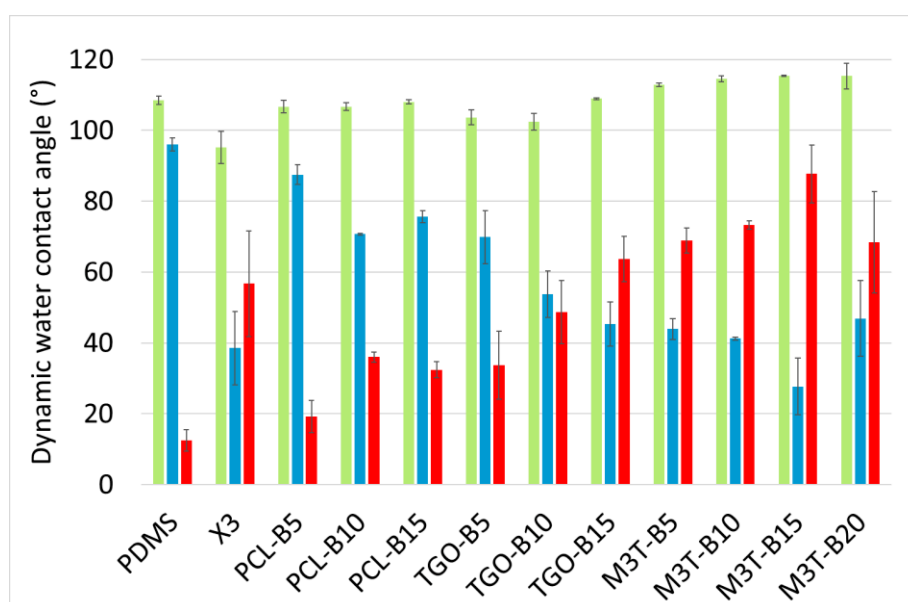


Figure II-15. Dynamic water contact angles of the silicone-based coatings (PDMS= reference, X3= commercial FRC) with the advancing contact angle (green), the receding contact angle (blue) and the contact angle hysteresis (red) before immersion.

Chapter II. Hydrolyzable polymer additive-based silicone elastomers

TGO-BX had $\theta_{w,rec}$ around 50-70° indicating that PCL segments were present on the TGO-BX surfaces and influenced the PDMS surface wettability ($\theta_{w,rec}$ of the pure PCL-*b*-PDMS-*b*-PCL was of $55.4 \pm 2.7^\circ$, cf. § II.2.5). The difference of $\theta_{w,rec}$ between PCL-BX and TGO-BX suggests that the PDMS block of the PCL triblock copolymer increased the availability of PCL segments at the coating surface.

M3T-BX coatings exhibited receding contact angles even lower (with $\theta_{w,rec} = 30-50^\circ$) certainly due to the presence of carboxylate groups generated after the fast hydrolysis of the trialkylsilyl ester pendant groups located at the near surface.

In case of TGO-BX, the contact angle hysteresis ($\Delta\theta \approx 30-60^\circ$) was rather due to the surface heterogeneity (variation of hydrophilic and hydrophobic blocks) whereas in case of M3T-BX, the contact angle hysteresis ($\Delta\theta \approx 70-90^\circ$) was rather due to the fast hydrolysis of PMATM2 in contact with water.

Additionally, it is worth noting that by increasing the amount of hydrolyzable polymer additives within the silicone coating, the contact angle hysteresis was even higher.

TGO-B10, TGO-B15 and the M3T-BX coatings showed a very similar wettability profile as the commercial hydrogel-based FRC (X3) before immersion suggesting they may be promising amphiphilic surfaces for marine applications.

- After immersion

After 3 weeks of immersion in ultrapure water, the advancing contact angles of the experimental coatings were comprised between 95° and 110° (Figure II-16). Thus, after 3 weeks, the coatings remained mostly hydrophobic. $\theta_{w,adv}$ were not influenced by the siliceous phases and/or salts (mentioned in § II.4.2.1 preliminary study).

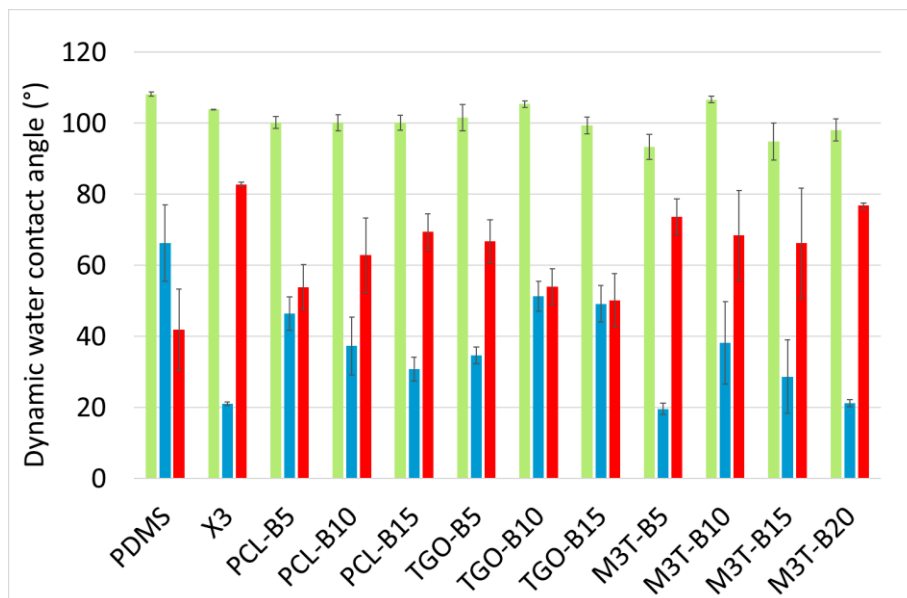


Figure II-16. Dynamic water contact angles of the silicone-based coatings (PDMS= reference, X3= commercial FRC) with the advancing contact angle (green), the receding contact angle (blue) and the contact angle hysteresis (red) after 3 weeks of immersion in ultrapure water.

The $\theta_{w,rec}$ values were all comprised between 20° and 55° while the PDMS reference had a $\theta_{w,rec}$ value of *ca.* 70° suggesting that the effect of the additives became even more apparent after 3 weeks of water immersion. The lowest values of $\theta_{w,rec}$ (*ca.* 20°) were obtained with M3T-BX coatings and X3. This result can be correlated with the mass loss test: at 3 weeks of immersion, there were still numerous potential hydrolyzable trialkylsilyl ester pendant groups able to generate hydrophilicity to the surface after water exposure. Thus, M3T-BX could still provide an amphiphilic surface similar to that of X3 after 3 weeks of immersion (although the involved chemistry is not the same) which is promising for antifouling applications. PCL-BX and TGO-BX showed $\Delta\theta$ superior to 50° indicating a chemical surface reorganization and a surface heterogeneity respectively. These surface behavior patterns may also disrupt, probably to a lesser extent than M3T-BX, the adhesion of fouling organisms.

The increase of $\Delta\theta$ (*ca.* 40°) for the PDMS reference was unexpected, and attributed to the presence of siliceous domains and salts (as seen in § II.4.2.1 preliminary study).

II.4.2.3.2. Surface free energy

The surface free energy (SFE) is an important parameter for FRCs as a low value makes difficult for the bioadhesives to strongly adhere on their surface (cf. Chapter I, § 1.5.1.3.1.2.). PDMS are known to have low SFE value (around 20-25 mJ/m^2) and to be mainly dispersive surfaces.

Figure II-17 shows the surface free energy of the PDMS reference, X3 and all the hydrolyzable polymer additive-based coatings before their immersion in deionized water. All the silicone-based coatings exhibited SFE values between 18 and 25 mJ/m^2 mainly due to the dispersive component (γ_S^D) since the polar contribution was almost zero (γ_S^P).

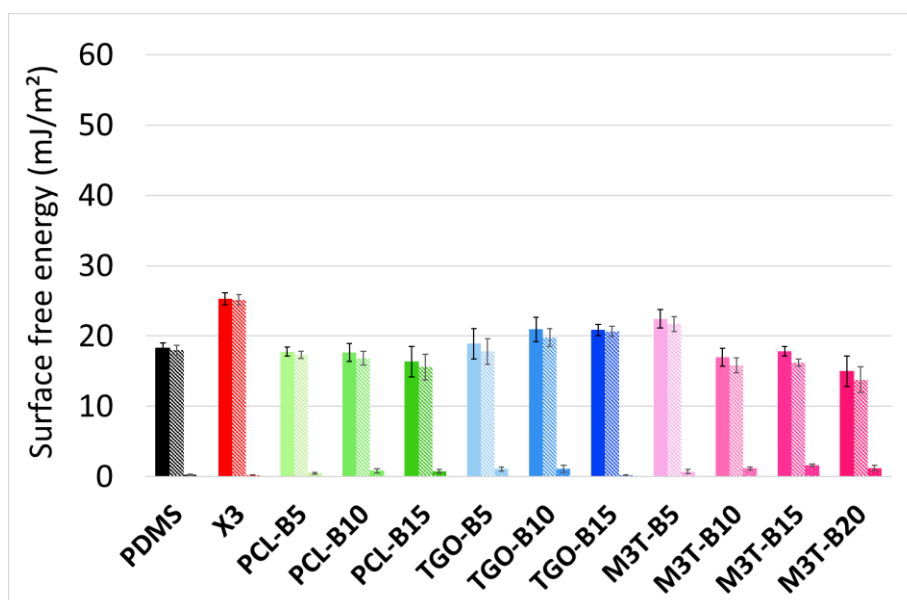


Figure II-17. Surface free energy values of the silicone-based coatings with total surface free energy (full color), its dispersive component (ribbed color) and its polar component (spotted color) before immersion.

The following figure shows SFE values of the experimental coatings after 12 weeks of immersion (Figure II-18). This immersion time was selected as the mass loss of M3T-BX was at its maximum (cf. § II.4.1).

After 12 weeks of immersion, an increase of SFE (from 20 to 30-50 mJ/m^2) was observed for the PDMS reference and the PCL-based coatings (Figure II-18).

Chapter II. Hydrolyzable polymer additive-based silicone elastomers

This was mainly due to the increase of the polar component from 0 to 10 mJ/m² or more. This polarity rise can again be explained by the siliceous phases and/or salts on the surface after water exposure.

M3T-BX did not seem to be affected by the white layer as the SFE values remained around 20-25 mJ/m² (with $\gamma_S^p = 0$). The release of degradation products from M3T-BX could have dragged the particles away. At 12 weeks, the PMATM2 pendant groups were all hydrolyzed according to § II.4.1, leading to remaining PMAA chains embedded in the PDMS elastomer matrix. The SFE values were assessed from static contact angle values which highlights the contribution of the hydrophobic phases at the polymer surface as the advancing contact angle. Thus the SFE values of M3T-BX could be mostly attributed to the PDMS elastomer matrix. The commercial FRC X3 also remained at 25 mJ/m².

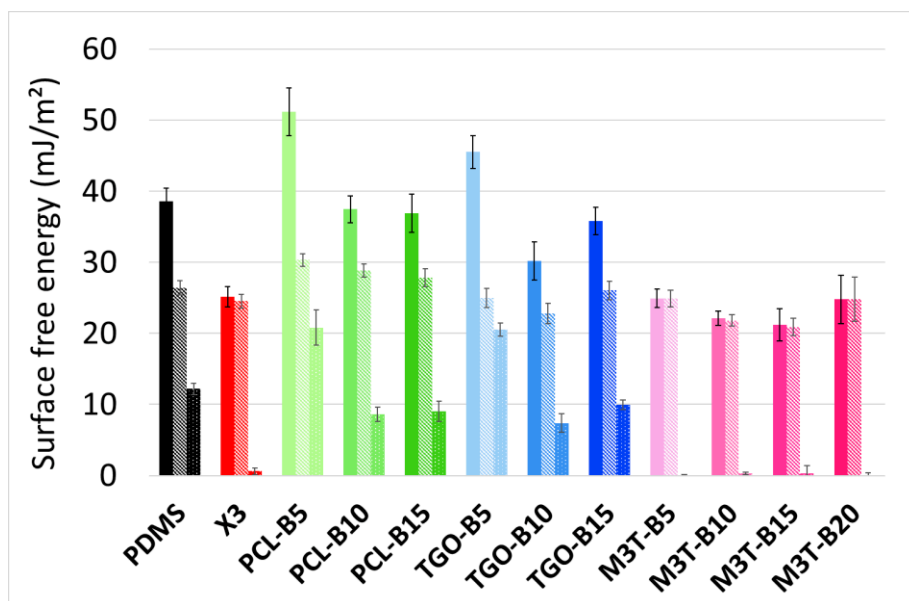


Figure II-18. Surface free energy values of the silicone-based coatings with total surface free energy (full color), its dispersive component (ribbed color) and its polar component (spotted color) after 12 weeks of immersion in ultrapure water.

II.4.2.3.3. Modified time lag method

Static contact angle measurements can be used to assess the presence of hydrophobic or hydrophilic functions on the surface of materials. In this test, the objective is to assess the tendency of the polymer additives to migrate through a PDMS network. A modified time lag test was performed, as described by Noguier et al. [4] (cf. Chapter I, § I.5.1.2.), in which a thin PDMS membrane was deposited onto all our coatings. A water droplet of 25 μL was then placed on top of the PDMS membrane and monitored for 1 h. Further details of the protocol in the experimental section (§ VI.5.1.1.1.). Thanks to this test, Noguier et al. highlighted the ability of small polymer additives of 200 to 3,000 g/mol to migrate through this additive-free PDMS membrane and to finally appear on top of it. Figure II-19 shows the evolution of the contact angle of the coatings containing 15 wt.% of additives, the PDMS reference and X3, all overlaid with the PDMS membrane.

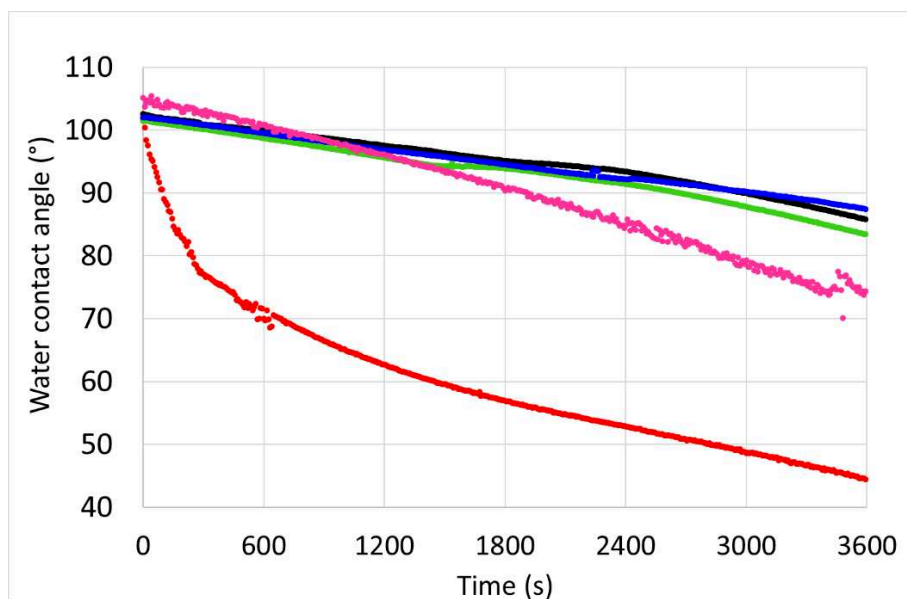


Figure II-19. Contact angle evolution over time of a water droplet on top of the additive-based coatings overcoated with a thin PDMS membrane. PCL-B15, TGO-B15 and M3T-B15 are respectively represented by green, blue and pink lines. The PDMS reference (black line) and the commercial hydrogel-based FRC X3 (red line) were also analyzed in the same conditions.

Chapter II. Hydrolyzable polymer additive-based silicone elastomers

After 1 h, the 25 μL -droplet placed on the [PDMS membrane + PDMS reference] showed a contact angle decrease of 16° (from 102 to 86°) likely due to water droplet evaporation or to the water droplet relaxation (caused by its weight).

M3T-B15 showed a contact angle decrease of 33° (from 107 to 74°), suggesting there were some PMATM2 able to migrate through the PDMS membrane and which had generated hydrophilicity through hydrolysis. Commercial FRC X3 (hydrogel-based FRC) exhibited the highest water contact angle drop from 102 to 44° , attributed to the diffusion of PEG-based additives through the PDMS membrane.

PCL-B15 and TGO-B15 showed the same pattern as the PDMS reference. This means the PCL-based additives were not able to diffuse through the PDMS membrane within the 1 h time or if they did, the water contact angle was not affected. The hydrophobic nature of PCL-based additives and their higher molar mass may be limiting parameters making this test not appropriate for these PCL-based coatings. A 2 h duration test was carried out on PCL-based coatings to validate this assessment, but the water evaporation became too important to eventually draw a conclusion.

Thus, this water contact angle test revealed that for M3T-B15, the PMATM2 additive could diffuse through the upper PDMS membrane, revealing a certain mobility of PMATM2 within the PDMS elastomer.

The results for coatings containing 5 and 10 wt.% additives were not shown as they did not give significant difference of water contact angle evolution with time compared with the PDMS reference.

II.4.2.4. Infrared spectroscopy

The coated glass slides were analyzed by Attenuated Total Reflectance-Fourier Transform Infrared (ATR-FTIR) spectroscopy with a diamond crystal before and after different immersion times (t_i) in deionized water. Right after water withdrawal, the coatings were rinsed with fresh deionized water and consecutively dried for 3 h in ambient air before analysis.

These FTIR analysis allowed to follow the surface chemistry of the silicone-based coatings and determine if there is any enrichment or depletion of the polymer additives at the surface.

Chapter II. Hydrolyzable polymer additive-based silicone elastomers

The analysis of each pure polymer was performed to identify the absorption bands of interest required to detect the polymer additives on the PDMS surfaces (Table II-6).

Table II-6. Main infrared absorption bands of the polymers.

Polymer	Wavelength (cm ⁻¹)/Vibration mode/Chemical bond assignment
PDMS elastomer	800 /stretching/ <u>-O-Si(CH₃)₂-O-</u> 1020-1091 /stretching/-Si-O-Si- 1260 /bending/ <u>-O-Si(CH₃)₂-O-</u> 2963 /stretching/-CH ₃ , -CH ₂ , -CH- 3292 /stretching/-SiOH
PCL	1172 /stretching/C-O (ester) 1723 /stretching/C=O (ester) 2963 /stretching/-CH ₃ , -CH ₂ , -CH-
PCL- <i>b</i> -PDMS- <i>b</i> -PCL	800 /stretching/Si-CH ₃ 1021-1090 /stretching/-Si-O-Si- 1260 /bending/ <u>-O-Si(CH₃)₂-O-</u> 1723 /stretching/C=O (ester) 2963 /stretching/-CH ₃ , -CH ₂ , -CH-
PMATM2	756 and 843 /stretching/ <u>-O-Si(CH₃)₃</u> 1250-1270 /bending/ <u>-O-Si(CH₃)₃</u> and <u>H₃C-Si(OR)₃</u> 1723 /stretching/C=O (silyl ester) 2963 /stretching/-CH ₃ , -CH ₂ , -CH-

The PDMS reference displayed all the characteristic bands described in Table II-6 before and after water immersion (Table II-7). There was no significant change of the PDMS reference surface chemistry, which is not surprising given that the PDMS surface does not rearrange a lot upon immersion. The presence of a small bands at 1414, 1653, 1734 cm⁻¹ more visible at $t_i = 32$ weeks could come from the presence of the tin-based catalyst on the surface (Figure II-20).

Chapter II. Hydrolyzable polymer additive-based silicone elastomers

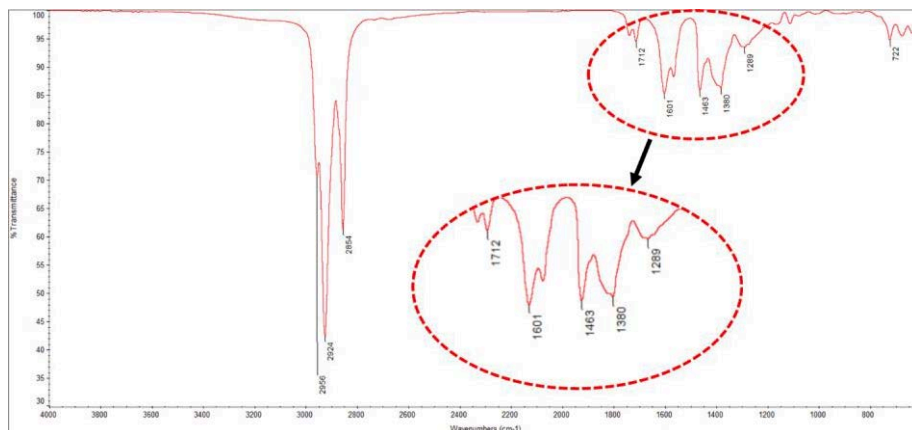
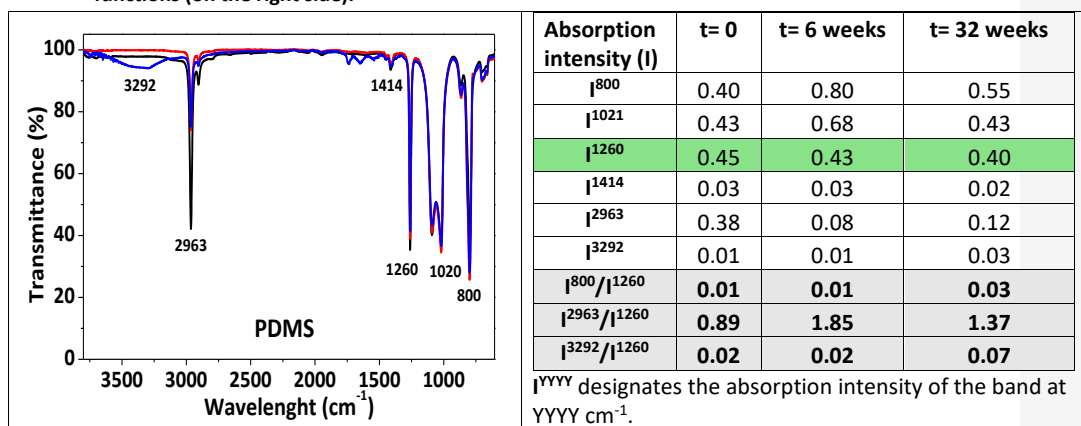


Figure II-20. ATR-FTIR spectra of DOTDL catalyst at $t_i = 0$.

A slight change after 32 weeks of immersion was observed with the appearance of a large band at $3292\text{--}3479\text{ cm}^{-1}$, which could be attributed to the diffusion of -SiOH groups of hydrolyzed ethoxysiloxane functions (from PDES) on top of the surface.

Table II-7. ATR-FTIR spectra of the PDMS reference at different times of immersion, $t_i = 0$ (black line), $t_i = 6$ weeks (red line) and $t_i = 32$ weeks (blue line) on the left side. Absorption intensity values (I) at different times of immersion as well as the ratios of absorption intensity of the targeted chemical functions (on the right side).



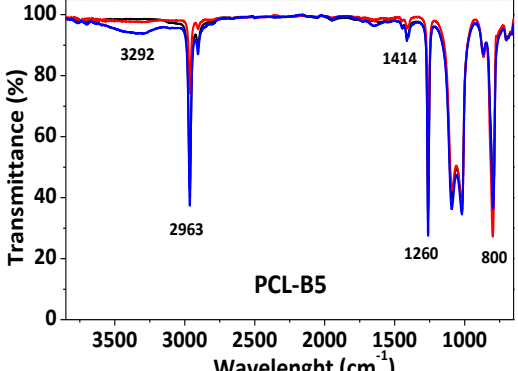
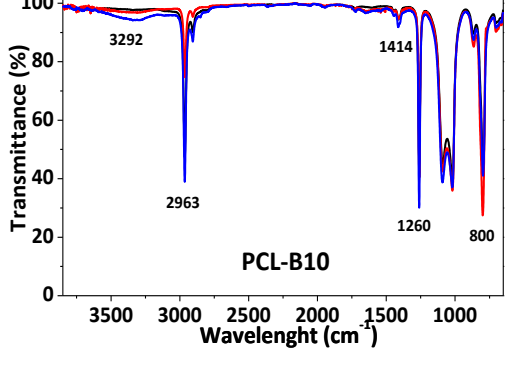
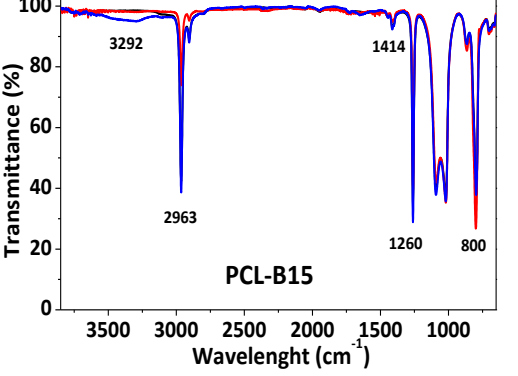
Chapter II. Hydrolyzable polymer additive-based silicone elastomers

To follow the changes of chemistry of all the other coatings, the absorption intensity at 1260 cm^{-1} was taken as a reference since it did not vary significantly through immersion for the PDMS reference (highlighted in green in Table II-7). To evaluate the variation of certain chemical functions on the surface, the ratios of absorption intensities are used. They were indicated by I^{YYYY}/I^{1260} in which I^{YYYY} is the absorption intensity of a band of interest usually characteristic of a chemical function from any hydrolyzable polymer additives.

In Table II-8, PCL-BX (5, 10 and 15 wt.%) did not show a vibration absorption band at 1723 cm^{-1} (ester carbonyl) before immersion traducing the absence of poly(ϵ -caprolactone) on the surface. After immersion, I^{1723}/I^{1260} ratio was still constant revealing there is no appearance of PCL near the surface (highlighted in red in Table II-8). This suggests the PCL molecules cannot diffuse towards the surface of the coating because they are “trapped” in the bulk of the PDMS matrix. PCL-BX coatings behave like the PDMS reference in terms of surface chemistry.

Chapter II. Hydrolyzable polymer additive-based silicone elastomers

Table II-8. ATR-FTIR spectra of PCL-BX at different times of immersion, $t_i=0$ (black line), $t_i=6$ weeks (red line) and $t_i=32$ weeks (blue line) on the left side. Absorption intensity values (I) at different times of immersion as well as the ratios of absorption intensity of targeted chemical functions (on the right side).

 <p>PCL-B5</p>	<table border="1"> <thead> <tr> <th>Absorption intensity (I)</th> <th>$t=0$</th> <th>$t=6$ weeks</th> <th>$t=32$ weeks</th> </tr> </thead> <tbody> <tr> <td>I^{800}</td> <td>0.41</td> <td>0.56</td> <td>0.43</td> </tr> <tr> <td>I^{1260}</td> <td>0.46</td> <td>0.39</td> <td>0.56</td> </tr> <tr> <td>I^{1414}</td> <td>0.03</td> <td>0.02</td> <td>0.04</td> </tr> <tr> <td>I^{1723}</td> <td>0.01</td> <td>0.00</td> <td>0.01</td> </tr> <tr> <td>I^{2964}</td> <td>0.37</td> <td>0.13</td> <td>0.43</td> </tr> <tr> <td>I^{3292}</td> <td>0.01</td> <td>0.01</td> <td>0.03</td> </tr> <tr> <td>I^{1414}/I^{1260}</td> <td>0.07</td> <td>0.05</td> <td>0.07</td> </tr> <tr> <td>I^{1723}/I^{1260}</td> <td>0.02</td> <td>0.01</td> <td>0.02</td> </tr> <tr> <td>I^{3292}/I^{1260}</td> <td>0.01</td> <td>0.03</td> <td>0.05</td> </tr> </tbody> </table>	Absorption intensity (I)	$t=0$	$t=6$ weeks	$t=32$ weeks	I^{800}	0.41	0.56	0.43	I^{1260}	0.46	0.39	0.56	I^{1414}	0.03	0.02	0.04	I^{1723}	0.01	0.00	0.01	I^{2964}	0.37	0.13	0.43	I^{3292}	0.01	0.01	0.03	I^{1414}/I^{1260}	0.07	0.05	0.07	I^{1723}/I^{1260}	0.02	0.01	0.02	I^{3292}/I^{1260}	0.01	0.03	0.05
Absorption intensity (I)	$t=0$	$t=6$ weeks	$t=32$ weeks																																						
I^{800}	0.41	0.56	0.43																																						
I^{1260}	0.46	0.39	0.56																																						
I^{1414}	0.03	0.02	0.04																																						
I^{1723}	0.01	0.00	0.01																																						
I^{2964}	0.37	0.13	0.43																																						
I^{3292}	0.01	0.01	0.03																																						
I^{1414}/I^{1260}	0.07	0.05	0.07																																						
I^{1723}/I^{1260}	0.02	0.01	0.02																																						
I^{3292}/I^{1260}	0.01	0.03	0.05																																						
 <p>PCL-B10</p>	<table border="1"> <thead> <tr> <th>Absorption intensity (I)</th> <th>$t=0$</th> <th>$t=6$ weeks</th> <th>$t=32$ weeks</th> </tr> </thead> <tbody> <tr> <td>I^{800}</td> <td>0.38</td> <td>0.56</td> <td>0.38</td> </tr> <tr> <td>I^{1260}</td> <td>0.39</td> <td>0.39</td> <td>0.52</td> </tr> <tr> <td>I^{1414}</td> <td>0.02</td> <td>0.02</td> <td>0.04</td> </tr> <tr> <td>I^{1723}</td> <td>0.01</td> <td>0.01</td> <td>0.01</td> </tr> <tr> <td>I^{2964}</td> <td>0.32</td> <td>0.13</td> <td>0.41</td> </tr> <tr> <td>I^{3292}</td> <td>0.01</td> <td>0.01</td> <td>0.03</td> </tr> <tr> <td>I^{1414}/I^{1260}</td> <td>0.06</td> <td>0.06</td> <td>0.07</td> </tr> <tr> <td>I^{1723}/I^{1260}</td> <td>0.02</td> <td>0.02</td> <td>0.03</td> </tr> <tr> <td>I^{3292}/I^{1260}</td> <td>0.03</td> <td>0.04</td> <td>0.05</td> </tr> </tbody> </table>	Absorption intensity (I)	$t=0$	$t=6$ weeks	$t=32$ weeks	I^{800}	0.38	0.56	0.38	I^{1260}	0.39	0.39	0.52	I^{1414}	0.02	0.02	0.04	I^{1723}	0.01	0.01	0.01	I^{2964}	0.32	0.13	0.41	I^{3292}	0.01	0.01	0.03	I^{1414}/I^{1260}	0.06	0.06	0.07	I^{1723}/I^{1260}	0.02	0.02	0.03	I^{3292}/I^{1260}	0.03	0.04	0.05
Absorption intensity (I)	$t=0$	$t=6$ weeks	$t=32$ weeks																																						
I^{800}	0.38	0.56	0.38																																						
I^{1260}	0.39	0.39	0.52																																						
I^{1414}	0.02	0.02	0.04																																						
I^{1723}	0.01	0.01	0.01																																						
I^{2964}	0.32	0.13	0.41																																						
I^{3292}	0.01	0.01	0.03																																						
I^{1414}/I^{1260}	0.06	0.06	0.07																																						
I^{1723}/I^{1260}	0.02	0.02	0.03																																						
I^{3292}/I^{1260}	0.03	0.04	0.05																																						
 <p>PCL-B15</p>	<table border="1"> <thead> <tr> <th>Absorption intensity (I)</th> <th>$t=0$</th> <th>$t=6$ weeks</th> <th>$t=32$ weeks</th> </tr> </thead> <tbody> <tr> <td>I^{800}</td> <td>0.41</td> <td>0.57</td> <td>0.42</td> </tr> <tr> <td>I^{1260}</td> <td>0.46</td> <td>0.40</td> <td>0.54</td> </tr> <tr> <td>I^{1414}</td> <td>0.03</td> <td>0.02</td> <td>0.03</td> </tr> <tr> <td>I^{1723}</td> <td>0.01</td> <td>0.01</td> <td>0.01</td> </tr> <tr> <td>I^{2964}</td> <td>0.37</td> <td>0.13</td> <td>0.41</td> </tr> <tr> <td>I^{3292}</td> <td>0.01</td> <td>0.01</td> <td>0.02</td> </tr> <tr> <td>I^{1414}/I^{1260}</td> <td>0.07</td> <td>0.06</td> <td>0.06</td> </tr> <tr> <td>I^{1723}/I^{1260}</td> <td>0.02</td> <td>0.02</td> <td>0.02</td> </tr> <tr> <td>I^{3292}/I^{1260}</td> <td>0.01</td> <td>0.02</td> <td>0.04</td> </tr> </tbody> </table>	Absorption intensity (I)	$t=0$	$t=6$ weeks	$t=32$ weeks	I^{800}	0.41	0.57	0.42	I^{1260}	0.46	0.40	0.54	I^{1414}	0.03	0.02	0.03	I^{1723}	0.01	0.01	0.01	I^{2964}	0.37	0.13	0.41	I^{3292}	0.01	0.01	0.02	I^{1414}/I^{1260}	0.07	0.06	0.06	I^{1723}/I^{1260}	0.02	0.02	0.02	I^{3292}/I^{1260}	0.01	0.02	0.04
Absorption intensity (I)	$t=0$	$t=6$ weeks	$t=32$ weeks																																						
I^{800}	0.41	0.57	0.42																																						
I^{1260}	0.46	0.40	0.54																																						
I^{1414}	0.03	0.02	0.03																																						
I^{1723}	0.01	0.01	0.01																																						
I^{2964}	0.37	0.13	0.41																																						
I^{3292}	0.01	0.01	0.02																																						
I^{1414}/I^{1260}	0.07	0.06	0.06																																						
I^{1723}/I^{1260}	0.02	0.02	0.02																																						
I^{3292}/I^{1260}	0.01	0.02	0.04																																						

Chapter II. Hydrolyzable polymer additive-based silicone elastomers

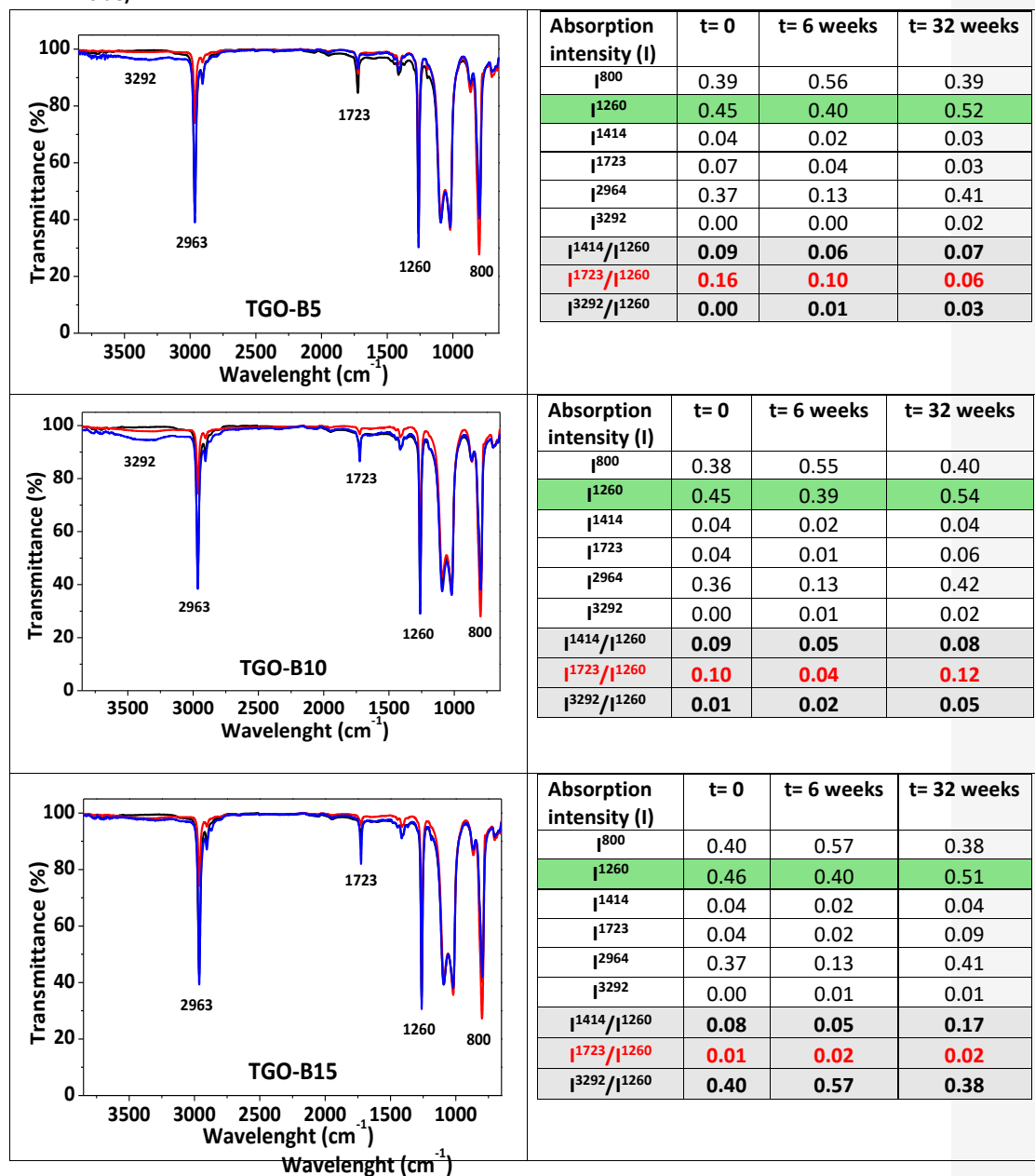
On the contrary, all TGO-BX coatings showed a vibration absorption band at 1723 cm^{-1} (ester carbonyl) before immersion traducing the presence of poly(ϵ -caprolactone) blocks on the surface (Table II-9).

After 6 weeks of immersion, the I^{1723}/I^{1260} ratio decreased for TGO-B5 and TGO-B10 indicating a depletion of PCL blocks on the surface. This may be due to the surface rearrangement while drying, causing the siloxane functions to rotate towards the air and hiding the PCL functions. Regarding TGO-B15, the I^{1723}/I^{1260} ratio remained constant upon immersion which tends to indicate the stationary state of the PCL block on the surface (non-hydrolyzed PCL).

After 32 weeks, the I^{1723}/I^{1260} ratios were similar to those at $t_i=0$ for TGO-B10 and TGO-B15 suggesting the slight decrease at 6 weeks was maybe just due to the surface heterogeneity (the infrared measurements were not taken at the exact same location on the coated glass slide for each immersion time).

Chapter II. Hydrolyzable polymer additive-based silicone elastomers

Table II-9. ATR-FTIR spectra of TGO-BX at different times of immersion, $t_i=0$ (black line), $t_i=6$ weeks (red line) and $t_i=32$ weeks (blue line) on the left side. Absorption intensity values (I) at different times of immersion as well as the ratios of absorption intensity of targeted chemical functions (on the right side).



Chapter II. Hydrolyzable polymer additive-based silicone elastomers

Regarding M3T-BX coatings, they all displayed an absorption band at 1723 cm^{-1} before immersion indicating the presence of PMATM2 on the surface (Table II-10).

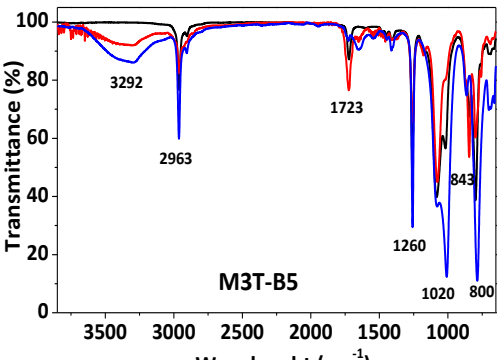
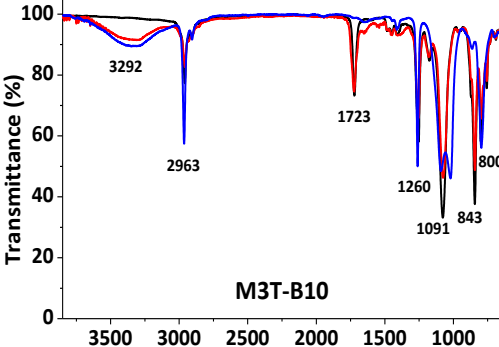
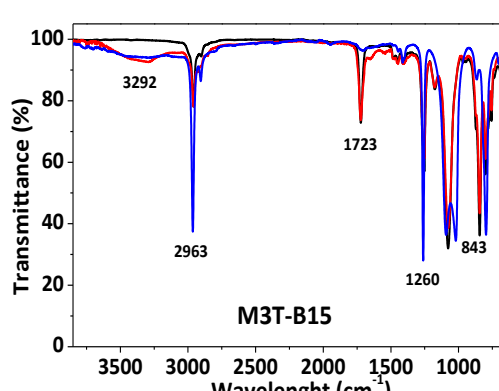
After 6 weeks of immersion the I^{1723}/I^{1260} and I^{843}/I^{1260} ratios are multiplied by 3 for M3T-B5. A significant increase of the infrared absorption band at 3292 cm^{-1} (-OH groups) was also noticed. These observations highlighted a surface enrichment of PMATM2 for M3T-B5, possibly both in its hydrolyzed form (revealed by the band at 3292 cm^{-1}) and non-hydrolyzed form (revealed by the bands at 843 cm^{-1}).

For M3T-B10 and M3T-B15, the I^{1723}/I^{1260} and I^{843}/I^{1260} ratios are quite constant after 6 weeks of immersion suggesting the surface is probably already saturated with PMATM2 from the beginning and could not be further enriched with PMATM2. The increase of the absorption band intensity at 3292 cm^{-1} is also attributed to the accumulation of hydrolyzed PMATM2 with -OH groups.

After 32 weeks, there was a drop of the I^{1723}/I^{1260} and I^{843}/I^{1260} ratios. These observations indicate the complete depletion of PMATM2 after 32 weeks of immersion. This highlighted the time-limited reservoir effect of PMATM2 which is confirmed by the mass loss test (cf. § II.4.1.) where a maximum mass loss was achieved only up to 12 weeks of static immersion. The shortage of the PMATM2 in the bulk of the coating could no longer replenish the surface. The absence of a band at 1711 cm^{-1} (C=O of a carboxylic acid) revealed the absence of poly(methacrylic) acid. The increase of the I^{1020}/I^{1260} ratio and apparition of a band at 800 cm^{-1} also indicated the recovery of the polysiloxane functions on the surface, which were partially hidden by PMATM2 until now.

Chapter II. Hydrolyzable polymer additive-based silicone elastomers

Table II-10. ATR-FTIR spectra of **M3T-BX** at different times of immersion, $t_i=0$ (black line), $t_i=6$ weeks (red line) and $t_i=32$ weeks (blue line) on the left side. Absorption intensity values (I) at different times of immersion as well as the ratios of absorption intensity of targeted chemical functions (on the right side).

 <p style="text-align: center;">M3T-B5</p>	<table border="1"> <thead> <tr> <th>Absorption intensity (I)</th> <th>$t=0$</th> <th>$t=6$ weeks</th> <th>$t=32$ weeks</th> </tr> </thead> <tbody> <tr> <td>I^{843}</td> <td>0.17</td> <td>0.27</td> <td>0.09</td> </tr> <tr> <td>I^{1021}</td> <td>0.25</td> <td>0.10</td> <td>0.70</td> </tr> <tr style="background-color: #e0ffe0;"> <td>I^{1260}</td> <td>0.30</td> <td>0.18</td> <td>0.53</td> </tr> <tr> <td>I^{1414}</td> <td>0.03</td> <td>0.03</td> <td>0.04</td> </tr> <tr> <td>I^{1723}</td> <td>0.06</td> <td>0.12</td> <td>0.03</td> </tr> <tr> <td>I^{2964}</td> <td>0.12</td> <td>0.08</td> <td>0.21</td> </tr> <tr> <td>I^{3292}</td> <td>0.00</td> <td>0.04</td> <td>0.07</td> </tr> <tr style="background-color: #ffe0e0;"> <td>I^{843}/I^{1260}</td> <td>0.57</td> <td>1.49</td> <td>0.17</td> </tr> <tr style="background-color: #ffe0e0;"> <td>I^{1723}/I^{1260}</td> <td>0.20</td> <td>0.64</td> <td>0.05</td> </tr> <tr style="background-color: #ffe0e0;"> <td>I^{3292}/I^{1260}</td> <td>0.00</td> <td>0.20</td> <td>0.12</td> </tr> </tbody> </table>	Absorption intensity (I)	$t=0$	$t=6$ weeks	$t=32$ weeks	I^{843}	0.17	0.27	0.09	I^{1021}	0.25	0.10	0.70	I^{1260}	0.30	0.18	0.53	I^{1414}	0.03	0.03	0.04	I^{1723}	0.06	0.12	0.03	I^{2964}	0.12	0.08	0.21	I^{3292}	0.00	0.04	0.07	I^{843}/I^{1260}	0.57	1.49	0.17	I^{1723}/I^{1260}	0.20	0.64	0.05	I^{3292}/I^{1260}	0.00	0.20	0.12
Absorption intensity (I)	$t=0$	$t=6$ weeks	$t=32$ weeks																																										
I^{843}	0.17	0.27	0.09																																										
I^{1021}	0.25	0.10	0.70																																										
I^{1260}	0.30	0.18	0.53																																										
I^{1414}	0.03	0.03	0.04																																										
I^{1723}	0.06	0.12	0.03																																										
I^{2964}	0.12	0.08	0.21																																										
I^{3292}	0.00	0.04	0.07																																										
I^{843}/I^{1260}	0.57	1.49	0.17																																										
I^{1723}/I^{1260}	0.20	0.64	0.05																																										
I^{3292}/I^{1260}	0.00	0.20	0.12																																										
 <p style="text-align: center;">M3T-B10</p>	<table border="1"> <thead> <tr> <th>Absorption intensity (I)</th> <th>$t=0$</th> <th>$t=6$ weeks</th> <th>$t=32$ weeks</th> </tr> </thead> <tbody> <tr> <td>I^{843}</td> <td>0.42</td> <td>0.34</td> <td>0.04</td> </tr> <tr> <td>I^{1021}</td> <td>0.05</td> <td>0.06</td> <td>0.34</td> </tr> <tr style="background-color: #e0ffe0;"> <td>I^{1260}</td> <td>0.19</td> <td>0.20</td> <td>0.30</td> </tr> <tr> <td>I^{1414}</td> <td>0.03</td> <td>0.04</td> <td>0.02</td> </tr> <tr> <td>I^{1723}</td> <td>0.14</td> <td>0.15</td> <td>0.01</td> </tr> <tr> <td>I^{2964}</td> <td>0.11</td> <td>0.11</td> <td>0.24</td> </tr> <tr> <td>I^{3292}</td> <td>0.01</td> <td>0.03</td> <td>0.05</td> </tr> <tr style="background-color: #ffe0e0;"> <td>I^{843}/I^{1260}</td> <td>2.20</td> <td>1.72</td> <td>0.14</td> </tr> <tr style="background-color: #ffe0e0;"> <td>I^{1723}/I^{1260}</td> <td>0.70</td> <td>0.73</td> <td>0.02</td> </tr> <tr style="background-color: #ffe0e0;"> <td>I^{3292}/I^{1260}</td> <td>0.03</td> <td>0.17</td> <td>0.16</td> </tr> </tbody> </table>	Absorption intensity (I)	$t=0$	$t=6$ weeks	$t=32$ weeks	I^{843}	0.42	0.34	0.04	I^{1021}	0.05	0.06	0.34	I^{1260}	0.19	0.20	0.30	I^{1414}	0.03	0.04	0.02	I^{1723}	0.14	0.15	0.01	I^{2964}	0.11	0.11	0.24	I^{3292}	0.01	0.03	0.05	I^{843}/I^{1260}	2.20	1.72	0.14	I^{1723}/I^{1260}	0.70	0.73	0.02	I^{3292}/I^{1260}	0.03	0.17	0.16
Absorption intensity (I)	$t=0$	$t=6$ weeks	$t=32$ weeks																																										
I^{843}	0.42	0.34	0.04																																										
I^{1021}	0.05	0.06	0.34																																										
I^{1260}	0.19	0.20	0.30																																										
I^{1414}	0.03	0.04	0.02																																										
I^{1723}	0.14	0.15	0.01																																										
I^{2964}	0.11	0.11	0.24																																										
I^{3292}	0.01	0.03	0.05																																										
I^{843}/I^{1260}	2.20	1.72	0.14																																										
I^{1723}/I^{1260}	0.70	0.73	0.02																																										
I^{3292}/I^{1260}	0.03	0.17	0.16																																										
 <p style="text-align: center;">M3T-B15</p>	<table border="1"> <thead> <tr> <th>Absorption intensity (I)</th> <th>$t=0$</th> <th>$t=6$ weeks</th> <th>$t=32$ weeks</th> </tr> </thead> <tbody> <tr> <td>I^{843}</td> <td>0.44</td> <td>0.36</td> <td>0.05</td> </tr> <tr> <td>I^{1021}</td> <td>0.07</td> <td>0.07</td> <td>0.46</td> </tr> <tr style="background-color: #e0ffe0;"> <td>I^{1260}</td> <td>0.20</td> <td>0.18</td> <td>0.55</td> </tr> <tr> <td>I^{1414}</td> <td>0.03</td> <td>0.04</td> <td>0.03</td> </tr> <tr> <td>I^{1723}</td> <td>0.14</td> <td>0.13</td> <td>0.02</td> </tr> <tr> <td>I^{2964}</td> <td>0.11</td> <td>0.11</td> <td>0.35</td> </tr> <tr> <td>I^{3292}</td> <td>0.00</td> <td>0.03</td> <td>0.03</td> </tr> <tr style="background-color: #ffe0e0;"> <td>I^{843}/I^{1260}</td> <td>2.17</td> <td>2.02</td> <td>0.08</td> </tr> <tr style="background-color: #ffe0e0;"> <td>I^{1723}/I^{1260}</td> <td>0.68</td> <td>0.74</td> <td>0.03</td> </tr> <tr style="background-color: #ffe0e0;"> <td>I^{3292}/I^{1260}</td> <td>0.01</td> <td>0.19</td> <td>0.05</td> </tr> </tbody> </table>	Absorption intensity (I)	$t=0$	$t=6$ weeks	$t=32$ weeks	I^{843}	0.44	0.36	0.05	I^{1021}	0.07	0.07	0.46	I^{1260}	0.20	0.18	0.55	I^{1414}	0.03	0.04	0.03	I^{1723}	0.14	0.13	0.02	I^{2964}	0.11	0.11	0.35	I^{3292}	0.00	0.03	0.03	I^{843}/I^{1260}	2.17	2.02	0.08	I^{1723}/I^{1260}	0.68	0.74	0.03	I^{3292}/I^{1260}	0.01	0.19	0.05
Absorption intensity (I)	$t=0$	$t=6$ weeks	$t=32$ weeks																																										
I^{843}	0.44	0.36	0.05																																										
I^{1021}	0.07	0.07	0.46																																										
I^{1260}	0.20	0.18	0.55																																										
I^{1414}	0.03	0.04	0.03																																										
I^{1723}	0.14	0.13	0.02																																										
I^{2964}	0.11	0.11	0.35																																										
I^{3292}	0.00	0.03	0.03																																										
I^{843}/I^{1260}	2.17	2.02	0.08																																										
I^{1723}/I^{1260}	0.68	0.74	0.03																																										
I^{3292}/I^{1260}	0.01	0.19	0.05																																										

II.4.3. Bulk properties

The bulk properties of the elastomer coatings were also investigated as they play a major role in the fouling release ability. Thermal and mechanical analysis (DSC and DMA) were performed to evaluate the influence of polymer additives on the silicone network.

II.4.3.1. Differential scanning calorimetry analyses

Differential scanning calorimetry (DSC) analysis were useful to evaluate the influence of the hydrolyzable polymer additives on the silicone network organization. DSC also enabled to determine if the semi-crystalline polymer additives were still able to crystallize once embedded in the PDMS elastomer. The values of crystallinity (X_c) of both the PDMS and semi-crystalline polymer additives when blended all together are important to study since they can explain the viscoelastic properties of the coatings as well as their ability to be hydrated.

Through DSC measurements, it can usually be observed a glass transition at -127°C which explains the viscoelastic properties or rubbery behavior of silicone elastomers at ambient temperature [44,45]. At low temperature (-65 and -80°C), the crosslinked PDMS elastomer also presents a crystalline organization with formation of large spherulites [46]. These crystalline structures melt around -45°C [44,45]. The crystallinity values of some silicone elastomers at low temperature vary from 59 % to 79 % [47–51].

The crystallinity coming from the PDMS chains is calculated according to **Eq. 1** and the crystallinity coming from the PCL polyester segments is calculated using **Eq. 2**:

$$X_c(\text{PDMS}) = (\Delta H_m^{\text{PDMS}} \times w_{\text{PDMS}}) \times 100 / (\Delta H_m^{\text{PDMS,th}}) \quad \text{Eq. 1}$$

$$X_c(\text{PCL}) = (\Delta H_m^{\text{PCL}} \times w_{\text{PCL}}) \times 100 / (\Delta H_m^{\text{PCL,th}}) \quad \text{Eq. 2}$$

With $X_c(\text{PDMS})$, the crystallinity of the cured PDMS, $X_c(\text{PCL})$, the crystallinity of PCL, ΔH_m^{PDMS} is the measured melting enthalpy of PDMS, ΔH_m^{PCL} is the measured melting enthalpy of PCL. $\Delta H_m^{\text{PDMS,th}}$ is the theoretical melting enthalpy of an unfilled cured PDMS rubber taken equal to 25.35 J/g [47]. $\Delta H_m^{\text{PCL,th}}$ is the equilibrium melting enthalpy of 100 % crystalline PCL taken

Chapter II. Hydrolyzable polymer additive-based silicone elastomers

equal to 139.3 J/g [8]. w_{PDMS} and w_{PCL} represent the mass fractions of PDMS elastomer and PCL respectively in the dry coatings.

The DSC analyses were able to determine the crystallinity (X_c) of PDMS and PCL (Table II-11). The detailed thermal conditions are described in the experimental section (§ VI.5.5.1.).

Table II-11. Thermal information of the coatings obtained by DSC analyses.

Coating ID	ΔH_m (PDMS) (J/g)	T_m (PDMS) (°C)	X_c (PDMS) (%)	ΔH_m (polyester) (J/g)	T_m (polyester) (°C)	X_c (PCL) (%)
PDMS reference	21	-44	74	-	-	-
PCL-B5	18	-44	60	2	50	0.1
PCL-B10	18	-44	57	9	51	0.6
PCL-B15	18	-44	54	14	51	1.5
TGO-B5	19	-44	64	3	52-55	0.1
TGO-B10	17	-45	54	4	52-55	0.2
TGO-B15	13	-44	39	7	52-55	0.5
M3T-B5	20	-44	67	-	-	-
M3T-B10	16	-44	51	-	-	-
M3T-B15	16	-44	48	-	-	-
M3T-B20	16	-43	45	-	-	-

The PDMS reference coating showed a crystallinity at -44°C of 74 % similar to the literature values. The glass transition temperature (T_g) of PDMS could not be visualized as the minimal temperature achieved by the DSC equipment was -90°C.

The PCL additive seemed to not disturb the PDMS matrix at -44°C given that PCL-BX showed very similar PDMS melting enthalpy. A possible explanation of that is the microscopic phase separation between PCL and PDMS. Indeed, being separated from the PDMS, PCL would not disturb the crystallization of PDMS at -44°C.

The PDMS melting enthalpy values of M3T-BX and TGO-BX decreased when increasing the additives content suggesting that the presence of amorphous (PMATM2) and semi-crystalline

Chapter II. Hydrolyzable polymer additive-based silicone elastomers

(PCL-*b*-PDMS-*b*-PCL) polymer additives disrupted the network organization at low temperatures. TGO-B15 showed a lower PDMS crystallinity than PCL-B15 probably because the PCL blocks were more intimately dispersed within the PDMS network thanks to its central PDMS block. Besides, as PMATM2 chemical structure and amorphous state is similar to the polysiloxane chain, PMATM2 additives could penetrate easier the network and thus disturbing the PDMS crystallization.

PCL-BX showed a melting temperature around 50°C indicating the PCL was able to crystallize even embedded in a soft PDMS elastomer. Nevertheless, the X_c values of PCL were very low (less than 1.5%) compared to the original crystallinity of PCL 3000 of 62 %. It can thus be supposed that PCL should not influence the viscoelastic properties of the PDMS coating. TGO-BX also showed a PCL melting temperature at 52-55°C. However, the X_c values of PCL were almost 2 times less important (less than 0.5%) than for PCL-BX. This confirms that in TGO-BX, the PCL blocks are better dispersed in the PDMS matrix and thus are unable to crystallize. As PMATM2 is an amorphous polymer, M3T-BX did not display any PMATM2 melting enthalpy. The T_g of PMATM2 was also not visible probably due to the very low heating rate of 1°C/min.

II.4.3.2. Elastic modulus

The measurement of elastic modulus was obtained with a DMA equipment in tension mode. The rectangular free films samples were mechanically deformed at low oscillation amplitudes (5-50 μm) to remain in the linear viscoelastic domain of the elastomer. The elastic modulus (or storage modulus) is a reliable parameter to investigate the effect of loading various amounts of hydrolyzable polymer additives on the viscoelastic properties of the silicone elastomer.

Before immersion, the resulting elastic moduli (E') for all prepared elastomers were between 0.9 and 2.1 MPa (Table II-12). The incorporation of 5 wt.% of any polymer additive had no influence on the elastomeric behavior of the silicone elastomer. Beyond 10 wt.% of additive content, the elastomers containing polyester-based additives (PCL-B15 and TGO-B15) were the most rigid elastomers compared with the PDMS reference. This reveals the influence of the semi-crystalline PCL in the matrix which was already highlighted by the DSC analysis (§ II.4.3.1.).

Chapter II. Hydrolyzable polymer additive-based silicone elastomers

Table II-12. Elastic modulus before and after 32 weeks of immersion.

	E' (MPa) at $t_i=0$	E' (MPa) at $t_i=32$ weeks
PDMS reference	0.9 ± 0.1	0.98 ± 0.03
Hempasil X3	0.99 ± 0.01	0.99 ± 0.02
PCL-B5	1.2 ± 0.3	1.6 ± 0.2
PCL-B10	1.5 ± 0.1	1.9 ± 0.3
PCL-B15	1.9 ± 0.1	2.0 ± 0.2
TGO-B5	1.1 ± 0.1	1.0 ± 0.1
TGO-B10	1.2 ± 0.1	1.3 ± 0.2
TGO-B15	2.09 ± 0.04	2.0 ± 0.1
M3T-B5	1.0 ± 0.1	0.79 ± 0.02
M3T-B10	1.2 ± 0.3	0.67 ± 0.05
M3T-B15	1.3 ± 0.3	0.62 ± 0.05
M3T-B20	1.6 ± 0.2	0.78 ± 0.04

Regarding M3T-BX, there was a slight increase of elastic modulus with the increase of the PMATM2 content. Nonetheless, the differences of elastic moduli between M3T-BX and the PDMS reference remained very low.

Generally, these DMA experiments revealed that the hydrolyzable polymer additives did not significantly modify the network integrity in the small deformation regime at ambient temperature.

DMA analysis were also performed after immersion of the materials in deionized water. After 32 weeks of immersion, there was no major change of elastic modulus for PCL-BX, TGO-BX suggesting there was no loss of additives and/or no increase of PCL crystallinity upon immersion. This corroborates the absence of mass loss from the hydrolytic degradation test (§ II.4.1). Since the PCL is likely to be trapped within the PCL-BX coating, the PDMS network can act as a protective matrix from water aging.

As mentioned with the DCA and infrared analyses (§ II.4.2.3.1 and § II.4.2.4), TGO-BX exhibited some PCL domains on their surfaces. The water aging of these PCL domains seemed not modifying the resulting elastic moduli of the coatings upon immersion. This is in good

agreement with the results reported in the literature where PCL were rarely affected by water aging [52,53].

A decrease of the elastic modulus was noticed for M3T-BX (two times lower than initially). This loss of stiffness could be attributed to the hydrolysis and release of PMATM2 degradation products during immersion as it led to the emptying of the network. A complementary explanation is that the PMATM2 could disturb the PDMS crosslinking process. Indeed, premature hydrolysis of some PMATM2 pendant groups during the formulation process could have generated -SiOH functionalities (coming from the degradation products) and which can further react with the bis-silanol PDMS. Thus, the resulting crosslinking density can be lower than that of the PDMS reference. The elastic modulus after 32 weeks of immersion corresponds to the elastic modulus of the “emptied” PDMS elastomer.

This can be confirmed by the DSC results in which a lower melting enthalpy of PDMS at -44°C was observed for M3T-BX (16 J/g against 21 J/g for PDMS, § II.4.3.1, Table II-11). The presence of PMATM2 additives was thus participating into the viscoelastic properties of the M3T-BX coating.

The loss of copolymer from Hemptasil X3 during immersion did not influence the elastic modulus, this suggests the copolymer did not intervene in the elastomer softness.

II.5. Conclusion

We have designed hydrolyzable polymer additives-based silicone coatings for AF/FR applications. The objectives of this study were to evaluate the hydrolysis ability of the polymer additives embedded in a silicone matrix as well as their influence on the surface and bulk properties.

Among the three experimental coatings, only the PMATM2-based PDMS displayed mass loss during 32 weeks of immersion contrary to PCL-based PDMS.

Depending on the chemical microstructure and molar mass of the polymer additives, there were different effects on the surface properties. PCL-BX surfaces seemed not to be covered with PCL as indicated by the contact angle and roughness (R_a) measurements. Thus PCL-BX had a similar behavior as the PDMS reference. There was also no obvious enrichment of PCL on the surface after 32 weeks of immersion, highlighted by the infrared analysis. This could explain why there was no hydrolytic degradation. Indeed, while trapped in the coating bulk, PCL chains had no access to water and so no possibility to be hydrolyzed.

TGO-BX surfaces were partially covered with PCL block as described by the dynamic contact angles and roughness measurements. The central PDMS block proved to have an essential role as it enabled the well dispersion of the PCL blocks throughout the coating. TGO-BX exhibited dynamic surface chemistry reflected by a water contact angle hysteresis up to 60° . Upon water exposure, there seemed to have no replenishment of polymer additives from the bulk according to the infrared analysis. This was confirmed by the Noguer's diffusion test in which the triblock copolymer could not migrate through a $90\text{-}\mu\text{m}$ PDMS layer after 1 h. The main reasons of the stationary state of the PCL-based copolymer were its high molar mass that limited its migration and the possibility that the PDMS central block acted as an anchor in the PDMS matrix preventing its departure from the coating. The hydrophobic nature of PCL also certainly limited its presence at the coating/water interface. This can be correlated with the mass loss test, where there was no mass loss for TGO-BX.

PMATM2-based coatings provided an interesting evolving surface chemistry thanks to a fast hydrolysis rate of the pendant ester group and a very dynamic surface chemistry reflected by a water contact angle hysteresis up to 90° . The diffusion of PMATM2 through the PDMS matrix was successful as demonstrated by the Noguer's diffusion test. The infrared analysis

Chapter II. Hydrolyzable polymer additive-based silicone elastomers

highlighted the enrichment or saturation of the surface with PMATM2 at least within the first 6 weeks of immersion. However, after 32 weeks, PMATM2 was almost totally absent on the M3T-BX surfaces. By combining the results from the mass loss test and infrared spectra, it was obvious that there was a reservoir effect of PMATM2 polymer additive upon immersion. The shortage of PMATM2 was limited to 12 weeks, after that the surface is mainly made of PDMS.

In this study, it was also observed the apparition on the PDMS surface of a thin white powder-like layer. This has raised some issues for the analysis of the surface properties such as contact angle and roughness measurements. At this stage, it is possible to say this white layer is made of siliceous phase and/or salt compounds.

Finally, the analysis of the bulk properties of the coatings enabled to conclude there was no major influence of the polymer additives on the elastic modulus, before and after immersion, which is promising to maintain fouling release properties upon immersion.

All these physico-chemical properties were important to characterize as they will be the key drivers of the antifouling and fouling release properties which are discussed in Chapter V.

II.6. Bibliographical references

1. Galli, G.; Martinelli, E. Amphiphilic Polymer Platforms: Surface engineering of Fflms for marine antibiofouling. *Macromolar Rapid Communications* **2017**, *38*, 1–20.
2. Mielczarski, J.A.; Mielczarski, E.; Galli, G.; Morelli, A.; Martinelli, E.; Chiellini, E. The Surface-segregated nanostructure of fluorinated copolymer–poly(dimethylsiloxane) blend films. *Langmuir* **2010**, *26*, 2871–2876.
3. Sundaram, H.S.; Cho, Y.; Dimitriou, M.D.; Finlay, J.A.; Cone, G.; Williams, S.; Handlin, D.; Gatto, J.; Callow, M.E.; Callow, J.A.; et al. Fluorinated amphiphilic polymers and their blends for fouling-release applications: The benefits of a triblock copolymer surface. *ACS Applied Materials & Interfaces* **2011**, *3*, 3366–3374.
4. Camós Noguera, A.; Olsen, S.M.; Hvilsted, S.; Kiil, S. Diffusion of surface-active amphiphiles in silicone-based fouling-release coatings. *Progress in Organic Coatings* **2017**, *106*, 77–86.
5. Oliva, M.; Martinelli, E.; Galli, G.; Pretti, C. PDMS-based films containing surface-active amphiphilic block copolymers to combat fouling from barnacles *B. amphitrite* and *B. improvisus*. *Polymer* **2017**, *108*, 476–482.
6. Rufin, M.A.; Barry, M.E.; Adair, P.A.; Hawkins, M.L.; Raymond, J.E.; Grunlan, M.A. Protein resistance efficacy of PEO-silane amphiphiles: Dependence on PEO-segment length and concentration. *Acta Biomaterialia* **2016**, *41*, 247–252.
7. Wei, C.; Zhang, G.; Zhang, Q.; Zhan, X.; Chen, F. Silicone oil-infused slippery surfaces based on Sol–Gel process-induced nanocomposite coatings: A facile approach to highly stable bioinspired surface for biofouling resistance. *ACS Applied Materials & Interfaces* **2016**, *8*, 34810–34819.
8. Azemar, F.; Faÿ, F.; Réhel, K.; Linossier, I. Control of hydration and degradation properties of triblock copolymers polycaprolactone- *b* -polydimethylsiloxane- *b* -polycaprolactone. *Journal of Applied Polymer Science* **2014**, *131*, n/a-n/a.
9. Marabotti, I.; Morelli, A.; Orsini, L.M.; Martinelli, E.; Galli, G.; Chiellini, E.; Lien, E.M.; Pettitt, M.E.; Callow, M.E.; Callow, J.A.; et al. Fluorinated/siloxane copolymer blends for fouling release: chemical characterisation and biological evaluation with algae and barnacles. *Biofouling* **2009**, *25*, 481–493.
10. Mazan, J.; Leclerc, B.; Galandrin, N.; Couarraze, G. Diffusion of free polydimethylsiloxane chains in polydimethylsiloxane elastomer networks. *European Polymer Journal* **1995**, *31*, 803–807.
11. Gent, A.N.; Tobias, R.H. Diffusion and equilibrium swelling of macromolecular networks by their linear homologs. *Journal of Polymer Science: Polymer Physics Edition* **1982**, *20*, 2317–2327.
12. Garrido, L.; Mark, J.E.; Ackerman, J.L.; Kinsey, R.A. Studies of self-diffusion of poly(dimethylsiloxane) chains in PDMS model networks by pulsed field gradient NMR. *Journal of Polymer Science Part B: Polymer Physics* **1988**, *26*, 2367–2377.
13. Lejars, M.; Margaillan, A.; Bressy, C. Synthesis and characterization of diblock and statistical copolymers based on hydrolyzable siloxy silylester methacrylate monomers. *Polymer Chemistry* **2014**, *5*, 2109.
14. Li, X.; Zhang, Q.; Li, Z.; Xu, S.; Zhao, C.; Chen, C.; Zhi, X.; Wang, H.; Zhu, N.; Guo, K. Tripodal hydrogen bond donor binding with sulfonic acid enables ring-opening polymerization. *Polymer Chemistry* **2016**, *7*, 1368–1374.

15. Faÿ, F.; Linossier, I.; Peron, J.J.; Langlois, V.; Vallée-Rehel, K. Antifouling activity of marine paints: Study of erosion. *Progress in Organic Coatings* **2007**, *60*, 194–206.
16. Lim, J.; Chong, M.S.K.; Teo, E.Y.; Chen, G.-Q.; Chan, J.K.Y.; Teoh, S.-H. Biocompatibility studies and characterization of poly(3-hydroxybutyrate-co-3-hydroxyhexanoate)/polycaprolactone blends. *Journal of Biomedical Materials Research* **2013**, *101B*, 752–761.
17. Ma, C.; Xu, W.; Pan, J.; Xie, Q.; Zhang, G. Degradable polymers for marine antibiofouling: optimizing structure to improve performance. *Industrial & Engineering Chemistry Research* **2016**, *55*, 11495–11501.
18. Azemar, F.; Faÿ, F.; Réhel, K.; Linossier, I. Development of hybrid antifouling paints. *Progress in Organic Coatings* **2015**, *87*, 10–19.
19. Ou, B.; Chen, M.; Huang, R.; Zhou, H. Preparation and application of novel biodegradable polyurethane copolymer. *RSC Advances* **2014**, *4*, 10000–10005.
20. Xie, Q.; Ma, C.; Zhang, G.; Bressy, C. Poly(ester)-poly(silyl methacrylate) copolymers: synthesis and hydrolytic degradation kinetics. *Polymer Chemistry* **2018**, *9*, 1448–1454.
21. Dai, G.; Xie, Q.; Chen, S.; Ma, C.; Zhang, G. Biodegradable poly(ester)-poly(methyl methacrylate) copolymer for marine anti-biofouling. *Progress in Organic Coatings* **2018**, *124*, 55–60.
22. Faÿ, F.; Linossier, I.; Langlois, V.; Renard, E.; Vallée-Réhel, K. Degradation and controlled release behavior of ϵ -caprolactone copolymers in biodegradable antifouling Coatings. *Biomacromolecules* **2006**, *7*, 851–857.
23. Duong, T.H.; Briand, J.-F.; Margailan, A.; Bressy, C. Polysiloxane-based block copolymers with marine bacterial anti-adhesion properties. *ACS Applied Materials & Interfaces* **2015**, *7*, 15578–15586.
24. Noguier, A.C. *Experimental investigation of the behaviour and fate of block copolymers in fouling-release coatings*; Technical University of Denmark (DTU): Kgs. Lyngby, **2016**.
25. Wang, Z.; Volinsky, A.A.; Gallant, N.D. Crosslinking effect on polydimethylsiloxane elastic modulus measured by custom-built compression instrument. *Journal of Applied Polymer Science* **2014**, *131*.
26. Vladkova, T.G.; Dineff, P.D.; Zlatanov, I.Y.; Kathioli, S.; Ramasammy, V.; Vasudeva, P.S.M. Composition coating for biofouling protection *WO2008/07102A1*, **2008**.
27. Olsen, S.M.; Yebra, D.M. Polysiloxane-based fouling release coats including enzymes *AU2012278332B2*, **2014**.
28. Jones, P.K.; Hamblett, P.J.; Hamilton, L. A, Method for coating an aged coating layer on a substrate, and a coating composition suitable for use in this method *US2017/0051159A1*, **2017**.
29. Mincheva, R.; Beigbeder, A.; Pettitt, M.E.; Callow, M.E.; Callow, J.A.; Dubois, P. Metal-free anti-biofouling coatings: the preparation of silicone-based nanostructured coatings via purely organic catalysis. *Nanocomposites* **2016**, *2*, 51–57.
30. Florio, J.; Ravichandran, R.; Switala, D.; Hsieh, B. Non-tin catalysts for alkoxy silane polymers. *European coatings journal* **2016**, *3*, 48–54.
31. Bressy, C.; Lejars, M. Marine fouling an overview. *The Journal of Ocean Technology* **2014**, *9*, 20–28.
32. Commission Regulation (EU) No 276/2010, *Official journal of the European Union*, 31 March **2010**, 86, 7-12.
33. Lee, J.N.; Park, C.; Whitesides, G.M. Solvent Compatibility of Poly(dimethylsiloxane)-Based Microfluidic Devices. *Analytical Chemistry* **2003**, *75*, 6544–6554.

34. Bordes, C.; Fréville, V.; Ruffin, E.; Marote, P.; Gauvrit, J.Y.; Briançon, S.; Lantéri, P. Determination of poly(ϵ -caprolactone) solubility parameters: Application to solvent substitution in a microencapsulation process. *International Journal of Pharmaceutics* **2010**, *383*, 236–243.
35. Vogel, G.E.; Stark, F.O. Mutual solubilities in water-permethysiloxane systems. *Journal of Chemical & Engineering Data* **1964**, *9*, 599–601.
36. Bullock, S.; Johnston, E.E.; Willson, T.; Gatenholm, P.; Wynne, K.J. Surface science of a filled polydimethylsiloxane-based alkoxy silane-cured elastomer: RTV11. *Journal of colloid and interface science* **1999**, *210*, 18–36.
37. Zhang, J.; Lin, C.; Wang, L.; Zheng, J.; Xu, F.; Sun, Z. Study on the correlation of lab assay and field test for fouling-release coatings. *Progress in Organic Coatings* **2013**, *76*, 1430–1434.
38. Berglin, M.; Wynne, K.J.; Gatenholm, P. Fouling-release coatings prepared from α,ω -dihydroxypoly(dimethylsiloxane) cross-linked with (heptadecafluoro-1,1,2,2-tetrahydrodecyl)triethoxysilane. *Journal of Colloid and Interface Science* **2003**, *257*, 383–391.
39. Wynne, K.J.; Ho, T.; Johnston, E.E.; Myers, S.A. Surface science and stability of networks prepared from hydroxy-terminated polydimethylsiloxane and methyltriethoxysilane. *Applied Organometallic Chemistry* **1998**, *12*, 763–770.
40. Ogoshi, T.; Fujiwara, T.; Bertolucci, M.; Galli, G.; Chiellini, E.; Chujo, Y.; Wynne, K.J. Tapping mode AFM evidence for an amorphous reticular phase in a condensation-cured hybrid elastomer: α,ω -Dihydroxypoly(dimethylsiloxane)/Poly(diethoxysiloxane)/fumed silica nanoparticles. *Journal of the American Chemical Society* **2004**, *126*, 12284–12285.
41. Johnston, E.; Bullock, S.; Uilk, J.; Gatenholm, P.; Wynne, K.J. Networks from α,ω -dihydroxypoly(dimethylsiloxane) and (tridecafluoro-1,1,2,2-tetrahydrooctyl)triethoxysilane: Surface microstructures and surface characterization. *Macromolecules* **1999**, *32*, 8173–8182.
42. Havrilla, G.J.; Miller, T. Micro X-ray fluorescence in materials characterization. *Powder Diffraction* **2004**, *19*, 119–126.
43. Thorlaksen, P.C.W.; Yebra, D.M.; Catala, P. Hydrogel-based third generation fouling release coatings. *Royal Belgium Institute of Marine Engineers* **2010**, 1-7.
44. Stricher, A.M.; Rinaldi, R.G.; Barrès, C.; Ganachaud, F.; Chazeau, L. How I met your elastomers: from network topology to mechanical behaviours of conventional silicone materials. *RSC Advances* **2015**, *5*, 53713–53725.
45. Andriot, M.; DeGroot, J.V.; Meeks, R.; Wolf, A.T.; Leadley, S.; Garaud, J.L.; Gubbels, F.; Lecomte, J.P.; Lenoble, B.; Stassen, S.; et al., Silicones in Industrial Applications. *Société Royale de Chimie* **2004**, 106.
46. Warrick, E.L.; Pierce, O.R.; Polmanteer, K.E.; Saam, J.C. Silicone elastomer developments 1967–1977. *Rubber Chemistry and Technology* **1979**, *52*, 437–525.
47. Kuo, A.C. Poly (dimethylsiloxane). *Polymer data handbook* **1999**, 411–435.
48. Wang, B.; Krause, S. Properties of dimethylsiloxane microphases in phase-separated dimethylsiloxane block copolymers. *Macromolecules* **1987**, *20*, 2201–2208.
49. Aranguren, M.I. Crystallization of polydimethylsiloxane: effect of silica filler and curing. *Polymer* **1997**, *39*, 4897-4903.
50. Lebedev, B.V.; Mukhina, N.N.; Kulagina, T.G. Thermodynamics of polydimethylsiloxane in the range 0–350°K. *Polymer Science U.S.S.R.* **1978**, *20*, 1458–1466.

Chapter II. Hydrolyzable polymer additive-based silicone elastomers

51. Ohlberg, S.M.; Alexander, L.E.; Warrick, E.L. Crystallinity and orientation in silicone rubber. I. X-ray studies. *Journal of Polymer Science* **1958**, *27*, 1–17.
52. Averous, L.; Moro, L.; Dole, P.; Fringant, C. Properties of thermoplastic blends: starch–polycaprolactone. *Polymer* **2000**, *41*, 4157–4167.
53. Rosa, D. dos S.; Rodrigues, T.C.; Graças Fassina Guedes, C. das; Calil, M.R. Effect of thermal aging on the biodegradation of PCL, PHB-V, and their blends with starch in soil compost: Biodegradation of PCL and PHB-V in Compost. *Journal of Applied Polymer Science* **2003**, *89*, 3539–3546.

Chapter III	Hydrolyzable PDMS/polyester hybrid networks	163
III.1.	<u>Introduction</u>	<u>163</u>
III.2.	<u>Hydrolyzable copolymers</u>	<u>164</u>
III.2.1.	Preparation of the hydrolyzable copolymers	164
III.2.1.1.	Synthesis of poly(D,L-lactide-co-glycolide).....	164
III.2.1.2.	Synthesis of PLGA-b-PDMS-b-PLGA.....	166
III.2.1.3.	Poly(ϵ -caprolactone)-based polymers.....	168
III.2.2.	Physico-chemical properties of the (co)polymers	169
III.2.2.1.	General description of the polymers.....	169
III.2.2.2.	Wettability of the polyester-based polymers.....	170
III.3.	<u>Elaboration of PDMS/polyester hybrid networks</u>	<u>171</u>
III.3.1.	Preparation of polyester macrocrosslinkers	173
III.3.1.1.	Preliminary investigations.....	173
III.3.1.1.1.	Alkoxysilylation reaction of polyester-based polymers.....	173
III.3.1.1.2.	Influence of the alkoxysilane functions.....	174
III.3.2.	Formation of PDMS/polyester hybrid networks	177
III.3.2.1.	Preliminary investigations.....	177
III.3.2.1.1.	Co-solvent	177
III.3.2.1.2.	Molar mass of the polyester-based polymer	178
III.3.2.1.3.	Catalyst amount	180
III.3.2.1.4.	Formulation preheating	180
III.3.2.1.5.	Curing conditions	180
III.3.2.1.6.	Conclusion on the optimal parameters.....	181
III.3.2.2.	Final coatings formulations.....	185
III.3.3.	Elaboration of self-crosslinked polyester-based networks	185
III.3.4.	Residue extraction test	186
III.3.5.	Thermal degradation of the networks	188
III.4.	<u>Conclusion</u>	<u>195</u>
III.5.	<u>Bibliographical references</u>	<u>197</u>

Chapter III Hydrolyzable PDMS/polyester hybrid networks

III.1. Introduction

The previous study in Chapter II, dealing with hydrolyzable additives-based coatings, showed a time-limited hydrolysis profile with PMATM2-based additives, or on the contrary, a hydrolysis resistance with PCL-based additives. In this new chapter, the aim was to find a system which is hydrolyzed on the long-term without risking the shortage effect of the use of hydrolyzable polymer-based additives.

The strategy was to design networks based on degradable polyesters. Such networks (e.g. hydrogels, interpenetrated and reversible networks) were already employed in the biomedical field to provide drug delivery systems or engineered tissue scaffolds [1]. The common properties of these networks are their biocompatibility, their biodegradability, their controlled internal architectures and their improved mechanical properties [2].

In this work, it was decided to use degradable networks as novel antifouling systems. The networks were obtained by condensing trialkoxysilane-terminated polyesters with bis-silanol polydimethylsiloxane chains. In this way, we could combine both fouling release (FR) and self-polishing (SP) mechanisms. The FR ability would be enabled by the presence of PDMS chains whereas the SP ability would be generated by the hydrolysis of the polyester material. These PDMS/polyester hybrid networks are expected to give a more gradual hydrolytic mass loss ensuring a continuous renewal of the surface chemistry.

In this chapter, different hydrolyzable copolymers were chosen according to their degradation kinetics and physico-chemical properties. Poly(D,L-lactide-co-glycolide) (PLGA) and a triblock copolymer PLGA-*b*-PDMS-*b*-PLGA (LGO) were synthesized. The hydrolytic degradation of PLGA segments are known to be faster than those of the poly(ϵ -caprolactone) ones, which make them more attractive for our final antifouling application. A new commercial PCL diol (2,000 g/mol) was introduced in this chapter and the commercial PCL-*b*-PDMS-*b*-PCL (TGO) copolymer, previously used in Chapter II, was also chosen as a candidate for the elaboration of hydrolyzable PDMS/polyester hybrid networks.

Chapter III – Hydrolyzable PDMS/polyester hybrid networks

All the polyester-based (co)polymers were end-capped with trialkoxysilane functions, and then crosslinked with bis-silanol PDMS to form the desired PDMS/polyester hybrid networks.

The optimal conditions of the crosslinking reaction were investigated. Various parameters such as the nature of the reactive terminal functions and the curing temperature had a crucial effect on the crosslinking of the polymers.

In addition to the design of the PDMS/polyester hybrid networks, the different trialkoxysilane-terminated polymers were also self-crosslinked to provide self-crosslinked polyester-based polymers as references.

III.2. Hydrolyzable copolymers

III.2.1. Preparation of the hydrolyzable copolymers

III.2.1.1. Synthesis of poly(D,L-lactide-co-glycolide)

Poly(D,L-lactide-co-glycolide) (PLGA) was synthesized by coordination-insertion ring opening polymerization of D,L-lactide and glycolide monomers at 140°C for 24 h (Figure III-1) [3]. The copolymer was prepared in the presence of stannous octoate catalyst with a monomers/catalyst feed molar ratio (M/C) of 400. The molar mass of PLGA was controlled by the monomers/initiator molar ratio (M/I) with 1,4-butanediol (BDO) as the initiator (§ VI.3.1.2.).

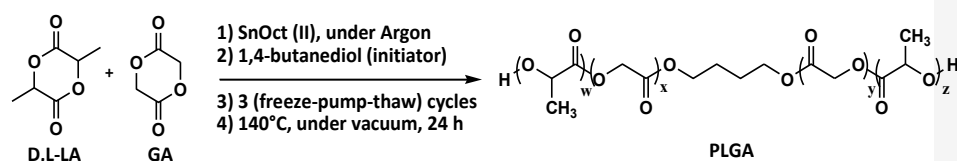


Figure III-1. Synthesis of poly(D,L-lactide-co-glycolide).

As reported in the literature, a linear relationship between M/I and the number-average molar mass (M_n) was established (Figure III-2).

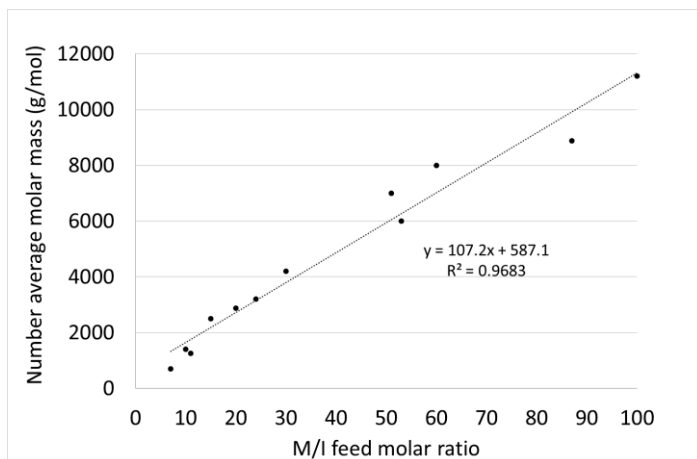


Figure III-2. Linear relationship between the number average molar mass (M_n) of the PLGA copolymer and the M/I ratio (the initiator nature varied depending on the literature source) [4–10].

The theoretical molar mass can also be found with the Eq. 1 [11]:

$$M_{n,th}(\text{g/mol}) = \frac{[M]}{[I]} \times M_{\text{monomer}} \times \text{Conversion} \quad (\text{Eq.1})$$

The molar mass of the obtained PLGA varied from 900 to 2,000 g/mol ($M_{n,SEC}$) with targeted M/I ratios ranging from 5 to 20 (Table III-1). These low molar masses were preferred to maximize the compatibility of PLGA with PDMS for the future formulations of hybrid networks.

The D,L-lactide was preferred to the D or L enantiomers as the polymers of the latter ones are semi-crystalline polymers whereas the polymerized racemic form is amorphous due to the irregularities in the polymer main chain [12]. The amorphous state of the poly(D,L-lactide-co-glycolide) is interesting since amorphous phases can be faster hydrated than crystalline phases, and thus will undergo faster hydrolytic degradation [13,14]. For example, the intrinsically amorphous racemic poly(D,L-lactic acid) has a mass loss of 90 % after 12 weeks in a buffered solution (pH = 7.4 and T = 37°C) whereas the amorphous poly(L-lactic acid) has a mass loss of 50 % after 110 weeks in the same conditions [15]. The mixture of LA and GA monomers gives more advantages regarding the hydrolysis kinetics. PLA is more hydrophobic than PLGA leading to a lower water absorption into the polymer [14,16]. The 75/25 and 80/20 (LA/GA) molar ratios were chosen given that the resulting PLGA copolymers display fast hydrolysis kinetics combined with good solubility in most organic solvents [3,16]. No residual 1,4-butanediol was found at the end of the polymerization (before precipitation). Mostly

residual lactide monomer was found (< 10 mol. %) in the reaction mixture but were eliminated during the precipitation step in cold pentane.

Table III-1. Synthesis of PLGA copolymers.

	M/I	Targeted molar ratio LA/GA in PLGA	Molar ratio LA/GA in PLGA (%/%) ^a	Conv.LA/GA (%) ^a	M _{n,th} (g/mol) ^b	M _{n,SEC} (g/mol) ^c	M _{w,SEC} (g/mol) ^c	Đ ^c	M _{n,NMR} (g/mol) ^d
PLGA (740)	5	75/25	74/26	98.2/99.5	690	880	980	1.1	740
PLGA (1,900)	10	75/25	75/25	91.3/96.9	1,400	1,600	2,500	1.5	1,900
PLGA (2,500)	20	80/20	80/20	97.7/99.3	2,800	1,500	2,200	1.4	2,500

^aCalculated by means of ¹H NMR before PLGA precipitation (Cf. experimental section, § VI.3.1.2.).

^bCalculated with $M_{n,th} \left(\frac{g}{mol} \right) = \frac{[M]}{[I]} \times M_{monomer} \times Conversion$ with $M_{monomer} = w_{LA}^{PLGA} \times M_{LA} + w_{GA}^{PLGA} \times M_{GA}$ and Conversion arbitrarily fixed at 100%.

^cDetermined by SEC (toluene, 30°C, PS standards).

^dCalculated by ¹H NMR after PLGA precipitation (Cf. experimental section, § VI.3.1.2.).

III.2.1.2. Synthesis of PLGA-*b*-PDMS-*b*-PLGA

PLGA-*b*-PDMS-*b*-PLGA (LGO) triblock copolymers were synthesized to investigate the influence of the central PDMS block on the network formation. To synthesize the triblock copolymer, a commercial bis(3-aminopropyl) polydimethylsiloxane (H₂N-(CH₂)₃-PDMS-(CH₂)₃-NH₂, with M_{n,SEC} = 1,400 g/mol, M_{w,SEC} = 2,100 g/mol, Đ = 1.5, M_{n,RMN} ≈ 3,000 g/mol) was used as a macroinitiator. Lactone rings were allowed to react on both sides of the central PDMS block by coordination-insertion ring-opening polymerization with stannous octoate catalyst (M/C = 400) at 150°C for 24 h (Figure III-3).

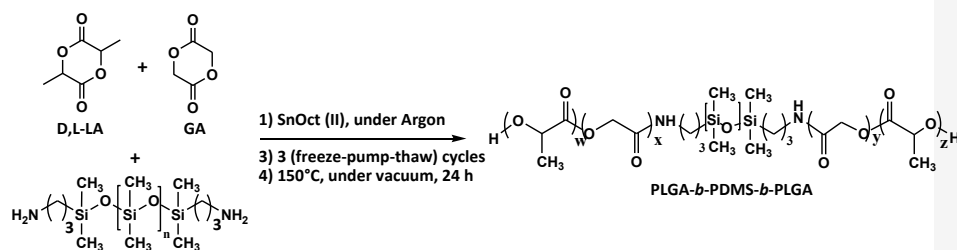


Figure III-3. Synthesis of PLGA-*b*-PDMS-*b*-PLGA.

The resulting triblock copolymers were yellowish viscous oils (Table III-2).

Table III-2. Syntheses of PLGA-*b*-PDMS-*b*-PLGA (LGO) triblock copolymers.

PLGA- <i>b</i> - PDMS- <i>b</i> -PLGA	M/I	Targeted molar ratio LA/GA in PLGA	Molar ratio LA/GA in PLGA (%/%) ^a	Conv.LA/GA (%) ^a	M _{n,th} (g/mol) ^b	M _{n,SEC} (g/mol) ^c	M _{w,SEC} (g/mol) ^c	Đ ^c	M _{n,NMR} (g/mol) ^a
LGO5200	18	75/25	76/24	94.9/99.9	5,500	6,700	16,600	2.5	1,100- <i>b</i> -3,000- <i>b</i> -1,100 (= 5,200)
LGO5800	20	80/20	79/21	97.2/99.6	5,800	10,700	24,400	2.3	1,400- <i>b</i> -3,000- <i>b</i> -1,400 (=5,800)
LGO6200	20	80/20	79/21	96.9/99.3	5,800	7,600	17,300	2.3	1,600- <i>b</i> -3,000- <i>b</i> -1,600 (= 6,200)

^aCalculated by means of ¹H NMR (Cf. experimental section, § VI.3.1.4.).

^bCalculated with $M_{n,th} \left(\frac{g}{mol} \right) = \frac{[M]}{[I]} \times M_{monomer} \times Conversion + M_{macroinitiator}$ with $M_{monomer} = w_{LA}^{PLGA} \times M_{LA} + w_{GA}^{PLGA} \times M_{GA}$, Conversion arbitrarily fixed at 100% and $M_{macroinitiator}$ the molar mass of the central PDMS block (3,000 g/mol).

^cDetermined by SEC (toluene, 30°C, PS standards).

The polymers were not purified by precipitation due to their oily physical state. Their purification by solid-phase extraction (or size exclusion chromatography) was not conducted as the monomers and the copolymer had very similar affinities with numerous solvents.

Figure III-4 shows the SEC curves of the three PLGA-*b*-PDMS-*b*-PLGA triblock copolymers compared to the bis(3-aminopropyl) polydimethylsiloxane macroinitiator. The synthesized PLGA-*b*-PDMS-*b*-PLGA (LGO) triblock copolymers displayed number-average molar masses ranging from 6,000 to 11,000 according to the size exclusion chromatography. Their dispersity values were particularly high (Đ ≥ 2.3) suggesting a heterogeneous polymer chains growth.

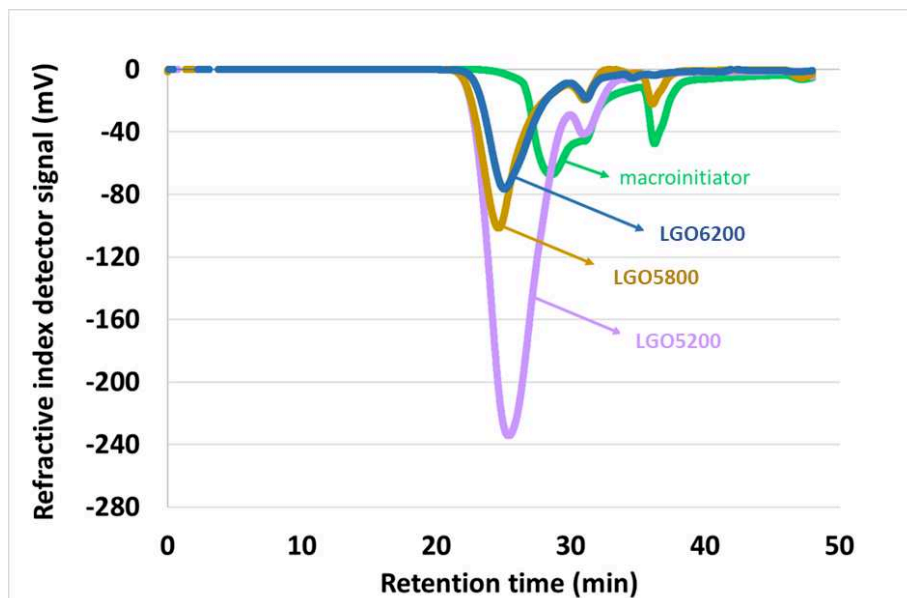


Figure III-4. SEC curves of the three PLGA-*b*-PDMS-*b*-PLGA triblock copolymers (LGO5200, LGO5800 and LGO6200) alongside with the bis(3-aminopropyl) polydimethylsiloxane macroinitiator.

The absence of remaining bis(3-aminopropyl) polydimethylsiloxane macroinitiator was confirmed by ^1H NMR analyses. Indeed, the ^1H NMR spectra revealed the total disappearance of a triplet at 2.68 ppm corresponding to $-\text{CH}_2-\text{NH}_2$ and appearance of a multiplet at 3.23 ppm corresponding to the $-\text{CH}_2-\text{NHCOR}$ (Cf. experimental section, § VI.3.1.4.).

III.2.1.3. Poly(ϵ -caprolactone)-based polymers

PCL (2,000 g/mol, Perstrop) was a white soft solid and was used as received without further purification. It was synthesized from the neopentyl glycol (NEO) initiator. PCL-*b*-PDMS-*b*-PCL (TGO6800) (6,800 g/mol, Evonik) was in the form of waxy solid pellets, also used without further purification.

III.2.2. Physico-chemical properties of the (co)polymers

III.2.2.1. General description of the polymers

Table III-3 summarizes the physico-chemical properties of the commercial and synthesized hydrolyzable copolymers used in this chapter. The crystallinity of the PCL-based polymers varied from 28 to 62 % with PCL block length comprised between 2,000 and 3,000 g/mol. The PCL homopolymers displayed a glass transition temperature (T_g) at ca. -60°C . The T_g of the PCL blocks within the triblock copolymer could not be detected with modulated DSC. The PLGA-based polymers were all amorphous polymers with T_g comprised between -20°C to 20°C . The more the molar mass ($M_{n,SEC}$) of the PLGA blocks increased, the more the T_g increased.

Table III-3. Summary of the physico-chemical properties of PCL-based and PLGA-based polymers.

Polymer nature	$M_{n,SEC}$ (g/mol)	$M_{w,SEC}$ (g/mol)	\bar{D}	$M_{n,NMR}$ (g/mol)	T_g ($^\circ\text{C}$)	T_m ($^\circ\text{C}$)	ΔH_m (J/g) ^a	X_c (%) ^a
PCL (2,000)	1,800	2,600	1.4	2,000	-67^b	40-44	70	50
PCL (3,000)	3,400	4,300	1.4	3,000	-60^b	51	87	62
PCL- <i>b</i> -PDMS- <i>b</i> - PCL (TGO6800)	7,300	9,600	1.3	2,300-2,200-2,300 (=6,800)	n.d. ^c	52-55	57	28
PLGA (740)	880	980	1.1	740	-24	-	-	-
PLGA (1,900)	1,600	2,500	1.5	1,900	-3	-	-	-
PLGA (2,500)	1,500	2,200	1.4	2,500	4	-	-	-
PLGA- <i>b</i> -PDMS- <i>b</i> -PLGA (LGO5200)	6,700	16,600	2.5	1,100- <i>b</i> -3,000- <i>b</i> - 1,100 (= 5,200)	-8	-	-	-
PLGA- <i>b</i> -PDMS- <i>b</i> -PLGA (LGO5800)	10,700	24,400	2.3	1,400- <i>b</i> -3,000- <i>b</i> - 1,400 (=5,800)	18	-	-	-
PLGA- <i>b</i> -PDMS- <i>b</i> -PLGA (LGO6200)	7,600	17,300	2.3	1,600- <i>b</i> -3,000- <i>b</i> - 1,600 (= 6,200)	18	-	-	-

^aCrystallinity of PCL, X_c (%) = $\frac{w(PCL) \times \Delta H_m \times 100}{\Delta H_m}$ with $\Delta H_m^\circ = 139.3 \frac{J}{g}$ [13] and $w(PCL) = 0.68$ (mass fraction of PCL) for PCL-*b*-PDMS-*b*-PCL.

^bDetermined by modulated DSC.

^c T_g value of the PCL blocks was not observed both with classic and modulated DSC. T_g value of the central PDMS block was not determined.

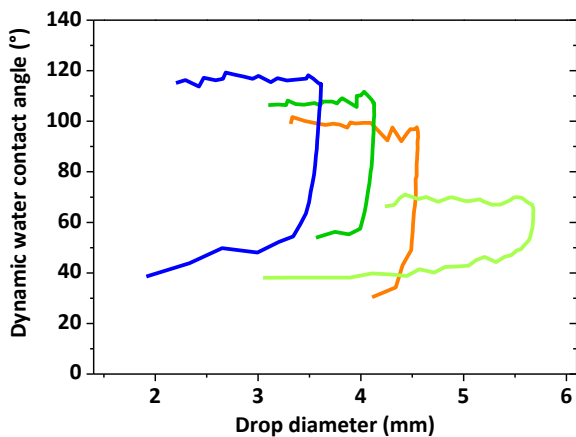
III.2.2.2. Wettability of the polyester-based polymers

The wettability of the polyester-based polymers was essential to assess as it is a key parameter for antifouling surfaces. The pure polyester films were obtained by dissolving the polymers in chloroform (50 wt.%), consecutively applied with a bar coater (100 μm wet) onto glass slides and dried for 48h at ambient air before contact angle analysis.

The PLGA-*b*-PDMS-*b*-PLGA (LGO) copolymers could not be analyzed as it was a very viscous oil. Regarding, the wettability of PLGA, only one copolymer candidate (740 g/mol) was selected in this study.

Figure III-5 showed that the four polymers were mainly hydrophobic in their pristine state (before immersion) except PCL (2,000 g/mol) which displayed a lower advancing contact angle ($\theta_{w,adv} \approx 70^\circ$) than PCL (3,000 g/mol) ($\theta_{w,adv} \approx 105^\circ$). This difference may be explained by a larger density of -OH terminal functional groups present on the surface.

All the hydrolyzable polymers exhibited a water contact angle hysteresis ($\Delta\theta = \theta_{w,adv} - \theta_{w,rec}$) higher than 30° (even higher than 60° for PLGA and PCL-*b*-PDMS-*b*-PCL). In the case of PCL-*b*-PDMS-*b*-PCL (TGO6800), the contact angle hysteresis was attributed to the surface chemical heterogeneity (as previously seen in Chapter II, § II.2.5.). In the case of PCL (2,000 g/mol) and PLGA, the contact angle hysteresis could be rather attributed to a chemical reorganization caused by the relocation of the polymers hydrophilic functions (such as ester or hydroxyl groups) towards the liquid.



	PCL- <i>b</i> -PDMS- <i>b</i> -PCL (TGO6800)	PCL (3,000)	PLGA (740)	PCL (2,000)
$\theta_{w,adv}$ (°)	115.8 ± 0.7	104.9 ± 2.8	101.0 ± 3.3	69.3 ± 0.5
$\theta_{w,rec}$ (°)	55.4 ± 2.7	49.0 ± 7.1	38.1 ± 3.2	38.3 ± 1.6

Figure III-5. Hysteresis curves of water contact angles for PCL-*b*-PDMS-*b*-PCL (TGO6800), PCL3000, PLGA740 and PCL2000, and the advancing and receding contact angle values (average of 3 advancing and receding cycles).

III.3. Elaboration of PDMS/polyester hybrid networks

The previous polyester-based polymers were all functionalized at their chain ends with alkoxy-siloxane groups to prepare the PDMS/polyester hybrid networks. This first step was essential to transform the polyester-based polymers into macrocrosslinkers. The second step was to substitute the polydiethoxysiloxane crosslinker (PDES, 744 g/mol), used for the condensation cure of the PDMS reference, with these polyester-based macrocrosslinkers. These two steps are illustrated in Figure III-6.

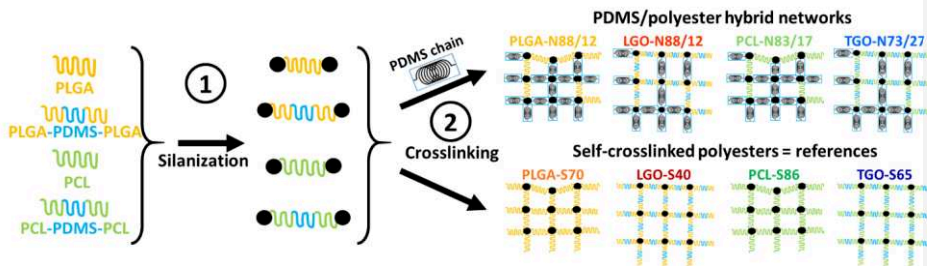


Figure III-6. Schematic pathway to obtain PDMS/polyester hybrid networks as well as their respective references (made of the self-crosslinked polyester-based polymers).

It should be noted that LGO-S40 (from Figure III-6) was not elaborated due to lack of polymer material and time. The formation of PDMS/polyester hybrid networks had required the investigation of various parameters to optimize the crosslinking reaction. A simple experimental set-up enabled to select the optimal conditions to obtain well-crosslinked PDMS/polyester hybrid networks. The different polymer candidates used to obtain hybrid networks are presented in Table III-4.

Table III-4. Overview table of the tested polyester-based candidates.

Nature of the polymer	Code name	$M_{n,NMR}$ (g/mol)
PLGA	PLGA740	740
PLGA	PLGA1900	1,900
PLGA	PLGA2500	2,500
PLGA- <i>b</i> -PDMS- <i>b</i> -PLGA	LGO5200	5,200
PLGA- <i>b</i> -PDMS- <i>b</i> -PLGA	LGO5800	5,800
PLGA- <i>b</i> -PDMS- <i>b</i> -PLGA	LGO6200	6,200
PCL	PCL2000	2,000
PCL	PCL3000	3,000
PCL- <i>b</i> -PDMS- <i>b</i> -PCL	TGO6800	6,800

III.3.1. Preparation of polyester macrocrosslinkers

III.3.1.1. Preliminary investigations

III.3.1.1.1. Alkoxysilanization reaction of polyester-based polymers

The selected polyester-based polymers were all functionalized at their chain ends with either 3-isocyanatopropyltriethoxysilane (IPTES) or 3-isocyanatopropyltrimethoxysilane (IPTMS) coupling agents in chloroform (Figure III-7). The detailed reaction protocols are described in the experimental section (§ VI.1.3.).

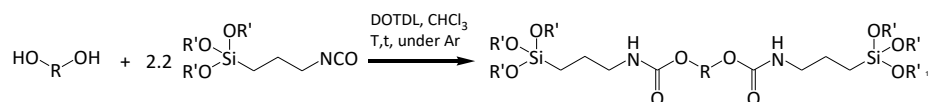


Figure III-7. General synthetic pathway of the alkoxysilanization reaction of the polyester-based polymers (referred as HO-R-OH). R' represents methyl or ethyl groups.

Depending on the nature of the polymer, the reactions were held at different temperatures and at different durations (Table III-5 and Table III-6). The lower reactivity of the LGO and TGO triblock copolymers (PCL-*b*-PDMS-*b*-PCL and PLGA-*b*-PDMS-*b*-PLGA copolymers respectively) was attributed to their higher molar masses and/or presence of a PDMS central block. Conversion rates above or equal to 80 % were achieved. The percentage of prematurely hydrolyzed alkoxysilane functions was monitored throughout the reaction with NMR analyses. A percentage of hydrolyzed alkoxysilane functions was considered too high when exceeding 10 %.

The reaction mixtures were precipitated in cold pentane (or heptane for PCL-*b*-PDMS-*b*-PCL). The precipitate was dried under vacuum overnight. The polymers which were functionalized with IPTMS were formulated within 2 days as the methoxysilane functions were much more sensitive to the air humidity than ethoxysilane functions. Exceeding these 2 days, the methoxysilane-functionalized polymers would react on themselves making it impossible to use them.

Table III-5. Methoxysilanization reactions of the polyester-based polymers.

Polymer code name	Time (h)	Temperature (°C)	Conversion (%) ^a	%-(SiOMe) ₃ hydrolyzed ^b	M _{n,calc.} (g/mol) ^c
PLGA740	4	35	89.5	1.2	1,150
PLGA1900	6	35	80	6.3	2,310
PLGA2500	4	35	100	2	2,910
LGO5200	4	65	100	12.3	5,610
LGO5800	4	65	100	1.8	6,210
LGO6200	5	65	100	12.3	6,610
PCL2000	4	65	100	0	2,410
PCL3000	3	65	100	0	3,410
TGO6800	6	65	100	0	7,210

^aThe conversion was calculated with ¹H NMR analysis before the polymer precipitation (Cf. experimental section, chapter VI, § VI.3.1.6.).

^bThe % -(SiOMe)₃ was calculated with ¹H NMR analysis after the polymer precipitation and drying (Cf. experimental section, chapter VI, § VI.3.1.6.).

^cM_{n, calc.} is the theoretical molar mass of the functionalized polymers, obtained with the addition of the molar mass of the end-capped trialkoxysilane functions to the molar mass (found with ¹H NMR) of the non-modified polymer.

Table III-6. Ethoxysilanization reactions of the polyester-based polymers.

Polymer code name	Time (h)	Temperature (°C)	Conversion (%) ^a	%-(SiOEt) ₃ hydrolyzed ^b	M _{n,calc.} (g/mol) ^c
PLGA740	3	65	81.5	0.6	1,240
PCL2000	1	60	100	0	2,500
PCL3000	1	70	90	5.7	3,500
TGO6800	7	75	91	6	7,300

^aThe conversion was calculated with ¹H NMR analysis before the polymer precipitation (Cf. experimental section, chapter VI, § VI.3.1.6.).

^bThe % -(SiOEt)₃ was calculated with ¹H NMR analysis after the polymer precipitation and drying precipitation (Cf. experimental section, chapter VI, § VI.3.1.6.).

^cM_{n,calc.} is the theoretical molar mass of the functionalized polymers, it was obtained with the addition of the molar mass of the end-capped trialkoxysilane functions to the molar mass (found with ¹H NMR) of the non-modified polymer.

III.3.1.1.2. Influence of the alkoxy silane functions

The sol-gel reaction used to obtain the hybrid networks is a two-step reaction: the alkoxy silanes are first hydrolyzed and then condensed. In this way, the well crosslinking of the network strongly depends on the hydrolysis kinetics of the first step. Thus, a preliminary ¹H

Chapter III – Hydrolyzable PDMS/polyester hybrid networks

NMR study was performed to evaluate the hydrolysis kinetics of the alkoxy silane-functions carried by the polyester-based polymers as described in the experimental section (§ VI.3.1.7.).

The study consisted in dissolving the freshly synthesized alkoxy silane-terminated polyester-based polymers (\approx 30-40 mg) in deuterated THF (1 mL) alongside with distilled water as a co-solvent (10 μ L) and dioctyltin dilaurate as a catalyst (1 μ L). The solution was immediately inserted in an NMR tube for direct NMR analysis at 23°C. The NMR spectra were recorded every 15 min for 24 h for the methoxy silane-terminated polymers. The NMR internal references and analyzed peaks are indicated in Table III-7.

Table III-7. NMR internal references and analyzed peaks to rate the hydrolysis kinetics of the -SiOR' functions.

Polymer	-SiOR' nature	Internal ref. (δ , ppm, fixed H number, attribution)	Observed peak (-SiOR') (δ , ppm, attribution)
PLGA740	-SiOMe	Singlet, 4.20 ppm, 4H, $-(\text{CH}_2)_2$ - BDO ^a	Singlet, 3.48 ppm, $-\text{SiOCH}_3$
	-SiOEt	Singlet, 4.20 ppm, 4H, $-(\text{CH}_2)_2$ - BDO ^a	Quadruplet, 3.79 ppm, $-\text{SiOCH}_2\text{CH}_3$
LGO5800	-SiOMe	Multiplet, 0.06 ppm, 244H, $-\text{Si}(\text{CH}_3)_2$	Singlet, 3.48 ppm, $-\text{SiOCH}_3$
	-SiOEt	Multiplet, 0.06 ppm, 244H, $-\text{Si}(\text{CH}_3)_2$	Quadruplet, 3.79 ppm, $-\text{SiOCH}_2\text{CH}_3$
PCL2000	-SiOMe	Singlet, 3.84 ppm, 4H, $-(\text{CH}_2)_2$ - NEO ^a	Singlet, 3.48 ppm, $-\text{SiOCH}_3$
	-SiOEt	Singlet, 3.84 ppm, 4H, $-(\text{CH}_2)_2$ - NEO ^a	Quadruplet, 3.79 ppm, $-\text{SiOCH}_2\text{CH}_3$
PCL3000	-SiOMe	Multiplet, 4.02 ppm, 50H, $-\text{OCH}_2$ -	Singlet, 3.48 ppm, $-\text{SiOCH}_3$
	-SiOEt	Multiplet, 4.02 ppm, 50H, $-\text{OCH}_2$ -	Quadruplet, 3.79 ppm, $-\text{SiOCH}_2\text{CH}_3$
TGO6800	-SiOMe	Triplet, 0.50 ppm, 4H, $-\text{Si-CH}_2\text{-CH}_2$ -	Singlet, 3.48 ppm, $-\text{SiOCH}_3$
	-SiOEt	Triplet, 0.50 ppm, 4H, $-\text{Si-CH}_2\text{-CH}_2$ -	Quadruplet, 3.79 ppm, $-\text{SiOCH}_2\text{CH}_3$

^aBD and NEO corresponded to the initiators used to synthesize PLGA and PCL respectively, their protons served here as internal references as they did not participate in the reaction and were easy to identify on the NMR spectra.

Figure III-8 showed that the triethoxysilane-terminated polymers required more than 24 h to be completely hydrolyzed. Thus, additional spectra were obtained until 168 h. Triethoxysilane-terminated PCL (3,000 g/mol) and triethoxysilane-terminated PCL-*b*-PDMS-*b*-PCL (TGO6800) solutions (contained in the NMR tube) were found gelled after *ca.* 80 h. This gelation was a good indication of the self-condensation of the functionalized polymers within the tube. After 168 h, some of the triethoxysilane-terminated polymers were still not completely hydrolyzed according to the ¹H NMR although the solutions were gelled. This showed that the hydrolysis kinetic was too slow and then limited by the gelling effect of the partially self-condensed polymers even if the gel was swollen in the deuterated solvent.

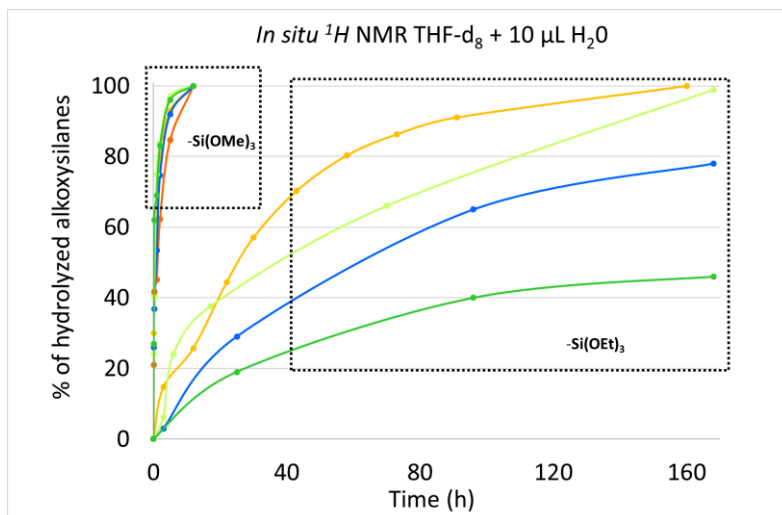


Figure III-8. Percentage of hydrolyzed alkoxy silane as a function of time (h) in deuterated THF. The 2 boxes differentiate the polymers modified at their chain ends with trimethoxysilane and triethoxysilane: PLGA740, PCL2000, PCL3000, TGO6800 and LGO5800.

Compared to the triethoxysilane-terminated polymers, the trimethoxysilane-terminated polymers were hydrolyzed at their chain ends within 8 hours. Some small variations of hydrolysis kinetics were observed between the homopolymers (PCL2000, PCL3000 and PLGA740) and the triblock copolymers (TGO6800 and LGO5800) (Figure III-9). The higher the molar mass was the slower the hydrolysis was. These results were very useful to determine the hydrolysis kinetics of the terminal alkoxy silane functions (≈ 8 h). The IPTMS coupling agent was thus selected for the design of the polyester-based networks as it provided the fastest hydrolysis of chain ends.

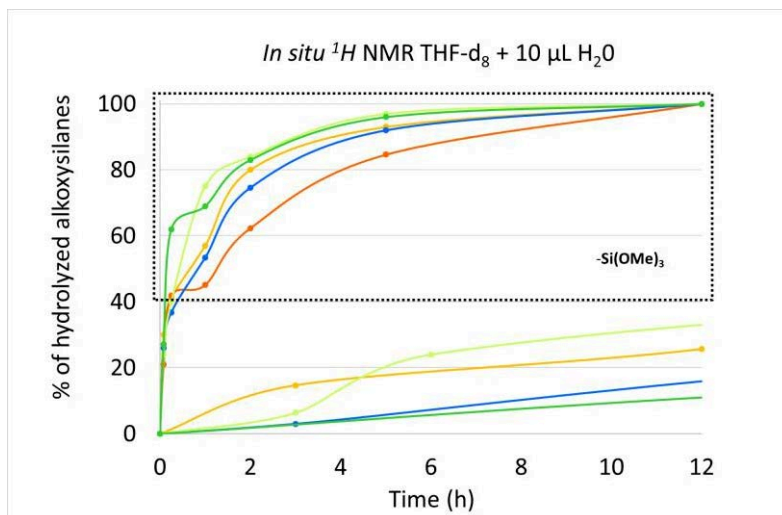


Figure III-9. Focus on the percentage of hydrolyzed trimethoxysilane as a function of time (h) in deuterated THF for PLGA740, PCL2000, PCL3000, TGO6800 and LGO5800 polymers.

III.3.2. Formation of PDMS/polyester hybrid networks

At this stage, the retained parameters are the trimethoxysilane crosslinking functions and the solvent (THF). In the following steps, different formulation and curing conditions were discussed always with the intention of optimizing the crosslinking of the PDMS/polyester hybrid networks.

III.3.2.1. Preliminary investigations

III.3.2.1.1. Co-solvent

The solvent/co-solvent ratio was kept at 1/100 (v/v) as previously fixed in the NMR kinetics study. Deionized water often led to fast coagulation of the mixtures as it hydrolyzed too fast the methoxysilane functions. Ethanol was the preferred co-solvent for the formulations as it could help the hydrolysis reaction initiate without risking phase separation issues.

III.3.2.1.2. Molar mass of the polyester-based polymer

The molar mass M_n of the hydrolyzable polymers and the functionality of the modified polymers (f) dictated the polyester content in the network. The number of reactive alkoxy silane functions (N) was kept identical to the one of the PDMS reference (with PDES as crosslinker with $M_n = 744$ g/mol and $f=12$)(Eq. 2). Given that the macrocrosslinkers used for the PDMS/polyester hybrid networks have various molar masses and a different functionality ($M_n = [1,000-7,200]$ g/mol and $f=6$), the networks are expected to have different crosslinking densities and inter-chain lengths (M_c) than the PDMS network reference.

$$N = \frac{m}{M_n} \times f \text{ (Eq. 2)}$$

The nomenclature used for the PDMS/polyester hybrid networks is ZZZZ-NX/Y where ZZZZ refers to the code name for the polyester-based polymer (PCL= poly(ϵ -caprolactone) diol, PLGA= poly(lactide-co-glycolide), LGO= PLGA-*b*-PDMS-*b*-PLGA and TGO= PCL-*b*-PDMS-*b*-PCL), N to “network”, X to the mass percentage of PDMS in the dry coating, and Y to the mass percentage of the polyester content in the dry coating.

Table III-8 describes the formulation recipes of the PDMS/polyester hybrid networks. A general trend was revealed by observing the appearance of the resulting coatings. The coatings based on low molar mass polyesters ($M_{n,NMR} \leq 2,000$ g/mol) rapidly showed good film properties whereas coatings based on higher molar mass polyesters ($M_{n,NMR} \geq 2,000$ g/mol) always led to macrophase separation, and thus to a crosslinking failure of the coating except for TGO6800-N73/27.

Table III-8. Formulation recipes of the PDMS reference (PDMS), and the PDMS/polyester hybrid networks.

ID coating	PDMS	PCL2000- N83/17	PCL3000- N77/23	PLGA740- N88/12	PLGA1900- N83/17	PLGA2500- N80/20	LGO5200- N88/12	LGO5800- N87/13	LGO6200- N83/17	TGO6800- N73/27
(Macro)crosslinker	PDES	PCL	PCL	PLGA	PLGA	PLGA	PLGA- PDMS- PLGA	PLGA- PDMS- PLGA	PLGA- PDMS- PLGA	PCL-PDMS- PCL
M_{n,NMR} (g/mol) of crosslinker	744	2,410	3,410	1,150	2,310	2,910	5,610	6,210	6,610	7,210
PDMS bis-silanol (wt.%)	74.9	53.6	51.2	55.7	53.8	52.4	39.2	38.4	37.7	27.1
DOTDL (wt.%)	0.2	0.2	0.2	0.2	0.2	0.2	0.2	0.2	0.2	0.2
THF (wt.%)	22.5	32.2	30.7	33.4	32.3	31.4	39.2	38.4	37.7	54.2
Ethanol (wt.%)	0.0	2.7	2.6	2.8	2.7	2.6	2.0	1.9	1.9	1.4
(Macro)crosslinker (wt.%)	2.5	11.4	15.4	7.8	11.0	13.4	19.6	21.1	22.6	17.2
TOTAL (wt.%)	100.0	100.0	100.0	100.0	100.0	100.0	100.0	100.0	100.0	100.0

III.3.2.1.3. Catalyst amount

The catalyst amount was set at 0.2 wt.% in the total formulation (corresponding to *ca.* 0.3 wt.% in the dry coating) to favor the condensation cure between the alkoxy silane macrocrosslinker and the bis-silanol PDMS.

III.3.2.1.4. Formulation preheating

To help the initiation of the hydrolysis reaction of the trimethoxysilane functionalities within the PDMS/polyester mixture, the formulations were stirred at 40°C for 15 minutes before their casting on the corresponding substrate. Assays with and without formulation preheating were performed and it was systematically noticed that the coatings which had their formulations preheated cured more rapidly (according to their less oily appearance). But this step was not sufficient to obtain fully dry coatings. Once applied on their substrate, the coatings required again other temperature and humidity conditions (see in the following § III.3.2.1.5).

III.3.2.1.5. Curing conditions

The curing conditions refer to the temperature, the humidity and duration during which the coatings crosslink. The coatings were cured at different temperatures (ambient temperature, 50 and 60°C). Although the crosslinking at ambient air was the most preferred way to minimize the processability constraints, it systematically led to partial crosslinking or crosslinking failures (with coatings more or less oily).

The heating of the coating could certainly increase the mobility and reactivity of the functional groups. Thus, the coatings were put in an oven at 50°C in an atmosphere saturated in moisture. At 50°C, the coatings showed promising results given that they were markedly less oily than the ones left at ambient temperature after the same amount of time (7 days). It was decided to cure all the hybrid coatings at 60°C as it could favor the mobility of the reactive chain ends. In fact, the curing temperature was intentionally set above the melting point of PCL-based polymers (which is around 50-55°C). The temperature was a strong influencing factor given that all the coatings were dry to the touch after 3 days at 60°C.

Chapter III – Hydrolyzable PDMS/polyester hybrid networks

III.3.2.1.6. Conclusion on the optimal parameters

Experiments which systematically led to defective coatings enabled to rapidly conclude on the optimal reaction conditions. What is meant by the term “defective” is the final aspect of the coating which could be:

- (1) oily, sticky or tacky (total or partial crosslinking failure),
- (2) brittle (happened mostly for PCL-based formulations),
- (3) coagulated (happened due to the premature hydrolysis of the polyester inducing its self-condensation following by a macrophase separation).

It appears that the polyester molar mass, the crosslinking functionalities, the solvent nature, and the curing temperature were the most critical factors for the crosslinking success.

The retained parameters and/or conditions for the next experiments were:

- The storage under vacuum of the freshly synthesized macrocrosslinkers in a sealed round-bottom flask for a maximum duration of 48 h before the formulation process.
- The dissolution of the polyester-based macrocrosslinker for 20 min in THF with a small quantity of ethanol (as the solvent and co-solvent respectively).
- The preheating of the formulations (after adding the solution of the macrocrosslinker, the bis-silanol PDMS and the DOTDL catalyst) for 15 min at 40°C under agitation.
- The curing of the coatings in an oven at 60°C, saturated with humidity for a minimum of 3 days.

PLGA-based networks showed promising film forming properties and could be easily detached from their substrates as long as the molar mass ($M_{n,NMR}$) of PLGA was strictly inferior to 2,000 g/mol (

Table III-9). By increasing the molar mass beyond 2,000 g/mol, the PDMS/PLGA networks displayed tacky surfaces which persisted after 1 month. This suggested the presence of

Chapter III – Hydrolyzable PDMS/polyester hybrid networks

partially unbound PDMS and/or PLGA which diffused towards the surface leading to a tacky touch. For this reason, PLGA2500-N80/20 failed the crosslinking reaction. Generally, the macrocrosslinkers were formulated the day following their synthesis (silanization reaction) to avoid premature hydrolysis of the methoxysilane functions. Nonetheless, in the case of PLGA1900-N83/17, the crosslinking reaction failed certainly due to the presence of hydrolyzed trimethoxysilane functions (6.3 %) before the formulation process (according to Table III.5). It is worth noticing that a slight change in the molar mass could also affect a lot the crosslinking efficacy. By increasing the PLGA molar mass ($M_{n,NMR}$) from 700 to 2,500 g/mol, the macrophase separation between PLGA and PDMS chains was markedly favored, and thus resulted in a failed crosslinking reaction.

Similarly, PCL3000-N77/23 failed the crosslinking reaction. The macrophase separation was also rapidly noticeable indicating that the molar mass and/or PCL content were too high. PCL2000-N83/17, on the contrary showed an elastomer aspect after 3 days at 60°C. The coating was slightly tacky but after rinsing the coating with deionized water and additional few hours at ambient air, this tackiness disappeared.

TGO6800-N73/27 was dry after 3 days at 60°C. The PDMS central block had a positive impact on the crosslinking reaction by improving the mobility of the copolymer.

All LGO-NX/Y coatings were systematically tacky and in worse cases, sticky. This tackiness or stickiness comes from the non-crosslinking or partial crosslinking of the copolymer PLGA-*b*-PDMS-*b*-PLGA. The main reason was undoubtedly the high degree of hydrolyzed trimethoxysilane functions (12.3 % for LGO5200 and LGO6200) before the formulation process (according to Table III.5). However, LGO5800-N87/13 also failed to crosslink even if its % -SiOMe was low (1.8 %). This was attributed to the residual LA monomers not eliminated from PLGA-*b*-PDMS-*b*-PLGA which could lead to undesired side reactions during the crosslinking reaction. Exposed to humidity, LA ring monomers may have opened and form lactic acid, the resulting acidic functions either accelerated the hydrolysis reaction of $-(SiOMe)_3$ or disrupted the crosslinking reaction by reacting with the terminal -SiOH groups. This assumption highlighted that the triblock copolymer should be purified from its residual starting reagents (mainly LA and GA monomers) before being crosslinked. PLGA-*b*-PDMS-*b*-PLGA also exhibited large dispersity values ($\bar{D} \geq 2.3$) with molar masses ranging from 6,000 to 11,000 g/mol (according to $M_{n,SEC}$). This important molar mass fluctuation may have caused a heterogeneous crosslinking. The lowest molar mass chains may have reacted first while the highest molar mass

Chapter III – Hydrolyzable PDMS/polyester hybrid networks

chains (non-crosslinked) may have been trapped in the bulk and/or may have remained on the surface and thus contributing to the coating tackiness.

Table III-9 summarizes the aspect of the PDMS/polyester hybrid networks.

Chapter III – Hydrolyzable PDMS/polyester hybrid networks

Table III-9. Summary of the success/failure of the crosslinking of PDMS/polyester hybrid networks.

ID coating	PDMS	PCL2000 -N83/17	PCL3000- N77/23	PLGA740- N88/12	PLGA1900- N83/17	PLGA2500- N80/20	LGO5200- N88/12	LGO5800- N87/13	LGO6200- N83/17	TGO6800- N73/27
(Macro)crosslinker	PDES	PCL	PCL	PLGA	PLGA	PLGA	PLGA-PDMS- PLGA	PLGA-PDMS- PLGA	PLGA-PDMS- PLGA	PCL-PDMS-PCL
$M_{n,NMR}$ (g/mol) of crosslinker	744	2,410	3,410	1,150	2,310	2,910	5,610	6,210	6,610	7,210
Visual aspect of the coating	Transparent,	Opaque white,	Macrophase separation	Yellowish,	Yellowish,	Yellowish,	Yellow, Translucent,	Yellow, Translucent,	Yellow, Translucent,	Opaque white,
Touch	Dry	Dry	Oily	Dry touch	Tacky	Tacky	Tacky	Very sticky	Very sticky	Dry
Crosslinking efficacy	Good	Good	Bad	Good	Bad	Bad	Bad	Bad	Bad	Good

III.3.2.2. Final coatings formulations

After the validation of all the parameters for the design of the hybrid networks, four final formulation recipes were made as well as a PDMS reference. The experimental protocol to obtain the PDMS/polyester hybrid networks is described in the experimental section (§ VI.4.2), it was based on the preliminary investigations (§ III.3.2.1.).

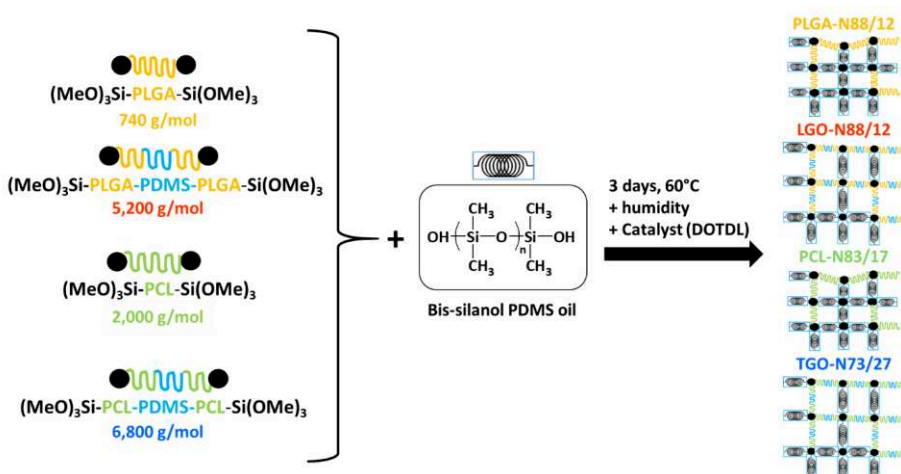


Figure III-10. General pathway of PDMS/polyester hybrid networks via a condensation cure between the polyester-based macrocrosslinkers and bis-silanol PDMS.

LGO5200-N88/12, newly named LGO-N88/12, was not fully characterized as for the others in the following Chapter IV due to its tackiness but could still bring some interesting physico-chemical information.

III.3.3. Elaboration of self-crosslinked polyester-based networks

Several self-crosslinked polyester-based networks were prepared to be compared with the PDMS/polyester hybrid networks. The same polyester-based polymers, modified at their chain ends by IPTMS, were prepared in THF with 0.1 wt.% DOTDL and ethanol. The solutions were casted onto glass slides for mass loss tests, contact angle, roughness and infrared analyses. They were also poured into polypropylene cups for DMA, AFM and SEM-EDX samples.

Chapter III – Hydrolyzable PDMS/polyester hybrid networks

The solutions were allowed to evaporate during 30 minutes at ambient air before being self-condensed in an oven at 60°C with a humidity-saturated atmosphere for 48h (Figure III-11). The resulting coating were dry and looked homogenous.

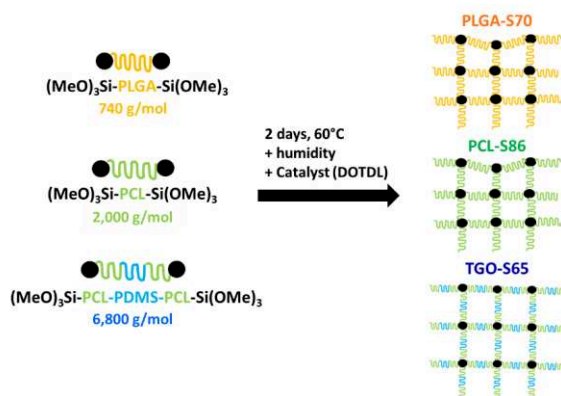


Figure III-11. General pathway of the elaboration of self-crosslinked polyester-based networks via a condensation cure reaction.

As regards the nomenclature of these self-crosslinked polyesters coatings (YYY-SX): YYY designates the polyester, S stands for self-crosslinked network and X corresponds to the polyester content in the dry coating.

PLGA-S70, PCL-S86 and TGO-S65 were introduced in Table III-10. The self-crosslinking of the triblock PLGA-*b*-PDMS-*b*-PLGA (LGO-S40) was not performed due to time and materials restrictions.

Table III-10. Details of the nomenclature of the self-crosslinked polyester-based networks.

	PLGA-S70	PCL-S86	TGO-S65
M _n Polyester (g/mol)	740	2,000	4,600
M _n of other segments than polyester (urethane linkage, PDMS block) (g/mol)	320	320	2,520 (=320 + 2,200)
Polyester mass fraction (wt.%) in the network	≈ 70	≈ 86	≈ 65

III.3.4. Residue extraction test

Once the PDMS/polyester hybrid networks were dried, a residue extraction test of each sample was carried out to verify the complete crosslinking of the polyester macrocrosslinkers

Chapter III – Hydrolyzable PDMS/polyester hybrid networks

with the bis-silanol PDMS oil. The protocol of the residue extraction test is described in the experimental section (§ VI.5.2.).

Swelling of PDMS elastomers is a technique to extract any uncrosslinked PDMS chains, small residual cyclic siloxane compounds but also catalysts. The extraction of the silicone matrix is achieved in organic solvents such as chloroform, hexane, diethyl ether, toluene but the most preferred ones (with the highest rate of swelling versus solubility) are dichloromethane, diethyl ether and tetrahydrofuran (THF) [17–20]. When the silicone elastomer swells, its volume significantly increases. The volume increase depends both on the crosslinking density and the affinity of the solvent towards the polymer nature. The generated free volume will ease the diffusion and migration of polymers which did not participate in the network crosslinking.

The results shown in Table III-11 indicate that the polyester macrocrosslinkers reacted well with the bis-silanol PDMS since less than 0.1 % of residue was found in the solvent of extraction. The self-crosslinked polyester-based polymers such as PCL-S86 and TGO-S65 also showed less than 0.1 % of residue. PLGA-S70 was the only network which released more than 1 % of residue.

No residue extraction test was performed for LGO-N88/12 due to a lack of polymer materials and time.

Table III-11. Residue content after extraction in deuterated chloroform.

	Coating ID	% silicone oil residue	% polyester residue
Reference PDMS	PDMS	0.063 ± 0.008	-
	PLGA-N88/12	0.09 ± 0.02	0.070 ± 0.005
PDMS/polyester hybrid networks	PCL-N83/17	0.021 ± 0.002	0.022 ± 0.003
	TGO-N73/27	0.05 ± 0.04	< 0.1
	PLGA-S70	-	1.3 ± 0.3
Self-crosslinked polyester-based networks	PCL-S86	-	0.047 ± 0.004
	TGO-S65	-	0.04 ± 0.01

III.3.5. Thermal degradation of the networks

Thermogravimetry analysis (TGA) was used to highlight the insertion of the polyester chains in the networks through monitoring their effects on the non-oxidative thermal stability of PDMS-rich networks. It will also be possible to compare the thermal degradations between the non-modified polyester-based polymers and the self-crosslinked polyester-based polymers. TGA could also help verify, when it was possible, the polyester content of each network.

The TGA experiments were carried out under N₂ atmosphere up to 800°C. The first derivatives of the weight percentages were graphically presented to better define the maximum peak degradation temperatures (T_{deg}^{max}) from Figure III-13 to Figure III-16 (B).

- **PDMS reference**

Under inert atmosphere, PDMS oils generally degrade in two steps [21]. The primary degradation is at 400 ± 50°C and is attributed to a series of terminal and internal intramolecular chain backbiting reactions (Si-O bond scissions) leading to formation of cyclic

siloxane oligomers of various ring sizes such as hexamethylcyclotrisiloxane (also named D3) (Figure III-12) [22,23].

The secondary degradation is at $500 \pm 50^\circ\text{C}$ and involves high temperature radically induced homolytic Si-CH₃ bonds scission reactions to form branched species (by crosslinking of radicals) and small molecules like methane through hydrogen abstraction [21,22].

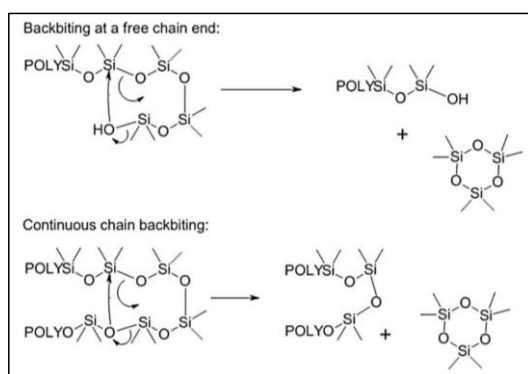


Figure III-12. Mechanisms of PDMS thermal depolymerization [24].

The thermal degradation of the PDMS elastomer is reported to be very similar to that of the PDMS oil, however, the crosslinking density, the catalyst and the nature and content of crosslinker can significantly change the thermal stability of the PDMS network [25]. Lewicki et al. also mentioned that the free chain end systems are generally *ca.* 50°C less stable than the fully crosslinked systems [21].

Figure III-13 displays the TGA curves of the bis-silanol PDMS oil and the crosslinked PDMS in presence of PDES and DOTDL (PDMS elastomer). The degradation of the oil and the elastomer both started at 390°C and showed a maximum degradation at 420-440°C. The two main thermal differences between the bis-silanol PDMS oil and its resulting elastomer were the presence of a second degradation peak for the PDMS oil (*ca.* 553°C, Figure III-13, B), and a greater amount of residue for the PDMS elastomer (in the form of a white powder). Apparently, the presence of DBTDL, which is a known reversible condensation catalyst, can cause premature degradation via rearrangement of a ring-chain equilibrium [25]. Thus, the presence of DOTDL in our case, could explain why the thermal degradation of PDMS elastomer ended earlier than the degradation of PDMS oil. As regards the residue observed in the PDMS elastomer TGA curve (14.2 %, Figure III-13, A), it was certainly made of silica (white powder).

The self-crosslinking of PDES (which was introduced in excess before the curing reaction) may be the cause of this remaining silica residue since there was no crosslinker in the case of the PDMS oil in the same inert atmosphere [21].

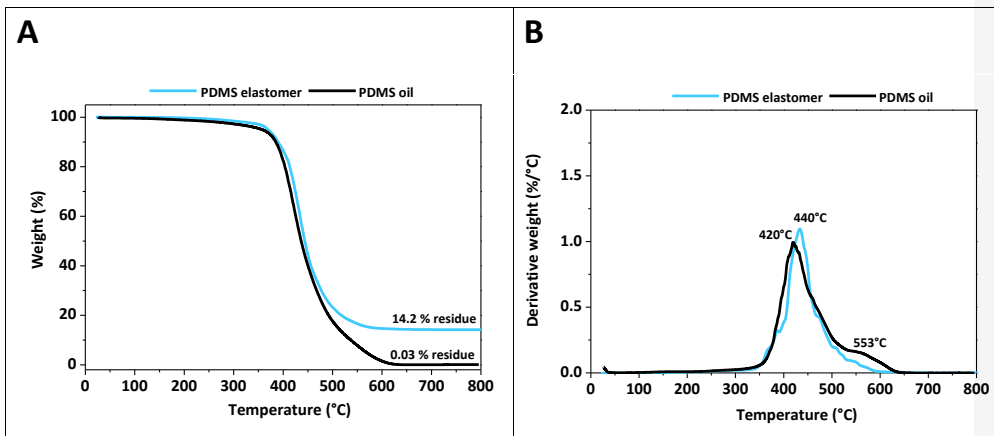


Figure III-13. Evolution of the weight percentage (A) and derivative weight (%/°C) (B) with temperature for PDMS oil and PDMS elastomer.

▪ PLGA-based networks

The TGA curves of the PDMS reference were intentionally shown again to observe the thermal degradation shift of the PDMS chains in the different networks (Figure III-14).

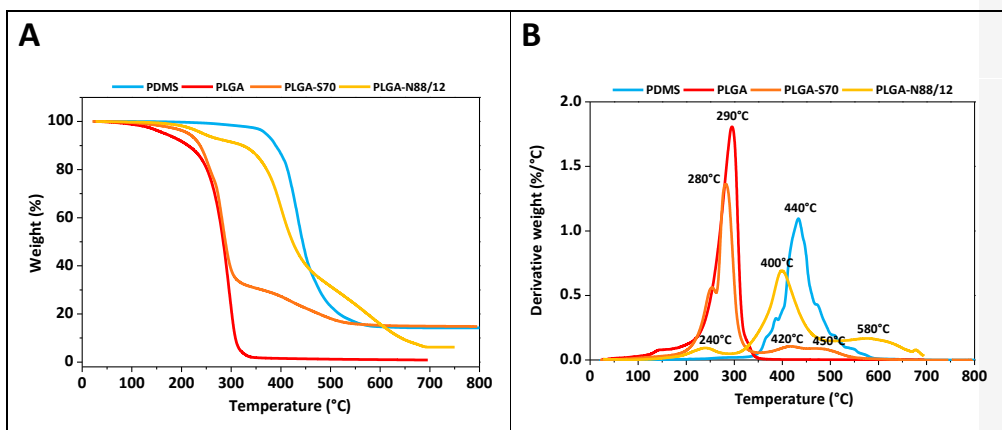


Figure III-14. Evolution of the weight percentage (A) and derivative weight (%/°C) (B) with temperature for PLGA740, PLGA-S70, PLGA-N88/12 and PDMS networks.

Chapter III – Hydrolyzable PDMS/polyester hybrid networks

Pure PLGA degraded itself between 180 and 340°C ($T_{deg}^{max} = 290^{\circ}C$) with no left residue which is similar to what is found in literature [26].

The self-crosslinked PLGA-S70 degraded in two steps with maximum peak degradation temperatures of 280°C and 420-450°C respectively. The first degradation at 280°C was likely due to the PLGA degradation and the associated weight loss percentage was of *ca.* 68 wt.% closed to the experimental PLGA content of 70 wt.%. The degradation occurring at *ca.* 420-450°C could come from the thermal degradation of the remaining siloxane crosslinking linkages.

The decomposition of PDMS/PLGA hybrid network (PLGA-N88/12) took place in three stages with maximum degradation peaks at 240°C, 400°C and 580°C. The first weight loss at 240°C was assigned to the PLGA decomposition and displayed a weight loss percentage of *ca.* 10 wt.% closed to the experimental PLGA content of 12 wt.%. The degradation of PLGA in PLGA-N88/12 was slightly faster than in PLGA-S70 ($T_{deg}^{max} = 240^{\circ}C$ in PLGA-N88/12 against $T_{deg}^{max} = 280^{\circ}C$ in PLGA-S70 and $T_{deg}^{max} = 290^{\circ}C$ for the initial PLGA740). The polysiloxane depolymerization started from 300°C. A majority of 60 wt.% weight loss happened between 300 and 500°C suggesting that the presence of PLGA may have altered the thermal stability of PDMS by acting as a “pro-degradant” maybe due to the generation of acidic functions during its degradation. Then, a weight loss of 24 wt.% occurred between 500 and 700°C. This degradation occurring between 500 and 700°C could be attributed to the depolymerization of PDMS-rich regions of higher crosslinking density [27,28]. The wide temperature interval during which occurred the PDMS degradation highlights the structural heterogeneity of the PLGA-N88/12 network.

The fact that PLGA-N88/12 showed different a thermogravimetric profile that those of PLGA740 and PDMS (based on the derivative weight curves) can confirm the well crosslinking of PDMS with PLGA. However, it is difficult to understand each thermal event given that they could be a combination of various complex degradation mechanisms.

▪ PCL-based networks

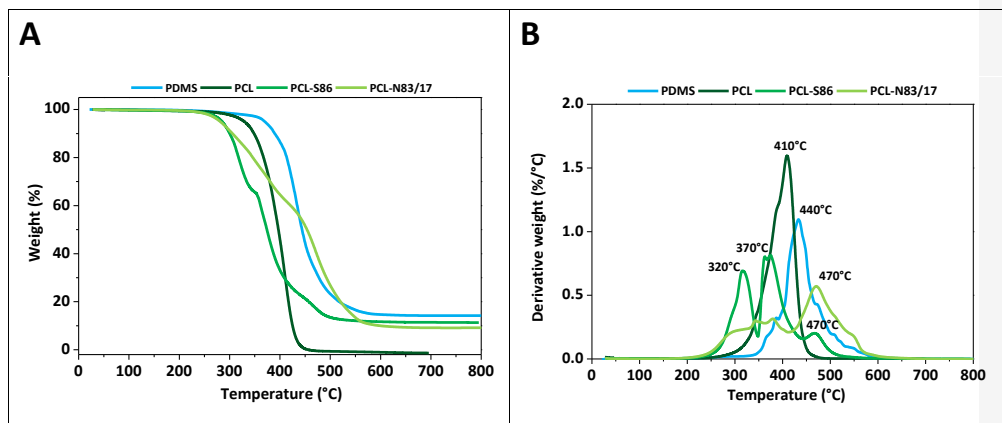


Figure III-15. Evolution of the weight percentage (A) and derivative weight (%/°C) (B) with temperature for: PCL2000, PCL-S86, PCL-N83/17 and PDMS networks.

Pure PCL2000 degraded itself between 320 and 450°C ($T_{deg}^{max} = 410^{\circ}C$) as a single peak and no residue was remained which is similar to what is found in literature [29].

The self-crosslinked PCL-S86 degradation took place in three stages: the first degradation occurred at 320°C, the second at 370°C and the third at 470°C. The derivative curve showed the degradation peaks were overlapped, making it difficult to separate the different thermal degradation events. The two degradation peaks at 320 and 370°C were certainly linked to the PCL decomposition. As it is expected for PCL to degrade in one step and at a higher temperature ($T_{deg}^{max} = 410^{\circ}C$), it can be assumed that the amorphous state of the PCL self-crosslinking accelerated its thermal decomposition. The degradation occurring at 470°C (*ca.* 11 % weight loss) certainly came from the thermal degradation of the remaining siloxane crosslinking linkages (which was theoretically of 14 % weight loss).

PCL-N83/17 displayed a first degradation from 250 to 400°C certainly due to the degradation of both PCL and PDMS (its beginning). PCL-N83/17 displayed a second degradation with maximum peak degradation temperature at 470°. This second degradation could be attributed to the depolymerization of PDMS-rich regions of higher crosslinking density [30], and thus more resistant to thermal degradation. But here again, the degradation mechanisms are not well-understood.

▪ PCL-*b*-PDMS-*b*-PCL-based networks

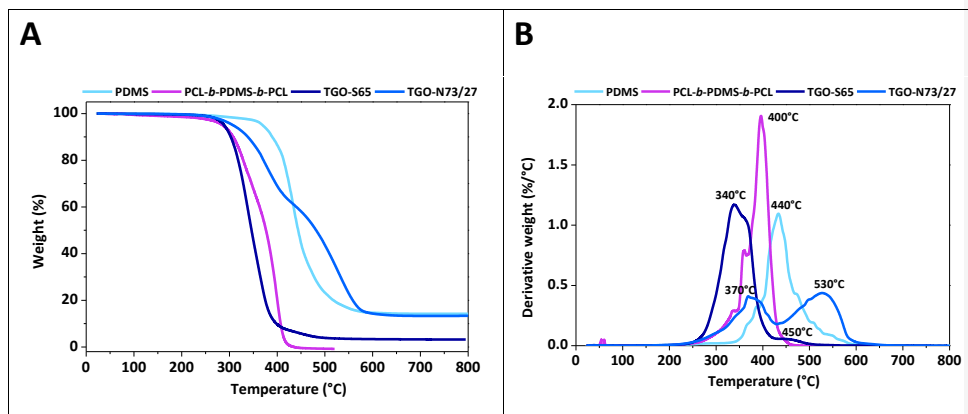


Figure III-16. Evolution of the weight percentage (A) and derivative weight (%/°C) (B) with temperature for: TGO6800, TGO-S65, TGO-N73/27 and PDMS networks.

Pure PCL-*b*-PDMS-*b*-PCL (TGO6800) with 68 wt.% of PCL degraded itself between 280 and 430°C ($T_{deg}^{max} = 400^{\circ}C$) in at least three unresolved steps, suggesting the degradation of PCL and PDMS blocks happened simultaneously.

The self-crosslinked copolymer (TGO-S65) showed a maximum degradation at 340°C and an overlapped one around 370°C. This indicated the crosslinking altered the thermal degradation of the triblock copolymer. As reported above, the thermal stability of PCL chains decreased when self-crosslinked with $T_{deg}^{max} = 340-350^{\circ}C$ lowered in comparison with the initial PCL-*b*-PDMS-*b*-PCL with $T_{deg}^{max} = 400^{\circ}C$. TGO-S65 also displayed a slight degradation peak at 450°C attributed to the thermal degradation of the remaining siloxane crosslinking linkages.

TGO-N73/27 degradation occurred in two steps. The first step at $T_{deg}^{max} = 370^{\circ}C$ was attributed to the copolymer and PDMS degradation. The second step at 530°C certainly referred to the second degradation of PDMS segments probably in more densely packed or crosslinked regions.

Chapter III – Hydrolyzable PDMS/polyester hybrid networks

For all the PDMS-based networks, a residue up to *ca.* 15 % was observed and attributed to the siliceous degradation products. A more moderate residue (*ca.* 5 %) was observed for the self-crosslinked polyester-based polymers. No residue was obtained from the degradation of the pure polyester-based polymers. Thus, the presence of siloxane functionalities favored larger amount of residue at 800°C.

Globally, the self-crosslinking of the polyester-based polymers accelerated the thermal degradation of the initial polyesters. The degradation of the PDMS/polyester hybrid networks occurred in multiple steps. Degradation above 450°C suggested the PDMS/polyester hybrid networks presented regions with higher crosslinking density and thus more resistant to the thermal degradation. Moreover, PDMS/polyester hybrid networks left more residues (mainly silica) than the self-crosslinked polyester-based polymers or initial polyester-based polymers. TGA was thus an interesting tool to distinguish between crosslinked and non-crosslinked polymers. The nature of the macrocrosslinker, the crosslinking density and/or inter-chain length were certainly the main influencing parameters of the PDMS chains thermal degradation. However, one question remains: Could there be some self-crosslinking of the macrocrosslinker within the PDMS/polyester hybrid network? TGA experiments only demonstrated that the polyester macrocrosslinkers were inserted in the PDMS/polyester networks. Further investigations combining TGA under isothermal conditions and pyrolysis-gas chromatography-mass spectrometry (Py-GC-MS) will be helpful to highlight the degradation mechanisms involved in each thermal step and to answer to the remaining question.

III.4. Conclusion

In this chapter, the synthesis of PLGA and its triblock copolymers were achieved by a ring opening polymerization. The M/I feed molar ratio enabled to target specific molar masses of 700-2,500 g/mol for the PLGA and 5,200-6,200 g/mol for PLGA-*b*-PDMS-*b*-PLGA, close to the molar masses of commercially available PCL and PCL-*b*-PDMS-*b*-PCL copolymer. PLGA was chosen for its faster hydrolytic degradation than PCL. This will serve in the following chapter to conclude on which hydrolysis kinetics favors the most the network erosion.

PLGA and PCL-based polymers were successfully transformed into telechelic macrocrosslinkers to further react with a bis-silanol PDMS to prepare PDMS/polyester hybrid networks. Several investigations were carried out to highlight the optimal conditions to obtain the crosslinked networks. The most important parameters were the crosslinker reactive functions, the solvent and the curing temperature. Low molar mass polyester and the triblock architecture were also favorable criteria to compatibilize the polyester chains with the PDMS. Eight final polymer networks were developed, among them a PDMS reference, four PDMS/polyester hybrid networks and three self-crosslinked polyester-based networks. The network done with PLGA-PDMS-PLGA (LGO-N88/12) displayed a sticky surface suggesting a partial crosslinking reaction. Despite that, it was decided to partially characterize it in the following chapter as it could still give some interesting information.

The elaboration of self-crosslinked polyester-based networks will allow, in the following chapter, to compare the physico-chemical properties of the networks with different polyester loadings.

To ensure that the polymer networks were well crosslinked, an extraction test in chloroform was conducted and it revealed there was no significant free polymer chains. The thermal analysis was another way to assess whether or not the PDMS and polyester reacted together. The PDMS degradation was indeed greatly influenced by the covalent addition of polyester into the silicone matrix.

III.5. Bibliographical references

1. Mangeon, C.; Renard, E.; Thevenieau, F.; Langlois, V. Networks based on biodegradable polyesters: An overview of the chemical ways of crosslinking. *Mater Sci Eng C Mater Biol Appl* **2017**, *80*, 760–770.
2. Tham, W.H.; Wahit, M.U.; Abdul Kadir, M.R.; Wong, T.W.; Hassan, O. Polyol-based biodegradable polyesters: a short review. *Reviews in Chemical Engineering* **2016**, *32*.
3. Avgoustakis, K. Polylactic-Co-Glycolic Acid (PLGA). *Encycl. Biomater. Biomedic. Eng.* **2005**, 1–11.
4. Park, C.W.; Lee, S.J.; Kim, D.; Lee, D.S.; Kim, S.C. Micelle formation and sol–gel transition behavior of comb-like amphiphilic poly((PLGA-b-PEG)MA) copolymers. *Journal of Polymer Science Part A: Polymer Chemistry* **2008**, *46*, 1954–1963.
5. Choi, S.H.; Park, T.G. Synthesis and characterization of elastic PLGA/PCL/PLGA tri-block copolymers. *Journal of Biomaterials Science, Polymer Edition* **2002**, *13*, 1163–1173.
6. Nederberg, F.; Connor, E.F.; Möller, M.; Glauser, T.; Hedrick, J.L. New Paradigms for Organic Catalysts: The First Organocatalytic Living Polymerization. *Angewandte Chemie International Edition* **2001**, *40*, 2712–2715.
7. Kim, M.S.; Seo, K.S.; Hyun, H.; Khang, G.; Cho, S.H.; Lee, H.B. Controlled release of bovine serum albumin using MPEG–PCL diblock copolymers as implantable protein carriers. *Journal of Applied Polymer Science* **2006**, *102*, 1561–1567.
8. Barakat, I.; Dubois, P.; Jérôme, R.; Teyssié, P. Macromolecular engineering of polylactones and polylactides. X. Selective end-functionalization of poly(D,L)-lactide. *Journal of Polymer Science Part A: Polymer Chemistry* **1993**, *31*, 505–514.
9. Ragheb, R.T.; Riffle, J.S. Synthesis and characterization of poly(lactide-b-siloxane-b-lactide) copolymers as magnetite nanoparticle dispersants. *Polymer* **2008**, *49*, 5397–5404.
10. Stridsberg, K.; Ryner, M.; Albertsson, A.-C. Dihydroxy-Terminated Poly(L-lactide) Obtained by Controlled Ring-Opening Polymerization: Investigation of the Polymerization Mechanism. *Macromolecules* **2000**, *33*, 2862–2869.
11. Dong, C.-M.; Qiu, K.-Y.; Gu, Z.-W.; Feng, X.-D. Synthesis of poly(D,L-lactic acid-alt-glycolic acid) from D,L-3-methylglycolide. *Journal of Polymer Science Part A: Polymer Chemistry* **2000**, *38*, 4179–4184.
12. D’Avila Carvalho Erbetta, C. Synthesis and Characterization of Poly(D,L-Lactide-co-Glycolide) Copolymer. *Journal of Biomaterials and Nanobiotechnology* **2012**, *03*, 208–225.
13. Azemar, F.; Faÿ, F.; Réhel, K.; Linossier, I. Control of hydration and degradation properties of triblock copolymers polycaprolactone- *b* -polydimethylsiloxane- *b* - polycaprolactone. *Journal of Applied Polymer Science* **2014**, *131*, n/a-n/a.
14. Ginpallli, K.; Shavi, G.V.; Averineni, R.K.; Bhat, M.; Udupa, N.; Nagaraja Upadhya, P. Poly(α -hydroxy acid) based polymers: A review on material and degradation aspects. *Polymer Degradation and Stability* **2017**, *144*, 520–535.
15. Li, S.M.; Garreau, H.; Vert, M. Structure-property relationships in the case of the degradation of massive aliphatic poly-(α -hydroxy acids) in aqueous media: Part 1: Poly(dl-lactic acid). *Journal of Materials Science: Materials in Medicine* **1990**, *1*, 123–130.

16. Park, T.G. Degradation of poly(lactic-co-glycolic acid) microspheres: effect of copolymer composition. *Biomaterials* **1995**, *16*, 1123–1130.
17. Lee, J.N.; Park, C.; Whitesides, G.M. Solvent Compatibility of Poly(dimethylsiloxane)-Based Microfluidic Devices. *Analytical Chemistry* **2003**, *75*, 6544–6554.
18. Rumens, C.V.; Ziai, M.A.; Belsey, K.E.; Batchelor, J.C.; Holder, S.J. Swelling of PDMS networks in solvent vapours; applications for passive RFID wireless sensors. *Journal of Materials Chemistry C* **2015**, *3*, 10091–10098.
19. Favre, E. Swelling of crosslinked polydimethylsiloxane networks by pure solvents: Influence of temperature. *European Polymer Journal* **1996**, *32*, 1183–1188.
20. Mark, J.E.; Sullivan, J.L. Model networks of end-linked polydimethylsiloxane chains. I. Comparisons between experimental and theoretical values of the elastic modulus and the equilibrium degree of swelling. *The Journal of Chemical Physics* **1977**, *66*, 1006–1011.
21. Lewicki, J.P.; Mayer, B.P.; Alviso, C.T.; Maxwell, R.S. Thermal Degradation Behavior and Product Speciation in Model Poly(dimethylsiloxane) Networks. *Journal of Inorganic and Organometallic Polymers and Materials* **2012**, *22*, 636–645.
22. Camino, G.; Lomakin, S.M.; Lagueard, M. Thermal polydimethylsiloxane degradation. Part 2. The degradation mechanisms. *Polymer* **2002**, *43*, 2011–2015.
23. Grassie, N.; Macfarlane, I.G. The thermal degradation of polysiloxanes—I. Poly(dimethylsiloxane). *European Polymer Journal* **1978**, *14*, 875–884.
24. Lewicki, J.P.; Liggat, J.J.; Patel, M. The thermal degradation behaviour of polydimethylsiloxane/montmorillonite nanocomposites. *Polymer Degradation and Stability* **2009**, *94*, 1548–1557.
25. Koerner, G. *Silicones, chemistry and technology*; CRC Press, 1992; ISBN 978-0-8493-7740-2.
26. Palacios, J.; Albano, C.; González, G.; Castillo, R.V.; Karam, A.; Covis, M. Characterization and thermal degradation of poly(d,l-lactide-co-glycolide) composites with nanofillers. *Polymer Engineering & Science* **2013**, *53*, 1414–1429.
27. Semsarzadeh, M.A.; Navarchian, A.H. Effects of NCO/OH ratio and catalyst concentration on structure, thermal stability, and crosslink density of poly(urethane-isocyanurate). *Journal of Applied Polymer Science* **2003**, *90*, 963–972.
28. Bhuvaneshwari, G, H. 3 - Degradability of Polymers. In *Recycling of Polyurethane Foams*; Thomas, S., Rane, A.V., Kanny, K., V.k., A., Thomas, M.G., Eds.; Plastics Design Library; William Andrew Publishing, **2018**; pp. 29–44 ISBN 978-0-323-51133-9.
29. Persenaire, O.; Alexandre, M.; Degée, P.; Dubois, P. Mechanisms and Kinetics of Thermal Degradation of Poly(ϵ -caprolactone). *Biomacromolecules* **2001**, *2*, 288–294.
30. Kweon, H.; Yoo, M.K.; Park, I.K.; Kim, T.H.; Lee, H.C.; Lee, H.-S.; Oh, J.-S.; Akaike, T.; Cho, C.-S. A novel degradable polycaprolactone networks for tissue engineering. *Biomaterials* **2003**, *24*, 801–808.

Chapter IV – Characterization of the PDMS/polyester hybrid networks

Chapter IV	Characterization of the PDMS/polyester hybrid networks	200
IV.1.	Introduction	200
IV.2.	Physico-chemical properties at $t_i=0$	201
IV.2.1.	Surface physico-chemical properties	201
IV.2.1.1.	<i>Microstructure of the coating surface</i>	201
IV.2.1.2.	<i>Surface chemistry</i>	208
IV.2.1.3.	<i>Surface micromechanics</i>	212
IV.2.2.	Thermo-mechanical bulk properties	223
IV.2.2.1.	<i>Thermal properties of the networks</i>	223
IV.2.2.2.	<i>Viscoelastic properties of the networks</i>	225
IV.2.2.2.1.	<i>Viscoelastic behavior at ambient temperature</i>	226
IV.2.2.2.2.	<i>Influence of the temperature on the viscoelastic properties of the networks</i>	227
IV.2.3.	Summarization of the key findings of the surface/bulk physico-chemical properties	233
IV.3.	Physico-chemical properties during immersion	235
IV.3.1.	Static immersion	235
IV.3.1.1.	<i>Mass loss test (and water uptake test)</i>	235
IV.3.1.2.	<i>Roughness</i>	240
IV.3.1.3.	<i>Wetting properties</i>	243
IV.3.1.3.1.	<i>Dynamic contact angle measurements</i>	243
IV.3.1.3.2.	<i>Surface free energy</i>	251
IV.3.1.4.	<i>Mechanical properties</i>	256
IV.3.2.	Dynamic immersion	256
IV.4.	Conclusion	264
IV.5.	Bibliographical references	267

Chapter IV Characterization of the PDMS/polyester hybrid networks

IV.1. Introduction

The Chapter III introduced the synthesis of hydrolyzable crosslinked PDMS/polyester networks which represent a novel category of erodible antifouling coatings. PDMS/polyester hybrid networks containing either poly(ϵ -caprolactone) or poly(D,L-lactide-co-glycolide) in proportions ranging from 12 to 27 wt.% were prepared (cf. Chapter III, § III.3.2.2.) as well as the corresponding self-crosslinked polyester-based networks (references) containing 65 to 86 wt.% of polyesters (cf. Chapter III, § III.3.3.).

The main objective of this Chapter IV is to characterize these networks by various techniques to study their surface and bulk physico-chemical properties before immersion. Image scanning electron microscopy with energy dispersive X-ray spectroscopy (SEM-EDX), infrared spectroscopy (FTIR) and atomic force microscopy (AFM) analyses were useful to evaluate the surface microstructure, surface chemistry and surface micromechanics, respectively. The bulk properties were analyzed through differential scanning calorimetry (DSC) and dynamic mechanical analysis (DMA) to better describe the microstructure of these peculiar networks (depending on the nature of the polyester, the content of polyester, the network inter-chain length and the network crystallinity). The comparative study between networks with different polyester loadings brought information on the influence of the polyester on the bulk properties.

A specific effort was made to focus on the antifouling key parameters of these coatings such as the elastic modulus, networks crystallinity, surface chemistry and topography which are known to markedly influence the antifouling and fouling release properties [1–4].

The physico-chemical properties of the PDMS/polyester hybrid networks during immersion were then studied (in static and dynamic conditions). Roughness, contact angles, surface free energy, mass loss, water uptake and thickness loss measurements at different immersion times gave precious information on the evolution of the surface topography and chemistry of the coatings when exposed to prolonged time in water.

Chapter IV – Characterization of the PDMS/polyester hybrid networks

As a reminder, LGO-N88/12 was a partially crosslinked network based on PLGA-*b*-PDMS-*b*-PLGA which exhibited a tacky surface. For that reason, it was not characterized as much as the other PDMS/polyester hybrid networks.

IV.2. Physico-chemical properties at $t_i=0$

IV.2.1. Surface physico-chemical properties

IV.2.1.1. Microstructure of the coating surface

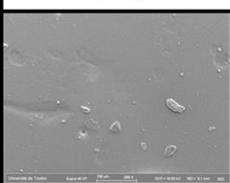
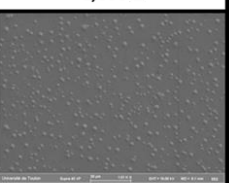
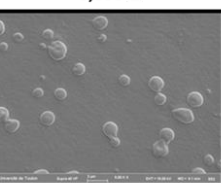
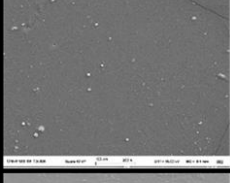
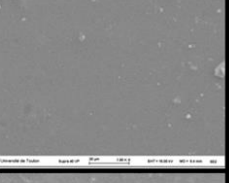
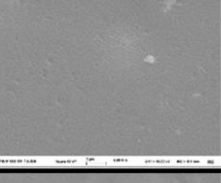
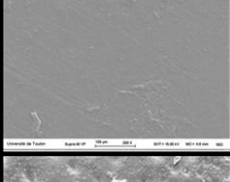
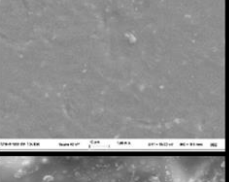
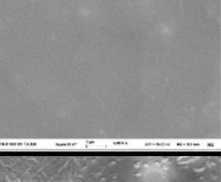
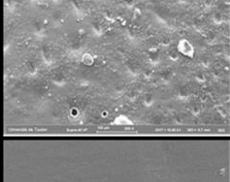
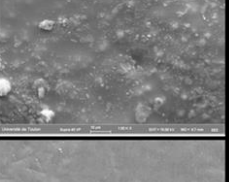
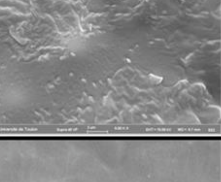
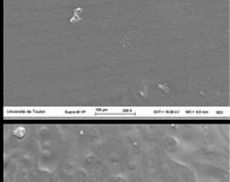
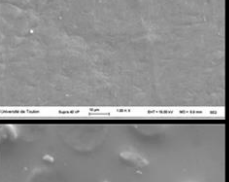
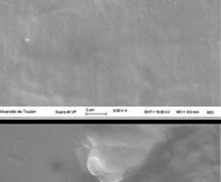
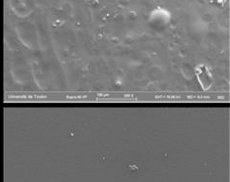
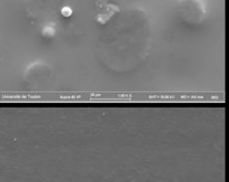
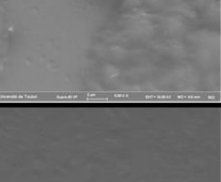
SEM-EDX is a useful tool to study the microstructure of polymer materials. The electron bombardment was produced with a 15-keV accelerating voltage. The coatings surface was metallized with gold before analysis (cf. experimental section, § VI.5.3.).

The surface of the PDMS/polyester hybrid networks and the self-crosslinked polyester-based networks were observed by using the secondary electrons detector to evaluate the topography and elemental composition of the surface (*ca.* 2 μ m depth). In this manner, it will be possible to assess the distribution of polyester and PDMS on the surface of the hybrid coatings as well as the size of the domains in case of a phase separation. The PDMS/polyester hybrid networks will be compared to the self-crosslinked polyester-based coatings to highlight the impact of the PDMS presence or absence on the chemical composition of the surface.

For each coating, the magnification range of the SEM images was from $\times 20$ to $\times 5,000$ (Table IV-1). The atomic surface composition of each coating was performed at the magnification of $\times 1,000$.

Chapter IV – Characterization of the PDMS/polyester hybrid networks

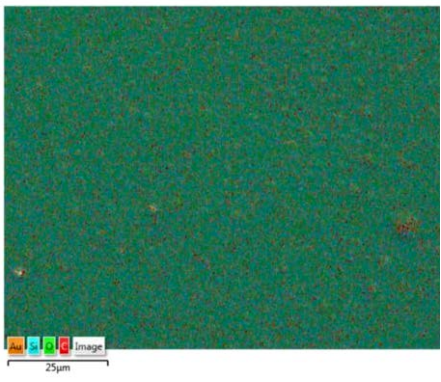
Table IV-1. SEM images of the polyester-based networks at different magnifications.

	× 200	× 1,000	× 5,000
PDMS			
PLGA-N88/12			
PLGA-S70			
PCL-N83/17			
PCL-S86			
TGO-N73/27			
TGO-S65			

Chapter IV – Characterization of the PDMS/polyester hybrid networks

The PDMS reference coating displayed a rather smooth surface covered with air bubbles of up to 2 μm in diameter. The atomic surface composition was of 59 % carbon, 19 % silicon and 22 % oxygen in accordance with the polydimethylsiloxane atomic structure (Table IV-2).

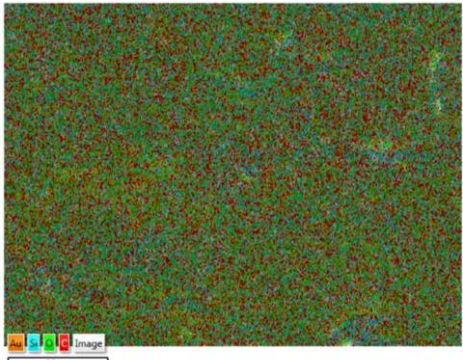
Table IV-2. EDX analysis of the PDMS reference. Mapping of the atomic composition on the picture. Atomic composition (%) on awaited atoms.

PDMS		
	Atomic composition (%)	
	C	58.8
	O	22.4
	Si	18.8
	N	0
	Sn	0
	Σ	100

PLGA-N88/12 showed a similar surface topography and atomic composition as the PDMS reference suggesting the small PLGA segments were hardly visible on the surface. PLGA-N88/12 was mainly composed of PDMS chains by contrast with PLGA-S70 for which there are more than 96 % of carbon and oxygen (Table IV-3). The nitrogen atom observed in PLGA-N88/12 came from the urethane functionalities.

Chapter IV – Characterization of the PDMS/polyester hybrid networks

Table IV-3. EDX analysis of PLGA-based coatings. Mapping of the atomic composition on the picture. Atomic composition (%) on awaited atoms.

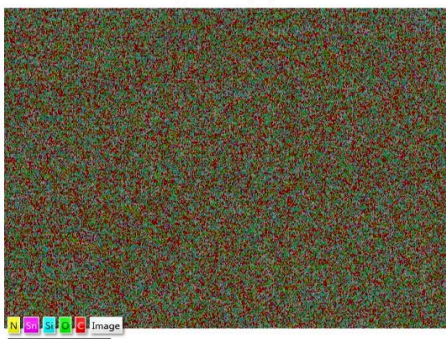
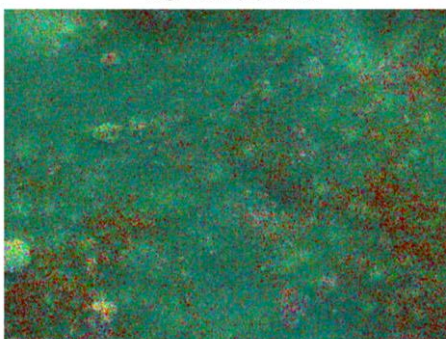
PLGA-S70		
		Atomic composition (%)
	C	66.7
	O	30.2
	Si	3.0
	N	0
	Sn	0.1
	Σ	100
PLGA-N88/12		
		Atomic composition (%)
	C	55.3
	O	23.5
	Si	19.5
	N	1.7
	Sn	0
	Σ	100

PCL-N83/17 exhibited some phase contrasts. Some irregular granular domains surrounded by smoother phases were observed (Table IV-4). The interdomain spacing was estimated in the range 100-200 µm. EDX analysis showed the rough domains were mainly made of carbon and oxygen whereas the surrounding smooth surface was richer in silicon and oxygen. The random

Chapter IV – Characterization of the PDMS/polyester hybrid networks

distribution of rough phases traduced the heterogeneous distribution of the polyester within the silicone matrix.

Table IV-4. EDX analysis of PCL-based coatings. Mapping of the atomic composition on left. Atomic composition (%) of awaited atoms.

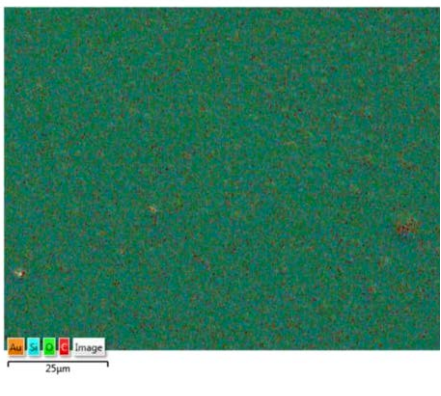
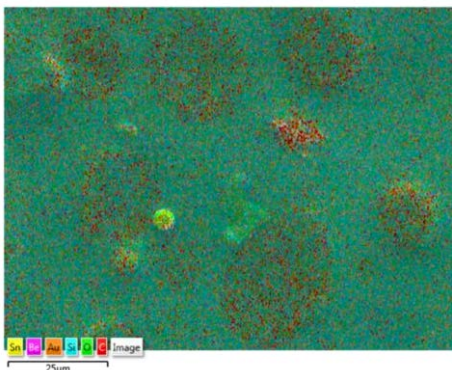
PCL-S86		
<p>Image EDS en superposition 3</p> 		Atomic composition (%)
	C	74.2
	O	22.5
	Si	2.1
	N	1.1
	Sn	< 0.1
	Σ	100
PCL-N83/17		
<p>Image EDS en superposition 10</p> 		Atomic composition (%)
	C	64.6
	O	22.9
	Si	12.3
	N	0
	Sn	0.2
	Σ	100

Chapter IV – Characterization of the PDMS/polyester hybrid networks

TGO-N73/27 surface also displayed some microdomains of variable sizes ranging from 10 to 200 μm , but their shapes were better defined than those of PCL-N83/17. These spherical domains were mainly made of carbon and oxygen traducing the presence of polyester domains (Table IV-5). The quite regular islets-shaped microdomains indicated the PCL segments were able to self-assemble. The self-assembly of PCL segments was thus not entirely prevented by the crosslinks, which supports the DSC results that showed the presence of remaining crystalline PCL in TGO-N73/27 (§ IV.2.2.1.). The central PDMS block in the linear triblock copolymer certainly helped the formation of these distinct phases. TGO-N35/75 showed some ridges of 2 μm -length all across the coating but major microphase separation was hardly perceptible. Generally, linear triblock copolymers such as PCL-*b*-PDMS-*b*-PCL (TGO6800) display crystalline lamellar structures at the nanoscale or spherulitic structures at the microscale [5]. The absence of regular ordering in the case of the self-crosslinked triblock copolymer (TGO-S65) suggested the presence of crosslinks could have disturbed the copolymer self-assembly morphology.

Chapter IV – Characterization of the PDMS/polyester hybrid networks

Table IV-5. EDX analysis of PCL-*b*-PDMS-*b*-PCL-based coatings.

TGO-S65		
	Atomic composition (%)	
	C	69.8
	O	23.3
	Si	6.9
	N	0
	Sn	0
	Σ	100
TGO-N73/27		
	Atomic composition (%)	
	C	60.3
	O	23.5
	Si	16.1
	N	0
	Sn	0.1
	Σ	100

Globally, contrary to the PDMS/polyester hybrid networks, the self-crosslinked polyester-based networks (references) appeared more homogeneous in terms of topography and chemical composition. They all showed less than 10 % of silicon confirming the well majority of polyester on the surface.

For the PDMS/polyester hybrid networks, the coexistence of PDMS and polyester undeniably favored microphase separation. This assessment is in accordance with the scientific work of

Chapter IV – Characterization of the PDMS/polyester hybrid networks

Patrickios et al. claiming that covalent amphiphilic polymer networks prefer to be in the microphase separated state [4].

Owing to their texturally and chemically heterogenous surfaces, the PDMS/polyester hybrid coatings could act as ambiguous surfaces towards marine species.

IV.2.1.2. Surface chemistry

The monitoring of the surface chemistry by Attenuated Total Reflectance-Fourier Transform Infrared (ATR-FTIR) spectroscopy was carried out to confirm the dual surface chemistry of the PDMS/polyester hybrid networks by comparison with the PDMS and the self-crosslinked polyester-based network references. Characteristic bands of the chemical functions of interest are displayed in Table IV-6.

Chapter IV – Characterization of the PDMS/polyester hybrid networks

Table IV-6. Main infrared absorption bands of the polymers.

Polymer	Wavelength (cm ⁻¹)/Vibration mode/Chemical bond assignment
PDMS elastomer	800 /stretching/-O-Si(CH ₃) ₂ -O- 1020-1091 /stretching/-Si-O-Si- 1260 /bending/-O-Si(CH ₃) ₂ -O- 2964 /stretching/-CH ₃ , -CH ₂ , -CH-
PCL2000 macrocrosslinker	1734 /stretching/C=O (ester) 2963 /stretching/-CH ₃ , -CH ₂ , -CH- 2866 /symmetric stretching/-CH ₂ - 2964 /stretching/-CH ₃ , -CH ₂ , -CH- 3447 /stretching/stretching/ -NH
PCL- <i>b</i> -PDMS- <i>b</i> -PCL macrocrosslinker (TGO6800)	800 /stretching/Si-CH ₃ 1021-1090 /stretching/-Si-O-Si- 1260 /bending/-O-Si(CH ₃) ₂ -O- 1725 /stretching/C=O (ester) 2866 /symmetric stretching/-CH ₂ - 2964 /stretching/-CH ₃ , -CH ₂ , -CH-
PLGA740 macrocrosslinker	1740 /stretching/C=O (ester) 2850 /symmetric stretching/-CH ₂ - 2964 /stretching/-CH ₃ , -CH ₂ , -CH- 3447 /stretching/stretching/-NH

Chapter IV – Characterization of the PDMS/polyester hybrid networks

Figure IV-1 showed PLGA-N88/12 did not show the characteristic band of carbonyl group of PLGA (at 1740 cm^{-1}) contrary to PLGA-S70. Indeed, PLGA-N88/12 showed a surface composition more similar to the PDMS reference which confirms what was observed in the EDX analysis (§ IV.2.1.1.). This may be due to the low content of PLGA within the network (12 wt.%). The large band at 3447 cm^{-1} visible on the spectrum of PLGA-S70 certainly came from the -NH stretching vibrations of the urethane linkages (*ca.* 30 wt.% in PLGA-S70). The stretching vibrations of the urethane carbonyl (C=O, usually around 1730 cm^{-1}) were certainly hidden by the large band at 1740 cm^{-1} .

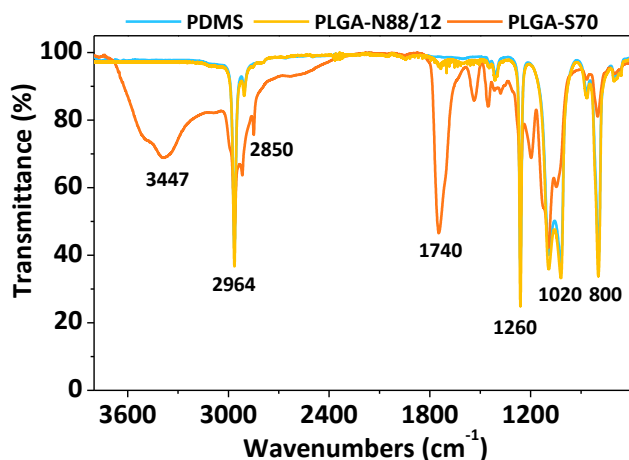


Figure IV-1. FTIR spectra of PDMS, PLGA-N88/12 and PLGA-S70.

Figure IV-2 and Figure IV-3 showed, for both PCL-N83/17 and TGO-N73/27, the presence of the characteristic bands of PDMS (1260 cm^{-1}) and of the polyester ($1725\text{-}1740\text{ cm}^{-1}$). The -NH stretching vibrations of the urethane linkages were visible on the PCL-S86, PCL-83/17 infrared spectra but not on those of TGO-S65 and TGO-N73/27 maybe because of the higher molar mass of the TGO6800 macrocrosslinker that “diluted” the urethane functionalities.

This again confirms the EDX analyses in which both chemistries were highlighted (§ IV.2.1.1.).

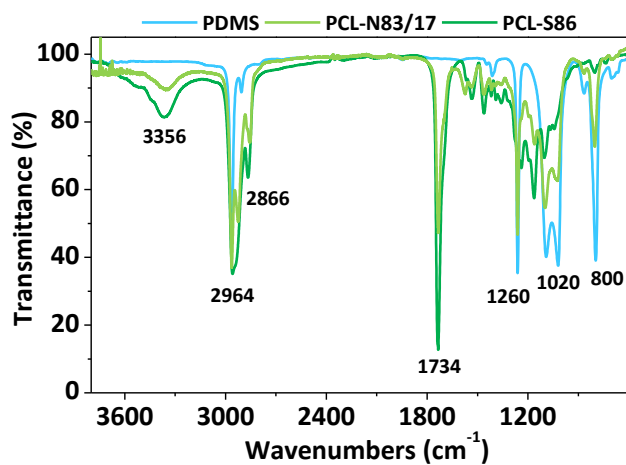


Figure IV-2. FTIR spectra of PDMS, PCL-N83/17 and PCL-S86.

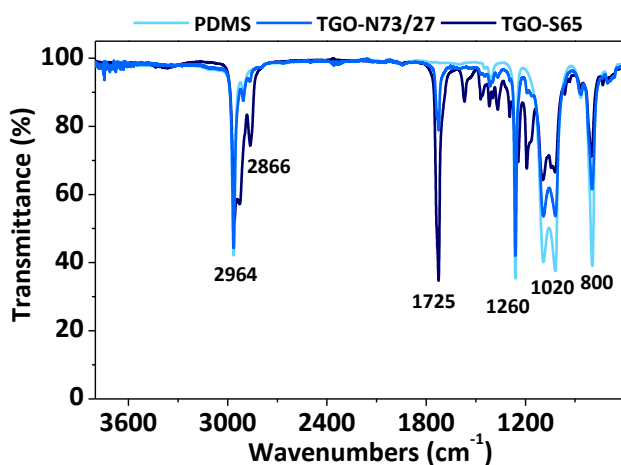


Figure IV-3. FTIR spectra of PDMS, TGO-N73/27 and TGO-S65.

Chapter IV – Characterization of the PDMS/polyester hybrid networks

IV.2.1.3. Surface micromechanics

AFM analysis can give valuable indications on the surface mechanical properties of coatings. The protocol of AFM analyses is described in the experimental section (§ VI.5.5.2.). The aim of using AFM was to highlight the effect of the polyester nature, polyester content and crosslinking density within the different coating samples.

The 20 μm -scaled surface images exhibit the topography, elastic modulus, adhesion force and deformation features of the coatings (from Figure IV-5 to Figure IV-12).

The PDMS surface showed homogenous micromechanics properties with an elastic modulus of *ca.* 1.4 MPa (Figure IV-4), an adhesion force of *ca.* 30 nN and a global deformation amplitude of *ca.* 50 nm (Figure IV-5).

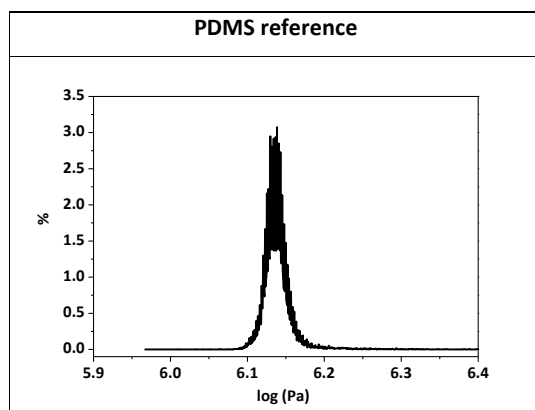


Figure IV-4. Spectral map of the surface elastic modulus (log) for the PDMS reference.

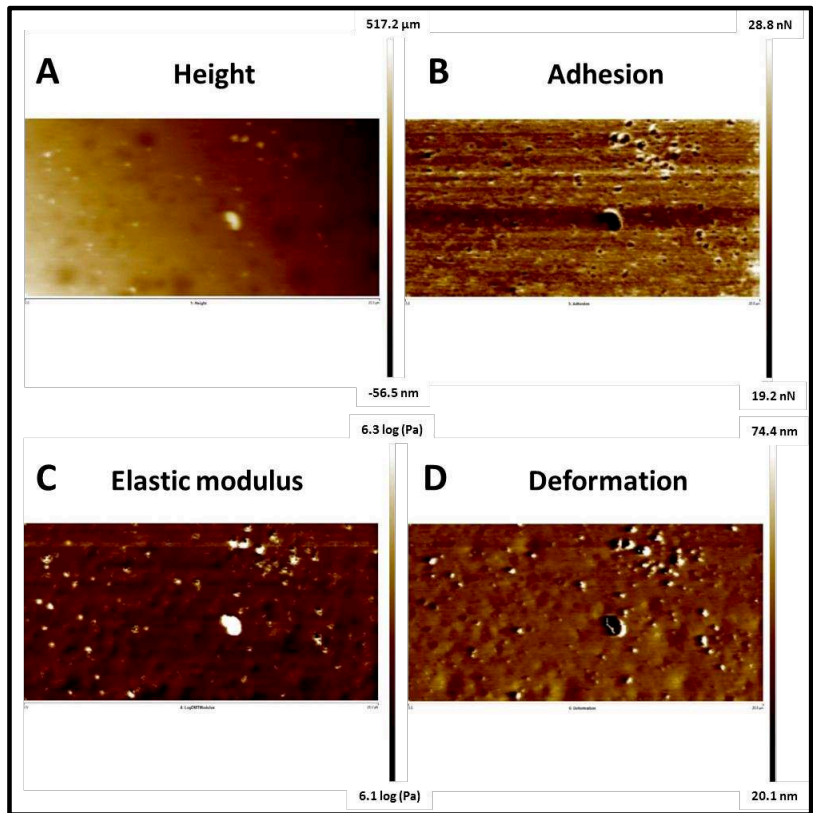


Figure IV-5. AFM images of the PDMS reference (20 μm scale).

Spectral maps of the surface elastic modulus of all the polyester-based coatings are shown in Table IV-7.

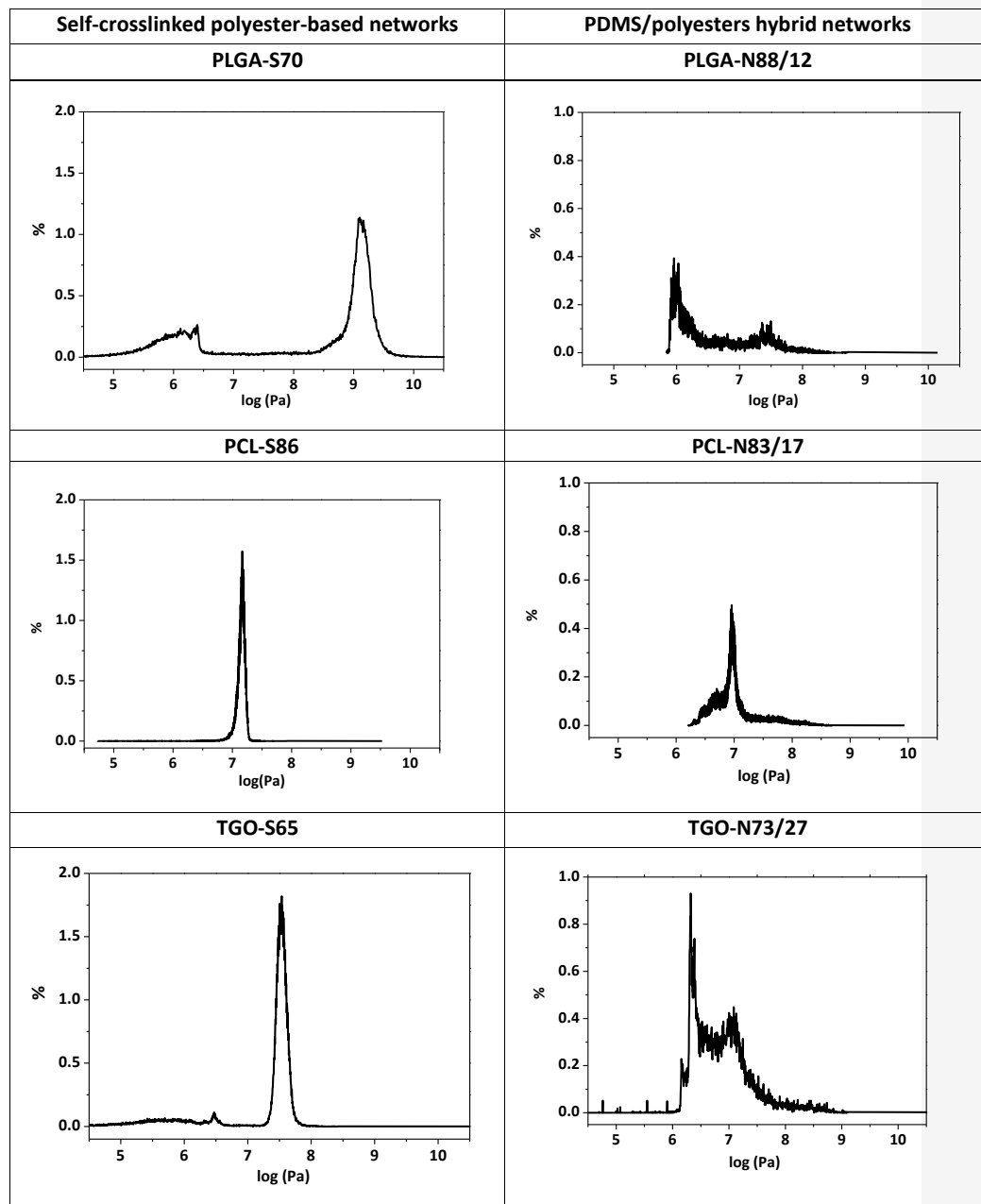
Chapter IV – Characterization of the PDMS/polyester hybrid networks

Globally, the self-crosslinked polyester-based networks (PCL-S86 and TGO-S65) displayed unimodal modulus distributions with elastic moduli of *ca.* 16 MPa and *ca.* 35 MPa, respectively. PLGA-S70 was an exception as it displayed a bimodal modulus distribution at *ca.* 2 GPa and *ca.* 1 MPa. The population of low elastic modulus (*ca.* 1 MPa) was probably due to some unbonded PLGA, observed with the extraction test in chloroform in Chapter III (§ III.3.4.) or some dangling PLGA chains.

The PDMS/polyester hybrid networks displayed more heterogeneous modulus distributions (bimodal) in accordance with their double chemistry with hard/soft segments. They displayed elastic modulus values ranging from 1 to 100 MPa which confirmed their multiphase nature.

Chapter IV – Characterization of the PDMS/polyester hybrid networks

Table IV-7. Spectral maps of the surface elastic modulus (log) for each coating.



Chapter IV – Characterization of the PDMS/polyester hybrid networks

▪ PLGA-based coatings

The self-crosslinked PLGA-S70 surprisingly exhibited a dual elastic modulus profile. There were regions with low elastic modulus of *ca.* 1MPa (dark zones, Figure IV-6, C) and high deformation values (bright zones, Figure IV-6, D) alternating with regions of high elastic modulus of *ca.* 1-3 GPa (bright zones, Figure IV-6, C) and low deformation values (dark zones, , Figure IV-6, D). These observations indicated that PLGA-S70 presented on its surface PLGA segments with more or less rigidity. Residual PLGA (not covalently bonded or partially bonded) observed in the residue extraction test in Chapter III (§ III.3.4.) could explain the regions with low elastic modulus.

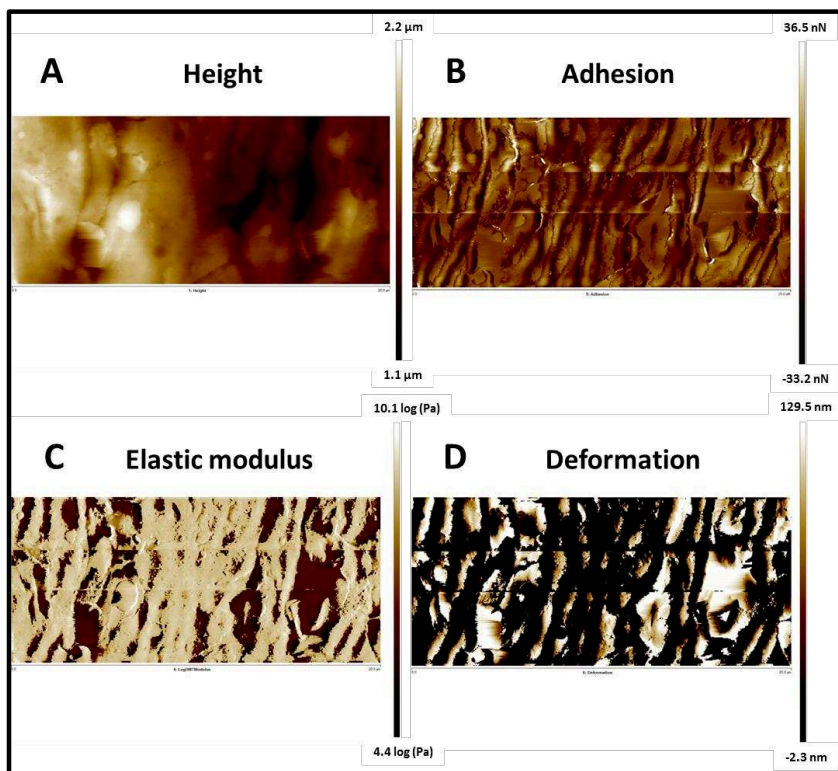


Figure IV-6. AFM images of PLGA-S70 (20 μm scale).

Chapter IV – Characterization of the PDMS/polyester hybrid networks

PLGA-N88/12 exhibited some small recurring globular phases of *ca.* 2 μm on the AFM images (Figure IV-7). PLGA-N88/12 surface showed large zones displaying an elastic modulus of *ca.* 500 kPa (dark phase, Figure IV-7, C), an adhesion force of *ca.* 30 nN (dark phase, Figure IV-7, B) and a deformation amplitude of *ca.* 100 nm (dark phase, Figure IV-7, D).

On the contrary, the small globular phases showed an elastic modulus of *ca.* 15 MPa (light phase, Figure IV-7, C), an adhesion force of *ca.* 10 nN (light phase, Figure IV-7, B) and a deformation amplitude of *ca.* 30 nm (dark phase, Figure IV-7, D). These values indicated a surface mostly made of PDMS but presenting some small PLGA clusters with distinctive micromechanics properties.

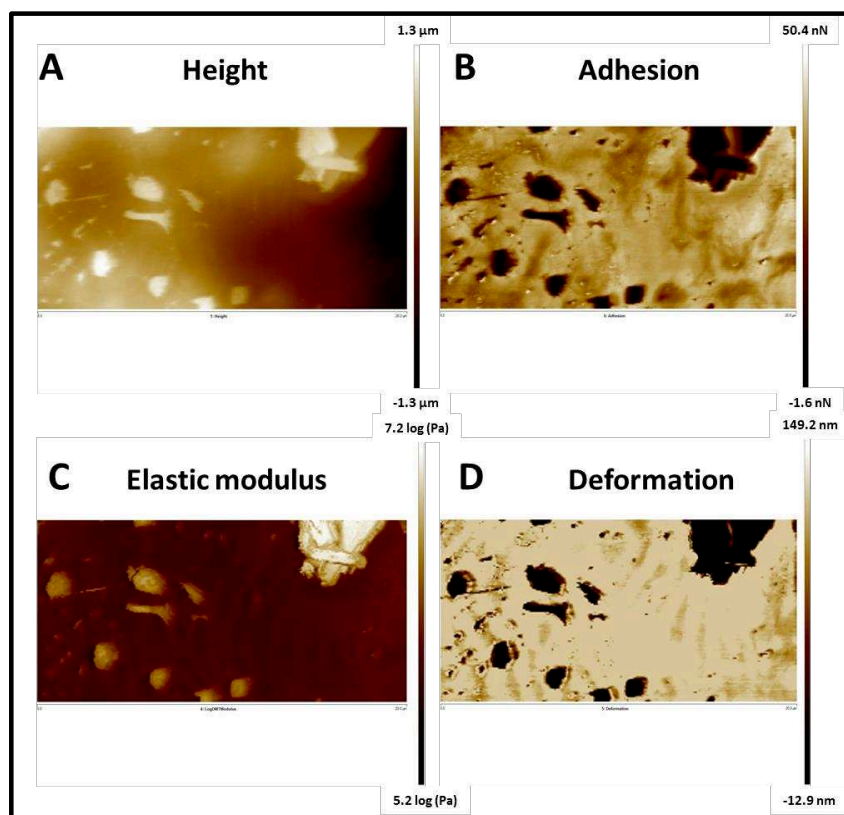


Figure IV-7. AFM images of PLGA-N88/12 (20 μm scale).

Chapter IV – Characterization of the PDMS/polyester hybrid networks

▪ PCL-based coatings

No large local variation in the height, adhesion, deformation and elastic modulus images was observed on PCL-S86 surface (Figure IV-8). According to the deformation and elastic modulus images, PCL-S86 exhibited an elastic modulus of *ca.* 16-20 MPa and maximum deformation of *ca.* 40 nm. No lamellar morphology was observed at a smaller scale (either 10 μm or 3 μm).

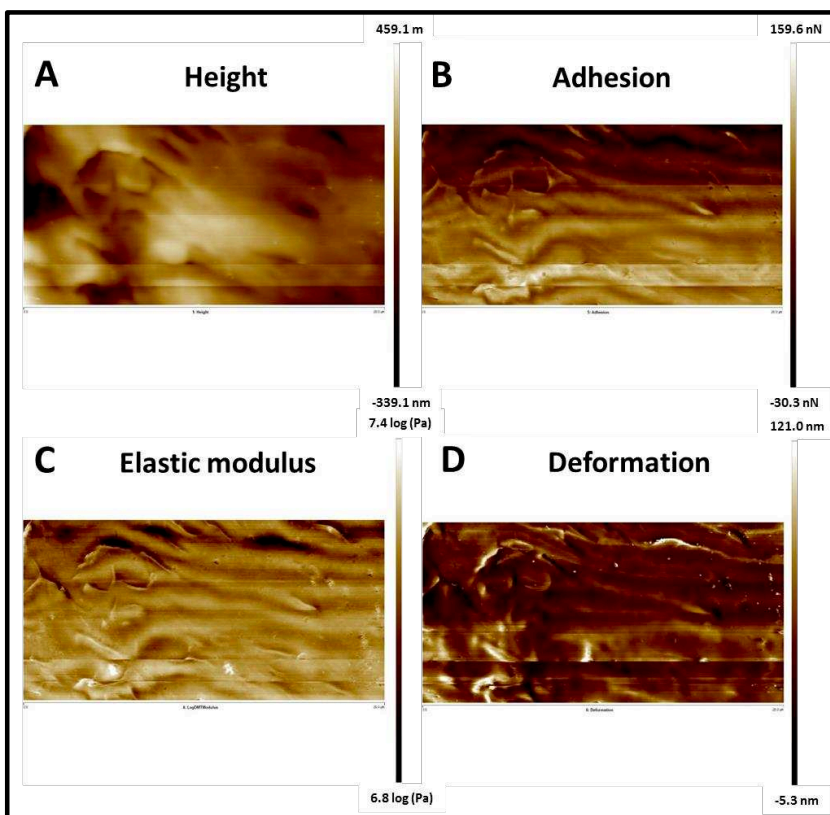


Figure IV-8. AFM images of PCL-S86 (20 μm scale).

Chapter IV – Characterization of the PDMS/polyester hybrid networks

Imaging AFM of PCL-N83/17 showed important variations in elastic modulus, deformation and adhesion (Figure IV-9). The presence of stiffer microdomains ($\geq 5 \mu\text{m}$ in width) of elastic modulus up to 30 MPa (Figure IV-9, C) and low deformation value ($\leq 10 \text{ nm}$, Figure IV-9, D) surrounded by a softer matrix traduced a microphase separation between PCL and PDMS confirming the SEM-EDX analysis (§ IV.2.1.1.). No lamellar morphology was observed at a smaller scale (either $10 \mu\text{m}$ or $3 \mu\text{m}$).

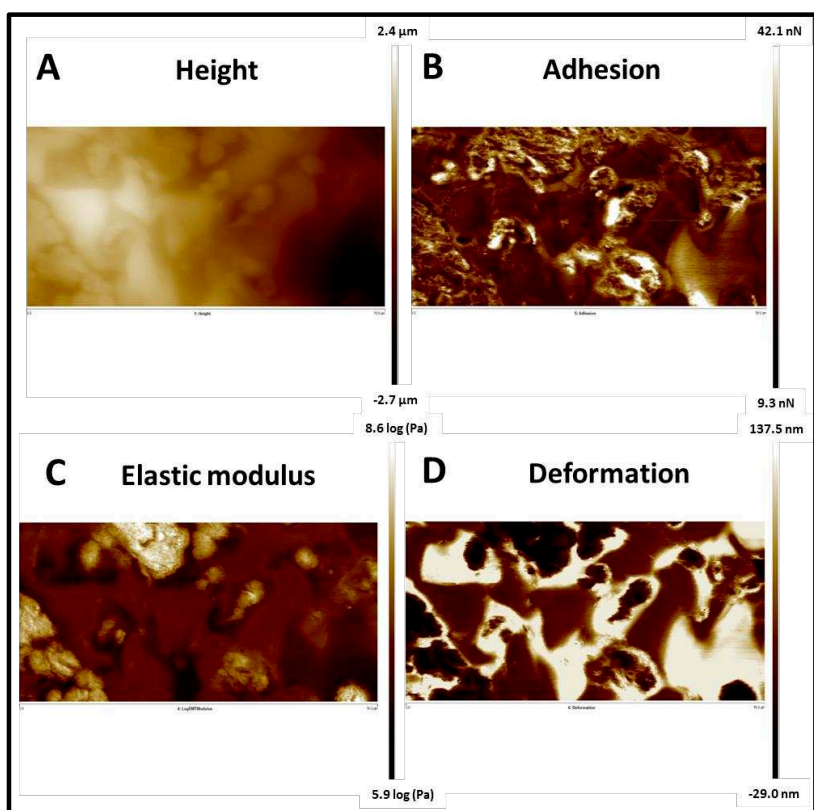


Figure IV-9. AFM images of PCL-N83/17 (20 μm scale).

▪ PCL-*b*-PDMS-*b*-PCL-based coatings

TGO-S65 displayed a more complex AFM imaging (Figure IV-10). Significant variations in the values of the modulus, adhesion and deformation at different points on the TGO-S65 surface highlighted a peculiar polymer arrangement. It should be noted that the “wavy” topography observed in Figure IV-10 was certainly due to the effect of the solvent evaporation during the drying of TGO-S65.

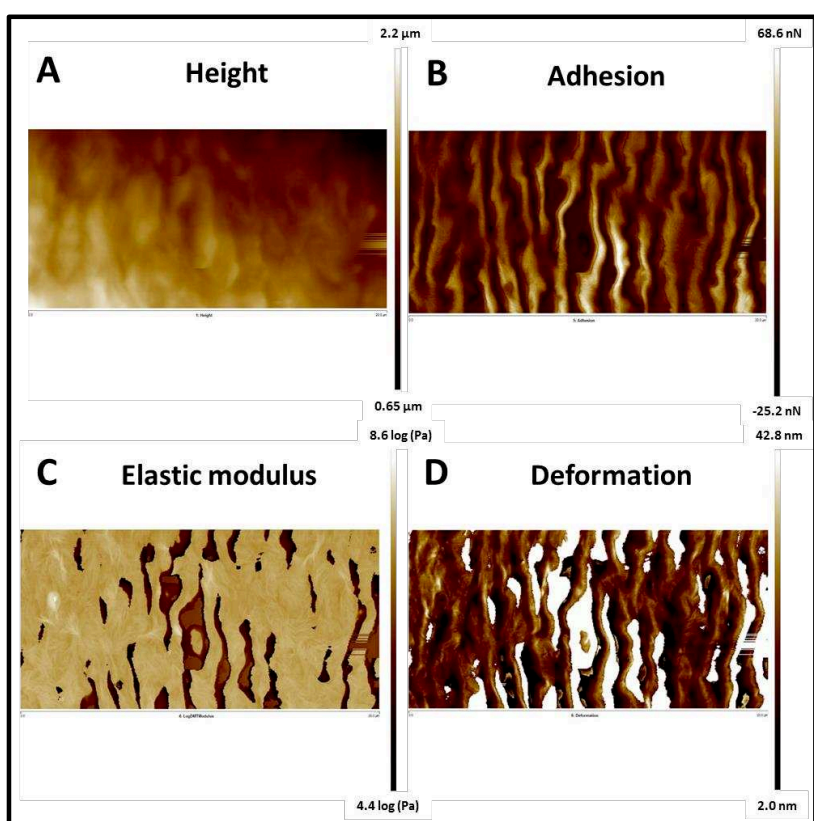


Figure IV-10. AFM images of TGO-S65 (20 μm scale).

The presence of organized clusters, more visible in Figure IV-11 at a smaller scale, suggested the triblock copolymer adopted a preferential organization in spherulitic structures. The spherulitic structures exhibited elastic modulus up to 35 MPa with lower adhesion and

Chapter IV – Characterization of the PDMS/polyester hybrid networks

deformation values than the PDMS reference indicating they were rather constituted of the semi-crystalline PCL.

The phases which exhibited lower elastic modulus (< 3 MPa), higher deformation and adhesion properties certainly corresponded to the grouping of the soft PDMS central blocks.

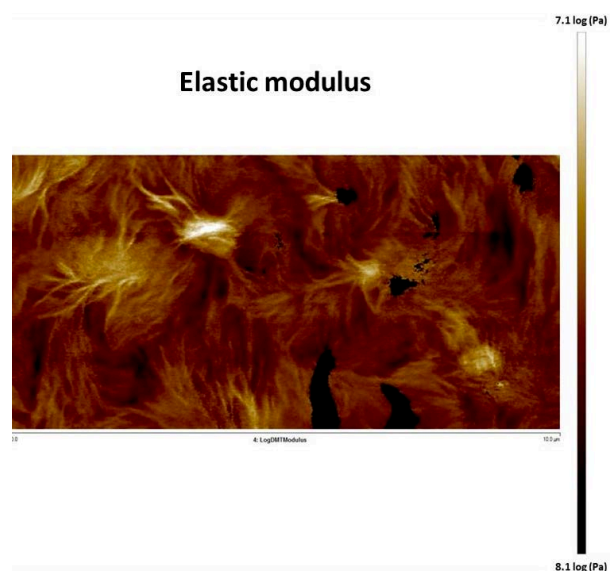


Figure IV-11. AFM image showing the elastic modulus variations of TGO-S65 at 10 μm -scale.

TGO-N73/27 exhibited some microphase separations visible on the AFM images (Figure IV-12). In details, TGO-N73/27 surface showed heterogeneous micromechanics properties with elastic moduli varying from *ca.* 4 MPa (dark phase, Figure IV-12, C) to *ca.* 30 MPa (light phase, Figure IV-12, C), adhesion forces varying from *ca.* 30 nN (dark phase, Figure IV-12, B) to *ca.* 10 nN (light phase, Figure IV-12, B) and a deformation amplitudes varying from *ca.* 30 nm (dark phase, Figure IV-12, D) to *ca.* 100 nm (light phase, Figure IV-12, D). The increase of elastic modulus, the diminution of adhesion and deformation are consistent with the transition from a silicone-rich phase to a densely packed polyester phase. The predominance of PDMS within the network seemed to have prevented the formation of spherulitic structures as seen in TGO-S65.

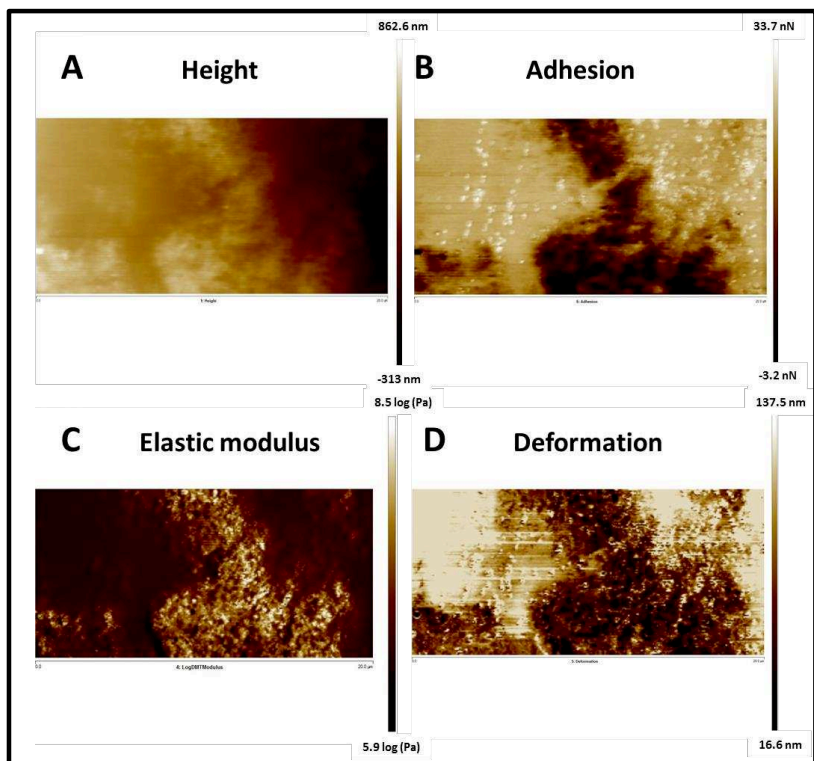


Figure IV-12. AFM images of TGO-N73/27 (20 μm scale).

Globally, the PDMS/polyester hybrid networks exhibited phase segregations with hard and soft domains with no defined geometry. The self-crosslinked polyester-based networks were stiffer than their corresponding PDMS/polyester hybrid networks traducing the effect of both the polyester content and shorter inter-chain molar mass. TGO-S65 was the only network presenting peculiar spherulitic microstructures due to the arrangement of semi-crystalline PCL.

Chapter IV – Characterization of the PDMS/polyester hybrid networks

IV.2.2. Thermo-mechanical bulk properties

The PDMS/polyester hybrid networks and the self-crosslinked polyester-based networks were characterized in terms of thermal and mechanical properties with various technical analysis such as DSC and DMA. These techniques can give valuable information on the polymer network crystallinity and elastic modulus.

IV.2.2.1. Thermal properties of the networks

Differential scanning calorimetry (DSC) analysis were performed to evaluate the influence of the crosslinking reaction on the thermal properties of the polyesters and/or PDMS segments. The main information provided by DSC was the crystallinity values of the PDMS and polyester segments (when present) within the networks.

The thermal conditions are reported in the experimental section (§ VI.5.5.). The crystallinity of the PDMS segments was calculated according to **Eq. 1** and the crystallinity of the PCL segments was calculated using **Eq. 2** as follows:

$$X_c(\text{PDMS}) = (\Delta H_m^{\text{PDMS}} \times w_{\text{PDMS}}) \times 100 / (\Delta H_m^{\text{PDMS,th}}) \quad \text{Eq. 1}$$

$$X_c(\text{PCL}) = (\Delta H_m^{\text{PCL}} \times w_{\text{PCL}}) \times 100 / (\Delta H_m^{\text{PCL,th}}) \quad \text{Eq. 2}$$

With $X_c(\text{PDMS})$, the crystallinity of the cured PDMS, $X_c(\text{PCL})$, the crystallinity of PCL, ΔH_m^{PDMS} the measured melting enthalpy of PDMS, ΔH_m^{PCL} the measured melting enthalpy of PCL. $\Delta H_m^{\text{PDMS,th}}$ is the theoretical melting enthalpy of an unfilled cured PDMS rubber taken equal to 28.35 J/g [7]. $\Delta H_m^{\text{PCL,th}}$ is the equilibrium melting enthalpy of 100 % crystalline PCL taken equal to 139.3 J/g [8]. w_{PDMS} and w_{PCL} represent the mass fractions of PDMS elastomer and PCL respectively in the dry coatings.

Table IV-8 showed that all the polyester-based networks were amorphous at ambient air except for the networks based on PCL-b-PDMS-b-PCL. The PDMS central block flexibility may have allowed the gathering of a small fraction of PCL segments in the form of clusters for TGO-N73/27. TGO-S65 showed a higher crystallinity value ($X_c(\text{PCL})$ around 14 %) than TGO-N73/27 ($X_c(\text{PCL})$

Chapter IV – Characterization of the PDMS/polyester hybrid networks

around 2 %) due to the predominance of PCL (65 % of PCL in TGO-S65 against 27 % of PCL in TGO-N73/27).

Table IV-8. Thermal characteristics of the experimental coatings obtained by DSC analyses.

Coating ID	$\Delta H_{m,PDMS}$ (J/g)	$T_{m,PDMS}$ (°C)	$X_c(PDMS)$ (%) ^a	$T_{g,polyester}$ (°C)	$\Delta H_{m,polyester}$ (J/g)	$T_{m,polyester}$ (°C)	$X_c(PCL)$ (%) ^c
PDMS elastomer	23	-45	81.1	-	-	-	-
PLGA-N88/12	22	-41	68.2	<i>n.d.</i> ^b	-	-	-
PLGA-S70	-	-	-	17	-	-	-
PCL-N83/17	19	-40	55.6	-56	-	-	0
PCL-S86	-	-	-	-54	-	-	0
TGO-N73/27	15	-40	38.6	<i>n.d.</i> ^b	10	30-40	2
TGO-S65	-	-	-	<i>n.d.</i> ^b	30	30-36	14

^aCalculated with Eq. 1

^bNot determined because the glass transition was hardly visible

^cCalculated with Eq. 2.

PLGA-N88/12 and PCL-N83/17 showed similar thermal behavior than the PDMS reference. The small polyester chains seemed not to have disrupted the crystallization of PDMS at -40°C. The T_g of PLGA in PLGA-N88/12 was hardly visible certainly because the PLGA content is too low to be detected.

PLGA-S70 displayed a broad glass transition temperature at around 17°C which is higher than the glass transition temperature of the pristine PLGA ($T_g = -24^\circ\text{C}$). This result shows the impact of the self-condensation of the PLGA with a decrease of the chains mobility. PCL-N83/17 and PCL-S86

Chapter IV – Characterization of the PDMS/polyester hybrid networks

presented no melting temperature near 50-55°C which proved that the crosslinking of PCL (2,000 g/mol) with PDMS completely prevent it from crystallizing (Figure IV-13).

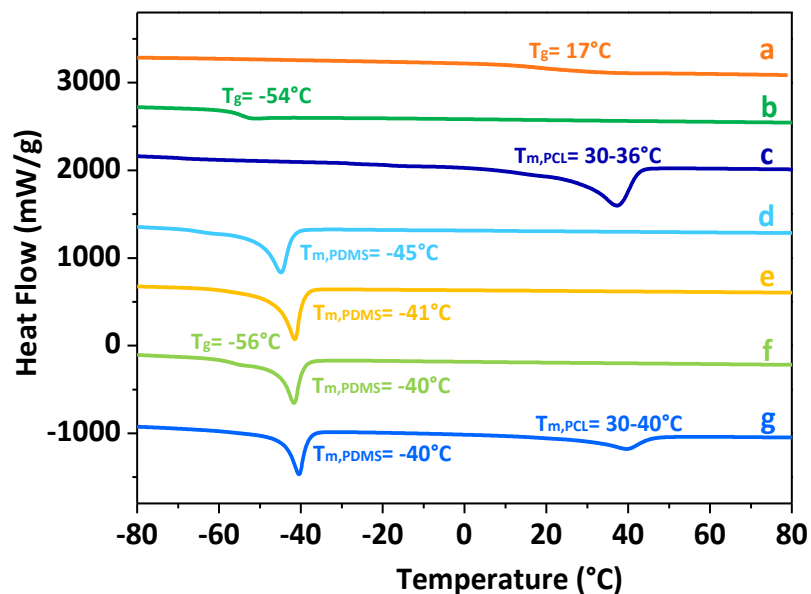


Figure IV-13. DSC thermograms of PLGA-S70 (a), PCL-S86 (b), TGO-S65 (c), PDMS (d), PLGA-N88/12 (e), PCL-N83/17 (f) and TGO-N73/27 (g) obtained at a heating rate of 10°C/min (second heating run).

IV.2.2.2. Viscoelastic properties of the networks

Dynamic Mechanical Analysis (DMA) were performed to study the elastic modulus of the polyester-based networks. Two protocols were tested on free films, one at ambient temperature and one with temperature varying from -150°C to 100°C. The elaboration of the rectangular free films is described in the experimental section (§ VI.4.2.) as well as the DMA protocols (§ VI.5.5.1.).

Chapter IV – Characterization of the PDMS/polyester hybrid networks

IV.2.2.2.1. Viscoelastic behavior at ambient temperature

The viscoelastic properties of free films of the PDMS/polyester hybrid networks and the self-crosslinked polyester-based networks were assessed by DMA. The elastic moduli were obtained at 25°C via the tension film mode (further details in § VI.5.5.1).

The elastic modulus of elastomeric materials depends on multiple parameters such as the crosslinking density, the inter-chain length and the nature of the crosslinked segments (semi-crystalline or amorphous).

The self-crosslinked polyester-based networks exhibited elastic modulus values ranging from 6 to 48 MPa depending on the polyester nature (Figure IV-14). At 25°C, TGO-S65 showed an elastic modulus of 48 ± 10 MPa highlighting the contribution of the crystalline PCL (not yet melted) in the bulk rigidity ($X_c(\text{PCL}) = 14\%$, § IV.2.2.1.). The elastic moduli of PLGA-S70 and PCL-N14/86 (around 6 MPa) were lower than that of TGO-S65 certainly due to their rubbery state at 25°C (above their glass transition temperature, § IV.2.2.1.). Their elastic moduli were higher than the PDMS reference because of the presence of the polyester segments.

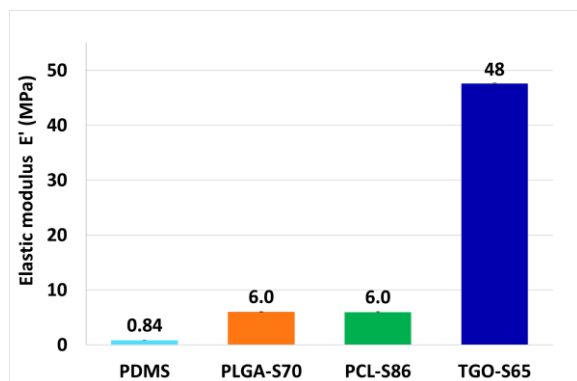


Figure IV-14. Elastic modulus of the self-crosslinked polyester-based networks obtained at 25°C.

FRCs usually exhibit elastic moduli ranging between 0.2 and 9 MPa [3]. Three of the PDMS/polyester hybrid networks displayed storage moduli below 1 MPa similar to the PMDS reference except TGO-N73/27 which showed an increase in rigidity (Figure IV-15). This notable

Chapter IV – Characterization of the PDMS/polyester hybrid networks

increase may be attributed to both the higher PCL crystallinity in the network and the high content of PCL in the dry coating (27 wt.%).

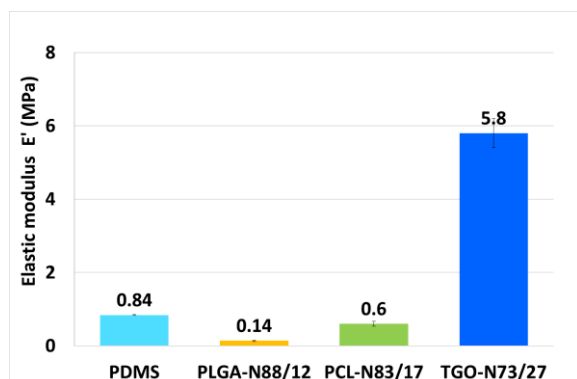


Figure IV-15. Elastic modulus of the hybrid PDMS/polyester hybrid networks obtained at 25°C.

On the contrary, PLGA-N88/12 exhibited an even lower storage modulus than the PDMS reference (0.7 MPa). A possible explanation of this very low elastic modulus would be the presence of some dangling chains within the network, since one-sided crosslinked chains could act as plasticizers in the network and making it more flexible. The elastic modulus of PCL-N83/17 (0.6 MPa at 25°C) was very similar to the PDMS elastic modulus (0.8 MPa at 25°C) suggesting there was no effect of the PCL segments onto the viscoelastic properties of the silicone elastomer.

TGO-N73/27 showed an elastic modulus almost ten times lower than that of TGO-S65. The long PDMS chains of TGO-N73/27 softened the network by disturbing the crystallization of the PCL segments ($X_c(\text{PCL})$ in TGO-N73/27 < $X_c(\text{PCL})$ in TGO-S65, Table IV-8). The elastic moduli of PLGA-N88/12 (0.2 MPa at 25°C) and PCL-N14/86 (0.6 MPa at 25°C) were also around ten times lower than those of PLGA-S70 and PCL-S86 (6 MPa at 25°C), highlighting the strong influence of the PDMS presence and the influence of the inter-chain length or crosslinking density.

IV.2.2.2. Influence of the temperature on the viscoelastic properties of the networks

DMA was performed to highlight the mechanical behavior of the polymer networks while varying the temperature. The polymer networks were tested between -150°C to 100°C at a rate of

Chapter IV – Characterization of the PDMS/polyester hybrid networks

3°C/min (further details in § VI.5.5.1.). The principal purpose of this program was to assess if the polyester segments were homogeneously distributed within the PDMS matrix. In that case, a single relaxation α would be detected, corresponding to an intermediate T_{α} with $T_{\alpha, \text{polyester}} < T_{\alpha, \text{network}} < T_{\alpha, \text{PDMS}}$. If the polyester segments were heterogeneously distributed with the PDMS chains, each polymer relaxation would be identified (at *ca.* -120°C for PDMS, *ca.* -60°C for PCL segments and *ca.* -20°C for PLGA). Given that these materials are designed for fouling release applications, the elastic modulus values within [5 - 30]°C were recorded (typical temperature range of the Mediterranean Sea water).

According to Figure IV-16, PDMS showed two thermal events: a glass transition temperature observed at *ca.* -120°C, and a melting temperature observed at *ca.* -40°C. Below -40°C, PDMS displayed an elastic modulus higher than 500 MPa. In the rubbery plateau region from -40 to 100°C, PDMS displayed a low elastic modulus of *ca.* 1 MPa. This confirmed the very soft nature of the PDMS elastomer within a large range of temperature.

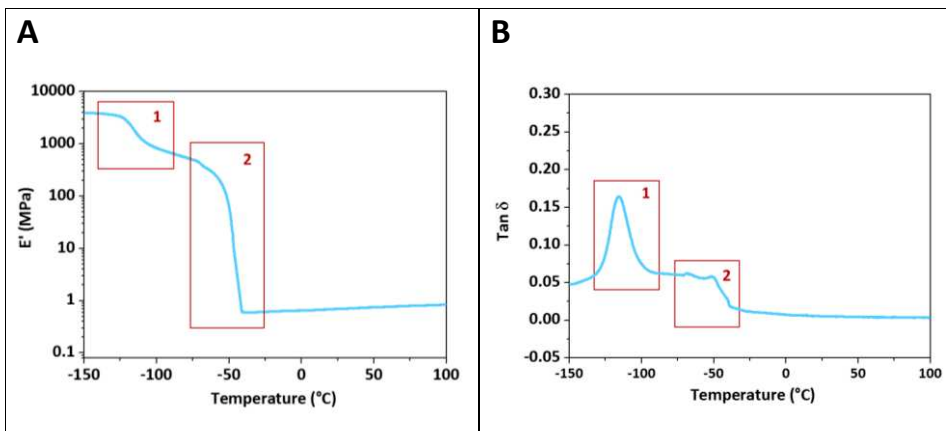


Figure IV-16. Variation of the elastic modulus (A) and $\tan \delta$ (B) with temperature for the PDMS elastomer reference (PDMS).

▪ PLGA-based networks

PLGA-S70 showed a broad α relaxation peak at 20-25°C indicating the self-crosslinking of PLGA strongly reduced the PLGA mobility compared to the pristine PLGA showing a glass-transition temperature at -24°C (from DSC results) (Figure IV-17, 3, A/B). The higher value of T_{α} of PLGA-S70

Chapter IV – Characterization of the PDMS/polyester hybrid networks

compared to PLGA-N88/12 could come from the decrease of the inter-chain molar mass resulting in a very tight network with less degree of liberty for the chains to move. PLGA-S70 also displayed a higher elastic modulus than the PLGA-N88/12 hybrid network between 0 and 100°C due to its higher crosslinking density.

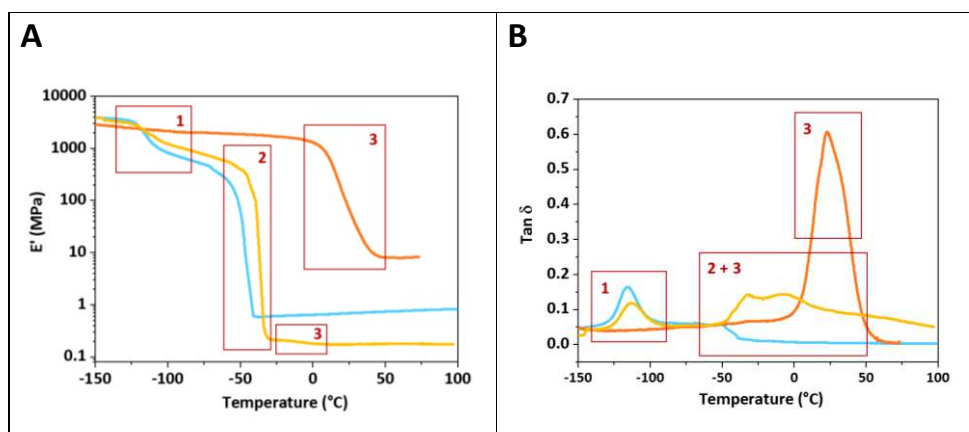


Figure IV-17. Variation of the elastic modulus (A) and $\tan \delta$ (B) with temperature for PLGA-S70, PLGA-N88/12 and PDMS.

PLGA-N88/12 showed a T_{α} at -115°C attributed to the PDMS relaxation (Figure IV-17, **1, A/B**). The melting of PDMS was also observed around -40°C for PLGA-N88/12 (Figure IV-17, **2, A/B**). A very large α relaxation at $T < 0^{\circ}\text{C}$ for PLGA-N88/12 interfered with the melting process of the PDMS according to the $\tan \delta$ curve (Figure IV-17, **2 + 3, B**). This suggested that the crosslinking of PLGA with PDMS caused mobility stress for the PLGA chains. PLGA chains showing T_{α} around -25°C were probably neighbors with flexible PDMS chains whereas chains showing T_{α} around 0°C were probably localized in a reduced-mobility domain. This domain could be composed of self-crosslinked PLGA segments within the network which are slightly more mobile than those formed in PLGA-S70 ($T_{\alpha} \approx 20\text{-}25^{\circ}\text{C}$, Figure IV-17, **3, B**). These DMA curves highlighted a random or heterogeneous distribution of PLGA within the PDMS matrix.

In addition, PLGA-N88/12 displayed a lower elastic modulus than the PDMS reference between 0 and 100°C due to its different crosslinking density. The presence of dangling chains within the network could also explained this lower value of elastic modulus

Chapter IV – Characterization of the PDMS/polyester hybrid networks

▪ PCL-based networks

Figure IV-18 highlighted the similar elastomer behavior of PCL-N83/17 and the PDMS reference. PCL-N83/17 showed a T_{α} at -115°C attributed to the PDMS relaxation (Figure IV-18, **1, A/B**). The melting of PDMS was observed at -40°C for the PDMS reference and the PDMS/PCL hybrid network (Figure IV-18, **2, A/B**). The strong peak at -38°C for PCL-S86 was referred to the α relaxation of PCL (Figure IV-18, **3, B**).

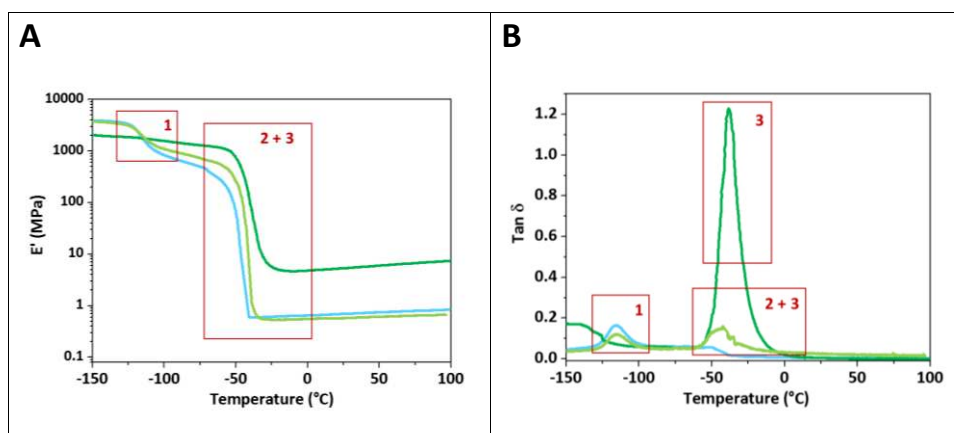


Figure IV-18. Variation of the elastic modulus (A) and $\tan \delta$ (B) with temperature for PCL-S86, PCL-N83/17 and PDMS.

Then, $\tan \delta$ curve indicated two events happening simultaneously at *ca.* -40°C : the PDMS melting and the PCL relaxation which enabled to differentiate PDMS from PCL-N83/17 (Figure IV-18, **2 + 3, B**). The observation of the characteristic relaxations of each polymer indicated a phase separation between PDMS and PCL.

The absence of transition around 50 - 55°C suggested the crosslinking of PCL prevented its crystallization in both PCL-S86 and PCL-N83/17 networks. The absence of PCL crystallinity in these coatings is in favor of a greater water uptake and faster hydrolysis.

In addition, PCL-S86 displayed a higher elastic modulus than the PCL-N83/17 hybrid network between 0 and 100°C due to its higher crosslinking density. PCL-N83/17 displayed a similar elastic

Chapter IV – Characterization of the PDMS/polyester hybrid networks

modulus than the PDMS reference between 0 and 100°C as already reported through tensile test (§ IV.2.2.2.1.).

▪ PCL-*b*-PDMS-*b*-PCL-based networks

TGO-N73/27 showed a T_{α} at -115°C attributed to the PDMS relaxation (Figure IV-19, **1, A/B**). TGO-S65 showed a very small α relaxation at -115°C given that the PDMS segments were in minority in the sample.

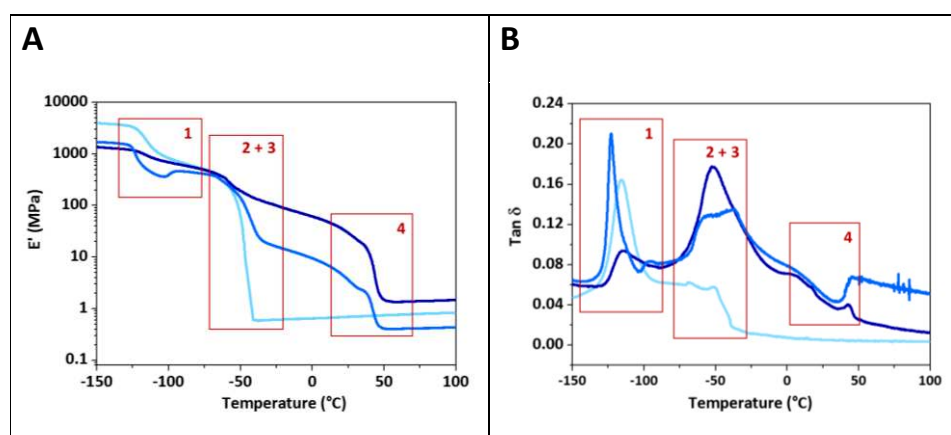


Figure IV-19. Variation of the elastic modulus (A) and $\tan \delta$ (B) with temperature for TGO-S65, TGO-N73/27 and PDMS.

Around -96°C, a cold crystallization of the hybrid network TGO-N73/27 was identified by a slight increase of E' looking like a shoulder on the modulus curve. The cold crystallization occurs when the polymer has reached enough molecular mobility to release the thermal and mechanical stress accumulated during the forced cooling [9]. This phenomenon can be explained by the presence of 27 wt.% PCL which changed from a rubbery to a glassy state during the cooling process, before the PDMS crystallization at -80°C. The glassy state of the PCL blocks certainly prevented the PDMS crystallization, by limiting the global polymer network mobility.

The melting of PDMS was observed at -40°C for the PDMS reference and the hybrid networks (Figure IV-19, **2, A/B**). Around -52°C, two simultaneous events occurred for TGO-N73/27

Chapter IV – Characterization of the PDMS/polyester hybrid networks

according to the $\tan \delta$ curve. The melting of PDMS was closely followed by the α relaxation of the PCL segments.

The decrease of E' at 43°C for both TGO-N73/27 and TGO-S65 was related to the melting of PCL segments (Figure IV-19, **3, A**).

Figure IV-19 highlighted the semi-crystalline state of PCL segments in the TGO-N73/27 film confirmed by DSC. The observation of the characteristic relaxations of each polymer segments meant there was phase separation.

In addition, TGO-S65 displayed a higher elastic modulus than the TGO-N73/27 hybrid network between 0 and 50°C due to its higher crosslinking density. TGO-N73/27 displayed a higher elastic modulus than the PDMS reference between 0 and 50°C due to the crystallinity of the PCL segments within the hybrid network.

To conclude, the elastic modulus values of the PDMS/polyester hybrid networks between 5 and 30°C (typical temperature range of the Mediterranean seawater) did not exceed 6 MPa indicating they behave like elastomer materials and are thus likely to display fouling release properties. The self-crosslinked polyester-based networks exhibited elastic moduli equal or higher to 6 MPa which would certainly limit their fouling release ability.

Chapter IV – Characterization of the PDMS/polyester hybrid networks

IV.2.3. Summarization of the key findings of the surface/bulk physico-chemical properties

Figure IV-20 gives an overview of the surface/bulk properties of the different PDMS/polyester hybrid networks and their corresponding self-crosslinked polymers. This schematic representation was based on the different findings in SEM-EDX, FTIR-ATR, AFM, DSC and DMA analyses. Some important characteristics are recalled, such as the crystallinity (X_c) and elastic modulus (E').

TGO-N73/27 and TGO-S65 were the only networks with some crystalline phases. This crystallinity was represented by “flower-shaped” clusters in Figure IV-20 and came from the local organization and/or self-crosslinking of the PCL-*b*-PDMS-*b*-PCL macrocrosslinker. PLGA-N88/12 and PLGA-S70 were amorphous networks easily distinguished from their low elastic modulus. Such viscoelastic variation was attributed to the difference in their network crosslinking density. PCL-N83/17 and PCL-S86 were also amorphous networks, the crystallinity of the initial PCL ($X_c = 50\%$, § III.2.2.1.) disappeared due to the PCL crosslinking.

The thermogravimetric analysis performed in Chapter III (§ III.3.5.) was not able to reveal if the polyester-based macrocrosslinkers could have reacted on themselves in the PDMS/polyester networks. While, PDMS could only attach on the polyester-based macrocrosslinkers as there was no PDES crosslinker (such as in the PDMS reference).

The possibility that these hybrid networks are interpenetrated networks (combination of PDMS/polyester and polyester/polyester networks) cannot be ruled out. DMA investigations showed that the self-crosslinking of PLGA macrocrosslinker within the PDMS/polyester hybrid network probably occurred. In doubt, we have drawn polyester macrocrosslinkers attached on themselves in the three PDMS/polyester hybrid networks in Figure IV-20.

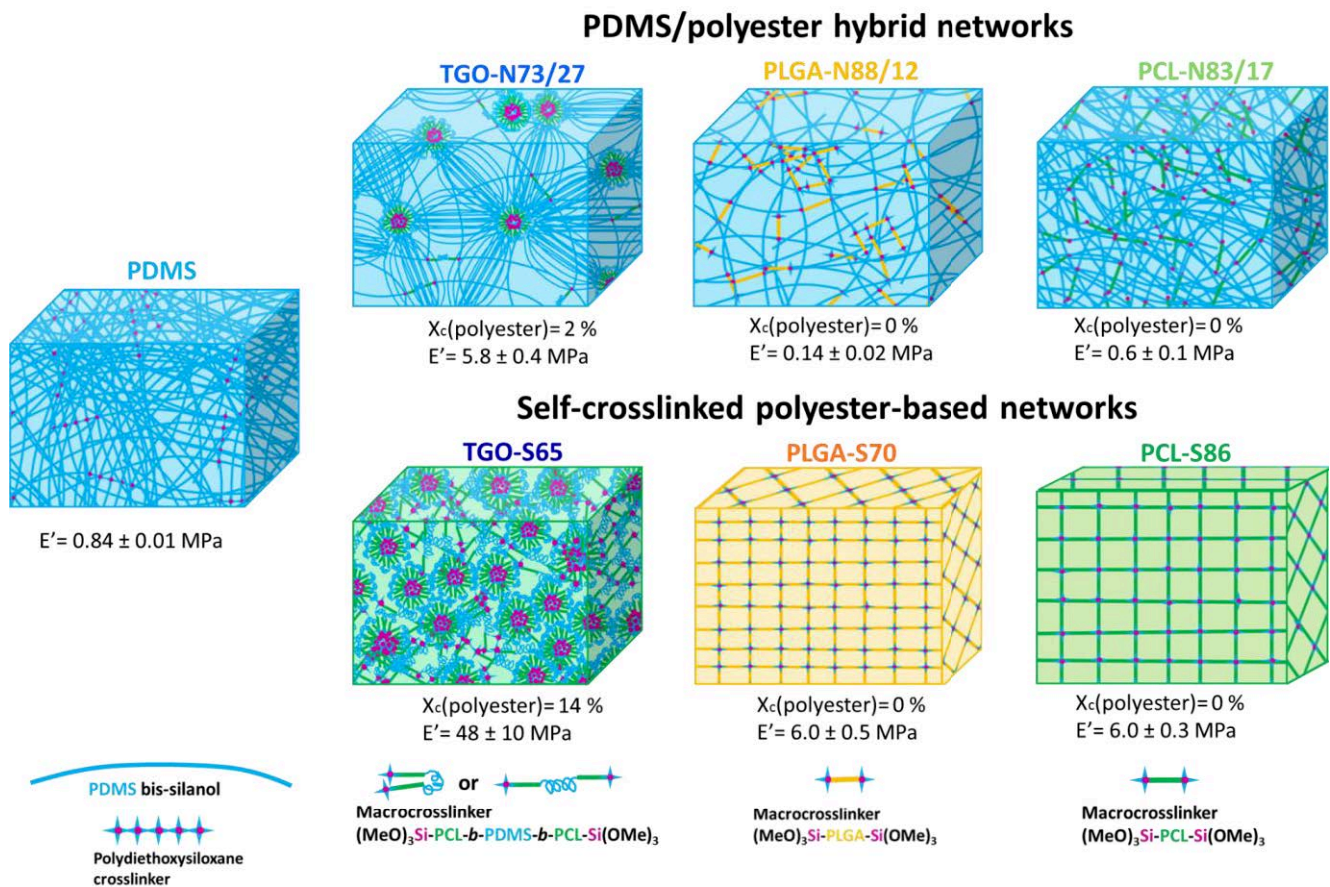


Figure IV-20. 3D schematic representation of the microstructure of the PDMS/polyester hybrid networks, the self-crosslinked polyester-based networks and the PDMS reference

IV.3. Physico-chemical properties during immersion

IV.3.1. Static immersion

IV.3.1.1. Mass loss test (and water uptake test)

The erosion properties of the PDMS/polyester hybrid networks and self-crosslinked polyester-based networks were investigated through a mass loss test in static conditions. The aim of this study was to evaluate the ability of the PDMS/polyester hybrid networks to hydrolyze in deionized water. A comparison with the self-crosslinked polyester-based networks was useful to estimate how much the presence of PDMS could impact on the mass loss of the hybrid PDMS/polyester hybrid networks.

The experimental coatings were immersed in deionized water at room temperature during 26 weeks (for the self-crosslinked polyester-based networks) and during 50 weeks (for the PDMS/polyester hybrid networks). They were removed from water every week to be weighted. to measure their water uptake and their mass loss (after 12 h of drying at ambient air). Further details of the protocol are described in the experimental section (§ VI.6.2. and § VI.6.3.).

The mass loss profile could reveal whether the erosion was a bulk erosion (profile presenting a brutal mass loss increase at the beginning of immersion) or a surface erosion (linear profile).

PDMS elastomers are known to be very resistant to hydrolysis as already discussed in Chapter II (§ II.4.1.). The hydrolytic degradation of silicone elastomers is possible but only at extreme pH-conditions, such as $\text{pH} > 11$ or $\text{pH} < 2.5$ [10]. By adding polyester chains within the PDMS networks, we aimed for promoting a gradual hydrolysis of the whole network.

Figure IV-21 showed the mass loss percentages of the PDMS/polyester hybrid networks (50 weeks), the self-crosslinked polyester-based networks (26 weeks) and the PDMS reference (50 weeks).

Chapter IV – Characterization of the PDMS/polyester hybrid networks

As expected, PDMS exhibited negligible mass loss (0.8 ± 0.1 wt.% after 50 weeks). PCL-N83/17 and TGO-N73/27 exhibited a similar mass loss profile with 13.9 ± 1.2 wt.% and 14.5 ± 0.2 wt.% mass losses respectively after 50 weeks of immersion.

PLGA-N88/12 mass loss was higher than the PCL-based coatings after 50 weeks. This higher mass loss of PLGA-N88/12 (16.2 ± 1.7 wt.%) compared to the PCL-based networks was likely due to the fastest hydrolysis of PLGA which compensated the lower polyester content (12 % of polyester against 17 and 27 % in the PCL-based coatings). The mass loss of PLGA-N88/12 also revealed the release of both PLGA and PDMS segments as the mass loss exceeded the initial PLGA content.

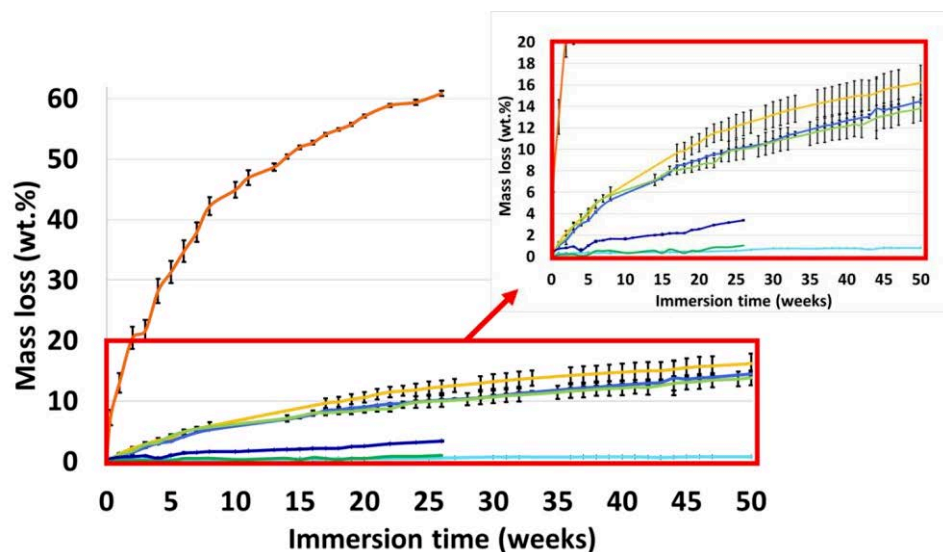


Figure IV-21. Mass loss percentage of PLGA-S70, PLGA-N88/12, PCL-S86, PCL-N83/17, TGO-S65, TGO-N73/27 and PDMS upon immersion in deionized water (before and after magnification of the area of interest).

The three hybrid coatings displayed curve profiles comprising two steps of different mass loss rates. The release of degradation products was faster within 10 weeks of immersion, and then slowed down. By extrapolating the mass loss results to 5 years, the hybrid coatings would reach *ca.* 70 wt.% of mass loss (considering the mass loss rate constant over time). Thus, the coatings would be totally degraded after 7 years of immersion. Taking this information into account, the service life of the coatings would be satisfying for antifouling applications.

Chapter IV – Characterization of the PDMS/polyester hybrid networks

The water uptake of the networks was also measured as it can be directly correlated to the hydrolysis kinetics of the networks (Figure IV-22). PLGA-S70 showed water uptake percentages varying from 3 to 1.5 wt.% which favored the fast hydrolysis (seen in Figure IV-21). TGO-S65 was the coating with the less water uptake during 20 weeks of immersion certainly due to its higher polyester crystallinity and presence of hydrophobic PDMS blocks. PCL-S86 did not absorb a significant amount of water.

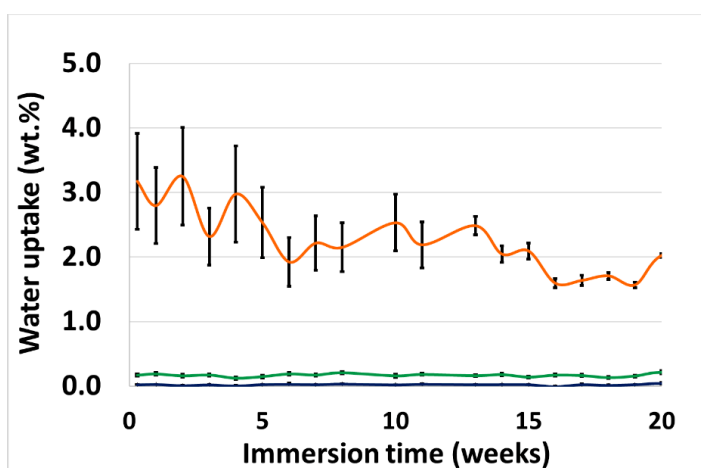


Figure IV-22. Water uptake percentages of the self-crosslinked polyester-based networks with PLGA-S70, PCL-S86 and TGO-S65, during immersion in water.

When comparing the water uptake and mass loss properties of the PDMS/polyester hybrid networks with the self-crosslinked polyester-based networks after 20 weeks, different trends were observed (Table IV-9 and Table IV-10).

Chapter IV – Characterization of the PDMS/polyester hybrid networks

Table IV-9. Water uptake of the experimental coatings after 20 weeks of immersion.

ID coating	Water uptake (wt.%)	ID coating	Water (wt.%)
PDMS	0.02 ± 0.01	PDMS	0.02 ± 0.01
PLGA-N88/12	0.26 ± 0.04	PLGA-S70	2.03 ± 0.03
PCL-N83/17	0.24 ± 0.01	PCL-S86	0.22 ± 0.02
TGO-N73/27	0.22 ± 0.01	TGO-S65	0.04 ± 0.01

Table IV-10. Mass loss of the experimental coatings after 20 weeks of immersion.

ID coating	Mass loss (wt.%)	ID coating	Mass loss (wt.%)
PDMS	0.47 ± 0.02	PDMS	0.47 ± 0.02
PLGA-N88/12	14.7 ± 3.1	PLGA-S70	57.1 ± 0.3
PCL-N83/17	8.5 ± 0.5	PCL-S86	0.53 ± 0.02
TGO-N73/27	9.0 ± 0.1	TGO-S65	2.56 ± 0.04

In the case of PLGA-based coatings, the water uptake and mass loss percentages were multiplied by 5 from PLGA-N88/12 to PLGA-S70. This indicated the crosslinking of PLGA with PDMS chains strongly reduced the ability of PLGA to hydrolyze. The hydrophobic PDMS was certainly the reason why the water penetration was reduced. By slowing down the water uptake, the erosion mechanism went from a bulk erosion (in the case of PLGA-S70, showing a brutal mass loss at the beginning of the immersion) to a surface erosion. Thus, the crosslinking of PLGA with PDMS allowed a more gradual hydrolysis mechanism.

Regarding PCL-N83/17 and PCL-S86, the water uptake percentages were similar but the mass loss percentage of PCL-N83/17 was higher than the mass loss percentage of PCL-S86. Given that both coatings showed PCL segments in an amorphous state, the explanation to this mass loss difference is the difference of crosslinking density between the two networks.

Chapter IV – Characterization of the PDMS/polyester hybrid networks

A hydrolytic cleavage of PCL-S86 will also release smaller degradation products (PCL oligoesters) compared to PCL-N83/17 which will release both high molar mass PDMS chains and PCL oligoesters. Another possible explanation is the entrapment of the degradation products in the PCL-S86 coating.

TGO-S65 displayed lower water uptake and mass loss percentages than TGO-N73/27. The most plausible explanation of this mass loss difference is the difference of crystallinity between the two coatings. TGO-S65 showed a PCL crystallinity of 14 % against 2 % for TGO-N73/27. The more amorphous state of PCL in TGO-N73/27 enabled more water uptake, leading to 7.4 ± 0.2 wt.% of mass loss against 2.1 ± 0.1 wt.% for TGO-S65.

Further physico-chemical characterizations of these coatings would be needed to understand the erosion mechanisms, such as the water diffusion within the coating using fluorescent probes or monitoring the release rate of fluorescent-based PDMS segments.

▪ LGO-N88/12

Figure IV-23 showed the evolution of LGO-N88/12 after 30 weeks in deionized water. The mass loss of LGO-N88/12 was linear and reached more than 8 wt.% after 30 weeks.

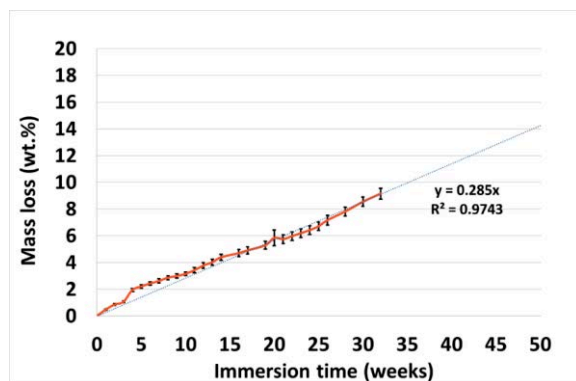


Figure IV-23. Mass loss percentage of LGO-N88/12 upon immersion in deionized water.

The non-crosslinked polymers were partly, if not totally, responsible for the mass loss for the first 20 weeks of immersion. After 20 weeks, the stickiness disappeared suggesting there was a surface renewal.

Chapter IV – Characterization of the PDMS/polyester hybrid networks

By comparing LGO-N88/12 to PLGA-N88/12, we noticed LGO-N88/12 mass loss at 32 weeks was lower than that of PLGA-N88/12. This may be surprising as they both contained the same content of PLGA, the difference was probably due to the initial presence of hydrophobic oils on the surface, which slowed down the mass loss by acting as a hydrophobic barrier.

IV.3.1.2. Roughness

The arithmetic average roughness (R_a) of the PDMS/polyester hybrid networks and the self-crosslinked polyester-based networks (references) was evaluated with a contact type stylus profiler. The mode of application (casting the solution on glass slides) was the same for each coating, since the mode of application influences significantly the roughness. The evolution of the coatings roughness during immersion in deionized water was investigated for 20 weeks for the self-crosslinked polyester-based networks and 50 weeks for the PDMS/polyester hybrid networks (Figure IV-24 and Figure IV-25). Every 5 weeks at least, the coated glass slides were removed from water, dried for 12 h before being analyzed with the profilometer.

▪ Self-crosslinked polyester-based networks

During 10 weeks of immersion, the self-crosslinked polyester-based networks displayed roughness values (R_a) below 2.5 μm except for PLGA-S70 (Figure IV-24). The surface of this coating was particularly affected by the water in the first 5 weeks with the apparition of hills and valleys caused by the fast erosion (seen in § IV.3.1.1.). TGO-S65 on the contrary exhibited the smoothest surface (R_a around 0.1 μm). After 20 weeks of immersion, all the self-crosslinked polyester-based networks coatings displayed roughness values below 5 μm . The topographies of TGO-S65 and PCL-S86 were not affected by the water immersion (no significant mass loss observed for these two networks in § IV.3.1.1.).

Chapter IV – Characterization of the PDMS/polyester hybrid networks

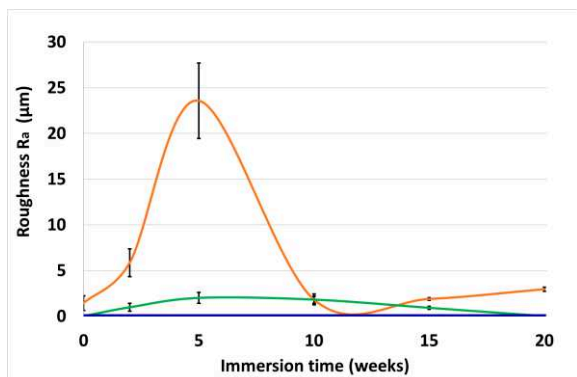


Figure IV-24. Roughness (R_a) of PLGA-S70, PCL-S86 and TGO-S65, during immersion in deionized water.

▪ PDMS/polyester hybrid networks

In Figure IV-25, the PDMS reference and PLGA-N88/12 coatings initially showed smooth surfaces ($R_a < 0.5 \mu\text{m}$). The roughness of PLGA-N88/12 was markedly lower than the self-crosslinked PLGA-S70, certainly thanks to the dominance of PDMS on the surface.

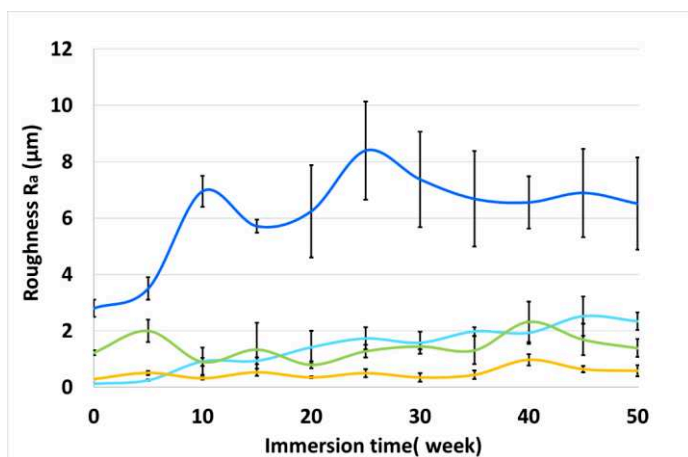


Figure IV-25. Roughness (R_a) of PLGA-N88/12, PCL-N83/17, TGO-N73/27 and PDMS, during immersion in deionized water.

Chapter IV – Characterization of the PDMS/polyester hybrid networks

PCL-N83/17 and TGO-N73/27 exhibited higher roughness ($>1-2\ \mu\text{m}$) meaning there was a strong effect of the PDMS/PCL surface micro-segregation (previously observed with the SEM and AFM images in § IV.2.1.1. and § IV.2.1.3.).

After 5 weeks of immersion in deionized water, a significant increase of R_a was observed for TGO-N73/27 ($R_a \geq 2\ \mu\text{m}$) which can be explained by the surface degradation of PCL (§ IV.3.1.1.) and/or polymer chains reorganization.

For the PDMS elastomer reference, the roughness increased probably due to the presence of a siliceous phase or salts [44–47] (as discussed in Chapter II, § II.4.2.1.).

Regarding PLGA-N88/12 and PCL-N83/17, the roughness values did not exceed $2\ \mu\text{m}$ during the 50 weeks of immersion. This indicated either a physical smoothing of the coatings allowed by their erosion (§ IV.3.1.1.), or no obvious changes of the surface topography after a prolonged water contact. The high roughness value of TGO-N73/27 (R_a around $7\ \mu\text{m}$) maintained until 50 weeks of immersion may certainly be a threat for the coating antifouling properties in the marine environment as it provides many crevices for the organisms to lodge in.

The typical roughness (R_a) of a sprayed silicone FRCs is usually lower than $2\ \mu\text{m}$ [6]. PCL-N83/17 and PLGA-N88/12 roughness values were thus representative to what is expected from a PDMS-based coating. The presence of polyester did not generate significant roughness in these two cases. However, there was an important influence of the polyester phases on the roughness of TGO-N73/27, certainly intensified by the greater content of PCL compared to PCL-N83/17.

▪ **LGO-N88/12**

LGO-N88/12 was not shown in this roughness analysis due to its initial surface tackiness. However, after 20 weeks of immersion, it was noticed a gradually diminution of this tackiness (which even disappeared at 25 weeks). Roughness measurements were thus performed between 20 and 30 weeks revealing roughness values (R_a) of $6.2 \pm 1.0\ \mu\text{m}$ at 20 weeks, $3.9 \pm 0.4\ \mu\text{m}$ at 25 weeks and $3.4 \pm 0.9\ \mu\text{m}$ at 30 weeks. The roughness values were above $2\ \mu\text{m}$ highlighting the heterogeneous surface topography of the PDMS/PLGA-*b*-PDMS-*b*-PLGA hybrid network. The

Chapter IV – Characterization of the PDMS/polyester hybrid networks

diminution of the stickiness and roughness after 20 weeks was certainly due to the release of unbonded PDMS or PLGA-*b*-PDMS-*b*-PLGA oils and/or hydrolysis of crosslinked PLGA-*b*-PDMS-*b*-PLGA.

IV.3.1.3. Wetting properties

IV.3.1.3.1. Dynamic contact angle measurements

As previously discussed in Chapter II, the advancing and receding water contact angles ($\theta_{w,adv}$ and $\theta_{w,rec}$) of the coatings can reveal information about the surface morphology or topography while exposed to water. In the literature, the contact angle hysteresis $\Delta\theta$ ($\Delta\theta = \theta_{w,adv} - \theta_{w,rec}$) of a coating is either explained by its surface roughness, by its surface chemical heterogeneity, or by the ability of its functional groups to reorganize or hydrolyze on the surface exposed to water [49–52]. In this study, the dynamic contact angles (DCA) were measured after different immersion times to assess the physico-chemical changes of the coatings.

▪ Self-crosslinked polyester-based networks

In Figure IV-26, **A**, PCL-S86 initially exhibited an advancing contact angle of 100° which is higher than that of the non-crosslinked PCL ($\theta_{w,adv} \approx 69^\circ$). The PCL network was more hydrophobic than the initial PCL diol certainly because the hydroxyl groups from PCL diol were end-capped with crosslinkable silylated functions.

PLGA-S70 initially exhibited an advancing contact angle of *ca.* 90° compared to *ca.* 101° for PLGA (§ III.2.2.). TGO-S65 initially exhibited an advancing contact angle of *ca.* 105° against *ca.* 116° for PCL-*b*-PDMS-*b*-PCL (§ III.2.2.). Thus, the self-crosslinking of PLGA740 and TGO6800 seemed to have decreased their initial hydrophobicity certainly due to the presence of some hydrophilic urethane linkages on the surface (cf. FTIR-ATR analysis, § IV.2.1.2.).

The $\theta_{w,adv}$ of PCL-S86 decreased down to *ca.* 80° after 5 weeks of immersion while TGO-S65 and PLGA-S70 maintained their $\theta_{w,adv}$ around 95-100°.

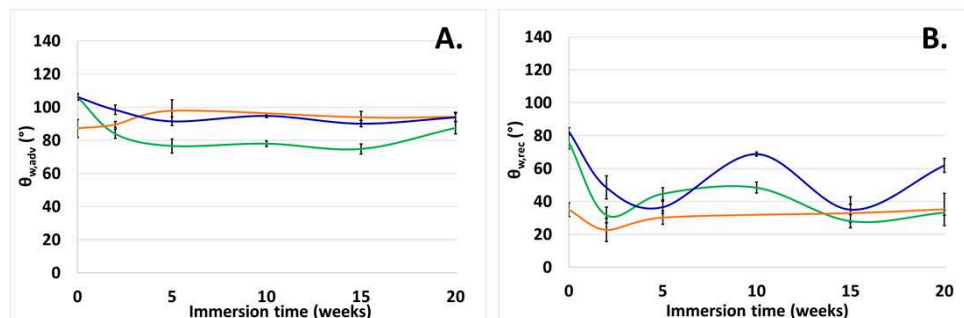


Figure IV-26. Advancing water contact angles ($\theta_{w,adv}$, **A**) and receding water contact angle ($\theta_{w,rec}$, **B**) of PLGA-S70, PCL-S86 and TGO-S65, during immersion in deionized water.

Before immersion, the receding contact angles of TGO-S65 and PCL-S86 were of *ca.* 80°, which was higher than that of the PLGA-S70 with $\theta_{w,rec}$ of *ca.* 35° (Figure IV-26, **B**). Thus, the PLGA chemistry influenced more the receding contact angle than the PCL chemistry before immersion. After 5 weeks of immersion, the $\theta_{w,rec}$ of PCL-S86 rapidly decreased to *ca.* 40° then *ca.* 30° after 20 weeks, showing the PCL network reorganized itself after immersion in water, and made it

Chapter IV – Characterization of the PDMS/polyester hybrid networks

easier for hydrophilic functions to relocate towards the coating/water interface. After 20 weeks, the $\theta_{w,rec}$ of PLGA-S70 was stable ($\theta_{w,rec}$ around 30°). Regarding TGO-S65, the receding contact angle was fluctuating between 40 to 70° during the whole period of immersion. These fluctuations were due to the heterogeneous copolymer blocks arrangement (previously discussed in § IV.2.1.3.).

The hysteresis contact angle of PLGA-S70 was the highest ($\Delta\theta \approx 60^\circ$) and was attributed to the PLGA hydrolysis (significant mass loss observed in § IV.3.1.1.) and also to the chemical reorganization of the crosslinked PLGA chains (Figure IV-27). PCL showed a $\Delta\theta$ value of 60° later at 20 weeks suggesting the PCL chains required more immersion time to gain mobility to rearrange while exposed to water. Finally, the fluctuations of $\Delta\theta$ of TGO-S65, showing no particular tendency, were attributed to the surface chemical heterogeneity.

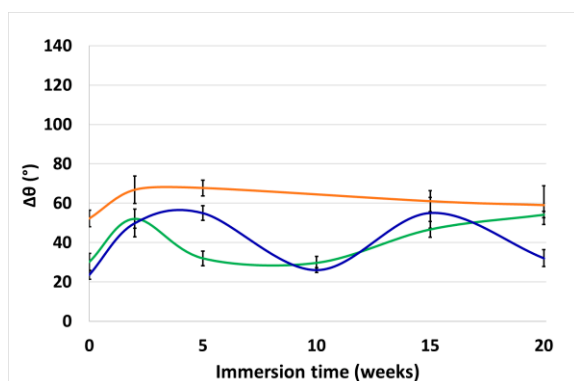


Figure IV-27. Contact angle hysteresis ($\Delta\theta$) of PLGA-S70, PCL-S86 and TGO-S65, during immersion in deionized water.

▪ PDMS/polyester hybrid networks

Roughness profiler analysis carried out before and after 5 weeks of immersion revealed that the changes in surface roughness were rather significant ($R_a \geq 2 \mu\text{m}$ in the case of PCL-based coatings), suggesting that the effect of roughness on water contact angles cannot be neglected. Roughness usually leads to two possible droplet states: the Wenzel state and the Cassie-Baxter state.

Chapter IV – Characterization of the PDMS/polyester hybrid networks

In the case of the Wenzel state, the droplet will fill in the crevices leading to a flatter water droplet. In the case of the Cassie-Baxter state, the droplet will lay on the top of asperities leading to high contact angles ($> 130^\circ$).

$\theta_{w,adv}$ remained essentially unaffected within the first 2 weeks of immersion for all the PDMS/polyester hybrid networks with $\theta_{w,adv} \approx 100\text{-}120^\circ$ (Figure IV-28).

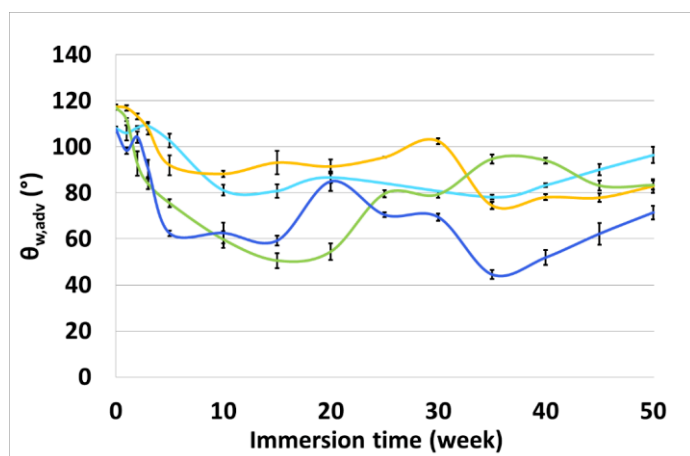


Figure IV-28. Advancing water contact angles ($\theta_{w,adv}$) of PLGA-N88/12, PCL-N83/17, TGO-N73/27 and PDMS, during immersion in deionized water.

After 4 weeks of immersion, the advancing contact angles rapidly decreased below 80° for the PDMS/PCL networks (Figure IV-28). As a reminder, PCL-S86 and TGO-S65 displayed $\theta_{w,adv}$ values equal or higher to 80° until 20 weeks of immersion, thus the strong decrease of $\theta_{w,adv}$ for PCL-N83/17 and TGO-N73/27 could not be attributed to the surface chemistry. This suggested the wettability of the PDMS/PCL networks was mainly influenced by their surface topography (with roughness more pronounced for TGO-N73/27 than PCL-N83/17, § IV.3.1.2.) and followed the Wenzel state.

Between 5 and 30 weeks of immersion, the advancing contact angle of PLGA-N88/12 stabilized around $90\text{-}100^\circ$. It is possible that both PDMS and PLGA chains contributed to this value of advancing contact angle given that PLGA-S70 displayed a $\theta_{w,adv}$ of 95° after 20 weeks of immersion. It is difficult to know which polymer had the most influence on the surface wettability.

Chapter IV – Characterization of the PDMS/polyester hybrid networks

The previous SEM-EDX and AFM analyses would indicate it was more likely the PDMS influence (since PLGA-N88/12 was mainly covered by PDMS at $t_i = 0$) but the previous mass loss study showed non-negligible mass loss between 5 and 30 weeks that could also have an impact on the wetting properties (§ IV.3.1.1.).

The PDMS reference partially lost its hydrophobicity (from 105 to 80°) due to the presence of a thin layer of siliceous phases/salts (cf. Chapter II, § II.4.2.1.).

After 30 weeks of immersion, different wettability profiles could be observed. Regarding PCL-N83/17, there was a hydrophobic recovery of the surface ($\theta_{w,adv} > 80^\circ$) maybe due to the removal of hydrophilic degradation products from PCL-N83/17 (cf. mass loss test, § IV.3.1.1.). On the contrary, the advancing contact angle of TGO-N73/27 coating was below 70° mostly due to the Wenzel state. PLGA-N88/12 showed a gain in surface hydrophilicity ($\theta_{w,adv} \approx 78^\circ$) which was revealing the apparition of PLGA segments onto the surface. This suggested that PLGA chains required some immersion time to cover the surface, probably due to the lower polyester content in PLGA-N88/12 compared with the two others. Maybe, the surface erosion of PLGA-N88/12 has also enabled a PLGA-rich underlying layer to appear.

Figure IV-29 shows the evolution of receding water contact angles with immersion time. During the first 2 weeks, $\theta_{w,rec}$ of all the PDMS/polyester hybrid networks were strongly decreased down to 20° while PDMS showed a decrease of its receding contact angle in a more progressive way down to 75°.

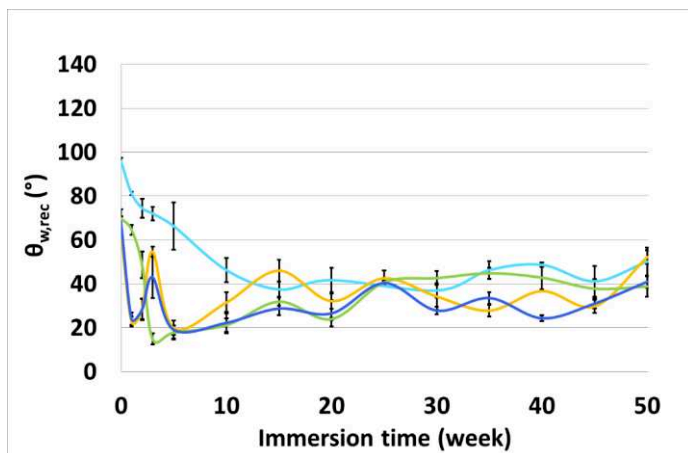


Figure IV-29. Receding water contact angles ($\theta_{w,rec}$) of PLGA-N88/12, PCL-N83/17, TGO-N73/27 and PDMS, during immersion in deionized water.

After 15 weeks, the $\theta_{w,rec}$ of the PDMS/polyester hybrid coatings ranged from 20 to 40° against *ca.* 40-50° for the PDMS reference. These low values of $\theta_{w,rec}$ can be related to surface chemical modification (*e.g.* erosion) and/or surface morphology changes of the coatings after water exposure.

Figure IV-30 shows the variation of $\Delta\theta$ during the 50 weeks of immersion in deionized water.

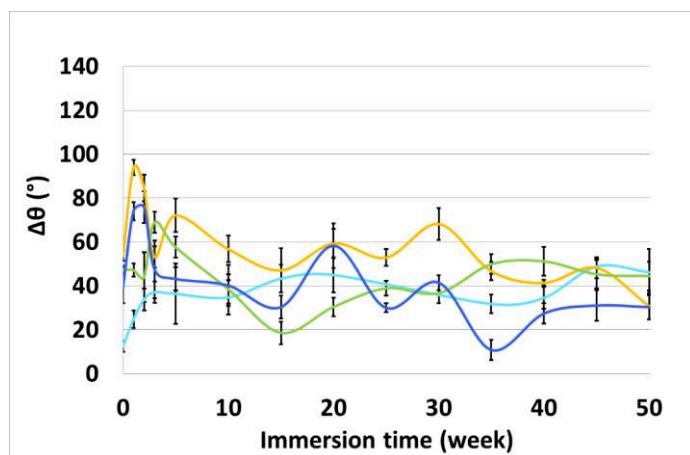


Figure IV-30. Contact angle hysteresis ($\Delta\theta$) of PLGA-N88/12, PCL-N83/17, TGO-N73/27 and PDMS, during immersion in deionized water.

The most stable evolution of $\Delta\theta$ was attributed to the PDMS reference ($\Delta\theta \approx 40^\circ$), highlighting its low propensity to reorganize.

PLGA-N88/12 was the coating exhibiting the highest values of $\Delta\theta$ (ca. $50\text{-}70^\circ$) upon immersion. Given that its roughness values were below $1\ \mu\text{m}$ upon immersion (§ IV.3.1.2.), the contact angle hysteresis was attributed to the ability of the PLGA to hydrolyze and to reorient its hydrophilic functions towards water such as carbonyl, carboxylic acid and hydroxyl functions.

Evolution of $\Delta\theta$ for PCL-N83/17 and TGO-N73/27 did not show any specific tendency. This was attributed to their erosion (§ IV.3.1.1.) and/or topography heterogeneity (§ IV.2.1 and § IV.3.1.2.).

- LGO-N88/12

Figure IV-31 shows the $\theta_{w,adv}$ of LGO-N88/12 immersed for 30 weeks in deionized water. $\theta_{w,adv}$ was initially very high ($\theta_{w,adv} \approx 136^\circ$) certainly due to the very hydrophobic nature of unbonded PDMS and/or PDMS central block of unbonded PLGA-*b*-PDMS-*b*-PLGA oils on the surface responsible of its stickiness.

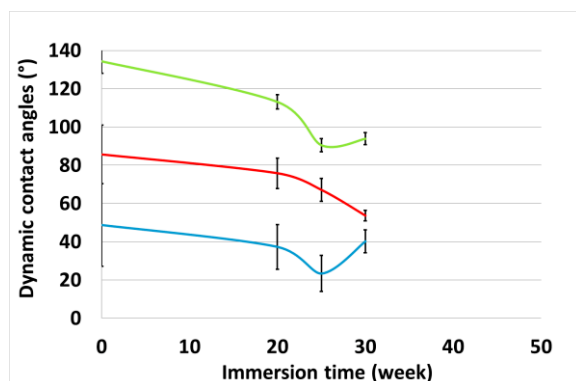


Figure IV-31. Dynamic contact angle of LGO-N88/12: $\theta_{w,adv}$ (green line), $\theta_{w,rec}$ (blue line) and $\Delta\theta$ (red line), during immersion in deionized water.

The gradual decrease of $\theta_{w,adv}$ down to 90° after 30 weeks suggests the partial if not total release of unbonded oils. It can be reminded that PLGA-N88/12 presented a similar $\theta_{w,adv}$ value ($\theta_{w,adv} \approx 90^\circ$) between 5 to 30 weeks as well as PLGA-S70 ($\theta_{w,adv} \approx 80-95^\circ$) during 20 weeks (§ IV.3.1.3.1.). This observation could confirm the PLGA contribution on the wetting properties of LGO-N88/12 and PLGA-N88/12. The roughness of LGO-N88/12 may also have an influence on the wetting properties. At the end, it is hard to say whether the chemistry prevailed over the roughness or the opposite, or whether they both influenced the wetting properties of LGO-N88/12 after 20 weeks of immersion.

$\theta_{w,rec}$ was initially around 48° indicating there was a significant hydrophilic contribution and thus a fast reorganization of the PLGA blocks on the upper surface after water contact. The values of $\theta_{w,rec}$ were stable upon immersion suggesting there were still some polar components on LGO-N88/12 surface. The $\Delta\theta$ values of LGO-N88/12 (from 86° to 54°) could be attributed to the PLGA reorganization onto the surface upon water exposure and/or PLGA hydrolysis and/or the roughness of the coating as previously mentioned.

Chapter IV – Characterization of the PDMS/polyester hybrid networks

IV.3.1.3.2. Surface free energy

In this study, the aim was to discuss the effect of the polyester on the coatings surface free energy during immersion in water.

▪ Self-crosslinked polyester-based networks

Initially, all the self-crosslinked polyester-based networks displayed a surface free energy (SFE) of 25-28 mJ/m² (Figure IV-32).

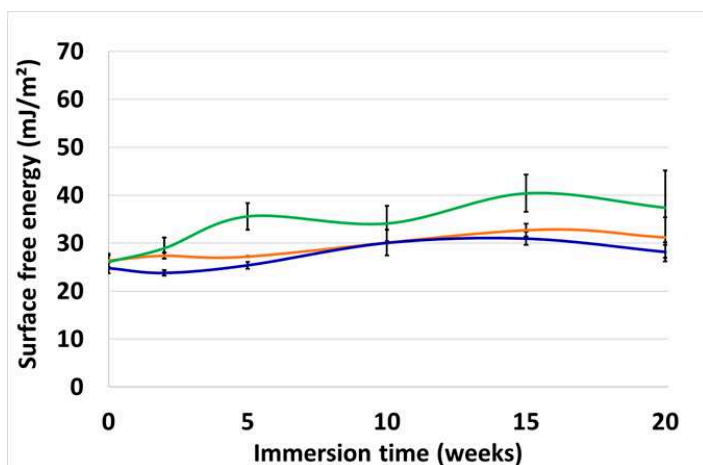


Figure IV-32. Surface free energy (γ_s) of PLGA-S70, PCL-S86 and TGO-S65, during immersion in deionized water.

After exposure to 5 weeks, PCL-S86 started to show an increase of SFE principally due to the increase of its polar component (Figure IV-33, B). After 20 weeks of immersion in deionized water, PCL-S86 reached 40 mJ/m². This revealed the hydrophilic nature of PCL when exposed to water.

PLGA-S70 and TGO-S65 showed similar SFE evolution upon immersion with a stable SFE value around 30 mJ/m² mainly due to dispersive forces ($\gamma_s^p \leq 5$ mJ/m², Figure IV-33, A). After 20 weeks, no significant increase of the polar component was revealed contrary to PCL-S86. Their lower content of polyester compared to PCL-S86 could explain this SFE difference.

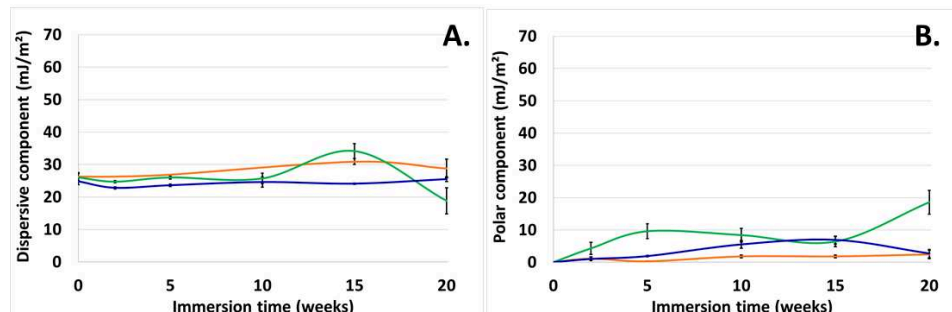


Figure IV-33. Dispersive component (γ_S^D , A) and polar component (γ_S^P , B) of the surface free energy of PLGA-S70, PCL-S86 and TGO-S65, during immersion in deionized water.

▪ PDMS/polyester hybrid networks

Before immersion, for all the PDMS/polyester hybrid coatings, the dominant contribution of the SFE was dispersive, typical of a non-polar silicone-based surface with $\gamma_S \approx \gamma_S^D \approx 18-26$ mJ/m² (Figure IV-34).

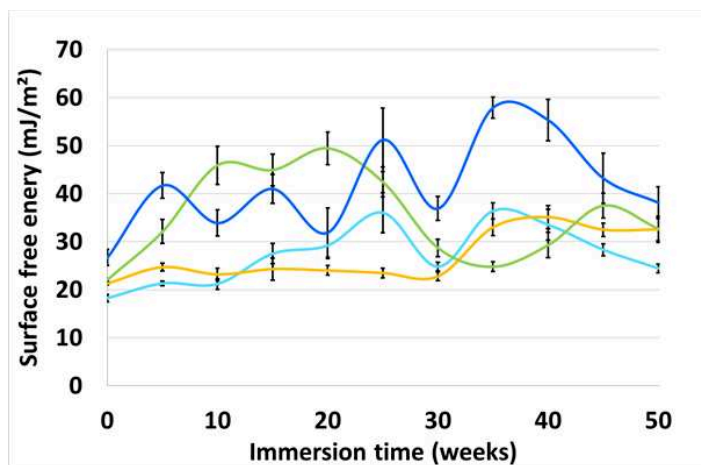


Figure IV-34. Surface free energies (γ_S) of PLGA-N88/12, PCL-N83/17, TGO-N73/27 and PDMS, during immersion in deionized water.

Chapter IV – Characterization of the PDMS/polyester hybrid networks

After 5 weeks of immersion in deionized water, PDMS and PLGA-N88/22 coatings showed SFE values lower or equal to 25 mJ/m² mainly due to dispersive interactions (Figure IV-35, A), whereas PCL- and TGO-based coatings exhibited higher values between 30 and 40 mJ/m². This SFE increase was due to the increase of its polar component only, as the dispersive component still remained the same as before immersion (Figure IV-35, B).

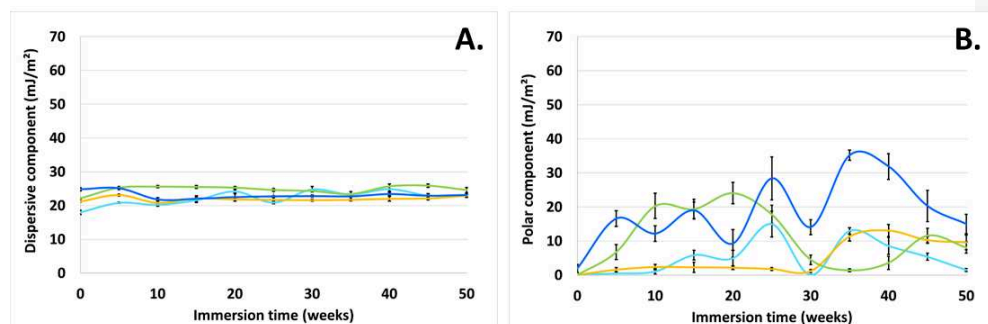


Figure IV-35. Dispersive component of surface free energy (γ_S^D , A) and polar component of surface free energy (γ_S^P , B) of PLGA-N88/12, PCL-N83/17, TGO-N73/27 and PDMS, during immersion in deionized water.

According to Figure IV-35, B, γ_S^P of TGO-N73/27 increased from 2 ± 1 to 17 ± 2 mJ/m² after only 5 weeks of immersion. This increase of the SFE polar component may not be due to the effect of polyester given that at 5 weeks, TGO-S65 exhibited a polar component below 2 mJ/m². The explanations to that were the non-negligible roughness and surface erosion of TGO-N73/27 which influenced the surface wetting properties according to the Wenzel theory (3-4 μm against *ca.* 0.1 μm , § IV.3.1.2.). Regarding PCL-N83/17, its SFE and its polar component were of *ca.* 32 mJ/m² and *ca.* 7 mJ/m² at 5 weeks of immersion respectively. Similarly, PCL-S86 presented at 5 weeks a SFE of *ca.* 35 mJ/m² and a polar component of *ca.* 10 mJ/m². This suggests PCL-N83/17 showed a higher SFE due to the presence of a more polar and/or partially hydrolyzed poly(ϵ -caprolactone) after exposition to water.

Between 5 and 20 weeks of immersion, the SFE dispersive components of all the coatings were constant ($\gamma_S^D \approx 25\text{-}28$ mJ/m²). The SFE variations were thus only attributed to the variations of the polar component (Figure IV-35, B). The SFE value of PLGA-N88/12 coating remained around 25

Chapter IV – Characterization of the PDMS/polyester hybrid networks

mJ/m² (against 30 mJ/m² for PLGA-S70) indicating that the surface was still mainly composed of PDMS segments (even if it was eroded by water). In the case of the PDMS elastomer reference, the SFE polar component increased due to the appearance of siliceous phases/salts on its surface as discussed in Chapter II (§ II.4.2.1.).

PCL-N83/17 and TGO-N73/27 exhibited SFE values around 35-50 mJ/m² with γ_S^P around 10-25 mJ/m² from 5 to 20 weeks of immersion. For PCL-N83/17, the increase of the SFE could be due to a surface enrichment in PCL segments and/or surface erosion and/or the effect of roughness ($R_a \approx 2 \mu\text{m}$), similar to the PCL-S86 coating during the same immersion period (with $\gamma_S = 35\text{-}40 \text{ mJ/m}^2$ and $R_a \approx 1.5 \mu\text{m}$).

The high roughness values of TGO-N73/27 around 7 μm obviously affected the liquid contact angles. Besides, TGO-S65 had a SFE value of 30 mJ/m² against 35-40 mJ/m² for TGO-N73/27. At this stage, it is thus difficult to differentiate the influence of the chemistry from the influence of the topography on the wetting properties of TGO-N73/27.

After 30 weeks of immersion, the surface energy of PLGA-N88/12 increased from *ca.* 25 to *ca.* 35 mJ/m² ($\gamma_S^P \approx 10 \text{ mJ/m}^2$) highlighting a surface enrichment in PLGA segments. The slow apparition of PLGA onto the surface may be explained by the low content of polyesters within the coating and as a result, a lower polyester concentration was available on the surface.

TGO-N73/27 coating showed strong fluctuations in its SFE (from 40 to 60 mJ/m²) mostly attributed to its heterogeneous topography and also to its mass loss which could renew the chemical composition of the surface.

The SFE polar component of PCL-N83/17 surprisingly decreased from *ca.* 20 to *ca.* 5-10 mJ/m² without changing the surface roughness. However, the mass loss is not negligible ($8.5 \pm 0.5 \%$ after 20 weeks) suggesting a complete modification of the surface chemistry in favor of PDMS-enriched phases. Further surface investigations such as SEM-EDX at this immersion time would be required.

- **LGO-N88/12**

Chapter IV – Characterization of the PDMS/polyester hybrid networks

LGO-N88/12 exhibited a SFE around 26 mJ/m² with $\gamma_S \approx \gamma_S^D \approx$ (Figure IV-36) indicating no significant polar contribution even after 30 weeks of immersion. This SFE profile is similar to PLGA-N88/12.

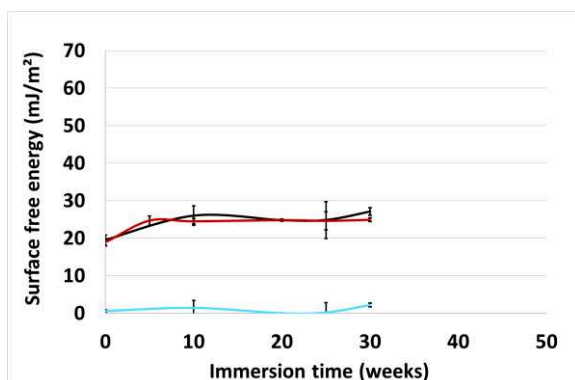


Figure IV-36. Surface free energy values of LGO-N88/12: γ_S (black line), γ_S^D (brown line) and γ_S^P (blue line), during immersion in water.

To conclude, this SFE study enabled to highlight some physico-chemical properties of the PDMS/polyester hybrid networks during immersion in deionized water. PLGA-N88/12 was globally the most hydrophobic PDMS/polyester hybrid network during immersion (even if it was eroded by water) due to the predominance of PDMS on its surface, which was however slightly altered after 30 weeks by the arrival of some hydrophilic PLGA. It was also the coating with the lowest roughness and the highest contact angle hysteresis upon immersion indicating PLGA could easily reorganize. PCL-N83/17 and TGO-N73/27 showed roughness values equal to or higher than 2 μm and chemical heterogeneities which may have affected a lot their wetting properties (but it is hard to know if it was a combination of both or just the effect of roughness). LGO-N88/12 was also very particular as it acted as a superhydrophobic coating at $t_i=0$, and became slowly similar to PLGA-N88/12 after immersion, except with higher roughness values.

Chapter IV – Characterization of the PDMS/polyester hybrid networks

IV.3.1.4. Mechanical properties

Additional experiments have started to study the effect of the water immersion on the elastic modulus of all networks but the results will not be presented in this manuscript.

IV.3.2. Dynamic immersion

A dynamic test was performed to accelerate the erosion of the PDMS/polyester hybrid networks. This erosion test was conducted in dynamic conditions using a Turbo eroder apparatus, at 650 rpm, in artificial sea water, at 40°C, for 1840 h. This accelerated erosion test enabled to evaluate the erosion rate of the coatings (when existing) by comparison with two commercial self-polishing coatings. The full protocol of the thickness loss test is described in the experimental section (§ VI.6.3.).

During the first 400 h, all the coatings showed no significant loss of thickness (Figure IV-37).

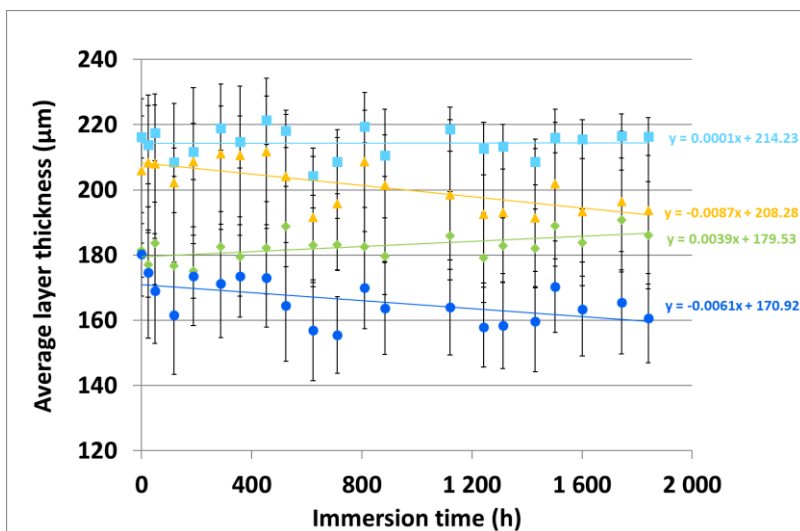


Figure IV-37. Evolution of the average layer thickness through immersion in dynamic conditions. PDMS, PLGA-N88/12, PCL-N83/17 and TGO-N73/27.

Chapter IV – Characterization of the PDMS/polyester hybrid networks

As expected, PDMS did not erode for the total duration test. PLGA-N88/12 and TGO-N73/27 displayed erosion rates of 0.21 $\mu\text{m}/\text{day}$ and 0.15 $\mu\text{m}/\text{day}$ respectively, indicating they both underwent erosion comparable to commercial self-polishing coatings such as Intersmooth 7460HS (0.14 $\mu\text{m}/\text{day}$) and Hempel Globic 9000 (0.15 $\mu\text{m}/\text{day}$) in the same conditions (600 h duration test). PCL-N83/17 showed no sign of erosion after 1840 h according to the slope of the regression line. As the slope of the regression line was positive, it could significate that the coating was slightly swollen by water.

After 1840 h, the coatings were definitely removed from the ASW, they were rinsed and dried for at least 1 week at ambient air, before the final measurement of the dry thickness (Table IV-11). PLGA-N88/12 and TGO-N73/27 lost at least 8 μm of coating thickness between the beginning and the end of the test (*ca.* 3 months). PCL-N83/17 lost a minimum of *ca.* 2 μm of coating thickness similar to the PDMS reference (minimum of *ca.* 1 μm). The absence of thickness loss during this test implies that the mass loss of PCL-N83/17 observed in static condition (chapter IV, Table IV-11) was rather due to a bulk erosion.

The linearity of the thickness loss PLGA-N88/12 and TGO-N73/27 revealed that these two coatings exhibited a surface erosion and could be classified as self-polishing coatings.

Table IV-11. Average dry layer thickness loss of the coatings before/after the 1840 hours of the erosion test.

	Average dry layer thickness loss (μm)
PDMS	2.8 ± 1.7
PLGA-N88/12	11.9 ± 4.2
PCL-N83/17	7.4 ± 5.8
TGO-N73/27	18.7 ± 10.1

In addition to the thickness measurements, the observation of the coatings brought information on the coatings aspect. All the hybrid PDMS/polyester hybrid networks displayed a decrease of brightness and an increase of roughness, less pronounced with the PDMS reference (Figure IV-38).

Chapter IV – Characterization of the PDMS/polyester hybrid networks

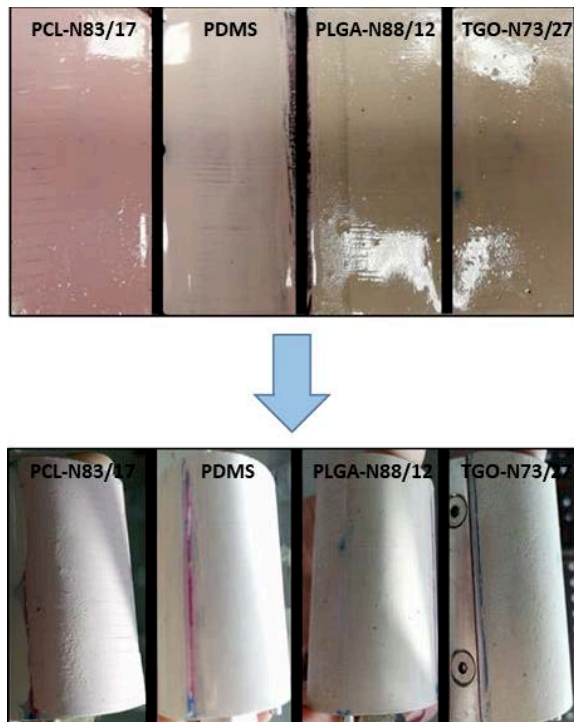


Figure IV-38. Coatings before/after the erosion test.

The matifying effect of the hybrid coatings could have several explanations:

- Roughness increase caused by erosion;
- Surface enrichment in polyester;
- Marine salts taking lodging inside the surface asperities.

According to Table IV-12, the most plausible explanation was the significant roughness increase (with $R_a \geq 6 \mu\text{m}$). The roughness values were higher than those observed in § IV.3.1.2. due to the more severe immersion conditions during the dynamic test. Table IV-12 also showed water contact angles higher than 130° for the hybrid coatings due to the roughness increase (Cassie-Baxter state). In this situation, the contact angles and surface energy values of the hybrid coatings were mainly governed by the surface topography. The PDMS reference displayed roughness and

Chapter IV – Characterization of the PDMS/polyester hybrid networks

contact angles values quite similar to what is usually described in literature, although slightly higher, indicating the PDMS coating did not undergo any major surface physico-chemical changes.

Table IV-12. Surface properties of the coatings after the erosion test.

	$R_a(\mu\text{m})$	$\theta_w(^{\circ})$	$\theta_{\text{hex}}(^{\circ})$	$\gamma_S(\text{mJ}/\text{m}^2)$	$\gamma_S^D(\text{mJ}/\text{m}^2)$	$\gamma_S^P(\text{mJ}/\text{m}^2)$
PDMS	1.1 ± 0.2	119.3 ± 1.9	17.0 ± 3.5	26.5 ± 0.7	25.9 ± 0.5	0.5 ± 0.2
PLGA-N88/12	6.3 ± 1.4	135.0 ± 1.4	10.4 ± 4.2	30.2 ± 0.7	26.7 ± 0.4	3.6 ± 0.4
PCL-N83/17	13.9 ± 1.4	137.5 ± 1.5	1.67 ± 2.0	31.3 ± 0.4	27.1 ± 0	4.3 ± 0.4
TGO-N73/27	16.0 ± 0.3	132.1 ± 2.5	10.1 ± 3.6	29.6 ± 0.9	29.6 ± 0.9	2.9 ± 0.6

However, an additional characterization of the coatings surface by SEM-EDX have invalidated previous interpretations. Indeed, all the surfaces exhibited numerous salt crystals coming from the artificial sea water (mainly CaCO_3), as shown in Figure IV-39, Figure IV-40, Figure IV-41 and Figure IV-42. The presence of salts suggests the measured values of thickness loss were inaccurate and underestimated values. The abundant rinsing of the coatings with deionized water was not sufficient to remove them. The salts may have also disturbed the erosion ability of the coatings acting as a physical barrier to water.

It was worth noticing that PCL-N83/17 and TGO-N73/27 displayed holes of $\approx 100\text{-}200\ \mu\text{m}$. The presence of these holes in addition to the presence of salts explained the higher values of roughness compared to PDMS and PLGA-N88/12. The generation of holes in the coatings indicated a heterogeneous surface erosion and thus invalidated the self-polishing ability of PCL-N83/17 and TGO-N73/27.

Chapter IV – Characterization of the PDMS/polyester hybrid networks

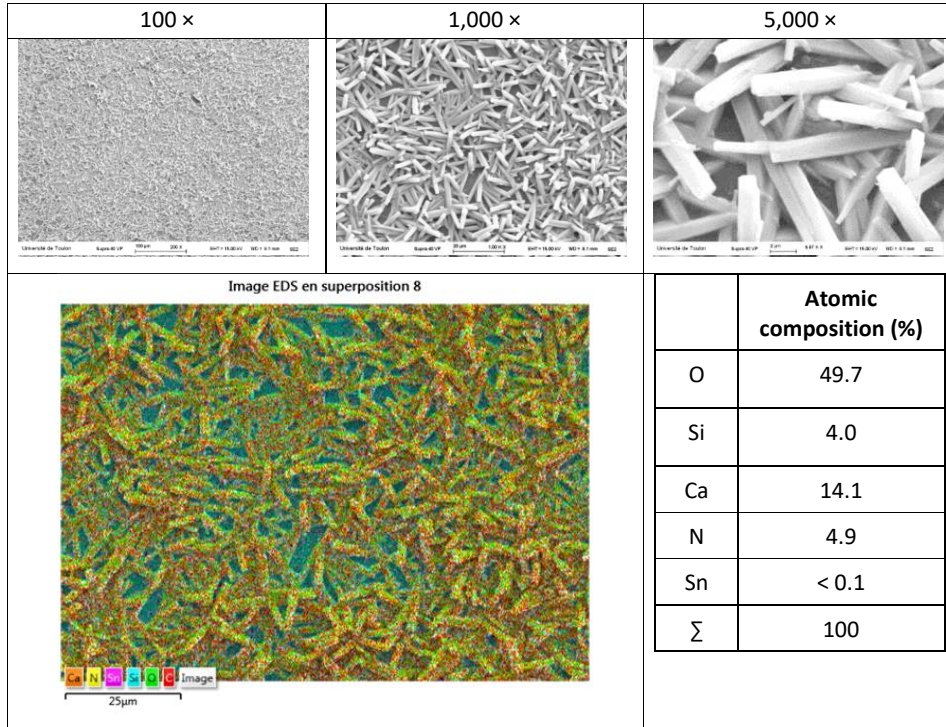


Figure IV-39. SEM-EDX images and surface atomic composition of PDMS coating after the erosion test in ASW.

Chapter IV – Characterization of the PDMS/polyester hybrid networks

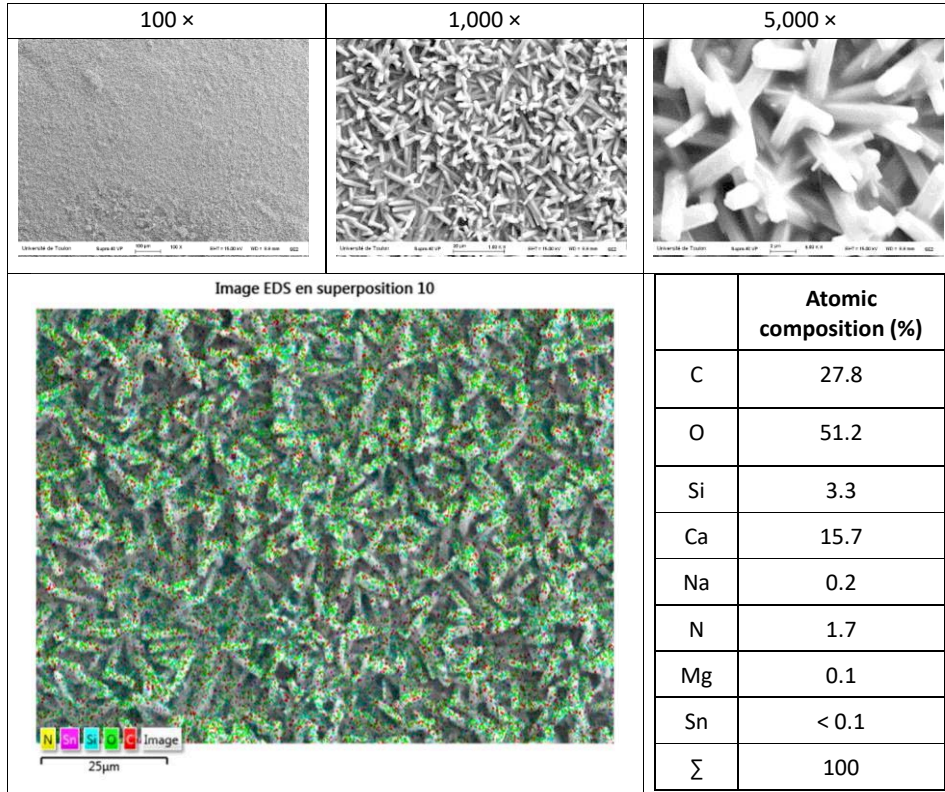


Figure IV-40. SEM-EDX images and surface atomic composition of PLGA-N88/12 coating after the erosion test in ASW.

Chapter IV – Characterization of the PDMS/polyester hybrid networks

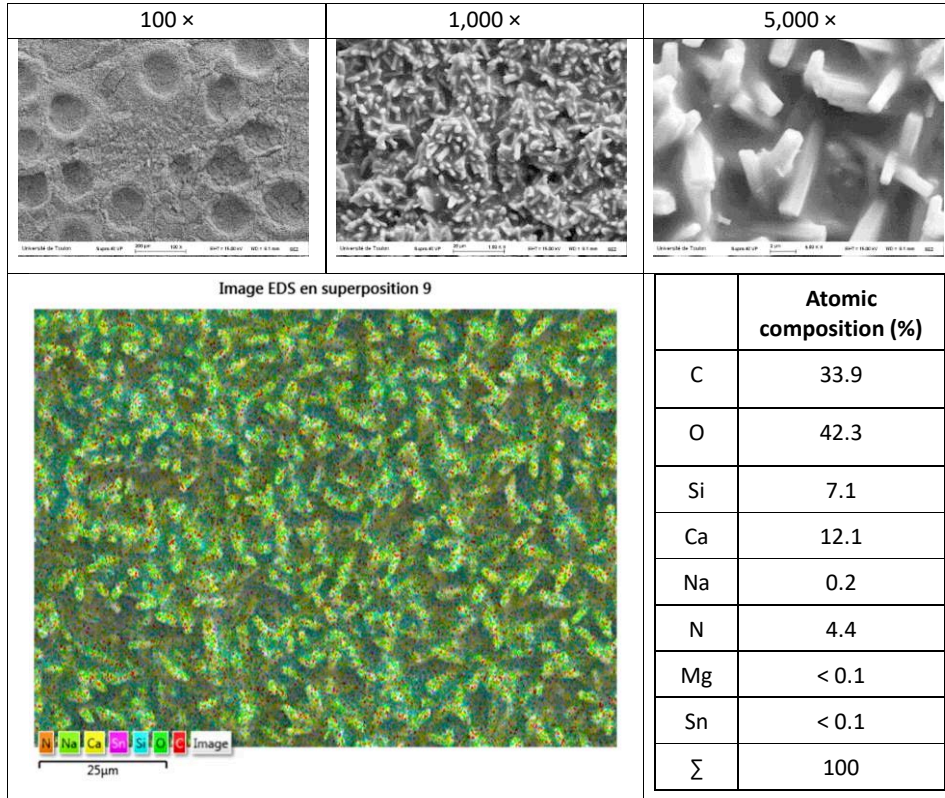


Figure IV-41. SEM-EDX images and surface atomic composition of PCL-N83/17 coating after the erosion test in ASW.

Chapter IV – Characterization of the PDMS/polyester hybrid networks

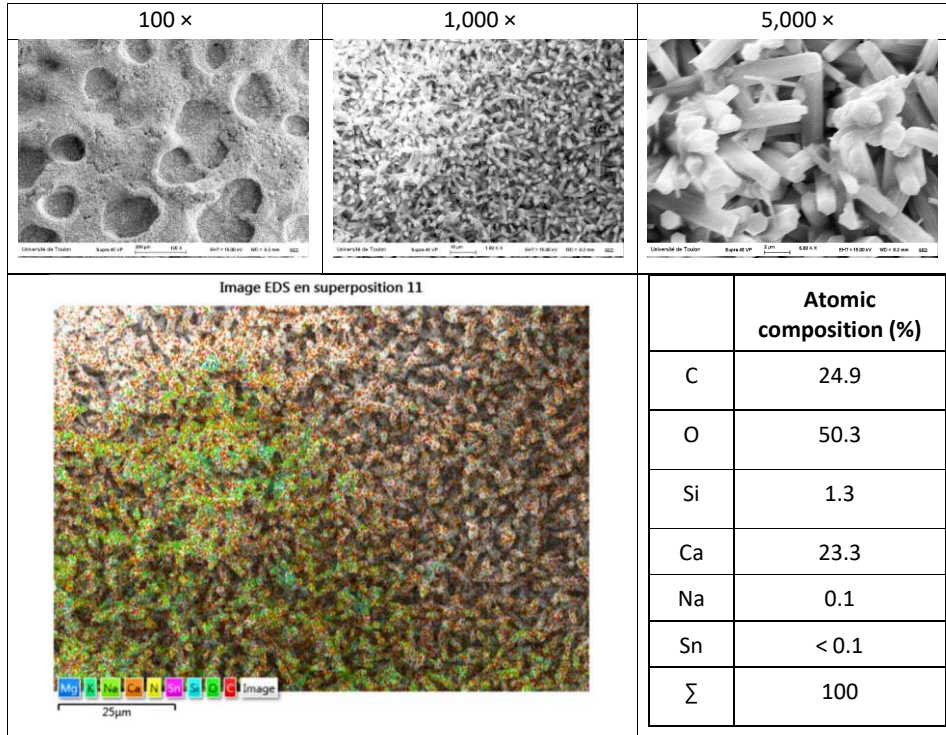


Figure IV-42. SEM-EDX images and surface atomic composition of TGO-N73/27 coating after the erosion test in ASW.

IV.4. Conclusion

In this chapter, the hybrid PDMS/polyester hybrid networks were characterized by various analytical techniques before or during immersion in aqueous media. The results highlighted the effects of the polymer network structure on its surface and bulk physico-chemical properties.

SEM-EDX and AFM results showed the presence of microphase separations of various sizes for all the PDMS/polyester hybrid networks (less pronounced in PLGA-N88/12). The presence of various shapes of polyester-rich domains suggested the local and random distribution of the polyester segments but also their inability to organize in a regular way due to the major presence of PDMS. The self-crosslinked PCL-*b*-PDMS-*b*-PCL-based network TGO-S65 was the only coating showing organized spherulitic phases, induced by the triblock copolymer architecture. Overall, the crosslinking of polyester with PDMS chains ended mostly in a microphase separated state without regular or specific morphologies. The crosslinks within the hybrid coatings also certainly led to distorted morphologies due to spatial and physical stress.

PLGA-N88/12 surface was mainly made of PDMS as revealed by SEM-EDX, AFM (only small PLGA clusters) and FTIR-ATR contrary to PCL-N83/17 and TGO-N73/27 which presented the dual hybrid chemistry (before immersion).

Polyesters incorporated within the PDMS networks had no significant effect on the elastic modulus at ambient air, suggesting the PDMS/polyester hybrid networks still displayed elastic behavior favorable to fouling release applications. The self-crosslinked polyester-based networks exhibited elastic modulus equal or higher than 6 MPa. The gain in rigidity for TGO-N73/27 (5.8 MPa) and TGO-S65 (48 MPa) was attributed to the PCL crystallinity (found by DSC analysis).

By combining SEM-EDX, AFM, ATR-FTIR, DSC and DMA results, it was possible to schematically represent the microstructure of the polyester-based networks in 3D. Such coatings microstructure could be beneficial for antifouling application as their chemical heterogeneity could prevent the marine species from settling.

The mass loss test presented similar linear profiles for the PDMS/polyester hybrid networks in favor of a progressive erosion. It has been demonstrated that the crosslinking promoted the

Chapter IV – Characterization of the PDMS/polyester hybrid networks

erosion process of the PDMS/PCL hybrid networks (PCL-N83/17 and TGO-N73/27). The hydrolysis of PLGA was markedly reduced in PLGA-N88/12 compared to PLGA-S70 which favored a more durable erosion.

The surface analyses during immersion revealed the impact of the polyester chemistry and/or topography on the wetting properties of the coatings. The wettability of PCL-N83/17 upon static immersion in deionized water showed various fluctuations of the water contact angles, attributed to the surface enrichment in polyester and/or erosion and/or effect of roughness. The decrease of water contact angles and the increase of the surface energy for TGO-N73/27 was rather due to its important surface roughness which generated a Wenzel wetting state. PLGA-N88/12 became hydrophilic later (after 30 weeks), mostly due to a less availability of PLGA within the coating. All hybrid coatings exhibited a surface reorganization either due to chemical and/or topographical changes, ensuring an interesting surface renewal upon immersion.

The thickness loss of the three targeted PDMS/polyester hybrid networks immersed in dynamic conditions showed promising results given that two coatings (PLGA-N88/12 and TGO-N73/27) displayed similar erosion rates to the ones of commercial SPC (0.15-0.20 $\mu\text{m}/\text{day}$). PLGA-N88/12 seemed to undergo a surface erosion or self-polishing whereas the presence of holes for PCL-N83/17 and TGO-N73/27 suggested they underwent heterogeneous bulk erosions. These holes certainly came from the hydrolytic degradation of the segregated PCL-rich domains (seen in the SEM images). The presence of salts observed at the end of the dynamic test suggested the thickness loss measurements were probably underestimated during the whole test duration. The erosion properties of the coatings were crucial to study as their antifouling performances could be strongly influenced by the surface renewal.

LGO-N88/12 using PLGA-*b*-PDMS-*b*-PLGA macrocrosslinker was studied separately to the others due to its particular tackiness issue. This coating appeared to be very hydrophobic at the beginning of the immersion test, but progressively showed similar trends to PLGA-N88/12 through dynamic contact angles and surface energy. The stickiness slowly disappeared after 20 weeks of water immersion suggesting the release of oils. The very linear mass loss profile of LGO-N88/12 in deionized water could be beneficial for a gradual surface renewal.

Chapter IV – Characterization of the PDMS/polyester hybrid networks

All these tests were essential to discuss the relationship between the microstructure and the antifouling property of the coatings which will be discussed in the following chapter.

IV.5. Bibliographical references

1. Brady, R.F.; Singer, I.L. Mechanical factors favoring release from fouling release coatings. *Biofouling* **2000**, *15*, 73–81.
2. Schmidt, D.L.; Brady, Robert F.; Lam, K.; Schmidt, D.C.; Chaudhury, M.K. Contact angle hysteresis, adhesion, and marine biofouling. *Langmuir* **2004**, *20*, 2830–2836.
3. Finlay, J.A.; Bennett, S.M.; Brewer, L.H.; Sokolova, A.; Clay, G.; Gunari, N.; Meyer, A.E.; Walker, G.C.; Wendt, D.E.; Callow, M.E.; et al. Barnacle settlement and the adhesion of protein and diatom microfouling to xerogel films with varying surface energy and water wettability. *Biofouling* **2010**, *26*, 657–666.
4. Faÿ, F.; Linossier, I.; Peron, J.J.; Langlois, V.; Vallée-Rehel, K. Antifouling activity of marine paints: Study of erosion. *Progress in Organic Coatings* **2007**, *60*, 194–206.
5. Lovinger, A.J.; Han, B.J.; Padden, F.J.; Mirau, P.A. Morphology and properties of polycaprolactone-poly(dimethyl siloxane)-polycaprolactone triblock copolymers. *Journal of Polymer Science Part B: Polymer Physics* **1993**, *31*, 115–123.
6. Lejars, M.; Margailan, A.; Bressy, C. Fouling release coatings: a nontoxic alternative to biocidal antifouling coatings. *Chemical Review* **2012**, *112*, 4347–4390.
7. Aranguren, M.I. Crystallization of polydimethylsiloxane: effect of silica filler and curing. *Polymer* **1997**, *39*, 4897–4903.
8. Azemar, F.; Faÿ, F.; Réhel, K.; Linossier, I. Control of hydration and degradation properties of triblock copolymers polycaprolactone- *b* -polydimethylsiloxane- *b* -polycaprolactone. *Journal of Applied Polymer Science* **2014**, *131*, 1–8.
9. Bosq, N.; Guigo, N.; Persello, J.; Sbirrazzuoli, N. Melt and glass crystallization of PDMS and PDMS silica nanocomposites. *Physical Chemistry Chemical Physics* **2014**, *16*, 7830–7840.
10. Goudie, J.L.; Owen, M.J.; Orbeck, T. A review of possible degradation mechanisms of silicone elastomers in high voltage insulation applications. In Proceedings of the 1998 Annual Report Conference on Electrical Insulation and Dielectric Phenomena (Cat. No.98CH36257); IEEE: Atlanta, GA, USA, **1998**; Vol. 1, pp. 120–127.

Chapter V	Antifouling and fouling release properties of the coatings	271
V.1.	Introduction	271
V.2.	Static field test	271
V.2.1.1.	<i>Antifouling efficacy duration.....</i>	273
V.2.1.2.	<i>Identification of the type of fouling organisms.....</i>	281
V.2.1.3.	<i>Fouling release properties.....</i>	287
V.3.	Biological assays.....	292
V.3.1.	Biological assay on <i>A. amphitrite</i> cypris larvae	292
V.3.1.1.	<i>Settlement of A. amphitrite on the hydrolyzable additive-based PDMS coatings</i>	292
V.3.2.	Bioassays on diatoms and algal spores	293
V.3.2.1.	<i>Diatoms Navicula incerta.....</i>	294
V.3.2.1.1.	<i>Initial attachment of diatoms on the PDMS/polyester hybrid networks</i>	294
V.3.2.1.2.	<i>Removal of diatoms on the PDMS/polyester hybrid networks</i>	295
V.3.2.2.	<i>Ulva spores.....</i>	296
V.3.2.2.1.	<i>Green alga Ulva rigida</i>	296
V.3.2.2.2.	<i>Green alga Ulva linza.....</i>	297
V.4.	Conclusion	301
V.5.	Bibliographical references.....	303

Chapter V Antifouling and fouling release properties of the coatings

V.1. Introduction

This chapter deals with the antifouling (AF) and fouling release (FR) properties of the coatings prepared in Chapter II and III. The hydrolyzable additive-based coatings and the PDMS/polyester hybrid networks were compared to determine the most promising strategy to combat biofouling.

To evaluate the AF and FR efficacy of the experimental coatings, coated PVC panels were immersed in the Toulon bay for 8 and 24 months. The macrofouling was observed and rated each month to finally indicate the service life of these coatings. The variations of the AF and FR properties during field immersions were correlated to the surface and bulk properties already covered by Chapter II and IV. The AF properties were further studied through biological assays to target the AF action against singular marine species such as diatoms, sporelings and barnacle larvae. Correlations of AF/FR performances with surface and bulk characteristics such as wettability, surface energy, elastic modulus, and surface roughness were investigated. The understanding of their mechanism of action enabled to give us a clear outlook on the development of future antifouling coatings.

V.2. Static field test

The coatings were immersed in static conditions in the Toulon bay (43° 06' 25" N; 5°55' 41" E) to evaluate their AF properties. The physico-chemical properties of the seawater in which the coatings were immersed between 2017 and 2019 showed pH variations from 7.48 to 8.64, temperature variations from 6 to 27°C and salinity variations from 26.8 to 38.4.

The evaluation of the macrofouling was performed by a monthly inspection of the percentage of surface coverage and the nature of the fouling species on the panels. Mechanical defects of the coatings were recorded. Panels were prepared in duplicates: one panel was never cleaned so that it indicated the antifouling efficacy, the other one was cleaned every three

Chapter V – Antifouling and fouling release properties of coatings

months with a wet sponge to assess the FR ability. The panels were photographed before and after cleaning to show the difference.

The experimental coatings were compared to a PDMS reference, a non-coated sandblasted PVC panel, and a commercial FRC (Hempasil X3, Hempel). The hydrolyzable additive-based PDMS coatings were immersed on July 2017 and the PDMS/polyester hybrid networks were immersed on October 2018. The AF activity was assessed by an efficacy factor (N), which takes into account the factors of intensity (IF) and severity (SF) of the foulant, based on the NF T 34-552 French standard (sept. 1996). The efficacy factor N was obtained as follows in Eq. 1:

$$N = \sum(IF \times SF) \quad \text{Eq. 1}$$

Further information is available in the experimental section (§ VI.7.1.).

Marine macroorganisms can be differentiated by their biological characteristics including:

- type (animal or plant),
- growth form (solitary or colonial),
- profile (erect or encrusting),
- structure (soft, hard or flexible)

These characteristics will determine the severity level of the fouling (SF). The marine fouling organisms known to easily colonize surfaces are organisms with colonial, encrusting, hard and/or flexible morphological characteristics [1].

Soft fouling can be easily removed with hydrodynamic forces. On the contrary, hard fouling like barnacles are difficult to remove due to their strong interaction with the underlying substrate [2]. Table V-1 summarizes the main organisms into these two categories.

Table V-1. Main hard and soft marine growths [3].

Hard fouling	Soft fouling
Mussel	Algae
Barnacle	Hydroid
Oyster	Soft coral
Tubeworm	Sponge
Encrusting sponge	Anemone

Chapter V – Antifouling and fouling release properties of coatings

The best AF efficacy is assigned to coatings with a N value of 5, which corresponds to a surface only covered by biofilm. The worse AF efficacy is attributed to the negative non-coated PVC control with a N value which tends to *ca.* 40. According to the laboratory expertise, an AF coating is considered efficient with the following condition: $N \leq N_{PVC}^{max} / 3 \cong 13$ where N_{PVC}^{max} is the maximal value for the non-coated PVC panel immersed in the same conditions. This non-coated PVC panel was used to highlight the biodiversity of marine macroorganisms able to colonize neutral surfaces in this coastal area. The photographs of coatings obtained from the two approaches at 0, 2, 4, 6 and 8 months (and 20 months for the hydrolyzable additive-based coatings) are presented in Table V-2 and Table V-3.

The physico-chemical studies performed in deionized water in Chapter II and IV gave information about the behavior of the coatings in aqueous media (wettability, chemistry, roughness, water uptake, mass loss, erosion rate, etc.). In the following sections, we tried to correlate these characteristics to the AF properties of the coatings immersed in seawater. However, it should be reminded that the natural marine environment is much more complex than the distilled water used in the laboratory. The temperature, the pH, the salinity, the dissolved oxygen, the water dynamics and the presence of microorganisms, all play a role on the coating surface properties, and thus on the coating AF efficacy.

V.2.1.1. Antifouling efficacy duration

▪ **Hydrolyzable additive-based PDMS coatings**

The AF properties of the hydrolyzable additive-based coatings are shown from Figure V-1 to Figure V-3. For easy viewing, each graph corresponds to the curves of one type of additive, at different content relative to the dry PDMS coating (5, 10, 15 wt.% and more for M3T-BX).

PVC panel (control) was rapidly fouled. At $t_i=2$ months, the PVC was already fouled on all its surface area. The commercial FRC (X3) showed good AF properties for the first 18 weeks of immersion then the AF properties decreased a little beyond 18 weeks (with $N \approx 25$). PDMS reference went from $N=20$ at $t_i=6$ months to $N=35-40$ at $t_i=24$ months, indicating limited AF properties upon immersion.

Chapter V – Antifouling and fouling release properties of coatings

The evolution of the N factor for M3T-BX coatings showed promising results for the first 3 months with enhanced AF properties compared to the PDMS reference and PVC (Figure V-1). The lower adhesion of marine species during these 3 first months could be directly correlated to the hydrolysis on the surface of the additive poly(bis(trimethylsilyloxy)methylsilyl methacrylate) (PMATM2). In Chapter II, it was observed a maximum mass loss during the first 12 weeks of immersion (3 months) followed by a plateau. The loss of AF properties for M3T-BX after 3 months of immersion can thus be explained by the shortage of PMATM2 within the bulk of the coating. It should be noted that the M3T-BX coatings with different loadings of PMATM2 did not exhibit differences in AF properties. This means that 5 wt.% of PMATM2 were sufficient to provide the expected surface chemistry renewal, at least for the first 3 months.

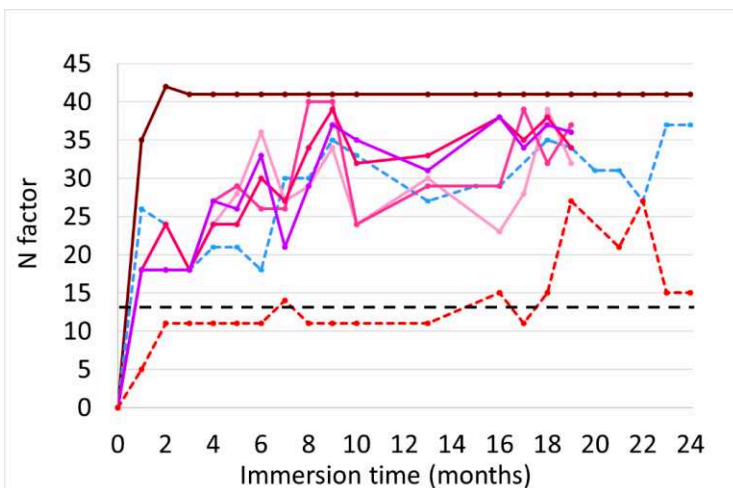


Figure V-1. Evolution of the N factor of M3T-BX coated panels immersed for 24 months in Toulon bay with PVC panel and PDMS reference. M3T-B5, M3T-B10, M3T-B15, M3T-B20 and commercial hydrogel-based FRC (dotted red line). The border line below which the AF efficacy is ideal (dotted black line).

Chapter V – Antifouling and fouling release properties of coatings

The PCL-BX coatings showed similarities with the PDMS reference in terms of AF properties for the first 6 months of immersion (Figure V-2). This observation is in accordance with the surface physico-chemical properties studied in Chapter II. The absence of mass loss for 8 months as well as a strong similarity of hydrophobicity and roughness compared to PDMS suggest there was no benefit of adding PCL additives for 8 months of immersions.

With longer immersion times (from 8 to 24 months), all the PCL-BX coatings exhibited a slightly better AF efficacy than the PDMS reference with an N factor stabilized at around 25 or below. This slight improvement could be attributed to the PCL additives that finally appeared on the surface and hydrolyzed. This assumption could not be verified by the mass loss test as it was stopped after 8 months of immersion. It should be kept in mind that the difference of AF efficacy between PDMS and PCL-BX remained low and thus not much conclusions can be inferred from these results. The difference of N factors between the different PCL-BX coatings was also not significant enough to draw a conclusion on the influence of the PCL additive content on the AF properties.

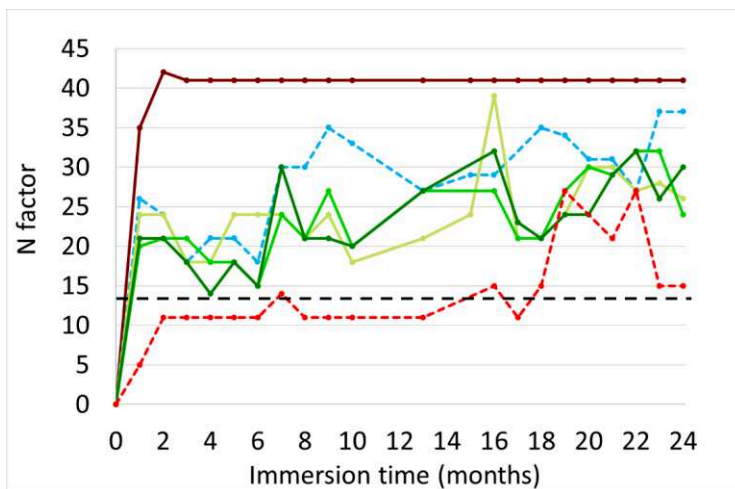


Figure V-2. Evolution of the N factor of PCL-BX coated panels immersed for 24 months in Toulon bay with PVC panel and PDMS reference. PCL-B5, PCL-B10, PCL-B15 and commercial hydrogel-based FRC (dotted red line). The border line below which the AF efficacy is ideal (dotted black line).

Chapter V – Antifouling and fouling release properties of coatings

TGO-BX coatings showed similar AF efficacy profiles to the PDMS reference during the 24 weeks of immersion (Figure V-3). Again, this observation is in accordance with the surface physico-chemical properties obtained in Chapter II. The absence of mass loss for 8 months as well as the strong similarity of hydrophobicity and roughness compared to PDMS suggest there was no real benefit of adding PCL-*b*-PDMS-*b*-PCL additives for 8 months of immersions. With longer immersion times (from 8 to 24 months), only TGO-B5 gave better AF properties than the PDMS reference with an N factor close to 20 or below. We are not able to explain why TGO-B10 and TGO-B15 showed a lower AF efficacy than TGO-B5, but the fact that TGO-B5 exhibited less phase segregations than the two other coatings could be one reason.

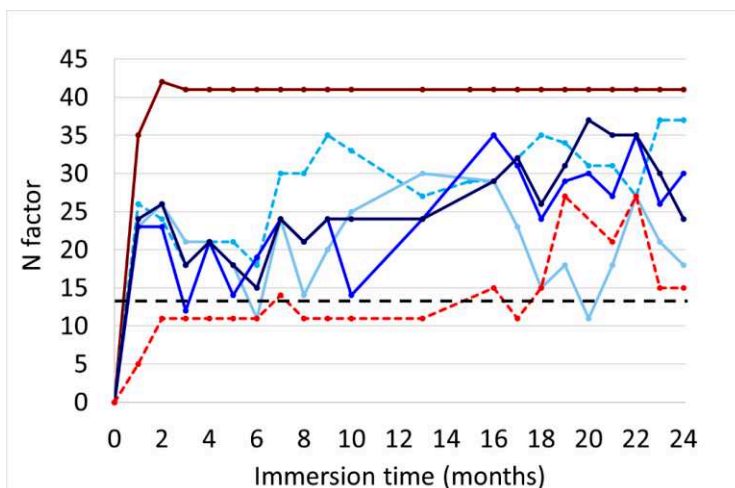
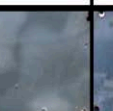
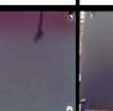
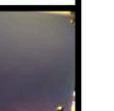
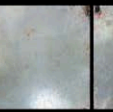
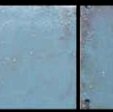
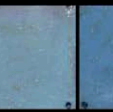
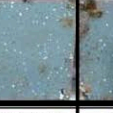
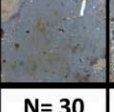
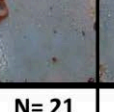
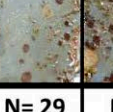
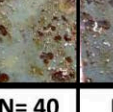
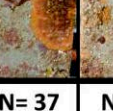


Figure V-3. Evolution of the N factor of TGO-BX coated panels immersed for 24 months in Toulon bay with PVC panel and PDMS reference (dotted light blue line). TGO-B5, TGO-B10, TGO-B15 and commercial hydrogel-based FRC (dotted red line). The border line below which the AF efficacy is ideal (dotted black line).

Chapter V – Antifouling and fouling release properties of coatings

Table V-2. Photographs of the coated and non-coated panels with the respective N efficacy factor.

t_i	PVC	PDMS	TGO-B5	TGO-B10	TGO-B15	PCL-B5	PCL-B10	PCL-B15	M3T-B5	M3T-B10	M3T-B15	M3T-B20
0												
	N= 0	N= 0	N= 0	N= 0	N= 0	N= 0						
2 months												
	N= 42	N= 24	N= 26	N= 23	N= 26	N= 24	N= 21	N= 21	N= 18	N= 18	N= 24	N= 18
4 months												
	N= 41	N= 21	N= 21	N= 21	N= 21	N= 18	N= 18	N= 14	N= 24	N= 27	N= 24	N= 27
6 months												
	N= 41	N= 18	N= 11	N= 19	N= 15	N= 24	N= 15	N= 15	N= 36	N= 26	N= 30	N= 33
8 months												
	N= 41	N= 30	N= 14	N= 21	N= 21	N= 21	N= 21	N= 21	N= 29	N= 40	N= 34	N= 29
20 months												
	N= 41	N= 34	N= 18	N= 29	N= 29	N= 24	N= 27	N= 24	N= 32	N= 37	N= 34	N= 36

▪ PDMS/polyester hybrid networks

Figure V-4 shows the evolution of the efficacy factor (N) upon immersion for the hydrolyzable network coatings. The N values were mean values of duplicates.

A new coating, which was not mentioned in Chapter III, was tested through the marine field test as a first trial. This coating was a combination of both strategies: a PDMS/PLGA hybrid network with the same content of PLGA than in PLGA-N88/12 but also containing 5 wt.% of PMATM2 additive relative to the dry coating. To simplify the nomenclature, this coating was named “PLGA+M3T”, its full description is found in the experimental section (§ VI.4.2.). This coating exhibited a very soft layer (almost gelatinous) certainly due to the PMATM2 additive which disrupted the crosslinking reaction.

The hybrid network coatings showed good AF properties for the 2 first months of immersion. During that immersion time, there was no significant difference of AF property between the hybrid network coatings and the PDMS reference except for LGO-N88/12 and PLGA+M3T coatings.

After 2 months, the N factor gradually increased from 15 to 30 at $t=4$ months, and up to 40 at $t=8$ months. According to the slope of the mass loss curves obtained in Chapter IV, the mass loss rate was at its maximum within the first 10 weeks (2 months $\frac{1}{2}$). By neglecting the difference of immersion conditions between the marine field test and the mass loss test, we could conclude that the decrease in erosion rate after 2 months $\frac{1}{2}$ was responsible for the gradual loss of AF properties.

The loss of AF property of TGO-N73/27 and PCL-N83/17 after 2 months could also be attributed to the increase of the roughness (mainly for TGO-N73/27 with $R_a \geq 6 \mu\text{m}$), an increase of surface free energy and a gain in hydrophilicity (at 2 months $\frac{1}{2}$, $\gamma_S \approx 40 \text{ mJ/m}^2$, $\theta_{w,adv} \approx 60^\circ$). The evolution of the N factor for PLGA-N88/12 displayed the same tendency as the PCL-based network coatings. This observation is difficult to understand given that PLGA-N88/12 showed promising physico-chemical properties at least until 30 weeks of immersion (8 months) with a smooth surface ($R_a \leq 0.5 \mu\text{m}$), a water contact angle higher than 90° , a low surface free energy ($\gamma_S \approx 23\text{-}24 \text{ mJ/m}^2$) as well as the highest erosion rate (self-polishing ability). The only conclusion that can be drawn from these results is that the surface erosion

Chapter V – Antifouling and fouling release properties of coatings

was not sufficient to refresh the upper layer of PLGA-N88/12, thus making it difficult to prevent the settlement of macroorganisms.

PLGA+M3T showed an AF efficacy similar to the PDMS reference. This coating showed a N value of 20 at 8 months against 40 for most of the PDMS/polyester hybrid networks.

LGO-N88/12 showed better AF properties than PDMS for the first 4 months of immersion. This could be attributed to the more hydrophobic nature of LGO-N88/12 (§ IV.2.5.1.) or its more linear mass loss profile (§ IV.4.1.) compared to the other PDMS/polyester hybrid networks (thus maintaining a minimum of surface replenishment). Another plausible reason could be that during the first 4 months, the leaching of some unboned oils from LGO-N88/12 deterred the adhesion between the macrofouling and the surface of the coating.

Due to the decrease of the AF properties of the hybrid network coatings (with N values comparable to the PVC panel), their inspections were suspended at 7 or 8 months.

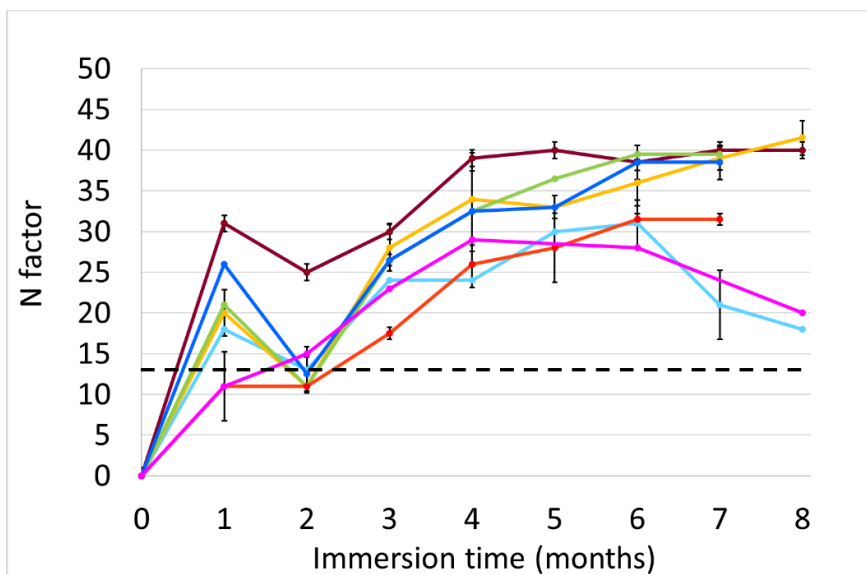
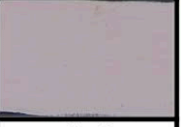
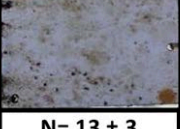
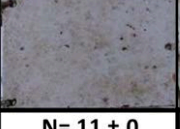
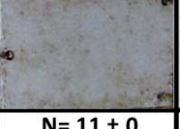
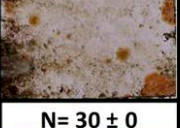
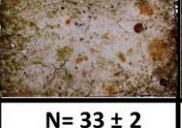
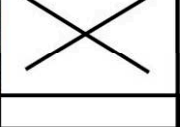
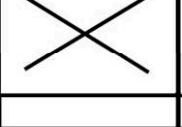
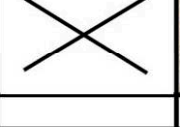


Figure V-4 Evolution of the N factor of the PDMS/polyester hybrid networks immersed for 8 months in Toulon bay with PVC panel, PDMS reference, PLGA-N88/12, PCL-N83/17, TGO-N73/27, LGO-N88/12 and PLGA+M3T. The border line below which the antifouling ability is ideal (dotted black line).

Chapter V – Antifouling and fouling release properties of coatings

Table V-3. Photographs of the coated and non-coated panels with the respective N efficacy factor.

t_i	PVC	PDMS	PLGA-N88/12	PCL-N83/17	TGO-N73/27	LGO-N88/12	PLGA/M3T
0							
	N= 0	N= 0	N= 0				
1 month							
	N= 31 ± 2	N= 18 ± 0	N= 20 ± 3	N= 21 ± 0	N= 26 ± 0	N= 11 ± 4	N= 11
2 months							
	N= 25 ± 3	N= 13 ± 3	N= 11 ± 0	N= 11 ± 0	N= 13 ± 2	N= 11 ± 0	N= 15
3 months							
	N= 30 ± 7	N= 24 ± 0	N= 28 ± 3	N= 27 ± 1	N= 27 ± 1	N= 18 ± 1	N= 23
5 months							
	N= 40 ± 0	N= 30 ± 0	N= 33 ± 2	N= 37 ± 4	N= 33 ± 2	N= 28 ± 4	N= 28
8 months							
	N= 40 ± 0	N= 18 ± 0	N= 42 ± 2				N= 20

V.2.1.2. Identification of the type of fouling organisms

The evolution of the type of marine fouling organisms settled on the coatings was assessed at 2 and 6 months of immersion (20 months as well for the hydrolyzable additives-based coatings). These immersion times were selected as they revealed significant variations of the biodiversity on the immersed panels. These changes in fouling species could indicate preferential AF trends towards certain species depending on the nature of the coating. The presence of different marine communities on two different substrates localized in the same immersion site can reveal the importance of the surface chemistry on the fouling process. In this way, we can find the most discouraging surfaces for macroorganisms.

Other information can be obtained from the relative abundance of marine species. Indeed, the accumulation of a wide range of marine species on the tested panel could predict a fast decrease of the AF efficacy through a cascading effect [4]. This cascading effect results from the settlement of species on top of other species giving a more secure anchorage for the newcomers to grow and colonize the remaining substrate.

▪ **Hydrolyzable additive-based PDMS coatings**

Figure V-5 shows the percentage of marine organisms on the hydrolyzable additive-based coatings after 2 months of immersion. Among all the tested panels, there was a clear difference of biodiversity depending on the nature of the additive: there were mainly brown algae (10-40 %) on the PCL-based coatings while there were mainly spirorbis (5-10 %) and red algae (≤ 5 %) on the PMATM2-based coatings. The fouling species of PCL-based coatings resembled to those of the PDMS reference (with 50 % of brown algae).

The influence of the PLGA chemistry on the AF properties was thus clearly highlighted in this figure.

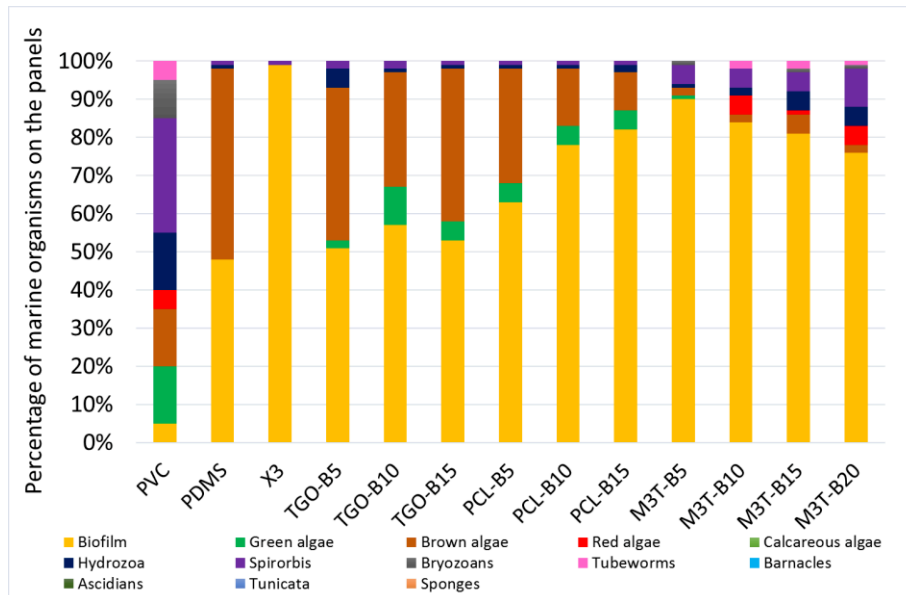


Figure V-5. Determination of the percentage of the additive-based PDMS coated surface covered by several type of marine organisms after 2 months of immersion.

After 6 months of immersion, the biofouling seemed to homogenize on the different coatings with mainly brown algae (ca. 5-10 %) and spirorbis (ca. 5-10 %) (Figure V-6). These results revealed that M3T-BX started to behave like the PDMS surface after the release of PMATM2. The higher amount of macrofoulers for M3T-BX could suggest some remaining hydrophilic PMAA that attracted more organisms. The amount of algae (green and brown) was strongly reduced between 2 and 6 months due to the effect of seasonality (most of the algae died during winter time).

The communities of marine species were relatively the same for PDMS, PCL-BX and TGO-BX traducing the PDMS influence on the marine species which colonize the surfaces.

After 6 months of immersion, the additive-based coatings were covered by less than 40 % of macrofouling. But PDMS showed less settled organisms (10 %) as well as the commercial FRC (< 5 %) indicating the developed coatings exhibited limited AF efficacy, especially compared to the commercially available hydrogel-based FRC.

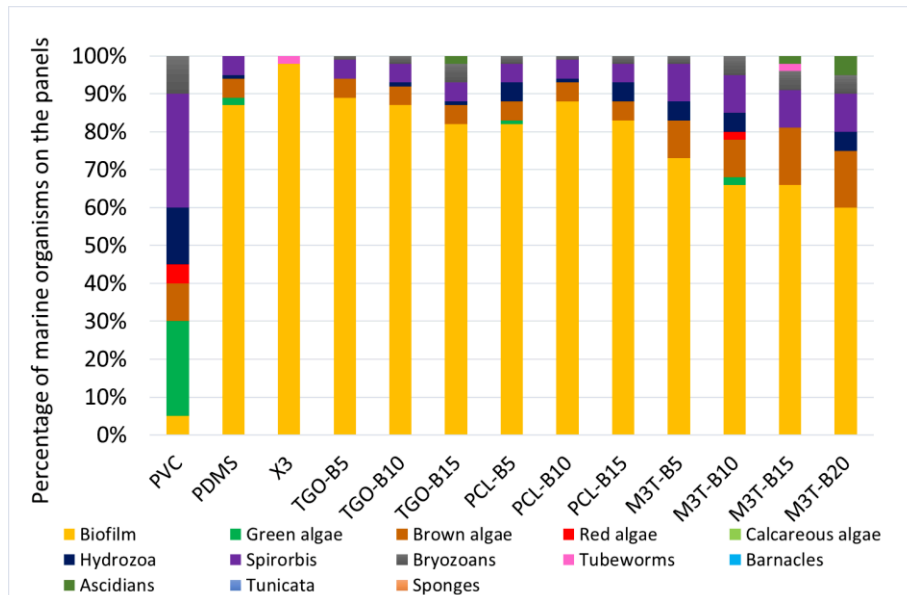


Figure V-6. Determination of the percentage of the additive-based PDMS coated surface covered by several type of marine organisms after 6 months of immersion.

Figure V-7 shows that the fouling was again quite similar for all the PDMS-based coatings after 20 months of immersion. They were all covered with macrofouling for over 40 to 80 % of the panel surface. One coating was however very different from the others, TGO-B5, with only few tubeworms and bryozoans settled. Between 6 and 20 months, the amount of bryozoans, red and green algae increased significantly on all the coatings excepting on TGO-B5.

The commercial FRC which displayed the best AF properties until 18 months of immersion (seen in Figure V-3) showed a decrease of antifouling efficacy with the arrival of 30 % of macrofouling.

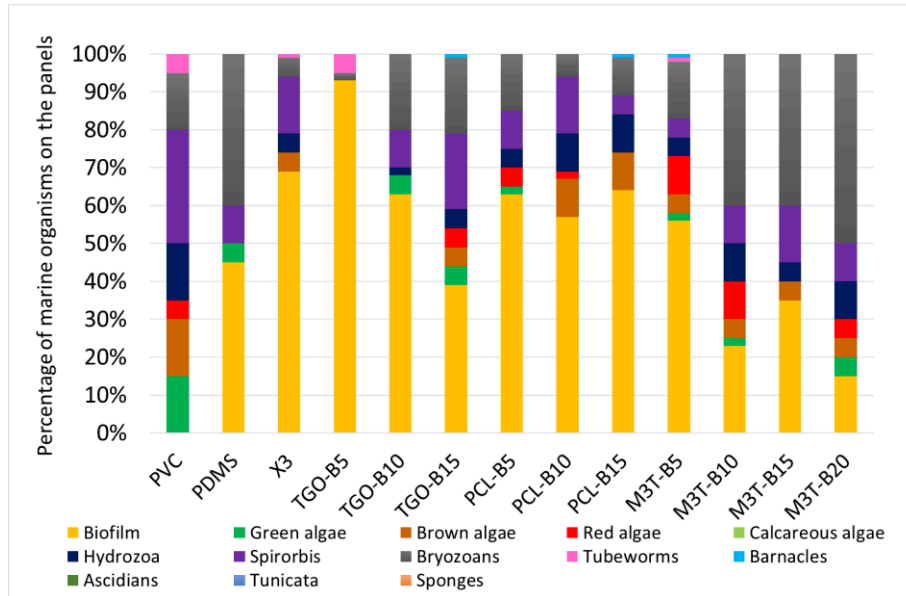


Figure V-7. Determination of the percentage of the additive-based PDMS coated surface covered by several type of marine organisms after 20 months of immersion.

▪ PDMS/polyester hybrid networks

Figure V-8 shows the percentage of marine organisms on the PDMS/polyester hybrid networks after 2 months of immersion. The predominant macroorganism was spirorbis ($\leq 10\%$ for the experimental coatings and 25 % for PVC panel) during this short-term immersion period.

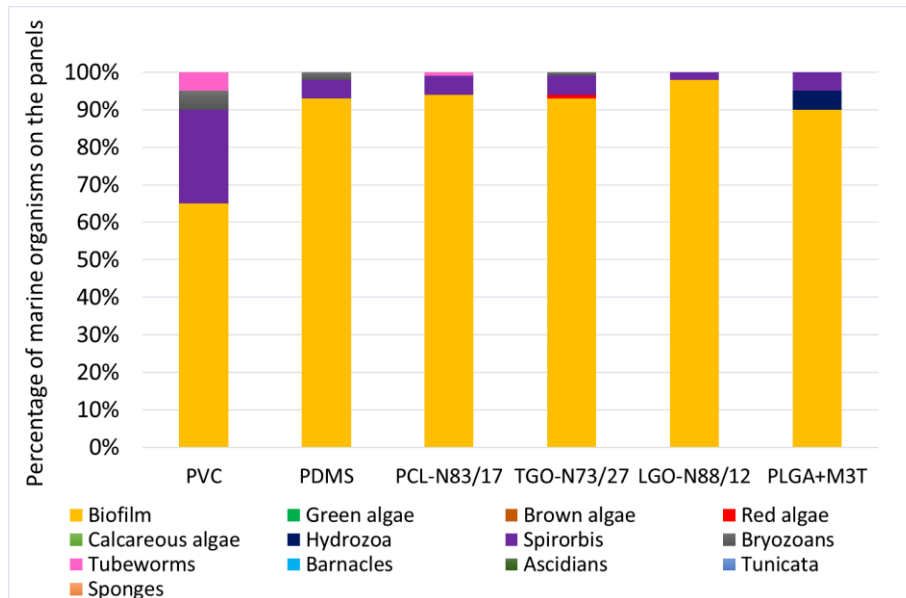


Figure V-8. Determination of the percentage of the PDMS/polyester hybrid networks area covered by several type of marine organisms after 2 months of immersion.

According to Figure V-9, the only organism that was present on the PDMS/polyester hybrid networks but absent on the PDMS was the green algae (10-60 %). Spirorbis and brown algae were the other main marine macroorganisms found on PDMS/polyester hybrid networks in similar proportions (20-30 %). At this stage of immersion, the PDMS/polyester hybrid networks were entirely covered with macroorganisms. It can be assumed that after 6 months of immersion, the AF property may definitely be lost given that the settled organisms can serve as an alternative substrate for the newcomers.

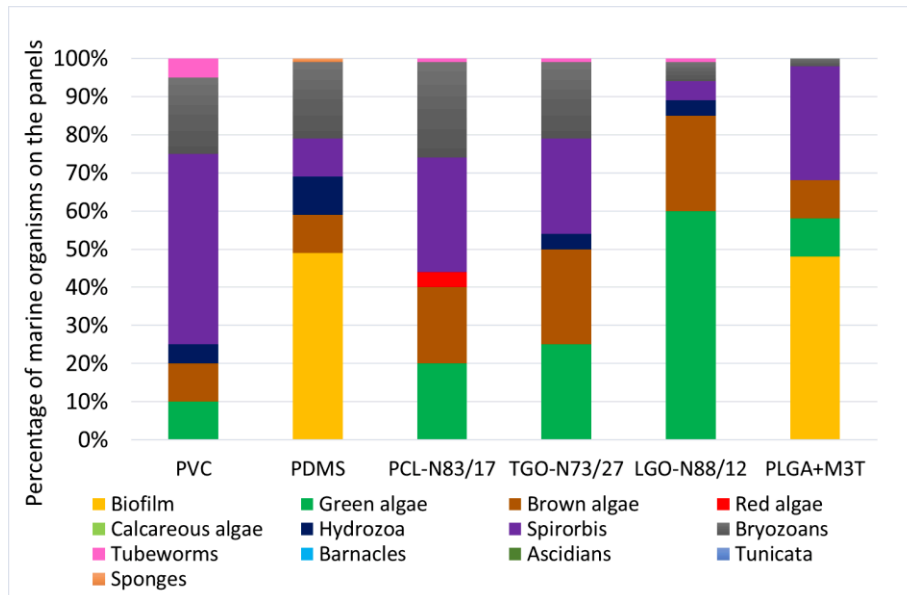


Figure V-9. Determination of the percentage of the PDMS/polyester hybrid networks area covered by several type of marine organisms after 6 months of immersion.

While comparing the evolution of settled marine organisms between the two approaches at 2 and 6 months, it was interesting to see that at 2 months of immersion, the PDMS/polyester hybrid networks showed less fouling coverage ($\leq 10\%$) than the hydrolyzable additive-based PDMS coatings (10 to 50 % other than biofilm). Whereas at 6 months the tendency was reversed with much more fouling for the PDMS/polyester hybrid networks than for the hydrolyzable additive-based PDMS coatings. The effect of seasonality also had a great impact on the fouling diversity. As a reminder, the hydrolyzable additive-based PDMS coatings and the PDMS/polyester hybrid networks were not immersed at the same period, thus resulting in different fouling trends.

Chapter V – Antifouling and fouling release properties of coatings

V.2.1.3. Fouling release properties

A coating could be classified as FRC as soon as soft and/or hard fouling could be easily removed under hydrodynamic forces. The FR property comes from the softness of an elastomer-based coating. The soft nature of silicone elastomers can indeed facilitate the peeling of settled organisms in presence of mechanical forces. A bad AF coating (a coating on which macroorganisms have settled) does not necessarily exhibit bad FR property.

The FR property was determined by the cleaning of the coatings with a wet sponge. According to the quantity and type of fouling removed, the FR ability of coatings was rated from 0 to 2:

- 0 corresponds to a coating exhibiting a bad FR property with no macrofouling removal
- 1 corresponds to a coating with a moderate FR property, with the removal of at least one type of fouling species
- 2 corresponds to a good FR property with the removal of all types of fouling species

▪ **Hydrolyzable additive-based PDMS coatings**

The cleaning of the second panel was performed every 3 months to allow any fouling accumulation between cleaning steps. Figure V-10 shows the FR values after 6 and 20 months of immersion. It should be mentioned that the panels at 20 months of immersion were already cleaned 6 times.

It was interesting to compare the FR ability at these two particular dates because the amount of biofouling was markedly different, and that we can conclude on the duration of the FR efficacy. The FR ability at $t_i=3$ months was performed but not shown as the fouling was not enough important to see any difference before and after the cleaning.

After 6 months of immersion, the FR properties of the hydrolyzable additive-based coatings were similar to the PDMS reference (except for M3T-BX coatings). This suggests they maintained their FR ability thanks to the effect of the soft PDMS matrix.

However, M3T-BX seemed to have weaker FR ability after 6 months of immersion. The apparition of hydrophilic functions coming from the hydrolyzed PMATM2 on the surface probably had favored chemical interactions between the organisms and the surface, making

Chapter V – Antifouling and fouling release properties of coatings

a stronger adhesion between them. Given that PMAA is released after 32 weeks (from FTIR analysis in Chapter II, § II.4.2.4.), it was expected to recover a hydrophobic surface once all the hydrolyzable additive is removed.

PCL-BX and TGO-BX still showed good FR properties after 20 months of immersion indicating the poly(ϵ -caprolactone) did not alter the FR ability of the PDMS elastomer matrix.

After 20 months, M3T-BX coatings completely lost their FR ability. This result is still not well understood given that it was expected for these coatings to retrieve their hydrophobicity and their FR ability once the additive degradation products were removed (as a reminder, the reservoir effect of M3T-BX lasted *ca.* 3 months). Maybe the presence of PMAA on the coatings has helped attracting more fouling and thus triggered the fouling cascading effect. It is then possible that some PMAA remained on the coating and could not be released due to its entrapment underneath the macrofouling layer.

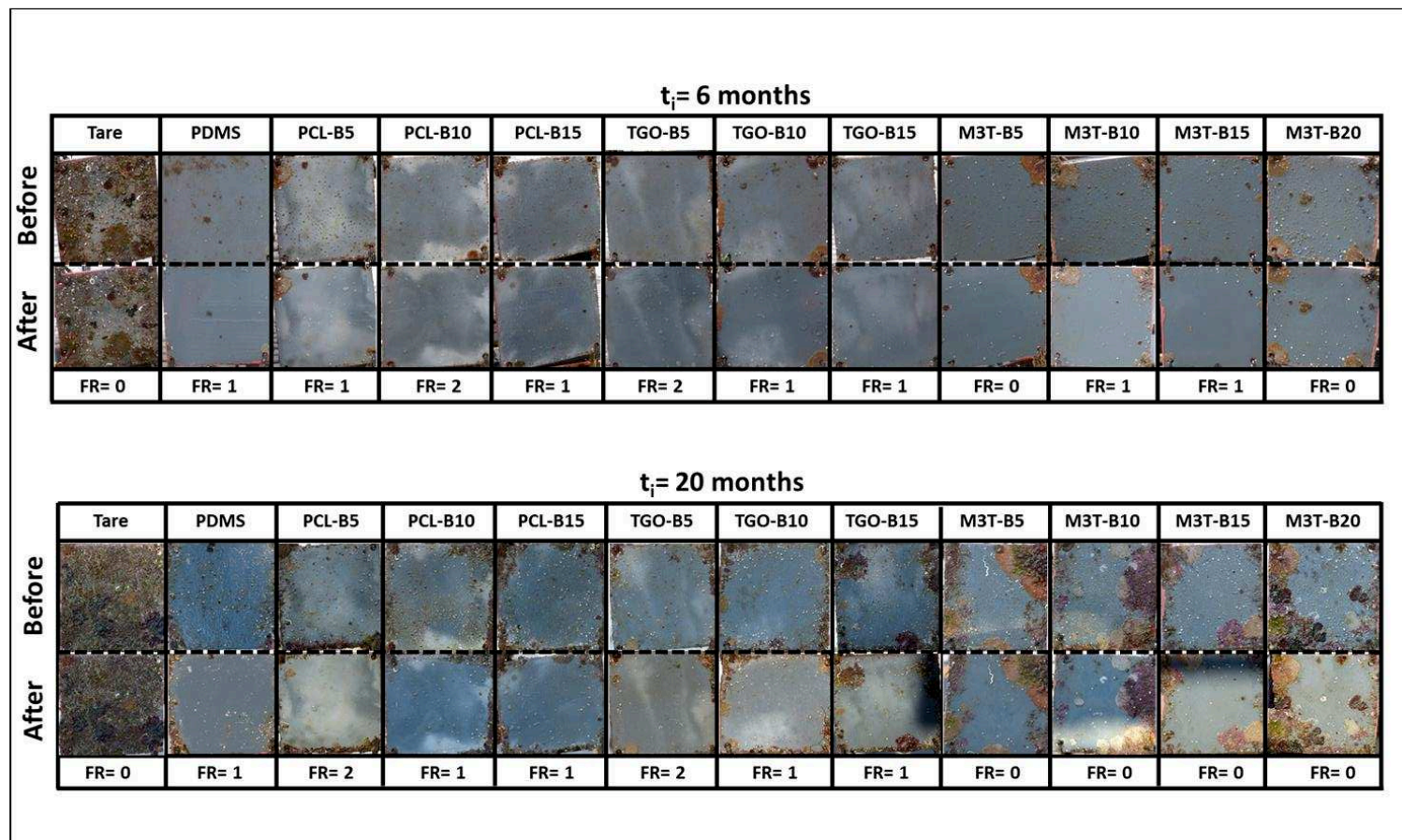


Figure V-10. Evaluation of the fouling release properties (noted FR) of the additive-based coatings before and after cleaning with a wet sponge at t_i= 6 and 20 months of immersion in Toulon bay.

Chapter V – Antifouling and fouling release properties of coatings

▪ PDMS/polyester hybrid networks

After 3 months, the FR properties of the coated panels were not ideal. Most of the settled organisms were hardly removed such as bryozoans and green algae. Only spirorbis could be removed (Figure V-11). The fact that even the soft green algae was not removed after the cleaning with a wet sponge means that the PDMS did not play its FR role (such as for PCL-N83/17). Coatings based on PLGA (PLGA-N88/12 and LGO-N88/12) were the most promising coatings in terms of FR ability at $t = 3$ months, probably because their polyester content was lower than those of PCL-N83/17 and TGO-N73/27. In these later two PDMS/PCL hybrid networks, the polyester segments certainly prevailed over the soft PDMS chains on the coating surface and thus reduced the FR ability (in Chapter IV, § IV.2.3.). The increase of elastic modulus during immersion was not necessarily the cause given that the elastic modulus of the PDMS/polyester hybrid networks (in the form of free films) was measured again after 2 months of immersion in deionized water and showed no difference.

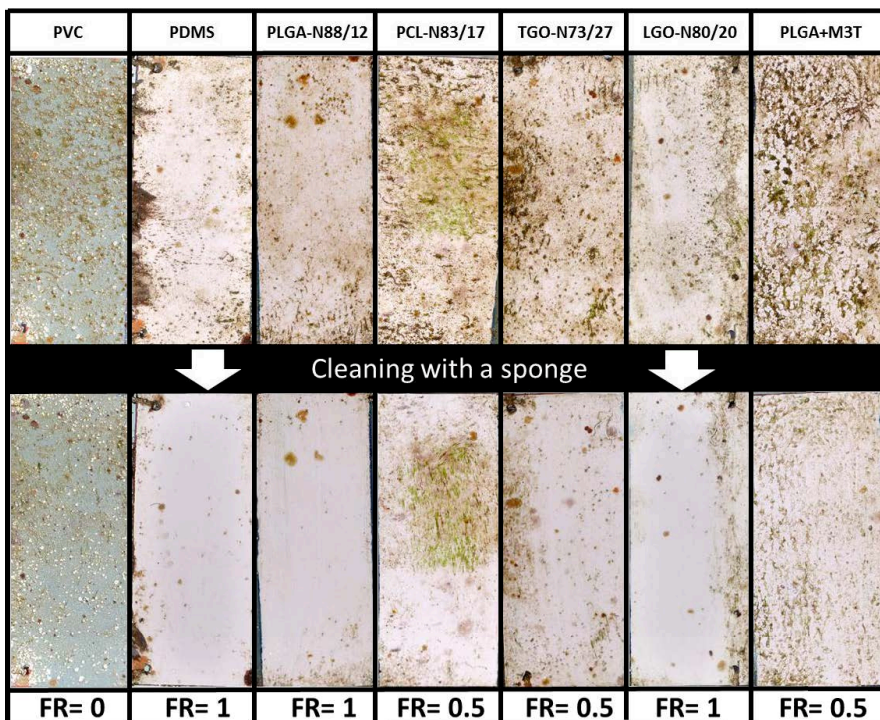


Figure V-11. Evaluation of the fouling release properties (noted FR) of the hydrolyzable PDMS-polyester networks after 3 months of immersion in Toulon bay.

Chapter V – Antifouling and fouling release properties of coatings

At 6 months of immersion, the FR ability of all PDMS/polyester hybrid networks was markedly altered (Figure V-12). The main explanations to that FR decrease are the increase of surface hydrophilicity and/or increase of roughness in contact with water.

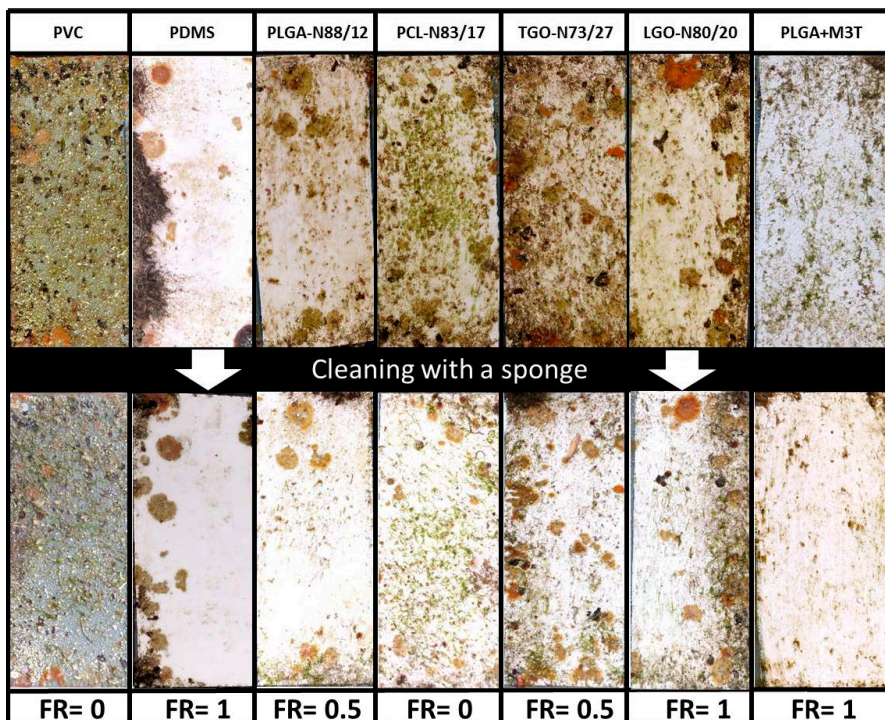


Figure V-12. Evaluation of the fouling release properties (noted FR) of the hydrolyzable PDMS/polyester hybrid networks after 6 months of immersion in Toulon bay.

We can notice that the PDMS reference which displayed rather good FR properties in Figure V-10 also seemed to be less efficient (the bryozoans were not removed at all). PLGA+M3T was the only PDMS/polyester hybrid network with a long-term FR ability certainly due to its very soft upper layer which must have discouraged a lot the settlement of marine species. A crosslinked network with both hydrolyzable additives and hydrolyzable polyester crosslinked chains could be a promising route to disturb fouling from settling.

V.3. Biological assays

Biological assays are useful to target the AF action against some specific marine organisms. *Amphibalanus* cyprids, *Ulva* spores and diatoms are all motile organisms that actively explore surfaces before choosing preferred sites [5]. Thus, it will be possible to know which coatings favor or dissuade their settlement.

V.3.1. Biological assay on *A. amphitrite* cypris larvae

A. amphitrite is a common member of the coastal fouling communities and has an extremely wide geographical distribution which is why it was interesting to target this marine organism. Several studies reported that *A. amphitrite* prefers hydrophilic and higher SFE surfaces [6]. Their settlement was linearly correlated with θ_w ($R^2= 0.84$) and γ_c ($R^2= 0.84$). The aim of this assay was to investigate the influence of variations in the surface chemistry of the silicone-based coatings on the settlement of hard macrofoulers such as barnacles.

V.3.1.1. Settlement of *A. amphitrite* on the hydrolyzable additive-based PDMS coatings

As a reminder, PDMS, PCL-BX, TGO-BX and M3T-BX coatings exhibited similar elastic moduli. Thus, any difference between the coatings in terms of barnacle attachment will be attributed to the different chemical compositions, achieved by the addition of hydrolyzable polymers in the PDMS elastomer. The *A. amphitrite* settlement assay adapted from Othmani et al. was relevant to determine the antiadhesive property of the coatings towards barnacle cypris larvae (Figure V-13) [7]. It was performed in partnership with the Paul Ricard oceanographic institute (France).

TGO-B15 and PCL-B15 both showed a statistically significant lower adhesion of barnacle cypris larvae than the PS control (Figure V-13). Thus, the presence of both hydrophobic and hydrophilic phases (revealed by dynamic contact angles analyses) potentially affected their adhesion. PMATM2-based coatings, M3T-B15 and M3T-B20, also showed significant effect on adhesion, with values lower than 30 % of adhered cypris larvae. This could be correlated with the mass loss recorded after 1 week of immersion given that the release of degradation products can make the surface brittle, and thus inhibit the macrofoulers settlement. During

Chapter V – Antifouling and fouling release properties of coatings

the incubation time of cypris larvae (7 days), M3T-B15 and M3T-B20 displayed mass losses of *ca.*2 wt.%. In addition, the surface chemistry changed. Both phenomena may explain the difficulty of barnacles to settle on the coatings. This study demonstrated that coatings containing at least 15 wt.% of hydrolyzable polymers displayed interesting anti-barnacle larvae settlement properties, as the surface chemical ambiguity tended to discourage the barnacle cypris larvae to settle. M3T-B20 showed very promising anti-barnacle properties, similar to that of the commercial X3 FRC.

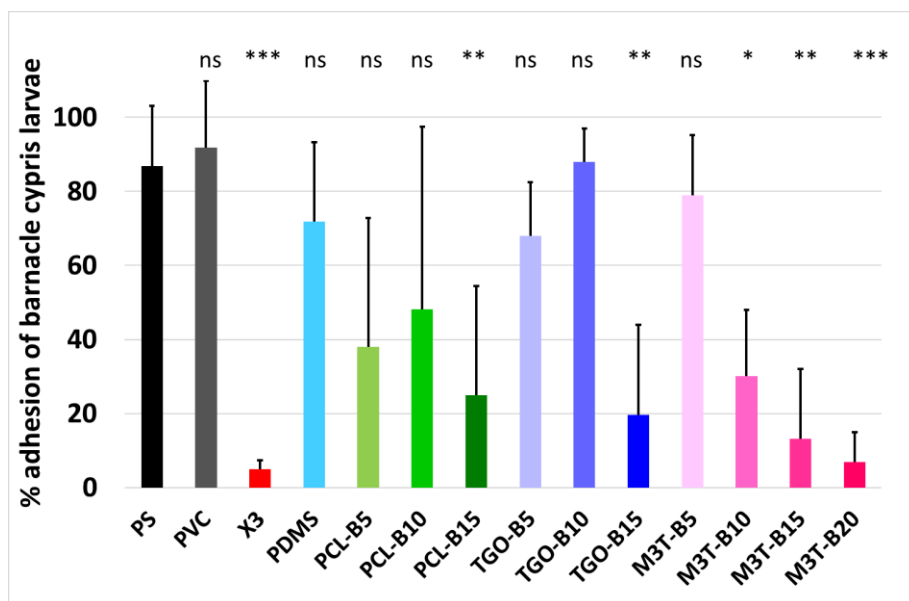


Figure V-13. Settlement of *A. amphitrite* larvae on controls (PS, PVC) and PDMS-based coatings. Error bars represent standard deviations and asterisks show values that are significantly different to the PS control (ns = not significant; * $p < 0.05$; ** $p < 0.01$; *** $p < 0.001$).

V.3.2. Bioassays on diatoms and algal spores

The aim of the following experiments was to assess if our coatings showed AF properties towards microorganisms thanks to their ambiguous chemical surfaces. Two organisms (*N. incerta* and *U. linza*) were chosen as they show opposite responses to coatings, with sporelings of *U. linza* being more easily removed from hydrophobic coatings while diatom *N. incerta* being hardly removed from hydrophobic coatings [6,8–11]. Microorganisms were used to study the coatings performance as they are typically the first organisms to appear on an

Chapter V – Antifouling and fouling release properties of coatings

underwater surface, and are responsible for forming a microbial slime layer on a ship's hull. It is important to assess the adhesion and removal of these microorganisms as they are partly responsible for the increase of hydrodynamic drag of ships [12].

*V.3.2.1. Diatoms *Navicula incerta**

A unicellular alga (diatom), *Navicula incerta*, was specifically targeted as it is known to attach and form adherent biofilms on hydrophobic surfaces including FRC [8,9,13,14]. This test was performed only on the PDMS/polyester hybrid networks in collaboration with the University of Newcastle (UK).

V.3.2.1.1. Initial attachment of diatoms on the PDMS/polyester hybrid networks

Diatoms sink in the water column and land on the surface of the coatings by gravity. Therefore, before washing, the cell density on all the test surfaces was the same, whatever the surface chemistry. The process of washing removes unattached and weakly attached cells and thus differences in initial attachment density reflect differences in the ability of cells to attach firmly to the surfaces and resist the hydrodynamic forces of washing. The full protocol of the initial attachment is described in the experimental section (§ VI.7.2.2.).

Initial attachment density on PLGA-N88/12 was lower than on PDMS (Figure V-14). TGO-N73/27 and PCL-N83/17 did not show significant difference compared with PDMS.

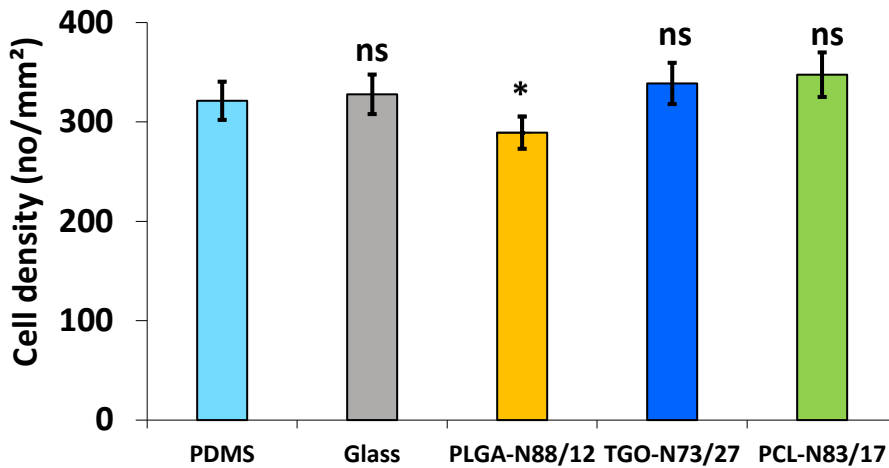


Figure V-14. The density of attached diatoms on coatings after 2 hours of incubation followed by washing. Each point is the mean of 90 counts from 3 replicate slides. Bars show 95 % confidence limits. Asterisks show values that are significantly different to the PDMS reference (ns = not significant; * $p < 0.05$; ** $p < 0.001$; *** $p < 0.0001$).

V.3.2.1.2. Removal of diatoms on the PDMS/polyester hybrid networks

To assess the percentage removal of diatoms, the coatings were exposed to 5 min of wall shear stress of 34 Pa in a turbulent flow water channel (§ VI.7.2.2.).

The percentage removal of diatoms was lower on the experimental coatings than on the glass reference (Figure V-15). Although the removal of diatoms from the PDMS/polyester hybrid networks were low, they were higher than from the PDMS coating. Initially, PLGA-N88/12 was the coating with the lowest diatoms settlement and it also presented the highest percentage removal. These results highlight the positive effect of the crosslinking of PLGA with PDMS chains. The presence of poly(ϵ -caprolactone) did not have a significant effect on the diatoms removal.

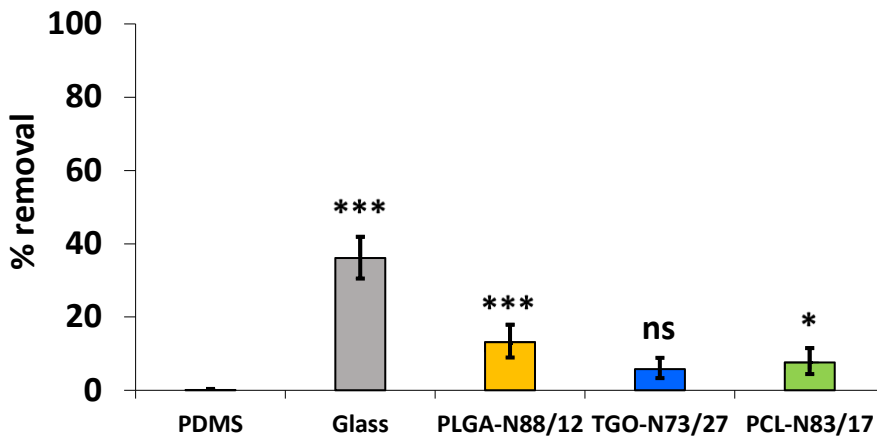


Figure V-15. Percent removal of diatoms from coatings due to a shear stress of 34 Pa. Each point is the mean of 90 counts from 3 replicate slides. Bars show 95 % confidence limits derived from arcsine transformed data. Asterisks show values that are significantly different to the PDMS reference (ns = not significant; * $p < 0.05$; ** $p < 0.001$; *** $p < 0.0001$).

V.3.2.2. *Ulva* spores

V.3.2.2.1. Green alga *Ulva rigida*

The settlement of *U. rigida* was tested on the hydrolyzable additive-based PDMS coatings. The spores were cultivated at the Paul Ricard Oceanographic Institute. The full protocol is available in the experimental section (§ VI.7.2.3.).

Figure V-16 shows the fluorescence intensity variations (ΔI) of the experimental coatings. A minimum of ΔI corresponds to a minimum of spore settlement.

The number of settled spores on PCL-B15, TGO-B15 and M3T-B15 were significantly higher compared to the PDMS reference (ANOVA, $p < 0.001$ and $p < 0.0001$). Thus, it appears that by increasing the content of hydrolyzable additive within the coatings, it favors the settlement of *U. rigida*. However, although ANOVA indicated no significant difference, the coating M3T-B15 seemed to show lower settlement of spores than PDMS reference (although ANOVA suggests no significant difference) suggesting the hydrolysis of PMATM2 (15 wt.%) could deter

Chapter V – Antifouling and fouling release properties of coatings

the spores from settling. Other coatings such as PCL-B5 and TGO-B5 showed similar results to PDMS suggesting there was no negative nor positive effects of adding 5 wt.% of PCL in PDMS on the spore settlement.

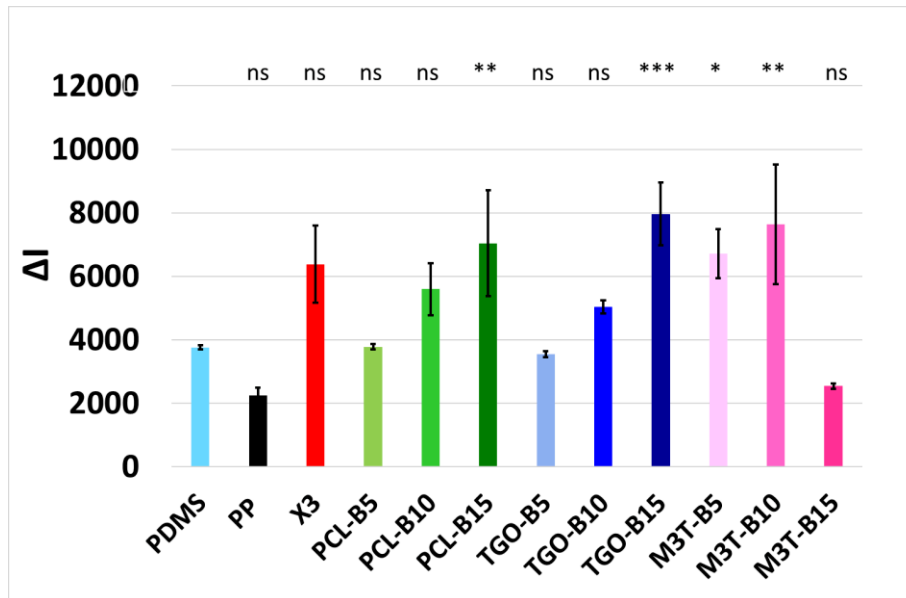


Figure V-16. Fluorescence intensity variations ($\Delta I = I_{\text{coating with spores}} - I_{\text{coating without spores}}$) of the experimental coatings showing the settlement of *U. rigida* spores on controls (PP and PDMS), on a commercial hydrogel-based FRC (X3) and on the hydrolyzable additive-based PDMS coatings. Error bars represent standard deviations and asterisks show values that are significantly different to the PDMS reference (ns = not significant; * $p < 0.05$; ** $p < 0.001$; *** $p < 0.0001$).

V.3.2.2.2. Green alga *Ulva linza*

Ulva linza is a green seaweed, which is reproduced by production of spores that rapidly develop into sporelings (young plants). Briefly, the spores of *U. linza* actively search a surface for suitable settlement sites before committing to irreversible attachment. Following this, the spores germinate and develop into sporelings (young plants) composed of a rhizoid (which attaches them to the surface) and a filament.

Sporelings of *Ulva* are known to adhere weakly on silicone-based FRC [10,15]. Thus, it will be possible with this bioassay to evaluate the impact of the crosslinked polyester segments (2nd strategy) on the settlement of *Ulva* spores.

▪ Settlement of spores on the PDMS/polyester hybrid networks

This bioassay was performed by the University of Newcastle (UK). The *Ulva* spores were collected from the Llantwit Major beach, Wales, UK. After incubation for 45 min darkness, the settled spores were counted by chlorophyll autofluorescence to assess the antifouling property of the coatings towards *Ulva linza* spores (further details in the experimental section, § VI.7.2.3.).

The density of settled spores was the highest on PCL-N83/17 and the lowest on PLGA-N88/12 and TGO-N73/27 (Figure V-17). The differences between the PDMS/polyester hybrid networks and the PDMS reference were however not significant suggesting that there was no important effect of the physico-chemical properties on the number of settled spores.

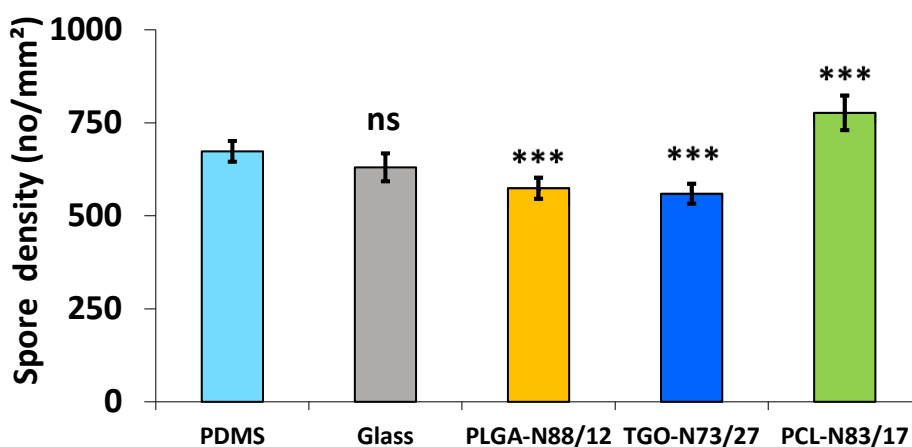


Figure V-17. The density of attached *Ulva linza* spores on coatings after 45 minutes of incubation followed by washing. Each point is the mean of 90 counts from 3 replicate slides. Bars show 95% confidence limits. Asterisks show values that are significantly different to the PDMS reference (ns = not significant; * $p < 0.05$; ** $p < 0.001$; *** $p < 0.0001$).

▪ Growth of sporelings (young plants) on the PDMS/polyester hybrid networks

The growth of sporelings was highest on PCL-N83/17 following the pattern of high spore settlement on this surface and lowest on PLGA-N88/12 (Figure V-18). No sporelings grew on the reference PDMS coating which traduces its toxicity towards sporelings. This toxicity may be due to DOTDL catalyst as already mentioned in some scientific papers [16]. The only way to avoid this toxicity would have been to let the tin-based coatings leach for long immersion periods like Martinelli et al. [17]. At this stage, it is thus difficult to conclude on the influence of the polyester chemistry on the growth of sporelings since the toxic effect of tin exposure cannot be ruled out.

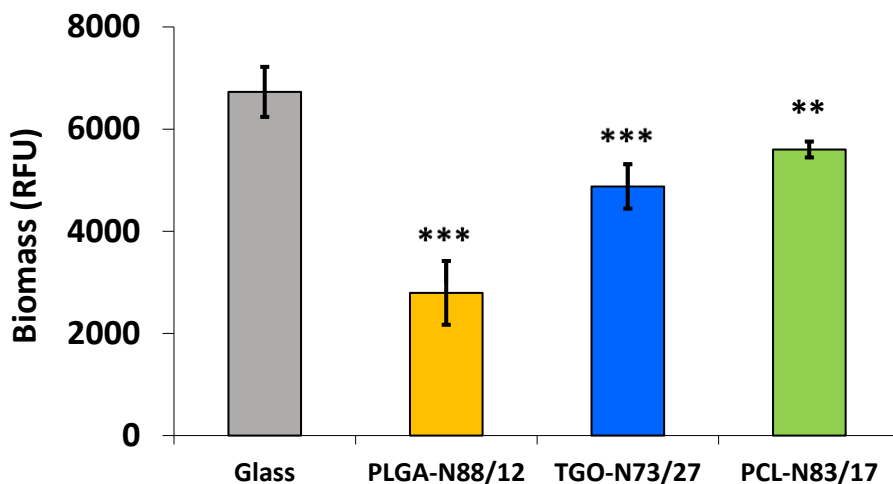


Figure V-18. The biomass of *Ulva linza* sporelings on test coatings after 7 days. Each point for the PLGA-N88/12, TGO-N73/27 and glass is the mean biomass from 6 replicate slides. For PCL-N83/17, the mean biomass was from 5 replicates. Measurements made using a fluorescence plate reader (RFU; relative fluorescence unit). Bars show standard error of the mean. Asterisks show values that are significantly different to the glass control (ns = not significant; * $p < 0.05$; ** $p < 0.001$; *** $p < 0.0001$).

▪ Removal of sporelings on the PDMS/polyester hybrid networks

The percentage removal of sporelings due to a shear stress of 60 Pa in a turbulent flow water channel was higher for PLGA-N88/12 and TGO-N73/27 than for PCL-N83/17 and the glass reference surface (Figure V-19). Again, it is difficult to conclude on the influence of the polyester chemistry since the toxic effect of tin exposure may also account for the higher release of sporelings from the tested surfaces.

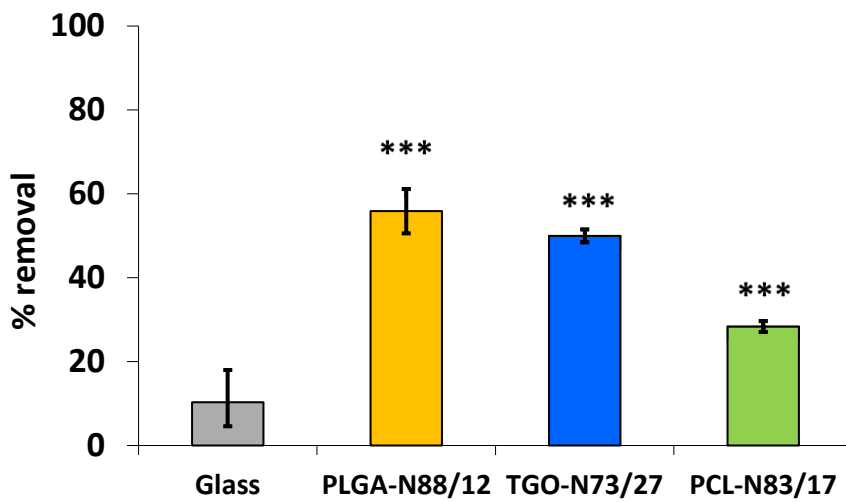


Figure V-19. Percent removal of 7 days old *Ulva linza* sporelings from the coatings due to a shear stress of 60 Pa. Each point for the PLGA-N88/12, TGO-N73/27 and glass is the mean biomass from 6 replicate slides. For PCL-N83/17 mean is from 5 replicates. Measurements made using a fluorescence plate reader (RFU; relative fluorescence unit). Bars show standard error of the mean derived from arcsine transformed data. Asterisks show values that are significantly different to the glass control (ns = not significant; * $p < 0.05$; ** $p < 0.001$; *** $p < 0.0001$).

V.4. Conclusion

To conclude on the antifouling efficacy of the two strategies (hydrolyzable additives-based PDMS and hydrolyzable networks), two main aspects were highlighted.

The first aspect is that the hydrolyzable additives-based approach can be rapidly limited by the additive shortage in case of polymer additives with fast hydrolytic degradations. The choice of additives with similar hydrolytic degradation kinetics to poly(ϵ -caprolactone) may be more suitable for long-term antifouling applications. However, it was hard to really notice a significant improvement of antifouling properties in static conditions compared to the PDMS reference. The hydrolyzable additive-based PDMS coatings remained satisfying as they maintained a rather good fouling release ability on the long term.

The second aspect is that PDMS/polyester hybrid networks did not show long-term antifouling properties in static conditions suggesting the erosion rate was insufficient. PLGA-N88/12 was the coating presenting the most promising physico-chemical properties according to the in-lab investigations performed in Chapter IV, but at the end did not show improved antifouling efficacy compared to the other PDMS/polyester hybrid networks and PDMS reference. The decrease of the erosion rate in deionized water after 2 months (cf. § IV.4.1.) and the increase in roughness and/or hydrophilicity of the PDMS/polyester hybrid networks (cf. § IV.2.4. and § IV.2.5.) were certainly responsible for the loss of the antifouling efficacy after 2 months.

Finally, it seems that by bringing a new property such as amphiphilic property (1st strategy) and/or erosion (2nd strategy), we have altered another property (i.e. smoothness, hydrophobicity of the PDMS elastomer). This reveals the complexity of finding the best antifouling coating.

The biological assays showed more positive antifouling results towards targeted marine organisms. In particular, M3T-B15/20 as well as PCL-B15 and TGO-B15 showed very good anti-barnacle larvae performance. PLGA-N88/12 showed good anti-settlement and removal properties towards *N. incerta* and *U. linza* microorganisms although the tin toxicity may have intervened at least in the bioassay towards *U. linza*. PCL-based coatings such as PCL-B15, TGO-B15 seemed to be more easily fouled by *U. rigida* compared to the PDMS reference suggesting poly(ϵ -caprolactone) may favor their settlement.

V.5. Bibliographical references

1. Coutts, A.D.M.; Piola, R.F.; Hewitt, C.L.; Connell, S.D.; Gardner, J.P.A. Effect of vessel voyage speed on survival of biofouling organisms: implications for translocation of non-indigenous marine species. *Biofouling* **2010**, *26*, 1–13.
2. Pinori, E.; Elwing, H.; Berglin, M. The impact of coating hardness on the anti-barnacle efficacy of an embedded antifouling biocide. *Biofouling* **2013**, *29*, 763–773.
3. Lehaitre, M.; Delauney, L.; Compère, C. Biofouling and underwater measurements. *Real-time observation systems for ecosystem dynamics and harmful algal blooms: Theory, instrumentation and modelling. Oceanographic Methodology Series. UNESCO, Paris* **2008**, 463–493.
4. Gutiérrez, J.L.; Palomo, M.G. Increased algal fouling on mussels with barnacle epibionts: a fouling cascade. *Journal of Sea Research* **2016**, *112*, 49–54.
5. Scardino, A.J.; Zhang, H.; Cookson, D.J.; Lamb, R.N.; Nys, R. de The role of nano-roughness in antifouling. *Biofouling* **2009**, *25*, 757–767.
6. Finlay, J.A.; Bennett, S.M.; Brewer, L.H.; Sokolova, A.; Clay, G.; Gunari, N.; Meyer, A.E.; Walker, G.C.; Wendt, D.E.; Callow, M.E.; et al. Barnacle settlement and the adhesion of protein and diatom microfouling to xerogel films with varying surface energy and water wettability. *Biofouling* **2010**, *26*, 657–666.
7. Othmani, A.; Bunet, R.; Bonnefont, J.-L.; Briand, J.-F.; Culioli, G. Settlement inhibition of marine biofilm bacteria and barnacle larvae by compounds isolated from the Mediterranean brown alga *Taonia atomaria*. *Journal of Applied Phycology* **2016**, *28*, 1975–1986.
8. Holland, R.; Dugdale, T.M.; Wetherbee, R.; Brennan, A.B.; Finlay, J.A.; Callow, J.A.; Callow, M.E. Adhesion and motility of fouling diatoms on a silicone elastomer. *Biofouling* **2004**, *20*, 323–329.
9. Cassé, F.; Ribeiro, E.; Ekin, A.; Webster, D.C.; Callow, J.A.; Callow, M.E. Laboratory screening of coating libraries for algal adhesion. *Biofouling* **2007**, *23*, 267–276.
10. Chaudhury, M.K.; Finlay, J.A.; Chung, J.Y.; Callow, M.E.; Callow, J.A. The influence of elastic modulus and thickness on the release of the soft-fouling green alga *Ulva linza* (syn. *Enteromorpha linza*) from poly(dimethylsiloxane) (PDMS) model networks. *Biofouling* **2005**, *21*, 41–48.
11. Finlay, J.A.; Callow, M.E.; Ista, L.K.; Lopez, G.P.; Callow, J.A. The influence of surface wettability on the adhesion strength of settled spores of the green Alga *Enteromorpha* and the Diatom *Amphora*. *Integr Comp Biol* **2002**, *42*, 1116–1122.
12. Schultz, M.P. Effects of coating roughness and biofouling on ship resistance and powering. *Biofouling* **2007**, *23*, 331–341.
13. Sommer, S.; Ekin, A.; Webster, D.C.; Stafslie, S.J.; Daniels, J.; VanderWal, L.J.; Thompson, S.E.M.; Callow, M.E.; Callow, J.A. A preliminary study on the properties and fouling-release performance of siloxane–polyurethane coatings prepared from poly(dimethylsiloxane) (PDMS) macromers. *Biofouling* **2010**, *26*, 961–972.
14. Finlay, J.A.; Bennett, S.M.; Brewer, L.H.; Sokolova, A.; Clay, G.; Gunari, N.; Meyer, A.E.; Walker, G.C.; Wendt, D.E.; Callow, M.E.; et al. Barnacle settlement and the adhesion of

Chapter IV – Characterization of the PDMS/polyester hybrid networks

protein and diatom microfouling to xerogel films with varying surface energy and water wettability. *Biofouling* **2010**, *26*, 657–666.

15. Finlay, J.A.; Fletcher, B.R.; Callow, M.E.; Callow, J.A. Effect of background colour on growth and adhesion strength of *Ulva* sporelings. *Biofouling* **2008**, *24*, 219–225.
16. Pretti, C.; Oliva, M.; Mennillo, E.; Barbaglia, M.; Funel, M.; Reddy Yasani, B.; Martinelli, E.; Galli, G. An ecotoxicological study on tin- and bismuth-catalysed PDMS based coatings containing a surface-active polymer. *Ecotoxicology and Environmental Safety* **2013**, *98*, 250–256.
17. Martinelli, E.; Sarvothaman, M.K.; Galli, G.; Pettitt, M.E.; Callow, M.E.; Callow, J.A.; Conlan, S.L.; Clare, A.S.; Sugiharto, A.B.; Davies, C.; et al. Poly(dimethyl siloxane) (PDMS) network blends of amphiphilic acrylic copolymers with poly(ethylene glycol)-fluoroalkyl side chains for fouling-release coatings. II. Laboratory assays and field immersion trials. *Biofouling* **2012**, *28*, 571–582.

Chapter VI	Experimental section	307
VI.1.	Synthesis protocols	307
VI.1.1.	Controlled radical polymerization	307
VI.1.2.	Ring opening polymerization	307
VI.1.3.	Silanization reactions	309
VI.2.	Preparation of polymer additive films	311
VI.3.	Analyses of the polymers	311
VI.3.1.	Nuclear Magnetic Resonance Spectroscopy	311
VI.3.1.1.	PMATM2	312
VI.3.1.2.	PLGA	314
VI.3.1.3.	PCL	315
VI.3.1.4.	PLGA-b-PDMS-b-PLGA	318
VI.3.1.5.	PCL-b-PDMS-b-PCL	320
VI.3.1.6.	Alkoxysilane-terminated polymers	322
VI.3.1.7.	¹ H NMR kinetics of the hydrolysis of trialkoxysilane functions	327
VI.3.2.	Size exclusion chromatography	329
VI.3.3.	Physico-chemical properties	330
VI.3.3.1.	Contact angle measurements	330
VI.3.3.1.1.	Dynamic contact angles	330
VI.3.3.1.2.	Surface free energy	331
VI.3.4.	Thermal properties	332
VI.3.4.1.	Differential scanning calorimetry analysis	332
VI.3.4.2.	Thermogravimetric analysis	333
VI.4.	Formulation of coatings	333
VI.4.1.	Formulation recipe of hydrolyzable additive-based PDMS coatings	333
VI.4.2.	Formulation recipe of the PDMS/polyester hybrid networks-based coatings	334
VI.5.	Characterization of the PDMS-based coatings	336
VI.5.1.	Physico-chemical properties	336
VI.5.1.1.	Contact angle measurements	336
VI.5.1.1.1.	Modified time lag method	336
VI.5.1.1.2.	Dynamic contact angles	337
VI.5.1.1.3.	Surface free energy	337
VI.5.1.2.	Roughness measurements	337

Chapter VI – Experimental section

VI.5.1.3.	<i>Infrared spectroscopy</i>	337
VI.5.2.	Residue extraction test	338
VI.5.3.	Scanning electron microscopy	338
VI.5.4.	Confocal laser scanning microscopy	338
VI.5.5.	Thermo-mechanical properties	339
VI.5.5.1.	<i>Dynamic mechanical analysis</i>	339
VI.5.5.2.	<i>Differential scanning calorimetry analysis</i>	339
VI.5.5.3.	<i>Thermogravimetric analysis</i>	340
VI.5.5.4.	<i>Atomic force microscope</i>	340
VI.6.	<u>Erosion properties</u>	341
VI.6.1.	Water uptake test	341
VI.6.2.	Mass loss test	341
VI.6.3.	Thickness loss test	342
VI.7.	<u>Antifouling properties</u>	343
VI.7.1.	Field test	343
VI.7.2.	Bioassays	344
VI.7.2.1.	<i>Larval barnacle culture and settlement assay of A. Amphitrite Cyprids</i>	344
VI.7.2.2.	<i>Settlement and removal assays of diatom N. incerta</i>	345
VI.7.2.3.	<i>Settlement and removal assays of Ulva spores</i>	345
VI.8.	<u>Bibliographical references</u>	349

Chapter VI Experimental section

VI.1. Synthesis protocols

VI.1.1. Controlled radical polymerization

The poly(bis(trimethylsilyloxy)methylsilyl methacrylate) (PMATM2) homopolymer was prepared by a Reversible Addition-Fragmentation chain Transfer (RAFT) polymerization in xylene with 2,2'-azobis(2-methylpropionitrile) (AIBN) from Sigma Aldrich as an initiator and 2-cyano-2-propyl dithiobenzoate (CPDB), purchased by Strem Chemicals, as the transfer agent [1].

MATM2 monomer was kindly supplied by PPG and was distilled under reduced pressure in presence of 2,6-di-tert-butyl-4-methylphenol before use. Xylene reagent was purchased from Carlo Erba Reagents and distilled under reduced pressure before use.

After introducing MATM2, CPDB, AIBN and xylene in a dry round-bottom flask, argon was bubbling for 30 min at r.t. (Table VI-1). The reaction mixture was then stirred at 75°C in anhydrous xylene for 20 h under argon. The synthesized polymer was precipitated in a great excess of cold methanol to provide a very sticky pink polymer.

Table VI-1. Quantities of reactants and solvent used for the synthesis of PMATM2.

Reactant/solvent	m (g)	n (mmol)	V (mL)
MATM2	25.2	82.5	28.5
CPDB	1.1693	5.3	-
AIBN	0.1735	1.1	-
Xylene	-	-	26.5

VI.1.2. Ring opening polymerization

Poly(D,L-lactide-co-glycolide) (PLGA) was prepared by a ring-opening polymerization using D,L-lactide (LA), glycolide (GA) and 1,4-butanediol (BD) as the initiator (all purchased from Alfa Aesar).

Chapter VI – Experimental section

LA, GA and BD were charged into a dry round-bottomed flask equipped with a stopcock (Table VI-2). Argon was bubbled into the solution for 20 min. A solution of anhydrous chloroform (15 mL) containing the stannous 2-ethylhexanoate catalyst (SnOctII) with a monomers/catalyst molar ratio of 400 was previously prepared in a nitrogen flushed flask and injected with a dried syringe into the round-bottomed flask. The resulting solution was degassed by three consecutive freeze-pump-thaw cycles. The reaction was then carried out in a preheated oil bath at 140°C under an argon atmosphere for 24 h with stirring. The product was dissolved in a small amount of chloroform and then precipitated in cold pentane. The precipitate was dried under vacuum overnight to provide a white solid.

Table VI-2. Quantities of reactants and solvent used for the synthesis of PLGA.

Reactant/solvent	PLGA740	PLGA1900	PLGA2500
LA	10.55 g (73.2 mmol)	3.12 g (21.7 mmol)	5.01 g (41.6 mmol)
GA	2.85 g (24.6 mmol)	0.82 g (7.1 mmol)	1.01 g (8.7 mmol)
BD	1.76 g (19.5 mmol)	0.26 g (2.9 mmol)	0.19 g (2.2 mmol)
SnOctII	79 μ L (0.24 mmol)	22 μ L (0.07 mmol)	35 μ L (0.11 mmol)

PLGA-*b*-PDMS-*b*-PLGA triblock copolymers were synthesized in the same manner but at 150°C and with bis(3-aminopropyl) polydimethylsiloxane (purchased from Alfa Aesar) as a macroinitiator (Table VI-3). The copolymers were yellow viscous oils, they were not purified due to their oily state.

Table VI-3. Quantities of reactants and solvent used for the synthesis of PLGA-*b*-PDMS-*b*-PLGA.

Reactant/solvent	LGO5200	LGO5800	LGO6200
LA	7.51 g (52.1 mmol)	5.02 g (34.9 mmol)	5.26 g (41.6 mmol)
GA	1.62 g (13.9 mmol)	1.05 g (9.02 mmol)	1.07 g (10.4 mmol)
Macroinitiator	10.93 g (3.6 mmol)	6.54 g (2.2mmol)	5.39 g (2.6mmol)
SnOctII	47 μ L (0.15 mmol)	35 μ L (0.11 mmol)	28 μ L (0.13 mmol)

VI.1.3. Silanization reactions

Polyester-based polymers were silanized at their chain ends with both (3-isocyanatopropyl)trimethoxysilane (IPTMS) and (3-isocyanatopropyl)triethoxysilane (IPTES) crosslinking agents (from Alfa Aesar).

The hydroxyl-terminated polyester-based polymers (1 eq) were first dissolved in anhydrous chloroform with the dioctyltin dilaurate catalyst in a round-bottomed flask equipped with a stopcock. The solutions were immediately degassed by two consecutive freeze-pump-thaw cycles. The crosslinking agent (either IPTMS or IPTES) was then injected in excess (2.2 eq) with a dried syringe into the round-bottomed flask through a rubber stopper and the solutions were again degassed by two consecutive freeze-pump-thaw cycles. All these precautions were important to prevent methoxysilane functions from early hydrolysis. The quantities of reactants and solvent used for the silanization reactions of the different polyester-based polymers with the triethoxysilane crosslinker are described in Table VI-4. The quantities of reactants and solvent used for the silanization reactions of the different polyester-based polymers with the trimethoxysilane crosslinker are described in Table VI-5, Table VI-6 and Table VI-7.

The solutions were then stirred under an argon atmosphere for 3 to 6 h either at 35°C or 65°C. In the case of the triblock copolymers, the silanization required a longer reaction time (up to 6 h) as well as a higher temperature (65°C) because of a slower reaction kinetic probably due to the higher molar mass of the copolymer (or due to the presence of the central PDMS block). The resulting products were precipitated in cold pentane. In the case of the trialkoxysilane-terminated PCL-*b*-PDMS-*b*-PCL (TGO), the precipitation solvent was heptane. The precipitates were finally dried under vacuum overnight. No precipitation was performed for the trialkoxysilane-terminated PLGA-*b*-PDMS-*b*-PLGA (LGO) given that it was oily.

Chapter VI – Experimental section

Table VI-4. Quantities of reactants and solvent used for the triethoxysilanization.

Reactant/solvent	PLGA740	PCL2000	PCL3000	TGO6800
Polymer	2.24 g (3.1 mmol)	4.10 g (2.3 mmol)	27.53 g (9.5 mmol)	20.06 g (3.0 mmol)
IPTES	1.6 mL (6.7 mmol)	1.4 mL (5.7 mmol)	5.1 mL (20.9 mmol)	1.5 mL (6.5 mmol)
DOTDL	2 μ L (0.002 mmol)	4 μ L (0.01 mmol)	28 μ L (0.04 mmol)	20 μ L (0.03 mmol)
Chloroform	10 mL	16 mL	60 mL	30 mL

Table VI-5. Mass and molar quantities of the reactants used for the trimethoxysilanization of PLGA.

Reactant/solvent	PLGA740	PLGA1900	PLGA2500*
Polymer	7.02 g (9.5 mmol)	1.41 g (0.74 mmol)	4.57 g (1.8 mmol)
IPTMS	4.19 mL (20.8 mmol)	330 μ L (1.63 mmol)	810 μ L (4.0 mmol)
DOTDL	7 μ L (0.01 mmol)	2 μ L (0.002 mmol)	5 μ L (0.006 mmol)
Chloroform	28 mL	6 mL	18 mL

Table VI-6. Mass and molar quantities of the reactants used for the trimethoxysilanization of PCL and TGO.

Reactant/solvent	PCL2000	PCL3000	TGO6800
Polymer*	8.02 g (3.0 mmol)	8.00 g (2.8 mmol)	8.02 g (1.2 mmol)
IPTMS	2.0 mL (9.8 mmol)	1.3 mL (6.1 mmol)	520 μ L (2.6 mmol)
DOTDL	8 μ L (0.01 mmol)	8 μ L (0.01 mmol)	8 μ L (0.01 mmol)
Chloroform	20 mL	30 mL	30 mL

Table VI-7. Mass and molar quantities of the reactants used for the trimethoxysilanization of LGO.

Reactant/solvent	LGO5200	LGO5800	LGO6200
Polymer	11.56 g (2.2 mmol)	3.09 g (0.5 mmol)	3.02 g (0.49 mmol)
IPTMS	1 mL (4.9 mmol)	240 μ L (1.2 mmol)	216 μ L (1.1 mmol)
DOTDL	12 μ L (0.016 mmol)	3 μ L (0.004 mmol)	3 μ L (0.004 mmol)
Chloroform	46 mL	12 mL	12 mL

VI.2. Preparation of polymer additive films

To assess the wetting properties of the hydrolyzable polymers alone (PCL, PCL-*b*-PDMS-*b*-PCL, PLGA and PMATM2), each polymer was dissolved in chloroform (50 wt.%) and consecutively applied with a bar coater (100 μ m wet) on a thin sandblasted poly(vinylchloride) (PVC) substrate (2 \times 4 cm²) previously cleaned with ethanol. The samples were dried for 48 h at room temperature before contact angles analysis.

To determine the mass loss kinetics of the hydrolyzable polymers, the chloroform-based solutions were also casted on glass slides (76 \times 26 mm cm²) previously cleaned with acetone. They were immersed in deionized water for a certain amount of time. Only PMATM2 films could give some conclusive mass loss results given that PCL-based and PLGA polymer films rapidly cracked into pieces during immersion. The wetting and mass loss properties of PLGA- *b*-PDMS-*b*-PLGA (LGO) copolymers were not evaluated given that they were all oily.

VI.3. Analyses of the polymers

VI.3.1. Nuclear Magnetic Resonance Spectroscopy

¹H Nuclear Magnetic Resonance Spectroscopy (NMR) spectra were recorded on a Brüker Avance 400 (400 MHz) spectrometer, mainly in deuterated chloroform (CDCl₃), but also in deuterated tetrahydrofuran (THF-*d*₆) or deuterated dimethyl sulfoxide (DMSO-*d*₆), always at room temperature.

Chapter VI – Experimental section

VI.3.1.1. PMATM2

The poly(bis(trimethylsilyloxy)methylsilyl methacrylate) (PMATM2) NMR spectrum is shown in Figure VI-1. This analysis was performed right before its precipitation to show the signals of the remaining MATM2 monomers (at 6.12 and 5.60 ppm), useful to calculate the reaction conversion.

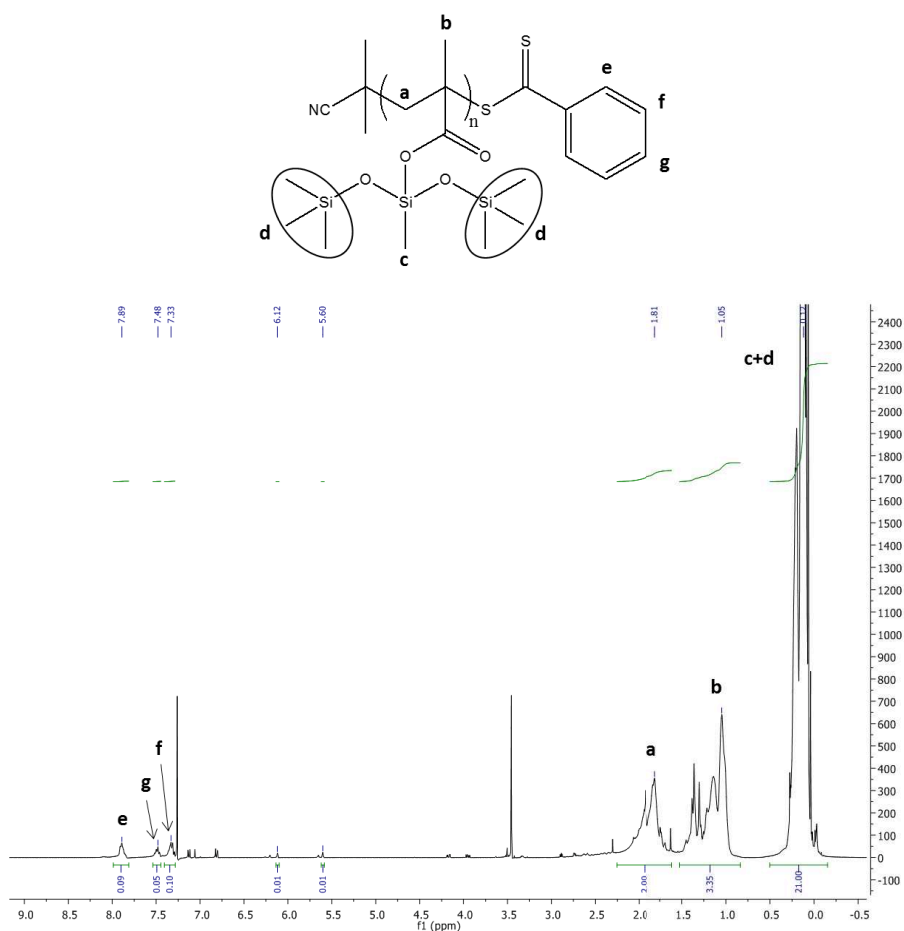


Figure VI-1. ^1H NMR spectrum of PMATM2 before its precipitation.

^1H NMR (400 MHz, CDCl_3 , δ , ppm) for PMATM2: 7.89 (e, 2H, aromatic -CH-), 7.48 (g, 1H, aromatic -CH-), 7.33 (f, 2H, m, aromatic -CH-), 6.12 (vinyl =CH-, residual MATM2 monomer), 5.60 (vinyl =CH-, residual MATM2 monomer), [1.71-2.23] (a, 2H, -CH₂-), [0.82-1.50] (b, 3H, -CH₃), [0.02-0.41] (21H, c+d, -SiCH₃ and -[(SiCH₃)₃]₂).

Chapter VI – Experimental section

The polymerization reaction was followed by ^1H NMR analysis to assess the conversion of the MATM2 monomer by measuring the disappearance of the vinyl proton at 5.60 ppm. Once the conversion no longer evolved, the reaction was stopped (Eq. 1).

$$\text{Conversion (\%)} = \frac{I_{0.02-0.41}^{\text{SiCH}_3}/21 - I_{5.60}^{\text{CH vinyl}}/1}{I_{0.02-0.41}^{\text{SiCH}_3}/21} \times 100 \quad \text{Eq. 1}$$

$I_{0.02-0.41}^{\text{SiCH}_3}$ corresponds to the intensity of the signal at [0.02–0.41] ppm, during the reaction, it includes the intensity of the protons in the trimethylsilyloxy methylsilyl moiety within the growing polymer and within the monomer. $I_{5.60}^{\text{CH vinyl}}$ corresponds to the intensity of the signal at 5.60 ppm (1H, s, vinyl –CH– of the MATM2 monomer).

The molar mass ($M_{n, \text{NMR}}$) of the purified PMATM2 (after precipitation and drying) was assessed by ^1H NMR analysis assuming that there is one CPDB molecule per polymer chain (Eq. 2).

$$M_{n, \text{NMR}} (\text{g/mol}) = \frac{I_{0.02-0.41}^{\text{SiCH}_3} / 21}{I_{7.9}^{\text{CH aromatic}} / 2} \times M_{\text{repeat unit}} + M_{\text{CPDB}} \quad \text{Eq. 2}$$

$I_{0.02-0.41}^{\text{SiCH}_3}$ corresponds to the intensity of the signal at [0.02–0.41] ppm (21H, m, –SiCH₃). $I_{7.9}^{\text{CH aromatic}}$ corresponds to the intensity of the signal at 7.9 ppm (2H, m, aromatic –CH–) corresponding to the CPDB moiety. $M_{\text{repeat unit}}$ corresponds to the molar mass of the repeat unit (305 g/mol). M_{CPDB} corresponds to the molar mass of the RAFT agent moiety (221.34 g/mol).

Chapter VI – Experimental section

VI.3.1.2. PLGA

One example of PLGA NMR spectrum is shown in Figure VI-2. It corresponds to PLGA1900 before its precipitation showing signals of remaining monomers (**d'**, **e'** and **c'**).

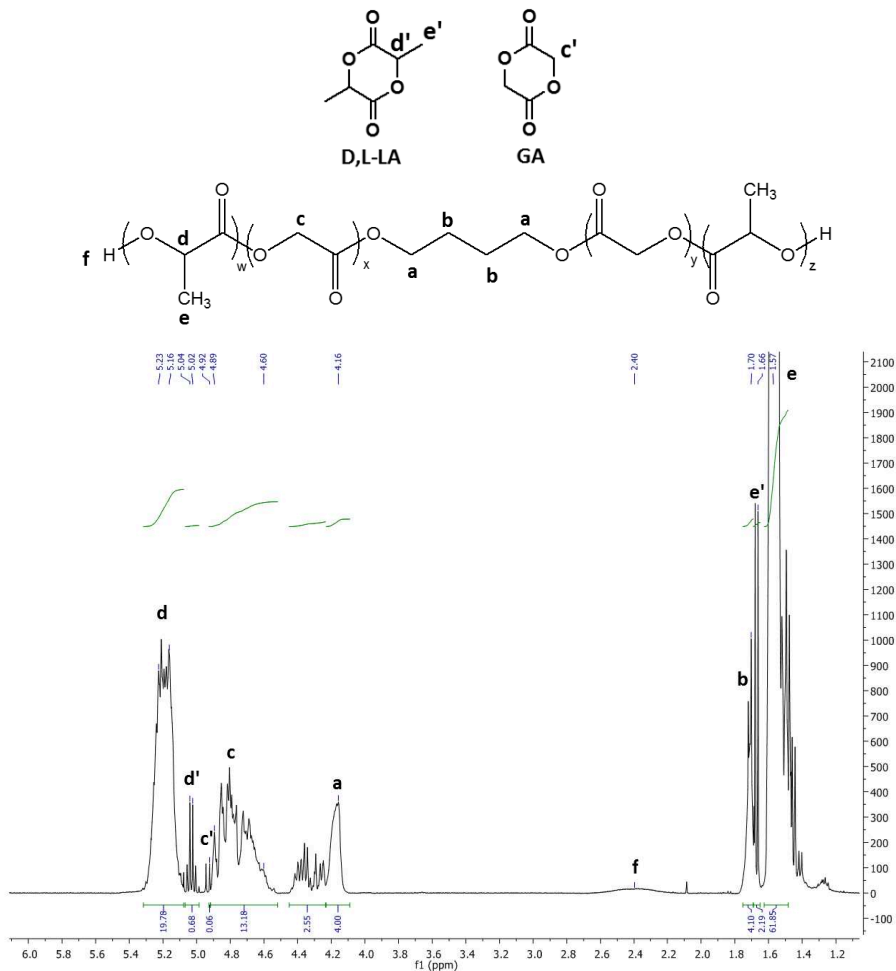


Figure VI-2. ^1H NMR spectrum of PLGA1900 before its precipitation.

^1H NMR (400 MHz, CDCl_3 , δ , ppm) for PLGA: [5.23-5.16] (**d**, ca.20H, $-\text{O}-\underline{\text{C}}\text{H}(\text{CH}_3)-\text{CO}-$), 5.02-5.04 (**d'**, quadruplet, $-\text{O}-\underline{\text{C}}\text{H}(\text{CH}_3)-\text{CO}-$, residual LA monomer), 4.92 (**c'**, singlet, $-\text{O}-\text{CH}_2-\text{CO}-$, residual GA monomer), [4.89-4.60] (**c**, ca.13H, $-\text{O}-\text{CH}_2-\text{CO}-$), 4.16 (**a**, 4H, $-\text{O}-\underline{\text{C}}\text{H}_2-\text{CH}_2-$, BD), 2.40 (**f**, -OH), 1.70 (**b**, 4H, $-\text{O}-\text{CH}_2-\underline{\text{C}}\text{H}_2-$, BD), 1.66 (**e'**, $\approx 2\text{H}$, doublet, $-\text{O}-\text{CH}(\underline{\text{C}}\text{H}_3)-\text{CO}-$, residual LA monomer), 1.57 (**e**, ca.62H, $-\text{O}-\text{CH}(\underline{\text{C}}\text{H}_3)-\text{CO}-$).

Chapter VI – Experimental section

^1H NMR was used to calculate the conversion of LA and GA monomers before precipitation (Eq. 3 and Eq. 4), the internal reference was the signal at 4.16 ppm assigned to the BD initiator (-CH₂-) and was fixed at 4H.

$$\text{Conversion LA (\%)} = 100 - \frac{I_{5.02-5.04 \text{ ppm}}^{d'}}{I_{5.02-5.04 \text{ ppm}}^{d'} + I_{5.23-5.16 \text{ ppm}}^d} \times 100 \quad \text{Eq. 3}$$

With $I_{5.02-5.04 \text{ ppm}}^{d'}$ the intensity of the quadruplet at 5.02-5.04 ppm and $I_{5.23-5.16 \text{ ppm}}^d$ the intensity of the ^1H NMR signal at [5.23-5.16] ppm for LA monomer and monomer unit, respectively.

$$\text{Conversion GA (\%)} = 100 - \frac{I_{4.92 \text{ ppm}}^{c'}}{I_{4.92 \text{ ppm}}^{c'} + I_{4.89-4.60 \text{ ppm}}^c} \times 100 \quad \text{Eq. 4}$$

With $I_{4.92 \text{ ppm}}^{c'}$ the intensity of the singlet at 4.92 ppm and $I_{4.89-4.60 \text{ ppm}}^c$ the intensity of the ^1H NMR signal at [4.89-4.60] ppm for GA monomer and monomer unit, respectively.

The molar mass ($M_{n,\text{NMR}}$) of PLGA was calculated according to Eq. 5 (with **a**, the internal reference set at 4H at 4.16 ppm):

$$M_{n,\text{NMR}} (\text{g/mol}) = \frac{I_{5.23-5.16 \text{ ppm}}^d \times M_{\text{LA}}}{2} + \frac{I_{4.89-4.60 \text{ ppm}}^c \times M_{\text{GA}}}{4} + M_{\text{BD}} \quad \text{Eq. 5}$$

With $I_{5.23-5.16 \text{ ppm}}^d$ the intensity of the ^1H NMR signal at [5.23-5.16] ppm and $I_{4.89-4.60 \text{ ppm}}^c$ the intensity of the ^1H NMR signal at [4.89-4.60] ppm. M_{LA} corresponds to the molar mass of the lactone monomer (*ca.*144 g/mol), M_{GA} corresponds to the molar mass of the glycolide monomer (*ca.*116 g/mol) and M_{BD} corresponds to the molar mass of the butane-1,4-diol initiator (*ca.*88 g/mol).

The molar percentage of LA in the resulting polymer was calculated according to Eq. 6:

$$\text{Molar \% of LA in PLGA} = \frac{I_{5.23-5.16 \text{ ppm}}^d}{I_{5.23-5.16 \text{ ppm}}^d + I_{4.89-4.60 \text{ ppm}}^c} \times 100 \quad \text{Eq. 6}$$

VI.3.1.3. PCL

The two poly(ϵ -caprolactone) diol were purchased from Perstrop and used without further purification. PCL (2,000 g/mol) and PCL (3,000 g/mol) were prepared using neopentyl glycol (NEO) and 1,4-butanediol (BD) as initiator, respectively.

- PCL (2,000 g/mol) shown in Figure VI-3

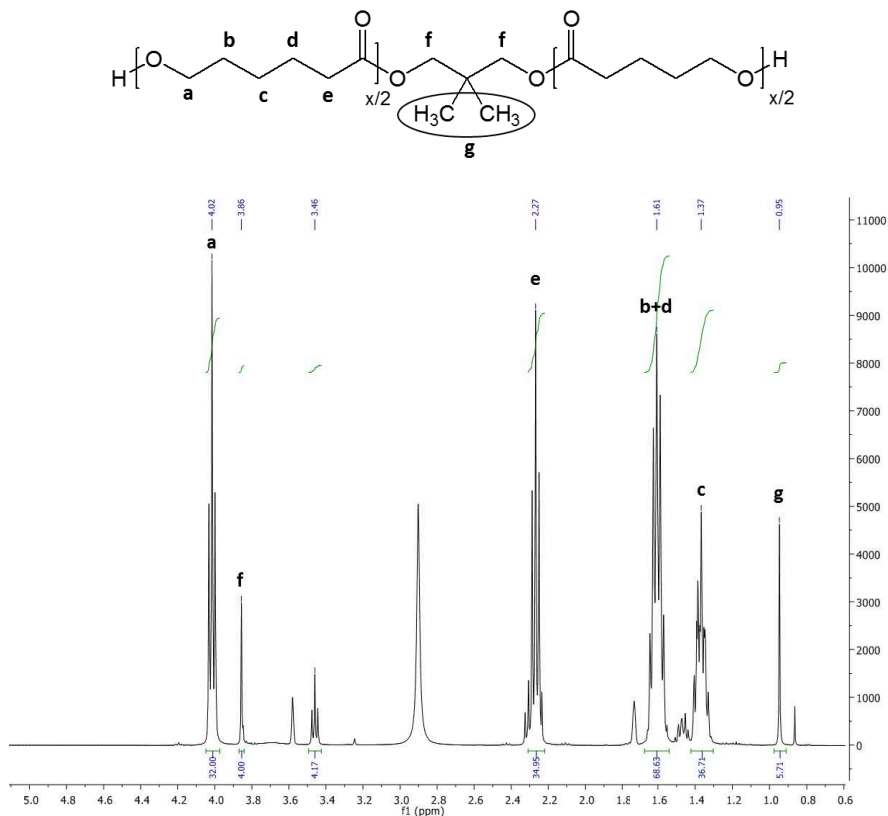


Figure VI-3. ^1H NMR spectrum of the commercial PCL2000.

^1H NMR (400 MHz, THF- d_8 , δ , ppm) for PCL2000: 4.02 (**a**, 32H, t, $-\text{CH}_2\text{-O}$), 3.86 (**f**, 4H, s, $-\text{CH}_2-$, NEO), 2.27 (**e**, *ca.* 35H, t, $-\text{CH}_2\text{-CO}$), 1.61 (**b+d**, *ca.* 69H, m, $-\text{CH}_2-$), 1.37 (**c**, *ca.* 37H, m, $-\text{CH}_2-$), 0.95 (**g**, 6H, s, $-\text{CH}_3$, NEO).

The molar mass ($M_{n,\text{NMR}}$) of PCL2000 was calculated according to **Eq. 7** (with **f**, the internal reference set at 4H at 3.86 ppm):

$$M_{n,\text{NMR}}(\text{g/mol}) = \frac{I_{4.02 \text{ ppm}}^a \times M_{\text{CL}}}{2} + M_{\text{NEO}} \quad \text{Eq. 7}$$

With $I_{4.02 \text{ ppm}}^a$, the intensity of the ^1H NMR signal at 4.02 ppm. M_{CL} corresponds to the molar mass of the ϵ -caprolactone repeat unit (*ca.* 114 g/mol) and M_{BD} , the molar mass of the neopentyl glycol initiator (*ca.* 104 g/mol).

Chapter VI – Experimental section

- PCL (3,000 g/mol) shown in Figure VI-4

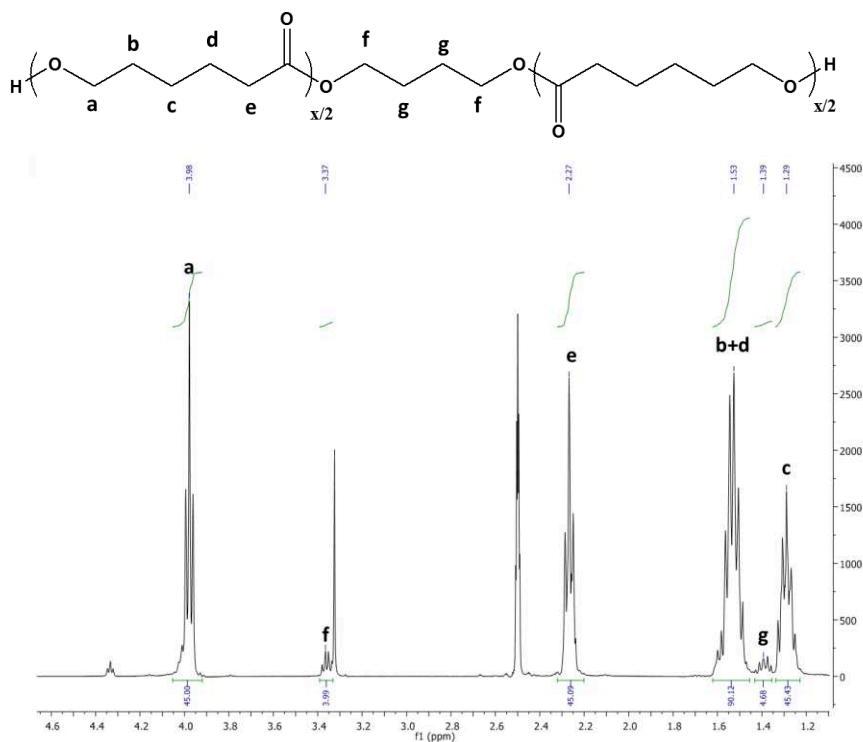


Figure VI-4. ^1H NMR spectrum of the commercial PCL3000.

^1H NMR (400 MHz, DMSO- d_6 , δ , ppm) for PCL3000: 3.98 (a, 45H, t, -CH₂-O-), 3.37 (f, 4H, t, -CH₂-, BD), 2.27 (e, 45H, t, -CH₂-CO-), 1.53 (b+d, 90H, m, -CH₂-), 1.39 (g, 4H, t, -CH₂-, BD), 1.29 (c, 45H, m, -CH₂-).

The molar mass ($M_{n,\text{NMR}}$) of PCL3000 was calculated according to Eq. 8 (with f, the internal reference set at 4H at 3.37 ppm):

$$M_{n,\text{NMR}}(\text{g/mol}) = \frac{I_{3.98}^a \times M_{\text{CL}}}{2} + M_{\text{BD}} \quad \text{Eq. 8}$$

With $I_{3.98}^a$, the intensity of the ^1H NMR signal at 3.98 ppm. M_{CL} corresponds to the molar mass of the ϵ -caprolactone repeat unit (ca. 114 g/mol) and M_{BD} , the molar mass of the butane-1,4-diol initiator (ca. 88 g/mol).

Chapter VI – Experimental section

VI.3.1.4. PLGA-*b*-PDMS-*b*-PLGA

One example of PLGA-*b*-PDMS-*b*-PLGA ^1H NMR spectrum was shown in Figure VI-5 corresponding to LGO6200.

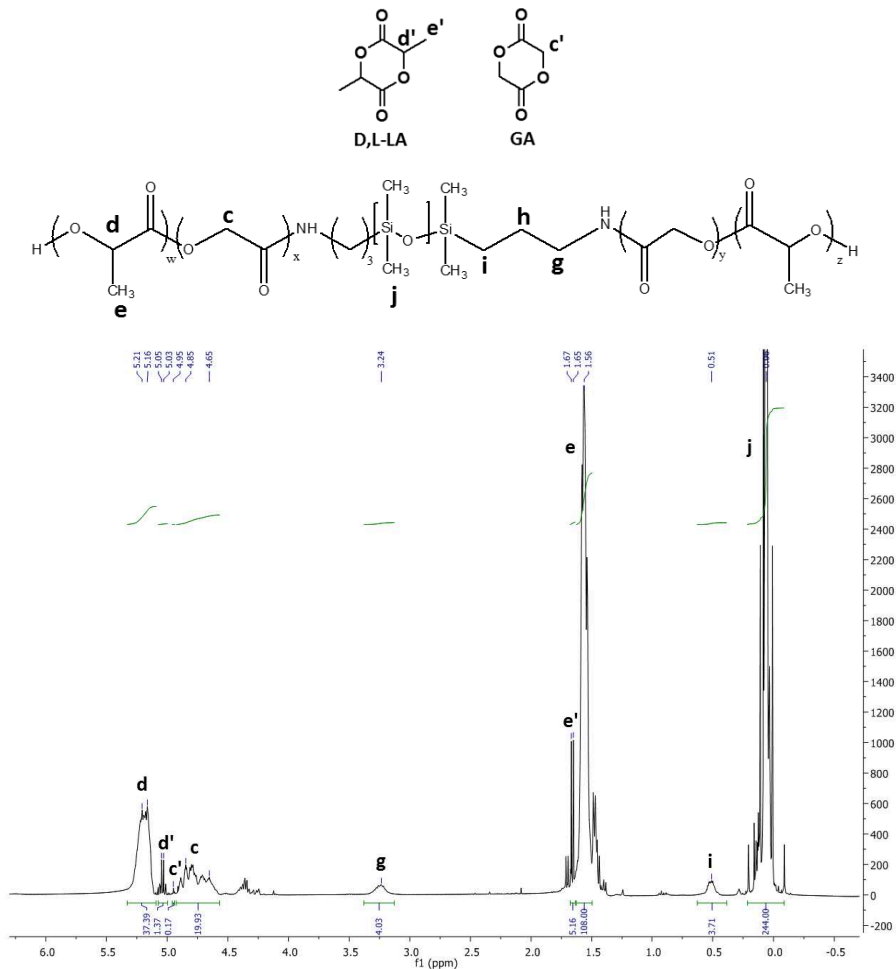


Figure VI-5. ^1H NMR spectrum of PLGA-*b*-PDMS-*b*-PLGA (LGO6200) without purification.

^1H NMR (400 MHz, CDCl_3 , δ , ppm) for PLGA-*b*-PDMS-*b*-PLGA: [5.23-5.16] (d, ca.38H, -O-CH(CH_3)-CO-), 5.02-5.04 (d', quadruplet, -O-CH(CH_3)-CO-, residual LA monomer), 4.92 (c', singlet, -O- CH_2 -CO-, residual GA monomer), [4.89-4.60] (c, ca.20H, -O- CH_2 -CO-), 3.25 (g, 4H, - CH_2 -NH-), 1.66 (e', doublet, -O-CH(CH_3)-CO-, residual LA monomer), 1.57 (e, 108H, -O-CH(CH_3)-CO-), 0.51 (i, 4H, -Si(CH_3) $_2$ - CH_2 -), 0.06 (j, 244H, -Si(CH_3) $_2$).

Chapter VI – Experimental section

^1H NMR was used to calculate the conversion of LA, GA (as previously seen in Eq. 3 and Eq. 4) and of the macroinitiator according to Eq. 9 (Figure VI-6) before precipitation. The internal reference was the signal at 0.06 ppm assigned to the $-\text{Si}(\text{CH}_3)_2$ of the macroinitiator and was fixed at 144H. The conversion was calculated based on the disappearance of the triplet at 2.65 ppm (\mathbf{x} , 4H, $\text{H}_2\text{N}-\underline{\text{CH}_2}$ -, Figure VI-6) coming from the macroinitiator.

$$\text{Conversion macroinitiator (\%)} = \frac{I_{2.65 \text{ ppm}/4}^{t_{\text{R}}=0} - I_{2.65 \text{ ppm}/4}^t}{I_{2.65 \text{ ppm}/4}^{t_{\text{R}}=0}} \times 100 \quad \text{Eq. 9}$$

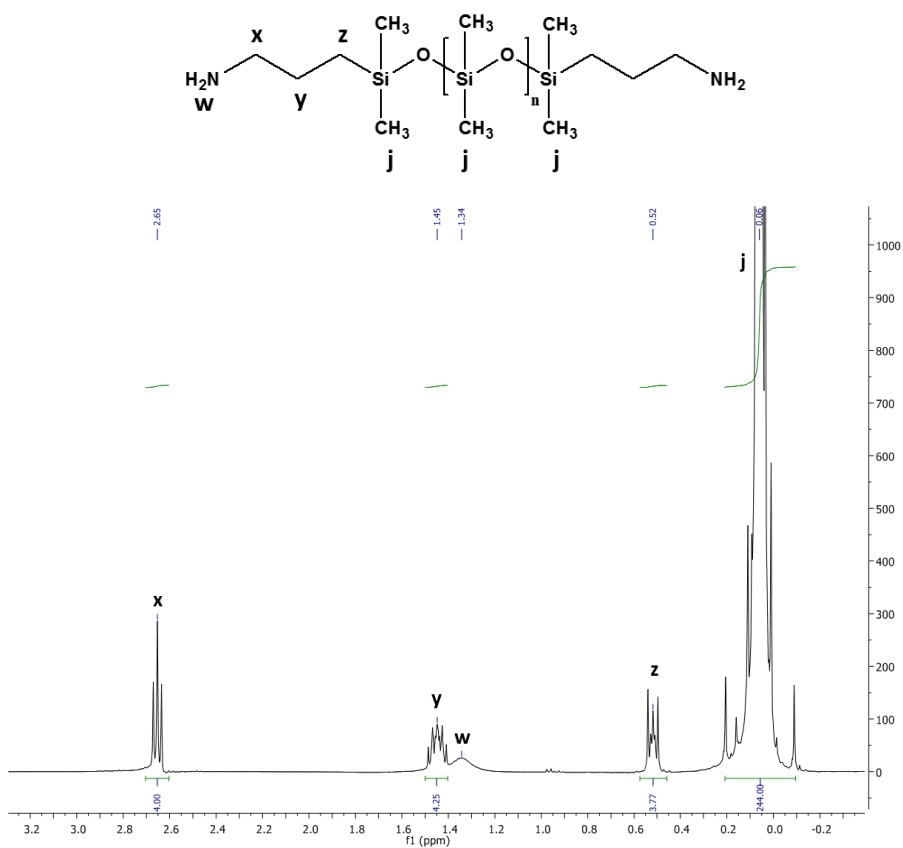


Figure VI-6. ^1H NMR spectrum of bis(3-aminopropyl) polydimethylsiloxane (macroinitiator).

^1H NMR (400 MHz, CDCl_3 , δ , ppm) for $\text{H}_2\text{N}-(\text{CH}_2)_3\text{-PDMS}-(\text{CH}_2)_3\text{-NH}_2$: 2.65 (\mathbf{x} , 4H, triplet, $\text{H}_2\text{N}-\underline{\text{CH}_2}$ -), 1.45 (\mathbf{y} , 4H, quintuplet, $-\text{CH}_2-\underline{\text{CH}_2}-\text{CH}_2-$), 1.34 (\mathbf{w} , wide signal, $\text{H}_2\text{N}-$), 0.52 (\mathbf{z} , 4H, triplet, $-\underline{\text{CH}_2}-\text{Si}(\text{CH}_3)_2-$), 0.06 (\mathbf{j} , 244H, $-\text{Si}(\text{CH}_3)_2$).

Chapter VI – Experimental section

The molar mass ($M_{n,NMR}$) of PLGA-*b*-PDMS-*b*-PLGA (LGO) was calculated according to **Eq. 10** (with j , the internal reference set at 244H at 0.06 ppm):

$$M_{n,NMR}(\text{g/mol}) = \frac{I_{5.23-5.16 \text{ ppm}}^d \times M_{LA}}{2} + \frac{I_{4.89-4.60 \text{ ppm}}^c \times M_{GA}}{4} + \frac{I_{0.06 \text{ ppm}}^j \times M_{\text{Si}(\text{CH}_3)_2\text{O}}}{6} \quad \text{Eq. 10}$$

With $I_{0.06 \text{ ppm}}^j$, the intensity fixed at 244H of the ^1H NMR signal at 0.06 ppm (internal reference), $I_{5.23-5.16 \text{ ppm}}^d$ the intensity of the ^1H NMR signal at [5.23-5.16] ppm and $I_{4.89-4.60 \text{ ppm}}^c$ the intensity of the ^1H NMR signal at [4.89-4.60] ppm. M_{LA} corresponds to the molar mass of the lactone monomer (*ca.* 144 g/mol), M_{GA} corresponds to the molar mass of the glycolide monomer (*ca.* 116 g/mol), $M_{\text{Si}(\text{CH}_3)_2\text{O}}$ corresponds to the molar mass of the PDMS repeating unit (*ca.* 74 g/mol).

VI.3.1.5. PCL-*b*-PDMS-*b*-PCL

The polyester modified polysiloxane triblock copolymer, PCL-*b*-PDMS-*b*-PCL (TGO6800), was kindly supplied by Evonik. Figure VI-7 shows its NMR spectrum.

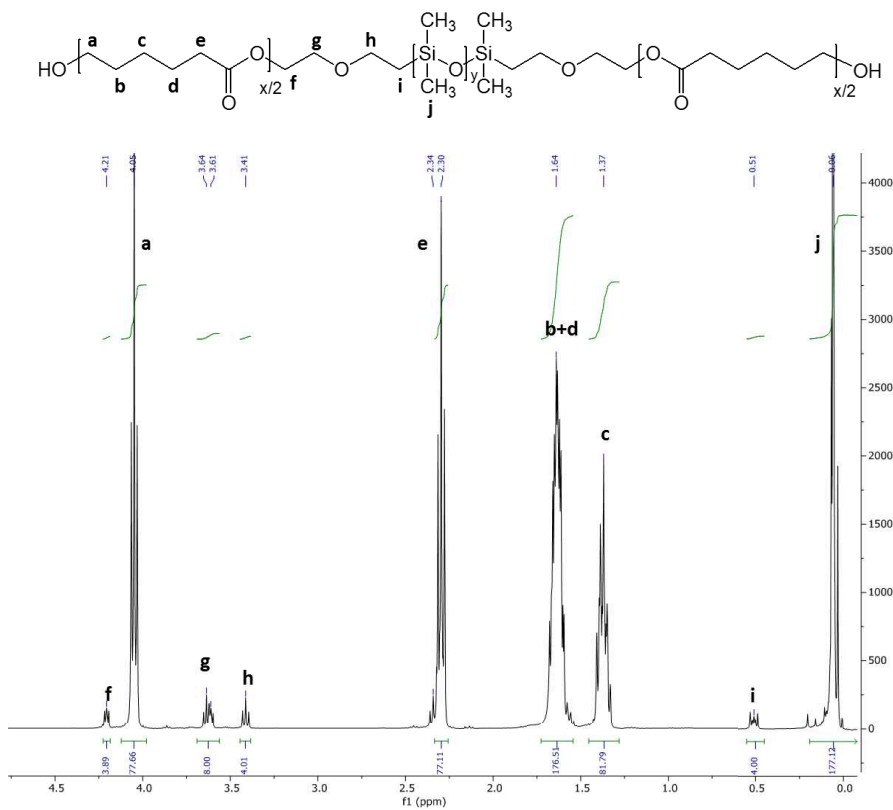


Figure VI-7. ^1H NMR spectrum of the commercial PCL-*b*-PDMS-*b*-PCL (TGO6800).

^1H NMR (400 MHz, CDCl_3 , δ , ppm) for PCL-*b*-PDMS-*b*-PCL: 4.21 (f, 4H, t, -O-CH₂-), 4.05 (a, 77H, t, -CH₂-O-), 3.64 (g, 4H, -CH₂-O-), 3.41 (h, 4H, t, -O-CH₂-), 2.30 (e, 77H, t -CH₂CO-), 1.64 (b+d, 176H, m, -CH₂- PCL), 1.37 (c, 82H, m, -CH₂- PCL), 0.51 (i, 4H, t, -CH₂- Si-), 0.06 (j, 177H, -[Si(CH₃)₂]₂).

The molar mass ($M_{n,\text{NMR}}$) of PCL-*b*-PDMS-*b*-PCL was calculated according to Eq. 11 (with i, the internal reference set at 4H at 0.51 ppm):

$$M_{n,\text{NMR}}(\text{g/mol}) = \frac{I_{4.05 \text{ ppm}}^a \times M_{\text{CL}}}{2} + \frac{I_{0.06 \text{ ppm}}^j \times M_{\text{Si}(\text{CH}_3)_2\text{O}}}{6} + 4 \times M_{\text{CH}_2} + 2 \times M_{\text{O}} \quad \text{Eq. 11}$$

With $I_{4.05 \text{ ppm}}^a$, the intensity of the ^1H NMR signal at 4.05 ppm and $I_{0.06 \text{ ppm}}^j$ the intensity of the ^1H NMR signal at 0.06 ppm. M_{CL} corresponds to the molar mass of the ϵ -caprolactone repeat unit (ca. 114 g/mol), $M_{\text{Si}(\text{CH}_3)_2\text{O}}$ corresponds to the molar mass of the PDMS repeat unit

Chapter VI – Experimental section

(ca. 74 g/mol), M_{CH_2} corresponds to the molar mass of methyl groups (ca. 14 g/mol) and M_{O} corresponds to the molar mass of the oxygen atom (ca. 16 g/mol).

VI.3.1.6. Alkoxysilane-terminated polymers

- Triethoxysilane-terminated PCL shown in Figure VI-8

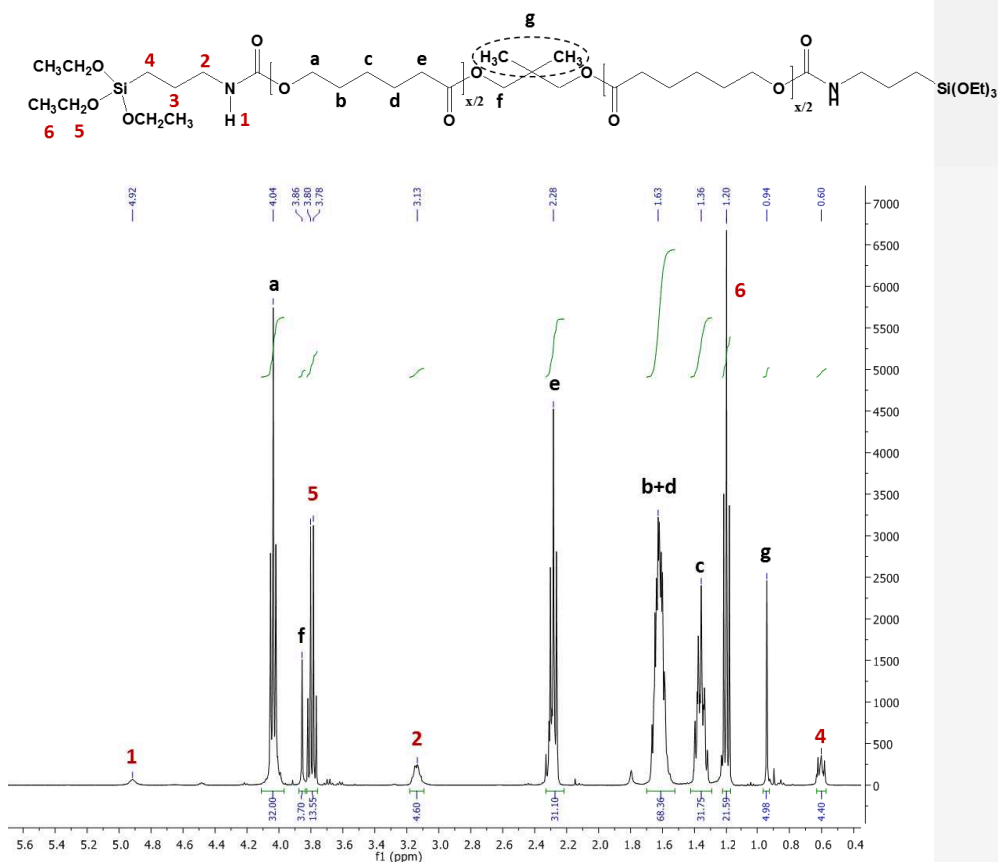


Figure VI-8. ^1H NMR spectrum of the triethoxysilane-terminated PCL2000 after precipitation and drying.

^1H NMR (400 MHz, CDCl_3 , δ , ppm) for triethoxysilane-terminated PCL2000: 5.14 (**1**, wide singlet, -NH-COO-CH₂-), 4.04 (**a**, 34H, t, -CH₂-O-), 3.86 (**f**, 4H, s, -O-CH₂-, NEO), 3.79 (**5**, 12H, s, -[Si(OCH₂CH₃)₃]₂), 3.13 (**2**, 4H, -CH₂-NHCOOR-), 2.28 (**e**, 34H, t, -CH₂-CO-), 1.63 (**b+d**, 72H, m, -

Chapter VI – Experimental section

CH₂-), 1.36 (c, 34H, m, -CH₂-), 1.20 (6, 12H, s, -[Si(OCH₂CH₃)₃]₂), 0.94 (g, 6H, s, -CH₃, NEO), 0.60 (4, 4H, t, -Si-CH₂-(CH₂)₂-NH-).

¹H NMR was used to calculate the conversion percentage of the silanized polymers. In the case of PCL2000, the internal reference was the signal at 3.86 ppm from PCL (f, 4H, s, -CH₂-, NEO) fixed at 4H. The conversion percentage was calculated based on the disappearance of the -CH₂-NCO from IPTES at 3.22 ppm (2', triplet, Figure VI-9), according to Eq. 12:

$$\text{Conversion IPTES (\%)} = \frac{I_{3.22 \text{ ppm}/4}^{t_{R=0}} - I_{3.22 \text{ ppm}/4}^t}{I_{3.22 \text{ ppm}/4}^{t_{R=0}}} \times 100 \quad \text{Eq. 12}$$

It was sometimes observed a premature hydrolysis of the triethoxysilane functions. The hydrolyzed -Si(OEt)₃ percentage was always verified before each formulation at a time *t*, calculated from Eq. 13 as follows:

$$\text{Hydrolyzed -Si(OEt)}_3 \text{ (\%)} = \frac{I_{3.79 \text{ ppm}/12}^{t_0} - I_{3.79 \text{ ppm}/12}^t}{I_{3.79 \text{ ppm}/12}^{t_0}} \times 100 \quad \text{Eq. 13}$$

With $I_{3.79 \text{ ppm}}^{t_0}$, the intensity of the ¹H NMR signal at 3.79 ppm (5, 12H, s, -[Si(OCH₂CH₃)₃]₂) of the freshly synthesized modified polymer and $I_{3.79 \text{ ppm}}^t$ the intensity of the same signal at a time *t* before the formulation process.

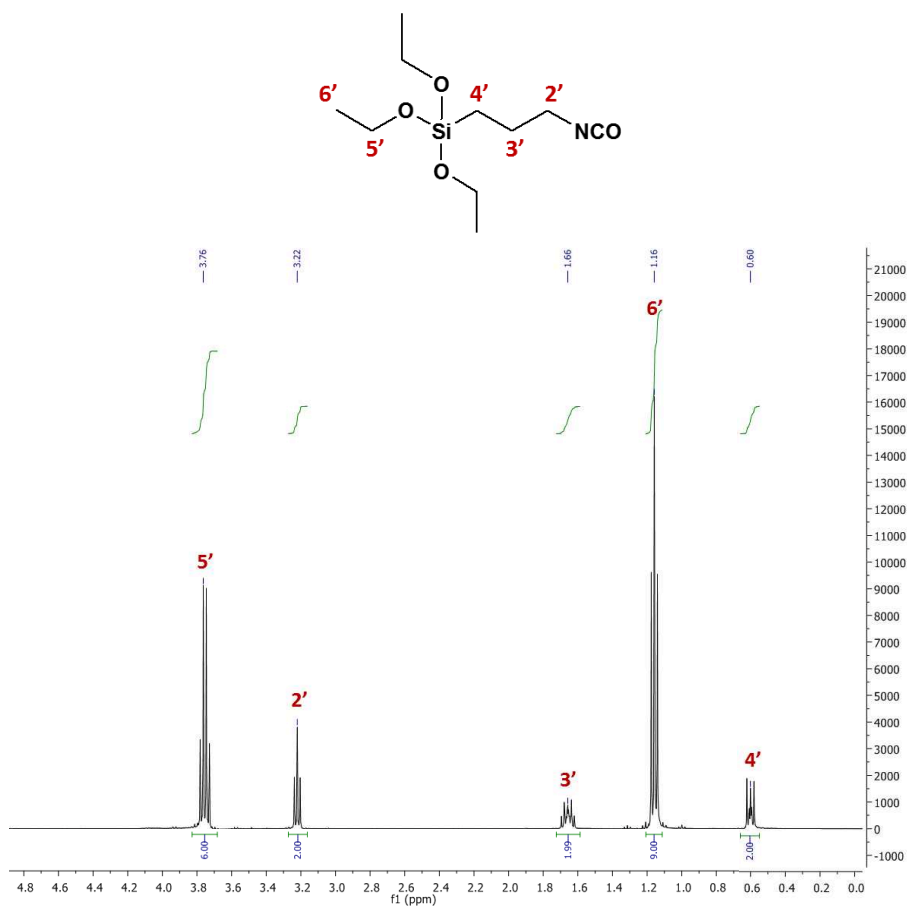


Figure VI-9. ^1H NMR spectrum of (3-isocyanatopropyl)triethoxysilane (IPTES) crosslinking agent.

^1H NMR (400 MHz, CDCl_3 , δ , ppm) for IPTES: 3.76 (**5'**, 6H, quadruplet, $-\text{Si}(\text{OCH}_2\text{CH}_3)_3$), 3.22 (**2'**, 2H, triplet, $-\text{CH}_2-\text{NCO}$), 1.66 (**3'**, 2H, quintuplet, $-\text{CH}_2-\text{CH}_2-\text{CH}_2-$), 1.16 (**6'**, 9H, triplet, $-\text{Si}(\text{OCH}_2\text{CH}_3)_3$), 0.60 (**4'**, 2H, triplet, $-\text{Si}-\text{CH}_2-$).

- Trimethoxysilane-terminated PCL shown in Figure VI-10

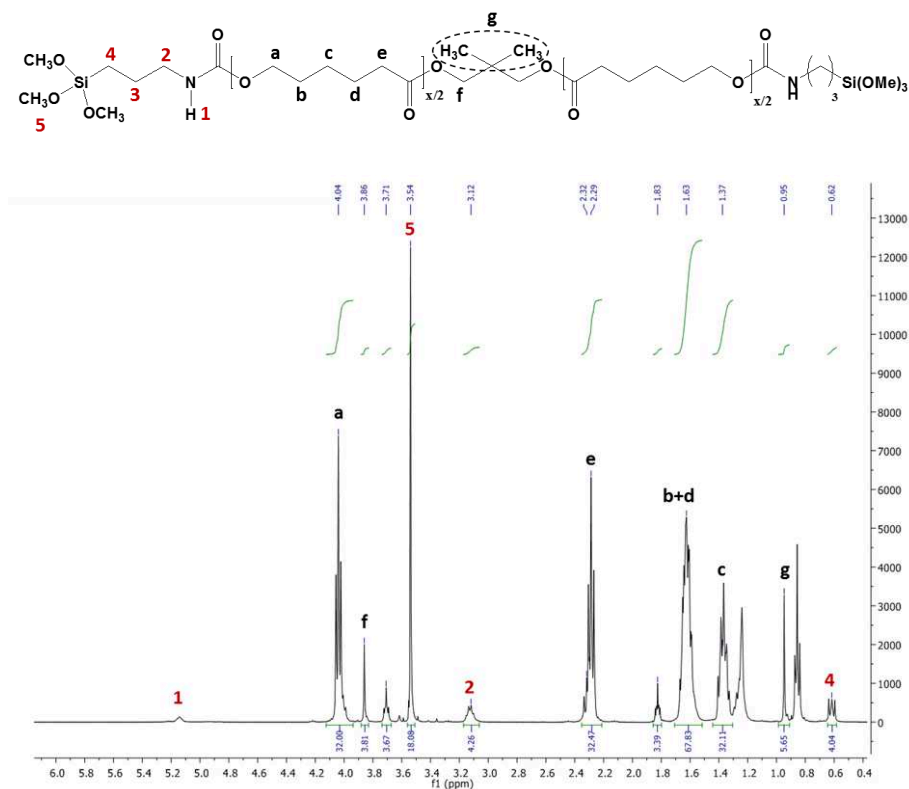


Figure VI-10. ^1H NMR spectrum of the trimethoxysilane-terminated PCL2000 after precipitation and drying.

^1H NMR (400 MHz, CDCl_3 , δ , ppm) for trimethoxysilane-terminated PCL: 5.14 (**1**, 2H, wide singlet, $-\text{NH}-\text{COO}-\text{CH}_2-$), 4.04 (**a**, 34H, t, $-\text{CH}_2-\text{O}-$), 3.86 (**f**, 4H, s, $-\text{CH}_2-$, NEO), 3.54 (**5**, 18H, s, $-\text{Si}(\text{OCH}_3)_3$), 3.12 (**2**, 4H, $-\text{CH}_2-\text{NHCOOR}-$), 2.29 (**e**, 34H, t, $-\text{CH}_2-\text{CO}-$), 1.63 (**b+d**, 72H, m, $-\text{CH}_2-$), 1.37 (**c**, 34H, m, $-\text{CH}_2-$), 0.95 (**g**, 6H, s, $-\text{CH}_3$, NEO), 0.62 (**4**, 4H, t, $-\text{Si}-\text{CH}_2-(\text{CH}_2)_2-\text{NH}-$).

^1H NMR was used to calculate the conversion percentage of the silanized polymers. In the case of PCL2000, the internal reference was the signal at 3.86 ppm (**f**, 4H, s, $-\text{CH}_2-$, NEO) fixed at 4H. The conversion percentage was calculated based on the disappearance of the $-\text{CH}_2-\text{NCO}$ from IPTMS at 3.28 ppm (**2'**, triplet, Figure VI-11), according to Eq. 14.

$$\text{Conversion IPTMS (\%)} = \frac{\frac{I_{3.28}^{t_R=0}}{4} - \frac{I_{3.28}^t}{4}}{\frac{I_{3.28}^{t_R=0}}{4}} \times 100 \quad \text{Eq. 14}$$

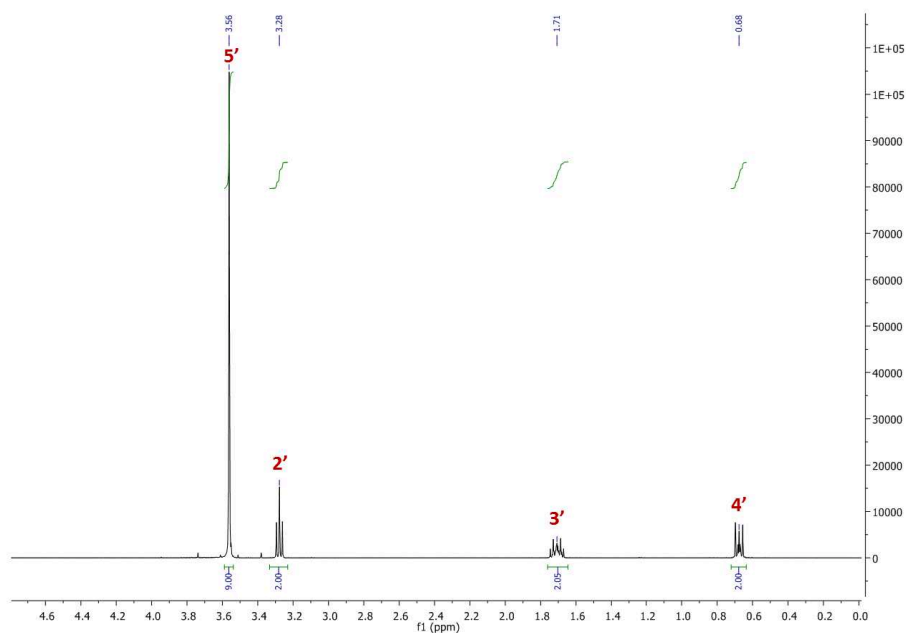
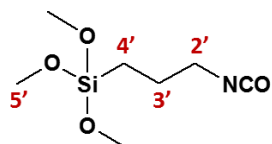


Figure VI-11. ^1H NMR spectrum of (3-isocyanatopropyl)trimethoxysilane (IPTMS) crosslinking agent.

^1H NMR (400 MHz, CDCl_3 , δ , ppm) for IPTES: 3.56 (**5'**, 9H, singlet, $-\text{Si}(\text{OCH}_3)_3$), 3.28 (**2'**, 2H, triplet, $-\text{CH}_2-\text{NCO}$), 1.71 (**3'**, 2H, quintuplet, $-\text{CH}_2-\text{CH}_2-\text{CH}_2-$), 0.68 (**4'**, 2H, triplet, $-\text{Si}-\text{CH}_2-$).

Chapter VI – Experimental section

It was sometimes observed a premature hydrolysis of the trimethoxysilane functions. The hydrolyzed $-\text{Si}(\text{OMe})_3$ percentage was always verified before each formulation at a time t , calculated as below in **Eq. 15**:

$$\text{Hydrolyzed } -\text{Si}(\text{OMe})_3 (\%) = \frac{I_{3.54 \text{ ppm}}^{t_0}/18 - I_{3.54 \text{ ppm}}^t/18}{I_{3.54 \text{ ppm}}^{t_0}/18} \times 100 \quad \text{Eq. 15}$$

With $I_{3.54 \text{ ppm}}^{t_0}$, the intensity of the ^1H NMR signal at 3.54 ppm (**5**, 18H, s, $-\text{Si}(\text{OCH}_3)_3$) of the freshly modified polymer and $I_{3.54 \text{ ppm}}^t$ the intensity of the same signal at a time t before the formulation process.

VI.3.1.7. ^1H NMR kinetics of the hydrolysis of trialkoxysilane functions

^1H NMR experiments were performed to control the hydrolysis kinetics of the trialkoxysilane functions at r.t. in solution with $\text{THF-}d_8$. The freshly prepared trialkoxysilane-terminated polymers (40 mg) were dissolved in 1 mL of $\text{THF-}d_8$ with 10 μL of deionized water to initiate the hydrolysis reaction. Figure VI-12 and Figure VI-13 show the evolution of the proton signals of $-\text{Si-O-CH}_2\text{-CH}_3$ and $-\text{Si-O-CH}_3$ respectively, after different reaction times (t_R) of PCL2000. During the hydrolysis of the triethoxysilane-terminated polymer, ethanol is generated (appearance of a quadruplet at 3.52 ppm) and the signal of the triethoxysilane functions (**5**) is decreasing (quadruplet at 3.79 ppm, Figure VI-12).

During the hydrolysis of the trimethoxysilane-terminated polymer, methanol is generated (appearance of a singlet at 3.26 ppm) and the signal of the trimethoxysilane functions (**5**) is decreasing (singlet at 3.54 ppm, Figure VI-13).

The hydrolysis percentages were calculated according to **Eq. 16** and **Eq. 17** by following the decrease of the signals at 3.79 and 3.54 ppm:

$$\text{Hydrolyzed } -\text{Si}(\text{OEt})_3 (\%) = \frac{I_{3.79}^{t_R=0}/12 - I_{3.79}^{t_R}/12}{I_{3.79}^{t_R=0}/12} \times 100 \quad \text{Eq. 16}$$

$$\text{Hydrolyzed } -\text{Si}(\text{OMe})_3 (\%) = \frac{I_{3.54}^{t_R=0}/18 - I_{3.54}^{t_R}/18}{I_{3.54}^{t_R=0}/18} \times 100 \quad \text{Eq. 17}$$

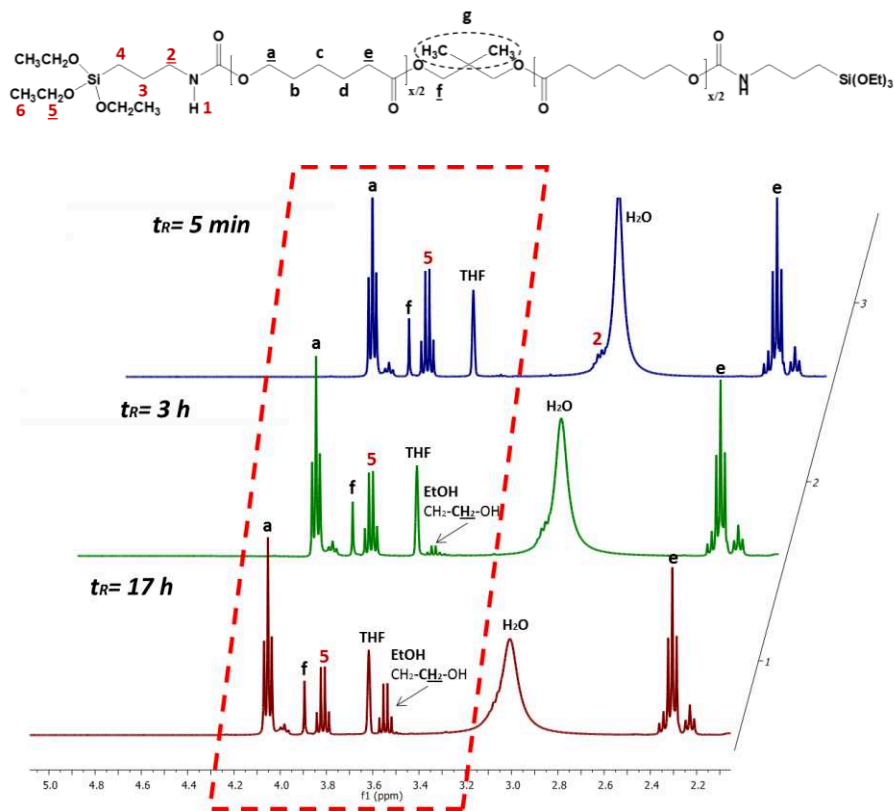


Figure VI-12. ^1H NMR spectra at different reaction times (t_R) for the triethoxysilane-terminated PCL2000 in presence of deionized water (THF- d_6).

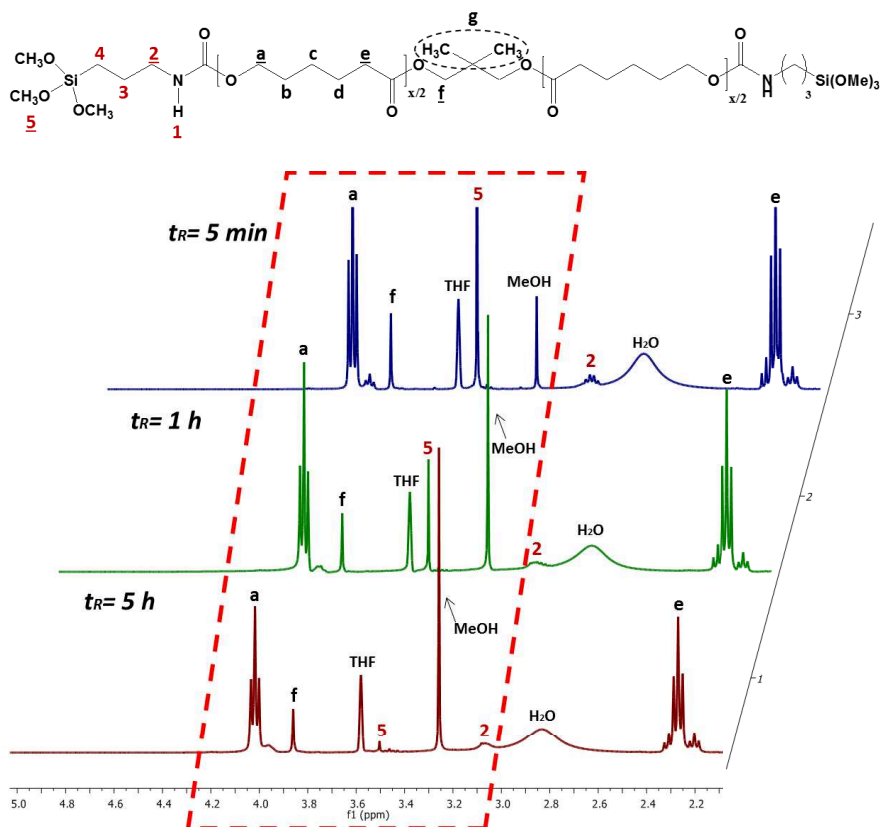


Figure VI-13. ^1H NMR spectra at different reaction times (t_R) for the trimethoxysilane-terminated PCL2000 in presence of deionized water (THF-d_8).

VI.3.2. Size exclusion chromatography

The number average molar mass (M_n) and dispersity (\mathcal{D}) of polymers were measured on a Triple Detection Size Exclusion Chromatography (TD-SEC) with OmniSEC software (Viscotek). The instrument is composed of a GPC Max (comprising a degazer, a pump and an autosampler) and a TDA-302 (RI detector, right and low angle light scattering detector at 670 nm and viscometer) and an UV detector (Knauer). The following Viscotek columns were used: a HHR-H precolumn, a GMHHR-H and a GMHHR-L ViscoGel columns. THF was used as the eluent with a flow rate of 1.0 mL/min at 30°C. Purified polymers were dissolved in THF at *ca.* 10 mg/mL and filtered on a 0.2 μm PTFE filter. Molar masses were calculated using the value of the

Chapter VI – Experimental section

refractive index increment dn/dc for PMATM2 ($dn/dc = 0.044$ mL/g in THF) and PCL ($dn/dc = 0.071$ mL/g in THF) using the OmniSEC software [1,2].

The analysis of the PCL-*b*-PDMS-*b*-PCL triblock copolymer was not possible by TD-SEC in THF due to its refractive index similar to n_{THF} , resulting in no monitored signal with the RI and light scattering detectors. This triblock copolymer was thus analyzed on a SEC apparatus (Waters, Milford, USA) equipped with a refractive index detector, with toluene as eluent at 30°C. The columns used were Styragel HR1, HR4, and HR5. Toluene was used as the eluent at a flow rate of 1.0 mL/min. Polystyrene standards (M_n values varying from 400 to 20,000 g/mol) were used to generate a conventional calibration curve. Data were analyzed using Breeze software (Waters).

VI.3.3. Physico-chemical properties

VI.3.3.1. Contact angle measurements

VI.3.3.1.1. *Dynamic contact angles*

Dynamic contact angles (DCA) experiments were carried out by the advancing-receding drop method using a DSA 30 apparatus (Krüss, Hambourg, Germany) under ambient conditions. A 4 μL -deionized water drop was first placed onto the coating with the syringe tip still immersed within the droplet, then the droplet was grown at a rate of 0.75 $\mu\text{L/s}$ until a final volume of 25 μL for the measurement of the advancing contact angle ($\theta_{w,\text{adv}}$). The receding contact angle ($\theta_{w,\text{rec}}$) was measured by withdrawing the liquid at the same rate (Figure VI-14). It has to be specified that the syringe tip was placed as close as possible to the coating surface to avoid any droplet distortion when aspirating the liquid. For each coating, the reported $\theta_{w,\text{adv}}$ and $\theta_{w,\text{rec}}$ were the average values obtained from 1 cycle of advancing-receding on 3 deionized water droplets (Figure VI-15).

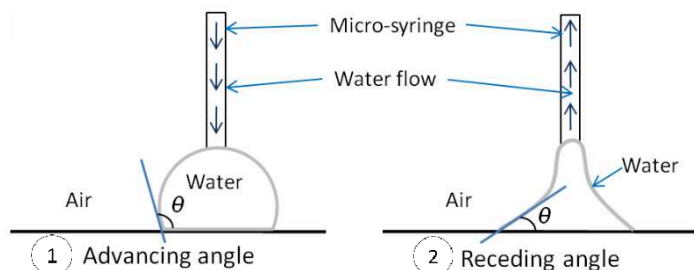


Figure VI-14. Advancing and receding layouts.

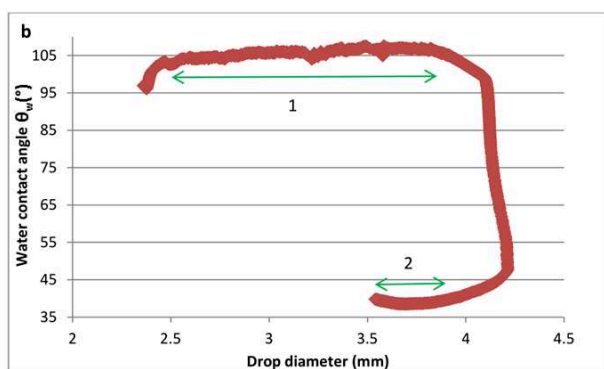


Figure VI-15. Tracking of the dynamic water contact angle as a function of the drop diameter. The means of all the contact angles within the arrows 1 and 2 represent the advancing and receding contact angle respectively.

VI.3.3.1.2. Surface free energy

Static contact angle measurements were performed using a DSA 30 apparatus (Krüss) by the sessile drop technique under ambient conditions. Five contact angle measurements were carried out with 2 μ L-droplets of deionized water (θ_w), diiodomethane (θ_{diiodo}) or *n*-hexadecane (θ_{hex}), after 4 s of stabilization. Diiodomethane and *n*-hexadecane were chosen because they are less polar than water. The SFE of the coatings (γ_s) was determined using the measured liquid contact angles and the surface tensions of the probe liquids (Table VI-8) according to the Owens Wendt method [3]. Both the dispersive (γ_s^D) and the polar (γ_s^P) components of the SFE were assessed ($\gamma_s = \gamma_s^D + \gamma_s^P$). Measurements were performed on pristine samples and samples immersed in ultrapure water (Chapter II) and in deionized water (Chapter IV).

Table VI-8. Surface tensions of the probe liquids [4].

	γ_L (mJ/m ²)	γ_L^D (mJ/m ²)	γ_L^P (mJ/m ²)
Water	72.8	21.8	51.0
Diiodomethane	50.8	48.5	2.3
n-hexadecane	27.6	27.6	0.0

VI.3.4. Thermal properties

VI.3.4.1. Differential scanning calorimetry analysis

The thermal behavior of polymers was analyzed on a Differential Scanning Calorimetry (DSC) equipment (TA Instruments) under a nitrogen flow of 50 mL/min.

To determine the crystallinity (X_c) of PCL and PCL-*b*-PDMS-*b*-PCL, samples (10–15 mg) were first heated at 100°C for 2 min, then cooled down to –90°C at a rate of 1°C/min, kept at –90°C for 2 min, and then reheated to 100°C at a rate of 1°C/min. All values were recorded from the second heating run.

To determine the glass transition temperature of the amorphous PMATM2, PLGA and PLGA-*b*-PDMS-*b*-PLGA, samples (10–15 mg) were cooled down to –90°C at a rate of 20°C/min, kept at –90°C for 2 min, and then reheated to 60°C at a rate of 20°C/min.

To determine the glass transition temperature of the semi-crystalline PCL (within PCL2000, PCL3000 and PCL-*b*-PDMS-*b*-PCL), modulated DSC were performed, samples (10–15 mg) were first heated at 100°C for 2 min then cooled down to –90°C at a rate of 5°C/min, kept at –90°C for 2 min, and then reheated to 100°C at a rate of 2°C/min (conventional DSC experiment did not allow a clear visualization of the PCL glass transition, regardless of the program choice).

Chapter VI – Experimental section

VI.3.4.2. Thermogravimetric analysis

All the thermogravimetric analysis (TGA) were carried out on a TA instrument system under a nitrogen flow of 100 mL/min. Around 20-30 mg of sample was introduced in an alumina crucible under N₂ atmosphere at a heating rate of 10°C/min from 25 to 800°C.

VI.4. Formulation of coatings

VI.4.1. Formulation recipe of hydrolyzable additive-based PDMS coatings

The hydrolyzable polymer additives were dissolved in xylene for 15 min under stirring. The xylene-based solutions were consecutively dispersed within the bis silanol-terminated PDMS at 1500 rpm for 20 min with a Dispermat® apparatus. The DOTDL catalyst was added using a micropipette. The PDES crosslinking agent was further added into the solution at 1500 rpm for 10 min. The mass ratio of PDMS/PDES/DOTDL was 100/4.4/0.1 for all the mixtures.

The solvent amount was adjusted to obtain a similar viscosity for all the formulations (21-26 wt.%) (full description in Table VI-9). The coatings were prepared immediately after mixing components (to avoid phase separation), by casting the formulation onto various substrates. The coatings were cured at room temperature for 24 h with a relative humidity of [38-48] %, measured by a hygrometer. For contact angle measurements, roughness measurements and the hydrolytic degradation tests, samples were prepared by casting *ca.* 2 g of the formulations onto cleaned glass microscope slides (76 × 24 mm²). Samples for dynamic mechanical analyses (DMA) investigations were 1 mm-thick free standing films obtained after casting the formulations onto 5 × 5 cm² cleaned smooth PVC panels, and gently detached from the substrate with a plastic tweezer. The samples for DMA analyses were also used for the hardness measurements by stacking 6 specimens together. Additional applications over 10 × 10 cm² sandblasted and cleaned PVC panels were performed with a bar coater (wet thickness of 300 μm) for field tests and biological assays. The nomenclature of the coatings is YYY-BX, where YYY is the type of hydrolyzable polymer additives (PCL for the PCL homopolymer, TGO for the triblock PCL-*b*-PDMS-*b*-PCL and M3T for the PMATM2 homopolymer), B stands for blend, and X corresponds to the mass fraction of the hydrolyzable polymer within the dry coating.

Table VI-9. Formulation recipes of the YYY-BX hydrolyzable additives-based PDMS coatings and the PDMS reference.

Coating ID	PDMS (wt.%)	Polymer additive (wt.%)	PDES (wt.%)	DOTDL (wt.%)	Solvent (wt.%)
PDMS	74.35	-	3.27	0.07	22.30
PCL-B5	71.43	3.93	3.14	0.07	21.43
PCL-B10	66.18	7.68	2.91	0.07	23.16
PCL-B15	61.37	11.32	2.70	0.06	24.55
TGO-B5	71.43	3.93	3.14	0.07	21.43
TGO-B10	66.18	7.68	2.91	0.07	23.16
TGO-B15	61.37	11.32	2.70	0.06	24.55
M3T-B5	71.43	3.93	3.14	0.07	21.43
M3T-B10	66.18	7.68	2.91	0.07	23.16
M3T-B15	61.37	11.32	2.70	0.06	24.55
M3T-B20	56.94	14.88	2.51	0.06	25.62

Due to the limited miscibility of PCL within the silicone matrix, the maximum amount of PCL was up to 15 wt.%. Above this quantity, the coatings with PCL-based additives displayed a macroscopic phase segregation, while coatings with 20 wt.% of PMATM2 could be achieved without incompatibility issues at the macroscale level.

VI.4.2. Formulation recipe of the PDMS/polyester hybrid networks-based coatings

The reference coating, pristine PDMS elastomer, was prepared by adding a solution of PDES in THF to the bis silanol-terminated PDMS with a SiOH/SiOEt molar ratio of 100/3.3, considering a PDES functionality of 12. PDMS/polyester networks were prepared using the polyester macrocrosslinkers with the same molar ratio of reactive functions [SiOH/SiOMe] = [100/3.3], with a macrocrosslinker functionality of 6.

The macrocrosslinkers were dissolved in THF and consecutively dispersed within the bis silanol-terminated PDMS for 20 min. The DOTDL catalyst (*ca.* 0.3 wt.% in the total solution) and the co-solvent (ethanol) were further added into the solutions. The formulations were

Chapter VI – Experimental section

preheated at 40°C for 15 min under agitation. The coatings were formed by casting 1.5 to 2 g of the 20-55 % (wt/wt) THF-based formulations onto cleaned glass microscope slides (76 x 24 mm²) for mass loss tests, contact angle, roughness and infrared analysis. To obtain free films of 1 mm-thickness for DMA, AFM and SEM-EDX analyses, *ca.* 3.5 g of the solutions were also casted onto smooth PVC substrate (5 × 5 cm²) to ease their removal from the substrate. The film coatings were dried for 3 days at 60°C in a humidity-saturated atmosphere with a daily renewal of the air to remove the released methanol and co-solvent. The dry coating thickness was 480-660 μm, measured by a micrometer gauge.

The nomenclature used for the four final PDMS/polyester hybrid networks is ZZZZ-NX/Y with ZZZZ the code name for the polyester-based polymer. With PCL= poly(ϵ -caprolactone) diol (2,000 g/mol), PLGA= poly(D,L-lactide-*co*-glycolide) (740 g/mol), LGO= PLGA-*b*-PDMS-*b*-PLGA (5,200 g/mol) and TGO= PCL-*b*-PDMS-*b*-PCL (6,800 g/mol). N refers to “network”, X refers to the mass percentage of PDMS in the dry coating and Y refers to the mass percentage of the polyester content in the dry coating.

The composition of the three self-crosslinked polyester-based networks was also shown in Table VI-10. The experimental procedure to obtain them was the same as for the PDMS/polyester hybrid networks

A particular coating named PLGA+M3T shown in Table VI-10 corresponds to the combination of both strategies: by adding 5 wt.% of the PMATM2 hydrolyzable additive (relative to the dry coating) within a the PDMS/PLGA hybrid network containing 12 wt.% of PLGA (relative to the dry coating).

Chapter VI – Experimental section

Table VI-10. Formulation recipes of the PDMS/polyester hybrid networks, the self-crosslinked polyester-based networks, the PDMS reference and the PLGA+M3T combining both hydrolyzable additives and a hydrolyzable network.

Coating ID	PDMS (wt.%)	(Macro)crosslinker (wt.%)	PMATM2 (wt.%)	DOTDL (wt.%)	THF (wt.%)	Ethanol (wt.%)
PDMS	74.9	2.5	-	0.2	22.5	-
PLGA-N88/12	55.7	7.8	-	0.2	33.4	2.8
LGO-N88/12	39.2	19.6	-	0.2	39.2	2.0
PCL-N83/17	53.6	11.4	-	0.2	32.2	2.7
TGO-N73/27	27.1	17.3	-	0.2	54.1	1.4
PLGA-S70	-	59.8	-	0.2	38.8	1.2
PCL-S86	-	59.8	-	0.2	38.8	1.2
TGO-S65	-	59.8	-	0.2	38.8	1.2
PLGA+M3T	53.1	7.7	4.5	0.2	31.8	2.7

VI.5. Characterization of the PDMS-based coatings

VI.5.1. Physico-chemical properties

VI.5.1.1. Contact angle measurements

VI.5.1.1.1. *Modified time lag method*

A modified time lag test was performed, as described by Noguier et al.[5], in which a free thin PDMS membrane of 90 μm was deposited onto the tested coating. The PDMS membrane had the same composition as the silicone-based coatings to maintain the same crosslinking density. Then a water droplet of 25 μL was placed on top of the PDMS membrane and protected from the surrounding environment by a glass cell to avoid both the contamination and the quick evaporation of the water droplet. The water contact angle of the droplet was monitored for 1 h with DSA 30 apparatus (Krüss) under ambient conditions.

Chapter VI – Experimental section

VI.5.1.1.2. *Dynamic contact angles*

The dynamic contact angles (DCA) of the coatings were measured the same way than the pure polymer films (§ VI.3.3.1.1).

VI.5.1.1.3. *Surface free energy*

The surface free energy (SFE) of the coatings was measured the same way than the pure polymer films (§ VI.3.3.1.2).

VI.5.1.2. Roughness measurements

Surface roughness profiles were measured by a contact type stylus profiler (Taylor Hobson, Ultra Version 6.1.12.1 software) using a 2 μm radius tip and a 0.1 μm radius diamond tip, with a minimum applicable 1 mN stylus load. The stylus moved across 15 mm length of the coating surface (40 mm if $R_a > 10 \mu\text{m}$), at a constant velocity of 0.50 mm/s to obtain surface height variations. R_a values were assessed from the average of three measurements. According to ISO 4288-1996, the selected cut-off wavelength (low-pass filter) was $\lambda_c = 0.08 \text{ mm}$ when $R_a < 0.02 \mu\text{m}$, $\lambda_c = 0.25 \text{ mm}$ when $0.02 < R_a < 0.1 \mu\text{m}$, $\lambda_c = 0.8 \text{ mm}$ when $0.1 < R_a < 2 \mu\text{m}$, $\lambda_c = 2.5 \text{ mm}$ when $2 < R_a < 10 \mu\text{m}$ and $\lambda_c = 8 \text{ mm}$ when $R_a > 10 \mu\text{m}$. The high-pass filter (λ_s) was fixed at 0.0025 mm for all the samples.

VI.5.1.3. Infrared spectroscopy

Fourier transform infrared spectroscopy (FTIR) of coatings was performed in the attenuated total reflection (ATR) mode by using a Nicolet iS50 FT-IR system equipped with an ATR cell with a diamond crystal. The coatings were applied directly onto the surface of the crystal. Spectra resulted from the accumulation of 32 scans at 4 cm^{-1} resolution. The measured wavenumber range was 4000–600 cm^{-1} . All the original spectra were baseline corrected using the Omnic™ Spectra software.

VI.5.2. Residue extraction test

Several pieces of the same elastomer coating (ca.50 mg) were introduced into three volumetric flasks (1 mL). They were filled with CDCl_3 and an internal reference (heptane) necessary to calculate the residue content. The elastomeric materials contained in the stoppered flasks were allowed to swell for 6 h in an ultrasonic bath, and further 6 h without ultrasound at room temperature. Then, the solvent of the volumetric flask was withdrawn and analyzed by ^1H NMR to quantify the residue content using **Eq. 18** (either for PDMS or polyester macrocrosslinker residues):

$$\% \text{ residue} = \frac{\frac{[\text{heptane}]}{I_{0.89}^{\text{heptane}}} \times \frac{I_{x \text{ ppm}}^{\text{residue}}}{n_{\text{H}}} \times V_0}{m_0} \times 100 \quad \text{Eq. 18}$$

Where n_{H} is the number of protons corresponding to the residue signal at x ppm, $[\text{heptane}]$ is the concentration of the internal standard heptane in the volumetric flask (in g/mL), V_0 is the volume of (THF + heptane) within the volumetric flask before the addition of the elastomeric pieces with a mass of m_0 . $I_{0.89}^{\text{heptane}}$ corresponds to the intensity of the signal at 0.89 ppm (t, 6H, $-\text{CH}_3$ of the heptane). $I_{x \text{ ppm}}^{\text{residue}}$ corresponds to the intensity of the signal at x ppm for the designated polymer and n_{H} the number of protons involved at this chemical shift.

VI.5.3. Scanning electron microscopy

Scanning electron microscopy was used in combination with energy dispersive X-ray spectroscopy (SEM-EDX). The electron bombardment was produced with a 15-keV accelerating voltage. The coatings surface was metallized with gold before analysis. The coatings surface was observed by using the secondary electrons detector (SE2). The samples used for SEM-EDX were the same used for AFM analyses and DMA.

VI.5.4. Confocal laser scanning microscopy

Confocal laser scanning microscopy (CLSM) was used with the He-Ne laser (with $\lambda_{\text{excitation}} = 594$ nm and $\lambda_{\text{emission}} = 633$ nm). The analysis was directly performed on the PDMS-

Chapter VI – Experimental section

coated microscope glass slide after 6 h of drying for the PDMS immersed at 1 day and 6 months in deionized water.

VI.5.5. Thermo-mechanical properties

VI.5.5.1. Dynamic mechanical analysis

The dynamic mechanical analysis (DMA) were performed using free standing films of 10–14 mm length, 8–10 mm width and 0.6–1.0 mm thick. The storage modulus E' of the samples was determined at 25°C with a dynamic mechanical analyzer (TA Instrument Q800) operating in tensile strain-sweep mode. A frequency of 1 Hz, a preload of 0.01 N, and amplitudes from 5 to 50 μm (within the linear viscoelastic region) were used. The results are the average of 5 measurements on 3 different samples.

In the case of the PDMS/polyester hybrid networks and self-crosslinked polyester-based polymers, the storage modulus (E') and $\tan \delta$ were also studied between -150°C and 100°C with the same apparatus at 3°C/min with a frequency of 1 Hz, a preload of 0.1 N, and amplitude of strain of 10 μm . To avoid undesired breaking of the free films during the experiments, the screws of the clamps were tightened once the temperature reached -150°C (at the end of the cooling process).

VI.5.5.2. Differential scanning calorimetry analysis

The thermal behavior of the hydrolyzable additive-based PDMS coatings, PDMS/polyester networks and self-crosslinked polyester-based networks were analyzed on a TA instrument system under a nitrogen flow of 50 mL/min.

To determine the crystallinity values, $X_c(\text{PCL})$ and $X_c(\text{PDMS})$, samples (10-15 mg) were first heated at 100°C at a rate of 20°C/min then cooled down to -90°C at a rate of 1°C/min, kept at -90°C for 2 min, and then reheated to 80°C at a rate of 10°C/min. All DSC values were obtained from the second heating. The very low cooling rate was chosen to maximize the crystallinity of PDMS and PCL.

Chapter VI – Experimental section

VI.5.5.3. Thermogravimetric analysis

The thermogravimetric analysis of the different coatings were performed the same way than the pure polymers (§ VI.3.4.2).

VI.5.5.4. Atomic force microscope

Atomic force microscope (AFM) with the Peak Force tapping mode was used to map the variations in material properties across the coatings surface. Briefly, the AFM probe, constituted of a tip and a cantilever, sweeps the surface. The information about the cantilever deflection and piezo position can be converted to force vs distance curves describing the tip-sample interaction during approach and separation (Figure VI-16). From such a force curve, the surface deformation amplitude (nm), surface adhesion force (nN) and surface elastic modulus (MPa) can be read. The elastic modulus was calculated based on the Derjaguin-Muller-Toporov (DMT) model (Eq. 19).

$$F = \frac{4}{3} \times E^* \times \sqrt{R \times d^3} + F_{adh} \quad \text{Eq. 19}$$

Where, F is the force, E^* is the effective elastic modulus, R is the tip radius, d is the deformation value at a given force and F_{adh} is the maximum adhesion force.

The mechanical properties of the PDMS/polyester hybrid networks were observed using a soft cantilever ($k \approx 0.54$ N/m) whereas the self-crosslinked polyester-based polymers were observed using a stiffer cantilever ($k \approx 15.92$ N/m). DMT model was used regardless of the coating nature for comparative purposes.

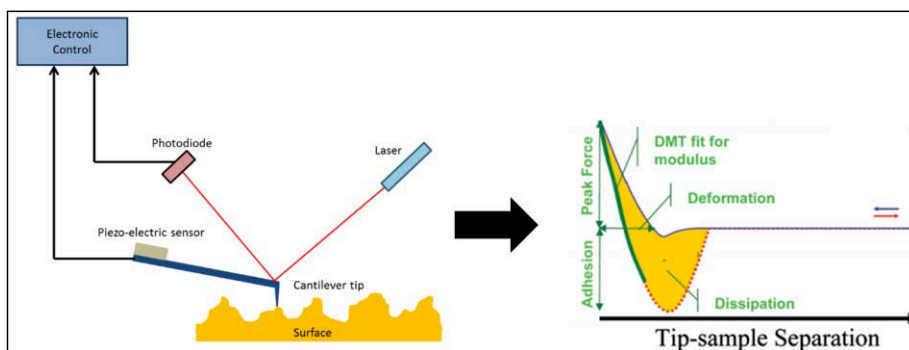


Figure VI-16. AFM operating principle.

VI.6. Erosion properties

VI.6.1. Water uptake test

The experimental coatings were immersed in deionized water at room temperature during 26 weeks (for the self-crosslinked polyester-based polymers) and during 50 weeks (for the PDMS/polyester hybrid networks). They were removed every week to be weighted. Once out of the water, they were rinsed abundantly to remove the residual degradation products. They were gently dabbed with a very thin paper to eliminate the exceeding water and subsequently weighted to measure the water uptake (Eq. 20). The reported water uptake results were the mean value of three replicates, weighted on an analytic balance (Denver Instrument) with a precision of 0.1 mg and calibrated prior to each measurement.

$$\text{Water uptake (\%)} = \frac{(W_{\text{wet},t} - W_{\text{dry},t})}{W_{\text{wet},t}} \times 100 \quad \text{Eq. 20}$$

Where $W_{\text{wet},t}$ is the mass of the wet coated glass slide (in g), $W_{\text{dry},t}$ is the mass of the dry coated glass slide after an immersion time t (in g).

VI.6.2. Mass loss test

The mass loss of silicone-based coatings was carried out by immersing coated glass slides for 24 weeks in deionized water. Before gravimetric measurements, the coatings were gently rinsed with deionized water and dried at room temperature for 12 h. The reported mass loss results were the mean value of three replicates, weighted on an analytic balance (Denver Instrument) with a precision of 0.1 mg and calibrated prior to each measurement. The mass loss (wt %) was calculated using Eq. 21.

$$\text{Mass loss (\%)} = \frac{(W_o - W_{\text{dry},t})}{(W_o - W_s)} \times 100 \quad \text{Eq. 21}$$

Where W_o is the initial mass of the coated glass slide (in g), $W_{\text{dry},t}$ is the mass of the dry coated glass slide after an immersion time t (in g) and W_s is the mass of the non-coated glass slide (in g).

VI.6.3. Thickness loss test

The coatings were applied onto a plastic foil using of a film applicator (bar coater) leaving 200 μm wet film thickness and subsequently dried for 3 days at 60°C. The plastic foil was previously cleaned with ethanol, scratched and coated with 20 μm wet film of a three-pack tie-coat Nexus (Hempel) in order to secure adhesion. The four coatings (7 \times 3 cm^2) were left to dry for 1 week at room temperature before testing. The coated plastic foil was then fixed onto a stainless steel cylindrical drum with a diameter of 45 mm. The cylindrical drum was then immersed within a 60 liters-tank filled with ASW at 40°C. During the first 24 h of test, a low speed of 350 rpm was chosen to allow the hydration of the coating. After this short hydration period, the speed was kept at 650 rpm for the total duration of the test.

Before each thickness measurement (using an Elcometer 276 measurement probe), the drum was rinsed and dried at room temperature for 15 minutes. The Elcometer was first calibrated with two standards (252 and 126 μm) on a second identical cylindrical drum (non-coated). A template was adapted on the cylindrical drum in order to always measure the coating thickness at the same place of the coating. To protect the coating from mechanical damage during thickness measurements, a 10 μm -thick foil was placed between the coating and the template. Dry coating thickness was measured at eight different positions, and ten thickness measurements were recorded for each of them (aberrant values were not taken into account). At the end of the measurements, the Elcometer device was checked again with the two standards to notice any unwanted deviations. Whenever the deviations were significant, the measures were performed a second time.

Salinity was measured every two days through conductivity measurements ($C \approx 58\text{-}62 \text{ mS/m}^2$, $\text{Sal.} \approx 30\text{-}32$). The seawater level in the tank was adjusted by adding demineralized water on demand to compensate any evaporation losses. The artificial seawater pH was controlled and corrected every 2 days by adding either NaOH (0.1 M) or HCl (0.1 M) solutions until the stabilization of pH at 8.20 ± 0.05 .

VI.7. Antifouling properties

VI.7.1. Field test

The coated panels (10 × 10 cm²) were fully immersed in a vertical position in the Mediterranean Sea, in the Toulon Bay (43°06'25"N; 5°55'41"E), at a relatively shallow depth of water (1-1.4 m). The antifouling (AF) performances in static conditions were evaluated every month. Two or three replicates of each coating were investigated, from which one was cleaned with a sponge, every 3 months, for assessing the fouling release (FR) properties. A sand-blasted uncoated PVC panel was also immersed as a negative control.

A French practice adapted from the French NF T 34-552 standard (sept. 1996) was used to assess the AF efficacy of the coatings [6]. This standard requires to report: (i) the type of macrofoulers attached to the surface, and (ii) the estimated percentage of the surface covered by each type of macrofoulers (intensity factor (IF), Table VI-11). The inspection was performed 1 cm from the edges of the panel. An efficacy factor N was defined as follows in Eq. 22.

$$N = \sum(IF \times SF) \quad \text{Eq. 22}$$

Where SF is defined as a severity factor (Table VI-11), which takes into account the frictional drag penalty of ship hulls attributable to increased surface roughness due to foulers [6]. The best antifouling efficacy is assigned to coatings with a N value of 5, which corresponds to a surface fully covered by a biofilm. The worse antifouling efficacy is attributed to the negative control with a N value which tends to *ca.* 40.

Table VI-11. Intensity factor value according to the % coverage of the panel.

% Coverage	Intensity factor IF
No fouling	0
0 ≤ % ≤ 10	1
10 ≤ % ≤ 20	2
20 ≤ % ≤ 40	3
40 ≤ % ≤ 60	4
60 ≤ % ≤ 100	5

Chapter VI – Experimental section

Table VI-12. Severity factor value according to the fouling type.

Fouling type	Severity factor SF
Biofilm	1
Algae (brown, red, green)	3
Non-encrusting species (hydrozoa, sponges, ascidians ...)	4
Encrusting species (barnacles, tubeworms, spirorbis, bryozoans, shells...).	6

The FR performance, ranging from 0 to 2 (0 = worst, 2 = best), was evaluated by cleaning the coating with a sponge on the lower half of the coated panel and assessing the level of detachment of the marine organisms.

These two inspection procedures provide meaningful information on both the AF/FR activity of the coatings and their long-term durability in an aggressive, real-world environment. However static immersion field tests may be susceptible to the seasonal diversity and abundance of fouling, at the test site.

VI.7.2. Bioassays

VI.7.2.1. Larval barnacle culture and settlement assay of *A. Amphitrite* Cyprids

Adult and larval barnacle cultures were performed with *Amphibalanus amphitrite* as described by Othmani et al.[7]. For anti-settlement assays, 2 mL of filtered sea water (FSW) were pipetted onto four different locations of each coating. Active cyprids were pipetted from the stock solution (~100 cyprids/mL) together with 200 µL of FSW. Thus, around 10 to 20 cyprids were allocated into each drop while adding 200 µL to the 2 mL drop of FSW. Incubation of cyprids on coating samples was carried out, at 22°C, for 7 days, in a humid chamber to avoid excessive evaporation of water in the dark. This procedure allowed efficient settlement and transformation of cyprids, after which time, attached or metamorphosed individuals were counted under a binocular microscope. A poly(styrene) (PS) plate was used as control to evaluate the ability of the larvae to settle. A one-way ANOVA (Analysis of Variance) followed by post-hoc tests (Tuckey) was performed to determine which of the coatings showed a significant difference compared to the control for cyprid adhesion. The adhesion percentage

Chapter VI – Experimental section

is defined as the number of alive fixed cyprids divided by the total number of tested cyprids. Barnacle larvae are prone to settle on the inert PS control surface with adhesion of 80%-100% of the larvae.

VI.7.2.2. Settlement and removal assays of diatom *N. incerta*

Standard protocols were used to measure the settlement and adhesion strength of cells of the diatom *N. incerta* which was isolated from rocks at Llantwit Major beach [8]. The PDMS/polyester hybrid networks were investigated. In brief, cells in log phase were washed three times in filtered ASW, resuspended, then filtered through 20 and 50 mm nylon meshes. The culture was diluted to a chlorophyll *a* content of 0.25 mg/mL. Six replicate slides of each experimental coating and control test surface were placed in compartments of QuadriPerm dishes and 10 mL of diatom suspension were added. After 2 h on the laboratory bench at room temperature, the slides were washed vigorously in filtered ASW to remove unsettled (unattached) diatoms. Three replicate slides of each experimental coating and control test surface were fixed and quantified as described previously in Mieszkin et al. [9] for spores of *U. linza* while the other three replicates slides were exposed for 5 min to a wall shear stress of 34 Pa in a calibrated water channel and processed as above. The number of cells remaining after flow was compared to the unexposed samples to evaluate the adhesion strength of cells on each test surface. The tested samples are given in Table VI-13.

Table VI-13. Characteristics of hybrid network-based coatings used in diatom *N. incerta* bioassays.

Sample n°.	Tested coating	Thickness	No. of slides
1	PLGA-N88/12	900 µm	6
2	TGO-N73/27	130 µm	6
3	PCL-N83/17	900 µm	6
4	PDMS reference	800 µm	6
5	Glass reference	n/a	6

VI.7.2.3. Settlement and removal assays of *Ulva* spores

▪ *Ulva rigida* cultures and sporulation

Ulva rigida specimens were collected on the coast of Cap Sicié (43°2.938'N, 5°50.791'E, Var, France) in Spring 2018. Thalli were maintained and allowed to grow until use in an outdoor 3000 L sea water tank under semi natural conditions (light and temperature) to which was

Chapter VI – Experimental section

added 30 μM NaNO_3 , 0.6 mM urea, 6 μM $\text{NH}_4\text{H}_2\text{PO}_4$ and 2 μM FeCl_3 final concentrations. To induce sporulation, mature thalli were transferred and maintained in a 10 L sea water tanks with gentle aeration during 24h in the dark at 25°C. Seawater was enriched with 191 μM K_2SO_4 , 56 μM $\text{NH}_4\text{H}_2\text{PO}_4$, 792 μM urea, 0.57 μM FeSO_4 (modified from Jimenez del Rio et al., 1996). After 24h, thalli were rinsed three times with fresh seawater, placed in 1L seawater beaker and hand-pressed to release zoospores. Spores were attracted to a light spot where they were pipetted into ice cold 0.2 μm filtered seawater (FSW, 38 psu). This step was repeated twice to wash and concentrate spores. Spores were verified under a microscope for the presence of four flagella and concentration of spores was determined using a Kova® slide.

▪ *In vitro* *Ulva rigida* spore settlement assays

Spore stock solutions were diluted into FSW to 2.10^5 spores per ml before assays. Polypropylene black microtiter 96-wells plates (Greiner®) containing the various coatings were filled with 100 μl of the spore working solution (2.10^4 spores per well) and incubated in the dark at 25°C overnight. Plates were then emptied by inversion and washed three times with FSW to remove unattached or weakly attached spores. Wells were refilled with 100 μl of FSW before measuring fluorescence emitted by chlorophyll presents in the zoospores using a TECAN® Infinite 200 plate reader (Bunet *et al.*, in preparation). Excitation and emission filters used to detect fluorescence were 430 nm and 670 nm respectively. Within each well, the fluorescence intensity was determined at the bottom of the well in five different spots. Attachment controls (FSW with or without spores) were performed in wells without coatings (polypropylene and polystyrene plates, Greiner®). The intrinsic autofluorescence of coatings was quantified in wells where only FSW with no spores was added.

▪ Settlement and adhesion strength of spores of *U. linza*

Standard protocols were used to measure the settlement of spores and their adhesion strength after settlement [9]. In brief, motile spores (zoospores) were released from fertile plants of *U. Linza* collected from Llantwit Major beach, Wales, UK (518400N; 38480W). The spore concentration was adjusted to $\text{OD}_{600\text{nm}} = 0.15$ (1.0×10^6 spore/mL) using filtered ASW. Twelve replicate slides for each experimental coating and control test surface were placed in individual compartments of QuadriPerm dishes (Greiner One) and 10 mL of spore suspension were added to each compartment. After incubation for 45 min in darkness at room

Chapter VI – Experimental section

temperature, all slides were washed in filtered ASW to remove unsettled (motile) spores. Three replicate slides of each coating and control test surface were fixed with 10 mL of 2.5 % (v/v) glutaraldehyde in filtered ASW and then washed and allowed to air-dry over-night. Settled spores were counted by chlorophyll autofluorescence using epifluorescence microscopy ($\times 20$ objective; λ excitation and emission: 546 and 590 nm, respectively) as described above.

To assess the adhesion strength of the settled spores, three replicate slides of each coating and control test surface were exposed for 5 min to a wall shear stress of 52 Pa in a calibrated water channel. Settled spores were fixed and counted as previously described. The number of spores remaining after flow was compared to the unexposed samples and the percentage removal of spores was calculated for each coating and control test surface. The six remaining slides for each test surface were used to cultivate sporelings (young plants). Ten milliliters of enriched seawater medium were added to each compartment of the QuadriPerm dishes, which were incubated at 18°C with a 16 h:8 h light:dark cycle with a light intensity of $40 \mu\text{mol}/\text{m}^2/\text{s}^2$, for 7 days to allow the growth of sporelings. The medium was refreshed after 24 h and then every 2 days.

- **Adhesion strength of sporelings of *U. Linza***

The biomass of sporelings after 7 days growth on each coating and control test surface was estimated by quantifying the fluorescence of chlorophyll in a plate reader (λ excitation and emission: 430 and 670 nm, respectively, TECAN Genios Plus). Fluorescence was measured as relative fluorescence units (RFU) and was the mean of a 168-point fluorescence reading taken within an area 6×1.9 cm along the middle of the slide. One slide for each test surface, previously hydrated in sterilized ASW, was used to blank the plate reader. RFU values from the TECAN are directly proportional to the concentration of DMSO-extractable chlorophyll *a* over the range of 0–2 mg chl *a*/cm². The six replicate slides per test surface were exposed for 5 min to a shear stress of 60 Pa (depending on the adhesion strength of the sporelings to each particular coating), in a calibrated water channel. Biomass remaining after flow was quantified as described above and was compared to the unexposed samples to evaluate the adhesion strength of sporelings as percentage removal of biomass on each test surface.

The tested samples are given in Table VI-14.

Chapter VI – Experimental section

Table VI-14. Characteristics of hybrid network-based coatings used in *U. linza* sporelings bioassays.

Sample n°.	Tested coating	Thickness	No. of slides
1	PLGA-N88/12	900 µm	6
2	TGO-N73/27	130 µm	6
3	PCL-N83/17	900 µm	6
4	PDMS reference	800 µm	6
5	Glass reference	n/a	6

VI.8. Bibliographical references

1. Lejars, M.; Margaillan, A.; Bressy, C. Synthesis and characterization of diblock and statistical copolymers based on hydrolyzable siloxy silylester methacrylate monomers. *Polymer Chemistry* **2014**, *5*, 2109-2117.
2. Li, X.; Zhang, Q.; Li, Z.; Xu, S.; Zhao, C.; Chen, C.; Zhi, X.; Wang, H.; Zhu, N.; Guo, K. Tripodal hydrogen bond donor binding with sulfonic acid enables ring-opening polymerization. *Polymer Chemistry* **2016**, *7*, 1368–1374.
3. Lejars, M.; Margaillan, A.; Bressy, C. Fouling Release Coatings: A Nontoxic Alternative to Biocidal Antifouling Coatings. *Chem. Rev.* **2012**, *112*, 4347–4390.
4. Kaelble, D.H. Dispersion-Polar Surface Tension Properties of Organic Solids. *The Journal of Adhesion* **1970**, *2*, 66–81.
5. Camós Noguer, A.; Olsen, S.M.; Hvilsted, S.; Kiil, S. Diffusion of surface-active amphiphiles in silicone-based fouling-release coatings. *Progress in Organic Coatings* **2017**, *106*, 77–86.
6. Bressy, C.; Brian, J.F.; Compère, C.; Réhel, K., Efficacy testing of biocides and biocidal coatings. *Biofouling Methods*, **2014**; John Wiley & Sons, Inc.: Hoboken, NJ, USA, Vol. 1, 12, 332-345, ISBN:9780470659854.
7. Othmani, A.; Bunet, R.; Bonnefont, J.-L.; Briand, J.-F.; Culioli, G. Settlement inhibition of marine biofilm bacteria and barnacle larvae by compounds isolated from the Mediterranean brown alga *Taonia atomaria*. *Journal of Applied Phycology* **2016**, *28*, 1975–1986.
8. Finlay, J.A.; Bennett, S.M.; Brewer, L.H.; Sokolova, A.; Clay, G.; Gunari, N.; Meyer, A.E.; Walker, G.C.; Wendt, D.E.; Callow, M.E.; et al. Barnacle settlement and the adhesion of protein and diatom microfouling to xerogel films with varying surface energy and water wettability. *Biofouling* **2010**, *26*, 657–666.
9. Mieszkin, S.; Martin-Tanchereau, P.; Callow, M.E.; Callow, J.A. Effect of bacterial biofilms formed on fouling-release coatings from natural seawater and *Cobetia marina* on the adhesion of two marine algae. *Biofouling* **2012**, *28*, 953–968.

CONCLUSION AND PERSPECTIVES

The objective of this PhD work was to develop hybrid antifouling coatings, at the frontier between FRC and SPC technologies, without using any biocide. These coatings had to combine erosion or hydrolysis properties such as those encountered in SPCs and low elastic modulus such as those encountered in PDMS based FRCs. To achieve this objective, two strategies were performed. In the first strategy, some hydrolyzable polymers were added into a PDMS elastomer at various content, in the second strategy, some hydrolyzable polymers were crosslinked with PDMS chains.

In the first Chapter, a bibliographic study reports on the major antifouling technologies used in the industry world as well as those developed in the academic research. This enabled to highlight the great rise of more environmentally friendly FRCs, and more precisely the rise of hybrid antifouling coatings. These complex coatings can combine silicone elastomers with various compounds such as amphiphilic copolymers, carbon nanotube, poly(urethane)s or even biocides. No antifouling systems comprising a silicone elastomer and hydrolyzable polymers were studied until now.

Chapter II dealt with the first strategy consisting in adding hydrolyzable polymers to a conventional condensation cure silicone elastomer. The three hydrolyzable polymers were either synthesized by RAFT (poly(bis(trimethylsilyloxy)methylsilyl methacrylate) = PMATM2) or kindly supplied (poly(ϵ -caprolactone)-based polymers). These polymers were first studied alone to characterize their surface physico-chemical properties before and after contact with water. This information was essential to understand the surface changes between the PDMS reference and the coatings containing 5 to 20 wt.% of hydrolyzable additives. The coatings displayed rather similar wetting properties, surface free energies, elastic moduli and roughness values to that of the PDMS reference. This enables to rightfully designate these hydrolyzable additive-based PDMS coatings as FRCs. DCA highlighted the very ambiguous surface chemistry of PMATM2-based PDMS coating (M3T-BX) as they still displayed hydrophobic surfaces after some times in water while showing a very important contact angle hysteresis due to the fast hydrolysis of PMATM2. PCL-BX and TGO-BX also showed higher hysteresis contact angles than the PDMS reference, mainly attributed to a chemical surface reorganization and surface heterogeneity, respectively. A mass loss test combined with a

Conclusion and perspectives

chemical surface analysis by FTIR-ATR highlighted two different trends. First trend was the reservoir effect of PMATM2-based coatings after 12 weeks of immersion as well as a complete release of both PMATM2/PMAA from the PDMS bulk. Second trend was, on the contrary, the absence of mass loss with no significant changes of surface chemistry for the PCL-based coatings, although some characteristic bands of polyester were observed on TGO-BX surfaces.

Chapter III introduced new hydrolyzable polymers obtained by ring opening polymerization such as PLGA and PLGA-*b*-PDMS-*b*-PLGA. These polymers were chosen as they exhibit intermediate hydrolysis kinetics between PCL and PMATM2. The optimal conditions to crosslink polyester-based polymers with a bis-silanol PDMS oil were then studied. The silanization agent, the curing temperature, nature of solvent and co-solvent played important roles in the crosslinking reaction. Other parameters were also studied such as the molar mass and architecture of the polyester-based polymers (homopolymer or triblock copolymer). At the end, the functionalization of the polymers chain ends was successfully carried out leading to the formation of trimethoxysilane-terminated polymers as new macrocrosslinkers. The resulting PDMS/polyester hybrid networks were analyzed through a residue extraction test to assess the % of non-crosslinked polymers. The results of the extraction test showed a well crosslinking of all the polyester-based networks.

Chapter IV presented the surface and bulk characterizations of the PDMS/polyester hybrid networks before water immersion. The behavior of the networks during water immersion was also investigated. The aim of this chapter was first to identify the microstructure of these peculiar networks. The dual chemistry was highlighted by different analysis such as SEM-EDX, AFM, FTIR-ATR, DSC and DMA. Results from the microscope analysis (SEM and AFM) revealed interesting microphase segregations, with some various sizes of hard-soft and/or rough-smooth domains, depending on the nature and content of the polyesters.

Surface physico-chemical analyses indicated different topographies and wetting profiles of coating surfaces during water immersion. Globally PLGA-N88/12 showed very promising results given that it maintained a long-term hydrophobicity (same for LGO-N88/12) and a very soft and smooth surface when immerse in water under static conditions.

DMA were useful to assess the elastic modulus, which is a key parameter for FR ability. All the PDMS/polyester networks exhibited satisfying viscoelastic properties (elastic modulus not exceeding 6 MPa). Finally, a mass loss test combined with a thickness loss test brought

Conclusion and perspectives

information on the erosion properties of the PDMS/polyester hybrid networks. LGO-N88/12 may have leached some unbonded PDMS or PLGA-*b*-PDMS-*b*-PLGA oils during the mass loss test due to its partial crosslinking. Nevertheless, the resulting linear mass loss profile of LGO-N88/12 could be very interesting for AF applications. All the quoted analyses suggested these PDMS/polyester hybrid networks could represent a novel category of hybrid FRCs, even though some FRCs properties were not maintained after immersion such as the low surface free energy and the smooth surface.

Chapter V showed the AF and FR properties of the experimental coatings from the two AF strategies. M3T-BX coatings as showed improved antifouling properties during the first 3 months of static immersion thanks to their chemical evolving surfaces, without the use of biocides. PCL-BX and TGO-BX showed very similar or slightly better AF/FR properties to those of PDMS reference suggesting there was a modest positive effect of the poly(ϵ -caprolactone) additive during prolonged static immersions. The bioassays revealed M3T-B15/20, PCL-B15 and TGO-B15 had very promising anti-barnacle larvae properties. The AF and FR properties of the PDMS/polyester hybrid networks decreased after 2 months of immersion suggesting the erosion rate was not sufficient to disrupt the fouling from settling. Generation of roughness or hydrophilic phases due to the surface erosion/renewal during immersion could also have altered their AF properties. PLGA-N88/12 showed better anti-settlement and removal of diatom *N. incerta* than the PDMS reference. This is interesting to know given that diatom *N. incerta* is usually hard to remove from hydrophobic PDMS coatings. Bioassays on *Ulva* spores (*rigida* and *linza*) showed no improvement of the anti-settlement properties for each strategy compared to the PDMS reference except for PLGA-N88/12 and TGO-N73/27, but this might have been due to a tin toxicity.

A logical progression of this PhD work would consist in optimizing the crosslinking of LGO-N88/12 to complete the study on the PDMS/polyester hybrid networks. The self-crosslinking of PLGA-*b*-PDMS-*b*-PLGA (LGO-S40) was also missing and could be another interesting erodible coating. Hydrolyzable additive-based PDMS coatings could be prepared with PLGA and/or PLGA-*b*-PDMS-*b*-PLGA additives to study their hydrolysis kinetics once embedded in the silicone elastomer.

To avoid future misinterpretations of contact angle/surface free energy/roughness results due to siliceous phases/salts, PDMS elastomers should be exempt of PDES (ES40). Besides, to avoid

Conclusion and perspectives

undesired tin toxicity, DOTDL catalyst should be replaced by a bismuth-based catalyst, for example. No issue of siliceous phases was observed in the PDMS/polyester hybrid networks given that PDES was substituted by the polyester-based macrocrosslinkers.

A more thorough study on the hydration and erosion mechanisms of the PDMS/polyester hybrid networks could be carried out by using fluorescent probes in water or fluorescent-based PDMS segments or by observing their lixiviation layer through SEM. The crosslinking density of these complex networks could also be investigated to be able to better control the elastic modulus of these networks (with an equilibrium swelling test or simply by following the relationship between the shearing modulus, the elastomer density and the crosslinking density).

Biodegradation tests and toxicological tests must be performed on all the experimental coatings to verify that these new coatings have low harmful impact on the marine environment. Indeed, although they do not contain biocides, they still release some degradation products in the aquatic environment that cannot be underestimated.

This PhD work opens up many new possibilities not yet explored such as new crosslinkable copolymer candidates based on PCL, PLGA, PEG and PDMS (for example) or such as the elaboration of partially crosslinked networks (this time made intentionally). A preliminary trial which combined the 1st and 2nd strategies was performed in this PhD work (PLGA+M3T coating) but would require further crosslinking improvements and further characterizations.

Globally, given that AF efficacy was lost after 6 months for the PDMS/polyester hybrid networks, the erosion rates of the PDMS/polyester networks should be increased, for example by increasing the glycolide content (GA) of PLGA in PLGA-N88/12. The self-crosslinked PLGA-S70 could also be tested in field immersion as it showed the highest mass loss after 60 weeks. If the surface erosion is too fast though, it would lead to a shorter coating service life. So, future efforts should be made to find the most suitable surface erosion rate that makes it impossible for the biofouling to settle on the long term.

Other approaches could be investigated such as combining not two but three or more AF strategies. For instance, a coating displaying a self-healing hydrogel upper layer (with PEG chemistry), an erodible surface thanks to PLGA or PLGA-*b*-PDMS-*b*-PLGA and some

Conclusion and perspectives

hydrophobic PDMS chains. By multiplying the strategies, we could achieve more durable unpredictable/unstable/ambiguous materials towards a wider range of marine organisms.

Finally, the marine industry may be not ready to abandon the use of dicopper oxide or booster biocides as they efficiently limit the biofouling. So, a last alternative could be to select biodegradable biocides, incorporated at low content in novel FRCs (for example, no more than 10 wt.% of Econea).

